

GC  
85.2  
.A4  
E57  
1980  
V.4

# Environmental Assessment of the Alaskan Continental Shelf

**Annual Reports of Principal Investigators  
for the year ending March 1980**

**Volume IV: Hazards**

**ARLIS**

Alaska Resources  
Library & Information Services  
Anchorage, Alaska



**U.S. DEPARTMENT OF COMMERCE  
National Oceanic & Atmospheric Administration  
Office of Marine Pollution Assessment**



**U.S. DEPARTMENT OF INTERIOR  
Bureau of Land Management**

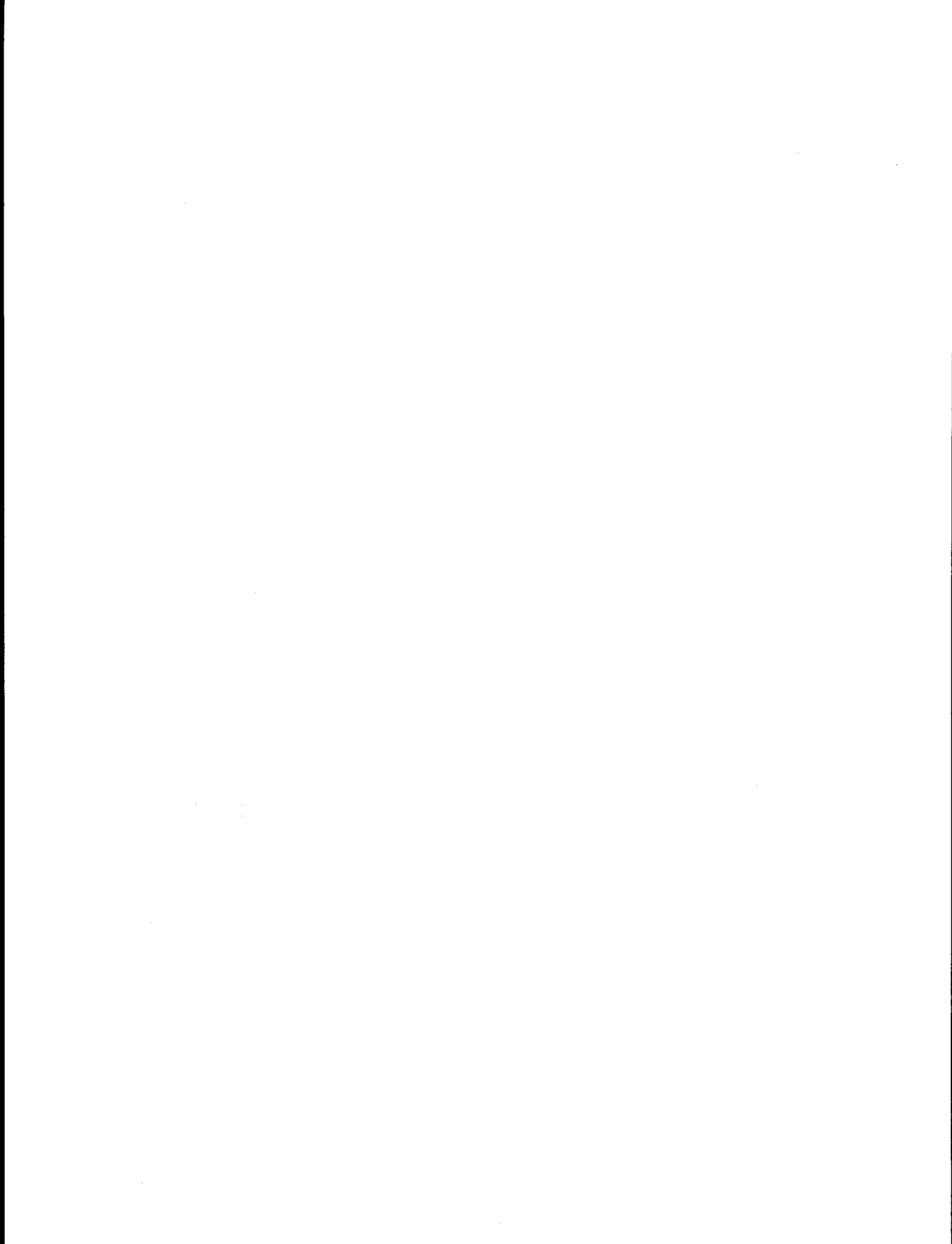


TABLE OF CONTENTS  
VOLUME IV: HAZARDS

<u>RU #</u>	<u>PI - Agency</u>	<u>Title</u>	<u>Page</u>	
16	Davies, J. K. Jacob	- Columbia University, N.Y.	A seismotectonic analysis of the Seismic and Volcanic Hazards in the Prbilof Islands - Eastern Aleutian Islands Region of the Bering Sea	001
105	Sellman, P., E. Chamberlain, A. Delaney	-U.S. Army Corps Engineers, N. Hampshire	Delineation and Engineering characteristics of Permafrost Beneath the Beaufort Sea	125
204/ 473	Smith, P. R. Hartz D. Hopkins	-USGS, California	Offshore Permafrost and Shoreline History as an aid to Predicting offshore permafrost conditions	159
205	Barnes, P. E. Reimnitz	-USGS, California	Geologic Processes and Hazards of the Beaufort Sea Shelf and Coastal Regions	257
210	Lahr, J. C. Stephens J. Rogers	-USGS, California	Eastern Gulf of Alaska Seismicity: Annual Report to the NOAA	357
212	Molina, B.	-USGS, California	Erosion, Disposition, Faulting, and Instability of Shelf Sediments: Eastern Gulf of Alaska	397
251	Pulpan, H. J. Kienle	-U. of Alaska, Fairbanks AK	Seismic and Volcanic Risk Studies Western Gulf of Alaska	427

Annual Report

A SEISMOTECTONIC ANALYSIS OF THE SEISMIC AND  
VOLCANIC HAZARDS IN THE PRIBILOF ISLANDS -  
EASTERN ALEUTIAN ISLANDS REGION OF THE BERING SEA

Contract: NOAA 03-50-022-70

Research Unit: 16

1 April 1979 through 31 March 1980

Principal Investigators

Dr. John N. Davies  
Dr. Klaus H. Jacob

Lamont-Doherty Geological Observatory  
of Columbia University in the City of New York  
Palisades, New York 10964

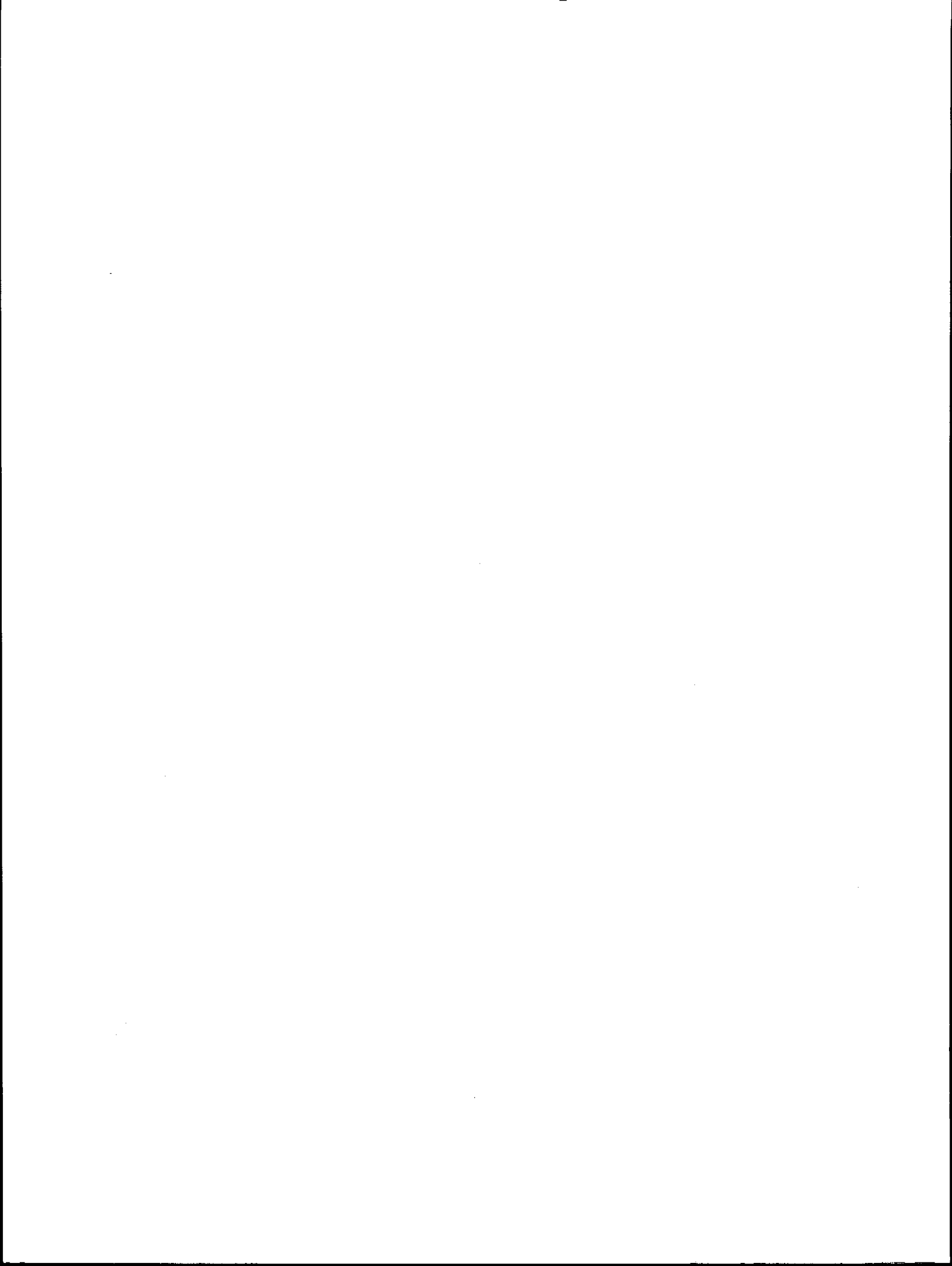


## TABLE OF CONTENTS

	<u>Page</u>
I. SUMMARY . . . . .	5
II. INTRODUCTION . . . . .	7
III. CURRENT STATE OF KNOWLEDGE . . . . .	9
IV. STUDY AREA . . . . .	11
V. SOURCES, METHODS AND RATIONALE OF DATA COLLECTION . . . . .	12
VI. RESULTS, VII. DISCUSSION, IX. NEED FOR FURTHER STUDY. . . . .	14
A. Historical Earthquakes Prior to 1938 and Repeat Times of Great Shocks ( <u>L. Sykes</u> ) . . . . .	14
B. Transverse Structural Boundaries: Their Geologic Control and Influence Upon the Dimensions of Rupture Zones of Great Earthquakes ( <u>J. Davies</u> ) . . . . .	27
C. The Pattern of Seismicity In and Near the Shumagin Gap ( <u>L. House</u> ) . . . . .	33
D. Refined Analysis of Microseismic Data: Hypocenter Locations, Crustal Structure and Focal Mechanisms ( <u>M. Reyners and K. Coles</u> ) . . . . .	43
E. Seismic Source and Strong-Motion Characteristics ( <u>K. Jacob and J. Mori</u> ) . . . . .	49
F. Pavlof Volcano Studies ( <u>S. McNutt</u> ) . . . . .	68
VIII. CONCLUSIONS . . . . .	80
X. SUMMARY OF FOURTH QUARTER OPERATIONS (January-March 1980) AND STATUS OF TECHNICAL WORK . . . . .	82
A. Field Work ( <u>D. Johnson</u> ) . . . . .	82
B. Operational Status of Remote Stations and Recording Centers ( <u>D. Johnson</u> ) . . . . .	83
C. Data Collection and Submission ( <u>J. Hauptman and J. Peterson</u> ) . . . . .	84
D. Computer System and Data Processing ( <u>E. Edsall and J. Peterson</u> ) . . . . .	102
XI. A. REFERENCES . . . . .	105
B. PAPERS PUBLISHED, SUBMITTED AND IN PREPARATION . . . . .	111
C. ABSTRACTS OF ORAL PRESENTATIONS . . . . .	113
D. ABSTRACT AND INTRODUCTION - "St. Elias Earthquake of February 28, 1979: Tectonic Setting and Precursory Seismic Pattern", by O. Perez and K. Jacob . . . . .	121
E. TENTATIVE ACTION PLAN FOR STRONG-MOTION PROGRAM ( <u>K. Jacob</u> ) . . . . .	123



## I. SUMMARY

Objectives. Through work carried out under this project we attempt to assess the volcanic and earthquake hazards that exist in the Eastern Aleutian Islands and Pribilof Islands region of the southeast Bering Sea and the western Gulf of Alaska. This assessment is made in the context of exploration for and possible future development of petroleum resources on the continental shelves which constitute most of the region. The present work focuses on the collection and analysis of new seismic data obtained from a seismic network jointly funded under this NOAA project and a companion project supported by D.O.E. During the past year, however, we have also analyzed historical data which have led to an increased estimate for the seismic potential of the Shumagin Gap. Through the companion D.O.E. and several smaller projects other geophysical, geodetic, and geologic and seismic engineering data are available to this study and the results relevant to hazards assessment are reported here to NOAA.

The Specific Objectives of the Current Work are: (1) to monitor seismic activity in the Shumagin Islands and Dutch Harbor regions of the Eastern Aleutian Island Arc and western Alaska Peninsula regions, and of the Pribilof Islands region of the southeast Bering Sea; (2) to relate this seismic activity to particular faults or fault zones, where possible; (3) to monitor seismically the eruptive activity of three volcanoes: Pavlof, Akutan and Makushin; (4) to evaluate these seismic and volcanic activities for their potential hazards to exploration for and development of petroleum resources on the continental shelves within the study area. An important aspect of seismic hazard assessments is that they require a long-term continuous and reliable data base.

Major Conclusions and Implications. The addition of new historical data and information on repeat times strengthens the conclusion that the Aleutian arc segment near the Shumagin Islands and the tip of the Alaska Peninsula is likely to be the site of one or more great ( $M \geq 7.75$ ) or large ( $M \geq 7$ ) earthquakes and related aftershock sequences within the next several years or a few decades. Such events have a high potential for producing destructive tsunamis and inducing hazardous submarine mudflows. At the present time this "seismic gap" is relatively quiescent, and we note occasional, moderate-sized earthquakes ( $m_b$  5 to 6.5)



associated with the unusually high stress drops (600 to 800 bars) and above-average levels of groundmotion. These events occur near the down-dip end (depths of about 40 km) of the inferred zone of contact between the North American and Pacific plates. They are located directly beneath fore-arc basins which have potential for petroleum exploration. Minor, probably shallow crustal activity appears to be associated with the Sanak Basin on the Pacific Side, and the southwesternmost portions of Bristol Bay, near the Black Hills (Alaska Peninsula) on the Bering-Sea side of the studied arc segment. The extent of rupture zones of past earthquakes appear to have been controlled by transverse structural features. This seismicity (especially in Sanak Basin) may be along a transverse feature that will control the extent of rupture of a future great earthquake in the Shumagin Gap. Other minor, shallow crustal seismicity in the overriding (North American) plate is apparently related to volcanic or magmatic activity. The Dutch Harbor region appears to be characterized by moderate seismicity typical of most portions of the former 1957 rupture zone, although data coverage was incomplete during this reporting period. Analysis of teleseismic data and tsunami arrival times lead us to the tentative conclusion that there is a seismic gap in the Dutch Harbor region. Some events were recorded in the southeast Bering Sea with a single seismic station located on St. Paul, in the Pribilof Islands. The distance range inferred from seismic travel times would indicate that some of these events are associated with the St. George Basin. The single-station limitation does not, however, allow any definite correlation with specific tectonic structures.

## II. INTRODUCTION

General Nature and Scope of Study. The present NOAA funded study, "A Seismotectonic Analysis of the Seismic and Volcanic Hazards in the Pribilof Islands - Eastern Aleutian Islands Region of the Bering Sea" is an amplification of the hazards aspects of a previously existing and concurrent seismotectonic study of the Aleutian arc, funded by D.O.E. The D.O.E. study is very broad in scope and as such includes hazards analysis, but at a low level of priority. NOAA funds are used to accelerate hazards analysis by providing (1) additional staff, (2) equipment for data collection for projects specifically or primarily directed toward hazards analysis, and (3) logistic support to maintain the extensive network of seismic stations and fieldwork required by the combined studies. The general goal of the present study is to monitor seismic and volcanic activity over a long time span and to evaluate this activity in terms of the hazard it implies for the exploration for and possible development of petroleum resources within the study area. The evaluation of this seismic and volcanic data requires a broad seismotectonic framework. This broad framework is provided by the D.O.E. study and by occasional special projects like the geologic investigation described in this report.

Specific Objectives. The specific objectives of the past year have been (1) to continue to monitor the seismic activity in the Sand Point, Dutch Harbor and St. Paul areas, (2) to attempt to relate this activity to specific faults, including a geologic investigation of the Shumagin Islands region for this purpose, (3) to monitor the activity of Pavlof, Akutan and Makushin Volcanoes, and (4) to begin to evaluate the data (where it is sufficient) in terms of its hazards implications.

Relevance to Problems of Petroleum Development. The relevance of this work to petroleum development is straightforward: The basic problem is to design structures that will withstand expected earthquakes, associated tsunamis, and volcanic activity within an acceptable level of risk. This design problem requires, as inputs, knowledge of the probable space-time distribution of large earthquakes, the acceleration vs. distances relations for those earthquakes and the distance to which various volcanic eruptions can be expected to be destructive. Prediction of the space-time distribution of large earthquakes requires a comprehensive understanding of the seismotectonic setting, knowledge of the distribution of pre-existing faults and the longest possible record of previous seismic activity. Deter-

mination of acceleration vs. distance relations requires actual measurements of accelerations within the region over as broad a range of distance and magnitude as possible. Specification of the minimum safe distance from a given volcano requires knowledge of the type of eruption to be expected and the frequency of eruption. The data being collected are essential to each of the above prerequisites to the inputs for the problem of designing safe and economical structures.

### III. CURRENT STATE OF KNOWLEDGE

Shumagin Islands Seismic Gap. Our present understanding of the seismic regime in the Shumagin Islands region is based on the concepts of plate tectonics (Isacks et al., 1968) and seismic gaps (Kelleher, 1970; Sykes, 1971; McCann et al., 1978). The Aleutian Island arc, of which the Shumagin Islands region is a part, is a convergent plate boundary between the Pacific and North American (Alaskan) plates. Along this plate boundary most of the seismic energy is released during great earthquakes ( $M \geq 7.8$ ) (Kanamori, 1977). The aftershock zones of these great earthquakes do not overlap, which suggests that the area left between recent aftershock zones, the seismic gaps, are the most likely sites of the next great earthquake. Other things being equal, the longer the time since the occurrence of a great earthquake in a given gap, the higher is the probability that the gap will be the site of the next great earthquake.

Davies et al. (1976) discussed the historic record of earthquakes in the Shumagin Gap and assessed various methods for estimating the occurrence time of the next great earthquake there. Unfortunately, the error limits on all such estimates are so large as to make them impractical as predictions. We reported in last years' annual report the results of the D.O.E. funded geodetic tilt measurements. While still preliminary, they suggest that the Shumagin Islands region is tilting trenchward at .4 to 4 microradians per year. This tilt rate, if substantiated, would be consistent with that observed in Japan for interseismic periods (Scholz, 1974); i.e. the period between great earthquakes during which strain energy is accumulating. This suggests that such an earthquake was not imminent (due within a few months) at the time of the last measurement (June, 1978).

Davies and House (1979) have compared the Benioff zone seismicity beneath the Shumagin Islands with that beneath other regions of the Aleutian arc and with some other subduction zones. This comparison suggests that the future fault plane of a great earthquake in the Shumagin Gap will be in the main thrust zone (MTZ), the shallowly dipping portion of the Benioff zone above 40 km depth. Below, we interpret most of the shallow seismicity (less than 80 km depth) as being the result of an edge effect of stress accumulation around the future fault plane. This is consistent with Mogi's (1969) observations of a "doughnut" pattern of seismicity around future fault planes in Japan.

The high stress levels implied by this ("our") interpretation have been observed in two studies. Archambeau (1977) computed the stress drop for several earthquakes in the Shumagin Islands region using  $M_s/M_b$  ratios. The high, kilobar stress drops that he obtained have been questioned by some seismologists. House and Boatwright (1980) obtained a maximum stress drop of 600-900 bars for the April 1974 Shumagin Islands earthquake. Additionally, we have recorded two more earthquakes ( $M_b = 5.5$  and  $6.5$ ) near the Shumagin Islands. Both of these events were located at the lower edge of the MTZ and triggered the strong-motion instrument at Sand Point. Unfortunately, these records are not suitable to the stress-drop analysis of House and Boatwright (1980). The strong motion accelerometer at Simeonof Island was not triggered by this event. Finally, we report below the analysis of several events by Mori that also show relatively high stress-drops within the Shumagin Gap. The occurrence of these events is consistent with the Mogi "doughnut" pattern described above and strengthens our conclusion that high stresses are accumulating in this region.

The high stress level observed in the main thrust zone probably implies relatively high stress in the upper crust. This stress will most likely be relieved along pre-existing faults. We are only just now beginning to acquire enough shallow seismicity data to identify active surface faults. If segmentation of the upper plate exists, there would be linear zones transverse to the arc that would have a high risk for large strike-slip or normal faulting earthquakes. We have also observed terraces (see the geologic results reported last year) that are evidence for episodic uplift. It may be that a study of uplifted terraces would allow us to define boundaries for crustal blocks. These boundaries, too, would be zones of high risk for fault motion during large earthquakes.

Pribilof Islands Region. We continue to record earthquakes at the St. Paul seismic station whose hypocenters are probably located in the St. George Basin. This basin is fault bounded (Marlow *et al.*, 1977) and these faults may extend northwesterly between St. George and St. Paul Island (Hopkins, 1976). We cannot determine the association, if any, of the earthquakes to these or other faults until we have more than one seismic station in the Pribilof Islands.

#### IV. STUDY AREA

In the combined D.O.E.-NOAA program, by far the strongest concentration of effort has been in the Shumagin Islands region. Within the OCSEAP program this region is classified as part of the western Gulf of Alaska. The specific area referred to as the Shumagin Islands region extends from the SW end of Kodiak Island to Sanak Island. Within this area is the 12 station network of seismic stations on Pavlof Volcano which is supported primarily by D.O.E. This area is also the same as the Shumagin Islands seismic gap in its broadest application; although there are some reasons to restrict the definition of the seismic gap to the western half of this area.

The Dutch Harbor area, also within the western Gulf of Alaska, receives the second highest level of effort. This area includes the NOAA funded stations on Akutan and Makushin Volcanoes.

Lastly we operate a single station on St. Paul Island, one of the Pribilof Islands. This station is in the Bering Sea region according to the OCSEAP classifications.

## V. SOURCES, METHODS, AND RATIONALE OF DATA COLLECTION

Seismic Data. Our primary emphasis in data collection is the operation of local, high gain, telemetered networks of short period seismic stations. These local networks allow the precise location of smaller magnitude earthquakes that is necessary for the timely and accurate delineation of tectonic features such as activity faults, segmentation of the subducted slab and patterns of volcanic activity. Precise locations are also critical for the evaluation of strong-motion records. The principal regional network is located in the Shumagin Islands. It consists of 15 remote (single component, vertical) stations and one 3-component station at the recording center, Sand Point.

Within this network we also operate a dense, 12 station network around Pavlof Volcano. The main purpose of this D.O.E. funded network is to provide data with which to study the geothermal potential of Pavlof Volcano. This network, in conjunction with the regional Shumagin Islands network, may also provide data that would allow us to study the relationship between variations in local volcanic activity and changes in the regional stress field as inferred from seismic activity. Several studies have suggested that such volcanic activity may be useful in predicting great earthquakes (Kimura, 1976; Nakamura et al., 1977; McCann, 1978).

At Dutch Harbor we record two local components (one vertical and one horizontal) and two remote stations (Akutan and Makushin Volcanoes). This three station "network" is very poorly distributed (geographically) and consists of the minimum number of stations to locate earthquake hypocenters. The local components are intended to complement the long period seismograph there and the remote stations are primarily intended to monitor volcanic activity on Akutan and Makushin volcanoes.

At St. Paul, in the Pribilof Islands, we operate a single, short period, vertical seismometer. This instrument monitors local activity levels as a function of distance and also complements the long period seismograph there.

Other sources of seismic data are the long period seismographs that we operate under D.O.E. funding at Sand Point, Dutch Harbor, and St. Paul, the broad band data that we discuss below in the hazard analysis section under "Results", and the World Wide Standard Seismograph Network.

Strong Motion Accelerographs. For the past few years (primarily under D.O.E. funding) L-DGO has operated Kinometrics SMA-1 accelerographs at Dutch

Harbor, Sand Point and Simeonof Island. The purpose of these instruments is to collect acceleration data with which to construct acceleration vs. distance relations that are essential to the safe engineering design of large structures such as drilling rigs, pipelines, and holding tanks.

Tilt Measurements. Under D.O.E. and NSF funding we annually reoccupy 1 km level lines at Sand Point (2 lines), Squaw Harbor (1 line) and Simeonof Island (1 line). These tilt measurements provide important data regarding the accumulation of stress in the Shumagin Seismic Gap.

Geologic Investigations. During June 1978 we employed two geologists in a reconnaissance of faults and terraces in the Shumagin Islands region. They mapped several minor new faults and tentatively identified several terraces. The identification and evaluation of faults is essential to the assessment of the activity level of faults within the study area. The ages, heights and distribution of terraces can provide extremely important data regarding past episodes of rapid uplift, perhaps during previous great earthquakes. These terraces may help to define block boundaries that may be particularly prone to relative motion during future earthquakes.

Because these investigations are not primarily seismologic in nature, we submitted a separate proposal to NSF for the geologic investigations. This work has been approved by NSF for two years. These geologic investigations are potentially extremely valuable to the purposes of seismic hazards evaluation.



## VI. RESULTS, VII. DISCUSSION, IX. NEED FOR FURTHER STUDY

### A. Historical Earthquakes Prior to 1938 and Repeat Times of Great Shocks (L. Sykes)

1898-1938. Except for the largest events, the record of felt earthquakes is quite short for most of mainland Alaska and is especially poor for the Aleutian Islands and the Alaska Peninsula prior to 1938. Limited instrumental data are available for great ( $M \geq 7.8$ ) earthquakes and for some but not all major ( $7 \leq M < 7.8$ ) shocks during the period 1898 to 1938. The epicenters, depth, and extent of rupture in these shocks, however, are often poorly known prior to the 1920's.

Figure 1 shows the epicenters and inferred extent of rupture of all known shallow (depths less than 70 km) earthquakes of magnitude 7.4 or greater along the plate boundary from British Columbia to southern Alaska and thence along the Aleutian arc to Kamchatka. The large shocks of March 7, 1929 ( $M_w = 7.8$ ) and March 30, 1965 ( $M_w = 7.6$ ) are omitted since they are known to have involved normal faulting in the trench rather than inter-plate motion [Kanamori, 1972; 1977; Abe, 1979]. It appears to be safe to conclude that shocks of magnitude greater than about 7.5, in fact, were absent from the entire arc from 1907 to 1938 except for the event of magnitude 7.6 in the western Aleutians on December 17, 1929. Eight shocks of  $M_s$  7.4 to 8.2 affected the central and western Aleutians from 1898 to 1907. If  $M_s$  is equated to  $M_w$  and is converted to seismic moment using

$$M_o = 1.5 (M_w + 10.7) \quad (1)$$

from Kanamori [1977], the sum of the seismic moments of the eight events is  $5.4 \times 10^{28}$  dyne-cm, which is about half the measured seismic moment of the Rat Island shock of 1965 of  $M_w = 8.7$ . Since data of periods longer than 20 sec are generally not available for those eight events, the total seismic moment is probably underestimated considerably. Hence, it does seem reasonable that a sizable segment of the arc ruptured between 1898 and 1907. The apparent absence of large tsunamis in the Pacific for those shocks suggests, however, that individually they were not as large as the great earthquakes of 1957, 1964 and 1965 [Abe, 1979; Kanamori, written communication, 1979].

The two shocks of magnitude 7.5 in the central Aleutians occurred on December 31, 1901 and January 1, 1902 only 20 hours apart. It is improbable, although not impossible, that the two events are unrelated. A tsunami reported at Kenai on Cook Inlet appears to have been associated either with these events or with an eruption of St. Augustine Volcano [Reid, 1912; Cox and Pararas-Carayannis, 1976]. Two great shocks in September 1899 of  $M_s$  8.2 ruptured all or most of the present seismic gap near Yakataga (Figure 1) in the Gulf of Alaska [Tarr and Martin, 1912; McCann *et al.*, 1979]. McCann *et al.* [1979] conclude that another large shock of  $M_s$  8.1 on October 9, 1900, which Richter placed near Yakataga, was most strongly felt on Kodiak Island. Also, the greatest number of aftershocks was reported from Kodiak Island. Hence, the rupture zone of that shock is shown in Figure 1 as extending from Kodiak Island an indefinite distance to the southwest.

Richter [1958] lists a shock on June 2, 1903 of magnitude 8.3 with a questionable depth of 100 km near what appears to be the eastern end of the aftershock zone of the 1938 earthquake. We are not able to ascertain the extent of rupture for that shock or whether it was, in fact, a deeper event or one that broke the plate interface at a shallow depth. Kanamori and Abe [1979] calculate an  $M_s$  of 7.7 for a shock on July 14, 1899 for which the location that they quote— $60^\circ\text{N}$ ,  $150^\circ\text{W}$ —appears to be very uncertain. Tarr and Martin [1912] list felt reports for that event from Unalaska in the eastern Aleutians and from Unga in the Shumagin Islands. The shock is plotted in Figure 1 as a questionable event in or near the Shumagin gap.

Hence, the events of July 14, 1899, October 9, 1900, January 1, 1902 and June 2, 1903 are possible candidates for large shocks that may have ruptured either the Unalaska or Shumagin gaps or may have previously ruptured the area involved in the earthquake of 1938. Thus, the Shumagin gap has not been the site of a large earthquake for at least 77 years (1980-1903).

#### Earthquakes Prior to 1897

The record of great historic shocks is generally poor and is certainly incomplete for the Aleutians and the Alaska Peninsula prior to the advent of a global instrumental record in 1897. Two large shocks of  $M = 7.5 \pm 0.7$  took place somewhere in the Commander gap in the westernmost Aleutians (Figure 1) in 1849 and 1858 [Kondorskaya and Shebalin, 1977]. Large events are inferred by us to

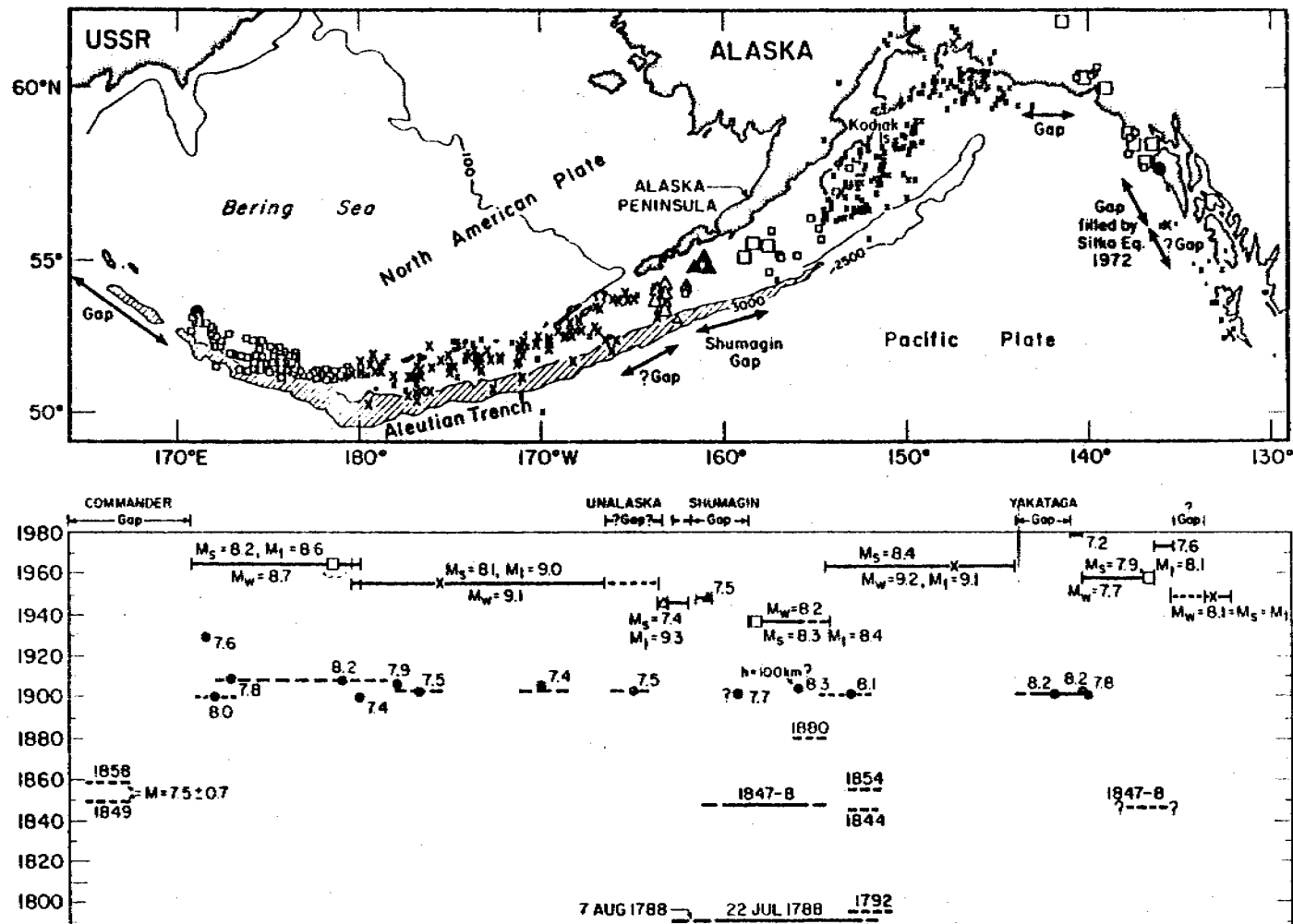


**Figure 1.** Above: Aftershocks of earthquakes of magnitude  $M > 7.4$  from 1925–1971 along plate boundary in Aleutians, southern Alaska and offshore British Columbia, after Sykes (1971). Contours in fathoms. Various symbols denote individual aftershock sequences as follows: crosses, 1949, 1957 and 1964; squares, 1938, 1958 and 1965; open triangle, 1946; solid triangle, 1948; solid circles, 1929, 1972. Largest symbols denote most precise locations. Aftershock dimensions usually could not be determined before about 1925. Below: Space-time diagram showing lengths of rupture zones, magnitudes and locations of mainshocks for known events of  $M > 7.4$  from 1784 to 1980. Dashes denote uncertainties in size of rupture zones. Magnitudes pertain to surface wave scale,  $M_s$  unless otherwise indicated.  $M_w$  is ultra-long period magnitude of Kanamori (1977);  $M_t$  is tsunami magnitude of Abe (1979). Large shocks in 1929 and 1965 that involve normal faulting in trench are omitted. Absence of shocks before 1898 along several portions of plate boundary reflects lack of an historic record of earthquakes for those areas. Magnitudes after Richter (1958), Kanamori (1977), Kondorskaya and Shebalin (1977), Kanamori and Abe (1979) and Perez and Jacob (1980).

have ruptured segments of the plate boundary near the Alaska Peninsula (Figure 1) in 1788, 1792, 1844, 1847, 1854, 1880 and possibly in 1848. Portions of the arc--including Kodiak Island, the Shumagin Islands, the Alaska Peninsula and Unalaska--were settled by the Russians in the late 18th century. Permanent settlements date from 1784. Hence, that part of the Alaska-Aleutian arc possesses the longest known historic record of large earthquakes. The general lack of large events along most other parts of the plate boundary prior to 1897 in Figure 1 is undoubtedly an artifact of the near absence of an historical record.

Criteria for Recognizing Large Historical Shocks. In Figure 1 we attempt to extend the record of large shocks that appear to have ruptured the plate boundary at shallow depths along the Alaskan-Aleutian zone back to the beginning of Russian settlement in the late 18th century. We omit shocks that from various historical descriptions appear to be related to volcanic eruptions or those that appear to have been felt at only a single location. We take one or more of the following criteria as indicative of an earthquake that appears to have broken a considerable ( 100 km) portion of the plate boundary: extremely strong shaking ( $MM \geq IX$ ) at two or more points a considerable distance apart [Kelleher, 1972], strong motion continuing for a matter of minutes, permanent changes in elevation (or in sea level), a large tsunami associated with the shock, numerous fissures or landslides, and reports of aftershocks lasting a period of weeks to months (especially when observed at two or more localities). Places experiencing these effects are taken to have been located adjacent to the zone of rupture.

Earthquakes of 1880 and 1868. G. Plafker (written communication, 1971) brought to our attention a published account [Newlander, 1883] of a large earthquake off the Alaska Peninsula near Chirikof Island ( $55.8^{\circ}N$ ,  $155.6^{\circ}W$ ) on September 28, 1880. The report cites the following observations by Mr. Alexander Newlander: three heavy successive shocks followed by a series of aftershocks that lasted until October 16, 1880; numerous deep fissures on the island with a width of from 15 to 20 inches (38 to 51 cm); shelves wrenched from the walls, and flooring twisted out of shape in his log house; no one able to stand on their feet out-of-doors during the strong motion that lasted for at least 20 minutes, several seawaves travelled inshore about 60 yards (55 m); an increase in sealevel on the south side of the island and a decrease on the west side.

Moore [1962; written communication, 1979] believes that the northwest part of Chirikof Island, which is bounded by a northeast trending fault, tilted abruptly to the southeast during the earthquake of 1880; the vertical displacement on the

southeast boundary fault was 6 feet (2 m), and evidence of the faulting is still preserved in dammed streams and uplifted wave-cut terraces. The above evidence for a tsunami, very strong ground shaking, aftershock activity and vertical deformation lead us to conclude that the shock of 1880 should be regarded as a major earthquake, which probably ruptured both the plate boundary and a nearby imbricate fault within the upper lithospheric plate. The extent of rupture along the arc, however, is uncertain and is indicated as indefinite in Figure 1.

Tarr and Martin [1912] quote Becker [1898] to the effect that during a slight earthquake in 1868 the elevation is said to have amounted locally to over 20 feet (7 m) at Unga in the Shumagin Islands. Becker, however, references Dall [1870] as the source of this information who states:

"Captain Riedell, of the bark Constantine, states that in the inner portion of the south harbor of Unga Island, one of the Shumagins, where he had previously obtained four fathoms, muddy bottom, after the slight earthquake shock of May, 1868, he sounded, obtaining only four feet in the same place. The lower portion of the harbor retained, however, abundance of water. Careful and exact charts of given localities are needed to determine with accuracy the rate of the gradual elevation."

We regard this quote as poor evidence for the existence of a large earthquake near Unga in 1868. Hence, we do not include that event in Figure 1.

Shumagin-Kodiak Earthquake of 1788. Descriptions of the earthquake of July 22, 1788 lead us to interpret it as a great shock that appears to have ruptured at least a 600 km segment of the plate boundary (Figure 1). Since many accounts of this event [e.g. Coffman and vonHake, 1973] are third or fourth-hand, we examined some of the original descriptions in Russian of this and other historic Alaskan earthquakes.

The oldest reference to this event is contained in a letter dated 2 May 1789 from W. Merkul'ev to G.I. Shelikov as quoted by Solov'iev [1968] and translated by G.W. Moore:

"On 11 [22] July 1788 here on Kodiak there was a great earthquake, and we thought that the ground would soon collapse. It was impossible to stand up, and we had not even managed to recover after the quake before a flood came in from the sea, and in our bay [Three Saints Bay] it caused a deluge. Everyone searched then for a place to save his life. The deluge caused extensive damage. First, my cabin was swept away, with the remaining goods belonging to Shelikof, along with a small building and stockade. In your kitchen garden, the soil and vegetables together were swept away, and in place of them rock particles were brought in and dug out holes were left in the soil. The water raised almost halfway up the upper windows of your room. It was swift and remained for only a short time: there were two large waves and the remainder were smaller. After that, the earth trembled

every day for a month or even longer, once, twice, three times, even more. After the earthquake, our place by the bay, compared to formerly, became lower."

The items in brackets in this and other references below are either those of the translator or our own explanations and additions. Note that 11 July in the Julian calendar as used in the letter is equivalent to 22 July in the modern Gregorian calendar. In the remainder of this article dates on the Julian calendar are followed by the modern date in brackets or parentheses unless otherwise noted.

Davydov [1812, p. 154-156] as translated by W.L. Klawe states:

"Furthermore, this is corroborated by earthquakes that occur every year on Kodiak. In 1788, this island and the adjacent land suffered from a strong earthquake, which continued for 17 days. At that time an opening appeared in the side of the volcano [Augustine Volcano] that is located behind Alaska [Peninsula] on Kamishak Bay, from which smoke exudes until this day. The earthquake on Kodiak Island was frightful. After the first shocks, the sea suddenly withdrew from the shore. Then the Koniags and the Russians fled into the mountains. After a few minutes, water with great speed and appearing like a mountain surged against the shore. This tide tore a vessel from its mooring lines (ropes used to fasten ships to shore) and placed it on top of a cabin. Some of the cabins were entirely carried away by the water. During the same day, two similar flood and ebb tides took place. In the course of 17 days, severe shocks occurred, which caused landslides in the mountains and slides along the shores. As a result of collapse of promontories, many stones were loosened.

Once on the Kuril Islands there was a still more terrible earthquake. The sea receded from shore then smashed against it with such swiftness that many people drowned, not having time to flee to the mountains. The craft of a Russian merchant that was lying by the shore was tossed three or four versts [3-4 kilometers] from the shore to where it remains forever.

In the year 1792, there was a still more severe earthquake, continuing for 18 hours. Because of this, all cabins collapsed, and some stones slid down. A vessel, which at that time was proceeding from the open sea into Three Saints Bay [Kodiak Island], encountered a strong agitation and suffered greatly from the unusual and highly anomalous wave patterns.

The earthquakes on Kodiak always occur at the same time as on Alaska [Peninsula], from the direction of which they commence. The cause of this may lie in Kamishak [Augustine] Volcano, located north from Kodiak."

A translation from Veniaminov [1888, vol. 2, p. 22] by J. Kisslinger indicates:

"There have not been extremely strong earthquakes here (excluding one on the Pribilovs) for a long time, but one record seen by me states that: 'on July 11 [22], 1788 (i.e. 16 days before the flood on Unga) here on Unga [Shumagin Islands] there was an earthquake so strong that it was impossible to stand on one's feet, and many mountains crumbled, and after this after a

little time had passed, there was a horrible flood.' It is remarkable that such strong earthquakes (as, for example, that which occurred on the Pribilovs) took place on islands far removed from volcanoes."

The phrase "after this after a little time" in Veniaminov is indefinite about the timing of what is termed the "horrible flood". It is not clear from the above quote if that flood, in fact, differs from the one that occurred 16 days after the earthquake, i.e. on July 27 (Julian) = August 7 (modern calendar). The above quotes from Merkul'ev and Davydov, however, are definitive in describing a tsunami on Kodiak that was associated with the earthquake of July 22.

The following quotations from Veniaminov [1840 or 1888] as translated by J. Kisslinger et al. [1980] refer to a flood that occurred on Unga 16 days after the earthquake. The page numbers refer to the same passage in the 1840 and 1888 editions, respectively.

[p. 27, 20]. "The tradition of the Aleuts...reports that during the flood which took place on Sanak around the year 1790 the water came in large and infrequent waves. In addition to this, I saw a remark in a church book, written in old-fashioned handwriting, which stated that on 27 July [August 7] 1788 there was such a terrible flood on Unga Island that many Aleuts were killed, though God spared the Russians, and the oldtimers say that (at this or the other time) the water rose to 50 sazhen". [91 or 107 m]."

[p.217, 154]. "The deluge or flood which took place on Unga and on the southern side of Alaska [Peninsula] in 1788 did not have any effect on the northern side of Unimak."

[p. 242, 171]. "The flood which took place on Sanak around the year 1788 was much smaller here [Pavlof Bay, south coast of Alaska Peninsula]."

The following are taken from the above quotes as strong evidence for a great earthquake in the Shumagin-Kodiak area on July 22, 1788: very strong ground motion and landslides on both Kodiak Island and Unga, a tsunami accompanying the earthquake on Kodiak, what appears to have been a tsunami on Unga, aftershocks lasting a month or more on Kodiak, and land subsidence on Kodiak. Almost all of Kodiak Island also subsided during the great Alaskan earthquake of 1964 [Plafker, 1965]. Thus, the rupture zone of the shock of July 22, 1788 is shown in Figure 1 as including at least half of the Shumagin gap, the entire rupture zone of the 1938 earthquake and the southwestern portion of the 1964 rupture zone. Solov'iev [1968] estimates that the average height of the tsunamis along the rupture zone was about 5 m (Figure 2) and that the magnitude was no less than 8. The actual extent of rupture, which appears to be at least 600 km, is uncertain and may have continued as far to the southwest as Sanak Island near 163°W.

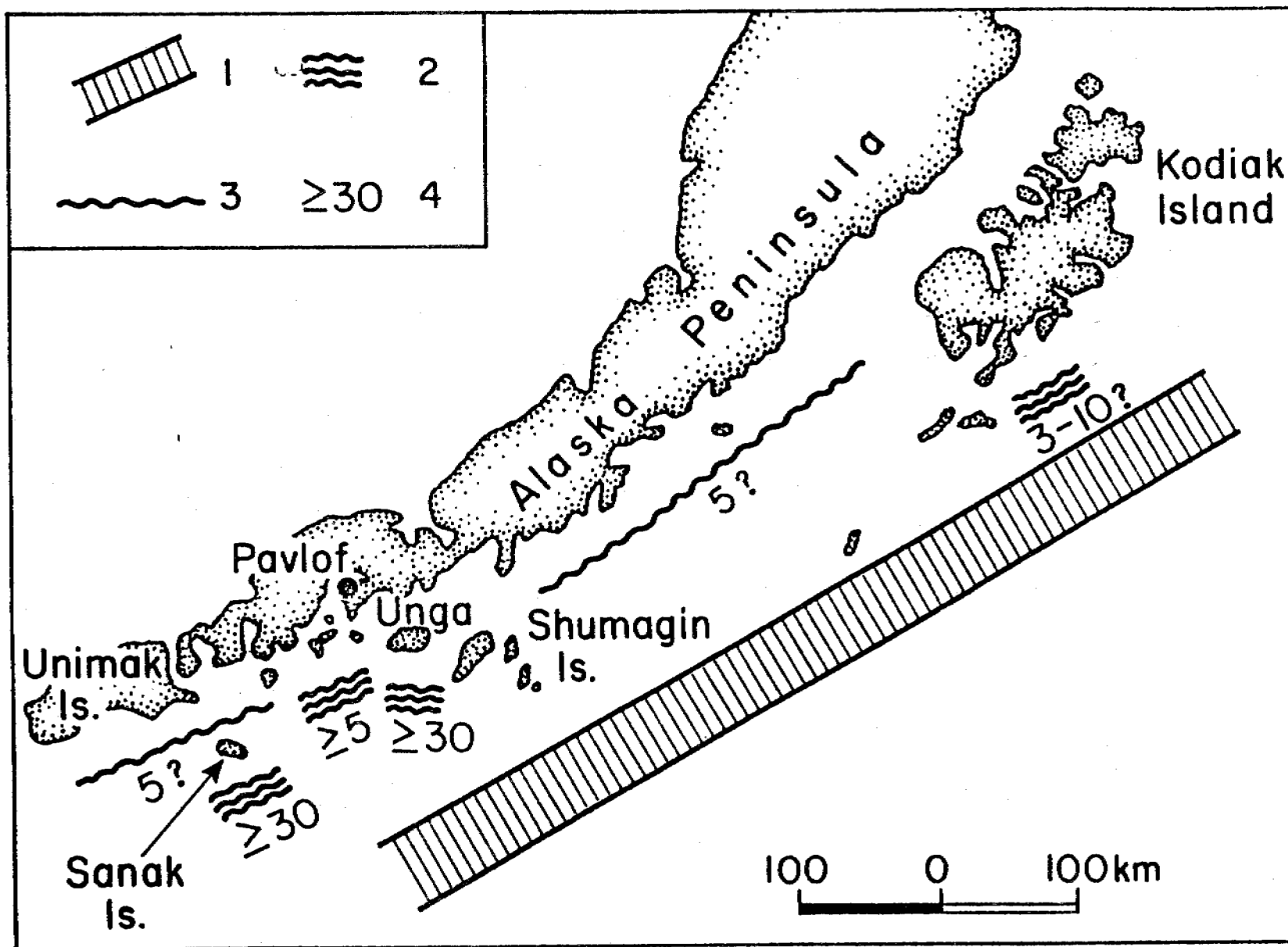


**Figure 2.** Diagram of earthquakes and tsunami of 1788, after Soloviev (1968). 1 - hypothetical location of rupture zone; 2 - positive known places of appearance of tsunami, 3 - probable places of appearance of tsunami; 4 - approximate height of tsunami in meters.



Solov'iev [1968] infers that a second large earthquake 16 days later on August 7, 1788 caused the second flood on Unga, ruptured the segment of the arc from Unga to Sanak (the western half of the Shumagin gap) and created sea waves that reached heights of more than 30 m on Unga and Sanak. He concludes that waves generated by that event did not affect Kodiak Island. It is difficult to attribute a wave height of 30 m to anything other than a tsunami. The term "strong and infrequent walls" in the above quote from Veniaminov [1840 or 1888] seems to us to be most readily interpreted as a tsunami on Sanak Island. For this reason it is also hard to imagine that the source of a large tsunami could be anything other than that of an earthquake.

None of the Russian texts we examined state that the second flood was accompanied by an earthquake or give the date of the flood on Sanak Island. The following quote from Dall [1870], however, is more specific on these points. Solov'iev [1968] concludes that Dall had access to other original documents as well as the work of Veniaminov [1840 or 1888].

"1788. An earthquake, attended with a tidal wave visited the Shumagins. On the 27th of July [about 7 August] the water overflowed Sannak Island, destroying the hogs which had been placed there. From this point the inundation extended to Aliaska [Peninsula]."

While it seems reasonable to conclude that the western portion of the Shumagin gap may well have broken in a large shock on August 7, the evidence is not definitive and comes in part from a secondary source, Dall.

The historic descriptions seem most compatible with rupture extending from Kodiak Island to near Unga on July 22 and from Unga to Sanak on August 7. A second large shock conceivably could have involved normal faulting in the trench seaward of the rupture zone of shock of July 22. Wave heights of tens of meters in the Alaska-Aleutian zone, however, are only known to have been associated with large events that occur along or north of the inner wall of the trench, as in 1946 and 1957. The evidence from the 1946 earthquake suggests that a 30 m wave was associated with a rupture zone at least 100 km on a side. This would include a substantial portion of the western half of the Shumagin gap. Obviously, the credibility of a seismic seawave with a height of 30 m on Unga in 1788 has great implications for the assessment of tsunami risk. The source of a wave of 30 m at Unga in 1788 must be sought nearby and not as distant as the zone farther west that ruptured in 1946.

Other Earthquakes During Russian Ownership: 1792, 1844, 1847, 1848 and 1854. An important paper by Doroshin [1870; translated by Kisslinger et al., 1980]

contains what appear to be unique descriptions of a number of earthquakes in the Alaska-Aleutian arc during the mid-19th century. Using the criteria listed in the last section, earthquakes in 1844, 1847 and possibly that of 1848 appear from the following quotes to be large shocks that may have ruptured considerable segments of the plate boundary as inferred in Figure 1 near Kodiak Island, Chirikof Island (Ukamok), the Shumagin Islands (Unga), and the Alaska Peninsula.

"[p.41]. On April 1 [13], 1844 at midnight, there was a large earthquake at Pavlof harbor on Kodiak Island. It continued for more than two minutes, and was accompanied by a loud noise. The local inhabitants ran from their homes. Earthquakes on Kodiak are frequent in general, but even the oldest inhabitants could not remember any earthquake there that was so strong as this."

"[p. 41]. On April 4 [16], 1847, 6 AM, there was a large earthquake on Ukamok. It began to the south, and continued from the east at about 10:00 AM. It continued, although considerably more weakly, until May 10 [22]. The ground cracked in many places on the island, and rocks slid."

"Early in the morning of the same date there was a fairly large earthquake on Unga. At 10:00 AM it grew to the point that one couldn't remain standing. At about this same time a fairly large earthquake was felt several times on the Alaskan Peninsula."

"[p. 42]. On June 18 [30], 1848, there was an earthquake on Ukamok. It began at midnight and continued for nearly half an hour. After a pause of several minutes it then struck again in the earth 'as if it were a strong breaker wave', and shook so strongly that one could not stand on one's feet. After fifteen minutes it grew quieter, but the 'earth still shook, like the ocean swells after a large storm'. The earthquake was accompanied by a sound like that of the wind, and by a rumble."

"[p. 43]. On January 16 [28], 1854, shortly after 8:00 AM there was an earthquake at Pavlov Harbor on Kodiak Island. It continued constantly for more than a minute; then, in the course of one hour there were up to six perceptible earthquakes, and weak earthquakes continued all day. On the night of the 17th [29] there were two earthquakes: one shortly after 1, one right after 5, and weak vibrations occurred repeatedly until January 21 [February 2]. At the first onset of the underground rumble on January 16th [28], the water in the harbor rose anomalously, and then subsided after two or three minutes, during which time there was a strong rip."

The above reports from Unga, the Alaska Peninsula and Chirikof (Ukamok) Island suggest that the earthquake of 1847 ruptured at least a 500 km segment of the arc including at least half of the Shumagin gap and all of the zone that broke in 1938. Since the shocks of 1792, 1844 and 1854 are only known to have been felt on Kodiak Island, the dimensions of their respective rupture zones are uncertain. These shocks as well as that of 1788 appear to have ruptured portions of the zone that broke in 1964. While the shock of 1844 conceivably could have been of

intermediate depth; the numerous aftershocks, the presence of sea waves or surficial effects reported in conjunction with the shocks of 1788, 1792, 1847, 1848, and 1854 suggest that the latter five events were, in fact, of shallow focus.

### Repeat Times of Large Shocks in Shumagin Gap

Since the earthquakes of 1788 and 1847-8 appear to have ruptured at least half of the Shumagin gap, it now seems reasonable to assign it a seismic potential for a large shock in either category 1 or 2 of McCann *et al.* [1979], both of which denote a region that is known to have experienced a previous large shock. Their category 1 reflects a period of at least 100 years since the last large earthquake while category 2 represents a previous shock between 30 and 100 years ago. The historic data (Figure 1) indicate a minimum of 77 years and a maximum of 133 years (1980-1847) since the last large earthquake in the Shumagin gap. The Unalaska gap, however, is not known to have definitely ruptured in a past large shock. Nevertheless, the plate boundary in that region may have ruptured in 1957 or between 1898 and 1903. It is clear from Figure 1 that almost the entire plate boundary along the Aleutians, southern Alaska and British Columbia is known to have ruptured in large earthquakes. If any segments move in a totally aseismic manner, their length cannot total more than a few hundred kilometers.

Taken alone the dimensions of the rupture zones of the shocks of 1938 and 1946 (Figure 1) might suggest that the region between the aftershock zones of the great shocks of 1957 and 1964 may not rupture in the very greatest earthquakes; i.e. shocks with rupture dimensions,  $L$ , in excess of 500 km and magnitudes,  $M_w$ , as great as 9.0. The shock of 1788, however, appears to have broken about at least a 600 km segment of the arc and that of 1847, at least a 500 km segment. If the Shumagin gap itself of length,  $L$ , equal to 250 km ruptures in a single event, the magnitude and moment are expected to be similar to those of the 1938 earthquake, i.e.  $M_w = 8.2$ ,  $M_o = 4 \times 10^{28}$  dyne-cm. Larger magnitudes and moments could result if rupture also extends into the Unalaska gap or into the zone that broke in 1938.

Sykes and Quittmeyer [1980] obtain the relationship

$$T_R = \frac{1}{\alpha} \left[ \frac{\Delta\sigma}{\mu C} \right] \left( \frac{W}{V_c} \right) \quad (2)$$

for the repeat time,  $T_R$ , of great shallow earthquakes of the thrust type along convergent plate boundaries where  $\mu$  is the shear modulus,  $\Delta\sigma$  the stress drop which is approximately a constant of about 30 bars for large thrust events [Kanamori, 1977; Sykes and Quittmeyer, 1980],  $W$  is the downdip length of interaction between two plates,  $v_c$  the rate of plate convergence (perpendicular to the arc),  $C$  is a geometrical factor that is nearly a constant of 0.9 for  $L \geq W$ , and  $\alpha$  is the ratio of seismic slip to total slip (seismic plus aseismic).

For a constant stress drop process the quantity in brackets is a constant and  $T_R$  is proportional to  $W/v_c$ .

$$T_R = B W/v_c \quad (3)$$

where  $B$  is a constant if  $\alpha$  is a constant along and among subduction zones and the term in brackets is also a constant. Since  $W$  varies from about 75 to 200 km along the Alaska-Aleutian arc, equation (2) predicts that the repeat time of great shocks may vary by about a factor of three along the arc. For the 1964 rupture zone a repeat time of about 164 years is obtained from  $T_R = U_s/v_c$  using  $U_s = 10.9$  m for the average slip in the 1964 earthquake,  $v_c = 6.66$  cm/year and assuming  $\alpha = 1$ . We obtain a repeat time of 147 years from  $T_R = BW/v_c$  using  $B = 4.91$ ,  $W = 200$  km and  $v_c = 6.66$  cm/year. We calculate repeat times of 66 to 86 years for the Shumagin gap using the same value of  $B$ ,  $v_c = 7.4$  cm/year, and  $W = 100$  to 130 km. If the gap ruptured in 1903, this suggests the reoccurrence of a great shock between about 1969 and 1989.

Alternately a mean repeat time of 6.3 years for shallow shocks of  $M_s \geq 7.8$  along the Alaska-Aleutian arc, a distance of about 4100 km (140°W to 164°E), is obtained by dividing 82 years (1980-1898), the time interval over which the record is nearly complete, by the number of great events, 13. This yields a repeat time,  $T_R$  ( $M \geq 7.8$ ), of about 103 years for a 250 km segment of the arc equal to the size of the Shumagin gap. Similarly, repeat times of 2.2 years for major events ( $7.0 \leq M_s < 7.8$ ) for the whole arc and 36 years for the Shumagin Gap are obtained using the 28 events of that size from 1918 to 1980 between 140°W and 164°E. The last major event in the gap occurred 32 years ago (1980-1948). Obvious after-shocks, events deeper than about 70 km, shocks situated more than 100 km from the plate boundary or those involving normal faulting in the trench were omitted from the above calculations.

Probably the best estimate of repeat time for the Shumagin Gap, 60 years, is obtained by taking the time difference between the shocks of 1788 and 1847-8 which appear to have ruptured the plate boundary from Unga to at least Chirikof Island. This includes at least half of the Shumagin Gap and all of the 1938 rupture zone. Hence, from 1788 to 1938 (150 years) the latter zone re-ruptured in 1847 and 1938 and possibly another time between 1898 and 1903. Hence, the mean repeat time for that segment is either 50 or 75 years. The largest individual repeat time, 91 years, is obtained if that segment is assumed not to have ruptured between 1847 and 1938. The Shumagin gap, as mentioned earlier, has not broken in a great event for at least the last 77 years. That interval is somewhat greater than the mean repeat time of 50 to 75 years calculated for the adjacent segment of the arc that ruptured in 1938. It is still somewhat less than the largest possible repeat time for that segment, 91 years. Hence, to the extent that experience from the 1938 zone can be applied to the Shumagin Gap, it seems very likely that one or more large earthquakes will rupture the Shumagin Gap within the next two decades.

## B. Transverse Structural Boundaries: Their Geologic Control and Influence Upon the Dimensions of Rupture Zones of Great Earthquakes (J. Davies)

In an earlier section on Plate Motions and the General Tectonic Setting of the Shumagin Seismic Gap, we noted that the Aleutian arc is built upon, or is backed by, a collage of distinct tectonic blocks. We further noted that boundaries between these blocks may be important for the present tectonism of the Aleutian arc; in particular, they may influence the extent of the rupture zones of great thrust-type earthquakes. This section summarizes a number of possible transverse structural boundaries that appear to have partially controlled the extent of rupture of some recent great earthquakes along the Aleutian arc. Following this arc-wide summary, we focus on the tectonic setting of the Shumagin and Unalaska(?) seismic gaps within the eastern Aleutian arc. We consider evidence for transverse structural features that may control the extent of the seismic gaps.

### Transverse Structural Boundaries Along the Aleutian Arc

Many authors [Brazee, 1965; Jordan *et al.*, 1965; Sykes and Ewing, 1965; Mogi, 1968, 1969; Sykes, 1971; Stauder, 1972; Van Wormer *et al.*, 1974; Bruns and von Huene, 1977; Spence, 1977; Nishenko and McCann, 1979; Pulpan and Kienle, 1979] have observed that the ends of the aftershock zones of great Alaska-Aleutian earthquakes often coincide with the locations of major transverse structural features. The spatial relationship between aftershock zones of recent great earthquakes and large-scale transverse features is shown in Figure 3. We suggest that these transverse structural features bound tectonic blocks of the Alaska-Aleutian portion of the North American plate; and further that these blocks are mechanically distinct such that they can store and release strain energy nearly independently of adjacent blocks.

Shirshov Ridge. The north-south trend of Shirshov Ridge (which separates two distinct "backarc" regions, Figure 3) intersects the Aleutian arc at the western end of the aftershock zone of the Rat Islands earthquake of 1965 [Sykes and Ewing, 1965]. The origin of the Shirshov Ridge and its relation to Bowers Ridge are not well understood. Whether it is an ancient spreading center [Kienle, 1971], remnant arc [Karig, 1972] or some other relic of the plate tectonics that formed eastern Siberia [e.g. Fugita, 1978], it seems likely that the Shirshov Ridge and its

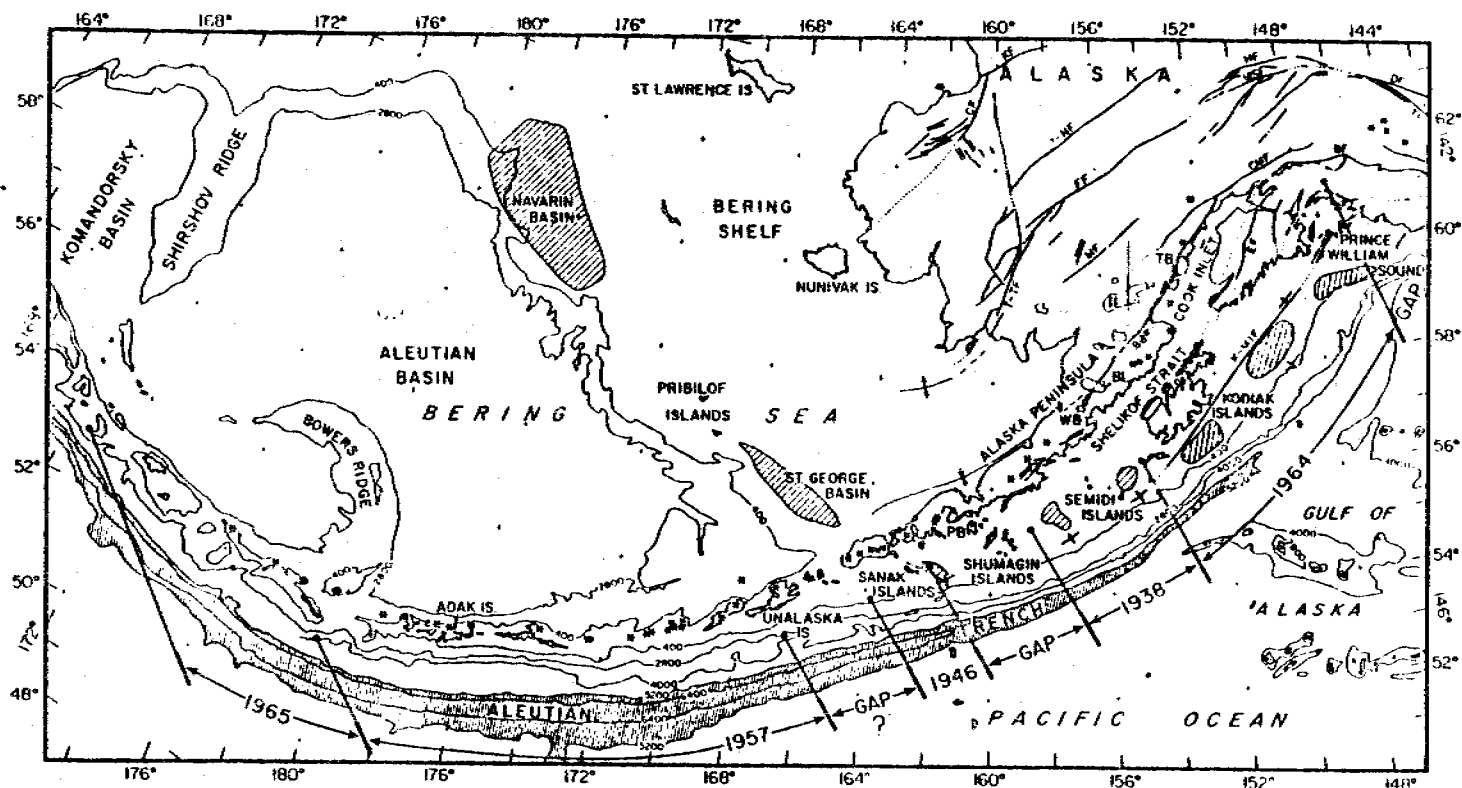


Figure 3. Location/tectonic map of the southern Bering Sea, central and eastern Aleutian Islands, Alaska Peninsula, southwestern and southcentral Alaska and the western Gulf of Alaska. The principal tectonic features are: (1) the central and eastern Aleutian Arc shown by the trends of the Aleutian Islands, the Alaska Peninsula and Cook Inlet, the historically active volcanoes (asterisks) and the subparallel Aleutian Trench (close hatchuring); (2) the Bering Shelf, its western margin shown by the subparallel 400 and 2800 m isobaths (all bathymetric contours are labeled in meters); (3) the shelf-edge basins are shown by the closed, hatchures of contours: Navarin and St. George on the Bering Shelf and six forearc basins along the Shumagin-Kodiak shelf, the first four, from west-to-east, being the Sanak, Shumagin, Tugidak and Albatros Basins. (4) the seamounts of the western Gulf of Alaska are shown by closed isobaths; (5) major faults are shown by heavy, solid lines. (6) the locations of the aftershock zones are shown by lines connecting solid dots and bars and are designated by the year of the earthquake. The dots indicate the boundary of the zone, the line is along the direction of relative plate motion.

southern extension to the Aleutian arc mark the boundary between two distinct tectonic blocks. Cormier [1975] attributes differences in sea-floor topography, heat flow, sedimentation and direction of relative plate motion to a distinct origin for the Komandorsky Basin as compared to the Aleutian and Bowers Basins. He further suggests that the highly oblique, relative plate motion in the far western Aleutians results in a release of compressive stress that allows formation of the Komandorsky Basin as a marginal basin with copious basaltic magmatism and attendant high heat flow. Thus, not only do the possible origins of the Shirshov Ridge suggest that it separates distinct tectonic blocks but so do direct geophysical observations of the blocks on either side. We conclude, therefore, that the western extent of the aftershock zone of the Rat Islands earthquake of 1965 was probably controlled by the boundary between portions of the arc backed by the Komandorsky Basin to the west of the trend of Shirshov Ridge and Bowers Basin to the east.

Bowers Ridge and Amchitka Pass. Bowers Ridge intersects the Aleutian arc at Amchitka Pass, near  $180^{\circ}$ , which coincides with the boundary between the aftershock zones of the Rat Islands earthquake of 1965 and the Andreanof-Fox Islands earthquake of 1957 (Figure 3). Bowers Ridge appears to be a remnant island arc that was underthrust from the present east-northeast [Kienle, 1971; Karig, 1972; Scholl *et al.*, 1975]. The intersection of this ancient convergent boundary with the Aleutian arc, continues to be a zone of weakness for present-day tectonism. Evidence for this are the existence of the deep Amchitka Pass and the occurrence of a large strike-slip earthquake [Stauder, 1972] whose causative fault was subparallel with the strike of the pass (i.e. transverse to the arc). Thus, it appears that a zone of weakness oriented by the intersection of Bowers Ridge with the Aleutian arc, controlled the formation of a major transverse boundary at Amchitka Pass. This boundary seems to have limited the extent of the rupture zones of the 1965 and 1957 Aleutian earthquakes.

Transverse Boundaries and the Rupture Zone of the Great Alaskan Earthquake of 1964. The Kodiak Islands are part of a tectonic block that is structurally high with respect to the shelf area to the southwest. The inferred structural discontinuity between the two is near the boundary between the 1964 and 1938 aftershock zones (see Figure 3). To the southwest of this boundary a series of sediment-filled basins (Tugidak, Shumagin and Sanak) interleave groups of islands (Semedi, Shumagin and Sanak) in a pattern of alternating structural lows and highs. This pattern is similar to that of a series of three anticlines described by Burk [1965] on the Alaska Peninsula which suggests a related origin. If so, the fact



that both patterns terminate near the southwest end of the Kodiak block strengthens the inference that a significant structural boundary exists there.

The northeast end of the 1964 aftershock zone is located near the region of transition from convergence along the Aleutian arc to transform motion along the Queen Charlotte-Fairweather fault system [e.g. Perez and Jacob, 1980]. This end of the 1964 aftershock zone lies south-southeast of the point where the Aleutian Benioff zone abruptly terminates beneath the central Alaska Range [Davies, 1975]. This abrupt termination of the Benioff zone and the position of the Wrangell volcanoes suggest that there may be a major tear in the Pacific lithosphere beneath the northeast shore of Prince William Sound. This implied tear in the downgoing lithosphere slab would be coplanar with the boundary in the overthrust plate between the Peninsular and Wrangellia terranes as mapped by Jones and Silberling [1979]. Thus, both ends of the rupture zone of the Great Alaskan earthquake of 1964 may have been controlled by transverse structural boundaries.

Indeed, all four of the rupture zones of the recent great Aleutian-Alaska earthquakes of 1965, 1957, 1938 and 1964 appear to have been controlled by transverse structural features that delimit tectonic blocks within the overthrust plate. We consider the eastern boundary of the 1957 zone and the western boundary of the 1938 zone in the next section. In that section we examine the question as to whether structural features delimit the Shumagin and Unalaska seismic gaps.

#### Transverse Structural Boundaries and Possible Future Rupture Zones

Shumagin Seismic Gap. We have defined the Shumagin Gap as the area between the 1938 and 1946 aftershock zones (Figures 3 and 4). The boundary between the Shumagin Gap and the 1938 aftershock zone falls between the uplifted Shumagin Islands [Winslow and Hickman, 1978] and the sediment-filled Shumagin Basin [Bruns and von Huene, 1977]. This boundary is also located along strike and to the southeast of a major discontinuity in the structures near Port Moller mapped by Burk [1965] on the Alaska Peninsula (shown in Figure 4 and based on an unpublished map by G. Bond). The boundary between the Shumagin Gap and the 1946 aftershock zone coincides with the Sanak Graben [Bruns and von Huene, 1977], which is filled with at least 7 km of sediments and is bounded by faults that trend subparallel to the strike of the Bering Shelf edge. Thus the Shumagin Gap

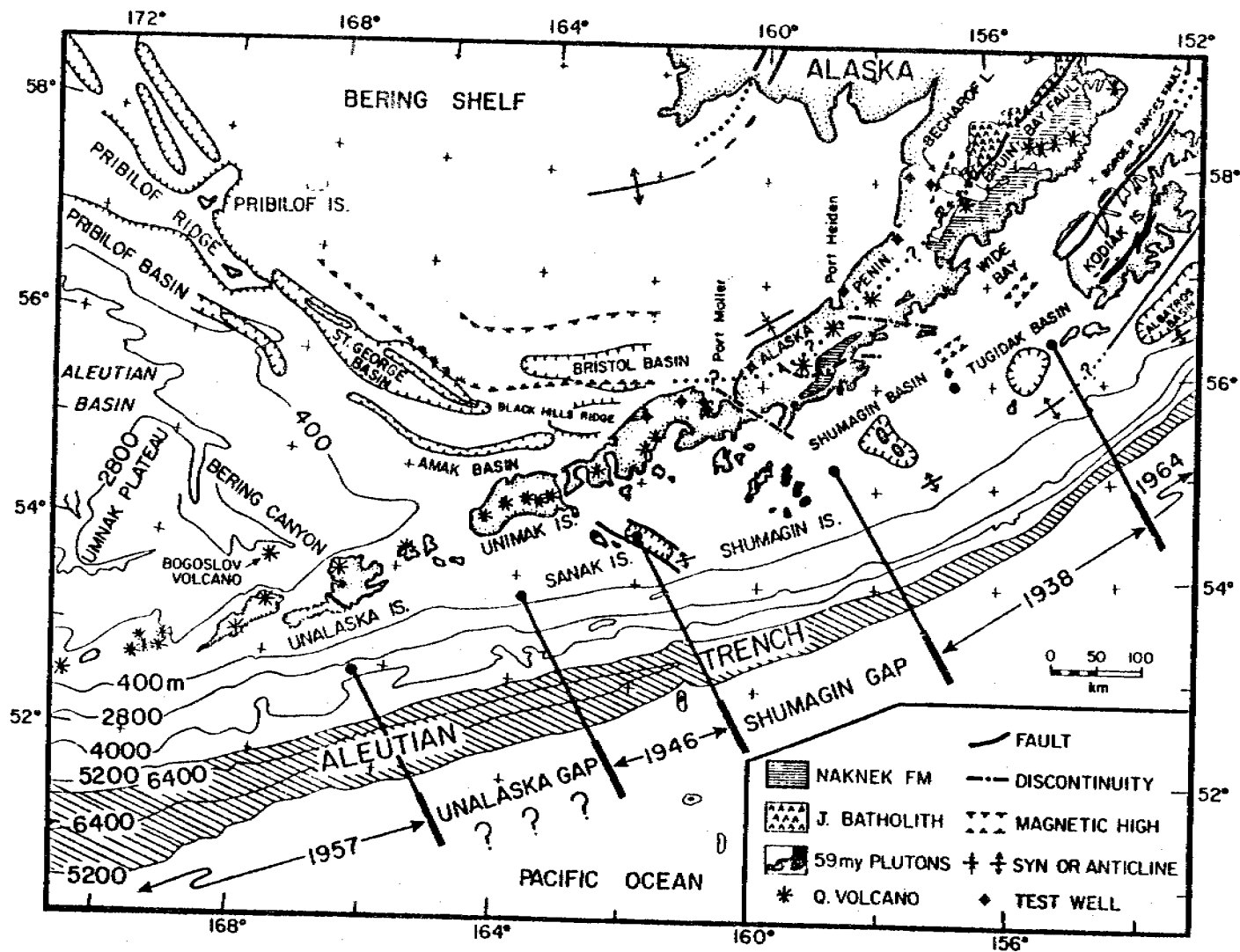


Figure 4. Tectonic map for eastern Aleutian-Alaska Peninsula region. Major, sediment-filled basins shown by closed, hatched contours. Discontinuities in geologic structures (from unpublished map by G. Bond, 1980) shown by heavy dash-dot lines. Locations of aftershock zones of great earthquakes (from unpublished map by G. Bond, 1980) shown by lines connecting heavy dot and bars; year of great earthquake is given. Note alignment of the ends of Shumagin Gap with direction of plate convergence, Moller to the east, and the trend of the Sanak Basin to the west. Also note alignment of the ends of the Unalaska Gap with the edge of the Bering Shelf to the east, and the trend of the Bering Canyon and Bogoslov volcano to the west.

appears to be bounded by transverse features that reflect discontinuities in the structure of the overthrust plate.

We noted above the similarity in the en-echelon structural pattern of the anticlines on the Alaska Peninsula to the sequence of structural highs and lows formed by the island groups and sediment-filled basins on the Shumagin-Kodiak shelf. This pattern is also similar to the overlapping pattern of basins and ridges seen on the Bering Shelf between the western tip of the Alaska Peninsula and the Pribilof Islands (Figure 4). The gross similarity suggests that this part of the Aleutian arc is being built upon a set of structures formed when the "basement" was part of the Beringian continental margin. If so, some of these older structures appear to exert important control upon the present tectonic regime of the eastern Aleutians. In particular, they may control the extent of the rupture zones of future great earthquakes.

Unalaska Seismic Gap. The Unalaska Gap is situated between the aftershock zones of the 1946 and 1957 earthquakes (Figure 4). A similar analysis to that applied to the Shumagin Gap could probably be applied to the region of the Unalaska Gap except that this area is not as well known in terms of marine seismic-reflection data and land-based geology.

We note, however, that the eastern boundary of the gap is aligned with Unimak Pass, immediately southwest of Unimak Island. Although it is not clear that Unimak Pass is structurally controlled, it does appear that Unimak Island is structurally low. This observation is based on the thick pile of Quaternary volcanic sediments on the island and the absence of outcrop of any formation older than the Tertiary. The abundance of volcanic activity of Unimak Island and its structural lowness may be controlled by its position over the older, Mesozoic continental margin. We also note that it is along strike of the St. George Basin and the Sanak Graben. The western boundary might be associated with the alignment of the Bering Canyon, and Bogoslov Volcano. The existence of the Unalaska Gap and its possible associations with transverse features need further study.

### C. The Pattern of Seismicity In and Near the Shumagin Gap (L. House)

During the past year, as a part of a study to define the area of the Shumagin gap [Davies et al., 1981], we undertook a study of the spatial and temporal trends of seismicity in and near the Shumagin Gap. Data from the Shumagin Islands network provide a detailed view of the pattern in the immediate vicinity of the gap, although for a relatively short time period. Seismicity data from teleseismic observations provide a more regional view of seismicity trends over a longer time period, although only earthquakes larger than  $m_b = 4.5$  generally are locatable. The seismicity patterns shown by network and teleseismic data are complimentary. We interpret the seismicity distribution within the Shumagin Gap to indicate that the area of the gap is probably in an advanced stage of preparation for a major earthquake. We cannot estimate from this data, however, how long it might be before a possible great earthquake occurs there. The pattern of seismicity of an area about 200 km long near Unalaska Island, in the eastern Aleutians, is nearly identical to that of the Shumagin gap. Other information, such as the lack of aftershocks, and lack of a tsunami generated in this area, suggest that this "Unalaska Gap" may not have broken during the great earthquake of 1957. It is possible that both these areas may be in advanced stages of earthquake preparation. It is also possible that were a great earthquake to initiate within one of the two areas - Shumagins or Unalaska - it would rupture into the other. Following is a brief description of the seismicity patterns, excerpted from the discussion of Davies et al (1981).

#### Seismicity Located by the Shumagin Islands Network

Figure 5 shows an epicentral plot of the earthquake set. Numbers of epicenters plotted at increasing distances from the network decrease rapidly both trenchward and to the northeast along strike of the arc. By comparison with the pattern to the southwest, which seems to represent the effect of decreasing detection ability, we infer a real decrease of seismicity in these two directions from the network. We consider the decrease of seismicity trenchward to result from the locking of the main thrust zone. This is discussed further in the context of a cross-section view presented below. The location of the rapid fall-off of shallow (depth  $\leq 60$  km) activity in the northeast direction coincides remarkably

### SHUMAGIN ISLANDS EPICENTERS

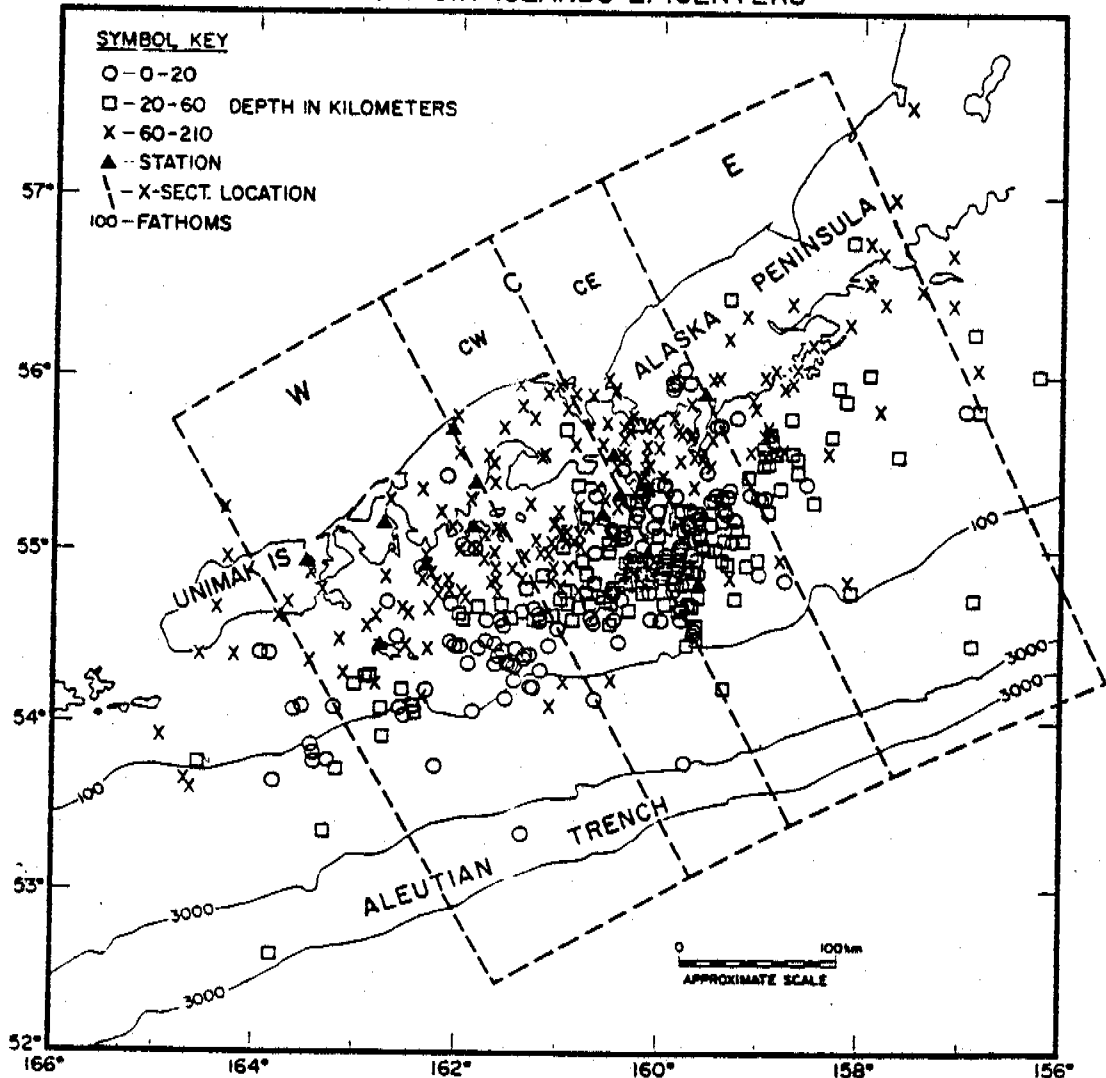


**Figure 5.** Map of epicenters in the Shumagin area obtained from the data of the Shumagin Islands network from the period July, 1973 through June, 1977 and April, 1978 through December, 1978. Epicentral locations have rms travel time residuals of 0.21 seconds or less and use 5 or more phase arrivals. Depths are coded as follows: open circle, 0-20 km; open square, 20-60 km; "x", 60-210 km. Stations of the Shumagin Islands Network are shown by solid triangles. Bathymetric contours are in fathoms. The dashed rectangle represents the location of the cross sections of Figures 4 and 5. "W", "C", and "E" are western, central, and eastern, respectively. The central section is divided into two additional cross-sections, "CW" and "CE", (central-west and central-east) that are about 75 km wide. Note the decrease of seismicity to the northeast of the cross-section; this corresponds to the eastern edge of the Shumagin Gap.

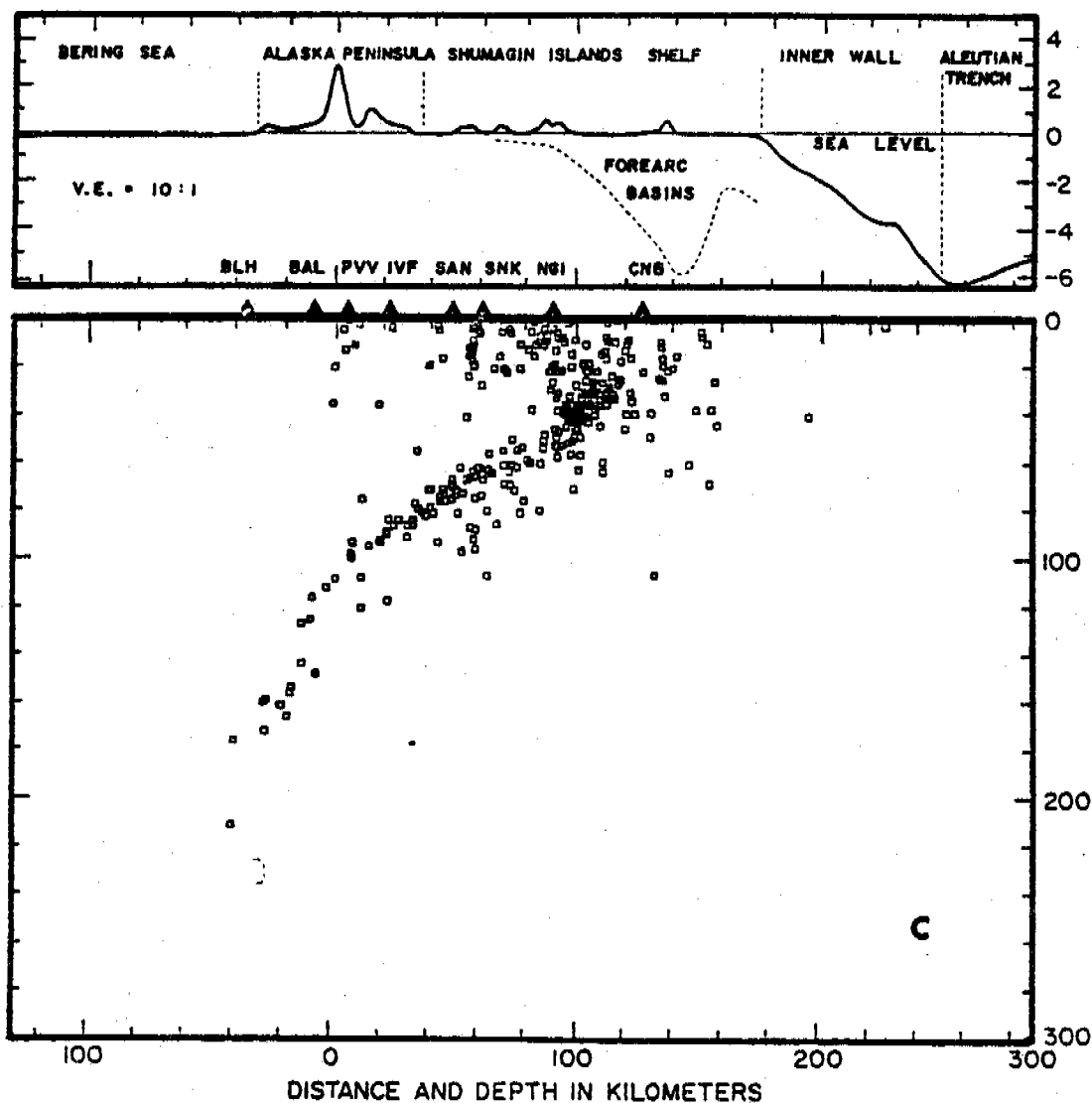
well with the northeastern margin of the Shumagin gap. Plots of epicenters obtained from teleseismic observations (Figures 7 and 8; discussed below) seem to show a similar pattern. Thus, the area immediately to the east of the gap, which is a part of the rupture area of the 1938 earthquake, presently produces little seismicity in the 0-60 km depth range. We consider the implications of this below.

Figure 6, a cross-sectional view of the hypocenters located by the local network, illustrates in more detail the geometry of plate interaction. This cross section includes earthquakes from a volume 150 km wide oriented normal to the strike of the volcanic line and centered on the network. Within that cross sectional volume earthquakes can be located most precisely and lowest magnitude events can be detected. A topographic profile taken along the center line of the cross section illustrates the relation between surface features and seismicity.

The cross-section demonstrates several important points about the seismicity distribution. First, most of the main thrust zone is currently aseismic. The main thrust zone extends from the trench axis downdip to the cluster of activity at about 40 km depth beneath NGI and CNB. Second, the downdip, arcward edge of the main thrust zone is highly active. The "knot" of activity at a depth of about 40 km beneath NGI and CNB seems to result from interplate deformation [Davies and House, 1979]. Thirdly, a large amount of seismicity is scattered throughout the overriding plate, in an area about 70 km wide centered above the downdip edge of the main thrust zone. We infer that this activity is a response of the overthrusting plate to compressional stresses that result from the accumulation of tectonic strain across the main thrust zone. Focal mechanisms of these earthquakes would provide a critical test of our interpretation [cf. Reyners, 1980].

We derive an interpretation of the shallow seismicity (depth less than 60 km) in the Shumagin Gap from studies of plate interaction in New Zealand. Walcott [1978] infers the behavior of the main thrust zone under the North Island of New Zealand from geodetic data. He deduces that the main thrust zone in the northern portion of the North Island is "unlocked" and slipping, whereas in the south portion it is "locked" and accumulating tectonic strain. Reyners [1980] notes differences in the seismicity of the northern and southern portions. In the northern portion he locates activity along the main thrust zone and within the Pacific plate that extends over at least the deeper 1/3 of the main thrust zone. The location of his network probably limits how far trenchward he could locate activity. Very little activity occurs within the overthrusting plate near the main thrust zone. In the southern portion of the North Island Robinson [1978] locates little activity along

## SHUMAGIN ISLANDS CROSS SECTION



**Figure 6.** Topographic and hypocentral cross-sections through the Shumagin Islands. All distances and depths in these figures are given in kilometers. The hypocentral section (bottom) is a view looking east-northeast through the volume indicated by the rectangle labeled "C" in Figure 4 with no vertical exaggeration. The topographic section (top) is a generalization of the relief along the axis of this rectangle; vertical exaggeration is 10:1. Approximate positions and depths of forearc basins are indicated by a dashed line. This line is based on a rough average of cross-sections of the Sanak, Shumagin and Tugidak Basins (Bruns and von Huene, 1977; Fisher, 1979). Station locations of the Shumagin seismographic network are shown by solid triangles along the top of the hypocentral section along with appropriate station codes. Earthquake hypocenters are shown by open squares. Hypocenters are from the same data set as that of Figure .

most of the main thrust zone, but a substantial amount of activity at the downdip edge and within the overthrusting plate above and landward of the main thrust zone.

Geodetic data comparable to that of Walcott [1978] are not available from the Shumagin gap. Lacking such information, we use the distribution of seismicity in the Shumagin gap to infer that the main thrust zone is "locked" in a fashion similar to that of the southern portion of the North Island of New Zealand. Critical to this interpretation are: the lack of seismicity along much of the main thrust zone; a concentration of seismicity (the "knot") at the lower edge of the main thrust zone; and large numbers of events that occur at shallow depths within the overthrusting plate.

We cannot determine the length of time that the main thrust zone has been locked, but we might crudely estimate it from the stress drops of earthquakes. Two high stress drop earthquakes occurred in 1974 within the "knot" of activity at the downdip edge of the main thrust zone [ $\Delta\sigma = 600-800$  bars, House and Boatwright, 1980]. These high stress drops may suggest that at least some portions of the plate interface have been locked long enough to accumulate substantial stresses. The lower amount of crustal and lower main thrust zone seismicity in the portion of the 1938 rupture adjoining the Shumagin gap suggests that the 1938 zone is not in the same state of earthquake preparation as the Shumagin Gap is. The 1938 zone may rerupture, however, as a result of earthquake deformation within the Shumagin Gap.

#### Seismicity Located by Teleseismic Observations

Hypocenters of earthquakes obtained from teleseismic observations, although not as precisely determined as those from the Shumagin Islands network, nevertheless extend both spatial and temporal coverage beyond that obtainable from the local network. The discussion that follows is concerned only with moderate to large size earthquakes ( $m_b \geq 5.0$ ) located at depths less than 80 km in the area from southern Alaska to the eastern Aleutians. We consider seismicity between 1945 and June 1979 in two time periods: 1965 to June 1979 (Figure 7), and 1945 to 1964 (Figure 8).

Seismicity In and Near the Shumagin Gap. Figure 7 shows that only one known earthquake of  $m_b = 5$  or larger occurred within the Shumagin gap in the past 14 years. In contrast, numerous events form a northeast-southwest trending



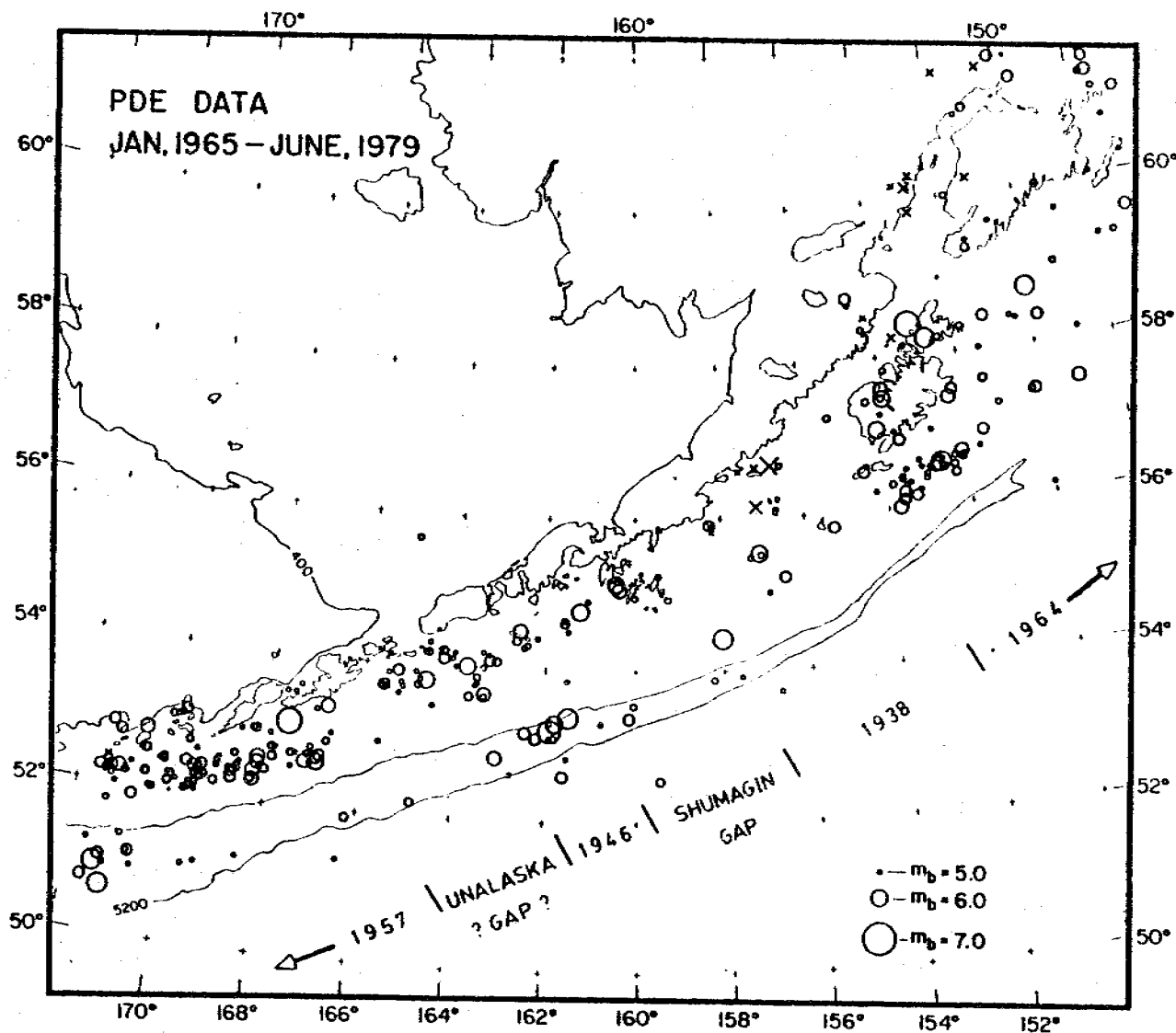


**Figure 7.** Epicentral plot of earthquakes shallower than 80 km in the eastern Aleutians and southern Alaska that occurred between 1965 and June 1979. Only earthquakes assigned magnitude 5.0 or greater are included. Epicenters are from the Preliminary Determination of Epicenters (PDE) of the U.S.G.S. Symbol size is scaled to magnitude shallow earthquakes (depth < 60 km) are indicated by a circle, earthquakes at depths between 60 and 80 km are indicated by an x. Bathymetric contours are in meters.

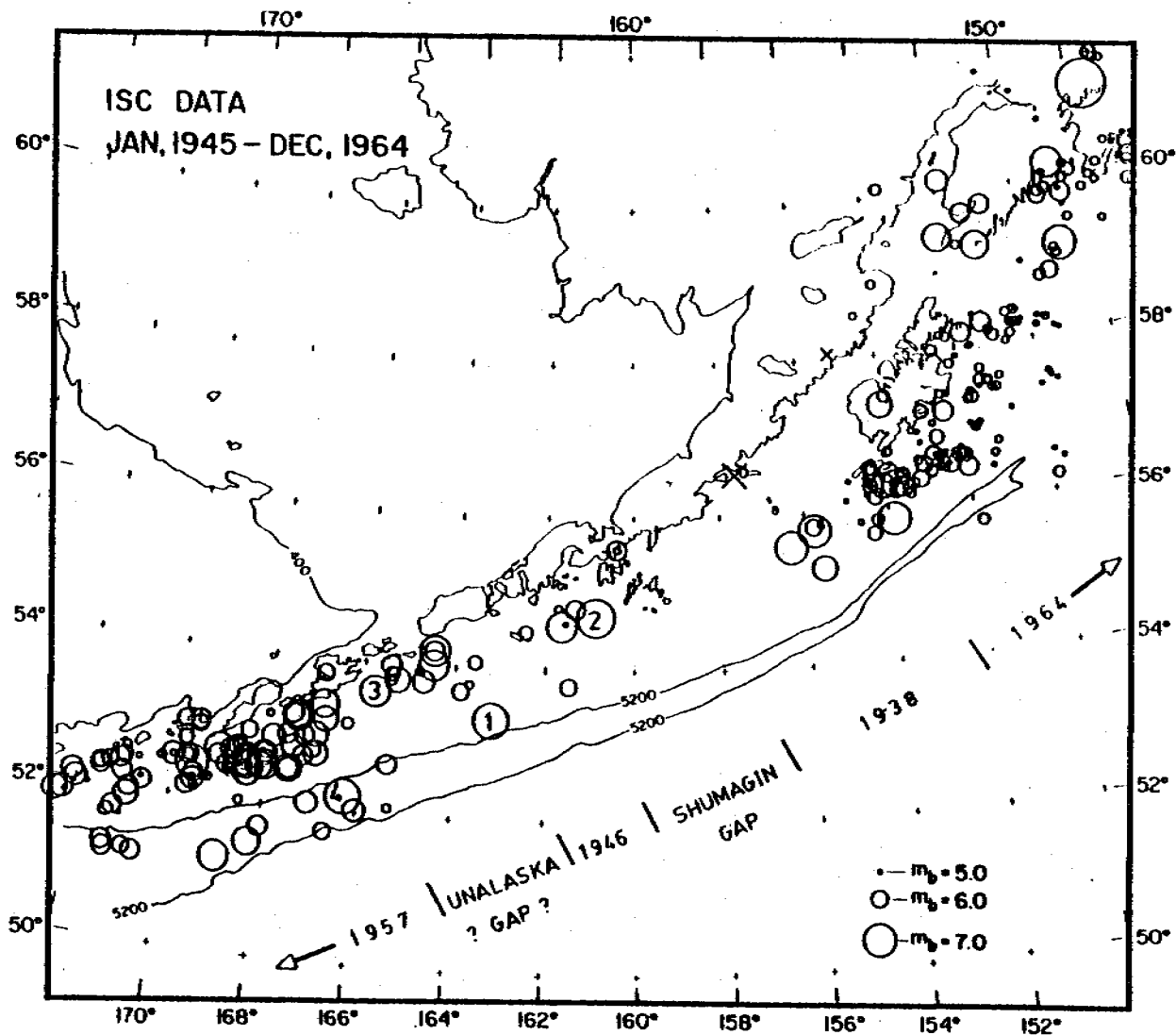


**Figure 8.** Epicentral p-ot similar to Figure , except of earthquakes that occurred between 1945 and 1964. Epicenters are from the relocations of Tobin and Sykes (1966), Sykes (1971) and from the locations of the International Seismological Center and the U.S. Coast and Geodetic Survey (PDE). Symbols are as Figure . The numbers 1 through 4 identify epicenters of particular interest: 1 - 1946 earthquake; 2 - 1948 earthquake (see previous section on historic earthquakes for a discussion of these two shocks); 3 - aftershock of 1957 earthquake on April 19, 1957; 4 - aftershock of 1957 earthquake on March 22, 1957.

lineation at what we infer to be the northern edge of the gap. Based on pP-P intervals published in the Bulletin of the International Seismological Center (BISC) all earthquakes larger than  $m_b = 6.0$  that are part of the lineation occurred at depths of 40-50 km. In addition, the Shumagin Islands network located two of these events at a depth of 40 km [Davies and House, 1979]. These two events were part of a sequence studied by House and Boatwright [1980] who estimated their stress drops to be about 600 to 800 bars. The depth of 40 to 50 km is about the deepest extent of the main thrust zone in the Shumagin Islands [Davies and House, 1979] and the epicenters of events at this depth probably represent the most northerly extent of rupture during a possible great earthquake in the Shumagin gap.

A cluster of earthquakes beneath the trench and elongate parallel to the trench axis occurred along the southern edge of the main thrust zone near the western margin of the Shumagin Gap. Focal mechanisms of these events showed normal faulting [Stauder, 1968; see Figure 12]. Several events near the western end of the Shumagin Gap suggest a trend that extends seaward from the alignment of 40-50 km deep events.

Seismicity located near the Shumagin gap between 1945 and 1964 (Figure 8) seems to be distributed in a pattern similar to that of the past 15 years. Because magnitudes were not routinely assigned to all earthquakes until 1964, only earthquakes of magnitude  $6 \frac{1}{4}$  and larger are uniformly included in this data set. The distribution of activity near the Shumagin Gap in Figure 8 may appear poorly developed because of incompleteness. The epicenter of the 1948 earthquake (labelled "2" in Figure 8), and several others nearby, may be part of a northeast-southwest trending lineation comparable to that observed in Figure 7.

The near quiescence within the gap and seismicity that occurs along its margins resemble the "doughnut" of seismicity that Mogi [1969, 1977] described in Japan. He noted that this "doughnut" pattern developed during a period of several to about 20 years before major earthquakes broke the interior of the "doughnut". Two details of the seismicity distribution near the Shumagin gap differ from the "doughnut" pattern of Mogi [1969, 1977]. First, the "doughnut" of seismicity contained activity spread over an area 100 km or more in width around the gap. In contrast, activity around the Shumagin gap defines a narrow zone only 50 km wide. Second, with the occurrence of the "doughnut" Mogi [1969, 1977] noted that the distribution of seismicity changed very noticeably. We do not observe a substantial change in the seismicity pattern since 1945. Thus, the pattern of seismicity we

observe is a stationary feature, or the "doughnut" pattern may have occurred prior to 1945.

Although the pattern of seismicity near the Shumagin gap may not exactly match the precursory pattern described by Mogi [1969, 1977], it differs substantially from that of other portions of the eastern Aleutians recently broken by great earthquakes. A zone extending about 300 km to the east of the Shumagin Gap broke during the earthquake of 1938. Relatively few earthquakes occurred within this area during the past 35 years. Nevertheless, as the recent 15 years' data of Figure 7 shows best, those that have occurred are scattered over much of the width of the main thrust zone.

Seismic activity of magnitude 5 and larger that occurred within the aftershock zones of two other great earthquakes in 1957 and 1964, also scatters throughout much of the respective widths of the main thrust zone. The Alaska earthquake of 1964 broke the plate margin from about the western end of Kodiak Island to the northeastern corner of Figures 7 and 8. Note that seismicity of the past 15 years (Figure 7) scatters over a zone 100-200 km wide and extends almost out to the trench. This band of seismicity occurs along much of the width of the main thrust zone. Seismicity from 1945-1964 plotted in Figure 8 includes numerous aftershocks of the 1964 earthquake. All events of magnitude 6.3 and larger located within the aftershock zone or north of it occurred before the 1964 earthquake.

The aftershock zone of the 1957 earthquake extends about 1200 km westward along the Aleutians from about the 1946 aftershock zone [Kelleher, 1970; Sykes, 1971; Mogi, 1968]. This is one of the longest aftershock zones known. Only the eastern 500 km of this zone plots within Figures 7 and 8. Except for the eastern 200 km of this zone, which is the possible Unalaska Gap, and is discussed more fully below, the recent seismicity plotted in Figure 7 scatters over much of the width of the main thrust zone. Some clustering of activity occurs, but there is no feature comparable to that of the prominent lineation in the Shumagin gap. Activity plotted within this zone in Figure 8 are largely aftershocks of the 1957 earthquake.

We conclude from this discussion that two prominent features of the distribution of recent seismicity in and near the Shumagin gap are: 1) the lack of seismic activity along most of the main thrust zone, and 2) a well-defined alignment of events at the lower edge of the main thrust zone. These features, as well as activity near the western edge of the gap and trenchward of it, may

represent a Mogi "doughnut" of seismicity around the Shumagin gap. The "doughnut" is seen most clearly in seismicity of the past 15 years, although seismicity of the past 30 years may show it as well. This pattern of seismicity differs markedly from that within the aftershock zones of three recent earthquakes that broke the plate margin in Alaska. The strong contrast between the distribution of seismicity in these areas with that in the Shumagin gap suggests that the Shumagin gap is in a more advanced stage of the earthquake cycle. The high stress drops of two earthquakes at the downdip edge of the Shumagin gap corroborate such a suggestion.

#### Seismicity In and Near the Possible Unalaska Gap

The easternmost 200 km of the aftershock zone of the 1957 earthquake [Sykes, 1971; see also Figure 8] experienced aftershocks along a narrow zone at its northern edge. In contrast to the area immediately west of it, this portion lacked known aftershocks along much of the width of its main thrust zone. We term this possible gap the "Unalaska Gap", since it is near Unalaska Island. House *et al.* [1981] discuss the Unalaska Gap in detail and note that since it did not generate an observable tsunami at the time of the 1957 earthquake it may have either ruptured with a time constant too long (order of several hundreds of seconds) to generate a tsunami, or it may not have ruptured at all in 1957.

Recent seismic activity plotted in Figure 8 shows little activity within the possible Unalaska gap, although many events occur at its northern margin. The alignment of this activity seems to be a westward extension of the faulting at the northern edge of the Shumagin Gap. From  $pP$ - $P$  times reported for many of these events (BISC) their depths range from 36 to 56 km. These events would seem to define the lower edge of the main thrust zone, as did comparable events in the Shumagin Gap.

Available data are therefore not conclusive, but the area of the possible Unalaska Gap may not have broken in 1957. This area probably has not broken since a possible major earthquake in 1903. The pattern of seismicity in and near this possible gap is very similar to that near the Shumagin Gap, and it may, therefore, be in a similarly advanced stage or preparation for a possible major earthquake.

D. Refined Analysis of Microseismic Data: Hypocenter Locations, Crustal Structure and Focal Mechanisms (M. Reyners and K. Coles)

An abiding problem in the analysis of microearthquake data from the Shumagin array is the rather incomplete knowledge we have of local crustal structure. No deep seismic sounding experiments have been undertaken in the area, and the crustal structure model routinely used for hypocenter determination is a synthesis of models determined by Matumoto and Page (1968) for the Cook Inlet area of Alaska, and Rowlett and Jacob (personal communication, 1974) for the central and eastern Aleutian Islands. The horizontally-layered crustal model used is clearly but a first approximation, given the rather large variations in structure one might expect at a converging plate boundary. In order to obtain a sample of hypocenters relatively free of model errors, hypocenters not critically dependent on the adopted velocity model have been grouped together. In practice, this has been achieved by requiring that the epicentral distance to the nearest station used in a hypocenter determination is less than or equal to twice the hypocentral depth. Such a procedure ensures good hypocentral depth control, as arrivals to the closest stations are interpreted as direct arrivals, the travel times of which are less prone to errors due to an inadequate crustal structure model than critically refracted arrivals, which may arrive first if the ratio of epicentral distance to hypocentral depth is large.

A depth section of the best-determined hypocenters satisfying the above condition and occurring during the period April 1978 to September 1979 is shown in Figure 9. The section is oriented perpendicular to the strike of the arc, and is centered on the station SAN. It differs somewhat from previous sections showing well-determined hypocenters selected in terms of goodness of fit criteria only (e.g. Figure 9 of last year's report); such differences can be ascribed to model-dependent errors in some hypocenters of the previous sections. Figure 9 shows the intense activity in the 25-45 km depth range of the main thrust zone to be more closely planar than previously - indeed, within their standard errors, these events could all originate on a single plane. Also, the marked absence of activity shallower than 25 km on the main thrust zone and in the overlying plate directly above it is much more pronounced than previously. Clearly the current lack of seismicity in the shallower part of the main thrust zone evident teleseismically extends down to the microearthquake level. Given the possibility that the plate boundary in the

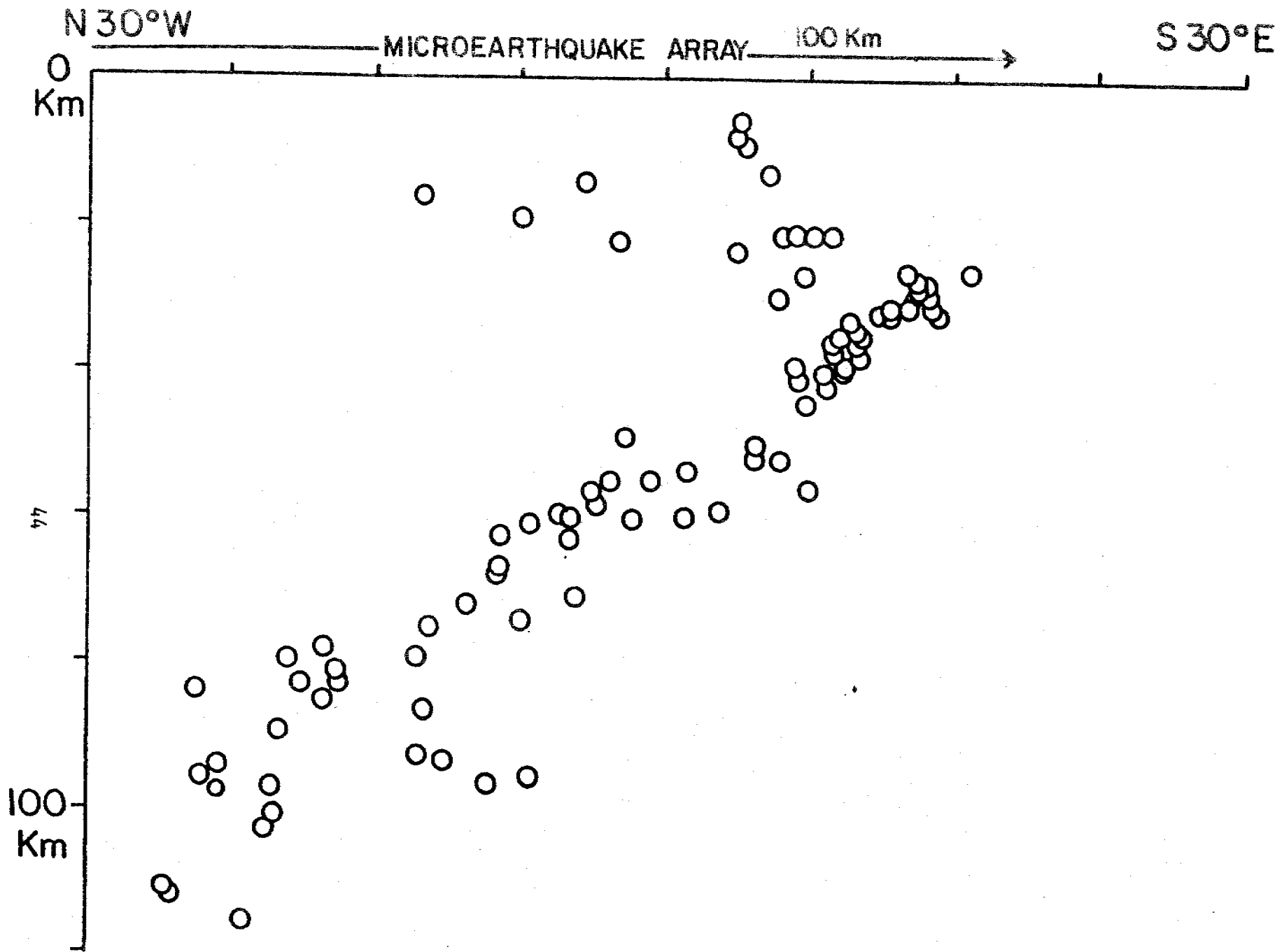


Figure 9. Depth section of best-determined microearthquake hypocenters shallower than 120 km for the period April 1978 to September 1979. For these solutions at least six phases (including 2 S-phases) are used, the RMS error in the time residuals  $\leq 0.15$  sec, standard errors in both epicenter and depth  $\leq 5$  km and the epicen-

Shumagin Islands region is in a preparatory phase of a large earthquake, it is important that a search be made for premonitory spatio-temporal patterns in the microseismicity located with the Shumagin array. To this end, catalogues of hypocenters relatively free of model errors (such as that plotted in Figure 9) have been compiled, and the spatio-temporal patterns shown by these hypocenters are currently being investigated.

The spatially localized nature of the activity shown in Figure 9 suggests that its location is structurally controlled. In an effort to elucidate such structure, seismograms have been scanned for phases other than P and S. It has been found that seismograms of microearthquakes shallower than 30 km and arcward of the main thrust zone (i.e. presumably occurring in the overlying plate) commonly show two additional phases, as illustrated in Figure 10. Preliminary modelling suggests that these are reflected P and S phases (PxP and SxS, respectively). Interpretation of the phases as reflections is supported by the slowness of the phases across the array and by the relative amplitudes of the phases on the two components of the seismograph SAN (P-phases are generally best recorded on a vertical component; S phases on a horizontal component). The inferred reflector apparently dips toward the trench, having a depth of about 20 km under SAN and about 30 km under NGI. If these phases are indeed PxP and SxS, they will be very useful in monitoring variations of the ratio of P-wave velocity ( $V_p$ ) to S-wave velocity ( $V_s$ ), since this ratio is simply given by the arrival time ratio  $\frac{SxS-S}{PxP-P}$  at a particular station, if Poisson's ratio is the same in all layers traversed by these waves (i.e. P and S travel the same path). Determination of  $V_p/V_s$  variations is important, as such variations have been shown to precede large earthquakes.

Events 25-45 km deep on the main thrust zone commonly show additional phases between P and S. The example illustrated in Figure 10 shows two such phases; these have both been interpreted as S to P converted phases ( $Sp$ ) because they are only obvious on the vertical component. The inferred  $Sp$  phase just preceding the S is apparent on most seismograms recorded at SAN (cf. the phase approximately 0.5 sec before S on SAN Z in Figure 10) and is probably produced at some very shallow crustal discontinuity directly under SAN station. Preliminary modelling of the phase approximately 3 sec after P in Figure 10 as  $Sp$  indicates a discontinuity at about the same depth as the reflector indicated by the PxP and SxS phases of overlying plate events. That both converted and reflected phases appear to be produced at about the same depth is encouraging. A relatively sharp discontinuity is suggested and, considering its depth, we may be seeing the



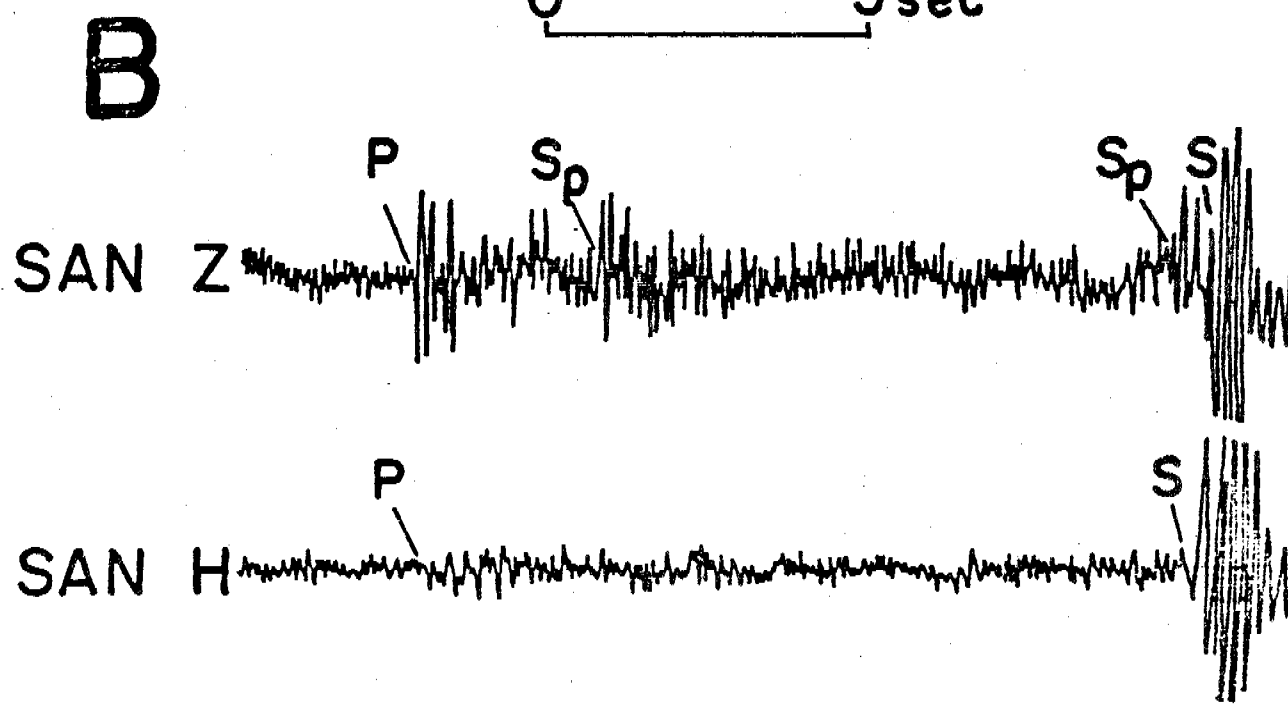
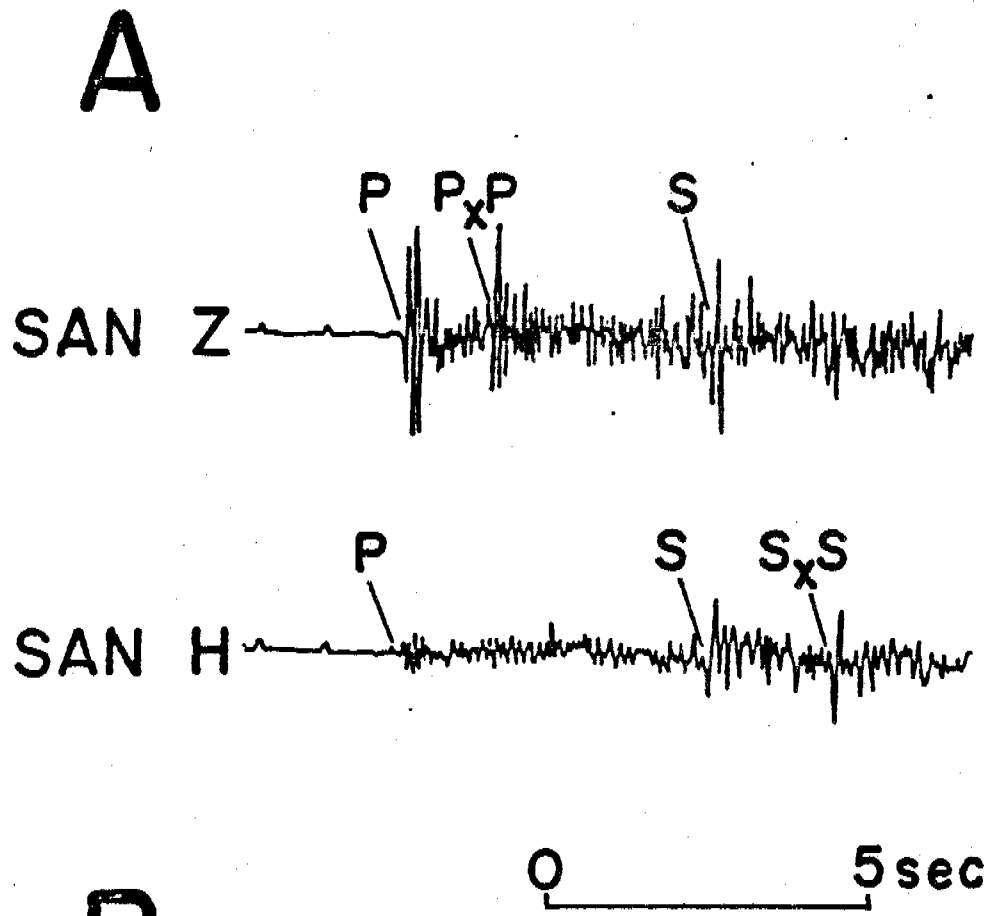
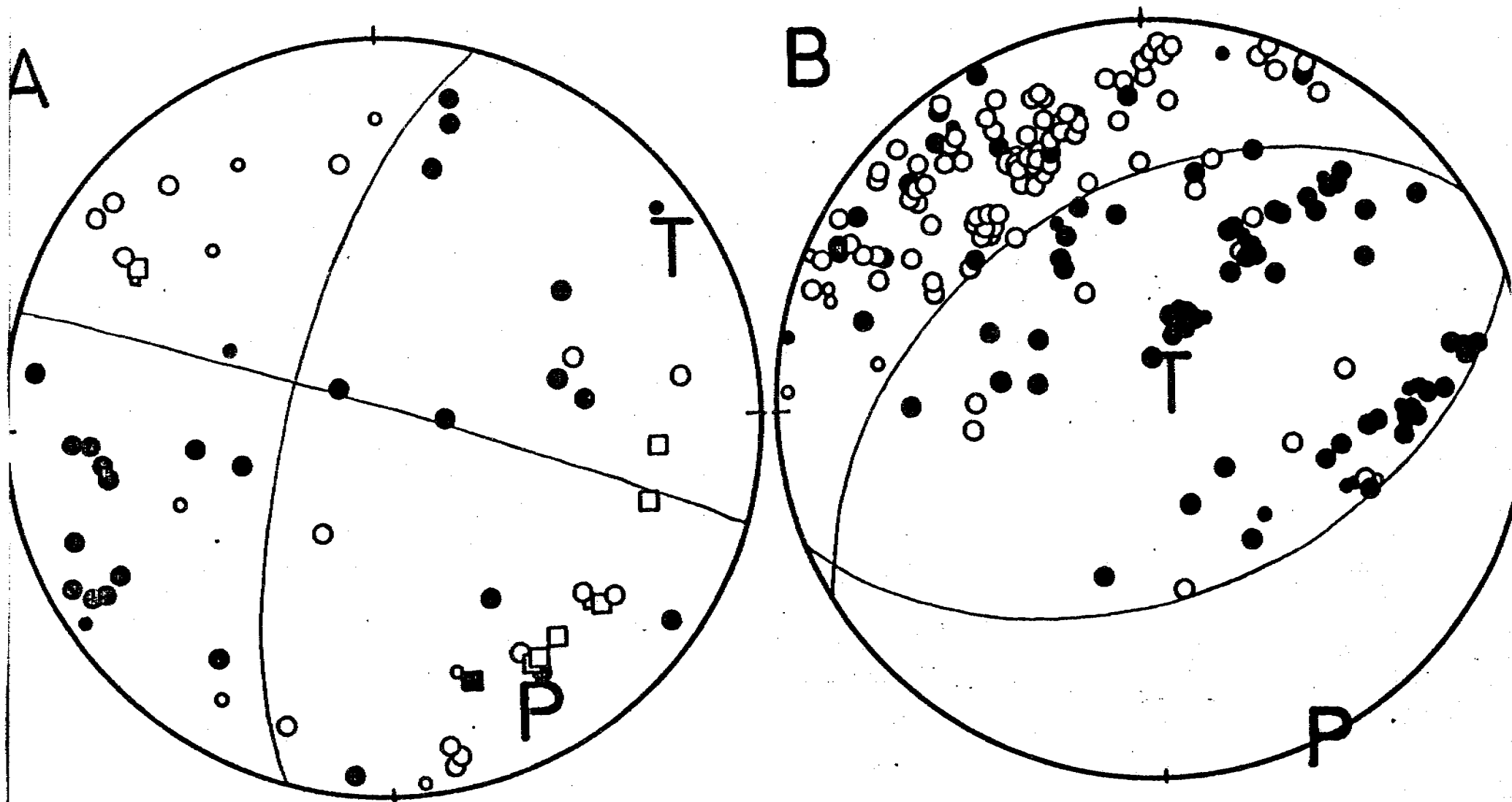


**Figure 10.** Tracings of seismograms showing phases additional to P- and S-phases. Seismograms in A are from a microearthquake in the overlying plate with a depth of 19 km; those in B are from a microearthquake on the main thrust zone at 31 km depth. Z and H refer to the vertical and horizontal components, respectively, of the seismograph SAN. For an explanation of phases additional to P and S, see text.



47

Figure 11. Upper-hemisphere, equal-area stereograms of first-motion directions for two groups of earthquakes: (A) those presumed to lie in the overlying plate (shallower than 30 km and arcward of the main thrust zone); and (B) those on the main thrust zone (25-45 km in depth). Solid circles represent compressional arrivals; open, dilatational. The axes of compression and tension are labeled P and T, respectively.

Mohorovicic Discontinuity of the overlying plate. Work is at present in progress to establish more rigorously the existence of this discontinuity, and to determine more precisely its location.

As individual events are recorded by insufficient stations for the determination of a fault plane solution, focal mechanisms of microearthquakes in the Shumagin Islands have been determined using composite fault plane solutions. The depth distribution of activity shown in Figure 9 suggests three obvious subsets into which to divide the events for the determination of such composite solutions, namely:

1. events presumed to lie in the overlying plate (those shallower than 30 km arcward of the main thrust zone);
2. events on the main thrust zone, 25-45 km deep; and
3. events deeper than 45 km.

Composite fault plane solutions constructed using well-determined hypocenters are shown in Figure 11. It is clear that the focal mechanisms of events both in the overlying plate and on the main thrust zone have been stable for the 1 1/4-year period shown. Both mechanisms have a near-horizontal P-axis oriented subparallel to the direction of plate convergence in the Shumagin Islands region. This result is consistent with the interpretation that the plate interface in the area is currently locked, with stresses due to plate convergence being transmitted to the overlying plate. Motion in the ESE-striking nodal plane of the predominantly strike-slip mechanism of microearthquakes in the overlying plate is in the correct sense to take up the slight obliquity of plate convergence in the Shumagin Islands. In addition, the fault plane solution for events on the main thrust zone is very similar to those of teleseismically recorded events in the same region (House and Boatwright, 1980).

## E. Seismic Source and Strong-Motion Characteristics (K. Jacob and J. Mori)

There are two very important elements of seismic hazards evaluation, i.e. to characterize the properties of (a) seismic sources and (b) of seismic ground motions from these seismic sources. During this reporting period we have made substantial progress in the first but little in the second task primarily due to absence of any new strong motion recordings from Aleutian earthquakes in this period. This regrettable situation points to the urgency that exists for deploying more strong-motion instruments in the Alaska-Aleutian seismic zone as soon as possible.

### Seismic Source Characterization

High Stress Drop Earthquakes in the Shumagin Gap. The study by House and Boatwright (1980) of two high-stress drop earthquakes in the Shumagin Islands was completed and a paper was submitted to the Bulletin of the Seismological Society of America. Since many of the technical details of this study were reported earlier we summarize here only the highlights of this study in the following abstract from the now completed paper.

Two moderate size ( $m_b = 5.8, 6.0$ ) earthquakes occurred within a local network of short-period seismograph stations in the Shumagin Islands, Alaska, on April 6, 1974. They were followed by 69 aftershocks recorded over the next two weeks. Both mainshocks triggered a strong-motion accelerograph (SMA) at Sand Point, 50 km NNW of their epicenters.

High quality locations obtained from local network arrivals for the mainshocks and 29 aftershocks yield depths between 35 km and 45 km and define a plane dipping about  $30^\circ$  to the NW. A nearly pure-thrust focal mechanism for the larger ( $m_b = 6.0$ ) earthquake was obtained from long-period data. The fault plane inferred from this mechanism dips  $30^\circ$  in the direction  $N16^\circ W$ . This sequence was located in the upper portion of the dipping seismic zone beneath the eastern Aleutians and was presumably related to underthrusting of the Pacific plate beneath the North American plate.

Estimates of the source parameters of these earthquakes were obtained from analysis of the SMA data and WWSSN short period data. The WWSSN data indicate that the earthquakes had approximately circular rupture areas. Modelling of the

SMA records with a quasi-dynamic source model provides the following estimates of the source parameters for the  $m_b = 5.8$  and  $6.0$  earthquakes, respectively: moments,  $M_0 = 3.6$  and  $6.6 \times 10^{24}$  dyne-cm and static stress drops,  $\Delta\sigma = 890$  and  $650$  bars. A high frequency spectral falloff of  $\omega^{-3}$  suggests that the ruptures stopped gradually.

The Shumagin Islands region is believed to have a high potential for a future large earthquake. The location of this earthquake sequence at what is inferred to be the deepest part of the zone of seismic interplate deformation and the high stress-drops of the main shocks may reflect a considerable accumulation of stress prior to a major earthquake in the Shumagin Islands region.

Stress Drop Determination From Other Eastern Aleutian Earthquakes (by Jim Mori). Using the set of earthquake focal mechanisms compiled by House and Jacob (Figure 12, Table 1), estimates of source parameters for several of these events were calculated. These earthquakes form a wide belt stretching from the Eastern Aleutians through the Alaska Peninsula, so they represent stress release in a wide variety of tectonic settings.

The P-arrival of events (with magnitudes  $m_b = 5.0$  to  $6.5$ ) have pulse shapes with dominant periods on the order of two seconds at teleseismic distances. Such frequencies are well recorded on WWSSN short-period instruments. Therefore, these records provide suitable data for an inversion to determine the size of the fault ( $a$ ), effective stress ( $\sigma_e$ ), stress drop ( $\Delta\sigma$ ), and moment ( $M_0$ ) of the source.

The method of analysis used is that developed by Boatwright (1979) for investigating a high stress-drop earthquake in the same region (#9, Figure 12). The major steps of this analysis are (Figure 13):

1. WWSSN records are researched for well recorded P-arrivals. Stations used are generally  $30^\circ$ - $90^\circ$  from the epicenter. The few stations which exist closer than  $30^\circ$  generally contain reverberating signals high-frequencies that make the interpretation of these crusts and upper mantle P-waves difficult to use for source-parameter analysis.
2. A photographic copy of the record is hand-digitized at a rate of about 10 samples a second. The digitization is processed by a set of computer programs which fits the data to a baseline and band-pass filters it (1.0 to .3 Hz). The low-pass part of the filter is a triangle smoothing operator and the high-pass is a third-order Butterworth filter which is run forward and backward over the data to ensure zero phase shift. Next a bilinear approximation for the instrument response of the

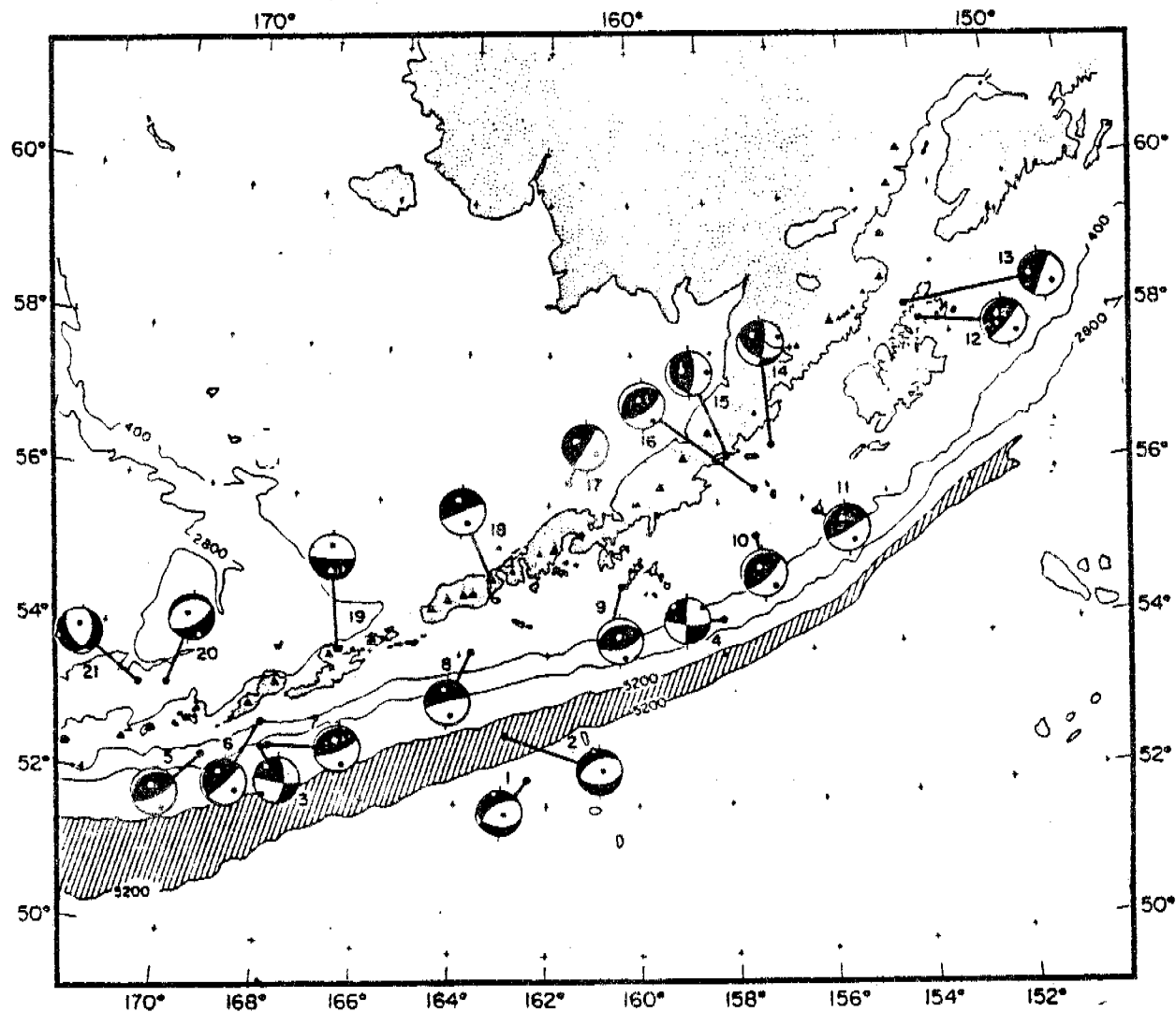


Figure 12. Compilation of mostly new or unpublished fault-plane solutions for the eastern Aleutian arc. For parameters and references regarding these solutions see Table 1. Lower-hemisphere equal-area projections of the focal spheres are shown. Solid black quadrants represent compressional P arrivals at stations; open quadrants, dilatational arrivals. Small open circle in the compressional quadrant represents T axis, small solid circle in the dilatational quadrant represents P axis. Note the following types of solutions: #1 and 2 normal faulting at shallow depths; #3 and 4, shallow strike-slip faulting; #5-13, shallow thrust faulting; #14-18, down-dip tensional solutions at intermediate-depth; #19-21, down-dip compressional solutions at intermediate-depth. Also note transition in the overriding North American plate from the oceanic portion in the Aleutian Basin west of 400 m isobath to the continental portion along the Alaska-Bering Sea margin east of this isobath. This transition coincides with the change in mechanism of intermediate depth shocks from down-dip compressional solutions in the western portion to down-dip tensional solutions in the eastern portion of the descending slab. Solid triangles are active volcanoes (large symbols) and Quaternary volcanoes (small symbols), respectively.

TABLE 1

## FOCAL MECHANISM PARAMETERS FOR DISCUSSED EARTHQUAKES IN THE EASTERN ALEUTIAN ARC

All hypocenter and magnitude information is taken from I.S.C. Bulletins unless other sources are indicated

EVENT NO.	HYPOCENTER INFORMATION							FOCAL MECHANISM INFORMATION													
	Y	M	D	h	m	s	LAT °N	Lon °W	DEPTH, km P	$m_b$	PLANE 1 Strike Dip	PLANE 2 Strike Dip	P Az. Pl.	T Az. Pl.	B Az. Pl.						
1 <sup>††</sup>	1969	06	20	02	37	51.8	53.31	162.41		41	5.8	225	49N	063	43S	074	80	322	01	234	09 (1)
2 <sup>††</sup>	1972	10	13	04	46	11.0	52.89	162.98		35	6.0	226	50N	070	42S	073	77	329	05	236	13 (1)
3	1967	01	18	08	18	22.3	52.55	168.24	33	37	5.7	091	78S	355	63E	221	10	316	28	113	60 (1)
4	1967	07	01	23	10	08.6	54.44	157.94		38	6.2	094	72S	005	85W	051	16	318	09	200	72 (1)
5	1967	01	28	13	52	58.3	52.40	169.54		42	6.0	052	68S	052	22N	142	23	322	67	052	00 (1)
6	1969	11	12	19	09	01.7	52.90	168.32	50	52	5.5	044	85S	341	12W	125	39	324	49	223	10 (1)
7	1967	07	06	13	42	27.6	52.58	168.13		49	5.9	061	74S	061	16N	151	29	331	61	061	00 (1)
8	1973	05	29	06	14	18.0	53.97	163.71	0	27	6.1	071	83N	071	07S	161	52	341	38	071	00 (1)
9	1974	04	06	03	56	01.8 <sup>†</sup>	54.92 <sup>*</sup>	160.28 <sup>*</sup>	41 <sup>*</sup>	40 <sup>†</sup>	6.0	254	30N	254	60S	164	15	344	75	254	00 (2)
10	1979	02	13	05	34	26.1 <sup>†</sup>	55.51 <sup>†</sup>	157.13 <sup>†</sup>	24 <sup>†</sup>		5.8 <sup>†</sup>	052	70S	052	20N	142	25	322	65	052	00 (1)
11	1964	02	06	13	07	23.1	55.72	155.95		13	6.1	216	12W	066	80E	151	35	342	54	245	05 (3)
12	1965	09	04	14	32	50.2	58.29	152.50		30	6.1	211	10W	050	80E	137	35	324	55	229	03 (3)
13	1965	12	22	19	41	21.6	58.35	153.15	37	49	6.4	301	13S	209	90	133	44	285	43	029	14 (3)
14	1979	05	20	08	13	56.6 <sup>†</sup>	56.68 <sup>†</sup>	156.74 <sup>†</sup>		72 <sup>†</sup>	6.5	009	75E	122	34S	078	24	314	50	182	30 (1)
15	1963	01	01	23	39	06.0	56.57	157.56		80 <sup>§</sup>	6.5 <sup>§</sup>	156	23W	008	71E	089	25	295	62	184	11 (3)
16 <sup>††</sup>	1972	03	24	03	38	24.1	56.14	157.14	42	68	6.0	327	39E	121	54W	222	08	342	75	130	13 (1)
17	1968	06	10	12	41	04.3	56.29	161.55	165	182	5.5	033	86E	033	04W	123	41	303	49	033	00 (1)
18	1971	09	04	15	53	25.7	54.94	163.35	110	123	5.7	064	90	064	00	154	45	334	45	064	00 (1)
19	1972	04	21	01	28	08.2	53.95	166.82	91	104	5.8	086	86S	266	04N	356	49	176	41	086	00 (1)
20	1971	04	05	09	04	42.3	53.26	170.53	150	148	5.8	053	64S	248	27N	310	70	148	19	056	05 (1)
21	1963	04	02	16	18	57.0	53.14	171.71	157		6.5 <sup>§</sup>	003	46E	318	54W	349	65	249	04	157	25 (4)

†† = graphical solution from S waves - no nodal plane constraint from P arrivals.

\* = hypocentral parameters obtained from local network data.

† = hypocentral parameters obtained from PDE.

§ = source parameter given by author of fault plane solution instead from I.S.C. data.

(1) = House; (2) = House and Boatwright, 1980; (3) = Akasche, 1968; (4) = Stauder, 1968.

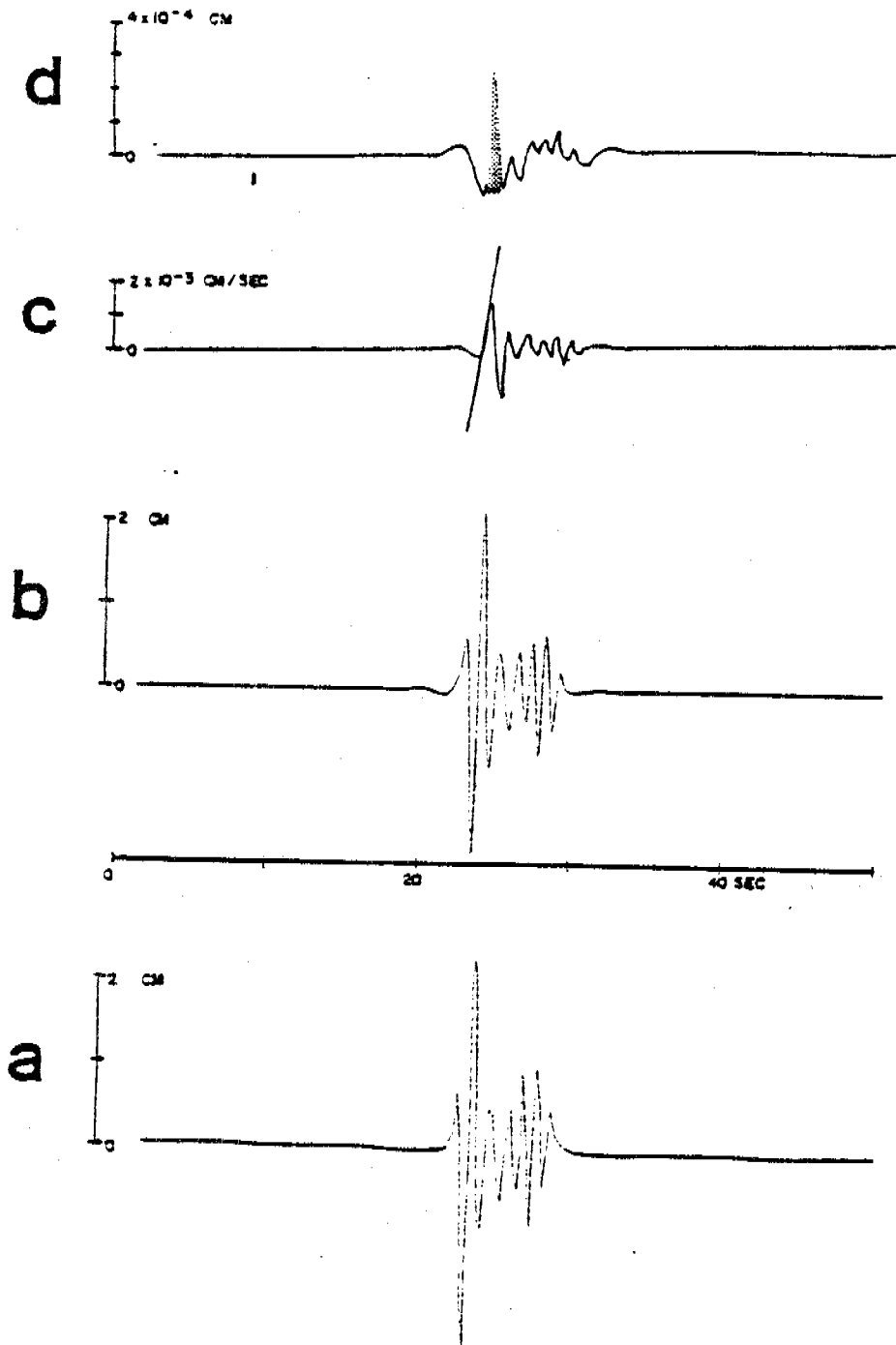


Figure 13. Steps in processing seismograms: (a) Plot of digitization of the first 10 seconds of event 17 as recorded at WSSN station PNG; (b) Digitization has been interpolated to equal time intervals and band passed filtered (1.0 to 0.3 Hz); (c) Deconvolved velocity plot. The slope of the line is

$$\left\langle \frac{\dot{u}_c(x,t)}{t} \right\rangle$$

which is used to determine effective stress; (d) Deconvolved displacement plot. Shaded section is the area of displacement pulse,  $u_c(x,0)$ , which is used to determine the moment.



WWSSN short-period system is deconvolved from the signal and the resultant signal is a time function of ground displacement. The displacement trace is then differentiated to obtain a velocity plot.

3. Assuming the self-similar circular rupture model Boatwright (1979) derives equations for obtaining source parameters from these plots. The moment is given by

$$M_0 = 4\pi(\rho(\xi_0)\rho(x)c(x))^{1/2}c(\xi_0)^{5/2} \frac{R(x,\xi_0)}{F^C(\theta,\phi)} \bar{u}_c(x,0).$$

where  $\rho(\xi_0)$  and  $\rho(x)$  are densities at the source and receiver, respectively;  $c(\xi_0)$  and  $c(x)$  are P-wave velocities at the source and receiver, respectively.  $R(x,\xi_0)$  is the geometrical spreading and  $F^C(\theta,\phi)$  is the radiation pattern.  $\bar{u}_c(x,0)$  is the pulse area of the displacement seismogram.

Effective stress, that is the stress drop during rupture, is given by

$$\tau_e = \frac{(\rho(\xi_0)\rho(x)c(x))^{1/2}c(\xi_0)^{5/2}}{v^3} \left( \frac{R(\xi_0,x)}{F^C(\theta,\phi)} \right) (1-\zeta^2)^2 \left\langle \frac{\dot{u}_c(x,t)}{t} \right\rangle$$

where  $v$  is rupture velocity and  $\zeta$  is the apparent Mach number defined as  $\zeta = \frac{v}{c(\xi_0)} \sin \theta$ , where  $\theta$  is take-off angle measured from the fault normal.

$$\frac{\dot{u}_c(x,t)}{t}$$

is the slope of the rupture phase taken directly off the velocity seismogram.

The fault radius is given by  $a = T^{1/2} v (1-\zeta)$  where  $T^{1/2}$  is the duration of the rupture phase, or equivalently the rise time of the displacement pulse. The (static) stress drop is given by Brune (1970)

$$\Delta\sigma = \frac{7}{16} \frac{M_0}{a^3}$$

The non-causal part of the processed signal which can be seen as a precursor on the velocity trace, and which becomes greatly amplified on the displacement trace, is a result of the high-pass filter which has a cut-off frequency close to the corner frequency of the P-wave. Unfortunately it is necessary to severely filter the signal in this manner in order to separate a clear unipolar displacement pulse from the slightly longer-period noise prevalent in the short period system.

This analysis has been carried out for four events and the results are summarized in Table 2. There is considerable scatter in source parameters derived for the same event but different stations. Some of this scatter could be caused by the crustal structure near the stations which can greatly change the amplitudes of a signal in the frequency band studied. The fact that many stations are used is a check on the effects of propagation in determining source parameters. By comparing several events at the same set of stations, empirical station corrections can be made.

Comparing source parameters obtained for the four events so far analyzed, the most apparent result is that the effective stresses and stress drops are almost an order of magnitude larger for event 8 than for the other events. Event 8 is a shallow ( $h = 27$  km) located on the main thrust zone between the trench and oceanic front. Events 17 and 20 are intermediately deep earthquakes within the portion of slab of descending Pacific plate landward of the volcanic front, and event 1 is a normal faulting mechanism located near the trench axis. The high stress drop for event 8 is consistent with the high stress drops of two events analyzed by House and Boatwright (1980), which were also shallow thrust events. One of these previously analyzed events is #9 (Figure 12). The obtained distribution of low- and high-stress drop events is consistent with Archambeau's (1978) stress contour map, in which (static) stress drops of earthquakes were inferred from  $M_s$  to  $m_b$  ratios. This map (Figure 14) shows an area of high stress earthquakes located south of the western end of the Alaska Peninsula. Lower stress events surround this area on all sides. Further analysis of the events in our remaining data set is necessary in order to see if the high stress events are indeed localized as suggested by Archambeau's map or if they are more a function of location within certain typical features of the subduction zone, e.g. trench, thrust zone, of within descending slab.

In making the calculation of source parameters, one of the more dominant factors is the P velocity at the source which enters into the equation as velocity raised to the power of 5/2. Velocity is strongly depth dependent. Hence, to make

TABLE 2

Source Parameters for Eastern Aleutian Earthquakes So Far Analyzed

	<u>STATION</u>	<u>EFFECTIVE STRESS</u>	<u>STRESS DROP</u>	<u>MOMENT</u>	<u>FAULT RADIUS</u>
Event 17	COR	50 bars	45 bars	$6.0 \times 10^{24}$ dyne-cm	3.9 km
Depth = 191 km	GOL	139 bars	90 bars	$1.6 \times 10^{25}$ dyne-cm	4.2 km
$M_b = 5.5$	LON	41.4 bars			4.2 km
	QUE	30 bars	21 bars	$2.9 \times 10^{24}$ dyne-cm	3.9 km
	SCP	164 bars		$1.5 \times 10^{25}$ dyne-cm	4.2 km
	TUC	90 bars	77 bars	$7.5 \times 10^{24}$ dyne-cm	3.5 km
Event 24	GSC	26 bars	105 bars	$2.15 \times 10^{24}$ dyne-cm	2.5 km
Depth = 136	GOL	27 bars	41 bars	$2.09 \times 10^{24}$ dyne-cm	2.8 km
$M_b = 5.3$	KTG	131 bars	21 bars	$3.67 \times 10^{24}$ dyne-cm	3.3 km
Event 1	ATL	50 bars			
Depth = 8 km	FVM	116 bars			
$M_b = 5.8$	MDI	100 bars	197 bars	$5.9 \times 10^{24}$ dyne-cm	2.4 km
	PTO	167 bars			2.1 km
	SNG	189 bars			2.4 km
	TOL	99 bars	235 bars	$5.13 \times 10^{24}$ dyne-cm	2.1 km
	UHE	67 bars	138 bars	$9.14 \times 10^{24}$ dyne-cm	2.1 km
	OXF	107 bars			
	WES	129 bars	261 bars	$7.8 \times 10^{24}$ dyne-cm	2.4 km
Event 8	LON	1420 bars			2.1 km
Depth = 17 km	SNG	792 bars			1.4 km
$M_b = 6.1$	STU	1030 bars	948 bars	$1.4 \times 10^{25}$ dyne-cm	2.3 km
	TUC	860 bars	500 bars	$1.4 \times 10^{25}$ dyne-cm	2.3 km
	OXF		728 bars	$2.1 \times 10^{25}$ dyne-cm	2.3 km

## Events Analyzed by House and Boatwright (1979)

Depth = 40 km	SDP	1040 bars	840 bars	$3.5 \times 10^{24}$ dyne-cm	1.2 km
$M_b = 5.8$					
Depth = 40 km	SDP	780 bars	640 bars	$6.7 \times 10^{24}$ dyne-cm	1.65 km
$M_b = 6.0$					

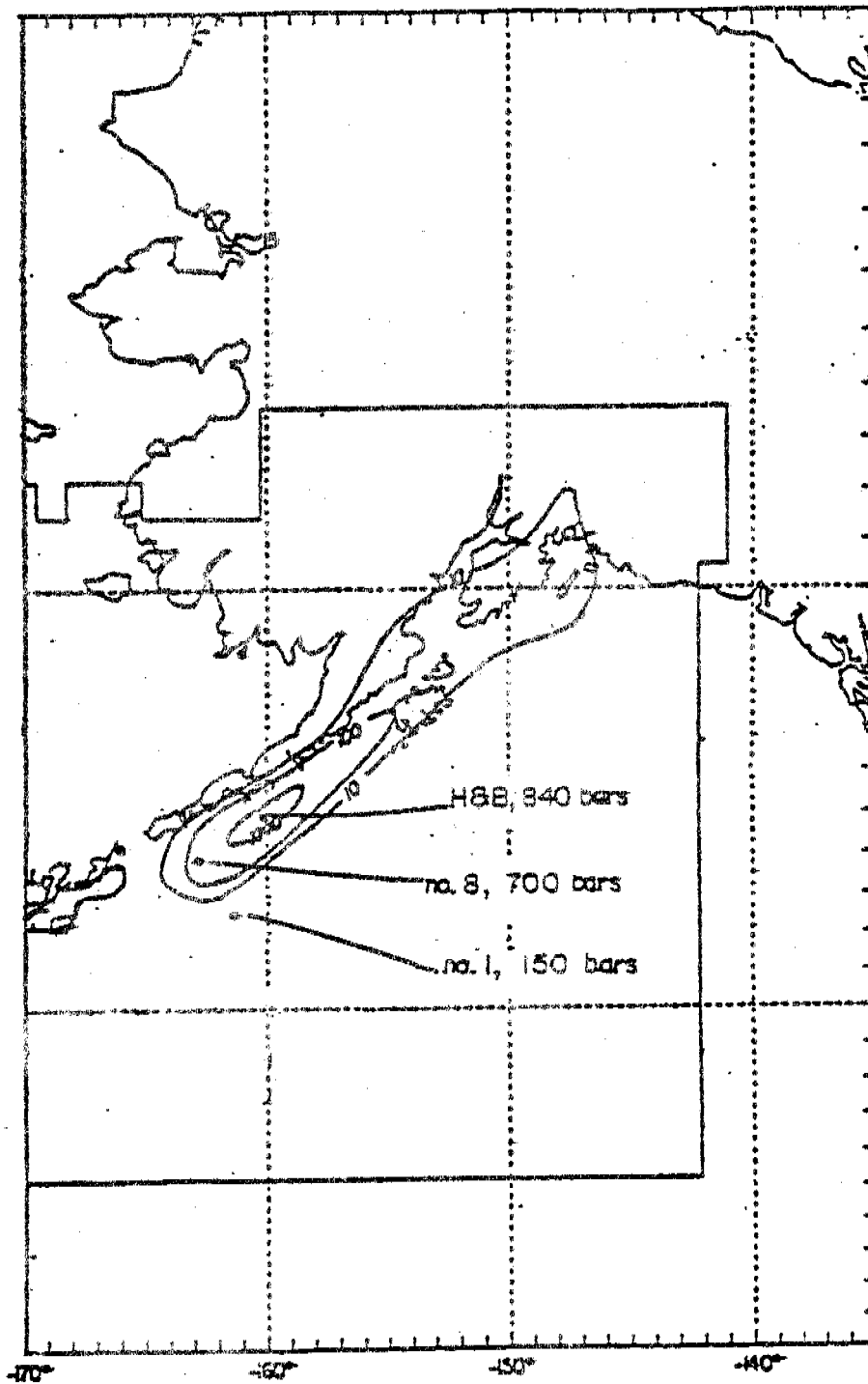


Figure 14. Part of stress contour map by Archambeau (1978) for earthquakes of focal depth 40-55 km. Plotted on the map are the locations and typical values of static stress drop for three events which were analyzed by the process described in the text. H&B is the event studied by House and Boatwright, which has a focal depth of 40 km. Events 1 and 8 have depths of 8 and 17 km, respectively.

accurate estimates of stress drop and moment one requires an accurate determination of depth. In general, the published ISC depths are not reliable. Inspection of numerous short-period records, and obtaining rough estimates of expected amplitudes of pP and sP, one can confidently identify depth phases including water boundes pwP, pwwP, and pWWWP. Depths for these events can then be constrained within a few kilometers.

Another more difficult problem is the determination of rupture velocity which appears as a factor cubed in the equation for effective stress. Following House and Boatwright a rupture velocity of 0.6 times the shear-wave velocity was used for the shallow thrust event. For the other events a rupture velocity of 0.75 times the shear velocity was used. In order to fix the rupture velocity more accurately one could follow the procedure of matching  $v^2$  plots of synthetics with the data as described by House and Boatwright (1980).

To extend this investigation of source parameters for events of magnitude greater than 6.5, one must turn from using short-period records to long-period records instead. The larger events have the advantage of reducing the station variations which so strongly effect the shorter-period signals. Essentially the analysis of long-period data follows the same procedure as for the short-period records, except the effect of depth phases must be compensated for in the long period pulse shape of the P-wave. Only a few events (see Table 2) will be large enough to be analyzed from long-period events.

Conclusions. This study is aimed to obtain for the Aleutian arc systematically static and dynamic source parameters (e.g. moment, source area, slip, stress drop and ambient stress) for as many earthquakes with magnitudes  $m_b - 5$  or larger as possible. Such data are important to understand the magnitudes of tectonic stresses in various parts of a subduction zone on the one hand; and--moreover--to categorize strength of seismic sources in the major seismogenic regions of the eastern Aleutian arc to obtain a set of 'typical sources' required in any scheme for seismic risk and hazards analysis.

#### Seismic Source Characterization in Gulf of Alaska (by J. Boatwright).

Although located outside the study area specifically assigned to this research unit we have studied the source properties of the St. Elias earthquake ( $M = 7.2$ ,

February 28, 1979) which ruptured a substantial portion of the plate boundary in the Gulf of Alaska. This region is of presently high interest to OCSEAP because of an imminent lease sale. Also this earthquake triggered 3 strong-motion instruments and these records will become available for analysis as soon as their digitization by the U.S.G.S. and/or industry is completed. In the meanwhile, J. Boatwright analyzed records from Lamont station (PAL) and WWSSN records. The following paragraphs provide a short description of the analysis technique and main results.

Employing a new technique for the body-wave analysis of shallow-focus earthquakes, we have made a preliminary analysis of the St. Elias, Alaska earthquake of February 28, 1979, using five long-period P- and S-waves recorded at three WWSSN stations and at Palisades, New York. Using a well determined focal mechanism and an average source depth of  $\approx 11$  km, the interference of the depth phases (i.e. pP and sP, or sS) has been deconvolved from the recorded pulse shapes to obtain velocity and displacement pulse shapes as they would appear if the earthquake had occurred within an infinite medium. These "approximate whole space" pulse shapes indicate that the rupture contained three distinct sub-events as well as a small initial event which preceded this sub-event sequence by about 7 seconds. From the pulse rise times of the sub-events, their rupture lengths are estimated as 13, 27 and 17 km, assuming that the sub-event rupture velocity was 3 km/sec. Overall, the earthquake ruptured  $\approx 60$  km to the southeast with an average rupture velocity of 2.2 km/sec. The cumulative body-wave moment for the whole event,  $1.2 \times 10^{27}$  dyne-cm, is substantially smaller than the surface-wave moments reported by Lahr *et al.* (1979) of  $5 \times 10^{27}$  dyne-cm. The moments of the sub-events are estimated to be .6, 3.2 and  $7.5 \times 10^{26}$  dyne-cm, respectively.

The analysis of large, shallow-focus earthquakes using body-waves is a difficult undertaking. Body-wave arrivals from these events are complicated by two distinct effects: first, the interference between the direct phase and the depth phases, and second, the generally complex nature of rupture in these events. In their analysis of the 1976 Guatemala earthquake, Kanamori and Stewart (1978) resolved these complications using a quasi-deconvolutional approach.

In this paper, we perform a direct deconvolution of five body-wave arrivals from the February 28, 1979, St. Elias, Alaska earthquake, recorded at three long-period WWSSN stations and on the Palisades, New York, broad-band Benioff instruments. This direct deconvolution is made possible by the specific focal mechanism of this earthquake; the technique is not generally applicable to all

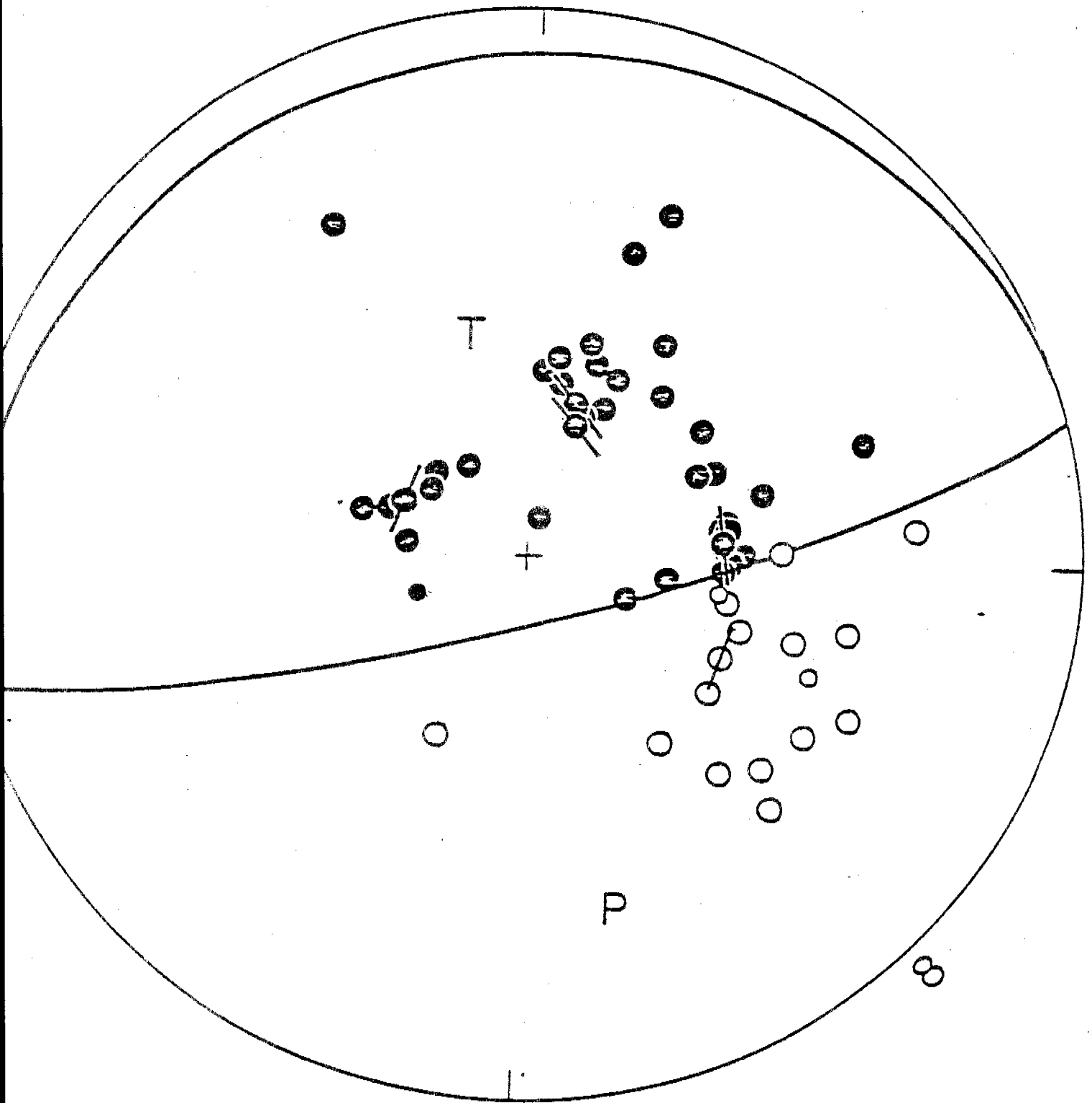
shallow-focus events. The pulse shape information retrieved includes both moments and rupture durations for the sub-events. An average rupture velocity and rupture direction for the whole event can also be estimated. This analysis provides a unique view of the complexity of rupture in this earthquake, in contrast to the descriptions of rupture determined from aftershock locations and surface-wave analysis.

Short samples (150-300 secs) of the seismograms were digitized and corrected to trace deflection against time by interpolating and correcting for the translation pitch of the recording drum. The corrected traces were bandpassed using a triangle smoothing operating and a second-order high-pass Butterworth filter (corner frequency at either 50 secs or 66 secs), run backwards and forwards over the trace. To obtain the bandpassed ground velocity, the band-passed seismograms were instrument-corrected using a recursive deconvolution derived from a bilinear approximation to the coupled galvanometer-seismometer systems.

Figure 15 shows the fault-plane solution for the earthquake as determined by Perez and Jacob (1979), who concluded on the basis of tectonic considerations that the plane which dips shallowly to the north is the fault plane. This nearly horizontal fault plane insures that the pulse shapes of the direct phase and the depth phases are nearly identical, and thereby permits the purely impulsive deconvolution.

A low-frequency baseline correction was then subtracted from the deconvolved velocity, giving the "approximate whole space" velocity trace. The AWS velocity was then integrated to obtain the AWS displacement, which has a unipolar displacement pulse shape and a flat baseline. The AWS displacement pulse shapes have three distinct pulses which we have indentified as sub-events 1, 2, and 3, preceded by a small initial event, labelled 0 where it can be identified.

Figure 16 illustrates the analysis process for the P wave arrivals at Palisades (PAL). The PAL P-wave is a nodal arrival, and the free-surface operator (FSO) has a somewhat longer and more detailed convolutional inverse. The seismogram as digitized, shown at the bottom of Figure 16, clearly details the initial event, which precedes the sharp onset of sub-event 1 by 7 seconds. It cannot be distinguished, however, in the AWS pulse shapes. Sub-event 1 is substantially stronger at PAL than at other stations studies, while sub-event 3 is weaker. Even more striking is the energetic arrival which separates sub-events 2 and 3. If a variation in the fault-plane solution is responsible for these differences, the fault plane must become somewhat more steep as the rupture proceeds, or the slip vector must rotate slightly counter-clockwise to decrease the amplitude of the sP arrival.



FEBRUARY 28 1979  
 60.62°N 141.50°W 11km

Figure 15. Lower-hemisphere, equal-area stereogram of first motion directions for the St. Elias earthquake of 28 February 1979. Solid circles represent compressional arrivals; open, dilatational. Bars through the circles indicate S-wave polarization directions. The axes of compression and tension are labeled P and T, respectively.



# P-WAVE AT PAL

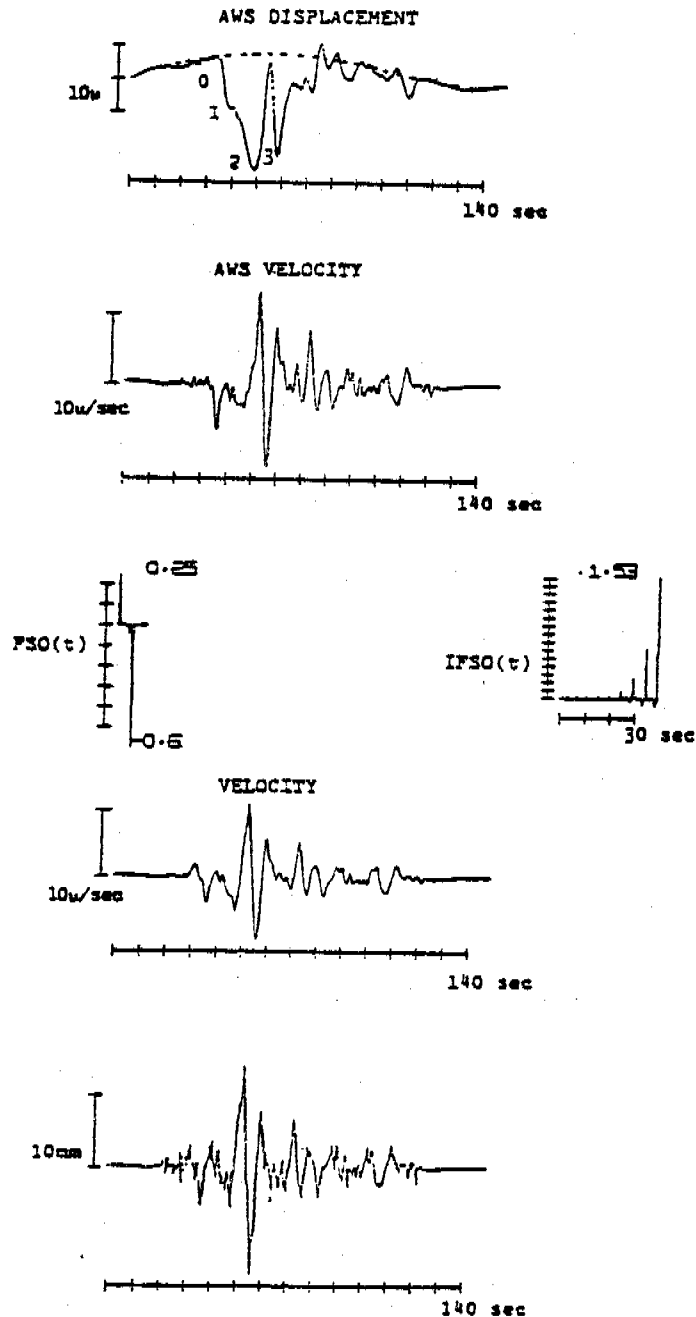


Figure 16. Analysis procedure for the P-wave at Palisades (PAL). Bottom trace is the digitized seismogram, next above is the integration to the velocity trace. In the middle are shown the Free Surface Operation (FSO) and the Inverse Free Surface Operators (IFSO). Second from the top and the top are the Average-Whole-Space (AWS) velocity and displacement traces, respectively.

Figure 17 summarizes the conclusions of our analysis. For comparison, the heavy dashed line is the estimate of aftershock area obtained by Lahr et al. (1979) from a U.S.G.S. array of 50 short-period seismic stations. The star is the location of the mainshock epicenter (what we have termed the initial event). Sub-events 1, 2, and 3 are plotted with dimensions and spatial separations as estimated from our analysis.

The total bodywave moment estimates from our analysis,  $11.6 \times 10^{26}$  dyne-cm, is a factor of 4 smaller than the surface wave moment estimated by Lahr et al. (1979). This discrepancy may result from focusing and amplification of the surface wave energy by a strong velocity contrast in the source region.

#### Summary on Source Characterization

Earthquakes in the magnitude range  $M = 5$  to  $7.2$  have been analyzed along the eastern Aleutian arc and in the Gulf of Alaska. Their source properties such as moment, source area, displacement and stress drops were determined where possible. Stress drops ranging from several tens to almost 1 kbar were observed with the highest stress drops reported at a depth of about 40 km near the down-dip end of the main thrust zone of the Shumagin seismic gap. These were simple sources with thrust mechanics and with magnitudes smaller than 6. The largest event ( $M_s = 7.2$ ), in the Gulf of Alaska, was a multiple event and has probably a much lower stress drop than the high-stress events in the Shumagin Islands. Considering their relative magnitudes, these stress properties may explain the relatively high level of ground motions excited by the Shumagin events versus the relatively low levels of motion excited by the St. Elias, Gulf of Alaska event.

#### SEISMIC STRONG-MOTION RECORDINGS

As pointed out earlier no new strong-motion recordings were collected from the 4 instruments operative in the eastern Aleutian arc between Unalaska Island and Shumagin Islands. The three records from the St. Elias earthquake in the NEOA region are expected to become available for analysis in the near future.

Since we believe that the availability of strong-motion records from the Alaska-Aleutian seismogenic belt is one of the foremost unresolved tasks within OCSEAP we have undertaken the following steps:

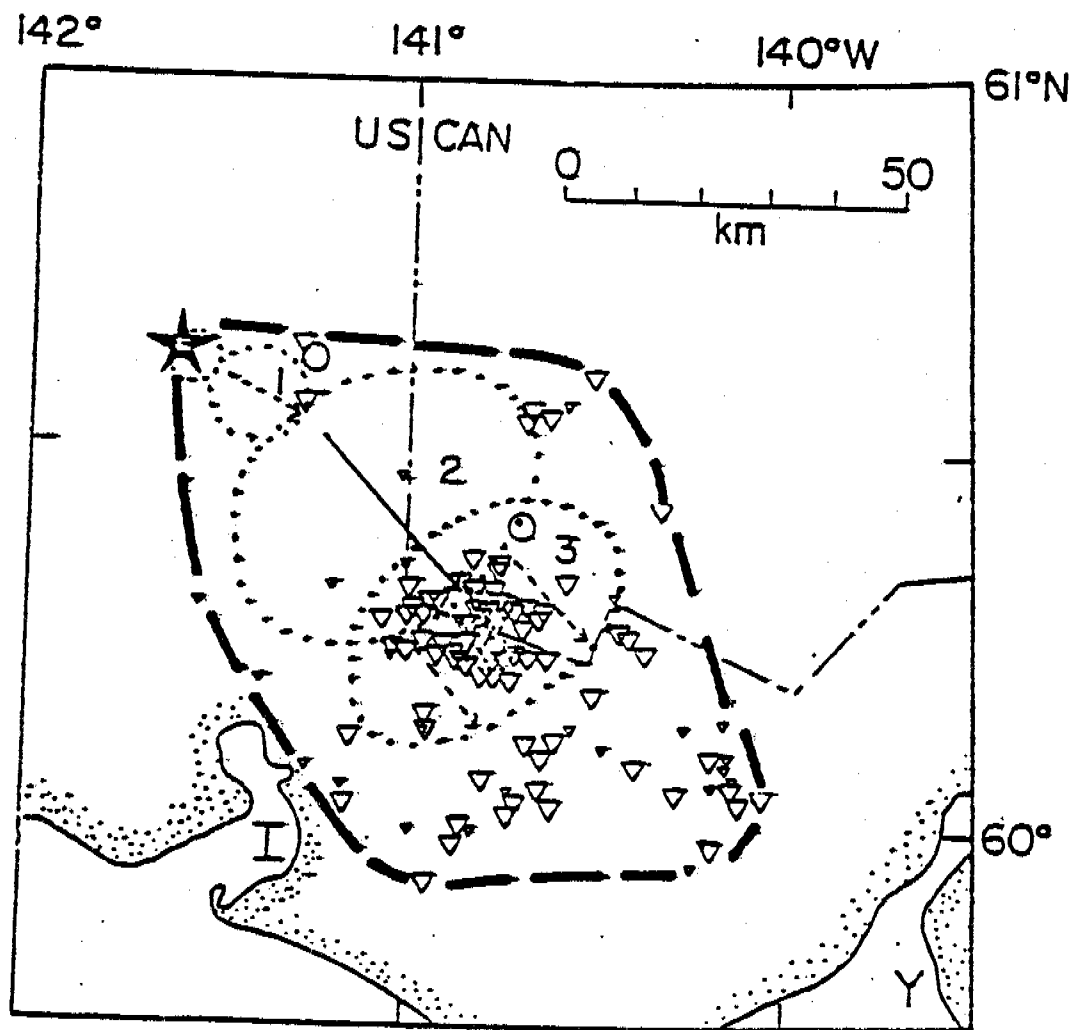


**Figure 17.** Rupture zones for the St. Elias earthquake of 28 February 1979 (star). Heavy dashed line from Lahr *et al.* (1979), zones 1, 2 and 3 are described in text. Icy Bay (I) and Yakataga (Y) are shown for reference.

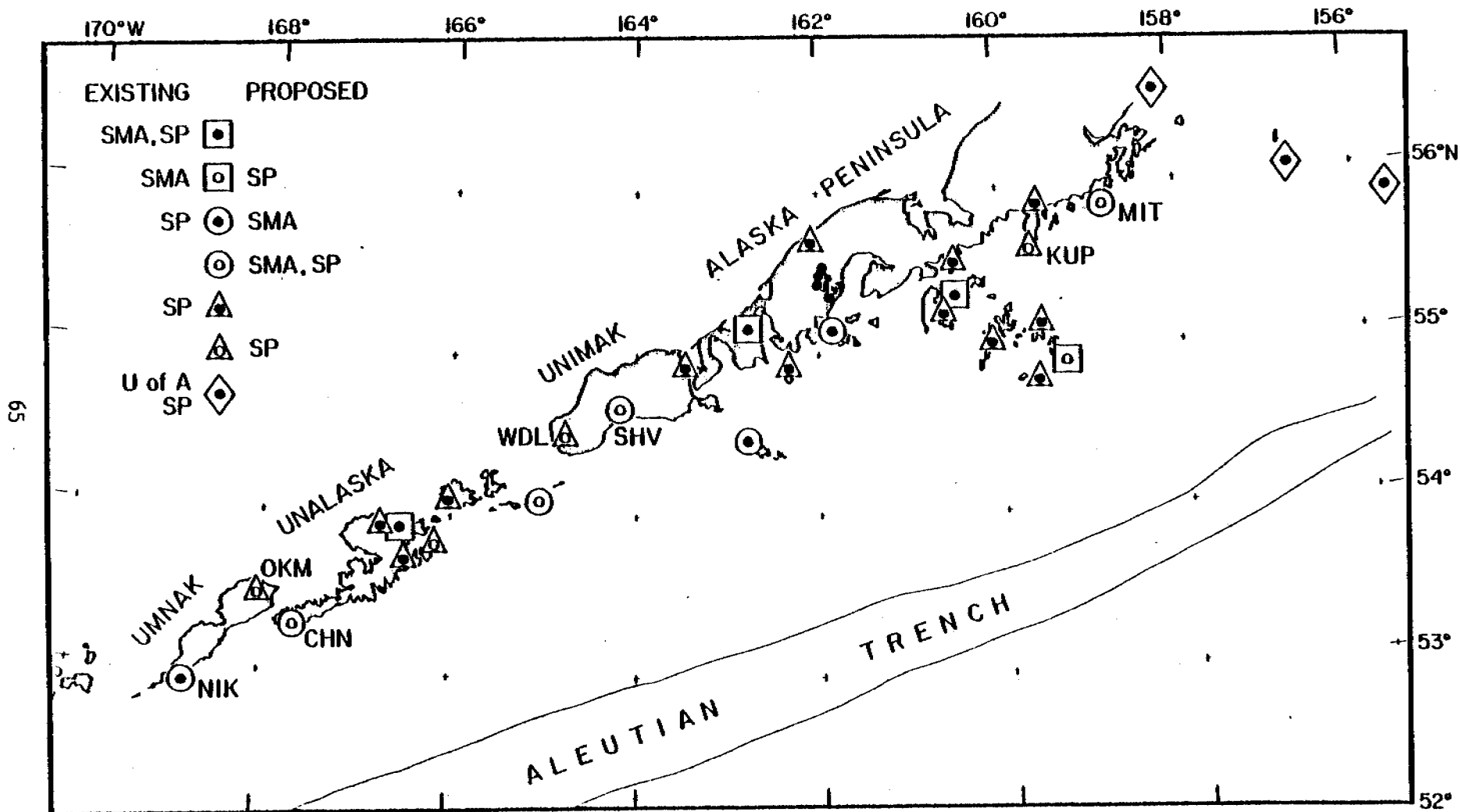


Figure 18. Suggested Eastern Aleutian Regional Network. This network is suggested to optimize the probability for recording useful strong-motion data. It is substantially based on existing stations. A possible time-table for completion of the network by summer of 1981 is given in Table III. All stations would have a short-period-vertical (SPZ) seismometer; existing SPZ sites are shown by a solid circle in the center of the symbols. Those with existing or proposed strong-motion recorders (SMA) are shown with the large square or circle, respectively. The large triangles denote stations, without SMA's, that are necessary to locate accurately the large events that trigger the strong-motion recorders. The strong-motion recorders will be provided through an approved contract with the USGS.

TABLE 3

POSSIBLE SCHEDULE FOR INSTALLATION OF EASTERN ALEUTIAN  
REGIONAL NETWORK

<u>Field Season</u>	<u>Station</u>	<u>Code</u>	<u>Component</u>	<u>Agency</u>
80	Sadanka Island	SDK	SPZ	D.O.E.
81	Shishaldin Volcano	SHV	SPZ/SMA	NOAA/USGS
80	Westdahl Volcano	WDL	SPZ	NOAA
80	Tigalda Island	TGD	SPZ/SMA	NOAA/USGS
80	Tanaskin Bay	TNB	SPZ	NOAA
80	Nikolski	NIK	SMA	NOAA
80	Sanak Island	SNK	SMA	NOAA
80	Dolgoi Island	DLG	SMA	USGS
81	Simeonof Island	SIM	SPZ	NOAA
81	Kupreanof Penn.	KUP	SPZ	NOAA
81	Mitrofanina Island	MIT	SPZ/SMA	NOAA/USGS
81	Okmok Volcano	OKM	SPZ	D.O.E.
81	Chernofsky	CHN	SPZ/SMA	NOAA/USGS

1. We have submitted a proposal and have been granted funding by the U.S.G.S. to add a minimum of 8 strong-motion instruments in the eastern Aleutian study area. Their deployment will be under NOAA/OCSEAP logistic support and with travel funding under this contract. At least four additional units will be installed in 1980 and the remainder in 1981. The accelerometers will be installed at remote sites of the Shumagin microseismic network (Figure 18, Table 3). A trigger signal will be transmitted through the existing radio links of the network and, hence, trigger times will be known with a precision not commonly found in strong motion instrumentation.
2. Early in 1980 we have arranged with the Strong Motion group of the U.S.G.S. in Menlo Park a visual on-site inspection of all Alaskan Strong Motion records in their archives. We expect to find at least 10 to 20 useful Alaska-Aleutian strong-motion records from which either source properties, or at least ground motion characteristics can be derived.
3. We have taken an initiative through the formation of SMAC (an informal group called Strong Motion Alaska Council) to bring together all OCSEAP and other seismic research groups active in Alaska for intensifying a concerted effort towards deployment of new strong-motion instruments and analysis of all existing Alaska strong-motion records (see Section XI.E). The quality of any quantitative estimates of seismic hazards from ground motion in Alaska OCS regions will strongly depend on how many of the SMAC goals can be realized soon. Until the few existing records, mostly in U.S.G.S. archives are analyzed and/or new recordings are collected little scientific progress can be expected.
4. A paper concerned with the tectonic setting of the St. Elias earthquake ( $M_s = 7.2$ ) of February 28, 1979, and its possible premonitory seismicity was prepared by Perez and Jacob (BSSA, 1980, in press). Since this paper is of potential interest to OCSEAP for the NEGOA lease area, we include the abstract and introduction of this paper in section XI.D.

## F. Pavlof Volcano Studies (S. McNutt)

During the past year we made substantial progress in our studies of the seismic activity of Pavlof volcano. Specific areas of study are: 1) several additional month's worth of helicorder data has been reduced; 2) an earth tide study has been nearly completed and is being prepared for publication; 3) frequency spectral analysis of some signals has been carried out; and 4) tapes from the Pavlof local array are being played back for the magma chamber study. Each of these areas will be described more fully in the following paragraphs, but first we present a brief review of the scope of relevance of our studies.

As the recent eruptive activity of Mt. St. Helens has shown, volcanoes can be quite unpredictable in their habits. Basic volcanic processes are only poorly understood, so an assessment of volcanic hazards must of necessity be extra cautious until some basis for a more relaxed outlook can be established. Fortunately, Pavlof Volcano is fairly remote from large population centers. Also, it tends to erupt mildly, based on observations and study over the past several decades. For these reasons we have focussed our attention on understanding details of eruption processes and cycles, rather than assessing hazards outright, as for example preparing a hazards map of the volcano showing areas of likely lava flows, directed blasts, ash accumulations, etc. Also, and perhaps more importantly, Pavlof sits in the Shumagin seismic gap (McCann et al., 1979); thus we are in an excellent position to study in detail interactions between tectonic and volcanic systems prior to and after an expected large earthquake. What we learn from volcanic activity may allow us to forecast tectonic earthquakes, or conversely, what we learn from earthquake activity may allow us to forecast the time and intensity of volcanic eruptions. Toward this end we are engaged in the following studies.

A. Volcanic Seismicity Plots Based on Helicorder Records. Figure 19 shows a map of Pavlof volcano and vicinity with station locations. Records from the PVV station are nearly continuous from October 1973 to the present. These data were collected in cooperation with Juergen Kienle of the University of Alaska. At Lamont-Doherty we have made a summary of the number of volcanic earthquakes per day for the first seven month's of the station's operation (15 October 1973 - 15 April 1974), for the period 1 September 1974 - 30 April 1975, and for the month of September 1975. We are continuing this count up to the present time.

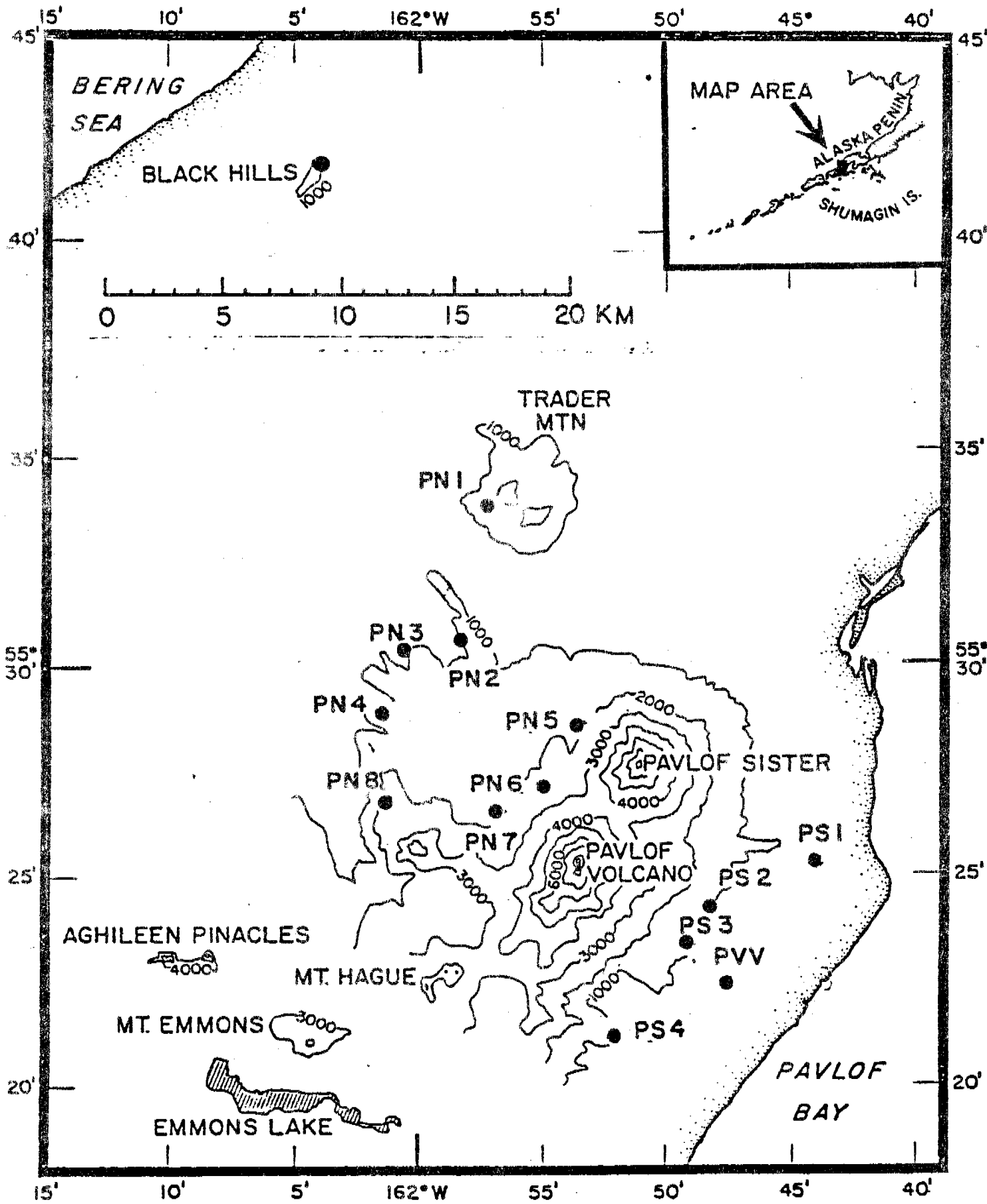


Figure 19. Locations of stations of the Pavlof seismograph array-



Histograms showing the number of events of four different types occurring during each 2 hour interval are also being routinely prepared for Pavlof Volcano. To date, helicorder records for the time period 1 September 1974 through 30 April 1975 and September 1975 have been systematically reduced. Number and size of b-type volcanic earthquakes, occurrence of air shocks, incidence and duration of harmonic tremor, and occurrence of high frequency tremor have been catalogued for each 2 hour interval for the entire period.

Figure 20 shows examples of each of these types of earthquakes as they appear on the PVV helicorder records. Plots have been prepared (ex. Figure 21) and the information has also been computerized so that statistical tests (such as moving averages, time series analyses, etc.) can be made. This information, together with visual eruption reports from local sources and others such as the Smithsonian Institution's Scientific Event Alert Network, provide us with solid data base to overview Pavlof's activity during the past eight years.

B. Earth Tide Study. Other workers (for example Mauk and Johnston, 1973) have shown that volcanic activity tends to be triggered by the solid earth tide. Certain episodes of volcanic earthquake activity at Pavlof show a positive correlation with both the fortnightly and semidiurnal components of the theoretical solid earth strain tide. In particular, swarms occurring 3-4 days before and 3-4 days after periods of mild eruptive activity correlate well with the horizontal component of the strain tide (Figure 21).

For comparative purposes, three tidal time series were generated: the vertical gravity tide, the horizontal strain tide parallel with the volcanic arc axis (azimuth  $45^\circ$ ), and the horizontal strain tide perpendicular to the axis (azimuth  $135^\circ$ ). The tide is calculated as a time series by Longman's (1959) method using the astronomy given by Munk and Cartwright (1966) and Cartwright (1968). There is no correction for height above sea level or for the ellipticity of the Earth (see Broucke et al., 1972). The Love and Shida numbers used are those of Longman (1966):  $h_2 = .612$ ,  $k_2 = .302$ ;  $l_2 = .083$ ,  $h_3 = .290$ ,  $k_3 = .093$  and  $l_3 = .014$ . The lunar tides are calculated for spherical harmonic orders 2 and 3, the solar tides for order 2 only. The lunar and solar tides are then added together (Beavan, personal communication).

The main results of the earth tide study are given in the abstract (Section XI.C) of a talk given at the Fall 1979 PNAGU Meeting. Additionally, Figure 21 shows a schematic diagram illustrating our interpretation of the data.

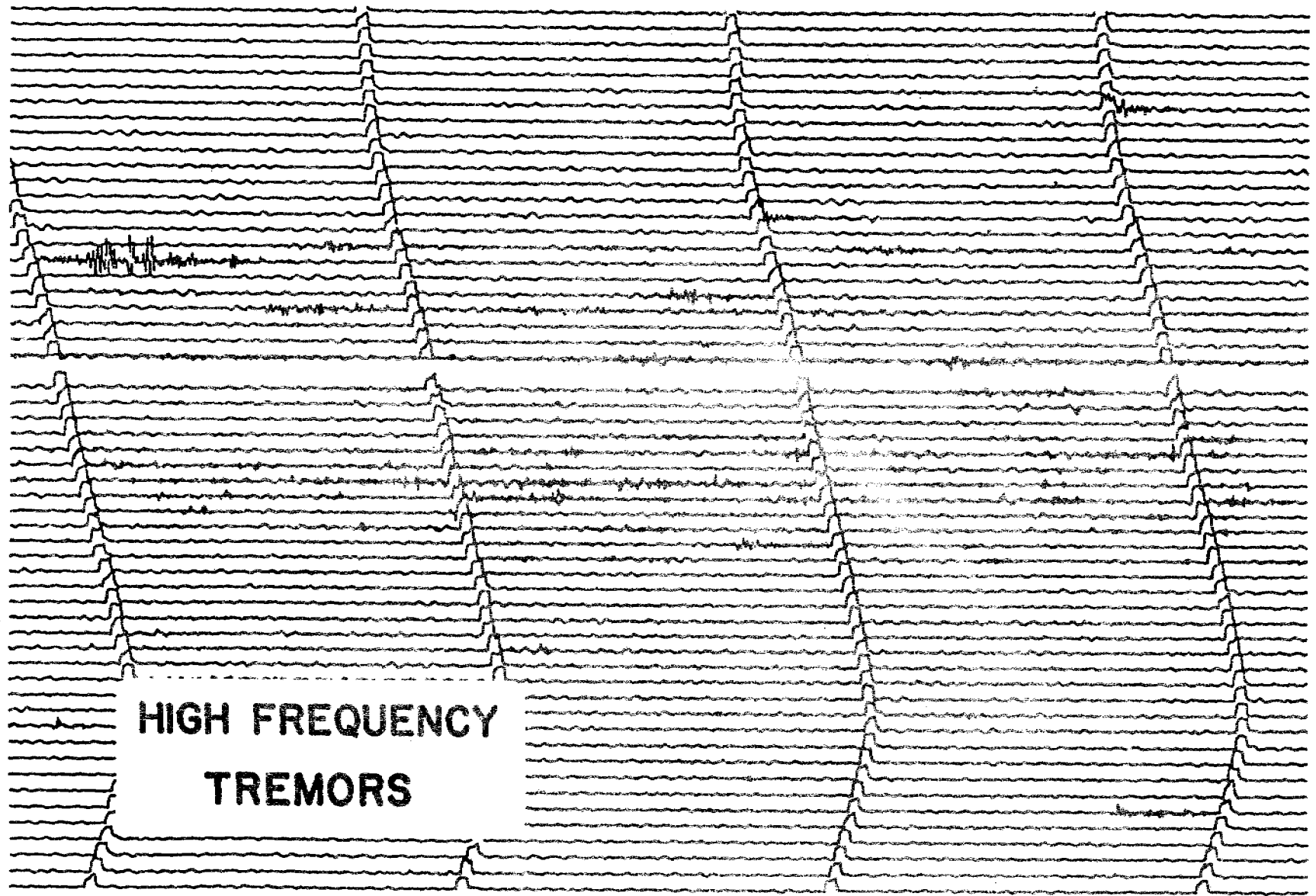


Figure 20A. Volcanic earthquakes as recorded on the PVV short period helicorder. High frequency tremors. The tick marks are one minute apart.

B

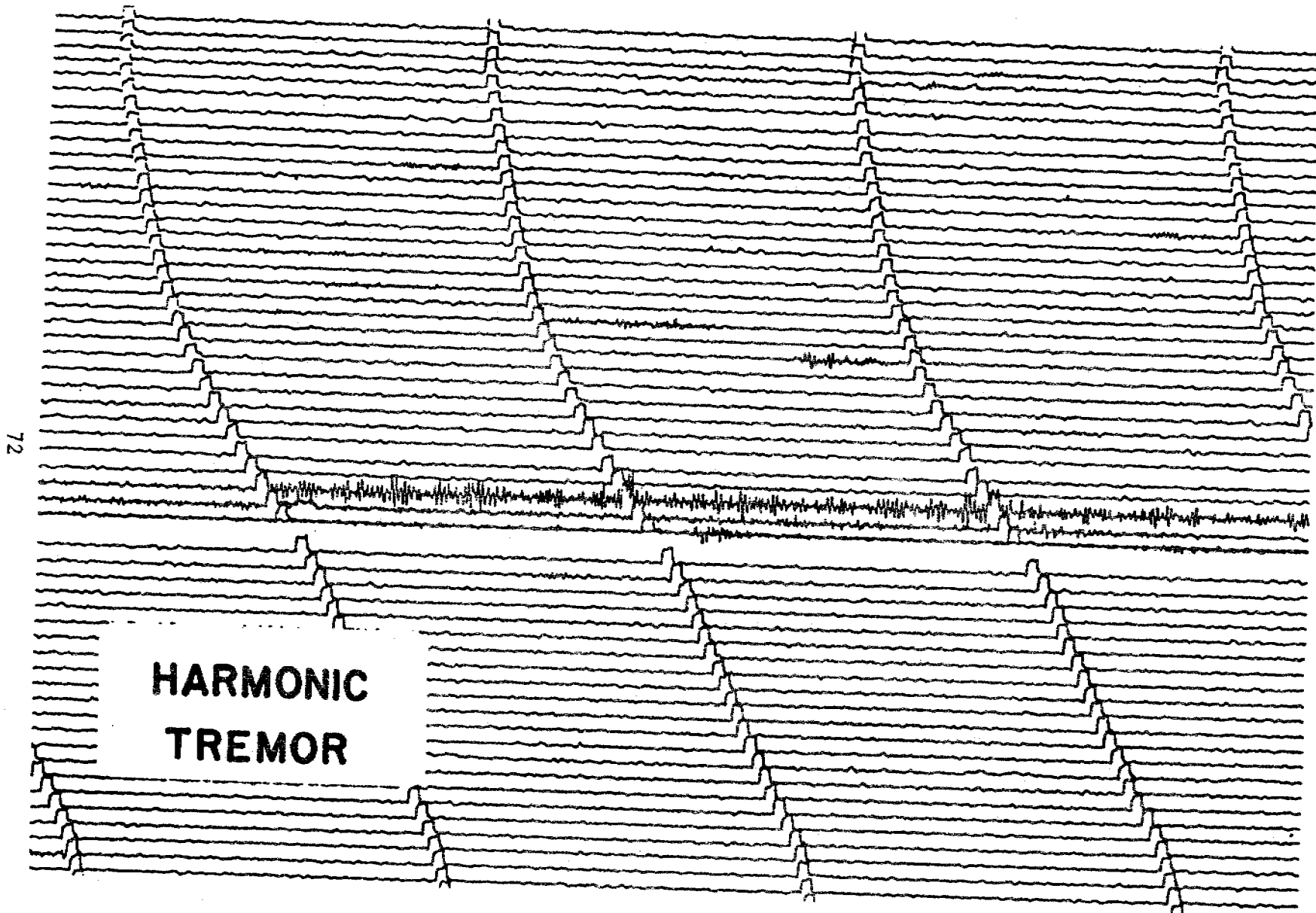


Figure 20 B. Volcanic earthquakes as recorded on the PVV short period helicorder. Harmonic tremor. The tick marks are one minute apart.

c

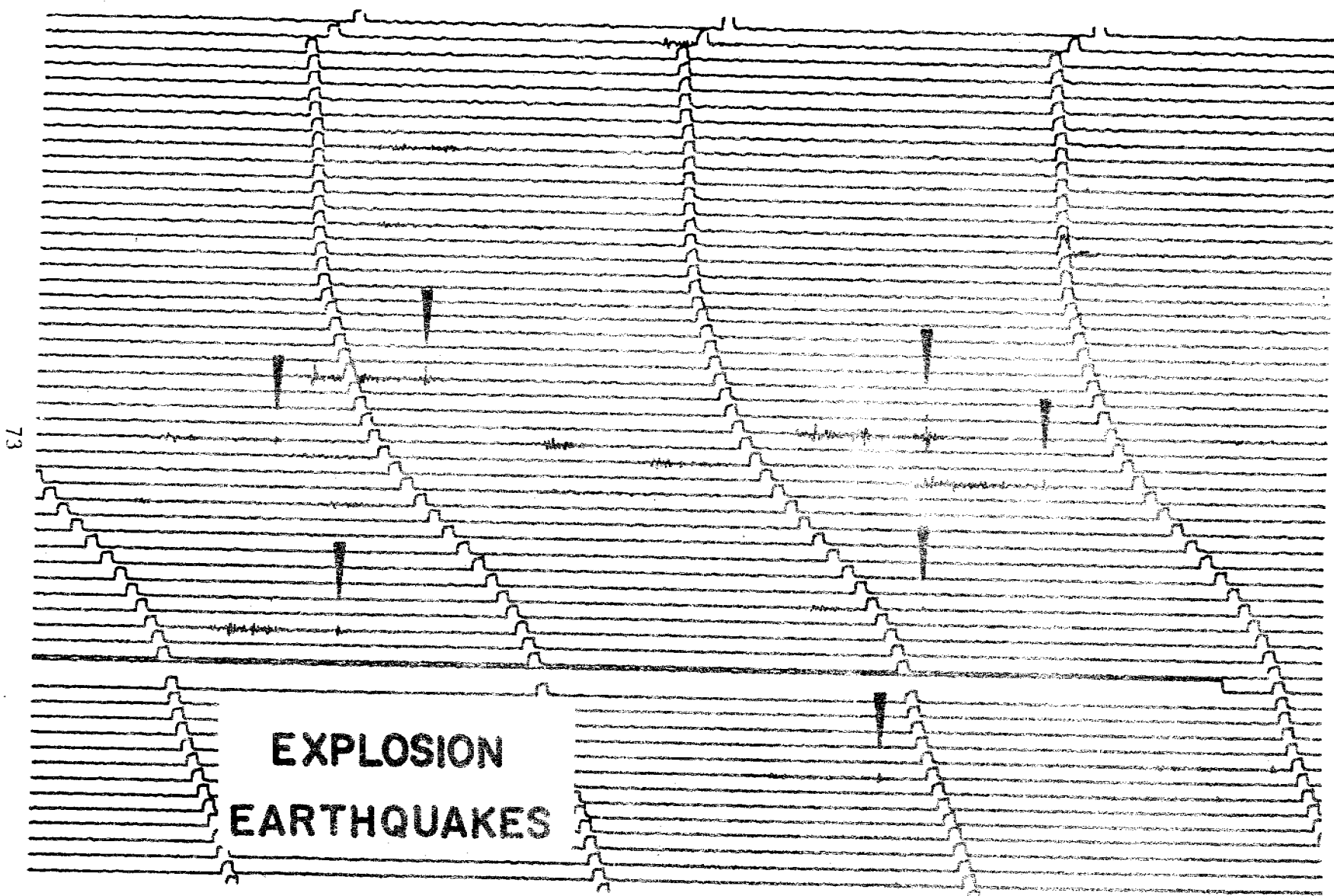


Figure 20 C. Volcanic earthquakes as recorded on the PVV short period helixer. Explosion earthquakes. The arrows point toward the air shock or explosion phase. The tick marks are one minute apart.

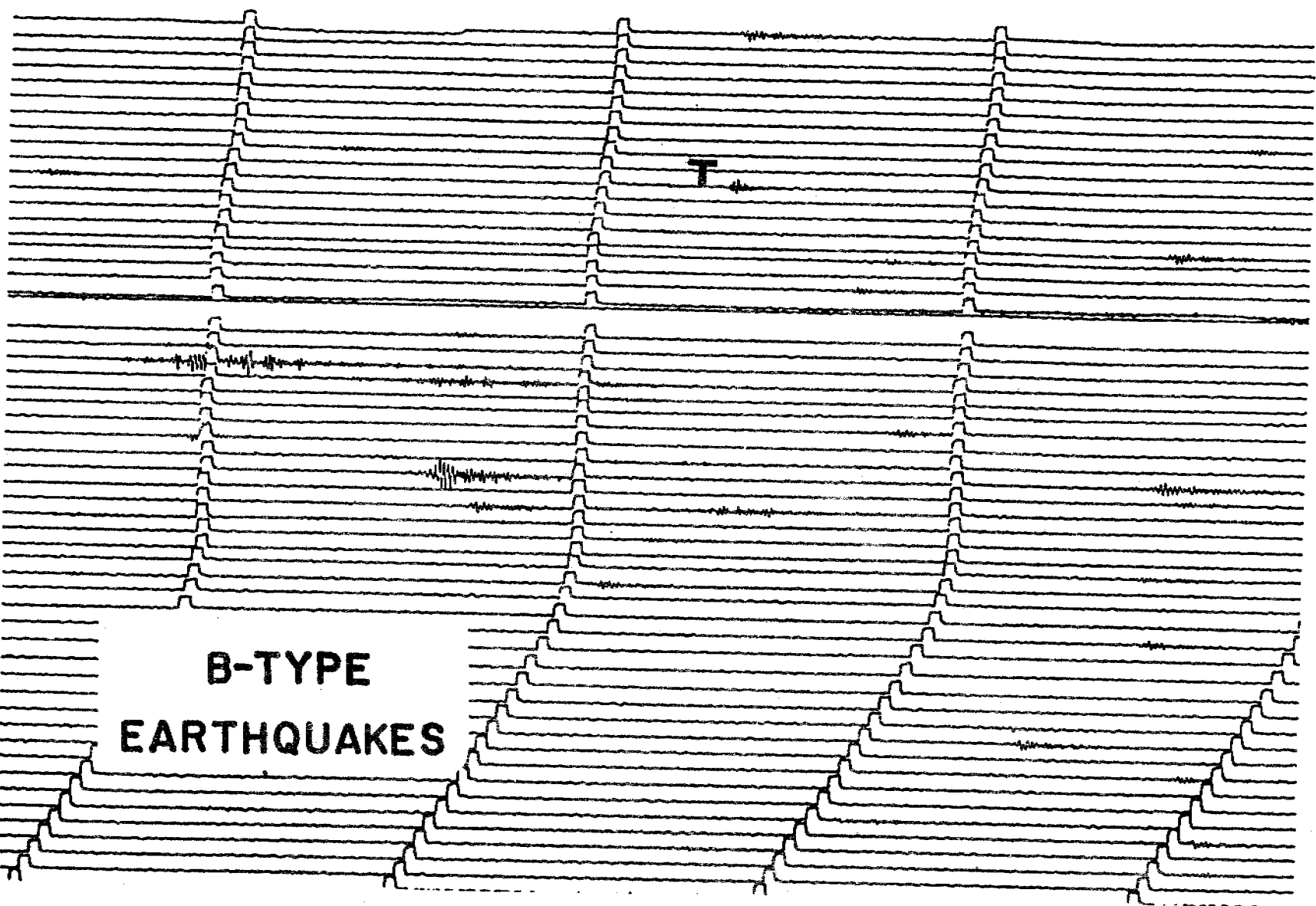


Figure 20D. Volcanic earthquakes as recorded on the PVV short period helicorder. Volcanic b-type earthquakes. The tick marks are one minute apart.

# PAVLOF VOLCANO SEISMICITY

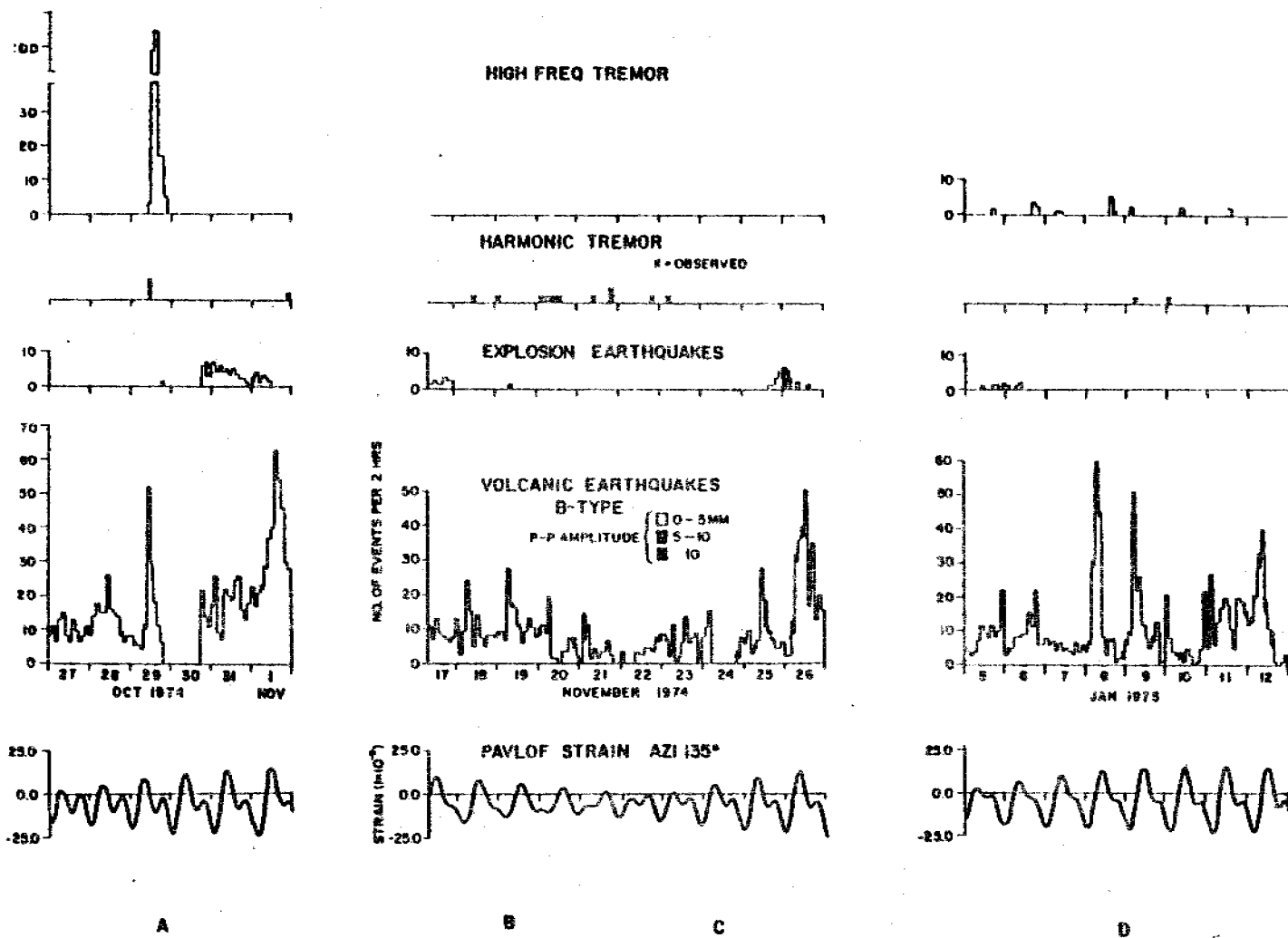
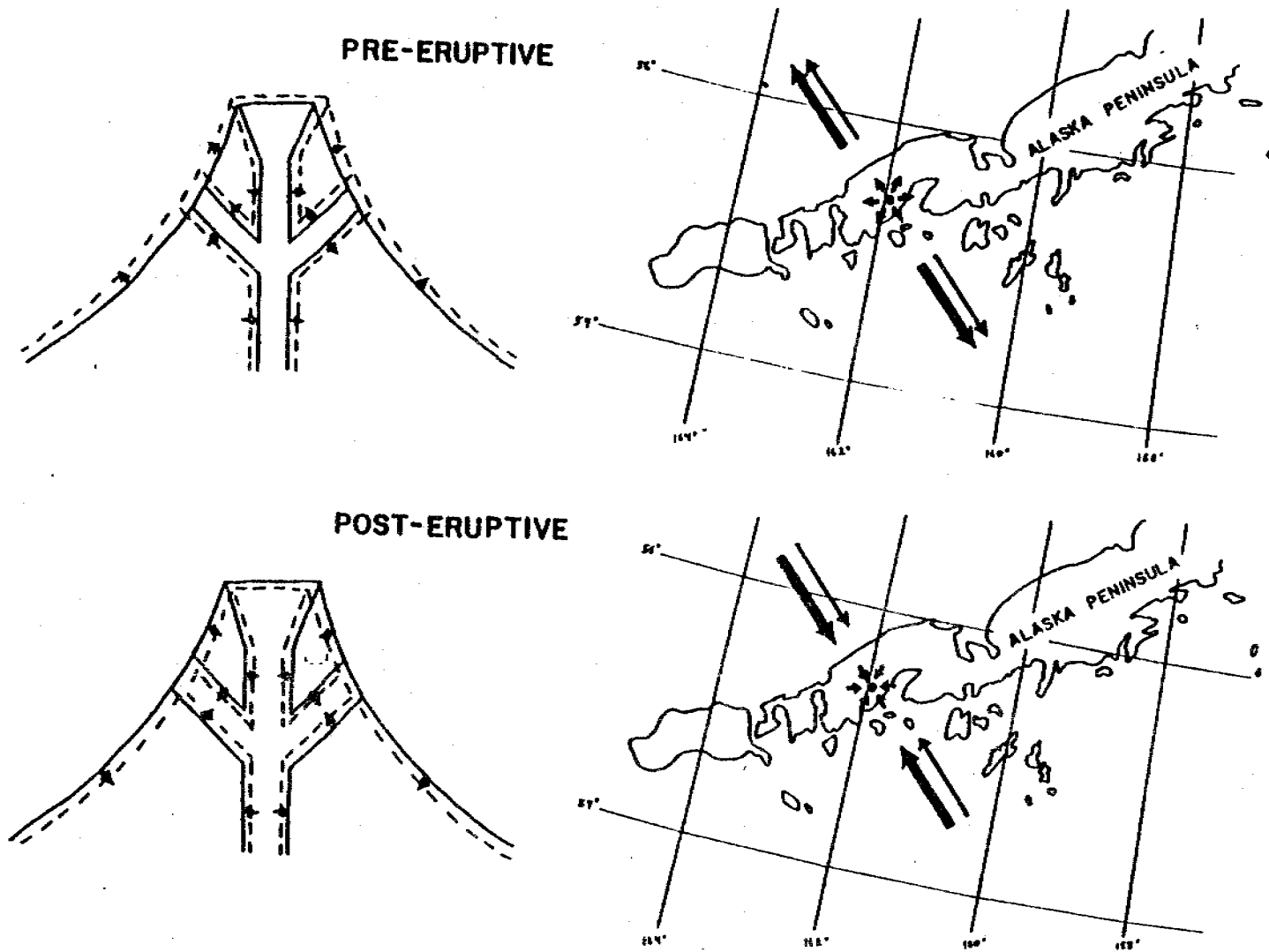


Figure 21. Pavlof volcano seismicity from PVV helicorder records:

- A) pre-eruptive period 27 Oct - 1 Nov 1974
- B) post-eruptive period 17 Nov - 21 Nov 1974
- C) pre-eruptive period 21 Nov - 26 Nov 1974
- D) post-eruptive period 5 Jan - 12 Jan 1975

The plots show the number of signals of each type recorded during each two-hour interval; the bottom is a theoretical horizontal strain tide for Pavlof at an azimuth of  $135^\circ$  ( $\approx N45^\circ W$ ). Note the correlation of b-type earthquake swarms with high tide (extension) at (A) and (C), and with low tide (compression) at (B) and (D).



**Figure 22.** Schematic diagram of Pavlof Volcano and the Alaska Peninsula. During pre-eruptive periods the earth tide acts to enhance inflation of the volcano, while during post-eruptive periods the earth tide acts to enhance deflation. The b-type earthquake swarms occur at tidal peaks, which suggests that b-type earthquakes are contraction/expansion events. The two sets of arrows perpendicular to the peninsula represent earth tide and ocean tide respectively, which are nearly in phase near Pavlof volcano.

All the data from the minor eruption of fall 1974 has now been reduced and plotted, so we are preparing the material for publication. We plan to continue this study with the entire PVV data set to verify the relationships already observed.

C. Frequency Analysis of Harmonic Tremor from Pavlof Volcano. Harmonic tremor signals from Pavlof volcano are observed on seismic records of eruptions. Signals resembling harmonic tremor are also observed on seismograms from stations near Tarbela dam and reservoir in Pakistan. Frequency analyses have been performed on both the Pavlof and Tarbela signals using two methods: Discrete Fast Fourier Transform and Burg maximum entropy. The Tarbela signals are shown to be organ pipe resonances in the outflow tunnels, with both even and odd harmonics present (i.e.  $\lambda = 1/4\ell, 1/2\ell, 3/4\ell, \ell, 5/4\ell, \text{etc.}$ ). The observed spectra (Figure 23) change with location around the reservoir and with the size of the outflow opening, which is gate controlled.

We infer that the Pavlof harmonic tremor signals are also organ pipe resonances, presumably of a magma-filled conduit. The spectra (Figure 23) exhibit well-recorded higher frequencies, representing overtones such as  $7/4, 2, 9/4, 5/2, \text{etc.}$ , but poorly recorded lower frequencies (including the fundamental modes). We infer that the source excites only higher frequency modes.

Several mechanisms are suggested for exciting oscillations within the conduit that cause harmonic tremor: 1) intermittent flow of magma through the pipe, 2) conduit extension/contraction, and/or 3) nearly continuous explosions. The inferred length of the tube depends on the velocity of p-waves in magma; reported values of 0.3-2.0 km/sec yield values for the conduit length of 0.5-3.2 km.

D. Magma Chamber Study. A study to determine the size of a magma chamber under Pavlof volcano is presently being funded by D.O.E. The study involves looking for travel time residuals and amplitude attenuation for ray paths of earthquake waves which travel through the root zone of Pavlof. A similar type of study by Iyers (1979) showed the presence of a low velocity zone under Yellowstone Park.

We now have data on magnetic tape from the 12-station Pavlof array (Figure 19) from summer 1976 to the present. We are in the process of playing back most of the tapes. This project was to have been begun by graduate student S. Hickman approximately one year ago. However, Hickman is presently on leave, and the project is being restarted by graduate student S. McNutt in cooperation with J.N. Davies.



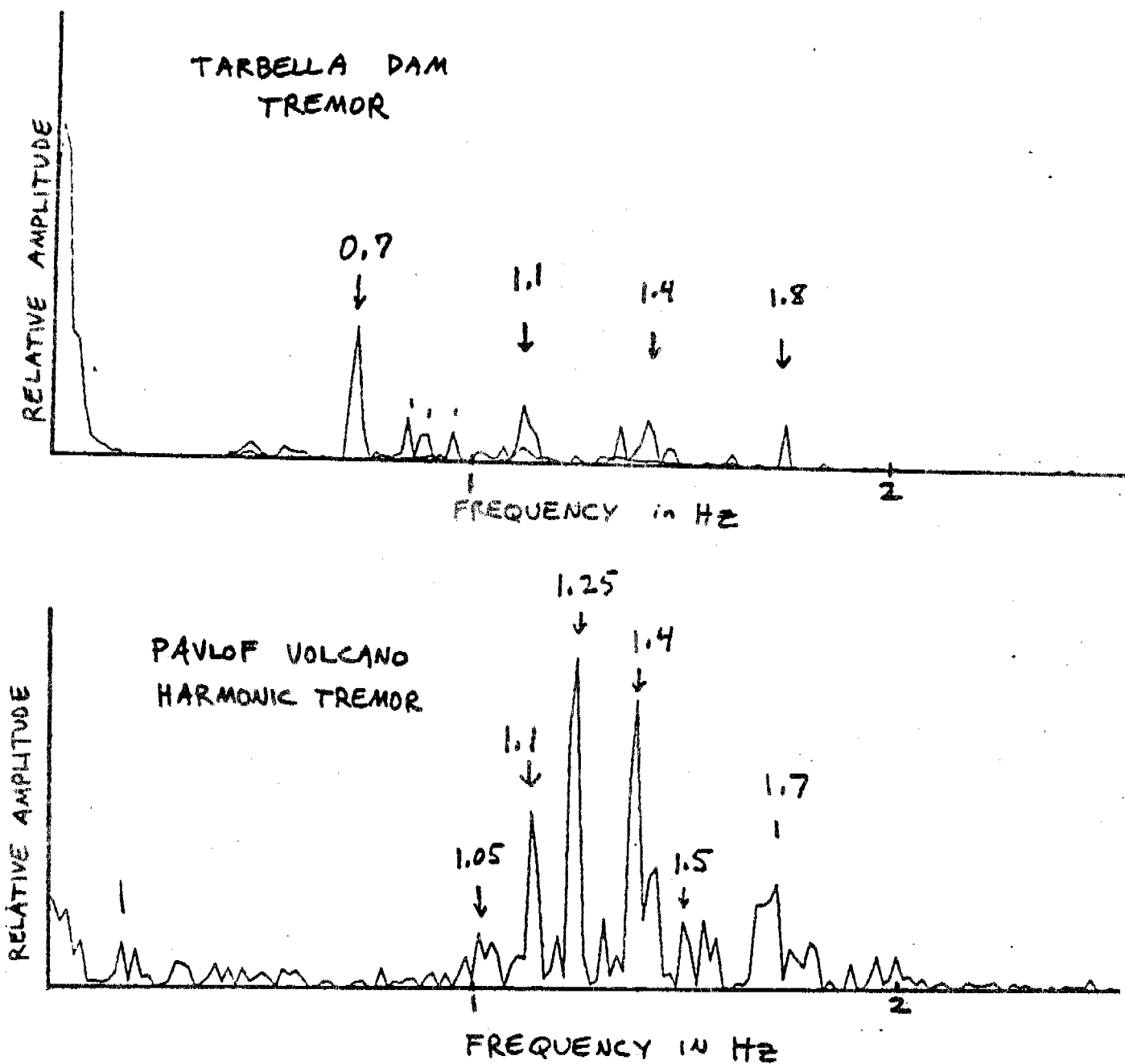


Figure 23. Discrete Fast Fourier Transform spectral analyses of signals from Tarbela Dam (Pakistan) and Pavlof Volcano (Alaska). Each plot shows the spectrum from one minute of record. Note the evenly spaced peaks in each spectrum, corresponding to standing waves of different modes set up in organ pipe-like resonators. The pipes are outflow tunnels at Tarbela dam and magma conduits at Pavlof volcano.

The study is relevant to volcanic hazards in that the presence, position and size of near surface magma chambers are some of the factors that determine how much magma is available for eruption. Thus, we hope to gain some insight into how intensity and type of eruption are related to the amount and chemical composition of magma. Also, the size and position of a magma chamber are important considerations in terms of potential for geothermal power.

## VIII. CONCLUSIONS

The studies reported above refine and strengthen our contention that the Shumagin Islands region is a seismic gap and that it has a high potential for a great earthquake or a series of very large earthquakes within the next one or two decades. This will be the controlling factor in any seismic hazard analysis for the broad region around the Alaska Peninsula; i.e. from lower Cook Inlet to Unalaska Island.

The studies of historical earthquakes greatly improve our understanding of the seismicity of the Alaska Peninsula region prior to the beginning of this century. In particular, they allow us to conclude that the Shumagin Islands region has a history of at least one great earthquake; the critical requirement for it to be considered to have a high potential for a future great earthquake. These historical studies, coupled with analyses of the seismicity of the Aleutian arc for this century and plate convergence rates for the eastern Aleutians improve, considerably, our estimates of repeat times for great earthquakes in the region of the Shumagin Gap. We conclude that there is a high probability for a great earthquake of a series of very large earthquakes within one to two decades. While there is no way to rigorously estimate this probability in the usual statistical sense, we mean about 60 to 80 percent by "high probability". Of course, this also implies a 20 to 40 percent "probability" that such earthquakes will not occur within two decades.

The studies of seismicity patterns and geological structures help us to define the expected fault plane for the future rupture. We conclude that the rupture will occur along the main thrust zone beneath the Shumagin Islands. The rupture will initiate at about 40 km depth and probably propagate upward and southwestward along the main thrust zone. The most likely extent of the rupture zone along the arc is from the Shumagin Basin offshore of Ivanof Bay to the Sanak Graben off of Cold Bay. A much longer rupture zone is also possible, however, should the rupture propagate into the adjacent zone of the 1938 earthquake to the east or the Unalaska Gap to the west; or both.

The detailed studies of the microseismic data and studies of the seismic source and strong motion characteristics are part of a several-year program to improve our estimate of the parameters used to describe strong ground motion to be expected for various kinds of earthquakes along the eastern Aleutian arc. These parameters will be important inputs to the calculation of seismic hazard maps.

During the coming summer we will install six new strong ground motion recorders. Presently, however, we are inventorying existing data that may be useful in characterizing the strong ground motion. Preliminary results from this work suggest that the Shumagin Gap region is characterized by high stress drops for moderate-sized events along the main thrust zone. This is consistent with our interpretation that the Shumagin Gap is in an advanced stage of preparation for a very large earthquake.

X. SUMMARY OF FOURTH QUARTER OPERATIONS (January-March 1980)  
AND STATUS OF TECHNICAL WORK

A. Field Work (D. Johnson)

D. Johnson and G. Gunther visited Sand Point and Dutch Harbor central recording stations per following schedule:

Leave New York - 3/18/80  
Arrive Sand Point - 3/19/80  
Leave Sand Point/Arrive Dutch Harbor - 3/28/80  
Leave Dutch Harbor - 4/1/80  
Arrive New York - 4/2/80

The work accomplished at each station was:

Sand Point:

1. Install analog event recording system.
2. Install satellite receiver clock.
3. Install 3 component intermediate period (IP) seismograph (this included installation of 2 horizontal SP components).
4. Repair and adjust existing equipment. In particular:
  - change 3 long period helicorders to short period config. (60 mm/min) for intermediate period recording.
  - Remove and ship to New York discriminator rack with non-operational power supply.
  - Align developorder traces.

Dutch Harbor:

1. Install new head assy. in loop machine of analog event recording system, and overhaul both machines.
2. Replace constant voltage power supply transformer.
3. Replace SMA-1
4. Locate site for new central recording station. This will be in a concrete building about 1/2 mile west of existing station, which was used as seismometer vault a number of years ago.

B. Operational Status of Remote Stations and Recording Centers (D. Johnson)

The status of the Shumagin and Unalaska networks was:

Shumagins:

Shumagin East Array (BKJ, SGB, IVF): Being received, but noisy, particularly BKJ.

Shumagin West (CNB, NGI, SQHZ, SQHH): All being received, good signals.

Cold Bay Array (FPS, BAL, SNK, DRR, DLG): All being received; noise varies: SNK shows evidence of multipath reception.

Pavlof South (PVV, PS1-4): Poor, intermittent reception.

Pavlof North (BLH, PN1-8): Very poor reception of BVB-1, reception of BVB-2 (RF, but no VCO signals evident)

Unalaska:

Makushin and Akutan both being received with good signal strength but no VCO modulation (i.e. no seismic signal). Local components operating.

Summary. In comparison to status at this time of the year, in previous years, the Shumagin network has about as many stations operational. Some changes to the station/network configuration on Pavlof (north and south) are indicated if performance is to be improved.

### C. Data Collection and Submission (J. Hauptman and J. Peterson)

Seismicity in the Bering Sea. Seismicity of the Bering Sea vicinity is monitored by one long period and one short period seismometer installed on Saint Paul Island, in the Pribilofs. These seismometers are recorded on helicorders located at the National Weather Service Observatory there.

At the time of this report we have received continuous records from April 1, 1979 through March 25, 1980. There are isolated daily gaps in the data due to missing records or high levels of noise.

The available records have been carefully scanned for earthquakes; Tables 4 and 5 (short and long period, respectively) list date, time, amplitude, period and S-P interval where these criteria exist for any earthquake or possible earthquake. Possible earthquakes refers to any cultural noise (i.e. trucks, surf, etc.) that resemble seismic events. Having records from only one station it is impossible to double-check these questionable cases.

Precise locations of earthquakes and their correlation with known regional tectonic features (i.e. Saint George Basin) is also not possible with only one station on Saint Paul Island. There were, however, a number of events detected within the past year which could fall within the proper distance range for a source in the Saint George Basin or various locations along the Aleutian Island arc. The approximate distances are obtained by applying the Jeffrey-Bullen Travel Time Tables (1958) to the S-P intervals where applicable and assuming a surface focus (0 depth). Using Table 4, two events had S-P intervals of 5 and 9 seconds, which corresponds to distance of about 40 and 70 km, respectively. These events may have occurred in the Saint Paul Island vicinity. Two events had S-P intervals of 27 and 30 seconds which corresponds to distances between 200 and 240 km. These distances would be consistent with the Saint George Basin as a source area. Fifty-four events had S-P intervals between 40 and 135 seconds (400-1000 km). These events could have occurred along the Aleutian arc between eastern Kodiak Island and the Near Islands. S-P intervals could not be determined for eleven events. Based on the dominant period of the wave trains, these events were classified as distant, originating on or beyond the Aleutian arc. Many of the above events are recorded on the long period instrument (Table 5) and/or have been located in the PDE published by the National Earthquake Information Service of NOAA (Tables 4 and 5).

In comparing this year's seismicity in the Bering Sea to the past 2 years, no significant changes are detectable. It still stands that there is a moderately low level of activity which falls within distance ranges consistent with possible active features, such as the Saint George Basin (NOAA Annual Report, 1978-1979).



TABLE 4

Saint Paul Short Period  
April 1979 - March 1980

<u>Date</u>	<u>Time</u>	<u>Amplitude</u> <u>mm P-P</u>	<u>Period</u> <u>(sec)</u>	<u>S-P</u> <u>(sec)</u>	<u>PDE Location</u> <u>or Comments</u>	<u>PDE</u> <u>mb</u>
<u>1979</u>						
Apr 8	21:43	3		15	Truck?	
Apr 10	01:53	2	1	?	Molucca Passage	6.3
Apr 16	08:34	3	.5	60		
Apr 16	11:56	2			Truck?	
Apr 16	20:58	2		~ 90		
Apr 21	13:24	7		60		
Apr 29	04:16	5		5		
May 1	13:15	2	1	?	Loyalty Is. Region	6.7
May 4	13:38	1		95		
May 5	00:32				Truck	
May 8	12:57	19		57		
May 12	19:14	2	1	60		
May 12	22:18	1.5		85?		
May 13	06:43	3	.5	57		
May 18	20:25	4	.5	132?		
May 20	08:15	60		85?		
May 23	13:46	2		82?	Alaska Peninsula	4.8
May 25	00:41	1.5		110?		
May 25	16:46	12	1	80		
May 25	18:23	5	.75	77	Fox Islands	5.9
May 26	08:37			22	Truck?	
May 29	01:13			?	Truck?	
May 29	02:13			?	Truck?	
May 29	21:54	4	.5	63?	Fox Islands	4.9
May 30	19:21	5	.5	70?	Alaska Peninsula	4.9
Jun 22	06:41	3	1	30?		
Jun 25	05:39	2	.50		Distant	

TABLE 4 (con't.)

<u>Date</u>	<u>Time</u>	<u>Amplitude</u> <u>mm P-P</u>	<u>Period</u> <u>(sec)</u>	<u>S-P</u> <u>(sec)</u>	<u>PDE Location</u> <u>or Comments</u>	<u>PDE</u> <u>mb</u>
Jul 4	06:13	2	1	?	Kuril Islands	6.1
Jul 4	18:58	1		105?	Fox Islands	4.6
Jul 11	12:32	2	1	?	Southeastern Alaska	
Jul 14	08:34	1		60?		
Jul 15	05:51	10	.50	58	Southern Alaska	
Jul 29	09:53	2		62	Andreanof Island	4.6
Aug 5	01:05	2	1	?	So. of Fiji Is.	6.2
Aug 10	07:26	4	.75	70?		
Aug 16	21:37	19	.75	112		
Aug 16	21:42	2	1	?	North Korea	5.7
Aug 20	04:01	2	.75	?	Hindu Kush	5.8
Aug 21	19:15	1		?	?	
Aug 22	18:33	12	1	?	Kamchatka	5.5
Aug 26	14:41	2	1	?	Philippines	5.9
Aug 31	20:43	3	.75	95?	Alaska Peninsula	5.0
Sep 1	05:28	52	1	53	Fox Islands	5.7
Sep 5	01:51	3		70		
Sep 5	09:20	3		55		
Sep 9	07:25	1		60?	Fox Islands	4.6
Sep 14	07:31	7	.75	131		
Sep 14	07:41	2		73?		
Sep 22	03:50	2		75?		
Sep 23	10:19	5	.50	115	Near Islands	5.7
Oct 2	06:27	2		100	Rat Islands	4.8
Oct 13	07:05	4	.75	86?	Andreanof Islands	4.6
Oct 15	06:25	13		73?	Andreanof Islands	4.8
Oct 17	05:51	9	1	135?		
Oct 18	03:37	10	.75	98	Rat Islands	5.7
Oct 23	10:02	2	.50	?	Solomon Islands	6.1
Oct 25	17:47	1.5		55		

TABLE 4 (con't.)

<u>Date</u>	<u>Time</u>	<u>Amplitude</u> <u>mm P-P</u>	<u>Period</u> <u>(sec)</u>	<u>S-P</u> <u>(sec)</u>	<u>PDE Location</u> <u>or Comments</u>	<u>PDE</u> <u>mb</u>
Oct 27	14:47	4	.75	?	Guatemala	5.5
Dec 9	22:26	13		50	Fox Islands	5.2
Dec 23	07:25	2		50		
<u>1980</u>						
Jan 12	08:55	1.5		67	Fox Islands	4.8
Jan 19	07:04	10	1	80	Andreanof Islands	5.8
Jan 22	09:17	8		57	Fox Islands	4.4
Jan 26	03:29	3		5	Truck?	
Jan 27	05:05	1.5		78	Andreanof Islands	4.9
Feb 6	10:45	3	.75	70	Andreanof Islands	5.1
Feb 8	13:38	10		9		
Feb 12	08:43	6	.5	58	Andreanof Islands	5.2
Feb 23	05:57	2		55?	Kuril Islands	6.4
Feb 23	22:45	1			Kuril Islands	5.9
Mar 11	03:48	5	.5	70		
Mar 12	23:05.	5	.5	70		
Mar 22	10:31	5		27		
Mar 24	02:18	2		55		
Mar 24	04:00	51		65	Main Shock	
Mar 24	04:11	2			Aftershock	
Mar 24	04:42	7		65	Aftershock	
Mar 24	04:49	1		65	Aftershock	
Mar 24	07:10	1		65	Aftershock?	
Mar 24	08:05	1		65	Aftershock?	

TABLE 5  
 Saint Paul Long Period  
April 1979 - March 1980

<u>Date</u>	<u>Time</u>	<u>Amplitude</u> <u>mm P-P</u>	<u>S-P Comments</u>	<u>PDE Location</u>	<u>PDE</u> <u>mb</u>
Apr 10	01:53	28	> 9 min.	*	
Apr 14	10:28	4	7 min.?		
Apr 15	06:31	17	~ 10 min.?	Yugoslavia	7.2
Apr 20	12:58	8	?	Southeastern Alaska	5.2
Apr 21	13:25	3	Local event?		
Apr 22	10:35	2	Surface waves		
Apr 29	14:26	2	Surface waves		
May 1	13:15	38	~ 10 sec.	*	
May 5	16:37	2	Surface waves		
May 8	12:57	9	Local event?		
May 13	06:44?	4	6 1/2 min.		
May 18	20:25	2		Loyalty Island	5.7
May 20	08:15	75	1 1/2 min.	Alaska Peninsula	6.5
May 21	22:49	2	Local? or surface waves		
May 23	00:44	2.5	3 3/4 min.	Kuril Islands	5.6
May 24	08:03	2	Surface waves		
May 25	16:46	85	1 1/2 min.?	Fox Islands	5.9
Jun 21	17:13	2	Surface waves		
Jun 22	06:41	10	9 min.	Chiapas, Mexico	6.2
Jun 25	05:40	4	~ 9 min.		
Jun 27	~10:30	2	Surface waves		
Jul 1	21:21	3	Surface waves		
Jul 4	18:58	3	Surface waves	*	
Jul 8	01:46	2	Surface waves		
Jul 9	16:19	2	Surface waves	New Ireland Region	5.8
Jul 11	12:36	2	Surface waves	*	
Jul 15	05:51	5	Local	*	

TABLE 5 (con't.)

<u>Date</u>	<u>Time</u>	<u>Amplitude</u> <u>mm P-P</u>	<u>S-P/Comments</u>	<u>PDE Location</u>	<u>PDE</u> <u>mb</u>
Jul 25	19:44	5	13 min.	South of Java	6.1
Aug 1	11:05	2	Surface		
Aug 5	01:05	2	Surface	*	
Aug 10	07:26	6	Surface		
Aug 16	21:37	12	2 min.?		
Aug 17	13:10	3	13 min.?	New Hebrides Islands	5.5
Aug 24	03:39	3	?		
Aug 25	09:05	3	?		
Aug 26	14:43	10	S-P ~ 9 min.?	*	
Aug 31	20:45	3	Local?	*	
Sep 1	05:28	5	Local	*	
Sep 12	05:29	85	9 1/2 min.	West Irian Region	7.8
Sep 14	07:34	5	Surface waves		
Sep 23	10:21	3	Surface waves	*	
Sep 29	18:50	6	3 1/2 min.?	W. Coast of North Sumatera	6.0
Oct 12	10:39	39	4 1/4 min.?	W. Coast of S. Island New Zealand	6.2
Oct 15	23:25	16	?	*	
Oct 17	05:51	5	Local?		
Oct 18	03:37	2	Local?	*	
Oct 22	06:10	4	10 min.?	Molucca Passage	6.2
Oct 23	10:02	15	9 1/2 min.	*	
Oct 27	14:47	7	9 1/2 min.	*	
Oct 27	21:54	5	9 1/2 min.	Guatamala	5.4
Nov 4	01:29	2	Surface waves		
Nov 5	02:03	3	10 min.?	Mona Passage	5.9
Nov 6	12:12	2	Surface waves		
Nov 9	13:52	3	Surface waves		
Nov 9	17:13	3	Surface waves		
Nov 13	20:01	3	Surface waves		

TABLE 5 (con't.)

<u>Date</u>	<u>Time</u>	<u>Amplitude</u> <u>mm P-P</u>	<u>S-P/Comments</u>	<u>PDE Location</u>	<u>PDE</u> <u>mb</u>
Nov 13	20:56	3	10 min.	Tonga Islands Region	6.6
Nov 14	02:44	23	?		
Nov 16	15:33	14	~ 11 min.?	Fiji Islands	6.3
Nov 24	19:40	5	S arrival and sur- face waves		
Nov 27	17:23	32	11 min.?	Iran	6.2
Dec 7	10:05	4	Surface waves		
Dec 9	20:27	3	Local		
Dec 11	17:34	4	5 min.?	Bonin Islands	5.9
Dec 12	08:12	Clipped	~ 11 min.	Equador	6.4
Dec 15	?00:22	4	?		
Dec 17	20:11	3	~ 11 min.	Sumbawa Island Region	5.7
Mar 8	15:06	3	Surface waves		
Mar 8	22:24	13	10 min.	Loyalty Is. Region	6.0
Mar 11	03:48	4	Local?		
Mar 22	10:31	4	Local?		
Mar 24	04:00	Clipped	1 min.		

---

\* = see Short Period, Table 4

Summary of Operations at Dutch Harbor. The recording site at Dutch Harbor uses two four-channel TEAC tape recorders. The first recorder contains a continuous tape loop, receiving short period vertical seismometers at Akutan Volcano (AKV) and Makushin Volcano (MKV). It also receives the local Dutch Harbor short period horizontal signal and a TS 250 clock with IRIG B time code. Whenever an event is detected by any 2 short period seismometers or the Dutch Harbor long period vertical seismometer, the contents of the loop are recorded on the second recorder. This provides a complete record of the event on the second recorder for playback and analysis. Problems involving RF/interference with this system, the lack of a station operator, and the failure of the remote stations prevent a complete assessment of seismicity.

With the acquisition of a new station operator in the summer of 1979, a complete inventory of long and short period vertical helicorder records for Dutch Harbor (DUT) begins on August 20, 1979. This compliment of records exists through March 8, 1980: due to a bad pen, short period records do not exist from October 16, 1979 through January 26, 1980.

After carefully scanning all existing helicorder records for earthquakes, two tables (6 and 7; short and long period, respectively) were constructed listing dates, times, amplitudes, periods and S-P intervals where applicable for each event or possible event. Due to the proximity of the station DUT to the airstrip it is susceptible to airplane and radio transmission noise. This noise can mimic earthquake signitures as well as obscure them. Also referenced on the tables are regional locations and magnitudes for events also located in the PDE, published by the National Earthquake Information Service of NOAA.

In summary, 104 events had S-P intervals of  $\leq 25$  sec; corresponding to distances within 200 km of Dutch Harbor. 31 events had S-P intervals of  $> 25$  sec; corresponding to distances of greater than 200 km. S-P intervals could not be determined for 22 events.

TABLE 6  
Dutch Harbor Short Period  
April 1979 - March 1980

<u>Date</u>	<u>Time</u>	<u>Amplitude</u> <u>mm P-P</u>	<u>Period</u> <u>(secs)</u>	<u>S-P</u> <u>(secs)</u>	<u>Comments</u>
Aug 20	04:02	20	.5	176	
Aug 20	12:16	1		?	
Aug 20	23:49	10		29	
Aug 21	11:14	2		81?	Andreanof Is. 3.6
Aug 21	16:56	13	.5	22	
Aug 21	19:13	1		73?	
Aug 21	23:25	3		?	Truck?
Aug 22	02:01	9	.5	22	
Aug 22	05:48	24		6	Radio Noise?
Aug 22	14:58	75		12?	
Aug 22	17:44	3		13?	
Aug 22	18:33	6	1.0	?	Kamchatka 5.5
Aug 22	22:16	45		6	
Aug 22	22:18	46		6	
Aug 22	22:20	37		6	
Aug 22	23:03	5		6	
Aug 22	23:34	2		6	
Aug 22	23:37	37	.5	6	
Aug 22	23:53	2		7	
Aug 23	00:53	6		7	
Aug 23	04:12	4		6	
Aug 23	05:35	36		10	
Aug 23	11:16	42	.5	7	
Aug 23	12:08	5		6	
Aug 23	15:54	34		6	
Aug 23	17:36	2		6	
Aug 23	18:27	80		6	
Aug 23	22:29	65		6	
Aug 23	23:41	5		18	



TABLE 6 (con't.)

<u>Date</u>	<u>Time</u>	<u>Amplitude</u> <u>mm P-P</u>	<u>Period</u> <u>(secs)</u>	<u>S-P</u> <u>(secs)</u>	<u>Comments</u>
Aug 24	04:38	3	1.0	?	Costa Rica 6.1
Aug 24	17:28	17	.5	15	
Aug 24	20:09	22	.75	32	
Aug 25	07:47	1		4?	
Aug 25	20:37	5	.5	33	
Aug 26	03:59	3		7	
Aug 26	14:41	1	.5	?	Philippines 5.9
Aug 27	04:41	4		?	
Aug 27	05:17	3		12	Noise?
Aug 28	00:29	?		6	
Aug 27	04:03	6		15	
Aug 28	04:03	2		7?	
Aug 28	21:41	3		18	
Aug 29	09:28	1		17	
Aug 29	10:20	6		53	Maybe 2 events?
Aug 29	10:57	23		27	
Aug 30	03:01	2		50?	
Aug 30	06:13	8		7	
Aug 30	08:19	3	.5	7	
Aug 30	18:53	4		61	
Aug 31	00:31	26		7	
Aug 31	01:22	Clipped		25?	Fox Islands 4.8
Aug 31	~21:30	8	.5	37	
Sep 1	22:56	2.5		24	
Sep 2	03:12	3	.5	43?	
Sep 2	08:04	2	1.0	?	Kamchatka 5.0
Sep 4	06:22	4		24	
Sep 4	10:07	4		20	
Sep 5	01:51	3		63?	
Sep 5	03:26	1		31	
Sep 6	15:22	4		?	Kamchatka? 4.9

TABLE 6 (con't.)

<u>Date</u>	<u>Time</u>	<u>Amplitude</u> <u>mm P-P</u>	<u>Period</u> <u>(secs)</u>	<u>S-P</u> <u>(secs)</u>	<u>Comments</u>
Sep 7	09:39	30		15	
Sep 8	04:39	1		26?	
Sep 8	05:08	1		22?	
Sep 8	10:01	11		11	
Sep 9	07:24	Clipped		15	Fox Islands 4.6
Sep 9	11:56	2		20?	
Sep 9	14:40	2		20?	
Sep 10	07:53	4		31	
Sep 10	15:33	3		45	
Sep 11	00:17	5		6	
Sep 12	05:29	8	1.0	?	W. Irian 6.2
Sep 12	09:38	28	.5	17	
Sep 12	12:18	5		15	
Sep 12	12:49	1		20	
Sep 12	16:40	2		47?	
Sep 12	23:22	40		20	
Sep 13	06:44	1		?	W. Irian 5.9
Sep 13	17:45	12		8	
Sep 14	01:31	4		30	
Sep 14	07:31	30	1.0	150	
Sep 14	16:40	1		32?	
Sep 15	09:20	34	.5	9	Noise?
Sep 16	18:07	4		?	Halmehera 5.9
Sep 17	07:28	5		8	
Sep 17	08:54	9		4	
Sep 17	11:25	12		24	
Sep 17	11:57	3		32	
Sep 17	15:14	4		12	
Sep 17	15:52	4		20	
Sep 18	19:28	2		35	
Sep 19	08:30	17		10	

TABLE 6 (con't.)

<u>Date</u>	<u>Time</u>	<u>Amplitude mm P-P</u>	<u>Period (secs)</u>	<u>S-P (secs)</u>	<u>Comments</u>
Sep 20	10:36	Clipped		10	
Sep 21	18:05	25		45	
Sep 22	03:48	25		7	Foreshock
Sep 22	03:49	Clipped		Saturated	Main Shock
Sep 22	03:50	Clipped		Saturated	Main Shock
Sep 22	03:54	?		?	Aftershock
Sep 22	04:03	10		7	Aftershock
Sep 22	04:07	15		7	Aftershock
Sep 22	04:14	?		7	Aftershock
Sep 22	04:24	29		7	Aftershock
Sep 22	04:30	6		6	Aftershock
Sep 22	04:30	Clipped		6	Aftershock
Sep 22	04:32	?		6	Aftershock
Sep 22	04:40	28		7	Aftershock
Sep 22	06:10	10		7	Aftershock
Sep 22	06:27	15		7	Aftershock
Sep 22	08:06	3		?	Hawaii 5.6
Sep 22	09:56	55		7	Aftershock
Sep 22	10:02	52		6	Aftershock
Sep 22	10:13	12		6	Aftershock
Sep 22	18:11	8		6	Aftershock
Sep 23	10:20	6	1.0	~135	Near Islands 5.7
Sep 23	21:42	28		7	
Sep 23	23:18	55		9	
Sep 24	00:35	25		6	
Sep 24	03:38	2		?	Nuclear Event Novaya Zemlya 5.7
Sep 24	04:28	8		7	
Sep 24	05:14	13		10	
Sep 24	07:00	3	1.0	?	
Sep 26	03:38	Clipped		10	
Sep 26	07:21	2		6	

TABLE 6 (con't.)

<u>Date</u>	<u>Time</u>	<u>Amplitude</u> <u>mm P-P</u>	<u>Period</u> <u>(secs)</u>	<u>S-P</u> <u>(secs)</u>	<u>Comments</u>
Sep 26	15:07	3		?	Nuclear Event Nevada 5.6
Sep 28	03:53	24		13?	
Sep 28	07:21	25		6	
Sep 28	23:16	5		6	
Sep 29	12:54	1	1.0	?	Sulawesi 5.9?
Sep 29	14:21	14		6	
Oct 1	14:24	8	1.0	?	Guatemala 5.4
Oct 2	06:27	1	.5	?	
Oct 2	15:39	5		14	
Oct 3	12:49	28		6	
October 16, 1979 records end - Resume January 26, 1980					
Jan 27	05:00	9	.5	54	Andreanof Is. 4.9
Jan 27	06:58	22		6	
Jan 27	07:45	38		5	
Jan 27	17:38	1	.5	55?	
Jan 29	07:16	5	.75	?	Halmehera 5.5
Jan 29	09:55	8		9	Event?
Jan 29	12:08	11		9	Event?
Jan 29	15:19	2		29	
Jan 29	15:21	12		5	Event?
Feb 5	04:28	33		6	
Feb 5	04:59	46		6	
Feb 5	05:05	23		8	Event?
Feb 6	08:45	1		9	
Feb 6	10:44	48	1.0	66	Andreanof Is. 5.1
Feb 6	14:53	50		Saturated	Local
Feb 8	03:55	Clipped		10?	Local
Feb 8	10:54	45		6	
Feb 8	13:15	3		?	Volcano Is. 5.4
Feb 10	08:02	1		38?	Possible event?
Feb 12	08:43	80	.75	53	Andreanof Is. 5.2

TABLE 6 (con't.)

<u>Date</u>	<u>Time</u>	<u>Amplitude</u> <u>mm P-P</u>	<u>Period</u> <u>(secs)</u>	<u>S-P</u> <u>(secs)</u>	<u>Comments</u>
Feb 13	02:18	Saturated		10?	
Feb 13	10:41	52	.5	12	
Feb 16	11:35	1		9	
Feb 17	14:41	20		7	
Feb 18	00:44	11		13	
Feb 18	10:25	Saturated		Saturated	
Feb 29	03:50?	47		10?	Saturated
Feb 29	12:25?	4.5?	1.0	30?	

TABLE 7

Dutch Harbor Long Period  
April 1979 - March 1980

<u>Date</u>	<u>Time</u>	<u>Amplitude mm P-P</u>	<u>S-P (min)</u>	<u>Comments</u>
Aug 20	19:26			Possible event
Aug 20	20:17			Possible event
Aug 25	09:28			Surface waves
Aug 26	11:59			New Hebrides 5.1
Aug 26	14:41	5	9	*
Sep 8	07:24	1	1	
Sep 9	07:24	4		*
Sep 12	05:29	46	9.5	W. Irian 6.2
Sep 14	07:31	9	2.5	
Sep 22	03:49	?	?	*
Sep 22	08:16			Event?
Sep 23	10:20	3	2	*
Sep 29	19:21			Surface waves
Oct 12	10:39	22	3.5	
Oct 15	23:36	10		S arrival
Oct 17	05:51	5	6	
Sep 18	03:37	3	2	
Oct 22	10:02	1	9	
Oct 26	14:47	1	9	
Nov 9	13:54			Surface waves
Nov 9	17:12			Surface waves
Nov 13	20:55	2	9	
Nov 14	02:45	2	9	
Nov 16	15:53	5		S arrival
Nov 24	19:40			Surface waves
Nov 27	17:57			Local event?
Dec 4	12:02			Possible event?
Dec 9	22:25	3		Local event?

TABLE 7 (con't.)

<u>Date</u>	<u>Time</u>	<u>Amplitude</u> <u>mm P-P</u>	<u>S-P</u> <u>(min)</u>	<u>Comments</u>
Dec 12	08:12	2	10	Coast of Ecuador 6.4
Jan 2	22:32			Surface waves
Jan 29	07:04	18		S arrival
Jan 23	01:56	2	3	Kamchatka 5.4
Jan 23	06:01			Surface waves
Feb 12	03:51			Surface waves
Feb 23	06:58	27	5.5	Kurils 5.7
Mar 8	22:25	6	~10	Loyalty Is. 6.0

---

\* = see Short Period, Table 6

### Data Submission

The last submission of hypocentral data was made in February 1980. It contained 225 events from July, August and September 1979. We are presently processing data from October, November and December 1979. Develocorder films for this period have been scanned and initial P and S arrivals have been picked for 168 earthquakes. We have also begun scanning January 1980 develocorder films.

During this last quarter's work we have been faced with converting our computer software to a new system and have received a preliminary version of a new hypocentral program which we intend to use as soon as possible. Although these changes are initially time consuming, we ultimately anticipate a reduction in time needed to process hypocentral data.

### Located Events During Annual Report Period

<u>Quarter</u>	<u>Date Submitted</u>	<u>Number of Events</u>
4Q78	Aug 9, 1979	203
1Q78	Sep 4, 1979	288
2Q79	Nov 16, 1979	108
3Q79	Feb 22, 1980	225
4Q79	(in process)	<u>168</u>
Total		<u>992</u>



SUBMISSION SCHEDULE

February 1980

Quarter	Original Due Date	Scheduled Due Date	Date Submitted	Phase Files	Bulletin Files	Hypocentral Files		
						S	STC	N**
7/73-6/75	Precontract	sub	10 May 76	C		T	No	T
3Q75	1 Jan 76	sub	10 May 76	C		T	No	T
4Q75	1 Mar 76	sub	10 May 76	C		T	*	T
1Q76	1 Jul 76	sub	10 May 76	C		T	*	T
2Q76	1 Oct 76		No Data					
3Q76	1 Jan 77	sub	1 Jul 77	C		T	No	T
4Q76	1 Mar 77	sub	28 Feb 77	C		T	*	T
1Q77	1 Jul 77	sub	27 Jul 78	C		T	*	T
2Q77	1 Oct 77	sub	27 Jul 78	C		T	*	T
3Q77	1 Jan 78	15 Jan 81						
4Q77	1 Apr 78	15 Jul 81						
1Q78	1 Jul 78	15 Jan 82						
2Q78	1 Oct 78	sub	25 Sep 78	C	T	T	T	T
3Q78	1 Jan 79	sub	20 Mar 79	C	T	T	T	T
4Q78	1 Apr 79	sub	9 Aug 79	C	T	T	T	T
1Q79	1 Jul 79	sub	4 Sep 79	C	T	T	T	T
2Q79	1 Oct 79	sub	16 Nov 79	T	T	T	T	T
3Q79	1 Jan 80	sub	22 Feb 80	T	T	T	T	T
4Q79	1 Apr 80	15 Apr 80						
1Q80	1 Jul 80	15 Jun 80						
2Q80	1 Oct 80	15 Sep 80						
3Q80	1 Jan 81	15 Nov 80						
4Q80	1 Apr 81	15 Mar 81						
1Q81	1 Jul 81	15 May 81						
2Q81	1 Oct 81	15 Sep 81						
3Q81	1 Jan 82	15 Nov 81						
4Q81	1 Apr 82	15 Mar 82						

Key:

S = in standard format

STC = standard format, time corrected

N = in NOAA format

C = data exists on cards

T = data exists on magnetic tape

\* = non-standard time correction exist for these quarters

\*\* = NOAA files are time corrected if there exists an STC file

#### D. Computer System and Data Processing (E. Edsall and J. Peterson)

Technical Status - Computer System (E. Edsall). June of 1979 marked the beginning of the installation of two computer systems here in the Seismology building at Lamont. The systems, a PDP 11/70 and a PDP 11/34, both manufactured by Digital Equipment Corporation, are funded by the USGS. The systems are one of originally six distributed by the USGS.

The PDP 11/34 consists of 96K bytes of memory with two TE16 tape drives (45 ips recording at 800 or 1600 bpi), two RL01 disk drives (5.2 megabytes each) and an LPA11-K controller for an A-D system.

The PDP 11/70 consists of 384K bytes of memory with two TE16 tape drives, one RP05 disk drive (88 megabytes), one RL01 disk drive, one CR11 card reader and an LPA11-K controller. The PDP 11/70 was delivered with one Versatec 1200A printer/plotter and one Tektronix 4014 graphics terminal.

Installation of the systems continued through August of 1979 with actual on-line usage beginning at the end of that month.

Since that time we have added on an additional Versatec 1200A and four Heath H19 terminals plus a Facal-Vadic 3467 modem which allows remote access to the PDP 11/70.

The PDP 11/34 under the RSX11M operating system is used primarily for creating digital tapes.

The PDP 11/70 is currently running primarily under the UNIX version 7 operating system. Under this programs are being developed in both the Fortran 77 and C languages. On the Versatecs we are able to create high resolution strip charts from digital tapes. The Tektronix 4014 can be used to take a closer look at seismic traces of interest.

Much software development is being done by the USGS in Menlo Park to enhance this system. The package we expect to obtain within the next few months is called GEOLAB.

GEOLAB is an interactive environment that extends the modular, tool approach of UNIX to a level that is based on an interpretive stack structure. It offers a wide variety of operators that can be readily combined to perform more complex tasks with the capability of handling large amounts of data. Like UNIX it is language independent. The elements of software being supplied are a database system, plotting package and tools package.

### Data Processing (J. Peterson)

During this last quarter we purchased a Heathkit H-19 CRT Terminal to streamline our daily processing routine. This has eliminated the use of computer cards. As we complete our transition to the UNIX system, our handling of supplementary data like time corrections and plotting will also improve.

A new hypocentral determination program, Hypo 79 (a precedent to Hypo 80) will replace our previous Hypo 8 and HypoEllipse routines which required the use of two (separate) computers.

As we receive a full working version of Geolab, Geobase and Geoplot, we will be able to handle large amounts of data more easily and quickly at the terminal. This USGS supplied system will help us standardize procedures for locating hypocenters as well as introducing time corrections, producing plots, etc. We also intend to publish a waveform bulletin or catalog of earthquakes as the data base system becomes available.

## XLA. REFERENCES

- Abe, K., 1979. Size of great earthquakes of 1837-1974 inferred from tsunami data, EOS, 60(2), p. 23, Amer. Geophys. Union.
- Akashe, B., 1968. Comparative investigation of the focal mechanism from short- and long-period seismograph records, Ph.D. thesis, University of Frankfurt.
- Archambeau, C.B., 1977. Earthquake predictions based on tectonic stress determinations, EOS, 57(4), p. 290, abstract.
- Archambeau, C., 1978. Estimation of non-hydrostatic stress in the earth by seismic methods: Lithospheric stress levels along Pacific and Nazca plate subduction zones, in: Proceedings of Conference VI; Methodology for Identifying Seismic Gaps and Soon-to-Break Gaps, 25-27 May 1978, Open-File Report 78-943, Menlo Park, California.
- Becker, G., 1898. Reconnaissance of the gold fields of Southern Alaska, U.S. Geol. Survey 18th Annual Rpt., pt. 3, 1-86.
- Boatwright, J., 1980. Preliminary body wave analysis of the St. Elias, Alaska earthquake of February 28, 1979, Bull. Seismol. Soc. Amer., 70, 419-436.
- Braze, R.J., 1965. A study of T phases in the Aleutian earthquake series of March and April 1957, Earthquake Notes, 34, 9-14.
- Broucke, R.A., W.E. Zurn, and L.B. Slichter, 1972. Lunar tidal acceleration on a rigid earth, in: Geophys. Mono Series 16, Flow and Fracture of Rocks, H.C. Heard, I.Y. Borg, N.L. Carter, and C.B. Raleigh (editors), Amer. Geophys. Union.
- Brune, J.N., 1970. Tectonic stress and the spectra of seismic shear waves from earthquakes, J. Geophys. Res., 75, 4997-5009.
- Bruns, T.R., and R. von Huene, 1977. Sedimentary basins on the Shumagin Shelf, Western Gulf of Alaska, paper presented at the Ninth Annual Offshore Technology Conference, Houston, Texas, May 2-5, OTC #2732, p. 41ff.
- Burk, C.A., 1965. Geology of the Alaska Peninsula: Island Arc and Continental Margin, Mem. 99, p. 150, Geol. Soc. Amer., New York.
- Cartwright, D.E., 1968. A unified analysis of tides and surges round north and east Britain, Phil. Trans. R. Soc. Lond., A-263, 1-55.
- Coffman, J.L., and C.A. von Hake (editors), 1973. Earthquake History of the United States, Publ. 41-1, U.S. Dept. of Commerce/NOAA, U.S. Gov't. Printing Office, Washington, D.C.

- Cormier, V., 1975. Tectonics near the junction of the Aleutian and Kuril-Kamchatka arcs, and a mechanism for middle Tertiary magmatism in the Kamchatka Basin, Geol. Soc. Amer. Bull., 86, 443-453.
- Cox, D., and G. Pararas-Carayannis, 1976. Catalog of Tsunamis in Alaska, U.S. Dept. of Commerce, NOAA/EDS, Asheville, N.C., 78 p.
- Dall, W.H., 1870. Alaska and Its Resources, Boston, Lee and Shepard, 627 p.
- Davies, J.N., 1975. Seismological investigations of plate tectonics in southcentral Alaska, Ph.D. thesis, Univ. of Alaska, Fairbanks, Alaska.
- Davies, J.N., L. House, K.H. Jacob, R. Bilham, V.F. Cormier, and J. Kienle, 1976. A seismotectonic study of the seismic and volcanic hazard in the Pribilof Islands - Eastern Aleutian Islands region of the Bering Sea, NOAA Annual Report, 1 April 1975 - 31 March 1976.
- Davies, J.N., and L. House, 1979. Aleutian subduction zone seismicity, volcano-trench separation and their relation to great thrust-type earthquakes, J. Geophys. Res., 84, 4583-4591.
- Davies, J.N., and K.H. Jacob, 1978-1979. NOAA Annual Report: A Seismotectonic Analysis of the Seismic and Volcanic Hazards in the Pribilof Islands - Eastern Aleutian Islands Region of the Bering Sea, Annual Report to NOAA/OCSEAP, Research Unit 16, 1 April 1978 - 31 March 1979.
- Davies, J.N., L. Sykes, L. House, and K.H. Jacob, 1981. Shumagin Seismic Gap, Alaska Peninsula: History of great earthquakes, tectonic setting, and evidence for high seismic potential, to be submitted to J. Geophys. Res.
- Davydov, G.I., 1812. Dvukratnoe puteshestvie v Ameriku [Double Voyage to America], [translated by W.L. Klauwe, provided by G. Moore, Oct. 1979] St. Petersburg Morskaya Tip., v. 2, 224 p.
- Doroshin, P., 1870. Onkotorykh vulkanakh, ikh izverzheniyakh: zemletryasenyakh v byvshikh Amerikamskikh vladenyakh Rossii, [Some volcanoes, their eruptions, and earthquakes in the former Russian holdings in America], Verh. Russ. Kais. Min. Ges. 2 ser., v. 25.44, St. Pbg.
- Fujita, K., 1978. Pre-Cenozoic tectonic evolution of Northeastern Siberia, Jour. Geology, 86, 159-172.
- Gedney, L., 1978. Summary of Alaskan Earthquakes/April, May, June 1978, Seismological Bulletin No. 4, Alaska Earthquake Analysis Center, Geophysical Institute, Univ. of Alaska, Fairbanks, Alaska.
- Hopkins, D.M., 1976. Fault history of the Pribilof Islands and its relevance to bottom stability in the St. George Basin, in: Environmental Assessment of

- the Alaska Continental Shelf, Principal Investigators Annual Reports, April 1975 - March 1976, NOAA/BLM OCSEAP, Geology Volume 13, 41-68.
- House, L., and J. Boatwright, 1980. Investigation of two high stress-drop earthquakes in the Shumagin seismic gap, Alaska, submitted to J. Geophys. Res.
- House, L., L.R. Sykes, J.N. Davies, and K.H. Jacob, 1981. Evidence for a possible seismic gap near Unalaska Island in the eastern Aleutians, Alaska, in preparation.
- Isacks, B., J. Oliver, and L.R. Sykes, 1968. Seismology and the new global tectonics, J. Geophys. Res., 73(18), 5855-5899.
- Iyer, H.M., 1979. Deep structure under Yellowstone National Park, U.S.A.: A continental "hot spot", Tectonophysics, 56, 165-197.
- Jones, D.L., and N.J. Silberling, 1979. Mesozoic Stratigraphy--the key to tectonic analysis of southern and central Alaska, U.S. Geol. Surv. Open-File Report No. 79-1200, 37 p. and 2 fig.
- Jordan, J.N., J.F. Lander, and R.A. Black, 1965. Aftershocks of the 4 February 1965 Rat Island earthquake, Science, 148, 1323-1325.
- Kanamori, H., 1972. Mechanism of Tsunami Earthquakes, Phys. Earth Planet. Interiors, 6, 346-359.
- Kanamori, H., 1977. The energy release in great earthquakes, J. Geophys. Res., 82(20), 2981-2988.
- Kanamori, H., and G.S. Stewart, 1978. Seismological aspects of the Guatemala earthquake, J. Geophys. Res., 83, 3427-3434.
- Kanamori, H., and K. Abe, 1979. Reevaluation of the turn-of-the-century seismicity peak, J. Geophys. Res., 84(B11), 6131-6139.
- Karig, D.E., 1972. Remnant arcs, Geol. Soc. Amer. Bull., 83, 1057-1068.
- Kelleher, J.A., 1970. Space-time seismicity of the Alaska-Aleutian seismic zone, J. Geophys. Res., 75, 5745-5756.
- Kelleher, J., 1972. Rupture zones of large South American earthquakes and some predictions, J. Geophys. Res., 77(11), 2087-2103.
- Kienle, J., 1971. Gravity and magnetic measurements over Bowers Ridge and Shirshov Ridge, Bering Sea, J. Geophys. Res., 76(29), 7138-7153.
- Kimura, M., 1976. Major magnetic activity as a key to predicting large earthquakes along the Sagams trough, Japan, Nature, 260, 5547, 131-133.
- Kimura, M., 1978. Significant eruptive activities related to large interplate earthquakes in the northwestern Pacific margin, J. Phys. Earth, 26, Suppl., S557-S570.

- Kisslinger, J., J. Davies, L. Sykes, L. House, and K. Jacob, 1980. Historical earthquakes of Alaska and the Aleutian Islands: A compilation of original references, some newly translated, manuscript in preparation.
- Kondorskaya, N.V., and N.V. Shebalin (editors), 1977. New Catalog of Strong Earthquakes in the Territory of the U.S.S.R., Nauka, Moscow, U.S.S.R., 347-433.
- Lahr, J.C., G. Plafker, C.D. Stephens, K.A. Fogleman, and M.E. Blackford, 1979. Interim report on the St. Elias earthquake of 28 February 1979, U.S. Geol. Surv. Open-File Report 79-670, Menlo Park, California.
- Longman, I.M., 1959. Formulas for computing the tidal accelerations due to the sun and moon, J. Geophys. Res., 64, 2351-2355.
- Longman, I.M., 1966. Computation of Love numbers and load deformation coefficients for a model earth, Geophys. J. Roy. astr. Soc., 11, 133-137.
- Marlow, M.S., D.W. Scholl, E.C. Buffington, and T.R. Alpha, 1973. Tectonic history of the Western Aleutian Arc, Geol. Soc. Amer. Bull., 84, 1555-1574.
- Marlow, M.S., D.W. Scholl, and A. Cooper, 1977. St. George Basin, Bering Sea Shelf: A collapsed Mesozoic margin, in: Island Arcs, Deep Sea Trenches and Back-Arc Basins, Talwani, M., and W. Pitman (editors), Maurice Ewing Series I, Amer. Geophys. Union, 211-220.
- Matumoto, T., and R. Page, 1968. Microaftershocks following the Alaskan earthquake of March 28, 1964: Determination of hypocenters and crustal velocities in the Kenai Peninsula-Prince William Sound Area, Bull. Seismol. Soc. Amer., 58(4), 1131.
- Mauk, F.J., and M.J.S. Johnston, 1973. On the triggering of volcanic eruptions by earth tides, J. Geophys. Res., 78, 3356-3362.
- McCann, W.R., S.P. Nishenko, L.R. Sykes, and J. Krause, 1979. Seismic gaps and plate tectonics: Seismic potential for major boundaries, PAGEOPH, 117, 1082-1147.
- Mogi, K., 1968. Development of aftershock areas of great earthquakes, Bull. Earthq. Res. Inst., Univ. of Tokyo, 46, 175-203.
- Mogi, K., 1969. Some features of recent seismic activity in and near Japan, 2, Activity before and after great earthquakes, Bull. Earthq. Res., Inst. of Tokyo Univ., 47, 395-417.
- Mogi, K., 1979. Two kinds of seismic gaps, Pure Appl. Geophys., 117, 1172-1186.
- Moore, G.W., 1962. Geology of Chirikof Island, Alaska, U.S. Geol. Surv. Techn. Lett., Aleut. 1, 10 p.

- Munk, W.H., and D.E. Cartwright, 1966. Tidal spectroscopy and prediction, Phil. Trans. R. Soc. Lond., A-259, 533-581.
- Nakamura, K., K.H. Jacob, and J.N. Davies, 1977. Volcanoes as possible indicators of tectonic stress orientation - Aleutians and Alaska, in: Stress in the Earth, M. Wyss (ed.), PAGEOPH, 115, 87-112.
- Newlander, A., 1883. Miscellaneous Phenomena, U.S. Signal Corps. Ann. Rpt. for 1882, pt. 2, p. 120.
- Nishenko, S., and W. McCann, 1979. Large thrust earthquakes and tsunamis: Implications for the development of forearc basins, J. Geophys. Res., 84, 573-584.
- Perez, O., and K. Jacob, 1980. Tectonic model and seismic potential of the eastern Gulf of Alaska and Yakataga Seismic Gap, submitted to J. Geophys. Res.
- Plafker, G., 1965. Tectonic deformation associated with the 1964 Alaskan earthquake, Science, 148(3678), 1675-1687.
- Pulpan, H., and J. Kienle, 1979. Western Gulf of Alaska Seismic Risk, presented at the Offshore Technology Conference, April 30-May 3, 1979, paper no. 3612, 2209-2213, 12 fig.
- Reid, H.F., 1912. List of strong shocks in the United States and dependencies, 16th Rpt., Comm. on Seismal Investig., Brit. Assn. Adv. Sci. Rpt. 81st Mtg., 1911, 41-45.
- Reyners, M., 1980. A microearthquake study of the plate boundary, North Island, New Zealand, submitted to Geophys. J. Roy. astr. Soc.
- Richter, C.F., 1958. Elementary Seismology, W.H. Freeman and Comp., San Francisco, California, 768 p.
- Robinson, R., 1978. Seismicity within a zone of convergence - the Wellington region, New Zealand, Geophys. J. Roy. astr. Soc., 55, 693-702.
- Scholl, D.W., E.C. Buffington, and M.S. Marlow, 1975. Plate tectonics and the structural evolution of the Aleutian-Bering Sea region, in: R. Forbes (ed.), Geology of the Bering and Adjacent Regions, Geol. Soc. Amer. Special Paper 151, 1-31.
- Scholz, C.H., 1974. Postearthquake dilatancy recovery, Geology, 2, 551-554.
- Solov'iev, S.L., 1968. Sanak-Kodiak Tsunami 1788, Probema Tsunami, Nauka, Moscow, 232-237.
- Spence, W., 1977. The Aleutian Arc: Tectonic blocks, episodic subduction, strain diffusion and magma generation, J. Geophys. Res., 82(2), 213-230.
- Stauder, W., 1968. Tensional character of earthquake foci beneath the Aleutian trench with relation to sea-floor spreading, J. Geophys. Res., 73, 7693-7701.



- Stauder, W., 1972. Fault motion and spatially bounded character of earthquakes in Amchitka Pass and the Delerof Islands, J. Geophys. Res., 77, 2072-2080.
- Sykes, L.R., and M. Ewing, 1965. The seismicity of the Carribean region, J. Geophys. Res., 70, 5065-5074.
- Sykes, L.R., 1971. Aftershock zones of great earthquakes, seismicity gaps, earthquake prediction for Alaska and the Aleutians, J. Geophys. Res., 76(36), 8021-8041.
- Sykes, L.R., and R.C. Quittmeyer, 1980. Repeat times of great earthquakes along convergent plate boundaries, to be submitted to Nature.
- Tarr, R.S., and L. Martin, 1912. The earthquake at Yakutat Bay, Alaska, in September 1899, U.S. Geol. Surv. Prof. Paper 69.
- Van Wormer, J.D., J. Davies, and L. Gedney, 1974. Seismicity and plate tectonics in southcentral Alaska, Bull. Seismol. Soc. Amer., 64(5), 1467-1475.
- Veniaminov, I., 1840. Zapiski: Parts 1-3, Published at the Exame of the Russian-American Company St. Pbg.
- Veniaminov, I., 1888. Zapiski of Ostrovakh Unalashkatska Otdeliela - vol. 2 of Tuoremya Innokentiya, Ivan Barsukov, ed., Sinodal'naya Tipografiya, Moscow.
- Walcott, R.L., 1978. Geodetic strains and large earthquakes in the axial tectonic belt of North Island, New Zealand, J. Geophys. Res., 83, 4419-4429.
- Winslow, M.A., and S.H. Hickman, 1978. Evidence for Quaternary uplifted terraces and tilting in a major seismic gap: the Shumagin Islands, Southwest Alaska, Amer. Geophys. Union. 1978 Fall Meeting, San Francisco, California.

## XI.B Papers Published, Submitted and in Preparation

### Papers Published

- (1) Davies, J.N., and L. House, Aleutian subduction zone seismicity, volcano-trench separation, and their relation to great thrust-type earthquakes, Jour. Geophys. Res., 84, 4583-4591, 1979.
- (2) Bilham, R., and J. Beavan, Satellite telemetry of sea-level data to monitor crustal motions in the Shumagin Islands Region of the Aleutian Arc., in: A. Vogel (editor), Terrestrial and Space Techniques in Earthquake Prediction Research; E.S.C.-E.G.S. Special, Conference Proceedings, F. Vieweg and Sons, Braunschweig/Wiesbaden, 269-283, 1979.
- (3) Boatwright, J., Preliminary body wave analysis of the St. Elias, Alaska earthquake of February 28, 1979, Bull. Seismol. Soc. Amer., 70, 419-436, 1980.

### Papers Submitted for Publication

- (1) McCann, W.R., O.J. Perez, and L.R. Sykes, Yakataga Seismic Gap, southern Alaska: History and earthquake potential, Science, in press, 1979.
- (2) Perez, O.J., and K.H. Jacob, Tectonic model and seismic potential of the eastern Gulf of Alaska and Yakataga Seismic Gap, submitted to Jour. Geophys. Res., October, 1979.
- (3) House, L., and J. Boatwright, Investigation of two high stress-drop earthquakes in the Shumagin Seismic Gap, Alaska, submitted to Jour. Geophys. Res., 1979.
- (4) Sykes, L.R., J.B. Kisslinger, L. House, J.N. Davies, and K.H. Jacob, Rupture zones of great earthquakes, Alaska-Aleutian arc, 1784-1980, submitted to Science, 1980.
- (4) Perez, O.J., and K.H. Jacob, St. Elias, Alaska, earthquake of February 28, 1979: Tectonic setting and seismic pattern prior to it, submitted to Bull. Seismol. Soc. Amer., 1980.

Papers in Preparation

- (1) Davies, J.N., L.R. Sykes, L. House, and K.H. Jacob, Evidence of a seismic gap in the Shumagin Islands region of the eastern Aleutian arc, Alaska, to be submitted to Jour. Geophys. Res., 1980.
- (2) House, L., and K.H. Jacob, Earthquake focal mechanisms and tectonics of the eastern Aleutian arc, in preparation, 1980.
- (3) House, L., L.R. Sykes, J.N. Davies, and K.H. Jacob, Evidence for a possible seismic gap near Unalaska Island in the eastern Aleutians, Alaska, in preparation, 1980.
- (4) Reyners, M., and K. Coles, Structure and subduction mechanics in the Shumagin Islands region of Alaska, in preparation, 1980.
- (5) McNutt, S., Volcanic earthquakes correlated with earth tides at Pavlof Volcano, in preparation, 1980.

SEISMOTECTONIC SETTING OF THE SHUMAGIN ISLANDS REGION, ALASKA: EVIDENCE FOR A SEISMIC GAP AND A REGION OF HIGH SEISMIC POTENTIAL

J.N. Davies (Lamont-Doherty Geological Observatory, Columbia University, Palisades, N.Y. 10964)

L. House (Lamont-Doherty Geological Observatory and Dept. of Geol. Sciences, Columbia University, Palisades, N.Y. 10964)

The Shumagin Islands are approximately in the center of a geographical area of the Aleutian arc that extends from Unalaska of the eastern Fox Islands to the western end of Kodiak Island. We present a study of the seismotectonic setting of this area that focuses on the Shumagin Islands region in which we have operated a local seismograph network since 1973. This area is bounded by the aftershock zones of the great earthquake of 1957 in the Andreanof-Fox Islands to the west and that of the 1964 in the Kodiak Island-Prince William Sound region to the east. The eastern half of this Unalaska-to-Kodiak area broke in the great earthquake of 1938. The tsunami earthquake of 1946 occurred in the western part of the area but most likely did not break much, if any, of the interplate boundary. It is along the interplate boundary above 50 km depth, i.e. along the main-thrust zone that great, thrust-type earthquakes occur. New maps of PDE and ISC epicenters for the eastern Aleutian arc suggest that within the past decade a "Mogi-Donut" pattern has become fairly well established around the Shumagin Islands region. The down-dip part of the donut pattern (at 40 km depth) is best developed and consists, at least in part, of events that have a very high stress drops (order of 1 kilobar) and which have focal mechanisms indicating underthrusting along a plane dipping at 30°. On the basis of these combined data, both historic and recent, we conclude that a seismic gap exists in the Shumagin Islands region which has a relatively high potential for an earthquake of magnitude  $\geq 8$  within the next few decades.

1. 1979 Fall Meeting AGU
2. 023052DAVIES
3. J.N. Davies  
Lamont-Doherty Geo. Obs.  
Palisades, N.Y. 10964
4. S
5. None
6. None
7. 40%
8. Mrs. Alma Kesner  
Purchasing Dept.  
Lamont-Doherty Geo. Obs.  
Palisades, N.Y. 10964
9. C

VOLCANIC EARTHQUAKES CORRELATED WITH EARTH  
TIDES AT PAVLOF VOLCANO

S. McNutt (Dept. Geol. Sci. and Lamont-Doherty  
Geological Observatory of Columbia University,  
Palisades, New York 10964)  
(Sponsor: Klaus Jacob)

A single short-period seismometer has been operated 7 km to the southeast of the summit of Pavlof Volcano since October 1973. Continuous helicorder records from an eruption sequence beginning 29 October 1974 and ending 13 January 1975 show four types of seismic signals: micro-earthquakes (A-type), volcanic tremors (B-type), explosion quakes with distinct air phases, and harmonic tremors. Histograms of the number of events of each type that took place during each two-hour interval are compared with the horizontal component of the theoretical solid-earth tidal strain, calculated for an azimuth of  $135^\circ$  (subparallel to the direction of plate convergence). For 3-4 days immediately before and after swarms of explosion quakes, a strong positive correlation is observed between B-type earthquake swarms and semi-diurnal tidal peaks. Before the explosions occur, swarms of B-type quakes correlate with the maximum tensional (high tide) peak, and after the explosions stop, swarms correlate with the maximum compressional (low tide) peak. This information strongly suggests that B-type earthquakes are caused by expansion and contraction, respectively, of shallow-depth magma conduits, and demonstrates that just before and just after eruptions the volcano is very sensitive and responsive to small changes in ambient stresses.

1. 021138JACOB (sponsor)
2. 1979 NW Section Meeting AGU  
Bend, Oregon
3. Volcanology
4. Volcanology
5. No
6. No
7. None
8. Bill to:  
Alma Kesner, Purchasing  
Lamont-Doherty Geol. Obs.  
Palisades, NY 10964

TELESEISMIC P-RESIDUALS AND RAY TRACING IN THE  
ALEUTIANS AND SOUTHERN ALASKA: EVIDENCE FOR  
LATERAL INHOMOGENEITIES IN THE CRUST AND UPPER  
MANTLE

J. Krause (Lamont-Doherty Geological Observatory  
of Columbia University and Dept. of Geol.  
Sciences, Palisades, N.Y. 10964)

K. Jacob (Lamont-Doherty Geological Observatory  
of Columbia University, Palisades, N.Y. 10964)

P-wave residuals with respect to a Herrin (1968) earth model for regional and teleseismic events recorded at stations in the Aleutians and southern Alaska show strong dependence on azimuth. For explosions on Amchitka Island, residuals are negative (i.e. arrivals are early) by up to 6 sec. Residuals from earthquakes in the Shumagin Islands region are generally positive by several seconds. Residuals from Soviet explosions on Novaya Zemlya range from negative by  $\leq 1$  sec. in the Aleutian arc to positive by 2-3 sec. in the Gulf of Alaska. Relative residuals for this source region with respect to station GMA in western Alaska are increasingly negative towards the west in the Aleutian arc. Residuals for the San Fernando, California, earthquake are positive by up to 5 sec.

Many of these variations in P-residuals can be explained by the high-velocity slab of lithosphere dipping beneath the Aleutians and southern Alaska. Rays which travel a large distance laterally along the dipping slab produce large negative residuals; those travelling up-dip along the slab produce small negative residuals; rays which miss the slab entirely appear to be influenced by other, weaker inhomogeneities in the upper mantle, and produce generally positive residuals.

We trace rays through a slab model derived from hypocenter locations to arrive at a velocity structure which approximately fits the observed travel times.

1. 1979 Fall Meeting AGU
2. 039516KRAUSE
3. Janet Krause  
Lamont-Doherty Geo. Obs.  
Palisades, New York 10964
4. S
- 5.
6. 0
7. 0%
8. Mrs. Alma Kesner  
Purchasing Department  
Lamont-Doherty Geo. Obs.  
Palisades, New York 10964

student rate applicable

SEISMIC HISTORY AND EARTHQUAKE POTENTIAL  
OF YAKATAGA SEISMIC GAP, SOUTHERN ALASKA

W. R. McCann

O. J. Pérez

L. R. Sykes (all at: Lamont-Doherty Geological  
Observatory and Department of Geological  
Sciences of Columbia University, Palisades,  
New York 10964)

Several authors have identified segments of the North American-Pacific plate boundary in southern Alaska and the Aleutians as seismic gaps. One gap is bounded by the rupture zones of the great earthquakes of 1958 and 1964. Only a small part of this gap, however, broke during the large ( $M_s \sim 7.7$ ) St. Elias earthquake of 28 February 1979. A re-evaluation of the seismic intensity data indicates that about 250 km of the plate boundary broke during the series of great events on September 4 and 10, 1899. Focal mechanisms of earthquakes in this region show shallow thrusting in a northerly direction. These mechanisms and geologic data indicate a décollement-style deformation with a series of imbricate thrusts in the upper plate. Moderate-size shocks since 1964 define a ring of activity surrounding a zone of near quiescence. This ring of activity is spatially similar to the "Mogi-donut" pattern observed before several great earthquakes. The average slip calculated for the 1899 sequence is comparable to the potential slip built up since then by plate movements. Although none of these methods yields a precise estimate of the time of occurrence of the next great earthquake in the Yakataga gap, the region merits intensive study for possible precursory effects.

1. 033692MC CANN
2. 1979 Spring AGU
3. Seismology
4. None
5. No
6. No
7. 0%
8. Bill to:  
Alma Kesner, Purchasing  
Lamont-Doherty Geol. Obs.  
Palisades, NY 10964

THE TECTONIC SETTING OF THE LARGE GULF OF  
ALASKA EARTHQUAKE OF FEBRUARY 28, 1979

Omar Perez (also at: Dept. Geological Sci.,  
Columbia University)  
Klaus H. Jacob (both at: Lamont-Doherty Geol.  
Obs., Columbia U., Palisades, NY 10964)

On February 28, 1979 at about 21h 27m a large earthquake ( $M_s$  near to 8.0) occurred in the Gulf of Alaska coastal region. The occurrence of this large earthquake was anticipated on the basis of the seismic gap theory (Sykes, 1971; Page, 1971; Kelleher et al., 1973). A study of all earthquakes during the period 1964-1975 which yielded fault-plane solutions using teleseismic information was completed just prior to this large event. All earthquakes indicated shallow-angle thrusting of the Pacific plate in a northerly direction both beneath the offshore Tertiary province (along a décollement zone) and on the onshore regions of the North American plate beneath the Chugach-St. Elias Ranges. From geologic evidence and from surface faulting related to the Sept. 10, 1899 earthquake in Yakutat Bay, it is known that steep-angle reverse faulting, associated with crustal-shortening and uplift of the northern blocks, can also occur in this region. Based on these interpretations we concur with McCann et al. (1979) in assigning a high seismic potential to this plate boundary segment, but we suggest that the area can be in general the site of two different types of earthquakes: shallow thrusting of Pacific Ocean floor in the offshore region and on-land, and steep-angle reverse faulting associated with the collisional boundary inland. It therefore seems possible that other large earthquakes following the February 1979 event may still occur in the region, similar to the series of great events that took place in the area around the turn of the century. In this interpretation the multiple events are related to successive rupture of the two stress-relieving features (décollement and boundary fault, respectively) at this plate margin.

1. 702418PEREZ
2. 1979 Spring Meeting AGU
3. Seismology
4. None
5. No
6. No
7. 0%
8. Bill to:  
Alma Kesner, Purchasing  
Lamont-Doherty Geol. Obs.  
Palisades, NY 10964



PRELIMINARY BODY WAVE ANALYSIS OF THE ST.  
ELIAS, ALASKA, EARTHQUAKE OF FEBRUARY 28, 1978

John Boatwright

Omar Perez (both at: Lamont-Doherty Geological  
Observatory and Department of Geological  
Sciences of Columbia University, Palisades,  
New York 10964)

We have made a preliminary analysis of the body waves radiated by the St. Elias earthquake, using long period P- and S-waves recorded at three WSSN stations and at Palisades, N.Y. The focal mechanism, determined from P-wave first motions and S-wave polarizations, shows a very shallow angle thrust striking 70°E and dipping 10°W. Using this mechanism and a best average source depth of = 11 km, we have directly deconvolved the interference of the depth phases (i.e., pP and sP, or sS) from the recorded pulse shapes, thus obtaining approximate whole space (AWS) velocity and displacement pulse shapes. These AWS pulse shapes show that the earthquake contained three distinct rupture events as well as a small initial event = 7 secs earlier. The earthquake propagated to the southeast. From the pulse rise times of these sub-events, the rupture lengths for these events are = 9, 24 and 16 km, assuming that the rupture velocity was 2.5 km/sec. The cumulative moment for the whole event obtained from this analysis,  $1.2 \times 10^{27}$  dyne-cm, is substantially smaller than the surface wave moments obtained by Hasegawa, and Stevens and Boore, of  $5 \times 10^{27}$  dyne-cm (personal communications). The moments of sub-events are estimated to be = .8, 3.5 and  $7.6 \times 10^{26}$  dyne-cm, respectively.

1. 702418PEREZ
2. 1979 Spring Meeting AGU
3. Seismology
4. Special Late Friday Sessl
5. No
6. No
7. None
8. (Mrs.) Alma Kesner  
Purchasing Dept.,  
Lamont-Doherty Geol. Obs.  
Palisades, NY 10964

SEISMOTECTONIC SETTING OF THE SHUMAGIN ISLANDS REGION, ALASKA:  
EVIDENCE FOR A SEISMIC GAP AND A REGION OF HIGH SEISMIC  
POTENTIAL\*

John Davies, Lynn Sykes, Leigh House  
and Klaus Jacob  
LamontDoherty Geological Observatory  
of Columbia University  
Palisades, New York 10964

The Shumagin Islands are approximately in the center of a geographical area of the Aleutian arc that extends from Unalaska of the eastern Fox Islands to the western end of Kodiak Island. We present a study of the seismotectonic setting of this area that focuses on the Shumagin Islands region in which we have operated a local seismograph network since 1973. This area is bounded by the aftershock zones of the great earthquake of 1957 in the Andreanof - Fox Islands to the west and that of 1964 in the Kodiak Island - Prince William Sound region to the east. The eastern half of this Unalaska-to-Kodiak area broke in the great earthquake of 1938. The tsunami earthquake of 1946 occurred in the western part of the area but most likely did not break much, if any, of the interplate boundary. It is along the interplate boundary above 50 km depth, i.e., along the main-thrust zone that great, thrust-type earthquakes occur. We show that the down-dip width of the main-thrust zone is proportional to the recurrence times for great thrust-type earthquakes along the Alaska-Aleutian convergence zone. In the Shumagin Islands region the width of the main-thrust zone is intermediate to those in the adjacent regions. This implies recurrence intervals on the order of 80 to 140 years as compared to 50 to 80 years for the central and western Aleutians and about 220 years for the Kenai Peninsula - Prince William Sound region. These estimates of recurrence intervals are based in part on new historic seismicity data and in part on rates of plate convergence. New maps of PDE and ISC epicenters for the eastern Aleutian arc suggest that within the past decade a "Mogi-Donut" pattern has become fairly well established around the Shumagin Islands region. The down-dip part of the donut pattern (at about 40 km depth) is best developed and consists, at least in part, of events that indicate a very high stress drop (order of 1 kilobar) and which have focal mechanisms indicating underthrusting along a plane dipping at 30°. On the basis of these combined data, both historic and recent, we conclude that a seismic gap exists in the Shumagin Islands region which has a relatively high potential for an earthquake of magnitude greater or equal to 8 within the next few decades. A questionable gap in the eastern Fox Islands region may have not broken in the great shock of 1957; it may or may not be connected with the Shumagin Gap.

---

\*Proceedings 30th Alaska Science Conference, September 19-21, 1979, Alaska

A TECTONIC MODEL FOR THE EASTERN GULF OF ALASKA  
AND ITS IMPLICATIONS FOR SEISMIC HAZARDS\*

Klaus H. Jacob and Omar J. Perez  
Lamont-Doherty Geological Observatory  
of Columbia University  
Palisades, New York 10964

A tectonic model is derived for the motions and deformations along the Pacific North American plate boundary in the Eastern Gulf of Alaska. The major data base consists of 13 new and several published fault-plane solutions, and of published regional plate-motion vectors obtained from global inversions.

The model predicts a component of about 1.3 cm/year of convergence across this predominant-transform boundary (associated with 5.3 to 5.7 cm/year of right-lateral strike-slip motion along the Queen Charlotte Fairweather fault systems). This small convergence leads, however, to a slow subduction of Pacific lithosphere beneath this western North American margin. A dipping Benioff zone is absent there but a weakly developed volcanic arc exists in the northern third of the boundary where the lithosphere is expected to extend deeper than 100 km into the mantle. West of Yakutat Bay convergence is dominant and is taken up along several imbricate thrust belts. Probably 80% of the 6 cm/year convergence are taken up on shallow-angle thrusts in the Chugach St. Elias fault system extending from the Pamplona zone offshore to the Border Ranges fault inland. A segment of this plate boundary has been identified as the "Yakataga seismic gap". It has not ruptured by a large earthquake for 80 years and is expected to rupture in a large quake in the not too distant future. Recurrence times at this plate-boundary segment are estimated to be near 100 years (with uncertainties ranging from 50 to 200 years). The St. Elias earthquake of February 28, 1979, ( $M = 7.7$ ) relieved stresses over an area much smaller than that of the Yakataga seismic gap.

A secondary shallow-angle thrust zone exists offshore along the northwest-trending shelf-edge connecting the Queen Charlotte fault (near Cross Sound) to the Aleutian trench (near Kayak Island). Slip is northeast-directed with rates estimated to be about 1.2 cm/year. Recurrence times are estimated to be 500 years but are highly uncertain.

Recurrence times for presently very weakly active faults inland (i.e., Denali fault, Totschunda Fault amongst others) may be even longer (approximately 1,000 years?).

---

\*Proceedings 30th Alaska Science Conference, September 19-21, 1979, Alaska.

XI.D. ABSTRACT AND INTRODUCTION

ST. ELIAS, ALASKA EARTHQUAKE OF FEBRUARY 28, 1979:

TECTONIC SETTING AND PRECURSORY SEISMIC PATTERN<sup>1</sup>

Omar J. Perez<sup>2</sup> and Klaus H. Jacob

Lamont-Doherty Geological Observatory of Columbia University

Palisades, New York, 10964

ABSTRACT

The St. Elias earthquake of February 28, 1979 and two earlier earthquakes in the St. Elias Range, Alaska, are shown to have involved thrust motion on gently NNW-dipping faults associated with subduction of the Pacific beneath the North American plate. The space-time patterns of the seismicity located within and in the immediate vicinity of the rupture zone of the St. Elias event in the sixteen years period prior to it, indicate approximately 6.3 years of relative quiescence before the main shock, interrupted by a burst of seismic activity about 3 years prior to the event. This observed seismic pattern resembles those reported for other large earthquakes, and therefore we suggest that the preceding burst of activity may have been a precursor.

---

<sup>1</sup>Lamont-Doherty Geological Observatory Contribution Number 0000.

<sup>2</sup>Also with the Department of Geological Sciences, Columbia University and FUNVISIS, Caracas Venezuela.

## INTRODUCTION

On February 28, 1979, an earthquake with a surface wave magnitude  $M_s = 7 \frac{1}{4}$  occurred in the Chugach-St. Elias Range near the eastern Gulf of Alaska, close to the international boundary between the U.S. and Canada (Figure 1). In this paper we investigate two aspects of the St. Elias earthquake. First, we present its focal mechanism and those of two earlier nearby earthquakes, and discuss some of their implications for the tectonics of the region. Second, we describe the behavior in space and time of the preceding teleseismically observable seismicity that took place within and in the immediate vicinity of the rupture zone of the St. Elias earthquake. Seismic events only above a cut-off magnitude of 4.2 and for the 16-year period preceding the main event are considered. The objective of the spatial-temporal study of seismicity is to find whether any pattern can be recognized which may contain premonitory information useful for understanding problems of earthquake prediction. Throughout this paper we rely on information obtained from teleseismic data that are limited in sensitivity and in hypocenter resolution. Hence, our results may need revisions as data from a local seismic network (Lahr *et al.*, 1979; Stephens *et al.*, 1980) become available. Local data almost certainly will reveal more complexities than this teleseismic study can address.

## TENTATIVE ACTION PLAN FOR STRONG MOTION PROGRAM

(Prepared for OCSEAP/ACST Workshop on Alaska Seismology, September 17 1979)

K. Jacob

A result of the OCSEAP Seismology and Earthquake Engineering Workshop in Boulder (March 26-29, 1979) was that a major effort must be launched to obtain more strong-motion records soon for the Alaska continental margin regions and that the few records existing must be analyzed speedily. Several recommendations were formulated, but with little visible results to date for the land-based program. The following points are listed and, after discussion and modification, are recommended for adoption into a plan of action.

1. Formation of a small, active Strong Motion Alaska Council (SMAC).
2. Formulate a realistic and timely SMAC plan for deployment of more strong motion sensors with clearly set priorities.
3. Go for funding of joint SMAC plan to agencies outside OCSEAP, i.e. USGS, NSF, Industry, State of Alaska.
4. Select qualified group of experts who in behalf of SMAC will put together ASMAF (Alaska Strong Motion Accelerogram File) consisting of (among other items):
  - a) listing of accelerometer sites, site description, and instrument characteristics (for all times).
  - b) copies of all Alaska analog strong-motion records and corresponding earthquake parameters.
  - c) digitizations of (b) on computer compatible tape and storage at a SMAC data bank.

- d) a standard library of computer programs for routine processing of (c).
  - e) a product-catalogue after applying (d) to (c) probably including the following: time histories of acceleration, velocity, displacement; peak values, durations, spectra; (rotated time series).
5. SMAC define procedures and algorithms to translate findings from (4) into hazards maps; define parameters to be mapped. (Needs other input than just from SM data).
  6. Establish Quality Control on SMAC by outside review.
  7. Establish Procedures which ensure new SM data are submitted to SMAC data bank in a timely and complete fashion.

Contract No. - 01-5-022-231  
Research Unit No. - RU105  
Reporting Period - 1 April 1979 -  
31 March 1980

Number of Pages - 31

ANNUAL REPORT

DELINEATION AND ENGINEERING CHARACTERISTICS OF  
PERMAFROST BENEATH THE BEAUFORT SEA

Principal Investigators:

P.V. Sellmann  
E. Chamberlain

Associate Investigators

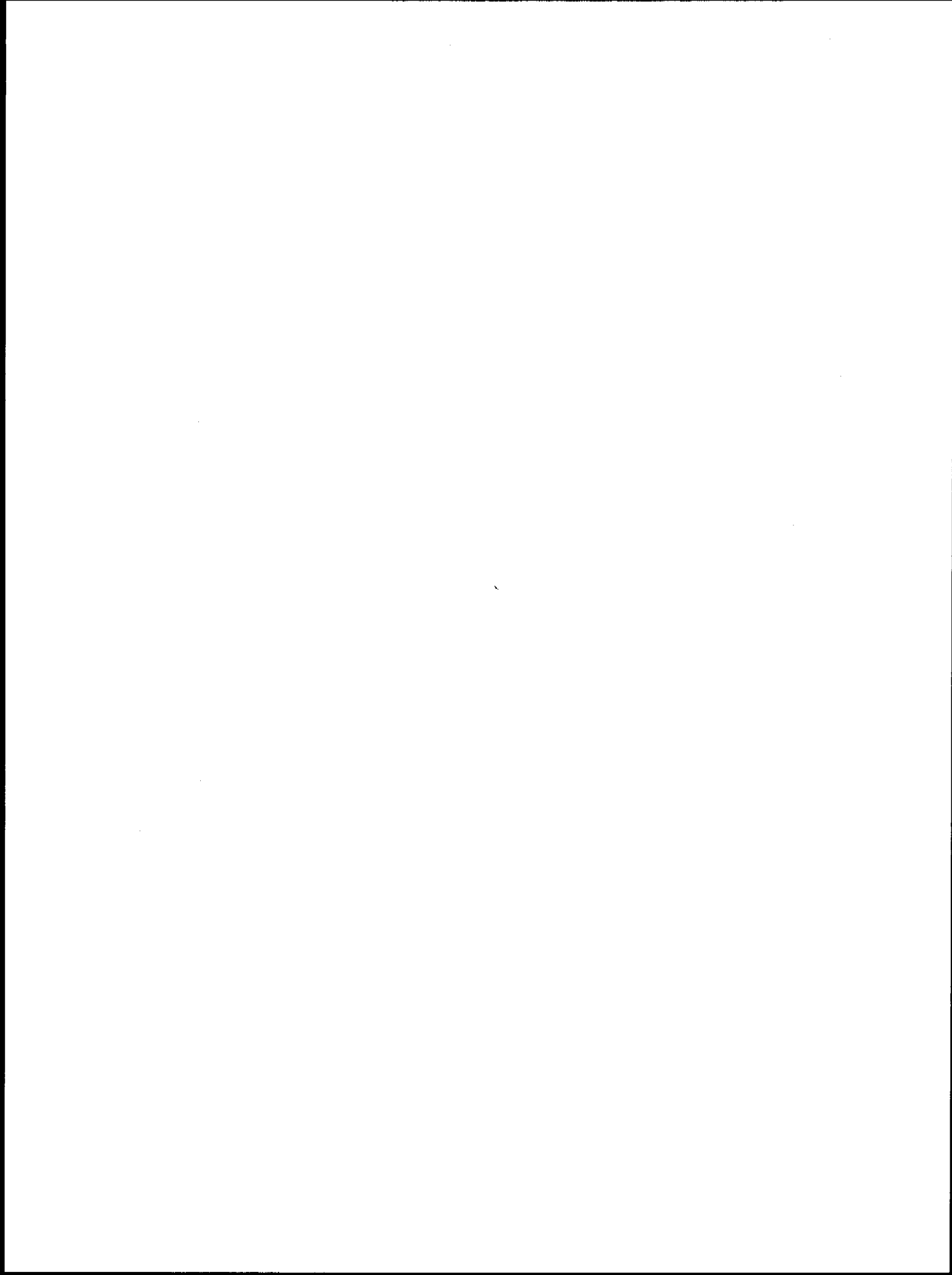
A. Delaney  
K.G. Neave

1 April 1980

Prepared for the BLM-NOAA Arctic Outer  
Continental Shelf Environmental Assessment Program

UNITED STATES ARMY CORPS OF ENGINEERS  
COLD REGIONS RESEARCH AND ENGINEERING LABORATORY  
HANOVER, NEW HAMPSHIRE, U.S.A.





## PREFACE

This preface was included in response to a request from the Arctic Project Office. It is intended to provide a short summary of past program results and projected goals. The summary included in the body of the annual report will cover only the past year's activities.

The objective of the CRREL program has been to obtain information on the distribution and properties of permafrost beneath the Beaufort Sea. It began with two seasons of drilling and penetrometer studies in the Prudhoe Bay region. This was a joint effort with the USGS, University of Alaska, and Robert Lewellen. The observations were based on information from 9 drill holes and 27 penetrometer sites. The deepest drill hole was 65.1 meters below the seabed, while a depth of 14.1 meters was reached with the penetrometer. The observations included determination of the engineering, chemical, and thermal properties of the sediments in this region. They also supported the geological studies conducted by the USGS. Temperatures below 0°C were observed at all the drill and penetrometer sites. Seasonal freezing of the seabed was common; strength was dependent on bed temperatures, with the greatest strength observed in shallow water areas (< 2 m). Of the eight holes drilled, four were deep enough to encounter ice-bonded permafrost. An attempt to integrate some of the results of the OCSEAP permafrost programs near Prudhoe Bay can be seen in the profile of the position of the top of ice-bonded permafrost shown in Figure 1.

Following this study the Conservation Division of the U.S. Geological Survey sponsored a drilling program that obtained information outside of the Prudhoe Bay area. Their observations extended the knowledge of the depth to the top of ice-bonded sediments and also contributed to the understanding of the properties of the ice-rich marine sediments (USGS, contract report, 1979).

The OCSEAP permafrost program and other non-industry studies such as Lewellen's conducted near Barrow provided the first quantitative data on the existence and extremely variable nature of offshore permafrost. They also served as an excellent starting point for the more widely spaced observations made by the USGS Conservation Division in the current lease area.

Our studies have found that the distribution and properties of the subsea permafrost are extremely variable. The large degree of variability makes generalizations about this permafrost environment extremely problematic. However, it can be stated that the marine permafrost exists at considerably warmer temperatures than does nearby land permafrost and so is more susceptible to thaw and its related problems. As the distance from shore increases, the marine permafrost becomes more similar to the permafrost found in the interior of Alaska. Because of the general lack of oil field development experience in this type of environment, construction activities in the area will probably encounter

- Refraction data (Rogers and Morack 1978)
- ▲ Reflection data (Rogers and Morack 1978)
- Refraction data (Rogers, in Barnes and Hopkins 1978)
- a Drilling, sampling, temperature and chemistry data (CRREL-USGS)
- b Drilling, sampling, temperature and chemistry data (Osterkamp and Harrison 1976)
- c Drilling and sampling (Humble C-1, unpublished)
- d Drilling (Osterkamp and Harrison 1978a)
- e Drilling and temperature data (Osterkamp and Harrison 1978b)

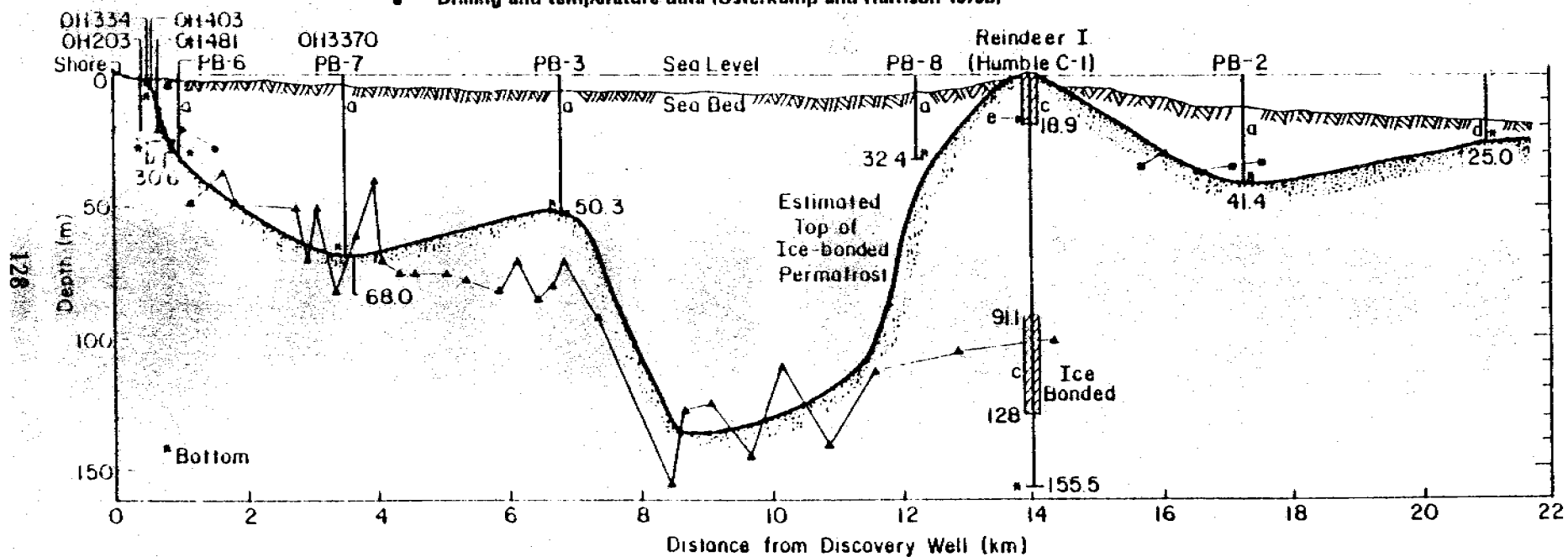


Figure 1. Summary of available data on depth of ice-bonded permafrost along a line from the West Dock at Prudhoe Bay through Reindeer Island. The dark shaded line is the estimated position of the top of ice-bonded permafrost (from Sellmann and Chamberlain, 1979).

more permafrost-related problems than are experienced in nearby onland sites. Site-specific investigations are therefore a necessity before any construction activities are begun in this area.

The extensive engineering property analysis conducted as part of this OCSEAP provided the first quantitative data on the properties of the sediments in this region. Probably the most significant observation was confirmation of the common occurrence of overconsolidated sediments. The distribution of these sediments is significant for more than one reason. Fine-grained overconsolidated sediments appear to influence the depth to the top of ice-bonded permafrost. Locations where shallow ice-bonded sediments were observed correspond with thick sections of overconsolidated material. Their distribution influences access to underlying, more desirable construction materials. The properties and extensive distribution of thick sections of fine-grained material will require site-specific investigations to ensure adequate supplies of materials for construction activities.

The permafrost distribution data were expanded by recent investigations of seismic data from the current lease area. The results of these investigations will be discussed in this annual report; they can help to establish where permafrost problems should be anticipated.

Significant gaps exist in the understanding of subsea permafrost and its properties in the lease area; however, the lack of information outside the current lease area is even greater. Many of the gaps in our knowledge are not likely to be answered because of the need for extremely expensive deep drilling. The data gaps are discussed in this report. A tabulation of all reports published as part of this program can also be found in Section VI.

A continued investigation of seismic records from this lease area and new proposed lease areas would provide additional information on permafrost distribution. In some cases it is possible that historical and property data can also be indirectly obtained.

## I. Summary

The objectives of the CRREL 1979-80 subsea permafrost program were to obtain additional information on the distribution and properties of permafrost in the current Beaufort Sea lease area. The property studies were to be based on cores obtained from the USGS Conservation Division Program. The distribution study was based on interpretation of seismic records.

Records from approximately 2350 kilometers of seismic line were examined for the area discussed in this report. The locations of these lines are shown in Figure 3. The lines along the coastline include both land and marine data from an ice survey, while the coverage from deeper water was from a conventional open water survey.

The data analysis included examination of the first arrival refraction data for the distribution of near surface sediment velocities and information on the velocity structure of materials that appeared to be ice-bonded. Surface wave velocities were also examined as a possible means of obtaining additional data on offshore sediment properties.

The high velocity materials observed offshore in the region covered by this report are assumed to represent ice-bonded permafrost, as opposed to unfrozen, high-velocity, chemically indurated materials. The direct wave velocities ranged from 1.6 to 4.6 km/s and formed three velocity groups (Fig. 2). The groups appear to be related to the degree of ice bonding in the permafrost caused by variations in temperature and possibly differences in material types. It was assumed that materials having velocities greater than 2.2 km/s are ice-bonded. The highest velocity group (3.3-4.6 km/s) represents well-bonded cold permafrost most commonly found on land, while the intermediate group (2.3 to 3.2 km/s) represents the bonded marine sediments in this study area. Offshore the highest velocity group was observed at considerable depth where velocity layering appeared to exist in the coastal ice-bonded permafrost. This deep high-velocity layer locally paralleled the coastline, with the depth to its top as much as 350-400 m below the seabed.

Direct wave velocity profiles all show a systematic variation when the shoreline is crossed. At the shoreline, or some distance seaward, the velocities decrease abruptly to values common to the intermediate velocity group.

A limited amount of surface wave data were obtained, but attempts to map the surface thaw zone using this information were hampered because less than half of the records had readable surface-wave signals. Low-frequency noise in the reflection part of the coastal records, interpreted to be scattered low-velocity surface waves, was used as a means of examining the continuity of the offshore thaw zone above ice-bonded permafrost. These data showed two anomalous offshore areas where bonded sediments are apparently at shallower depths than can be explained by the bathymetric data.

The maximum velocity data from the deeper water offshore seismic lines are all very similar and fell into the low-velocity group, ranging from 1.6 to 2.2 km/s. The velocities resolved in this region are too low for there to be any significant ice-bonding of the sediments in the upper part of the section.

The velocity profiles and maps included in this report suggest that offshore bonded permafrost is extremely extensive, evidently occurring along all of the lines examined from the coastal ice-shooting survey, since velocities are greater than 2.25 km/s. This lower limit should provide an estimate of the minimum extent of bonded sediments. Materials slightly colder than 0°C, possibly with some ground ice, can have far greater extent.

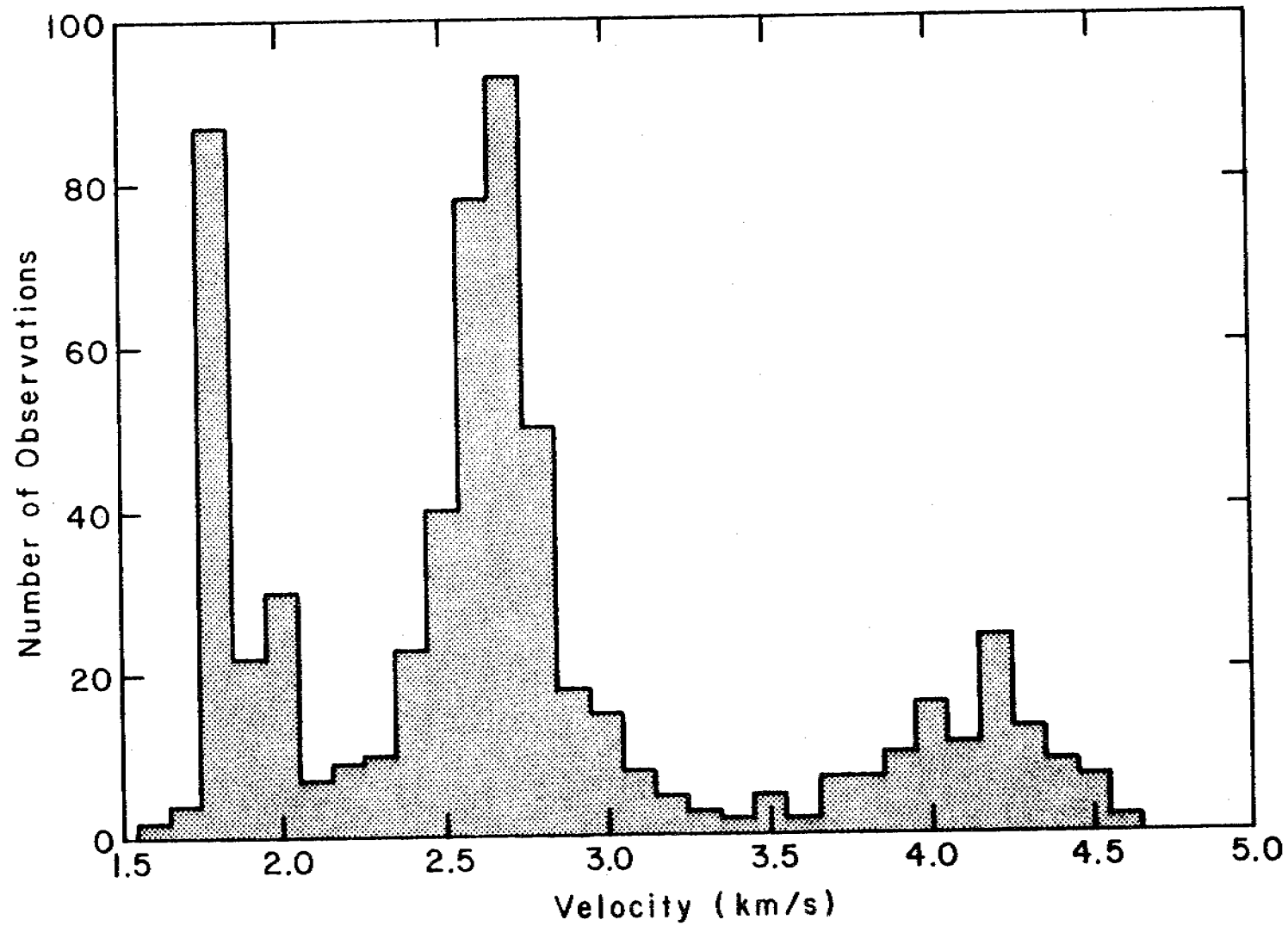


Figure 2. Histogram of direct wave velocity data.

The velocity layering noticed offshore can help establish the minimum thickness of ice-bonded sediments. The top of this deep high-velocity layer is around 300 to 400 m below the bed, suggesting that ice-bonded permafrost is at least this thick where this structure occurs more than 8 km off-shore.

In addition to the information on permafrost distribution the seismic data also appear to provide regional information on coastal processes. A comparison of the velocity structure and surface velocity data shows velocity patterns that could be related to differences in historical coastal erosion and transgression trends.

The areas where we observed velocity layering could have experienced changes in properties due to temperature differences in the permafrost. The differences may be related to transgression rates that were large enough that temperature modifications at depth could not keep pace with the rapid warming. Sections of the coast that show a sharp change in velocities at the coastline from high land values to lower values offshore are probably areas of active erosion. In contrast, areas that are probably more stable tend to show velocities that increase inland from the coastline, suggesting some landward modification due to prolonged exposure to the marine environment.

In general the velocity groups formed bands that paralleled the coastline and appeared to be related to corresponding variations in the subsurface temperatures. In addition to the noticeable contrast between the land and marine velocities, other less obvious zones exist, such as the narrow velocity band along the coast out to the 1-m water depth. Another similar zone appears immediately shoreward, forming a belt along the coastline with velocities that range from 3.5 to 4 km/s. It occurs primarily on land although it extends offshore in the delta regions.

Sediment type may influence the velocity pattern observed but this has not been confirmed.

The offshore limit of the bonded permafrost detectable by this type of analysis could not be precisely determined from this study because of the gap between the ice-shooting and marine records. The analysis suggests that the limit is someplace between these two groups of data. Emphasis is now being placed on acquiring records to fill this gap.

## II. Introduction

This year's study of subsea permafrost distribution was based on examination of seismic records originally acquired for petroleum exploration purposes. Records were selected for analysis from the 2350 kilometers of shotline shown in Figure 3. Minimum record spacing was 1 record per kilometer of line. USGS sparker data from the Prudhoe Bay area were also examined to determine the significance of the hyperbolas observed in these records. It was hoped that they might provide additional information on permafrost velocities or properties.

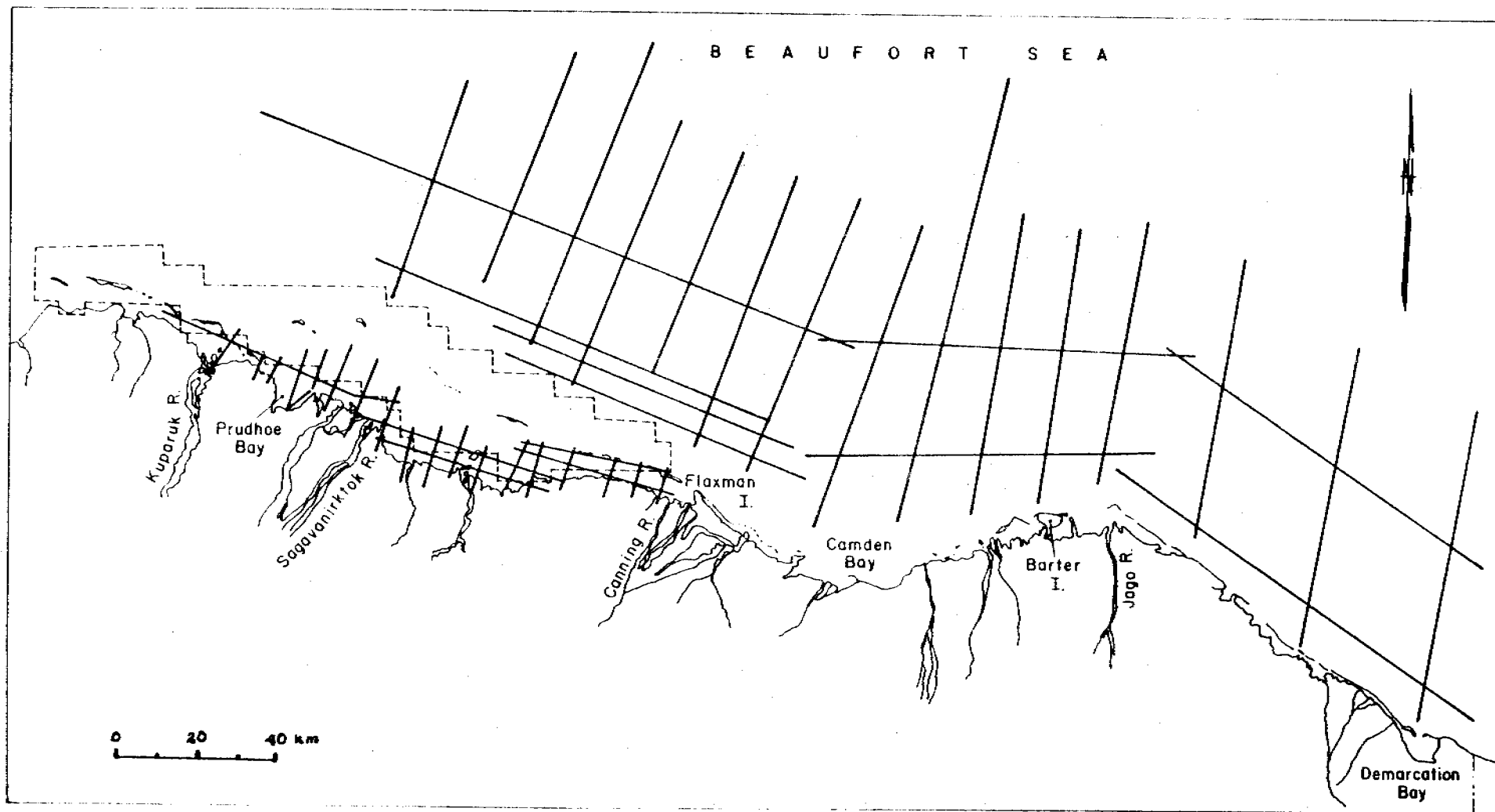


Figure 3. Map of seismic survey lines from which records were analyzed. Dashed line shows the limit of the current lease area.



Samples obtained during the USGS Conservation Division program were recently transferred to CRREL. There has been no opportunity yet to perform chemical and engineering property analyses.

### III. Current State of Knowledge

The greatest amount of available information on subsea permafrost in the U.S. Beaufort Sea is from the current lease area. This information primarily comes from studies supported by the OCSEAP program and the recent USGS Conservation Division drilling and sampling effort. Some of the major contributions these programs have made to our understanding of subsea permafrost in the current lease area are listed below.

- (1) Established the existence and common occurrence of subsea permafrost.
- (2) Determined that its properties and distribution are extremely variable.
- (3) Suggested some general limits for the areal distribution of bonded permafrost.
- (4) Determined information on the depth to bonded permafrost along one line near Prudhoe Bay and at spot locations in the lease area.
- (5) Provided some engineering property data on both ice-bonded and unbonded sediments.
- (6) Established the existence and properties of overconsolidated sediments in the Prudhoe Bay area as well as the widespread distribution of these sediments.
- (7) Obtained temperature data from the upper part of the permafrost section.
- (8) Developed information on the historical geology of this region.
- (9) Developed thermal and chemical models for subsea permafrost.

There still remain considerable gaps in knowledge from the current lease area. Only general information on permafrost distribution exists. Data are needed on:

- (1) offshore extent of both bonded and unbonded permafrost
- (2) thickness of bonded permafrost
- (3) the relationship between depth to the top of bonded sediments and various offshore conditions such as material types, proximity to islands and deltas, etc.

(4) engineering properties of the permafrost with emphasis on properties related to the ice content of the bonded sediments, including pore ice chemistry. (Some of this data will be coming from the USGS Conservation Division program.)

(5) local variations in permafrost distribution

(6) information on occurrence of gas hydrates offshore and in the adjacent land area.

(7) understanding of geological history and coastal processes.

Extremely little data is available from outside the lease area, except for information from Lewellen's studies near Barrow, and some observations made by Osterkamp and Harrison. It is possible the extension of the seismic data analysis to other parts of the Beaufort Sea would provide regional information on bonded permafrost distribution. Additional data analysis accompanied with geological and property data from local observations, would help to improve the current lack of information. It is unlikely that the OCSEAP program will fill all of the gaps mentioned above, since information from deep within the permafrost would require extremely high cost drilling activities.

#### IV. Study Area

The seismic records used for this years study were selected from the shotlines shown in Figure 3.

#### V. Sources, Methods and Rationale of Data Collection

The location of seismic records examined thus far was controlled by the availability of data that could be treated in a nonproprietary manner. The lines selected were intended to provide as much coverage as possible from the land to water depths as great as 90 m. The gaps between the coastal lines and the deeper water data will hopefully be filled in the near future.

The basis for this study is that noticeable changes in seismic velocities occur between frozen and unfrozen unconsolidated materials (Aptikaev, 1964). This contrast is often most apparent when the moisture content of the materials is near saturation. This fact and the existence of large amounts of seismic data from surveys conducted for petroleum exploration activities makes the study of the distribution of ice-bonded subsea permafrost by seismic techniques a reasonable approach. When records are available, and their quality and field recording parameters are appropriate, permafrost data can be extracted. These records can permit determination of direct wave velocities and refraction interpretation of the first returns for information on velocity structure. This velocity data can then provide the basis for predicting the distribution of ice-bonded permafrost and, when resolution is adequate, the depth to the top of the frozen sediments.

The offshore marine data used for this study was obtained by GSI using a 2350-m hydrophone array with a phone group spacing of 50 m, and multiple air guns for an energy source. The ice-shooting data was obtained with a 4800-m line on the ice surface, a group interval of 100 m, and explosive charges for the energy source.

This data is normally processed for petroleum exploration with emphasis on deep targets, commonly with first break suppression, increased gain with depth, and normal moveout corrections. These procedures tend to compromise the quality of the data from the near surface. In an attempt to obtain as much as possible from the records without costly processing, approximately the first two seconds of data were played back from the field tapes with expanded gain. They were printed in a wiggletrace or variable area format, without normal moveout corrections. The first arrival data from which velocity measurements can be made is easily seen on the ice survey record (Fig. 4), with a direct wave at 2.8 km/s and a refracted wave at 4.1 km/s.

It was possible to obtain direct wave velocity data from the records and refraction interpretation was possible, allowing velocity structure within the ice-bonded sediment to be determined. However, less conventional methods with greater resolution were required to study the thin thaw layer often found above the ice-bonded permafrost. Surface wave velocities were used for this analysis since their shorter wavelength permitted greater sensitivity. On these records the wavelength of the surface wave velocities was approximately 6 times less than the length of the compressional waves.

The attempt to map the thaw zone above the offshore bonded permafrost was hampered by the fact that less than half the records had readable surface wave signals. However, low-frequency noise on the reflection part of many of the offshore records was interpreted to be either scattered low-velocity surface waves, or scattered compressional wave modes in a near surface low-velocity wave guide. This low-frequency noise was contrasted with the high quality reflection records from land where no significant thaw is expected. By mapping the low-velocity noise distribution, it appears that the presence and qualitative information on the thickness of the surface thaw zone above the ice-bonded layer can be determined.

#### Resolution of Data

The resolution of this type of study is obviously not as great as can be obtained from a seismic investigation designed for the study of offshore permafrost. The resolution is variable and depends on a number of factors, including geophone spacing, signal frequency, and complexity of the subsurface. In general, the horizontal resolution of the data covered in this report, based on refraction interpretation of the compressional waves, should be a minimum of three phone spacings. This suggests that the minimum horizontal extent of a feature that can be

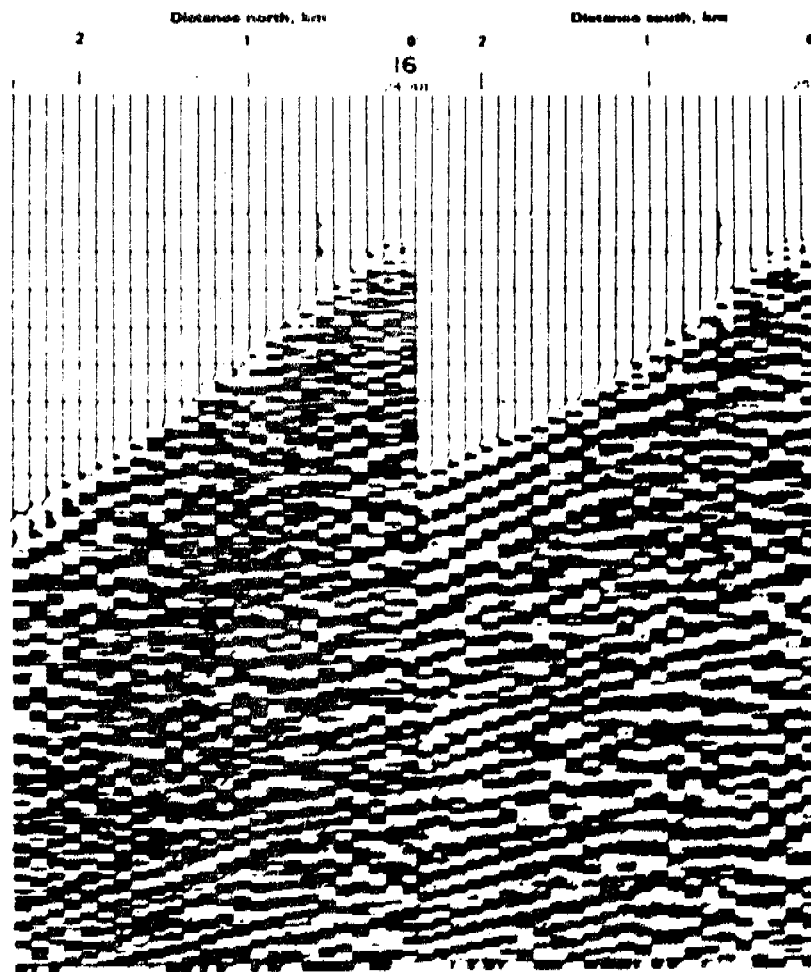


Figure 4. Sample ice-survey record.

detected is around 300 m for the ice-shooting data, and around 150 m for the marine survey data. The minimum vertical thickness of a detectable high-velocity layer is determined by the wavelength of the signal source, with resolution possibly around 1/2 wavelength (Sherwood, 1967). Therefore, the minimum vertical thickness of a detectable high-velocity layer is probably limited to about 50 m.

The resolution of the surface wave signal is also dependent on the wavelength involved. Ewing et al. (1957) showed that a layer must be thicker than 0.6 wavelengths in order to carry a signal which has no dispersion. Accordingly, the surface waves should be visible on the ice-shooting records where the surface thaw zone is approximately 25 m thick.

## VI and VII. Results and Discussion

The results of all aspects of the CRREL activities related to the previous drilling and sampling program have been covered in a variety of reports in addition to the usual OCS quarterly and annual reports. This year several other reports were published, and two others are nearly completed and will be published as part of the CRREL report series. Several review reports were also prepared for the USGS Department of Marine Geology which relied, for the most part, on past OCS studies. All of these reports are listed below, in some cases the citations are accompanied with explanatory comments.

(1) Sellmann, P.V., R.I. Lewellen, H.T. Ueda, E.J. Chamberlain, and S.E. Blouin 1976, Operational Report: 1976 USACRREL-USGS Subsea Permafrost Program, Beaufort Sea, Alaska, U.S. Army CRREL Special Report 76-12.

(2) Sellmann, P.V., E.J. Chamberlain, H.T. Ueda, S.E. Blouin, D.E. Garfield, and R.I. Lewellen, 1977, Operational Report: 1977 USACRREL-USGS Subsea Permafrost Program, Beaufort Sea, Alaska, U.S. Army CRREL Special Report 77-41.

(3) Sellmann, P.V., E.J. Chamberlain, S.E. Blouin, I.K. Iskandar and R.I. Lewellen, 1977, Field Methods and Preliminary Results of Subsea Permafrost Studies in the Beaufort Sea, Alaska, (Expanded Abstract) Proceedings of Symposium on Permafrost Field Methods & Permafrost Geophysics, NRC Technical Memorandum no. 124, p. 207-213.

(4) Page, F.W., 1978, Geochemistry of Subsea Permafrost at Prudhoe Bay, Alaska. Prepared as MA Thesis, for Department of Earth Sciences, Dartmouth College.

(5) Page, F.W. and I.K. Iskandar (1978) Geochemistry of Subsea Permafrost at Prudhoe Bay, Alaska, U.S. Army CRREL Special Report 78-14 (Published version of above Thesis).

(6) Chamberlain, E.J., P.V. Sellmann, S.E. Blouin, D.M. Hopkins, and R.I. Lewellen, 1978, Engineering Properties of Subsea Permafrost in the Prudhoe Bay Region of the Beaufort Sea, Proceedings of the Third International Conference on Permafrost, Vol. 1, 1978, p. 629-635.

(7) Iskandar, I.K., T.E. Osterkamp, and W.D. Harrison, 1978, Chemistry of Interstitial Water from Subsea Permafrost, Prudhoe Bay, Alaska, Proceedings of the Third International Conference on Permafrost, Vol. 1, p. 93-98.

(8) Blouin, S.E., E.J. Chamberlain, P.V. Sellmann, and D.E. Garfield, 1979, Determining Subsea Permafrost Characteristics with a Cone Penetrometer-Prudhoe Bay, Alaska, Cold Regions Science and Technology, Vol. 1, No. 1.

(9) Blouin, S.E., E.J. Chamberlain, P.V. Sellmann and D.E. Garfield, 1979, Penetration Tests in Subsea Permafrost, Prudhoe Bay, Alaska, USACRREL Report 79-7, 45 p. (This is a complete report containing all data - version (8) was condensed for the journal.)

(10) Sellmann, P.V. and E.J. Chamberlain, 1979, Permafrost Beneath the Beaufort Sea near Prudhoe Bay, Alaska, Proceedings of the Eleventh Offshore Technology Conference, Vol. 3, p. 1481-1488.

(11) Sellmann, P.V. & E.J. Chamberlain, 1980, Permafrost Beneath the Beaufort Sea: Near Prudhoe Bay, Alaska. Jour. of Energy Resources Technology, Transactions of the ASME, Vol. 102, N. 1, p. 35-48. (Journal publication of the above Offshore Technology Conference paper).

(12) Chamberlain, E.J., 1979, Overconsolidated Sediments in the Beaufort Sea, Northern Eng. Vol. 10, n. 3, p. 24-29.

(13) Neave, K.G., P.V. Sellmann and A. Delaney, 1980, Information on Subsea Permafrost Distribution from Seismic Data Interpretation - U.S. Beaufort Sea, USACRREL Report (in prep).

(14) Neave, K.G., 1980, Hyperbolic Reflections on Beaufort Sea Seismic Records, USACRREL Report (in prep).

The following reports were part of a review funded by the USGS. However OCSEAP experience and information contributed to them.

(15) Chamberlain, E.J., 1979, Site Investigation and Submarine Soil Mechanics in Polar Regions - Review of Problems and Practices - Contract Report prepared for Department of Marine Geology-USGS.

(16) Chamberlain, E.J., 1979, Foundations of Structures in Polar Waters - Review of Problems & Practices, Contract Report prepared for Department of Marine Geology - USGS.

(17) Sellmann, P.V., 1979, Regional Distribution and Characteristics of Bottom Sediments on Arctic Coastal Waters of Alaska - Review of Current Literature, Contract Report prepared for Department of Marine Geology - USGS.

### Seismic Data Interpretation

#### Velocity Data

The velocity data showed a great deal of variability, although when it is organized it groups into coherent patterns that appear to be related to the thermal history of the sediments found along this part of the coast. The histogram of compressional wave velocities from all the lines shown in Figure 3 form three groups that range from 1.6-4.6 km/s (Fig. 2).

The groups appear to indicate the degree of bonding of the permafrost and possibly the distribution of various material types. As mentioned earlier, materials having velocities greater than 2.2 km/s are assumed to be ice-bonded. The high-velocity group, with velocities that range from 3.3 to 4.6 km/s and average 4.1 km/s, represent the well-bonded cold materials with ice-saturated pores usually found on land and in some cases in the marine environment. The intermediate group, which ranges from 2.3 km/s to 3.2 km/s and has an average velocity of 2.7 km/s, possibly represents bonded marine permafrost that has undergone some changes in properties and may contain more unfrozen water than the high-velocity group. The high-velocity materials observed offshore in this region are assumed to represent ice-bonded permafrost as opposed to unfrozen high-velocity chemically indurated materials. This assumption appears to be supported by the coastal data, much of which provides velocity information across the land-sea transition. In general these survey lines contain a velocity gradient from the high onshore permafrost velocities to lower velocities offshore with the most significant change occurring near the shoreline. There appears to be no geological basis (Howitt, 1971) for this change in velocities other than the influence of the warmer marine environment on permafrost properties. This appears to be supported by the fact that the high-velocity material is not observed great distances from the shoreline in the marine seismic data.

The low-velocity group, which ranges from 1.6 km/s to 2.2 km/s with an average of 1.9 km/s, is thought to represent the unbonded sediments that could be colder than 0°C.

Seismic studies of offshore permafrost, conducted by Rogers and Morack (1978), observed a grouping of velocities similar to the two lowest categories. In their studies, they did not observe velocities in the highest velocity group, partly because they had no land data incorporated in their results. They observed that velocities in the offshore ice-bonded sediments systematically fell into the 2.5 km/s to 3.1

km/s range, which is comparable to our mid-velocity group. They reported that, for similar materials in an unfrozen state, velocities ranged from 1.6 km/s to 2.0 km/s. These velocities match very closely those observed in the low-velocity group obtained during our study.

In the subsea permafrost investigation conducted in the Canadian Beaufort Sea by Hunter, et al. (1976), the threshold velocity used for ice-bonded material was 2.5 km/s. This limit is in general agreement with the lower velocity end of our intermediate group.

In our study, offshore sediments in the highest velocity group were observed primarily where velocity layering appeared to occur in the bonded permafrost. A deeper second layer locally paralleled the coastline and in several locations provided velocities that were much like those observed on land. The top of this layer was as much as 350 - 400 m below the bed and apparently was too deep to be detected by Rogers and Morack because of their array geometry. In contrast, the ice-shooting array used to obtain data for this study detected the deeper high-velocity material, but lacked the required resolution to observe the thin unfrozen layer which overlies the bonded permafrost in this near shore area. The low-velocity values reported in Figure 2 were primarily from analysis of the marine data which is presumed to be sufficiently far offshore that bonded permafrost does not occur. The low-velocity values obtained by Rogers and Morack (1978) were from unfrozen sediments in the near shore region.

#### Near Surface Velocity Profiles

As previously mentioned, the near surface velocities from the ice-shooting data indicate a systematic variation when the shoreline is crossed. The nature of this variation is illustrated in the four sample profiles shown in Figure 5. These profiles were selected because they represent the velocity trends along the coastline. The profiles all show the high onland velocities. At the shoreline, or some distance seaward, the velocities decrease abruptly to values associated with the intermediate group, and remain at those values to at least the seaward limit of the ice-shooting data.

In most cases, the decrease in the near surface velocities occurs fairly near the coastline, as shown by the lines from Prudhoe Bay and Foggy Island Bay. A major exception is seen for the line on the Sagavanirktok River Delta where high velocities were observed to extend several kilometers beyond the limit of the delta. This offshore extension of high velocities occurs in the vicinity of all the major deltas in this study area.

In the Maguire Island region, in addition to the transition to the intermediate-velocity group at the shoreline, a velocity gradient also occurs on land. The higher land velocities decrease more gradually near the shoreline compared to the sharper transition seen in the other lines.



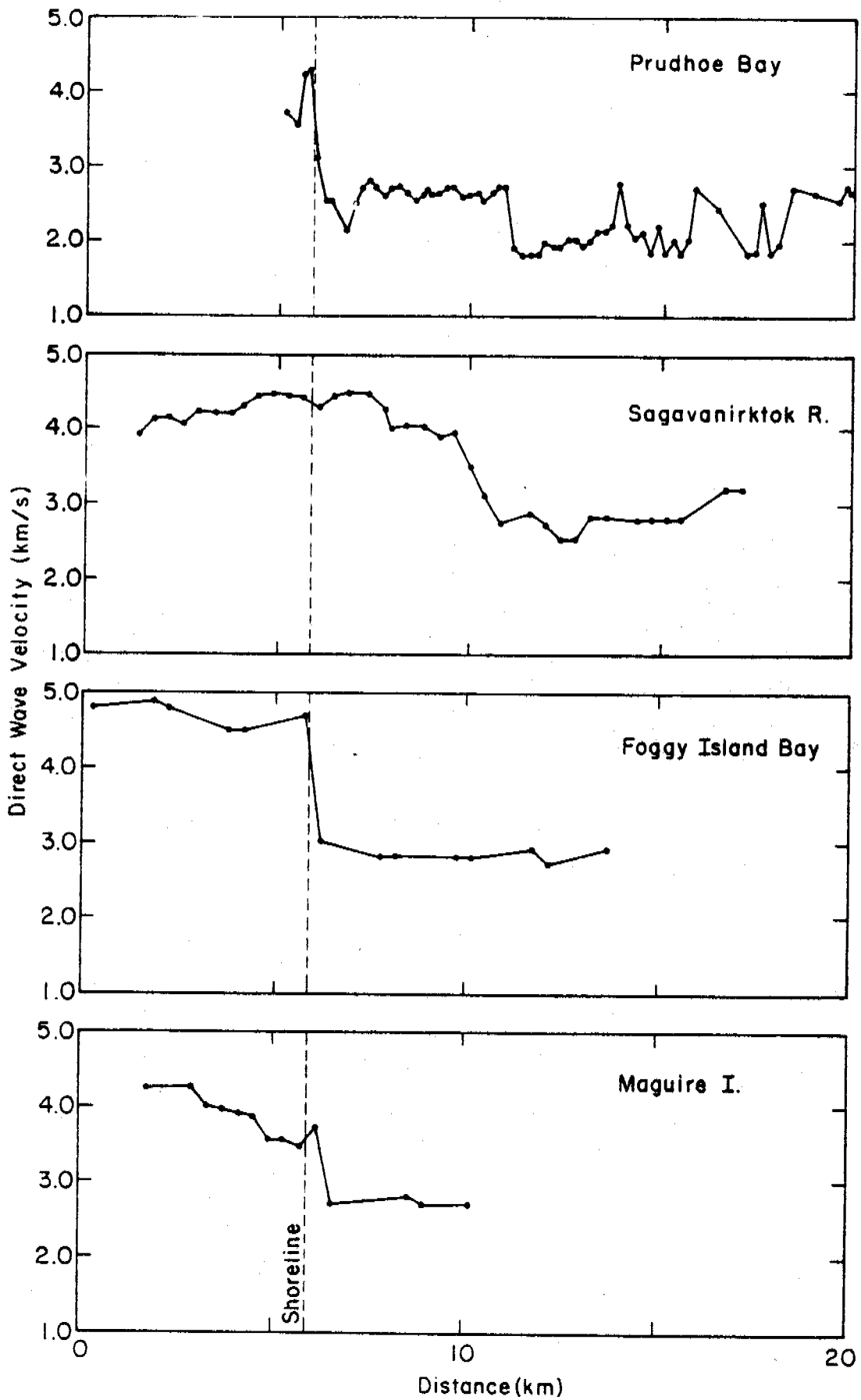


Figure 5. Typical direct wave velocity profiles selected from coastal lines in the current lease area.

The near surface velocity data from all of the lines was used to construct the velocity map for the upper part of the ice-bonded permafrost section shown in Figure 6. In general, the velocities shown on this map are average velocities for approximately the upper 100 m.

This map helps to illustrate the velocity contrast between the land and marine environment. It also shows the locations where onshore velocities begin to decrease prior to reaching the coastline. The onshore velocity zone in this region, which apparently is not greatly influenced by the marine environment, generally has permafrost velocities greater than 4.0 km/s. At locations where the on-land velocities decrease toward the coastline, velocities are between 3.5 km/s to 4.0 km/s. This zone also extends offshore, including the outer margins of major stream deltas and associated near-shore land masses such as Tigvariak Island. Areas where this zone occurs on land are characterized by the profile shown in Figure 5 from the Maguire Island area. The map also illustrates at least one area where the onland transition zone is absent, as indicated by the profile from Foggy Island Bay.

The middle-velocity zone occurs primarily offshore and ranges from 3.0 km/s to 3.5 km/s. The 3.0-km/s velocity contour generally follows the 1.0-m water depth contour, except in Prudhoe Bay where it does not extend that far offshore.

In the marine environment, the velocities from the ice survey data primarily fall within the 2.5-3.0 km/s range. Most of the offshore areas covered by this data are uniform with the exception of several lower-velocity zones. The largest and most continuous is a narrow zone inshore of the islands west of Brownlow Point. The other smaller zones on these data lines can be seen to the east of the Sagavanirktok Delta and the Kuparuk Delta. Only in several restricted areas were velocities lower than 2.25 km/s observed. Under some of the lower-velocity zones in the marine environment there apparently is high-velocity bonded permafrost, given the velocity structure data which will be discussed in the following section.

Velocity data was available from two offshore islands, Cottle Island in the western part of the area and Flaxman Island to the east. These islands both have higher velocities than the surrounding marine environment, with velocities in the 3.5 to 4.0 km/s range observed on Cottle Island. These values are similar to those in the transition belt along the coastline.

#### Velocity Structure

Refraction interpretation was used to obtain information on velocity structure in this area. In general, the structure in the offshore velocity data can be grouped into four general classes using the same sample lines discussed previously (Fig. 7). A common structure was a two-layer case with the underlying layer having high on-land velocities,

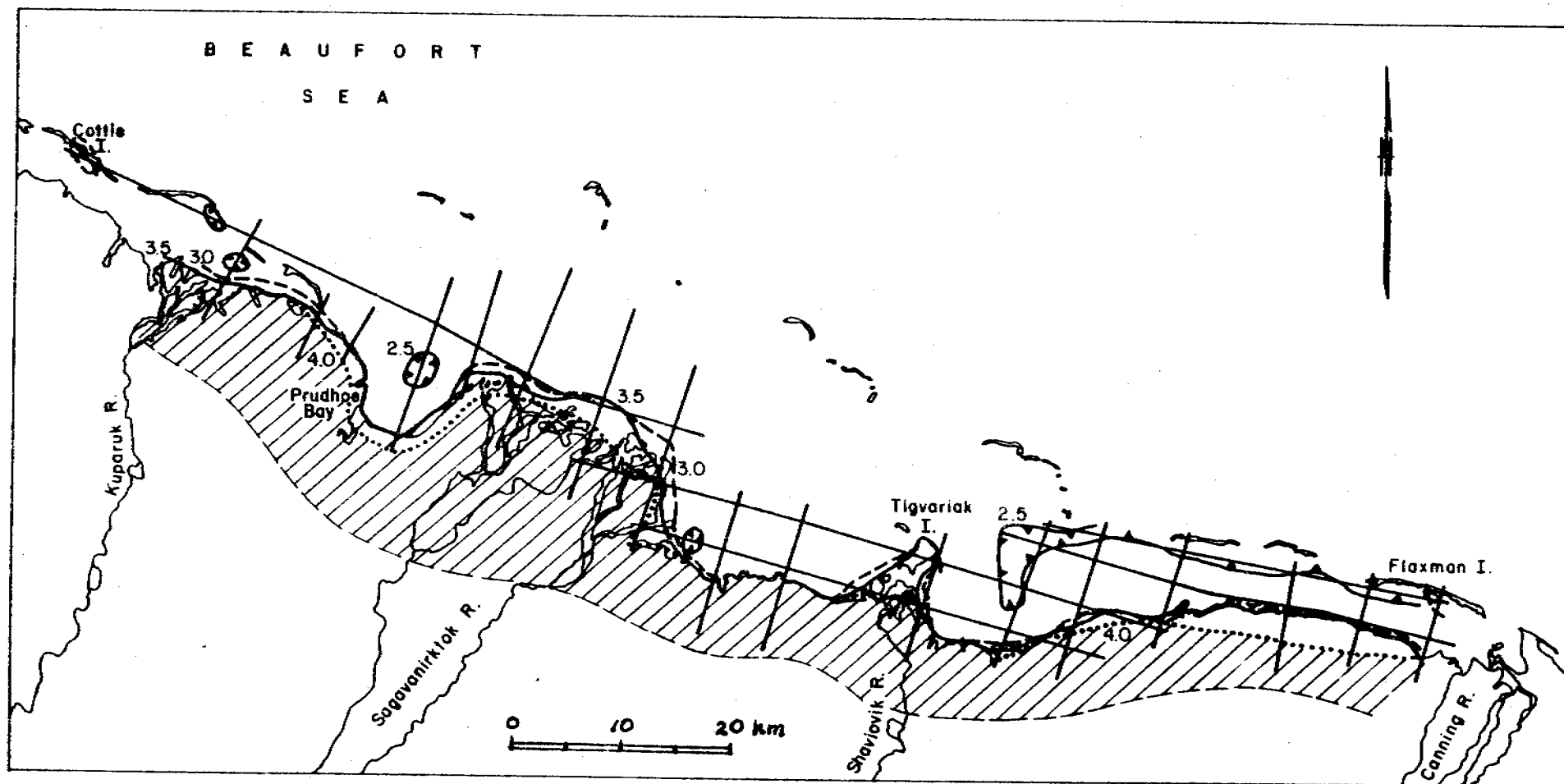


Figure 6. Contour map of direct wave velocities based on data from the seismic lines shown. Velocity contour values are in km/s, with a contour interval of 0.5 km/s. Velocities are greater than 2.5 km/s at the outer limits of the seismic lines except in local areas where they are shown to decrease to less than 2.5 km/s.

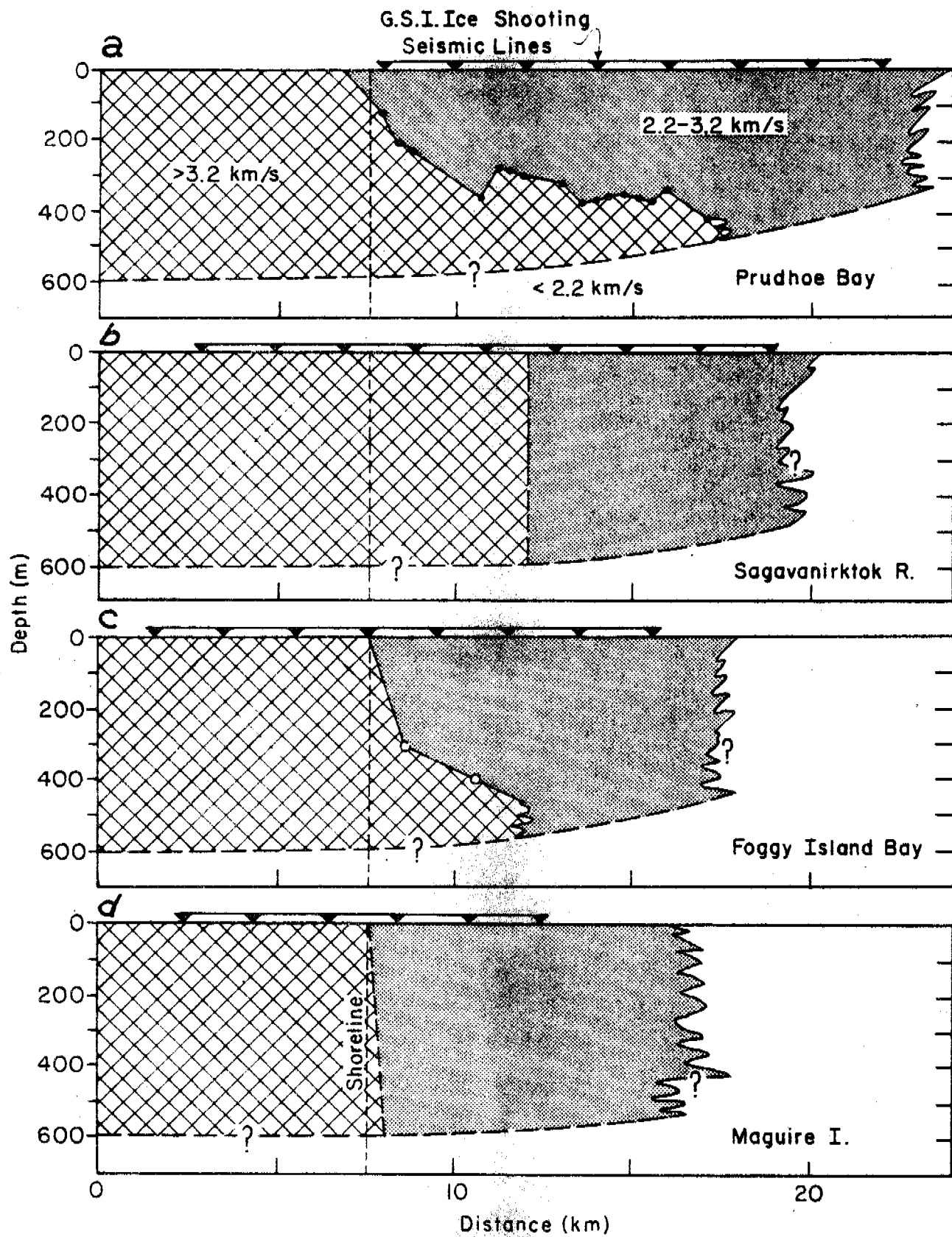


Figure 7. Typical velocity structure profiles selected from coastal lines in the current lease area.

it also has increasing depth seaward of the shoreline, (Fig. 6a) and the top layer having intermediate velocities. The depth to the higher-velocity second layer appears to increase offshore to as much as 400 m below the bed. This deeper high-velocity layer disappears with increasing distance from shore, leaving only the intermediate-velocity marine permafrost layer. An idealized drawing illustrating this type of structure is shown in Figure 8. In most cases, the near-shore transition to the lower-velocity marine permafrost appears to be rather abrupt. This layered case provides some information on the vertical limit of the bonded permafrost. Refraction analysis can normally provide thickness data only when velocities increase with depth. This case is not usual at the base of permafrost where the transition is from higher-velocity bonded permafrost to lower-velocity unfrozen materials. However, in this situation the bonded permafrost contains a higher-velocity layer, making it possible to at least obtain minimum thickness data. It appears that in much of this coastal zone where this structure occurs, bonded permafrost thickness must be greater than 350 to 400 m as far as 8 kilometers from the coastline.

The remaining three examples of the velocity structure found in the near-shore data (Figs. 7b,c,d) resemble each other except for the position of the velocity transition in relation to the shoreline. They also lack the extensive high-velocity second layer discussed in the previous example. In Figure 7b, the sharp transition from land to marine velocities occurs some distance offshore, a structure observed in the delta regions. The section shown in Figure 6c differs from the previous case in that the velocity transition occurs nearer the coastline. The contact between the two structural units also has a more gentle seaward slope than was noted in the previous case. The last example (Fig. 7d) is similar to Figure 7c except that the higher land velocities begin to decrease prior to reaching the coastline. In all of the seismic lines typified by these examples, the velocities normally associated with bonded permafrost apparently extend past the seaward end of the survey lines.

Our analysis permitted construction of the offshore velocity structure map shown in Figure 9. The shaded zones show the distribution of the velocity structure types just discussed and include: 1) the single layer of high-velocity bonded permafrost ( $> 3.2$  km/s) usually associated with most ice-saturated sediments found on land in areas of cold permafrost, 2) the offshore two-layer structure with intermediate velocities over a layer of high-velocity permafrost, and 3) the single layer of low-velocity bonded permafrost (velocity in the intermediate-velocity range between approximately 2.2 km/s and 3.2 km/s).

#### Maximum Velocity Data from the Marine Records

A contour map of maximum first-return velocities for the deep water area is shown in Figure 10. In general, the velocities are all very similar and fall into the low-velocity group between 1.6 and 2.2 km/s.

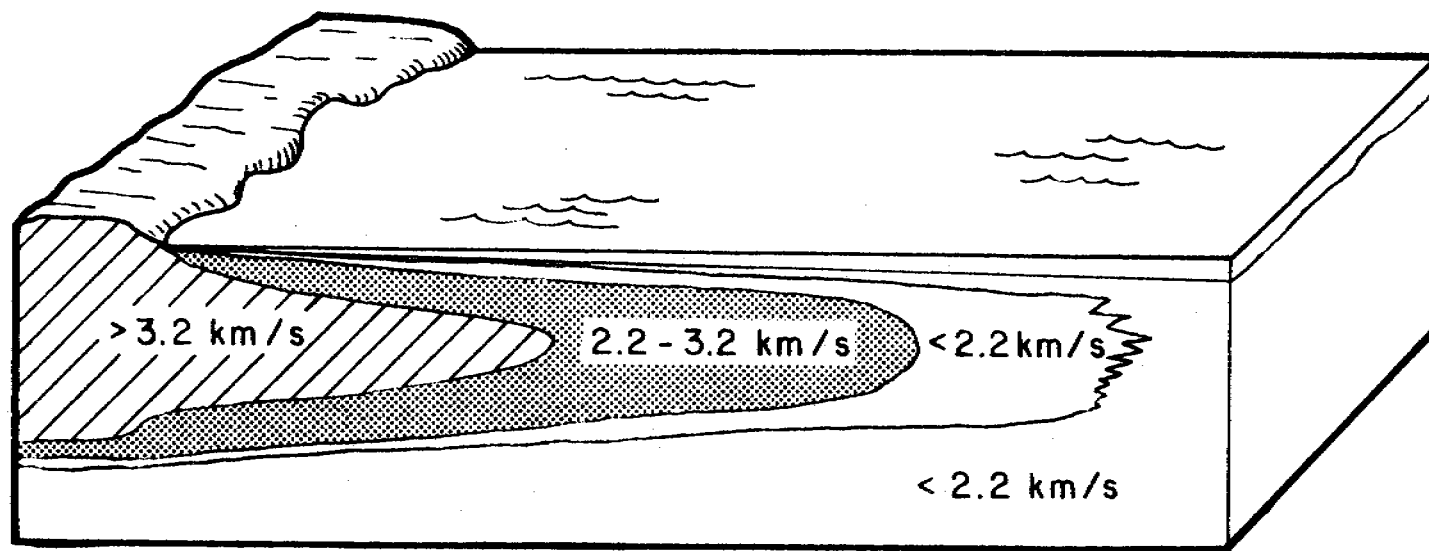


Figure 8. Idealized illustration of velocity distribution in offshore permafrost as controlled by temperature alone. The  $< 2.2$  km/s material outside of the permafrost lobe is thawed material above  $0^{\circ}\text{C}$ , while the similar velocity zone within the lobe is material below  $0^{\circ}\text{C}$  but warm enough to be very poorly ice-bonded and not detectable by the seismic technique.

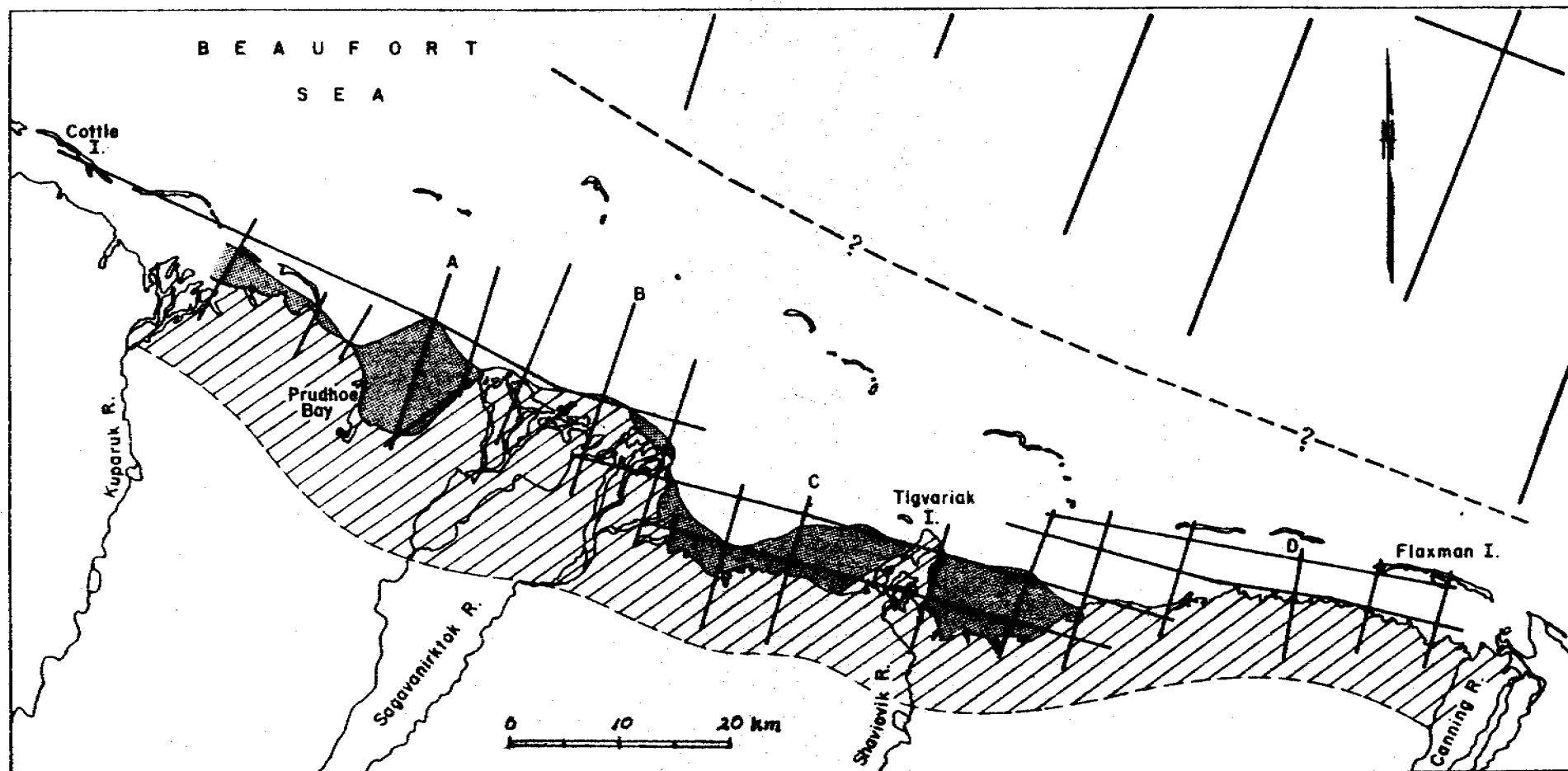


Figure 9. Velocity structure map showing three major structural units. The lined unit is a single layer of high velocity bonded permafrost  $> 3.2$  km/s, shaded area consists of two layers 2.2-3.2 km/s marine permafrost over higher velocity  $> 3.2$  km/s permafrost. The offshore plain area at least out to the limits of the coastal seismic lines, is a single layer with velocities between 2.2-3.2 km/s. Marine seismic lines are shown in the upper part of the figure. Their low velocities suggests that bonded permafrost terminates somewhere between the two sets of seismic data. The dashed line indicates the uncertain offshore limit of bonded permafrost.

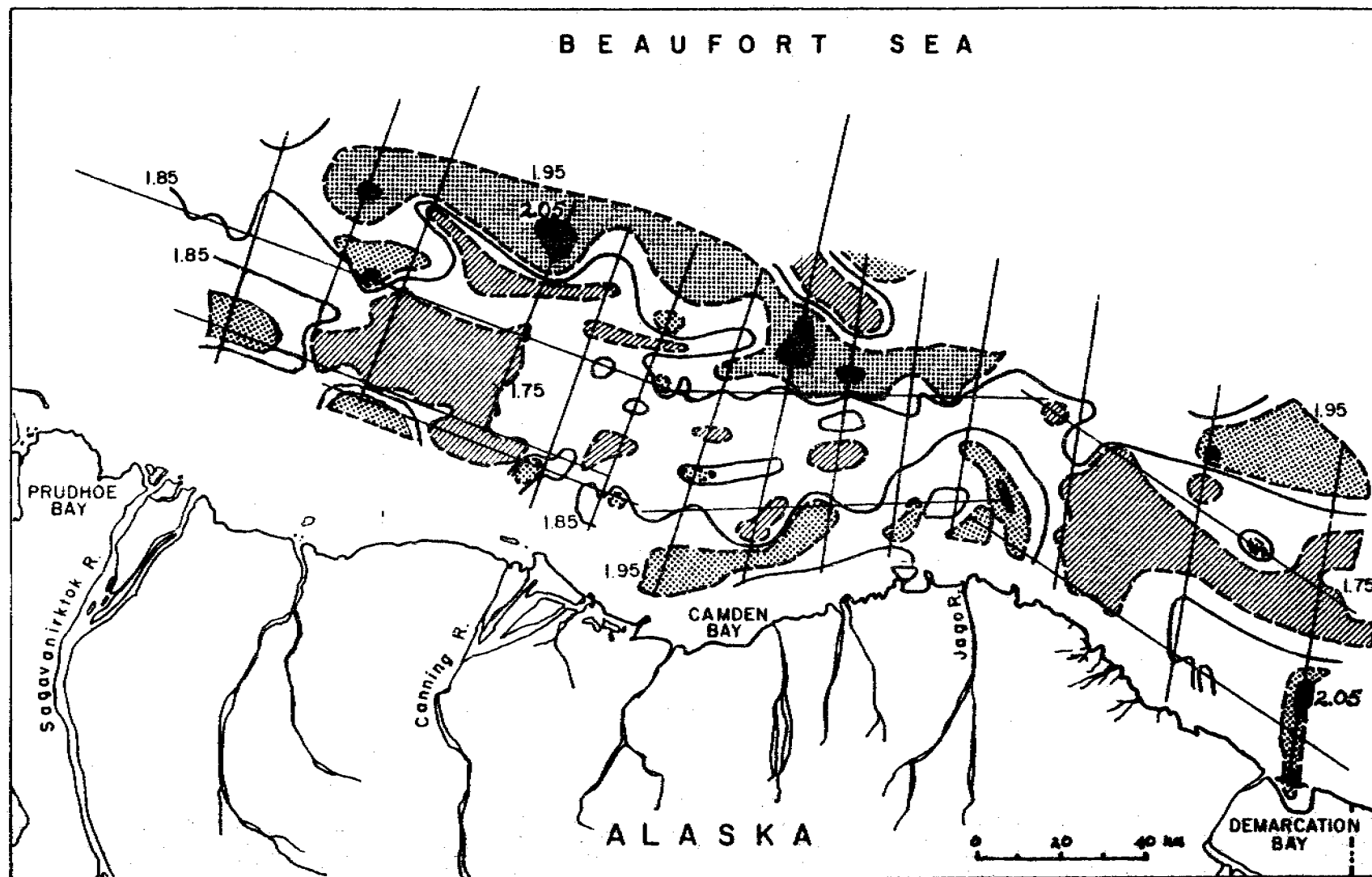


Figure 10. Contour map of maximum marine velocities. Velocity contour values are in km/s, with a contour interval of 0.10 km/s.



The lowest velocities in this area occur along a band through the central part of this region. Even though there appears to be some pattern to the velocities, it is felt that no significance can be attributed to the grouping at this time. The velocities observed in this area are too low for any significant ice bonding of the sediment in the upper part of the section.

#### Surface Wave Analysis (Rayleigh Velocities)

For the limited amount of near shore ice survey data for which surface wave velocity determinations were possible, a histogram of these values was prepared (Fig. 11). The velocities fall into two distinct groups. The lower group (0.1 - 1.1 km/s) corresponds to the range for all types of shallow unconsolidated sediments reported in the summary by Malotova and Vassilev (1960). Hamilton (1971) lists shear velocities for clay, silt, and sand in the 30 - 534 m/s range. Accordingly, most of the sediments in this low-velocity group can be interpreted as lacking ice-bonding. The highest velocity group represents values more usually associated with consolidated or ice-bonded sediments.

Values that fall in the low-velocity group are invariably found in the offshore segments of the velocity profiles. These low-surface-wave (Rayleigh wave) velocities can be associated with the same sediments which gave the low-velocity group of compressional waves observed by Rogers and Morack (1978) for the thaw zone above ice-bonded sediments in the Prudhoe Bay vicinity.

An attempt to map the zone containing thaw above the ice-bonded permafrost using this data was hampered by the fact that less than half of the records have readable surface-wave signals. However, as mentioned, low-frequency noise in the reflection part of the record was interpreted to be scattered waves in the thaw layer. Therefore, mapping the low-frequency noise distribution (Fig. 12) yields additional data on the presence of the surface thaw above the ice-bonded permafrost. The resulting map suggests that none of the mainland has significant thaw above the ice-bonded permafrost. It also indicates that several areas offshore also do not appear to have significant thaw, (> 25 m) including the shallow water offshore of the deltas and islands near the deltas. All four barrier islands intersected by seismic lines, as well strips on the lee of each island, appear to lack a significant surface thaw zone.

According to this analysis two areas have anomalous results which cannot be explained by the present bathymetry. The entrance to Prudhoe Bay, north and east of Gull Island, contains a mixture of the two types of records. Part of a line in Mikkelsen Bay shows this same variability. These locations, as a result, do not fit the general pattern that emerged elsewhere in the study area, i.e., thaw zones above bonded permafrost occurring where the water was more than a meter deep. Blouin et al. (1979) found that shoals near Gull Island influenced the shallow temperature regime, with unexplained decreases in sediment temperatures near the

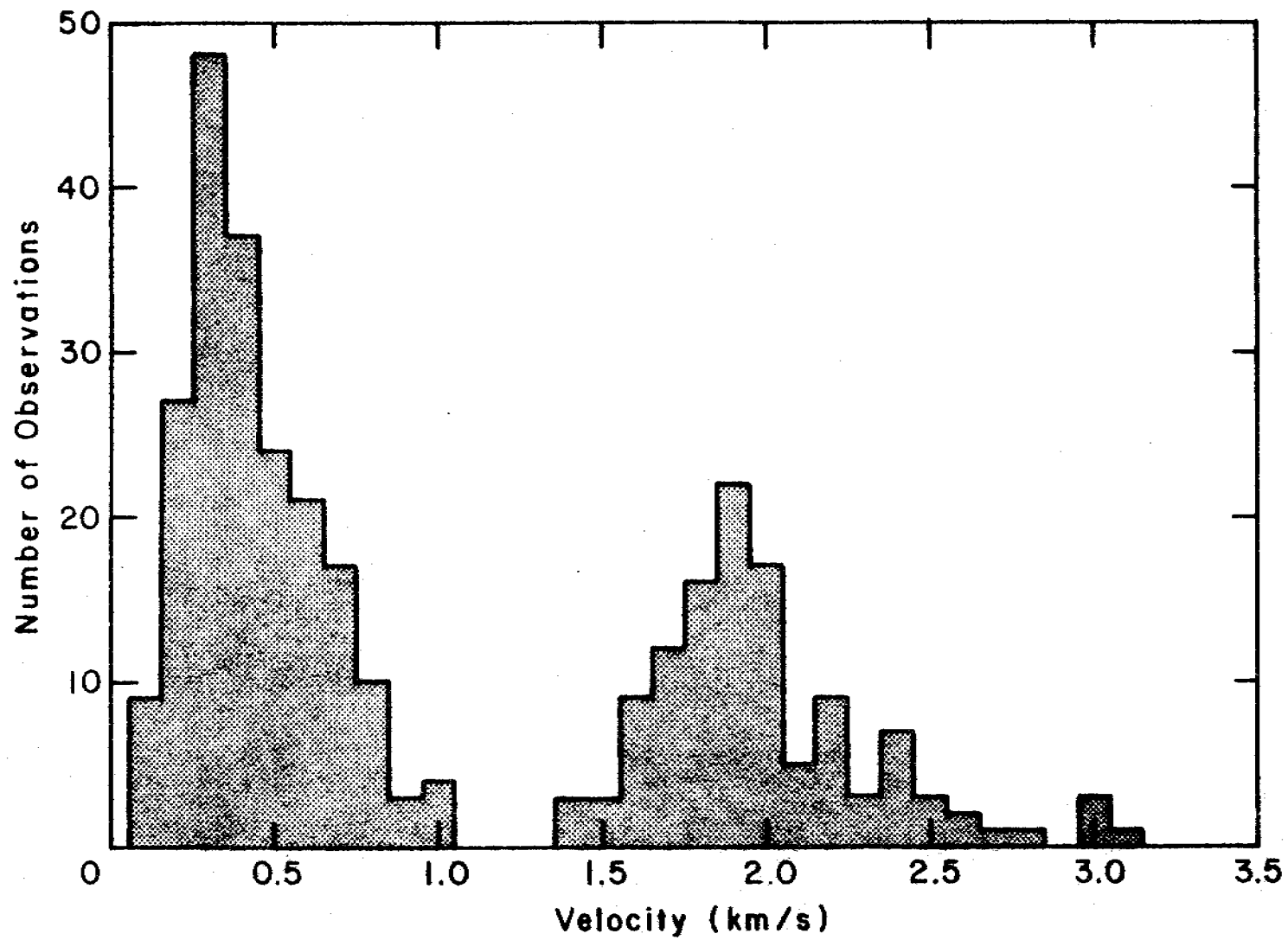


Figure // Histogram of surface wave (Rayleigh) velocities from the coastal lines.

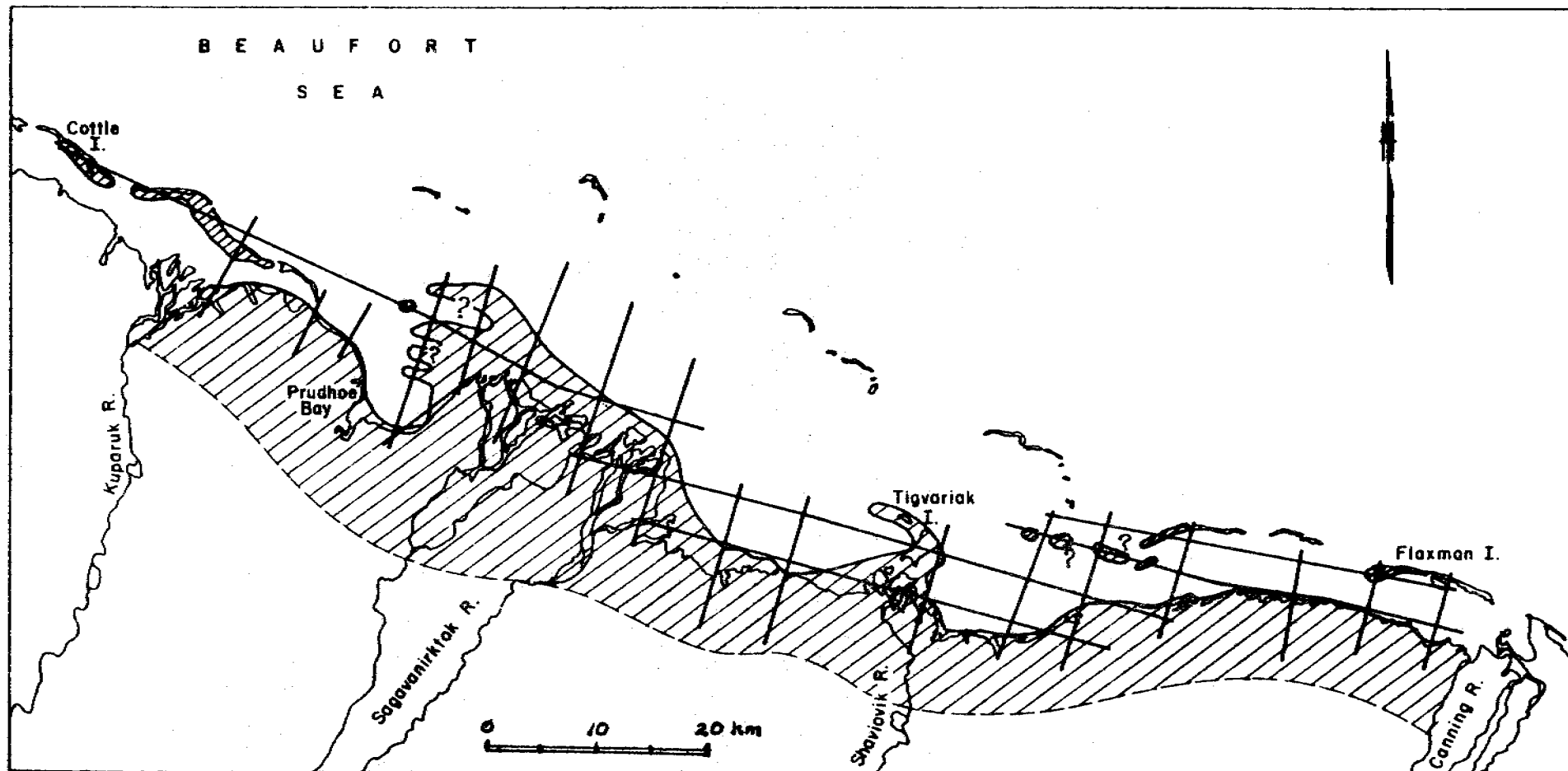


Figure 12. Map of low-frequency noise distribution. The lined zone was free of low-frequency noise in the reflection part of the records and was interpreted as being an area where minimum thaw depths occur above bonded permafrost.

Sagavanirktok Delta. It was suggested that low sediment temperatures north of Niakuk Island may be linked with shoals that have been recently destroyed. It is possible that the two anomalous areas outlined by the surface wave study may be linked to recent changes in the water depth in these regions. This would suggest that a large area of shallow water may have once extended to the north-west from the Sagavanirktok River delta much farther than at present, and the barrier islands may have extended further west from Maquire Islands toward Tigvariak Island.

### Hyperbolic Reflections

Hyperbolic reflections are a common feature on oil exploration marine seismic records from the Beaufort Sea. They were also found in abundance by Reimnitz et al. (1972) in their sub-bottom seismic profiles. These reflections have a two-fold significance in both types of seismic observations. First, they constitute a noise problem. The sub-bottom profiles from the Prudhoe Bay area can be saturated with hyperbolas. Structural features that may be present in the sediments are obscured completely by these reflections. Some oil industry records, similarly saturated with hyperbolas, would require considerable expensive enhancement if they were to be studied for geological structures. Consequently, it is of some economic interest to understand these signals so they can be eliminated from marine seismic records.

The second reason for examining the hyperbolic reflections is their potential significance. They must be caused by anomalies in the density or elastic properties of the sediments. Two possible causes were mentioned by Reimnitz et al. (1972): massive ice and erratic boulders. They felt that massive ice was the most probable cause from the evidence available. Rogers and Morack (1978) added gas pockets to the list of possible sources. It remains important to find the cause of these anomalies to assess the hazards to construction projects or drilling operations.

We examined these features; the evidence to date suggests that they are probably generated by anomalies that occur in the top few meters of the seabed and may be related to changes in bed properties caused by ice gouges. The complete results of this work will be available this coming quarter as a draft CRREL report.

### VIII. Conclusions

The velocity profiles and velocity structure map (Figs. 6 and 9) both suggest that the distribution of offshore bonded permafrost is extremely extensive; evidence indicates that it occurs along all the lines that were part of the ice-shooting survey. Bonded permafrost is assumed to exist when velocities in this region are greater than 2.25 km/s. As noted earlier, this velocity limit should provide an estimate of the minimum extent of bonded permafrost. Materials that contain some ice or have temperatures slightly lower than 0°C may be far more widely distributed than is indicated by this seismic approach.

These conclusions are supported by the data from the land-sea transition. In this region, logical changes in permafrost velocities occur that could be related to the temperature contrasts between the two environments. The results of the recent subsea permafrost investigations based on drilling activities also support the widespread distribution of the bonded permafrost.

In addition to the information on permafrost distribution, the seismic data analysis also appears to provide regional information on coastal processes. Comparison of the velocity structure and the surface velocity map indicates variations in velocity patterns along the coastline that could be related to differences in historical coastal erosion and transgression patterns.

A noticeable feature of the velocity structure data (Figs. 9) is the offshore zone which contains velocity layering. The layering helps to establish a limit on minimum thickness of ice bonded sediments. The top of the refracting layer, which occurs at around 300 to 400 m below the seabed, indicates that permafrost at least this thick extends more than 8 km offshore where this type of velocity layering is observed. If this layer can be attributed to changes in properties due to temperature differences in the permafrost, transgression rates in this region may have been high enough that thermal modification of the deeper sediment has not kept pace with the rapid transgression. However, the structure may also be related to material types with inherently higher velocities occurring at depth.

If temperature differences within the sediments have a dominant influence on velocity, the region with higher velocities at depth can be contrasted to adjacent areas where no obvious velocity structure is observed offshore. The lack of velocity structure could indicate that the rate of coastal retreat is much lower in these zones, permitting thermal modification of the deeper marine permafrost to keep pace with the slower transgression.

This hypothesis, that variation in offshore velocities in a region dominated by thick sections of sediment may be strongly related to variations in temperature, appears to be supported by comparison of the surface velocity and velocity structure map. The surface velocity map, as mentioned earlier, shows a discontinuous on-land lower-velocity belt that parallels the coastline. For the most part, this belt is absent or narrow along sections of the coastline where the velocity structure indicates extensive offshore distribution of the deep high-velocity second layer. This could indicate that coastal erosion is rapid enough in the zone with a second layer that onshore permafrost is not significantly warmed.

In contrast, in areas where the velocity structure does not occur offshore, a velocity transition exists on land. This could imply longer stability or lower transgression rates in these areas that permit the marine environment to modify the onshore permafrost temperatures.

The low-velocity zone inshore of the islands in the eastern part of the study area probably does not represent the ultimate seaward extent of bonded permafrost. This supposition can be supported by the observations made during the subsea permafrost study sponsored by the Conservation Division of the USGS, which reported bonded sediments as little as seven meters below the seabed on the seaward side of these islands (USGS Contract report 1979).

Unfortunately, the exact offshore limit of the bonded permafrost could not be precisely determined from this study because of the gap in records between the ice shooting and offshore marine records. Emphasis is now being placed on attempting to acquire data in these gaps. The marine data, shown in Figure 10 for the region offshore from the lease area and extending to near the Canadian border, indicates the low velocities associated with this region. The velocities for this entire region are between 1.6 and 2.1 km/s: values low enough to be considered representative of unfrozen material. In contrast, nearly all the data from the ice-shooting lines contained velocities associated with ice-bonded sediment.

Only additional detailed drilling data will determine if the velocity patterns observed along the coast are related to variations in permafrost temperatures, regional differences in the materials that make up the permafrost section, or some combination of these controlling parameters.

#### IX. Summary of 4th Quarter Operations

##### A. Laboratory Activities

This quarter was spent completing the necessary data analyses and preparing the following two reports for publication as part of the CRREL report series.

(1) Information on Subsea Permafrost Distribution from Seismic Data Interpretation - U.S. Beaufort Sea, by K.G. Neeve, P.V. Sellmann, and A. Delaney.

(2) Hyperbolic Reflections on Beaufort Sea Seismic Records, by K.G. Neeve.

Samples were also received from the USGS Conservation Division drilling program. Analysis of these samples will be during the next quarter.

B. Significant Problems - none.

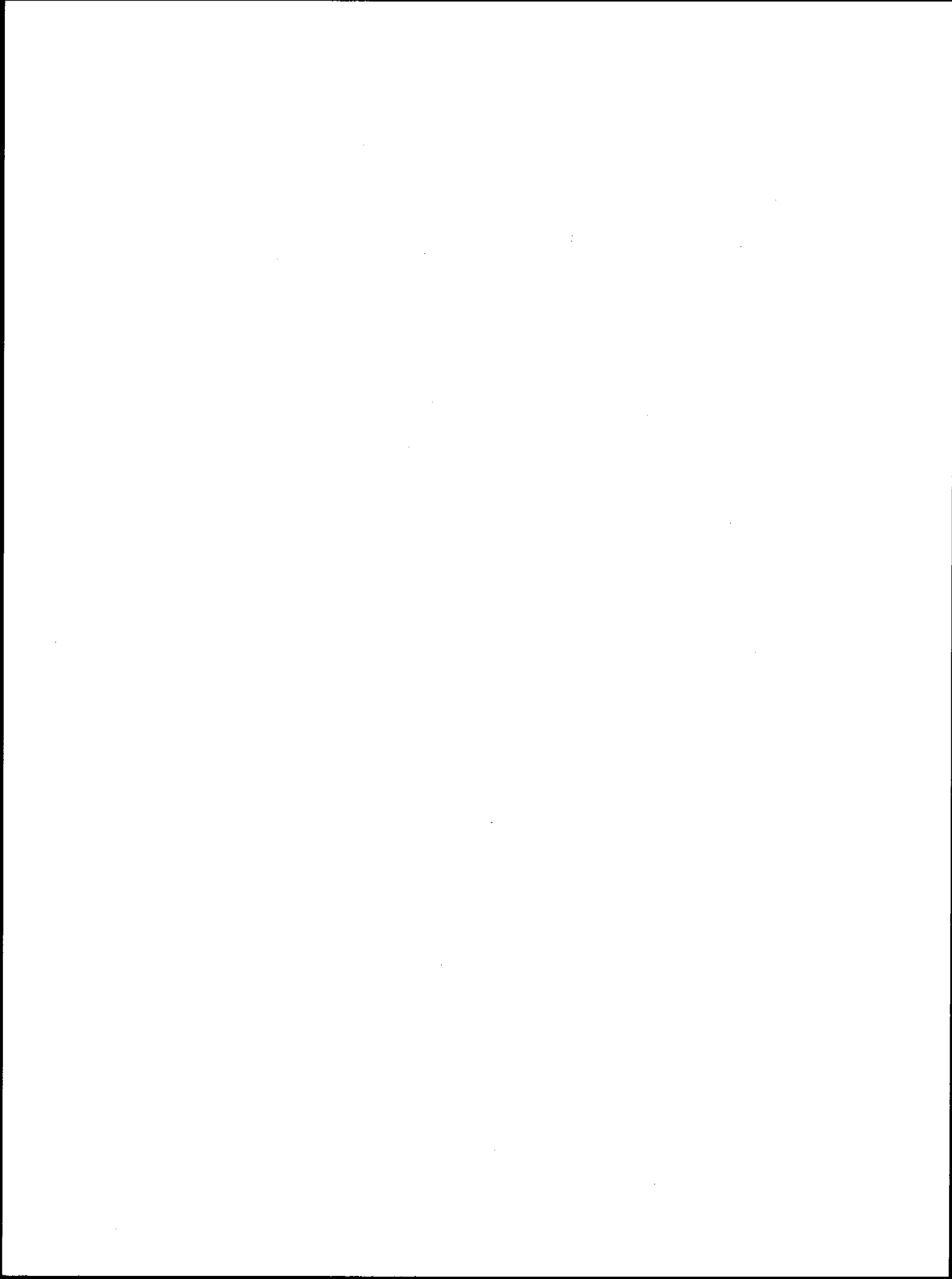
C. Estimate of Funds Obligated. As of 31 March a total of 20 K of this year's funds have been obligated.

## References

1. Aptikaev, F.F., 1964, Temperature field effect on the distribution of seismic velocities in the permafrost zone: Akad. Nauk SSSR Sibjrskoe otd-ie. Inst. Merzlotovedeniia. Teplovye protsesy v merzlykh porod.
2. Blouin, S.E., E.J. Chamberlain, P.V. Sellmann and D.E. Garfield, 1979, Penetration tests in subsea permafrost, Prudhoe Bay, Alaska, USACRREL Report 79-7, 45 p.
3. Ewing, W.M., W.S. Jardetzky and F. Press, 1967, Elastic Waves in Layered Media, McGraw-Hill, New York, 380 p.
4. Hamilton, E.L., 1971, Elastic Properties of Marine Sediments, Jour. Geophysical Res., Vol. 76, No. 2, p. 579-604.
5. Howitt, F., 1971, Permafrost geology at Prudhoe Bay: World Petroleum, v. 171, no. 4, p. 28-38.
6. Hunter, J.A., A.S. Judge, H.A. MacAulzy, R.M. Gagne, R.A. Burns and R.L. Good, 1976, The study of frozen seabed material in the Southern Beaufort Sea: Technical Report No. 22, Beaufort Sea Environmental Project, Environment Canada, Victoria, British Columbia.
7. Hunter, J.A., K.G. Neave, H.A. MacAulay, and G.D. Hobson, 1978, Interpretation of sub-sea bottom permafrost in the Beaufort Sea by seismic methods, Part 1: Seismic refraction methods: Proc. of the Third Inter Permafrost Conf. Vol. 1, p. 514-520.
8. Malotova, L.V. and Vassilev, Y.I., 1960, Velocity Ratio of Longitudinal and Transverse Waves in Rocks, Part II, EZV. Geophysical Series, p. 1097-1116.
9. Nakano, Y. and N.H. Froula, 1973, Sound and shock transmission in frozen soils. Proc. 2nd International Conf. on Permafrost. North American Contribution, Nat. Acad. Sci. Washington, p. 359-368.
10. Reimnitz, E., S.C. Wolf, and C.A. Rodeick, 1972, Preliminary Interpretation of Seismic Profiles in the Prudhoe Bay Area, Beaufort Sea Alaska USGS Open-File Report 548, 11p.
11. Rogers, J.C. and J.L. Morzck, 1978, Geophysical investigation of offshore permafrost at Prudhoe Bay, Alaska, Proc. Third Int. Conf. on Permafrost, Vol. 1, p. 560-566.
12. Sellmann, P.V. and E.J. Chamberlain, 1979, Permafrost Beneath the Beaufort Sea near Prudhoe Bay, Alaska, Proc. of the Eleventh Offshore Technology Conference, Vol. 3.

13. Sherwood, J.W.C., 1967, Refraction along imbedded high speed layer, In: Seismic Refraction Prospecting, Published by Society of Exploration Geophysics, p. 138-151.
14. USGS, Contract Report, 1979, Geotechnical Investigations, Beaufort Sea, conducted by Harding-Lawson Associates for the Conservation Division of the USGS. USGS data set AK-17718, Vol. 1-3.





Annual Report Task D-9  
Research Units 204 and 473  
April 1979 to March 1980

OFFSHORE PERMAFROST STUDIES AND SHORELINE HISTORY  
AS AN AID TO PREDICTING OFFSHORE  
PERMAFROST CONDITIONS

Prepared by

P. A. Smith, R. W. Hartz and D. M. Hopkins  
U.S. Geological Survey  
345 Middlefield Road  
Menlo Park, CA 94025

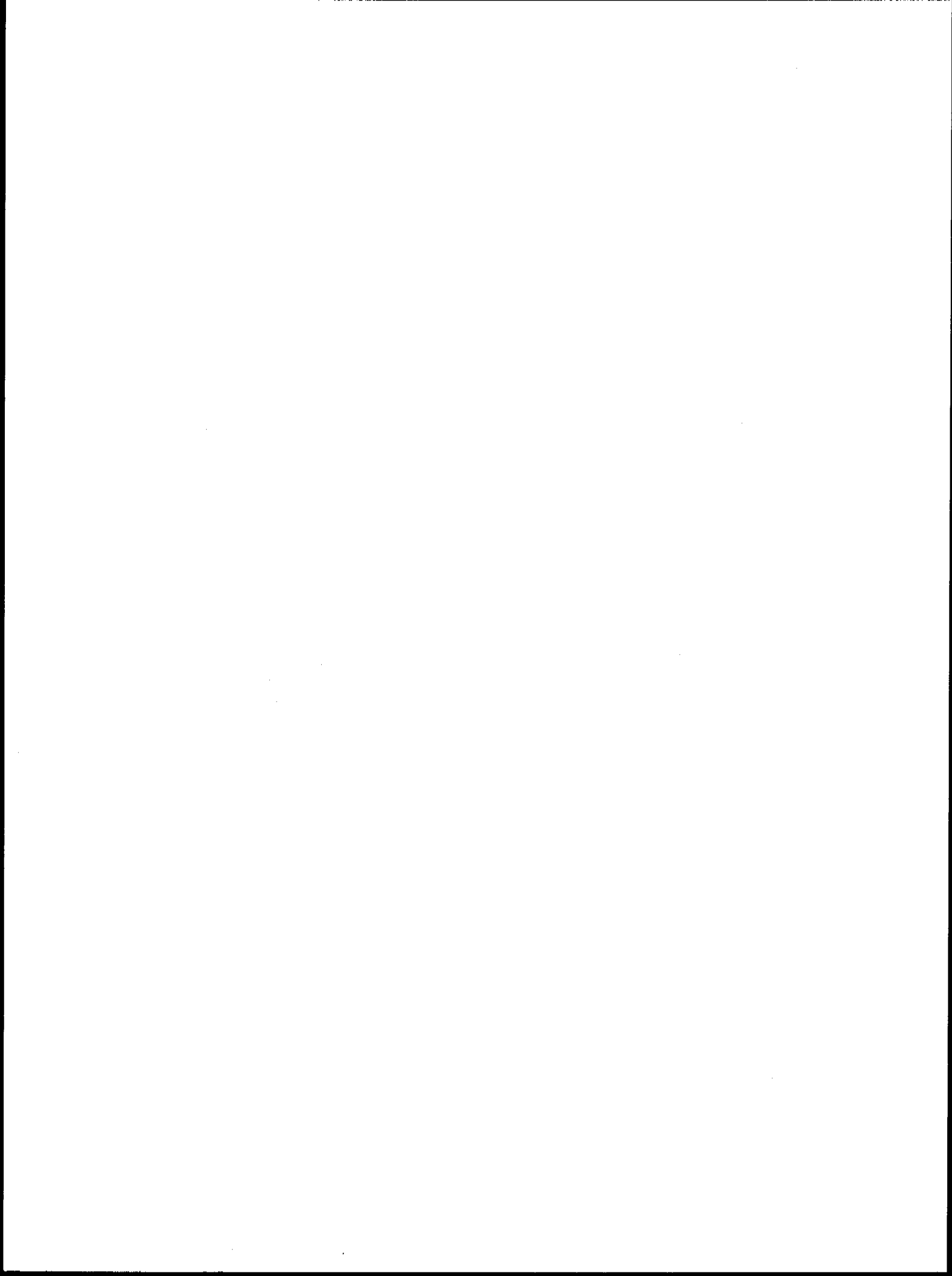


TABLE OF CONTENTS	PAGE
Summary -----	162
Introduction -----	163
Results and discussions -----	164
Summary of quarterly activities, January-March 1980 -----	166
Appendices:	
A. A review of offshore permafrost studies, Beaufort Sea, Alaska, 1976 to 1980, by R. W. Hartz and D. M. Hopkins -----	167
B. Coastal morphology, coastal erosion, and barrier islands of the Beaufort Sea coast, Alaska, by D. M. Hopkins and R. W. Hartz-----	178
C. Geological cross sections, by R. W. Hartz and D. M. Hopkins-----	182
D. Likelihood of encountering permafrost in submerged areas of northern Bering Sea, by D. M. Hopkins -----	187
E. Radiocarbon dates from the Beaufort and Chukchi Sea coasts (1979-80), by D. M. Hopkins, S. W. Robinson, and J. Buckley-----	203
F. Ostracodes from 1977 offshore boreholes in the Beaufort Sea, by Elisabeth M. Browsers -----	221
G. Microfossil studies of Pelukian and Flaxman deposits, Alaskan coast of Beaufort Sea, by D. M. Hopkins, Kristin McDougall and Elisabeth Browsers -----	230
H. Extinct and extra-limital mollusks in Pelukian deposits of Kogro River and Eskimo islands, by D. M. Hopkins and Louie Marincovich -----	240
I. Identified fossils from the Flaxman Formation, by J. T. Dutro, Jr.	246
J. The Flaxman Formation of northern Alaska: Record of Early Wisconsinan shelf glaciation in the high Arctic?, by D. M. Hopkins -----	248
K. Discrepancy in correlation of transgressive marine deposits of Alaska and the eastern Arctic, by D. M. Hopkins and L. D. Carter	250
L. Application of amino acid geochronology to deposits of the Arctic Coastal Plain, Alaska: Preliminary results and implications, by J. K. Brigham, D. M. Hopkins, L. D. Carter and G. H. Miller-----	252
M. Summary bibliography for year ending March 1980 -----	254

## SUMMARY

By integrating information obtained from the 1976, 1977, and 1979 offshore boreholes in the Prudhoe Bay/Beaufort Lease area, a reasonably detailed picture of the offshore stratigraphy and permafrost characteristics has been made possible. This information has been compiled as a series of maps and cross sections showing location of paleovalleys, depth and thickness of offshore permafrost and distribution and thickness of Holocene sediments.

Using both offshore and onshore work, sources of sand and gravel fill have been identified, and rates of coastal processes have been calculated. Radiocarbon dates received in the past year have provided rates of growth of ice wedges and thaw lakes, and ages of both fluvial and coastal terraces.

Microfossils from boreholes PB-1 through PB-8 are being re-examined and a USGS Open-File Report on the stratigraphy and paleontology of the Prudhoe Bay area as interpreted from these boreholes is being prepared,

Identifications of foraminifera and ostracodes from exposures along the Beaufort Sea coast from Cape Simpson to the Canning River have enabled us to characterize the microfauna of the Pelukian and Flaxman deposits. Identifications of mollusks collected in 1977 and 1978 along the Beaufort Sea coast have also been completed.

Some of the other activities that have overlapped with these projects, or have been outgrowths of our research are:

1. A study completed in 1975 by D. M. Hopkins on the recency of fault movement and frequency of eruptions on the Pribilof Islands. Improvements in the K/Ar geochronology of the islands proved unsuccessful.
2. A study of the Yukon Delta by W. Dupre undertaken from 1975 to 1979.
3. A report by D. M. Hopkins on the likelihood of encountering permafrost in Norton Sound, included in this report as Appendix D.

4. The organization of a Wenner-Gren Foundation symposium on the paleoecology of Beringia by D. M. Hopkins and others in 1979. A volume of papers that grew out of this symposium will be published in 1981.

5. The supervision of four doctoral candidates by D. M. Hopkins, and the provision of partial financial support for two of them. The students and their topics are:

- a) Pat Anderson: Late Quaternary palynology of northwestern Alaska
- b) Julie Brigham: Stratigraphic and amino acid studies at Skull Cliff
- c) R. E. Nelson: Paleoecological studies on NPRA
- c) Lee Porter: Vertebrate paleontology of Lost Chicken Mine

6. D. M. Hopkins is also a member of the U.S. National Committee/INQUA, Committee on New Initiatives for Cooperative Studies in Earth Science with the USSR, and the Geologic Names Committee, to name a few.

#### INTRODUCTION

Research units (R. U.) 473 and 204 have been closely tied together in an attempt to delineate the distribution and characteristics of offshore permafrost on the Beaufort Sea shelf, to identify possible sources of sand and gravel fill, and to determine the nature and rates of coastal processes in the arctic.

R. U. 204 is dedicated to the study of offshore permafrost studies through the drilling and examination of core samples from boreholes in the Beaufort Sea lease area. Detailed stratigraphic logs have been compiled for each borehole, and materials that are frozen, overconsolidated, or show other signs of disturbance are noted. Suitable core segments are sub-sampled for microfossil and mollusk examination, pollen studies, radiocarbon dating, and granulometry studies, all of which aid in a better understanding of the age and nature of the sediments encountered during drilling. Seismic and thermal information from other investigators (R. U. 105, 253, 271) is also utilized by this project in determining the thickness

of and depth to permafrost and in mapping paleo-drainages of major coastal rivers across the Beaufort Sea shelf.

R. U. 473 is involved with the study of coastal exposures along the Beaufort Sea from the Canning River to Point Barrow, and the Chukchi Sea from Barrow to Icy Cape. The work involves excavation of sections in coastal bluffs and fluvial terraces near the coast, then sampling these exposures for microfossil analysis radiocarbon dating, mollusk and bone identification, and grain size analyses. Mollusk collections from modern beaches have also been made in an attempt to define the living fauna in the arctic regions of Alaska. Driftwood lines along estuaries and bluffs were mapped in 1977 and 1978 to determine storm surge limits. Air photo and map analyses have been made to determine rates of coastal erosion and barrier island migration. During 1979 our attention has been focused especially on information provided to us on samples collected along the Beaufort Sea coast during 1977 and 1978. Much of the information available from this research unit is used in interpreting the offshore sedimentary sequence exposed by our boreholes.

#### RESULTS AND DISCUSSIONS

Results of our work over the past year have been so diverse that they have been written up as individual reports presented as appendices to this annual report instead of being presented in this section. The first three appendices represent our major accomplishments. Appendix A summarizes our information on offshore permafrost and presents maps showing the study area and locations of the probe holes and boreholes, as well as distribution of Holocene sediments and paleo-drainages. B discusses coastal morphology and processes involved in beach erosion and barrier island migration. C is a compilation of offshore cross sections showing thickness of sediments and depth to bonded permafrost as interpreted from borehole and probe hole data.

Appendix D is a report on the likelihood of encountering permafrost in Norton

Sound, prepared for NOAA by D. M. Hopkins, and E is a listing of all radiocarbon dates which have been received this past year, with a short discussion of their significance to our studies.

Appendices F through I present results of paleontological studies of borehole and coastal samples. F. presents tables of preliminary ostracode identifications received this year from boreholes PB-5 through 8, and a short discussion of their paleoecological significance. Location of samples may be obtained from Appendix I of the 1979 Annual Report for R. U. 204 and 473. It should be noted that both the ostracodes and the foraminifera from boreholes PB-1 through 8 are being carefully re-examined in preparation for inclusion as part of a USGS Open-File Report on the stratigraphy and paleontology of the Prudhoe Bay area. Appendix G presents microfossil identifications from two critical coastal bluff exposures (Cape Simpson and Drew Point) and from several smaller exposures along the Beaufort coast from Cape Halkett to the Canning River. Microfossil identifications have proven to be very useful in distinguishing the Flaxman Formation from Pelukian and Holocene deposits along the coast. Appendix H discusses the significance of several species of mollusks collected along the Beaufort Sea coast during 1977 and 1978. Appendix I contains two paleontological reports on fossils collected from a large dolomite boulder found in a Flaxman Formation exposure near Brownlow Point in 1977. It is hoped that identification of the fossils would help to define the source area for the Flaxman boulders by allowing us to examine areas in Canada and Alaska where similar lithologies and fossils are present. However, we can only say so far that the dolomite is probably of Silurian age. A K/Ar date from Flaxman granite was obtained recently by S. Naidu, and it shows that the granitic rocks of the Flaxman are Precambrian.

Appendices J, K, and L are abstracts that have been recently published. J is an abstract of a talk presented by D. M. Hopkins at the Pacific Science Congress



in Khavorvsk in August 1979. Appendices K and L provide the first interpretive results of amino acid racemization studies on shell samples submitted from the Arctic Coastal Plain.

Appendix E is a summary list of all publications published, in press, or submitted for publication this year.

#### SUMMARY OF QUARTERLY ACTIVITIES, JANUARY-MARCH 1980

No field activities were undertaken this quarter. Instead, we (D. M. Hopkins, R. W. Hartz, S. Pounder, and P. A. Smith, all of the U.S. Geological Survey, Menlo Park, CA) spent the time preparing and submitting samples for radiocarbon dating, microfossil examination, and clay mineralogy and granulometry studies. At this time, approximately 85 percent of the core samples from the 1979 offshore boreholes have been submitted for analysis. Preliminary results on the forams in the highest priority borehole have just been received, but are not yet ready for publication. They will be included in the next quarterly report. Sub-samples of 16 core segments were sent to S. Naidu and T. Osterkamp, University of Alaska, for their clay mineralogy and granulometry studies.

In addition to laboratory work, we have been attempting to synthesize information gained over the past several years, and especially that in the last year. This has led to the preparation of several short reports, maps, and offshore cross sections which are presented as appendices to this report.

## APPENDIX A

### A REVIEW OF OFFSHORE PERMAFROST STUDIES, BEAUFORT SEA, ALASKA, 1976 TO 1980

By

R. W. Hartz and D. M. Hopkins

The continental shelf of the Beaufort Sea is believed to contain as much as fifty percent of the estimated oil and gas reserves of the North Slope of Alaska. Preliminary exploration has shown that most of the petroleum reserves of the continental shelf are exploitable only from offshore drilling sites. The engineering problems associated with offshore drilling are further complicated by the occurrence of shallow sub-sea permafrost and its thermal vulnerability to engineering disruption.

Prior to 1975, ideas on the occurrence of bonded permafrost on the continental shelf of the Beaufort Sea were largely theoretical inferences drawn from land-based data and observations on seismic refraction profiles. Only a handful of investigators (Lewellen, 1974; Mackay, 1972; Ostercamp and Harrison, RU 253, 255, 256), had attempted in situ studies by drilling and sampling sub-sea sediments. By 1975 it was clear that an understanding of the properties, processes, history, and stability of the sedimentologic and permafrost regime could only be acquired by drilling and coring a number of shallow offshore boreholes.

During the summer of 1975, L. D. Carter, R. W. Hartz, D. M. Hopkins, and R. E. Nelson conducted a U.S. Geological Survey study of the exposures along the Colville River in order to gather data on the stratigraphy, age, distribution, paleontology, and palynology of the Gubik Formation of the Arctic Coastal Plain. The results of these studies led us to believe that the state and distribution of bonded permafrost on the continental shelf was directly related to fluctuations in Pleistocene sea level and the regional geologic history.

Through the joint efforts of the U.S. Geological Survey, the U.S. Army Cold

Regions Research and Engineering Laboratories, and Arctic Research Inc. an offshore borehole program was undertaken. The primary goal of this borehole program was to delineate the history, distribution, and thermal state of sub-sea permafrost on the inner shelf of the Beaufort Sea, Alaska. The secondary objectives were to define the stratigraphy, geotechnical properties of the offshore sediments, and the sea level history of the shelf in order to develop a preliminary model of offshore permafrost in the sub-bottom materials within Stefansson Sound.

During March and April, 1976, four shallow boreholes were drilled through the sea ice in the vicinity of Prudhoe Bay. The first two boreholes, PB-1 and PB-1A, were drilled near the center of Prudhoe Bay; a third borehole, PB-2, was drilled about 3 km seaward of Reindeer Island, and the fourth borehole, PB-3, was drilled in Stefansson Sound between Reindeer Island and ARCO's west dock (fig. 1). The boreholes were cored at intervals ranging from 0.5 m to 6.0 m, and samples of the drill cuttings were collected in the intervals not cored. Upon completion of drilling operations the boreholes were geothermally instrumented, and temperatures were recorded at various depth and time intervals until the hole returned to thermal equilibrium.

During the spring of 1977 four additional boreholes were completed offshore in the Prudhoe Bay area (fig. 1). Borehole PB-5 was drilled on Gull Island Shoal; a second borehole, PB-6, was drilled near the elbow of ARCO's west dock; a third borehole, PB-8, was drilled just south of Reindeer Island; the fourth borehole, PB-7, was drilled approximately 3 km offshore and due north of ARCO west dock. Ancillary information on stratigraphy and geothermal temperatures were provided through the utilization of engineering probes developed by CRREL engineers (RU-104). Upon completion of the boreholes, thermistor pipe was installed and downhole temperatures were logged immediately following drilling operations. The holes were then allowed time to return to thermal equilibrium, and once again the downhole temperatures were recorded.

Although logistic limitations restricted our drilling to the Prudhoe Bay area, this constraint had the effect of permitting us to obtain relatively detailed knowledge of distribution of permafrost in a restricted area. With these few holes, we were able to establish factors governing depths of thaw and ground temperatures of subsea permafrost that could be generalized to other areas of the Beaufort Sea shelf. The boreholes were supplemented by a series of auger, probe, and water-jetted holes completed by Ostercamp and Harrison (RU-253, 255, 256), and by seismic refraction profiles collected by J. C. Rogers (RU-271).

#### RESULTS OF THE 1976-1977 USGS CRREL BOREHOLES

Each of the offshore boreholes provided valuable insights into the sedimentologic history and distribution of sub-sea permafrost in the area immediately offshore from Prudhoe Bay and the Sagavanirktok River Delta. Sub-sea sediments in the boreholes within Stefansson Sound can be divided into three major stratigraphic units. They include, from top to bottom, a surficial sequence of one to ten meters of soft marine fine sand, silt, and clay overlying one to two meters of beach sand and gravel. Pollen spectra and microfossil faunas indicate that these sediments accumulated since the last rise in sea level, about 10,000 years ago; an underlying sequence of angular, sterile sand and gravel with numerous ventifacted pebbles is interpreted as glacial outwash deposited by the ancient Sagavanirktok River during the last major glaciation in the Brooks Range; and a deeper, finer sequence of interbedded pebbly sand and well-sorted sand and gravel containing scattered lenses of detrital plant material interpreted as alluvium deposited by the paleo Sagavanirktok River earlier in the last glaciation.

Although temperature measurements of the 1976 boreholes were consistently below 0°C, and although thermal gradients in all boreholes were negative (growing colder downward) indicating ice-bonded permafrost below, none of the holes drilled within Stefansson Sound encountered bonded permafrost. These anomalous thermal

conditions are believed to result from the presence of brine solutions in the relatively porous outwash and alluvial sequences. The boreholes drilled during 1977 encountered similar thermally anomalous conditions; even the deepest hole, PB-7, driven to a depth of 68 meters, failed to penetrate frozen sediments, although temperatures as cold as -2.2 C were recorded. The 1977 boreholes also penetrated thick sequences of porous outwash and alluvium with high brine concentrations.

Only borehole PB-6 encountered ice-bonded permafrost at 29 meters below the sea floor; this hole was close enough to the mainland coast and recently enough submerged so that shallow ice-bonded permafrost was preserved at relatively shallow depth even in coarse-grained material.

The sedimentary history and permafrost regime seaward of Reindeer Island proved to be quite different from that within western Stefansson Sound. During the 1976 drilling program borehole PB-2 encountered a sequence of stiff, overconsolidated marine silt and clay 3 km seaward of Reindeer Island. Initially we believed that the overconsolidated sediments were Holocene muds that had been overconsolidated as a result of Reindeer Island migrating over the site. But during 1977, borehole PB-8 was drilled about 1.7 km south and inland from Reindeer Island, and it, too, encountered stiff overconsolidated marine sediments. Pollen and foraminiferal analyses indicated that the overconsolidated silt and clay were deposited during the Sangamon interglacial when sea level was higher than present. Evidence suggests that these deposits formed an erosional surface during the last glacial maximum when the shoreline lay somewhere seaward of the 20-meter isobath. Exposure to seasonal freezing and thawing cycles at that time resulted in the overconsolidation of the marine sediments. They became overconsolidated as a result of segregation and later loss of interstitial water.

Thus the offshore permafrost data suggested that ice-bonded permafrost on the inner shelf was largely relict, having formed during the last reduction in

sea level, and that the depth to the ice-bonded layer was apt to be highly variable. The irregular nature of the ice-bonded surface and the stratigraphic history of the shelf suggest the following model of permafrost distribution on the Beaufort Sea continental shelf:

During the height of world-wide continental glaciation that culminated about 18,000 years ago, sea level was lowered. The Bering Sea shelf was exposed seaward to about the present-day 90-meter isobath. The position of the shoreline in the Beaufort Sea 18,000 years ago lay somewhere seaward of the 20-meter isobath and borehole data suggest, in fact, that relative sea level fell at least 90 m below present in the Beaufort Sea. The mantle of marine silt and clay, deposited during Sangamon time (approx. 120,000 years ago), became frozen as did the underlying gravels. The total thickness of bonded permafrost formed at any particular place depended partly upon the duration of exposure to subaerial temperatures, but thicknesses of several hundred meters were formed in most areas of the shelf landward of the present 20-meter isobath.

The major rivers draining the north slope of the Brooks Range aggraded and formed outwash fans extending across much of the present-day coastal plain, although the edges of most of the fans lay within a kilometer inland of or seaward of the present coastline. Seaward from the edges of the fans, the rivers removed the ancient marine silt and clay to form broad, shallow valleys graded to the shoreline of the time. By analogy with the braided gravel floodplains of present-day north slope rivers we may assume that the top of the ice-bonded layer lay at depths of several tens of meters beneath the river channels but at depths of less than a meter beneath uplands mantled with overconsolidated marine silt and clay.

As continental glaciers waned and sea level began to rise, the shallow river valleys were drowned. In the absence of a cover of ancient, overcon-

solidated marine silt and clay, the cold but salty sea water gained ready access to the underlying gravel. Ice in the gravel was thawed rapidly and deeply by salt advection. Ultimately these valleys began to collect Holocene sediments carried by current from the river mouths.

Although the sea transgressed over the slightly higher plains away from the sea valleys, salt water was prevented from gaining access to the potentially porous gravel substrate by the mantle of tight overconsolidated marine deposits. Consequently thawing of ice in the shallow bonded permafrost could progress only by heat diffusion and salt diffusion. The water temperatures were below zero and silt diffusion progressed very slowly. As a result, thawing has progressed extremely slowly and only to a very limited depths in most areas mantled by the overconsolidated marine silt and clay.

If this paleovalley model is correct, then areas of unbonded permafrost many tens of meters thick should be delineated by curvilinear belts of thick Holocene marine sediments. Conversely, shallow ice-rich permafrost should be encountered in areas mantled by the stiff overconsolidated Sangamon marine deposits.

Radiocarbon-dated samples from the deep gravel pits along the lower Putalagayuk River and from the offshore boreholes confirm that the ancient Sagavanirktok River once flowed through Prudhoe Bay and then turned westward through a broad valley carved in the area between ARCO's west dock and Reindeer Island. This valley was carved more than 42,000 years ago, then backfilled with several tens of meters of alluvium and fine outwash gravel. Slow filling or relative stability and a vegetated landscape is indicated by a paleosol, buried peat layers, and accumulations of wood (including poplar) dated 42,000, 36,000, and 26,000 years old in a gravel pit beneath the lower Putalagayuk River and in borehole PB-7.

The opportunity to test the validity of the paleovalley model materialized during the autumn of 1978 when we were invited to participate in a new Beaufort Sea geotechnical borehole program. Conservation Division of the U.S. Geological

Survey planned to drill a number of shallow offshore boreholes scattered throughout the proposed Beaufort Sea lease area. Drilling operations were scheduled during February and March of 1979; the primary objective was to recover sediment cores from a number of lease tracts in order to perform engineering and geochemical tests. The distribution of permafrost within the lease area was largely unknown, and, as the USGS-CRREL boreholes had demonstrated, only drilling could delineate its distribution.

A total of twenty boreholes were drilled through the sea ice between Flaxman Island and the Return Islands: eleven of the holes were located seaward of the barrier islands and nine holes were located in the lagoons between the mainland and the barrier islands (fig. 1). Sampling was continuous through the upper fine grained sediments and at 10-foot intervals through the coarse-grained sequences. Detailed stratigraphic logs were compiled for all the boreholes, sediment cores were examined upon recovery, and in the coarse grained units the drill cuttings were monitored continuously (RU-204, Quarterly Report, August to July 1979).

These boreholes have established that bonded permafrost is present everywhere, although at variable depths, throughout the Beaufort Sea lease area from the shoreline seaward to at least the 20-meter isobath. Bonded permafrost was encountered 22 km from the mainland at depths as shallow as 6.5 meters below the sea floor in overconsolidated silt and clay. On the other hand, unbonded sediments greater than 90 meters thick were found less than 5 km from shore just east of Tigvariak Island. Temperature measurements indicate that both bonded and unbonded sediments have temperatures well below zero in all of the boreholes and that all the boreholes have negative thermal gradients indicating that bonded permafrost is present at depth, even if not reached by the borehole.

Apparently, the thickness of the surficial unbonded layer is determined by differences in thermal history including the effects of the passage of migrating



barrier islands, differences in time since inundation by rising sea level, and differences in pore-water salinities. Salt advection following the entry of sea water into porous alluvium exposed upon the sea floor indeed seems to have been one important mechanism for inducing local deep thaw on the inner shelf.

The 1979 USGS Conservation Division boreholes seemed to verify our predictive model which is based on the assumption that thick unbonded permafrost occupies paleovalleys. With one exception (borehole HLA-14), all areas of deep thaw do, indeed, coincide with areas in which boreholes have encountered thick sandy and gravelly alluvium and outwash beneath Holocene marine deposits (fig. 2). Utilizing this assumption and all available borehole and seismic data we were able to construct an interpretive contour map of the thickness of unbonded sediments in the Beaufort Sea lease area (RU-204, Quarterly Report, October-December 1979) (see fig. 3). The resulting map can be used to assist in delineating gravel-filled Pleistocene valleys on the shelf and can be used as a guide in the search for accessible, unfrozen sand and gravel for the construction of artificial islands and causeways.

FIGURE 1 BOREHOLE LOCATION MAP

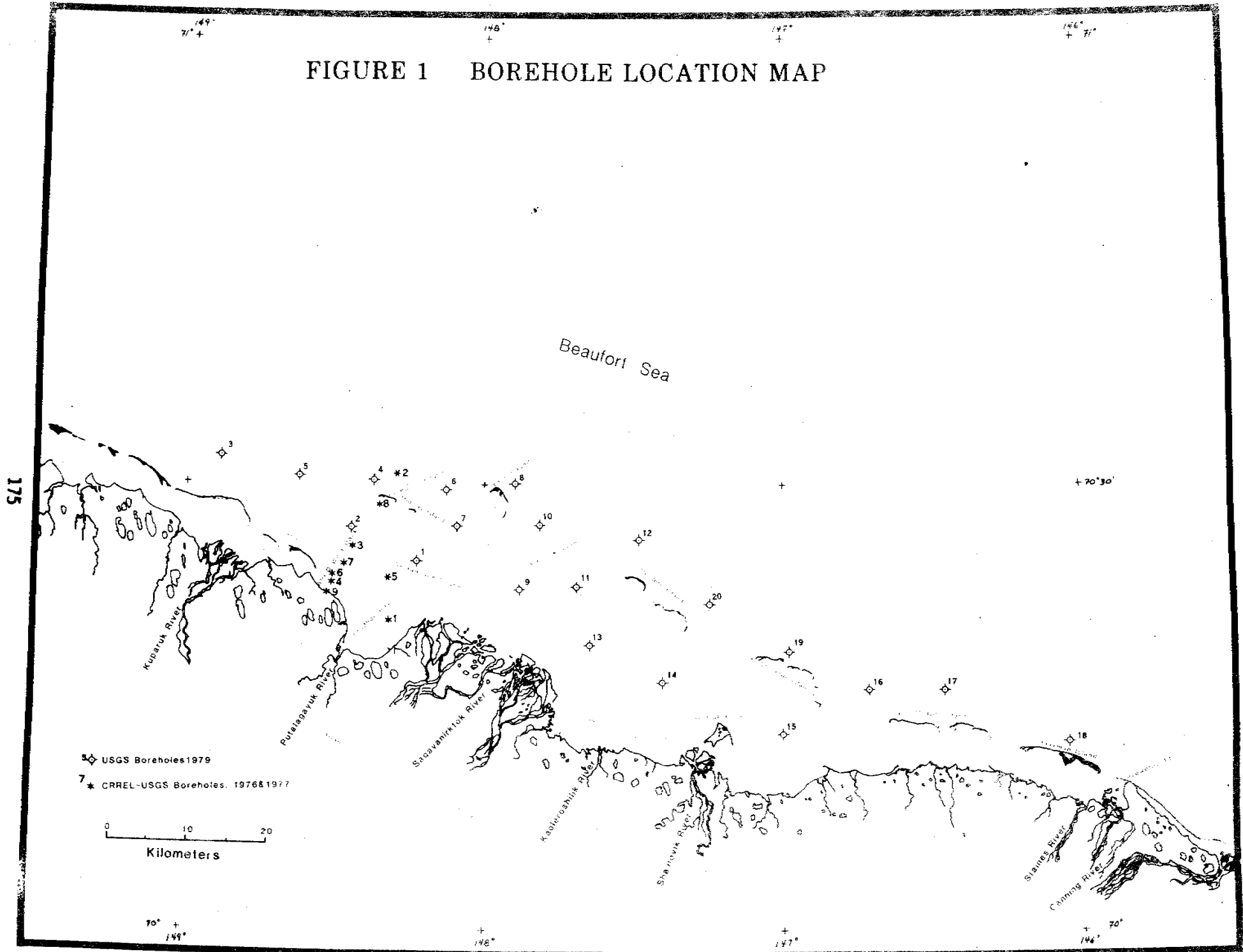


FIGURE 2 HOLOCENE UNIT THICKNESS

— Explanation —

Contour interval 5 meters

15 Borehole and thickness of Holocene sediments penetrated

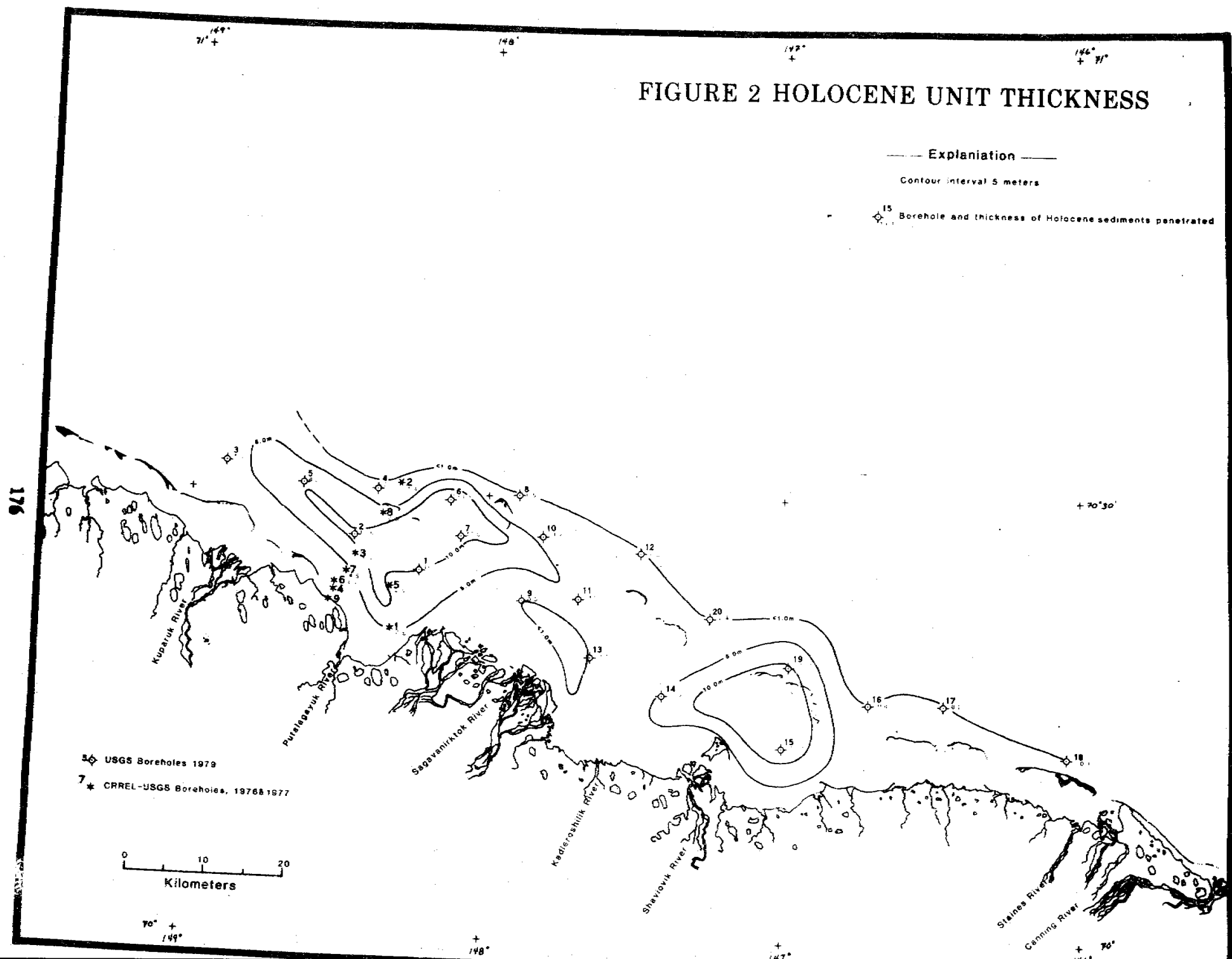
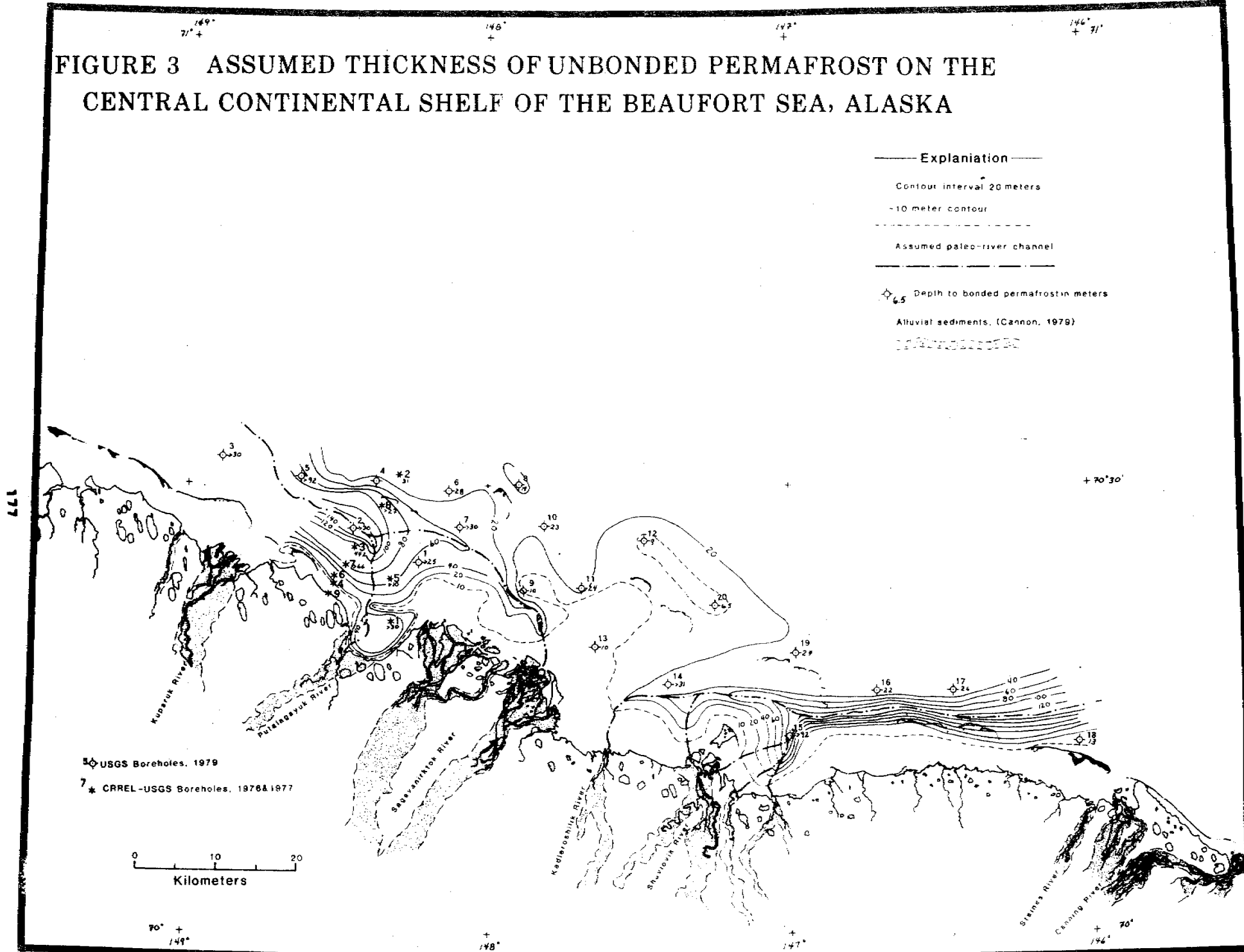


FIGURE 3 ASSUMED THICKNESS OF UNBONDED PERMAFROST ON THE CENTRAL CONTINENTAL SHELF OF THE BEAUFORT SEA, ALASKA



## APPENDIX B

### COASTAL MORPHOLOGY, COASTAL EROSION, AND BARRIER ISLANDS OF THE BEAUFORT SEA COAST, ALASKA

By

D. M. Hopkins and R. W. Hartz

The environment of the mainland coast and continental shelf of the Beaufort Sea is exceptional in that many of the processes affecting it are uniquely arctic. In order to assess the potential impact of petroleum exploration and development within the coastal zone of the Beaufort Sea it is necessary to define the relationship of coastal geologic and geomorphic processes to shoreline history and the occurrence of subsea permafrost.

The Beaufort Sea portion of the Arctic coastal plain is mantled in most places by thaw-lake deposits consisting of peat, fine sand, and silt a meter to a few meters thick; these deposits are generally younger than 10,000 years and are a major source of detrital organic matter supporting productivity in lagoons and near-shore areas. East of the Colville River, the thaw lake deposits are underlain in coastal bluffs by Pleistocene alluvial and outwash fans emanating from the Brooks Range and composed of large quantities of chert, graywacke, quartzite, and grit pebbles. West of the Colville River, the Holocene peaty deposits are underlain in most places by Pleistocene marine silt and sand of the Gubik Formation; these marine sediments are divided into an offshore and a lagoonal facies by a series of low mounds and ridges representing ancient barrier islands and extending eastward from Barrow to the Kogru River. An exception is in the segment of the coast along the south shore of Kogru River to the mouth of Fish Creek; ancient sand dunes underlie the surficial peaty deposits along this segment of the coast.

In some areas immediately adjacent to the coast the Flaxman Formation forms a thin veneer of marine silt or fine sand containing erratic cobbles and boulders

of red granite, dolomite, red quartzite, pyroxenite, and diabase. The source area of the Flaxman erratics is still uncertain but is clearly outside of northern Alaska.

#### COASTAL MORPHOLOGY

Deep embayments and crenulations characterize the mainland coast of the Beaufort Sea from Point Barrow to the Canning River. Embayments such as Harrison Bay and Smith Bay lack the protection of offshore islands and may be exposed to intense wave action during summer and autumn storm surges.

The beaches of the mainland coast are backed by bluffs from 1 to 10 meters high, and most if not all of the coarse beach sediment is derived from the coastal bluffs. As a result, mainland beaches tend to be narrow (rarely wider than 20 meters), low-lying, and only a few tens of centimeters thick. During periods of high surf it is not uncommon to find beach sediments tossed atop low-lying bluffs. In general, the beaches between Point McIntyre and the Canning River contain high percentages of gravel and coarse sand, while the beaches between Point Barrow and the Colville River are composed of fine sand and mud. The paucity of coarse sediments in the coastal bluffs between Harrison Bay and Barrow often results in no beach at all, exposing the toe of the bluffs to constant wave attack and rapid thermal erosion during the ice-free season.

#### COASTAL EROSION

In spite of the short ice-free period and the relatively low wave energy environment, the coast of the Beaufort Sea is retreating at a spectacular rate. This rapid rate of coastal erosion is in large part the result of two distinctly arctic processes; thermokarst collapse and thermal erosion. Thermokarst collapse results in the loss of volume due to the melting of ground ice in excess of normal porosity of the sediments, causing subsidence and collapse of the thawed materials. Thermal erosion is the result of undercutting of the coastal bluffs by wave action and may result in spectacular bluff retreat when frost cracks extend-

ing along the axes of ice wedges are intersected. Blocks as large as a house may be disjoined and fall onto the beach.

Rates of coastal retreat vary at different sites, depending on composition of the coastal bluffs, exposure to wave action, and the morphology of the adjoining sea bottom. Average rates of retreat are highest from Harrison Bay to Barrow; rates as high as 30 meters per year have been observed at Drew Point and Cape Simpson.

#### OFFSHORE ISLANDS

The discontinuous chains of offshore islands extending from Point Barrow to Brownlow Point profoundly affect water circulation and sediment transport on the inner shelf of the Beaufort Sea. These islands may be divided into three morphologic types; erosional remnants of the coastal plain, recent constructional features resembling barrier islands, and constructional islands with relict Pleistocene cores. The constructional islands are migrating shoreward and westward at rates which require only 30 to 40 years for them to cross a given point on the sea floor. On the other hand, islands which are erosional remnants of the coastal plain are rapidly being destroyed and dispersed by longshore drift (estimated longshore transport on the outer coast of Pingok Island was  $10,000 \text{ m}^3$  during the summer and autumn of 1972). The general westward movement of longshore sediment is accomplished by a number of littoral transport cells averaging less than 10 kilometers in length. These cells exert control over the movement of sediments within an entire island-shoal complex such as the Maguire Islands and the Stockton Islands, and tend to sustain the migration of sediment slugs such as Thetis Island.

Major passes within the Beaufort Sea island chains are barriers to sediment transport and serve to isolate the different island groups from one another. The arcuate shape of the island groups and their frequent terminations in compound recurved spits confirms that the major passes are sediment sinks, not sediment transmission belts. The presence of cobbles and gravel on Jeanette, Narwhal, and


Cross Islands much coarser than the gravel comprising islands that lie eastward and up-drift establishes that the source of sediment lies or once lay somewhere seaward on the continental shelf. The eastern islands within the Plover chain are or once were fed from the bluffs east of Cape Simpson DEWline station, while the peninsula leading from Eluitkak Pass to Point Barrow appears to be fed by sediment moving northward up the Chukchi Sea coast and eastward around Point Barrow, but the islands between Eluikrak and Eluitkak Passes differ enough to indicate that they originated from a sediment source that has now disappeared.

Long-term comparisons seem to indicate that the islands are migrating with little loss of area and mass. Wave overwash during storm surges helps to move sand and gravel from the nearshore zone onto the body of the island, and ice-push rakes the lagging coarser particles from deep water and returns them to the island surface. However, the islands will eventually disappear. Dinkum Sands seems to be an example of a member of the Midway Island chain that eventually lost mass and became completely submerged.

Because many of the islands in the Beaufort Sea island chains are mostly lag deposits derived from sand and gravel sources that have now disappeared, they must be regarded as irreplaceable. If they are quarried and removed, they would not be replaced by natural processes, and the local oceanographic and biologic regime would be irreversibly altered.

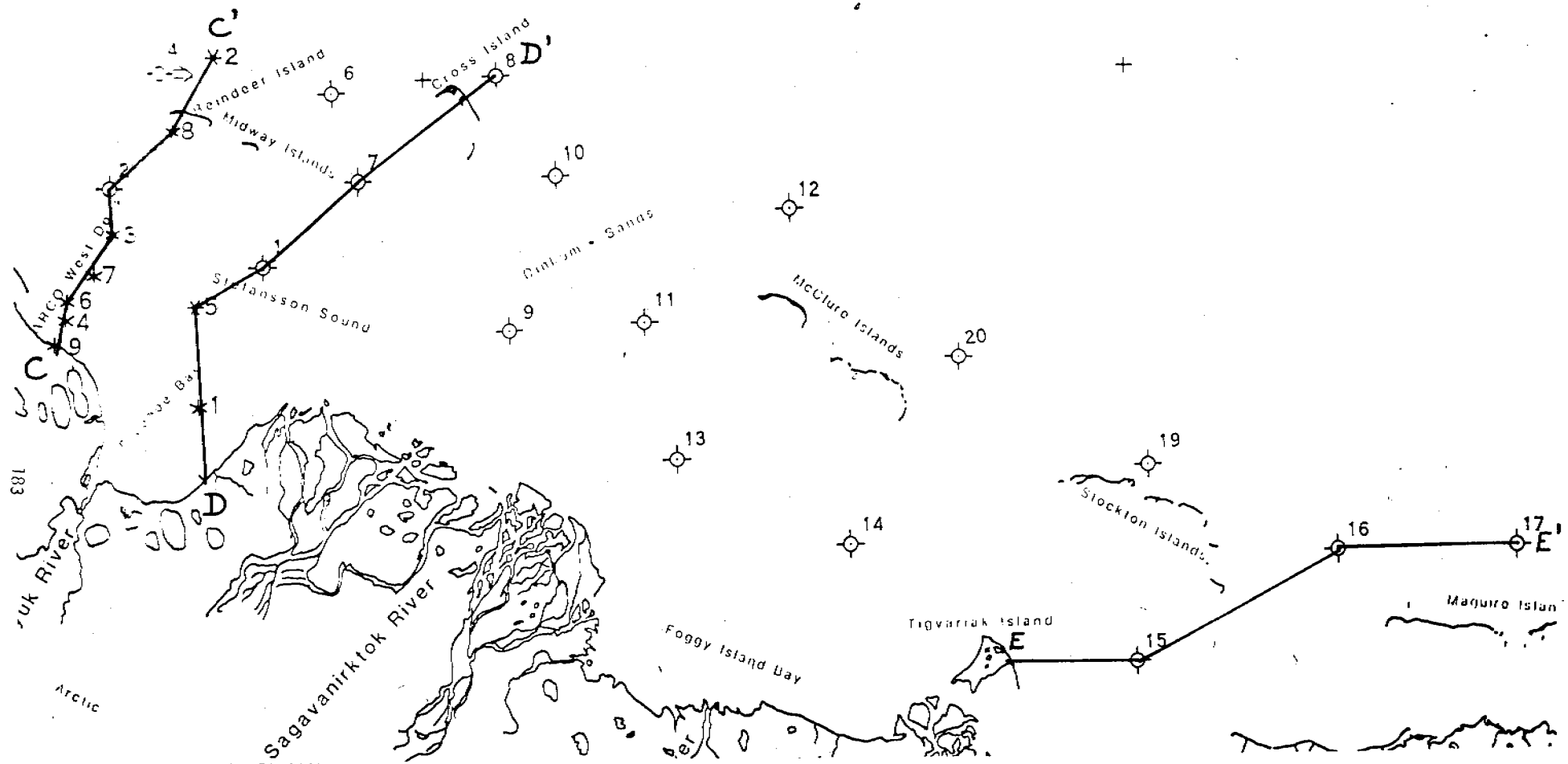


APPENDIX C  
 Geological Cross Sections  
 by R. W. Hertz and D. M. Hopkins

EXPLANATION		
Quaternary	Holocene	QHi- Holocene barrier island complex
		QHd- Holocene deltaic deposits
		QHm- Holocene marine deposits
		QHb- Holocene beach deposits
	Pleistocene	QFx- Flaxman Formation
		QSm- Sangamon marine deposits, usually overconsolidated
		Qsb- Sangamon beach deposits
		QPf- Pleistocene fluvial and glaciofluvial deposits
		Qpm- Pleistocene marine deposits
		
Ice bonded permafrost		

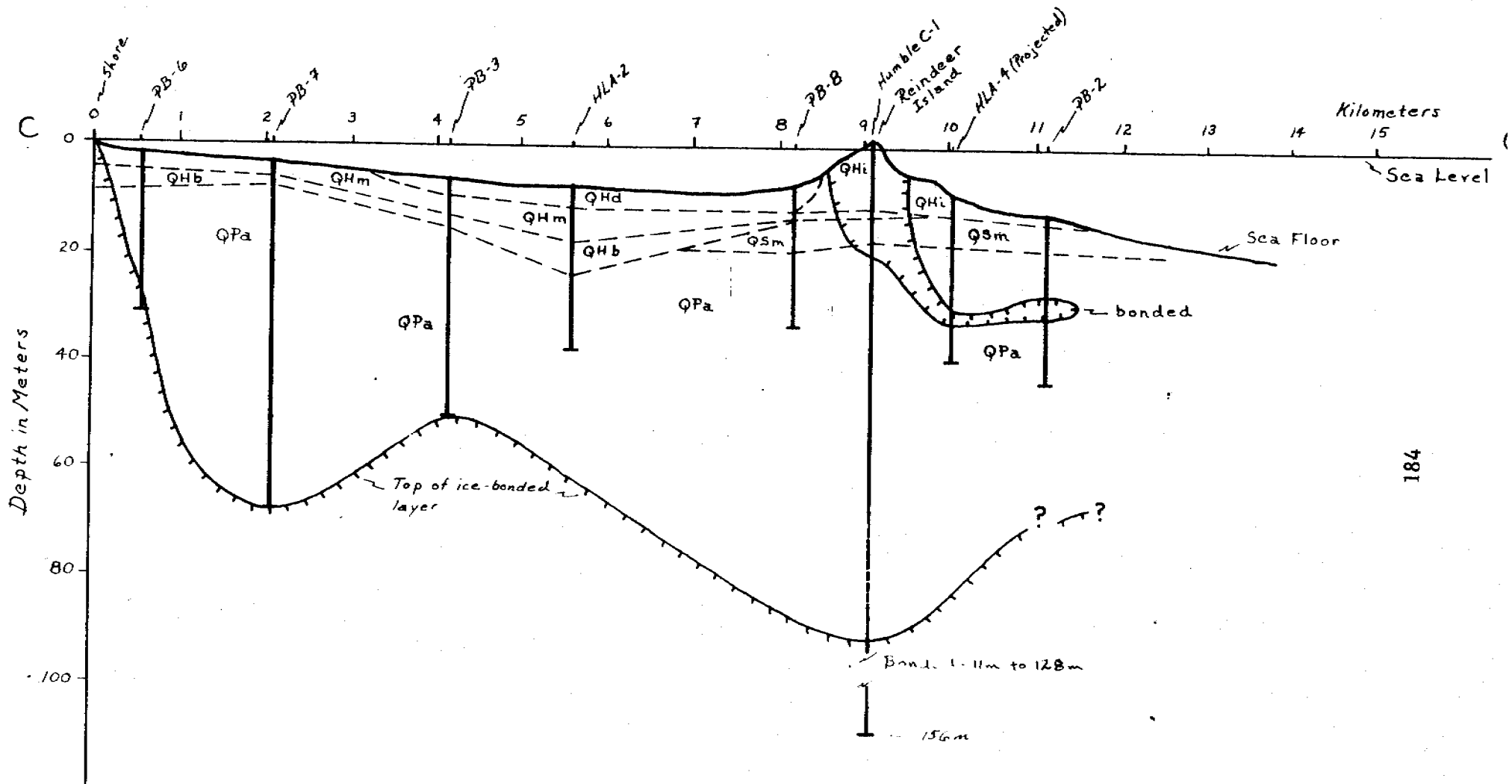
Horizontal scale 1:80,000

GEOLOGICAL CROSS SECTION LOCATION MAP

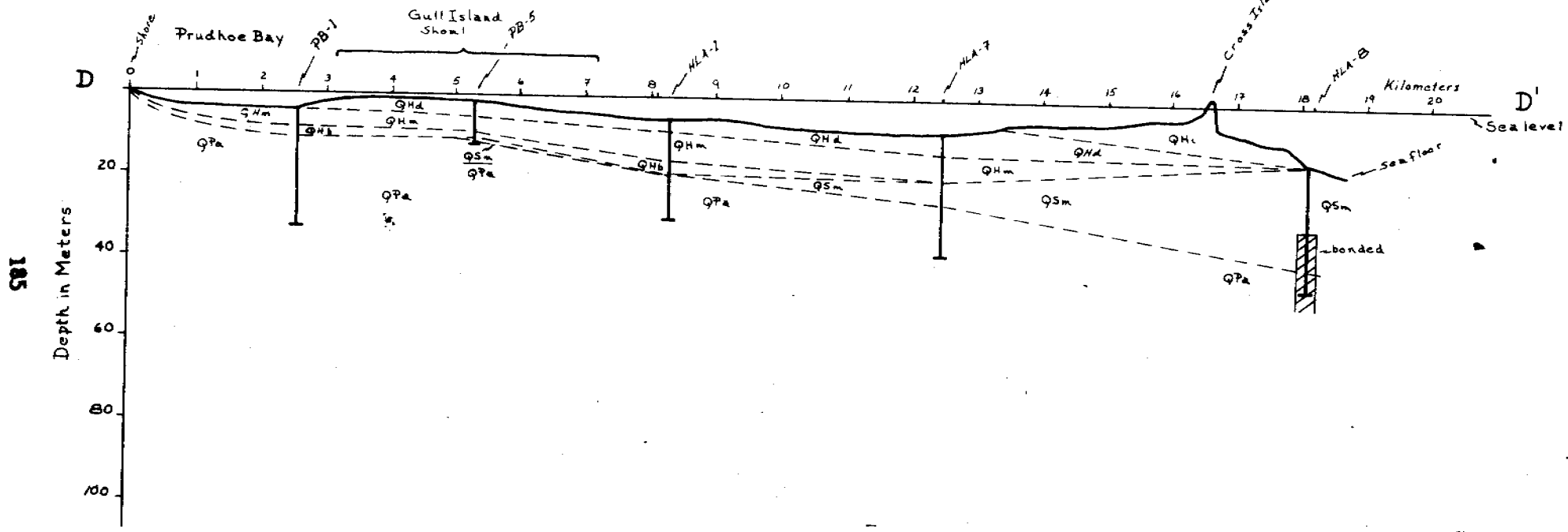


(scale aprox. 1:250,000)

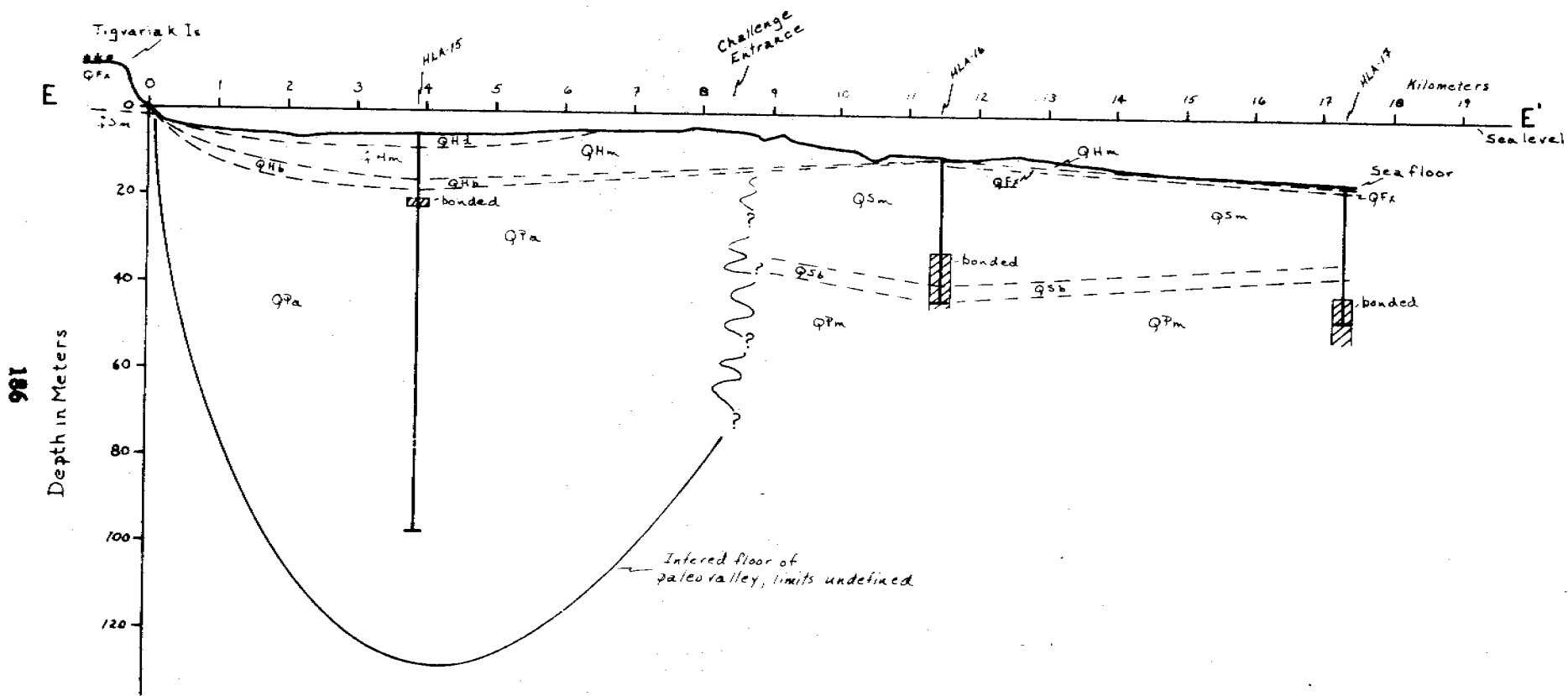
# Geological Cross Section-C



# Geological Cross Section - D



# Geological Cross Section-E



981

APPENDIX D

LIKELIHOOD OF ENCOUNTERING PERMAFROST IN  
SUBMERGED AREAS OF NORTHERN BERING SEA

by

David M. Hopkins

Abstract

Offshore ice-bonded permafrost is rare if present at all along the northern Bering Sea coast. Small initial thicknesses (probably less than 150 m), initial temperatures only a few degrees below zero, and presence of bottom waters a few degrees above zero should result in rapid destruction of permafrost upon submergence. Thawing should be accelerated by salt-water intrusion into the prevailing sandy and gravelly nearshore sediments. Many segments of the coast are cut into bedrock or into coarse Pleistocene sediments with only a small ice content; in these areas, the ground seems to become thawed prior to submergence due to coastal retreat.

Rapid coastal retreat in areas of ice-rich Pleistocene or Holocene sediment may result in a narrow nearshore belt of submerged permafrost in coastal segments between the Koyuk River and Cape Denbigh, between St. Michael and Apoon Pass of the Yukon River, and between Kwikloak Pass and Cape Romanzof. Planning for offshore construction or excavation in these areas should include a study of nearshore permafrost conditions.

LIKELIHOOD OF ENCOUNTERING PERMAFROST IN  
SUBMERGED AREAS OF NORTHERN BERING SEA

by

David M. Hopkins

Although offshore permafrost has never been reported beneath northern Bering Sea (figure 1) the possibility that it might be present cannot be altogether ignored, since no studies have ever been directed toward detection of ice-bonded sub-bottom sediment there. Consideration of regional history suggests at first glance that permafrost could be present. The entire area of the Chirikov Basin and Norton Sound (the two physiographic provinces making up Bering Sea north of St. Lawrence Island--Hopkins and others, 1976) was emergent for many millenia, becoming gradually submerged between 14,000 and 5,000 years ago (Hopkins, 1973). Several lines of paleoclimatic evidence indicate that mean air and ground temperatures were well below freezing (Hopkins, 1979), and presumably the ground became frozen to depths of a hundred meters or more. Nevertheless, consideration of the character and condition of present-day onshore permafrost, bottom water temperatures in northern Bering Sea, rates of coastal retreat, character of sub-bottom sediment, and results of offshore drilling suggests that ice-bonded material, if present, must be restricted to a very few, narrow areas lying within a few hundred meters of the present strand.

Conditions favoring persistence of  
permafrost beneath Beaufort Sea

Consideration of the likelihood of encountering ice-bonded permafrost beneath northern Bering Sea will be facilitated by comparison of conditions there with the conditions that have led to the preservation of thick and extensive areas of subsea permafrost on the Beaufort Sea shelf.

The widespread ice-bonded permafrost beneath the Beaufort Sea shelf is relict, having formed prior to submergence at times when sea level was lower and the continental shelf was exposed to cold subaerial temperatures at least as far seaward as the 100-m isobath. Rising sea level and rapid coastal retreat have brought a vast area of relict ice-bonded permafrost beneath sea level. The process continues; shoreline retreat along the Beaufort Sea coast is rapid, generally exceeding 2 m/yr (Hopkins and Hartz, 1978).

Onshore permafrost on the Arctic coastal plain generally is thicker than 500 m. Offshore boreholes have penetrated ice-bonded permafrost extending to depths of more than 100 m (Hartz and others, 1979), and analysis of seismic records indicates that the ice-bonded layer is as thick as 500 m at a distance of 10 km from the present shore (P. V. Sellmann and E. Chamberlain, Quarterly Report to OCSEAP, July-September, 1979). Farther offshore the ice-bonded layer gradually thins; nevertheless, ice-bonded permafrost several hundred meters thick is present 20 km off Prudhoe Bay (Sellmann and Chamberlain, op. cit.).

Bottom waters in the Beaufort Sea are at subzero mean annual temperatures (Lachenbruch and Marshall, 1977), and consequently are not warm enough to thaw fresh-water ice by heat conduction alone. Onshore permafrost at Prudhoe Bay is very cold, reaching temperatures of  $-10^{\circ}\text{C}$  at the level of zero annual change (Gold and Lachenbruch, 1973, fig. 1). The relict offshore permafrost beneath the Beaufort Sea shelf must originally have been as cold or colder, but temperature measurements in offshore boreholes indicate that at shallow depths, at least, the submerged permafrost has warmed to temperatures near  $-1^{\circ}\text{C}$  (Lachenbruch and Marshall, 1977; Bruggers and England, 1979). Seismic velocities confirm that most of the offshore permafrost is warmer than onshore permafrost (Sellmann and Chamberlain, op. cit.). The effect of the overlying sea water has evidently been to warm but not necessarily to thaw the relict permafrost.

Such thawing as has taken place has been the result of diffusion or advection of salt water into the underlying frozen sediments (Osterkamp and Harrison, 1976). Salt diffusion is a slow process, and where tight, impermeable, overconsolidated marine clay is at the sea bottom, ice-bonded material commonly lies at a depth of 10 or 15 m (Hopkins and others, 1979; Bruggers and England, 1979; R. W. Hartz and D. M. Hopkins, Quarterly Report to OCSEAP, September-December, 1979). Salt water advection is more rapid, and where thick sand and gravel layers lie at or near the sea bottom, salt water has penetrated and thawed interstitial ice to depths of 100 m or more.

In summary, the presence of thick and widespread permafrost on the Beaufort Sea shelf reflects initial very great thicknesses of very cold ice-bonded permafrost prior to submergence; rapid sea level rise, and then rapid coastal retreat which has constantly brought new permafrost beneath the sea; very low bottom-water temperatures; and a prevalence of impermeable bottom sediments which in many places has limited the potential intrusion of salty sea water.

#### Conditions in northern Bering Sea

Onshore permafrost.--The lands adjoining northern Bering Sea lie within the discontinuous permafrost zone, a zone in which permafrost is thin, warm, and commonly interrupted by thawed zones beneath lakes, river channels, and steep south-facing slopes (Péwé, 1975). Permafrost was encountered in 73 out of 83 wells and borings reported by Williams (1970, figs. 3, 4, 6, 7) within 160 km of the Bering Sea coast north of the Kuskokwim River. The median thickness of ice-bonded permafrost encountered in these wells and borings was 30 m, and the thickest permafrost encountered extended to a depth of about 135 m. There is no pronounced latitudinal gradient in permafrost thicknesses, and, in fact, permafrost thicker than 100 m is reported more commonly on the southern part of the Yukon-Kuskokwim Delta than at any point within the area of figure 1.

Little data is available concerning ground temperatures. Although mean annual temperatures of  $-2^{\circ}$  to  $-4^{\circ}\text{C}$  in this region would suggest that ground temperatures at the level of zero annual change should be only slightly below zero (Brown and Péwé, 1973), colder ground temperatures near  $-5^{\circ}\text{C}$  are suggested by the presence in many places of young ice wedges apparently actively forming at the present time. Active ice wedges are fairly widely distributed in interior Seward Peninsula and inland on the Yukon-Kuskokwim Delta but they



are rarer near the coast. However, active or recently developed ice wedges within a few hundred meters of the present shore have been seen near Nome (Hopkins and others, 1960; D. M. Hopkins, unpublished field notes, 1949-50), north of the mouth of the Yukon River near Cape Romanof (Dupré, in press), and Yukon-Kuskokwim Delta south of Kwikloak Pass (Ager, in press; W. R. Dupré, oral communications, 1976-79).

Much of the ice-bonded frozen soil on the shores of northern Bering Sea may be relict, having frozen initially during the colder climates of late Wisconsinan time. Large ice wedges seen by the author at the mouth of Agnagak Lagoon, northwestern St. Lawrence Island and near Teller and Cape Douglas on Seward Peninsula and reported to the author in coastal bluffs around Norton Bay by the late Ivar Skarland (University of Alaska, oral communication, 1948) probably formed during past times when the ground was colder and frost-cracking more frequent than at present.

Water temperatures.--Bottom waters in northern Bering Sea are at temperatures above 0°C throughout most of the year, varying from local winter minima of -0.5°C to summer maxima in the range 1.5°-2.0°C (Coachman and others, 1975). Consequently one would expect that relict ice-bonded subsea permafrost would be unstable and that frozen earth materials would eventually thaw after inundation due to rising sea level or coastal erosion.

Bottom sediments.--Surficial sediments on the northern Bering Sea floor consist predominantly of poorly sorted silty very fine sand (McManus and others, 1977, figs. 9 and 14). Gravel and coarser sand is common, however, in many nearshore areas (Nelson and Hopkins, 1972, fig. 10) (figure 4). Extensive areas of silt are confined chiefly to Norton Bay, which receives considerable amounts of fine Yukon River sediment (McManus and others, 1974). In contrast to the Beaufort Sea floor, there are no extensive areas of overconsolidated clay and silt at the sea bottom in northern Bering Sea. Rates of marine sedimentation are generally low, and over wide areas the surficial sediments are subject to resuspension during storm surges with recurrence intervals of a few years to a few decades (Nelson, 1978; Larsen and others, 1979).

The generally thin cover of Holocene sediment is underlain by a thick sequence of Pleistocene and late Tertiary bedded sediment throughout much of northern Bering Sea (Johnson and Holmes, 1978). More than half of the northern Bering Sea coast is adjoined, however, by a submerged belt as much as several kilometers wide in which schist, limestone, granite, or thoroughly lithified and folded sandstone and shale are exposed at the sea bottom or lie beneath sandy and gravelly surficial sediments only a few meters thick (Grim and McManus, 1970; D. M. Hopkins, unpublished data, 1967-1971) (figure 2).

The nature of subsea rocks and sediments in northern Bering Sea is not conducive to prolonged preservation of relict ice-bonded permafrost. The predominating loose, sandy sediments provide much better avenues for salt-water intrusion than does the overconsolidated clay that underlies large tracts on the Beaufort Sea shelf, and consequently, one would expect that relict ice-bonded permafrost within a few tens of meters below the sea floor would undergo rapid thawing after submergence. In rocky substrates, ground ice initially would have been confined to joints and through-going fractures and would be especially vulnerable to rapid thawing by intruding salt water soon after submergence.

Rates of coastal retreat.--Few studies have been made of long-term rates of coastal retreat around the shores of northern Bering Sea. The coast can be classified, however, into segments backed by coastal bluffs cut in hard, resistant rock; segments with coastal bluffs cut in Pleistocene gravel, glacial till, peat, or silt; segments in which the coast consists of spits, barrier bars, and prograded beach ridges; and segments in which deltas are advancing into the sea (figure 2).

Deltaic areas comprise about 15% of the coast. The active delta of the Yukon River between Kwikloak and Apoon Passes is by far the largest of these, but smaller prograding deltas are found at the head of Golovnin and Norton Bays. New land created by deposition of mud is being built out over areas previously long submerged. No offshore permafrost would be expected in these areas.

Rocky coastal segments occupy about 50% of the Alaskan mainland coast of northern Bering Sea. No observations have been made concerning long-term retreat rates, but coastal erosion is certainly generally slow, probably considerably less than 1 m/year. No offshore permafrost would be expected in these areas, either.

Holocene spits, barrier bars, and prograded beach-ridge complexes occupy about 10% of the Alaskan mainland coast of northern Bering Sea. Some of these coastal segments may be prograding and others may be stable, but some are retreating or migrating shoreward at substantial rates. Study of sequential maps and air photos of a barrier-bar system south of Cape Romanof indicates a shoreward migration rate of 12-20 m/yr (Dupré, 1977). Because permafrost is thin or lacking in these sandy and gravelly Holocene marine sediments and because they are quickly penetrated by salt water after submergence, ice-bonded permafrost is unlikely to be encountered offshore.

The remaining 25% of the coast consists of segments backed by unconsolidated gravel, sand, silt, peat, and glacial till. These segments are, indeed, susceptible to rapid coastal erosion, mainly concentrated during autumn storms. Storm surges coinciding with onshore winds have been a constant threat to the Nome town site. The spectacular and unprecedented storm surge of 1974 resulted locally in as much as 45 m of coastal retreat along portions of the Nome coast unprotected by a breakwater (Ralph Hunter and Asbury Sallenger, Jr., oral communication, 2/80). Although rapid coastal retreat can be anticipated in other, similar coastal segments, the only other estimates of retreat rates known to the author is W. R. Dupré's (oral communication, 1980) estimate of 8-10 m/yr for the segment between Cape Romanof and Apoon Pass and Dupré's estimate of 2-4 m/yr for a portion of the active Yukon Delta immediately west of Apoon Pass (figure 3). This very sparse data suggests that retreat rates for segments of the northern Bering Sea coast backed by unconsolidated sediments are comparable to the highest coast-retreat rates recorded for the Beaufort Sea.

Boreholes.--Many boreholes have probed the sea bottom in nearshore waters in the vicinity of Nome and a few have been placed near Bluff, 90 km east of Nome, in connection with gold-placer prospecting activities during the late 1960's and early 1970's. A Geological Survey party under my direction was present and prepared lithologic cores during drilling of 50 boreholes from the R/V VIRGINIA CITY as part of a U.S. Bureau of Mines-U.S. Geological

Survey gold exploration effort in 1967. The boreholes were placed at distances of 500 to 8,000 m offshore in water 10 to 30 m deep and probed to depths of 30 to 100 m below bottom. A variety of substrates ranging from clay to gravel were encountered (figure 3). Permafrost was not expected, and consequently, no temperatures were measured in these boreholes, nor was any special attention given to other criteria that might indicate presence or absence of ice-bonded layers. It remains noteworthy, nevertheless, that no indications of ice, ice-bonded sediment, or extremely cold sediment were seen.

Some hundreds of boreholes, some in very shallow, nearshore waters were drilled from shorefast ice in this same region during a gold-exploration program conducted by Shell Oil Company and later by American Smelting and Refining Company in the 1960's and 1970's. I have discussed the results of this drilling extensively with the engineers in charge and have examined lithologic logs for boreholes drilled during the early phase of this project. Permafrost is not mentioned in the logs and was never reported to me by the engineers in charge.

Several boreholes were drilled from shorefast ice in a gold placer deposit that extends several thousand meters offshore at Bluff by a series of operators interested in the possibility of offshore mining, there. I have only a general familiarity with the results of this drilling, but the presence of offshore permafrost seems never to have been suspected on the basis of the exploratory drilling.

It is common knowledge at Nome and an experience shared with other settlements on the south coast of Seward Peninsula that houses placed on land within a few tens of meters of the beach will have no difficulty with settling foundations due to thawing of ground ice, that septic tanks and drain fields can be installed, and that in some places, fresh-water can be obtained from wells.

Where these observations apply, it is clear that ice-bonded permafrost is lacking not only beneath the nearshore waters but also beneath a belt extending a few tens of meters inland from the shoreline bluffs.

#### Conclusions

Based on analogy with the better-studied permafrost situation on the Arctic coastal plain of northern Alaska, it seems likely that the thickest persisting layers of permafrost on land reflect approximate original thicknesses of permafrost formed in the northern Bering Sea region during the last cold period. It is unlikely that bonded permafrost was ever thicker than 150 m anywhere on the continental shelf of the Bering Sea.

Given the relatively small initial thicknesses and the warm temperatures of ice-bonded permafrost and the relatively warm bottom-water temperatures in northern Bering Sea, one would expect rapid thawing after submergence. In many regions, thawing will be accelerated as salt water intrudes into sandy and gravelly nearshore sediments or into fractures in bedrock ledges at the sea bottom. Ice-bonded permafrost seems to be destroyed before submergence within rock or sediment immediately adjoining the coast in those segments of the northern Bering Sea shore in which coastal retreat is slow as well as in those in which the initial ground-ice content is low. Ice-bonded

permafrost is likely to be encountered offshore only in those areas where ice-rich sediments underlie bluffs that are subject to exceptionally rapid coastal retreat, and one would expect submerged permafrost, even in these areas, to be limited to a belt extending no wider than a few hundred meters wide.

Three segments of the northern Bering Sea coast are subject to rapid coastal retreat which potentially may bring ice-rich sediments below sea level. These include the low-lying coast of Norton Bay between the delta of the Koyuk River and Cape Denbigh, the narrow coastal lowland between St. Michael and Apoon Pass, and the coast of the older part of the Yukon River delta south of Kwikloak Pass (figure 1). Any construction or excavation planned in nearshore waters along these coastal segments should be preceded by studies to determine the presence or absence, the extent, and the ice-content of bonded permafrost beneath nearshore waters.

## References cited

- Ager, T. A., in press, Vegetational history of western Alaska during the Wisconsinan glacial interval and Holocene time, in Hopkins, D. M., Matthews, J. V., Jr., Schweger, C. E., and Young, S. B., eds., *Paleoecology of Beringia*: Academic Press.
- Brown, R. J. E., and Péwé, T. L., 1973, Distribution of permafrost in North America and its relationship to the environment: a review, 1963-1973, in *Permafrost: the North American Contribution to the Second International Conference*: National Academy of Sciences, p. 71-100.
- Bruggers, D. E., and England, J. M., 1979, U.S.G.S. geotechnical investigations, Beaufort Sea, Alaska - 1979: Harding-Lawson Associates Job No. 9619-005.08, Contract No. 14-08-0001-1718, 3 vols.
- Coachman, L. K., Aagaard, K., and Tripp, R. B., 1975, *Bering Strait: the regional physical oceanography*: University of Washington Press, 172 p.
- Dupré, W. R., 1977, Yukon Delta coastal processes study: U.S. Department of Commerce, National Oceanic and Atmospheric Administration, Environmental Assessment of the Alaskan Continental Shelf: Annual Reports of Principal Investigators for the year ending March, 1977, v. XIV Transport, p. 508-553
- \_\_\_\_\_ in press, Yukon Delta coastal processes study: U.S. National Oceanic and Atmospheric Administration, Outer Continental Shelf Environmental Assessment Program: Annual Reports of Investigators for the year ending March 31, 1979.
- Gold, L. W., and Lachenbruch, A. H., 1973, Thermal conditions in permafrost--a review of North American literature, in *Permafrost--North American Contributions: 2nd International Conference, Yakutsk, U.S.S.R., July, 1973*: National Academy of Science, Washington, p. 3-25.
- Grim, M. S., and McManus, D. A., 1970, A shallow seismic-profiling survey of the northern Bering Sea: *Marine Geology*, v. 8, p. 293-320.
- Hartz, R. W., Holden, K., Hopkins, D. M., and Shearer, G., 1979, Location map and summary logs for the Geological Survey's 1979 Beaufort Sea Over-the-ice drilling program: U.S. Geological Survey Open File Report 79-1303.
- Hopkins, D. M., ed., 1967, *The Bering Land Bridge*: Stanford University Press, 495 p.
- \_\_\_\_\_ 1973, Sea level history in Beringia during the last 250,000 years: *Quaternary Research*, v. 3, p. 520-540.
- \_\_\_\_\_ 1979, Landscape and climate of Beringia during late Pleistocene and Holocene time, in Laughlin, W. L., and Harper, A., eds., *Origins and affinities of the first Americans*: Fischer-Verlag (in press).
- Hopkins, D. M., and Hartz, R. W., 1978, Coastal morphology, coastal erosion, and barrier islands of the Beaufort Sea, Alaska: U.S. Geological Survey Open File Report 78-1063, 54 -

- Hopkins, D. M., MacNeil, F. S., and Leopold, E. B., 1960, The coastal plain at Nome, Alaska--a Late Cenozoic type section for the Bering Strait region: Dept. 21st International Geological Congress, Copenhagen, Norden, pt. 4, p. 46-67.
- Hopkins, D. M., Nelson, C. H., Perry, R. B., and Alpha, T. R., 1976, Physiographic subdivisions of the Chirikov Basin, northern Bering Sea: U.S. Geological Survey Professional Paper 759-B, 7 p.
- Hopkins, D. M., Sellmann, P. V., Chamberlain, E., Lewellen, R. E., and Robinson, S. W., 1979, Buried valleys as a possible determinant of deeply buried permafrost on the continental shelf of the Beaufort Sea, App. 2, in Smith, P. A., and Hopkins, D. M., eds., Offshore permafrost and shoreline history of Chukchi and Beaufort Seas as an aid to predicting offshore permafrost conditions: Environmental Assessment of the Alaskan Continental Shelf: Annual Reports, Principal Investigators for year ending March, 1979 (in press).
- Johnson, J. L., and Holmes, M. L., 1978, Report on surface and subsurface faulting in Norton Sound and northeastern Chirikov Basin, Alaska, in Environmental Assessment of the Alaskan Continental shelf: Annual Report of Principal Investigators for the year ending March, 1978, v. 12, p.
- Lachenbruch, A. H., and Marshall, B. V., 1977, Sub-sea temperatures and a simple tentative model for offshore permafrost at Prudhoe Bay, Alaska, app. VIII, in Hopkins, D. M., and others, eds., Offshore permafrost studies, Beaufort Sea: U.S. National Oceanic and Atmospheric Administration, Outer Continental Shelf, Environmental Assessment Program: Annual Reports of Principal Investigators for the year ending March 31, 1977, v.
- Larsen, M. C., Nelson, H., and Thor, D. R., 1979, Geological implications and potential hazards of scour depressions on Bering shelf, Alaska: Environ. Geol., v. 3, p. 39-47.
- McManus, D. A., Kolla, V., Hopkins, D. M., and Nelson, C. H., 1977, Distribution of bottom sediments on the continental shelf, northern Bering Sea: U.S. Geological Survey Professional Paper 759-C, 31 p.
- McManus, D. A., Venkatarathnam, K., Nelson, C. H., and Hopkins, D. M., 1974, Yukon sediment in the northernmost Bering Sea shelf: Journal of Sedimentary Petrology, v. 44, p. 1052-1060.
- Nelson, Hans, 1978, Faulting sediment instability, erosion, and deposition - hazards of the Norton Basin sea floor, in U.S. National Oceanic and Atmospheric Administration, Outer Continental Shelf Environmental Assessment Program: Annual Reports of Principal Investigators for the year ending March 31, 1978, v. 12, p.
- Nelson, C. H., and Hopkins, D. M., 1972, Sedimentary processes and distribution of particulate gold in the northern Bering Sea: U.S. Geological Survey Professional Paper 689, 27 p.

Osterkamp, T. E., and Harrison, W. D., 1976, Subsea permafrost at Prudhoe Bay, Alaska: drilling report and data analysis: University of Alaska Geophysical Institute Report No. 76-5, 67 p.

Péwé, T. L., 1975, Quaternary geology of Alaska: U.S. Geological Survey Professional Paper 835.

Williams, J. R., 1970, Ground water in the permafrost regions of Alaska: U.S. Geological Survey Professional Paper 696.

Figure D-1. Location Map. Heavy sinuous line parallel to coast indicates areas in which ice-bonded permafrost is likely to be encountered in the nearshore zone.



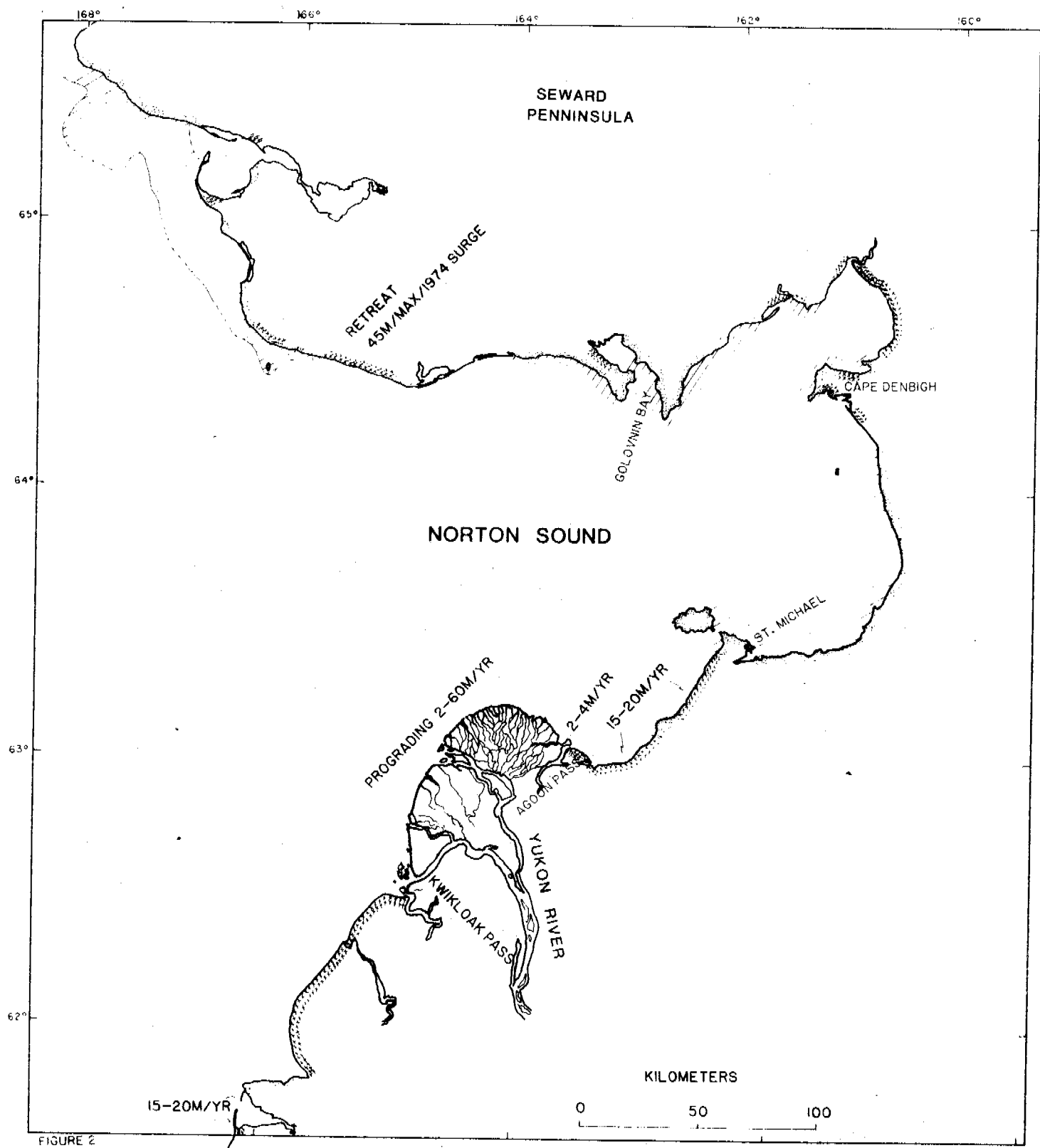


FIGURE 2

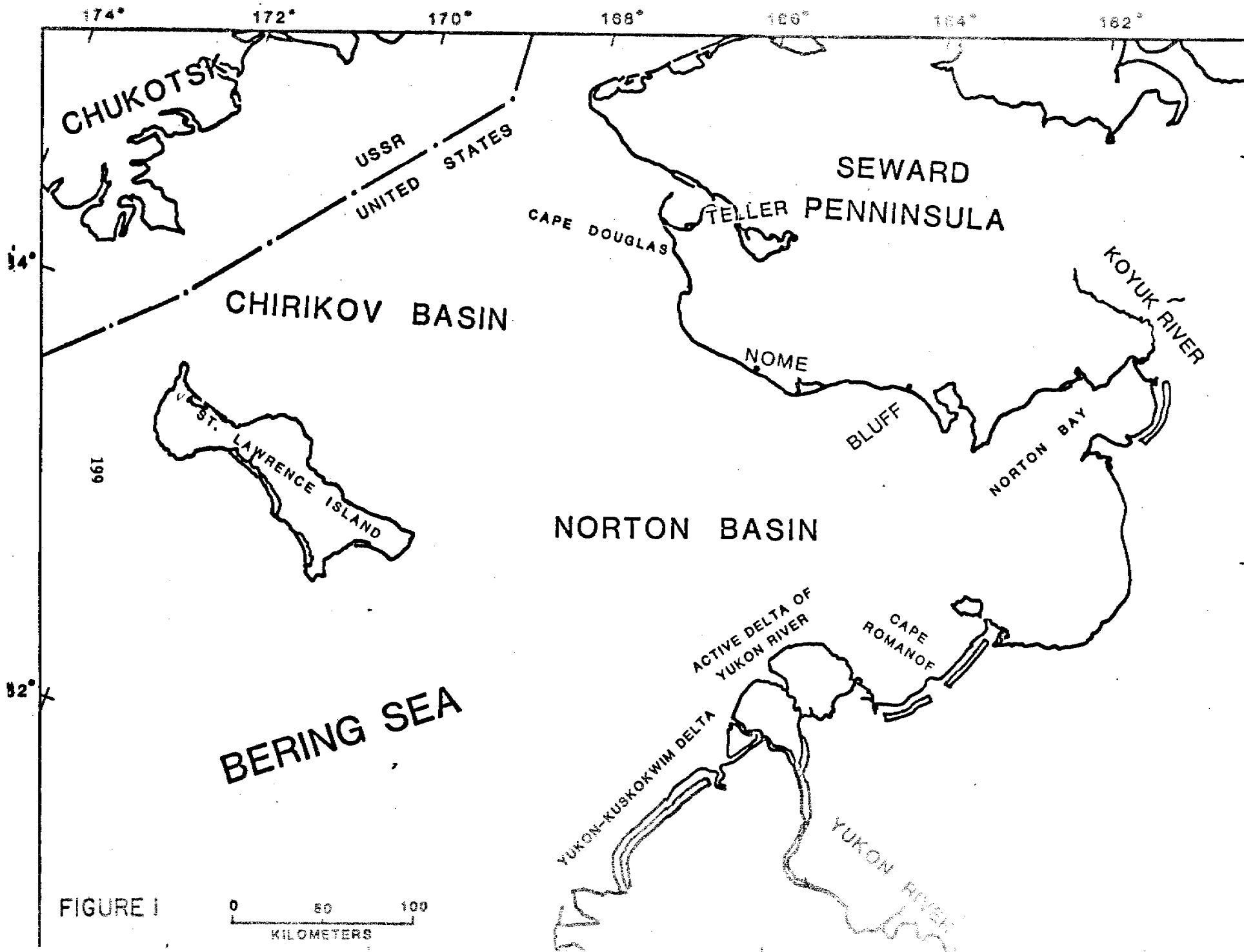


Figure D-2. Classification of coast and nearshore zone of mainland coast of northern Bering Sea. Stippled pattern: coastal segment cut in bedrock. Coarse hatched pattern: submerged areas underlain at shallow depth by bedrock. "X"'s: coastal segments adjoined by bluffs cut in Pleistocene or Holocene sediment (numbers indicate rates of coastal retreat). Fine cross-hatched pattern: fronts of prograding deltas (numbers indicate rate of progradation). Coastal segments with no pattern consist of spits, barrier bars, and prograded beach-ridge complex.

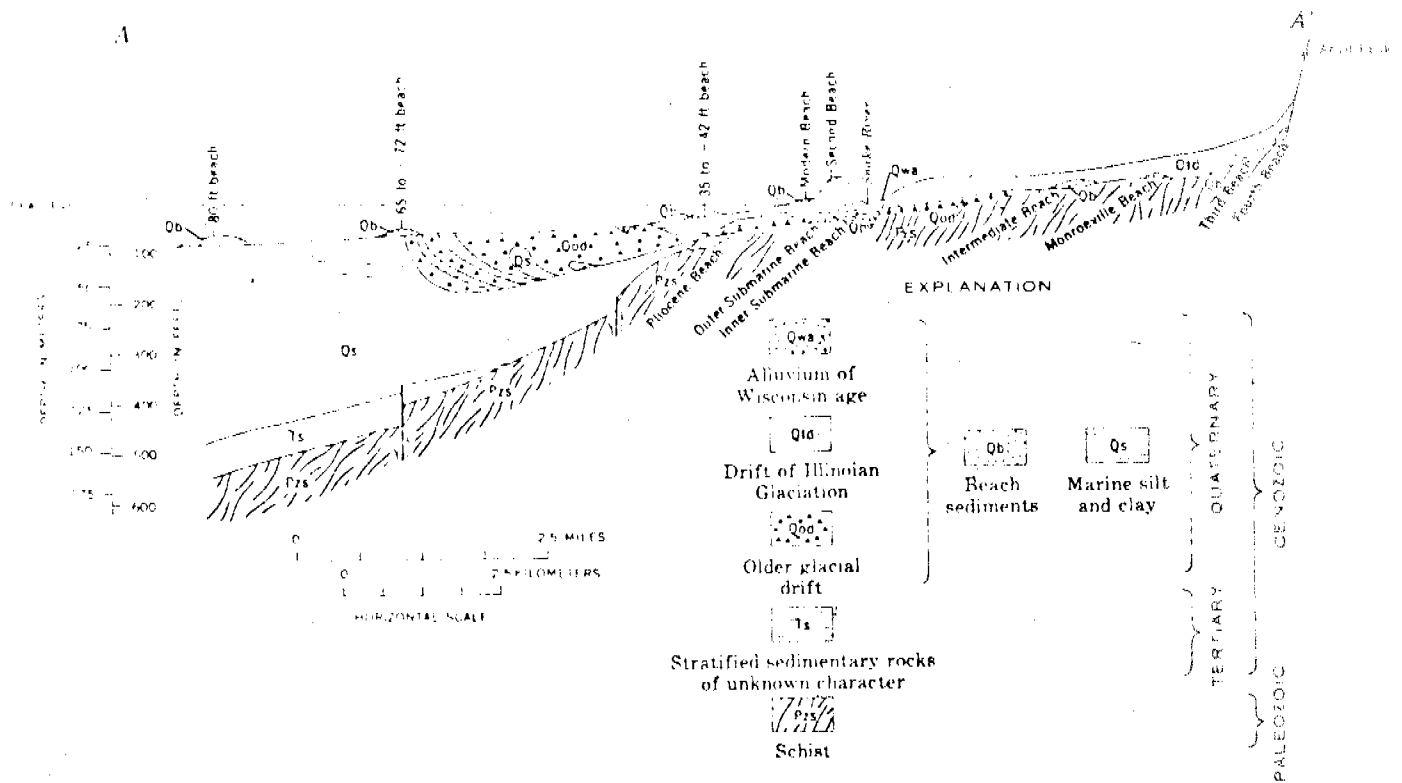
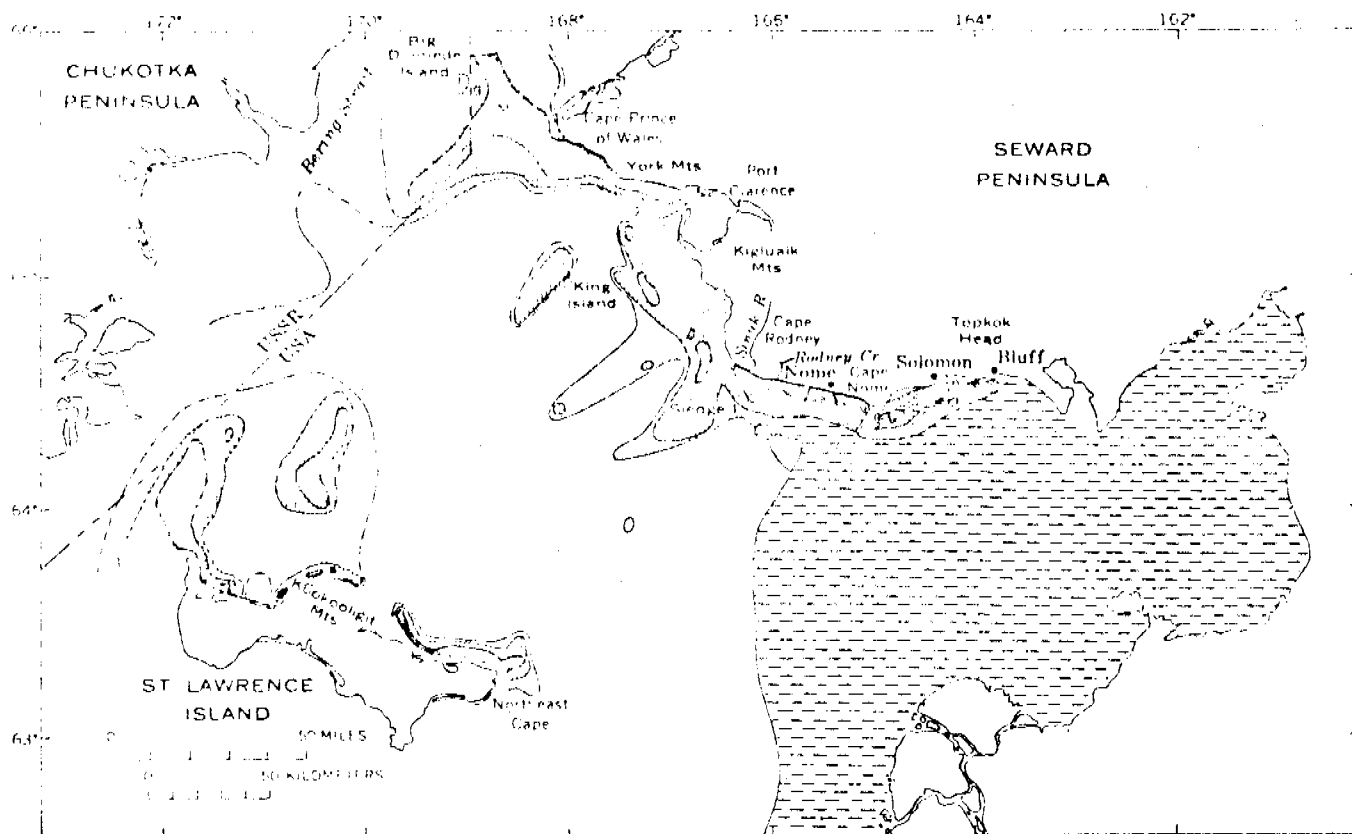
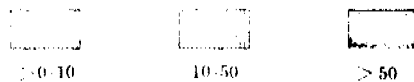


Figure D-3. Geologic section across the coastal plain area at Nome. Onshore geology from Hopkins (1967) and based in part on unpublished results of exploratory drilling by United States Smelting, Refining, and Mining Co. Offshore geology based on seismic-reflection profiles by A. R. Tagg and H. G. Greene, 1970, and results of exploratory drilling by Shell Oil Co. and U.S. Bureau of Mines.



EXPLANATION



Percentage of gravel in surface sediments

Fine silty sand

Yukon silts

Figure D-4. Distribution of sediments in the northern Bering Sea (from Nelson and Hopkins, 1972).

APPENDIX E

RADIOCARBON DATES FROM THE BEAUFORT AND CHUKCHI SEA COASTS (1979-80)

D. M. Hopkins<sup>1/</sup>, S. W. Robinson<sup>1/</sup>, and J. Buckley<sup>2/</sup>

---

<sup>1/</sup>U.S. Geological Survey, Menlo Park, CA 94025

<sup>2/</sup>Isotopes, Inc., Westwood, NJ 07675

We report here the results of radiocarbon dating of 24 samples from coastal areas of the Chukchi and Beaufort Seas and the continental shelf of the Beaufort Sea as a contribution to the Outer Continental Shelf Environmental Assessment Program (OCSEAP) funded by the U.S. Bureau of Land Management and managed by the U.S. National Oceanographic and Atmospheric Administration. The report supplements and in a few cases amends information given in a previous list of 22 dates (Hopkins and Robinson, 1979). Locality data, stratigraphic notes, and some discussion are given in table E-1 and localities are shown on figures E-1 to E-3. Additional discussion is given below for some of the conclusions that can be drawn from the two date lists.

Interglacial deposits.--An alluvial terrace of the Kaolak River and a thaw-lake deposit on Baldwin Peninsula dating from the last interglacial interval are identified by contained organic remains and by infinite radiocarbon dates (USGS-690, I-10622). Closer study of these localities could provide valuable paleoclimatic and paleoecological information concerning the last interglacial interval in northwestern Alaska.

Interstadial deposits.--Pleistocene studies in Siberia (e.g., Kind, 1967) have shown that the last glaciation was preceded by a relatively mild interval, the Kargin Interstadial, which lasted from about 24,000 to 45,000 years ago. This interval corresponds to isotope stage 3 of deep-sea cores

(Shackleton and Opdyke, 1973) and evidently was experienced throughout the world as a remission of the severer climates that preceded and followed during the early and late parts of the last glacial interval. So far, this interstadial interval has been little studied, however, in Alaska. Consequently, it is interesting that several of our samples date a cycle of alluviation and organic accumulation in northern Alaska during this interval 45,000-24,000 years ago.

A 7-m terrace on the Kaolak River (USGS-689, preliminary date reported by S. W. Robinson, written commun., 4/80) and a 10-m terrace of the Colville River (LSU-7345, Hopkins and others, in press) date from this interval. In the Prudhoe Bay area, alluvium from this cycle of aggradation has been buried beneath younger glacial outwash, but the relatively mild interval is recorded by wood-bearing alluvium, a paleosol, and buried peat exposed in 1978 in a deep gravel pit on the lower Putulagayuk River (USGS-504, -505) and in a widespread organic horizon encountered in offshore boreholes between Prudhoe Bay and Reindeer Island (USGS-210, -249, -638). The presence of a marine amphipod (Charlotte Holmquist, Naturhistoriska Riksmuseet, Stockholm, written commun., 7/22/77) associated with 42,800-year-old peat at -13.5 m in borehole PB-7 (USGS-249) suggests that sea level may have been only a few meters lower 42,000 years ago. Of additional interest is the fact that wood of Populus (cottonwood or aspen) has been identified in the "Kargin" deposits of the lower Colville terrace and the Put River gravel pit.

Warmer, wetter climate at beginning of Holocene.--Many observers have recognized that a unique vegetation rich in Populus trees and various shrubs extended into present-day tundra areas in western and northern Alaska about

10,000 years ago and that this event coincided in many places with thawing of permafrost by as much as 2 m below the present-day frost table (McCulloch and Hopkins, 1966; Brown, 1967; Detterman, 1970; Hopkins et al., in press). Continuing and partly unpublished studies indicate that the warming and vegetation change probably began as early as 11,000 years ago and was ended between 8,000 and 8,500 years ago. The exact nature of the climate and the reasons for its differences from present-day climates remain unknown and should be elucidated. A better understanding, for example, probably would assist in attempts to anticipate the environmental consequences of the projected warming of the Arctic in the near future due to an increase in the amount of CO<sub>2</sub> in the atmosphere.

We have sampled at least five thaw-lake sequences dating from this interval at Nokotlek Point (I-10328), 9 km south of Wainwright Inlet (I-10368), near the head of the Kuk River delta (USGS-517 and -518), at Drew Point (USGS-692), and on Flaxman Island (I-10639 and -10640). Most are rich in identifiable organic remains, including wood of large shrubs. More detailed studies of the fossil organisms preserved in these deposits would provide valuable paleoclimatic information.

Thaw lake evolution and history.--Our geochronologic and stratigraphic studies have provided considerable incidental information on the thaw-lake cycle in northern Alaska. Geochronologic and stratigraphic studies near the Arctic Circle on northern Seward Peninsula (Spieker and others, 1978; D. M. Hopkins, unpub. data) indicate that thaw lakes have been a feature of the landscape during glacial as well as interglacial intervals, although lakes may have been less abundant during interglacial and interstadial intervals than at the present time. In northern Alaska, however, thaw lakes seem to have



been entirely absent during the interval 24,000 to 11,000 years ago, and we do not know enough about the earlier "Kargin" interstadial interval, 24,000-45,000 years ago, to state whether thaw lakes were present or not. In any case, the radiocarbon-dated samples reported here and by Hopkins and Robinson (1979) provide age estimates for at least 16 different thaw-lake sequences, and all are less than 11,000 years old. Thaw lakes in northern Alaska seem to have had their inception during the 11,000-9,000-year-old climatic event.

Carson (1968) shows that several lakes on the low-lying coastal plain near Barrow have persisted, though with changing levels, for at least 2,700 and possibly 4,200 years. Unpublished palynological studies by P. M. Anderson (Brown University, written commun., 1979) indicate that Teshekpuk Lake and Square Lake (a small lake in the foothills at the inner edge of the Arctic coastal plain) have also been in existence for many thousand years. Our results, however, suggest that long-lived lakes may be exceptional and that thaw lakes are generally short-lived. None reported here seem to have persisted longer than 2,000 years.

We have encountered several sites where young Holocene lake deposits are superposed upon lake deposits several centuries to several millenia older. Examples are found at the east end of Flaxman Island (I-10637, -10638, and -10639), at Drew Point (USGS-692 and unpublished dated sample of D. L. Carter), I-10328 and -10329 (Robinson and Hopkins, 1979), and at the coal-diapir site 9 km south of Wainwright Inlet (USGS-507, I-10620). Most of these examples evidently record distinct episodes of lake development separated by lengthy intervals when no lake was present, but the coal-diapir sequence probably reflects several occupations of the site by the fluctuating shoreline of a

single lake. Where they occur, these successive, superposed lake deposits obviously record net aggradation of (that is, addition of material to) the surface of the coastal lowland during the last 10,000 years. The added material consists partly of accumulated peaty plant remains, but much of it is fine-grained mineral material. The source of the silt and sand is uncertain, but we speculate that east of Colville River it may consist largely of wind-blown silt and sand swept from the larger river channels, and west of the Colville that it consists mostly of material blown from the exposed bottoms of other, nearby drained thaw lakes.

Time of initiation of accumulation of peat and organic-rich detritus.--

OCSEAP studies have shown that organic detritus eroded from peat and from the plant remains in peaty sand and gravel exposed in coastal bluffs of Beaufort Sea contributes significantly to productivity in nearshore waters such as Simpson Lagoon (Don Schell, Univ. Alaska, oral commun., 1979). A better understanding of nutrient resources and cycling on the Beaufort Sea shelf can be gained, therefore, through better knowledge of the age and origin of organic deposits exposed in the coastal bluffs. Interestingly enough, our date lists (Table E-1 and Hopkins and Robinson, 1979) show that practically all of the exposed peaty deposits in coastal areas of the northern Chukchi and Beaufort Seas are younger than 11,000 years. In situ peat beds are unknown and detrital organic accumulations are extremely rare in deposits between 11,000 and 24,000 years ago, and deposits older than 24,000 years lie below sea level near the Beaufort Sea coast and cannot contribute organic debris to the present-day Beaufort shelf. If organic detritus eroded from coastal bluffs is now an important contributor to marine productivity on the continental shelf of the Beaufort

Sea, it would seem to follow that shelf productivity must have been considerably lower prior to 11,000 years ago.

Surface turf aside, the organic deposits exposed in Beaufort Sea coastal bluffs consist of the bottom deposits of drained thaw lakes and in situ peat that accumulated in a low-center ice-wedge polygons. The thaw lake deposits, discussed above, range in age from 10,600 (USGS-517) to as young as 500 years (USGS-506), but all of the in situ polygon peat accumulations that we have seen are less than 8,500 years old (I-10330, -11052).

We suspect that this changing record of organic accumulation reflects a series of climatic changes in northern Alaska. Certainly, as we noted above, the initiation of organic-rich lake sedimentation about 11,000 years ago clearly records a climatic shift toward a wetter and probably warmer climate than that which had prevailed in northern Alaska during the preceding 13,000 years. The apparent initiation, about 8,500 years ago, of peat accumulation, facilitating development of low-center ice-wedge polygons and impounding shallow ponds, coincides with the end of the episode of more widespread poplar and large-shrub growth in northern and western Alaska and evidently records a further increase in available moisture, probably accompanied by cooler summers.

Canning ash.--Hopkins and Robinson (1979) show that the thin ash layer encountered in lacustrine and alluvial deposits in several places between the Canning and Kuparuk Rivers is a useful stratigraphic marker whose age is reasonably well defined at Canning Point on the west side of the mouth of the Canning River as less than  $3,945 \pm 115$  years (I-10369) and more than  $3,315 \pm 115$  years (I-10370). New data presented in table E-1 is consistent with this dating but fails to refine it. However, the ash has proved useful in defining times of

drainage changes (discussed below) and of initiation of thick cliff-head dune accumulations.

Holocene history of the Putulagayuk River.--Both D. M. Hopkins (in Smith and Hopkins, 1979) and Cannon and Rawlinson (1979) have recognized evidence that a major branch of the Sagavanirktok River once flowed down the present-day course of the Putulagayuk River. Hopkins postulated that this stem of the Sagavanirktok River fed the large paleovalley recognized through drilling on the continental shelf and suggested that Prudhoe Bay is the estuary of this large stream, somewhat widened by thermoarst collapse. The terrace lacks thaw lakes and large ice wedges and for that reason seems very young (and also very desirable as a building site). Samples I-10642 confirms that the terrace was being built by the Sagavanirktok River as recently as 5,500 years ago. Sample I-10643 confirms that the terrace had been abandoned and the Putulagayuk River incised by 2,150 years ago, but if the pink layer in the ox-bow fill at locality I-10642 is really the Canning ash, then the terrace was abandoned and the smaller Putulagayuk River incised by 3,900 years ago.

Redeposition of organic debris.--Because thaw lakes enlarge by thawing and collapse of their steep banks, one intuitively assumes that their bottom sediments consist largely of redeposited material, and, indeed, the belief that the bottom sediments must contain much redeposited pollen has resulted in their general avoidance in palynological studies. Our radiocarbon dates confirm that wood and peaty remains several hundred years old can be recycled into a thaw lake. For example, sample USGS-508, collected 60 cm above the base of thaw-lake deposits at the coal diapir locality, is 800 years older than sample USGS-507, collected at the base of the sequence, and a similar stratigraphic

inversion was encountered in thaw-lake deposits on Flaxman Island, where wood collected 45 cm above the base of the sequence (I-10371) is 600 years older than wood collected at the base. That alluvium, too, may contain redeposited wood seems to be indicated by the 7,200-year age (I-10644) for a sample from a terrace in the inner valley of the Putulagayuk River that can hardly be older than 5,500 years.

The confirmation that wood in alluvium and thaw-lake deposits may be centuries or even millenia older than the enclosing sediments should be kept in mind in detailed studies of palynological sequences and alluvial history in Arctic Alaska.

#### References Cited

- Brown, Jerry, 1967, Tundra soils formed over ice wedges, northern Alaska: Soil Science Society of America Proceedings, v. 31, p. 686-691.
- Cannon, P. J., and Rawlinson, S. E., 1979, The environmental geology and geomorphology of the barrier island-lagoon system along the Beaufort Sea coastal plain: U.S. National Oceanographic and Atmospheric Administration, Environmental Assessment of the Alaskan Continental Shelf, Annual Reports of Principal Investigators, March 1979, v. X, p. 209-321.
- Carson, C. E., 1968, Radiocarbon dating of lacustrine strands in Arctic Alaska: Arctic, v. 21, p. 12-26.
- Detterman, R. L., 1970, Early Holocene warm interval in northern Alaska: Arctic, v. 23, p. 130-131.
- Hopkins, D. M., and Robinson, S. W., 1979, Radiocarbon dates from the Beaufort and Chukchi Sea coasts: U.S. Geological Survey Circular 804-B, p. 44-47.
- Hopkins, D. M., Smith, P. A., and Matthews, J. V., Jr., Dated wood from Alaska and the Yukon: implications for forest refugia in Beringia: Submitted to Quaternary Research. (in press)
- Kind, N. V., 1967, Radiocarbon chronology in Siberia, in Hopkins, D. M., The Bering land bridge: Stanford University Press, p. 172-192.
- McCulloch, D. S., and Hopkins, D. M., 1966, Evidence for an early recent warm interval in northwestern Alaska: U.S. Geological Society of America Bulletin, v. 77, p. 1089-1108.

- Shackleton, N. J., and Opdyke, N. D., 1973, Oxygen isotope and paleomagnetic stratigraphy of equatorial Pacific core V28-238: oxygen isotope temperatures and ice volume on a  $10^5$  year and  $10^6$  year scale: *Quaternary Research*, v. 3, p. 39-55.
- Smith, P. A., and Hopkins, D. M., 1979, Offshore permafrost studies and shoreline history of Chukchi and Beaufort Seas as an aid to predicting offshore permafrost conditions: U.S. National Oceanic and Atmospheric Administration, Environmental Assessment of the Alaskan Continental Shelf, Annual Reports of Principal Investigators, March 1979, v. IX, p. 116-163.
- Spieker, E., Kelley, L., and Rubin, M., 1978, U.S. Geological Survey radiocarbon dates XIII: *Radiocarbon*, v. 20, p. 139-156.

TABLE E-1

## RADIOCARBON AGE DETERMINATIONS FROM THE BEAUFORT AND CHUKCHI SEA COASTS (1979-80)

Laboratory number (Field no.)	Location (Quadrangle)	Longitude W. Latitude N.	Material	Age determination	Stratigraphic setting and significance
USGS-504 (77Ahp84d)	9.5 m below sfc., gravel pit beneath ox-bow of Putuli- gayuk River (Beechey Pt. B-3)	70°17'25" 148°38'24"	Twigs	35,600 ± 550	Dates lower and older of two organic horizons (buried soil, local compressed peat, ice-wedge pseudomorphs containing accumulations of detrital wood of <i>Salix</i> <sup>a</sup> and <i>Populus</i> <sup>b</sup> ) interbedded with gravel, probably Sagavanirktok River outwash. Upper horizon previously dated as 26,300 ± 370 years (USGS-505, Hopkins and Robinson, 1979).
USGS-507 (76Ahp84a)	Terrace-like flat about 2 m above sea level 8 km south of Wain- wright Inlet (Wainwright C-3)	70°32'01" 160°15'03"	Tangle of rooted heaths with attached leaves	6,260 ± 80	These two samples and I-10620 (below) date activity of small diapirs of shattered Cretaceous coal intruded upward into early Holocene thaw-lake deposits about 1 m thick. Tangle of rooted and leafed heaths ( <i>Cassiope</i> sp. <sup>c</sup> ) once were living plants undercut by expanding thaw lake 6260 years ago (USGS-507) and now lie at base thaw-lake sequence. <i>Salix</i> <sup>b</sup> twigs are in detrital peat lens 60 cm higher that was deformed by rising diapir. Age of 7,040 years indicates they were dead and buried when undercut by bank expanding lake. Diapirs are truncated by younger thaw lake sequence with basal date of 5,410 ± 110 years (I-10620) and diapir activity ceased before that time.
USGS-508 (76Ahp84e)	-----Ditto-----	--Ditto---	Twigs ( <i>Salix</i> )	7,040 ± 90	
USGS-510 (77Ahp14le)	North shore of Kogru River (Harrison Bay C-4)	70°34'30" 152°17'12"	Peat	4,580 ± 75	From depth of 30 cm in mass of detrital peat 2.0 m thick resting on Gubik Formation of Pelukian (last interglacial) age. Peat mat contains interbeds of silt, scattered pebbles, and large twigs and roots and represents marginal shoreline deposit of large, drained thaw lake. Sample gives approximate time of initiation of ice wedges now 1.5-1.75 m thick.

USGS-512 (77Ahp178a)	Bluff, 2.75 m SW Cape Bakkett (Harrison KV D-4)	70°47'34" 152°15'12"	Peat	5,980 ± 50	Collection near middle of ancient thaw-lake deposit consisting of well-bedded fine sand and detrital peat 1.5 m thick. Underlain at sea level by beach deposits of Pelukian or Flaxman age and overlain by peat 1.5 m thick and surficial loess 25 cm thick. This lake deposit is truncated laterally by deposits of slightly younger, lower thaw lake, 2,900-3,100 years old (USGS-501, -503, Hopkins and Robinson, 1979), which is evidently the source of surficial loess. This locality is another example of repeated Holocene thaw lake cycles on Arctic coastal plain.
USGS-514 (76Ahp146b)	Coastal bluff about 7 m high on shore of Baldwin Peninsula near Arctic Circle (Kotzebue C-1)	66°39'27" 162°17'24"	Wood ( <u>Salix</u> <sup>a</sup> )	150 ± 40	Dates a low alluvial terrace resting on marine silt of Kotzebuan (middle Pleistocene age) about 5 m above sea level. The terrace is incised through a thaw-lake deposit which overlies Kotzebuan deposits at 8 m. Bones of mammoth, bison, and caribou <sup>d</sup> on the beach seem to be washing out of the alluvium but evidently were originally derived from the undated thaw-lake deposits.
USGS-515 (76Ahp90e)	3.5-m terrace, Kaolak River, 3.5 m above mouth (Wainwright A-2)	70°05'00" 159°40'15"	Wood	Less than 100	Collected 30 m below surface, this sample shows that 4.5 m terrace is the active flood plain of the Kaolak River. Another sample 1,730 ± 40 years old (USGS-499) was collected at 3.7-3.8 m below surface of this same terrace (Hopkins and Robinson, 1979).
USGS-516 (76Ahp87a)	4-m bluff on right bank of Kuk River at head of delta (Wainwright C-3)	70°13'55"	Wood ( <u>Salix</u> <sup>a</sup> )	9,590 ± 80	This sample and USGS-517 (10,600 ± 180) (Hopkins and Robinson, 1979) date a thaw-lake deposit consisting of olive, loess-like silt and yellow fine sand with peaty interbeds, cut by vertical stringers (diapirs?) of shattered coal. Ice-wedge pseudomorphs at base of sequence very woody and contain willow stems up to 4 cm thick--much larger than willows presently growing on lower Kuk River. Dates confirm field interpretation that this woody deposit accumulated during early Holocene warm period of McCulloch and Hopkins (1966). A distal humerus of <u>Equus</u> sp. <sup>d</sup> found on beach may be derived from this deposit



USGS-638 (PB-7, 62.4-63.3 m)	Borehole 3.3 km offshore near ARCO West Dock, Prudhoe Bay	70°28'30" 148°21'36"	Organic debris	31,600 ± 600	This sample consists of discrete organic particles (twigs and shreds of wood) screened and handpicked from a wash sample near the bottom of borehole PB-7. A sample higher in the hole at 13.3-13.6 m yielded a date of 42,800 ± 1,440 (USGS-249, Hopkins and Robinson, 1979), but a nearby borehole yielded organic material dated at 22,300 ± 1,200 at a depth of about 13.5 m (AU-115) and presumably from the same horizon (Hopkins and Robinson, 1979). Contamination of USGS-638 by modern wood slivers entrained in circulation water is possible, but real significance of these dates cannot be assessed until additional samples have been analyzed.
USGS-690 (76Ahp92c)	14-m fluvial terrace of Kaolak River, 1.5 km above mouth (Wainwright A-2)	70°06'48" 159°40'30"	Detrital peat	More than 30,000	Sample was collected 12.5 m below top of the highest of three terraces of lower Kaolak River. Terrace sediments consist of well-bedded sand and silt with lenses of twigs, large willow leaves. Nearby 7-m terrace yields a preliminary age of about 37,000 years (USGS-689).
USGS-692 (78Ahp15o & 78Ahp15p)	1 km east of Drew Point (Teshekpuk D-2)	70°16'36" 161°56'30"	Wood	10,300 ± 70	When collected, the two twigs were thought to represent driftwood in Flaxman Formation but later micropaleontological study (Appendix <u>  </u> ) indicates that sediments containing dated wood were deposited in early Holocene thaw lake, and these two samples date the period of existence of the lake.
I-10620 (76Ahp84c)	Terrace-like flat above 2 m above sea level 8 km south of Wainwright Inlet (Wainwright C-3)	70°32'01" 160°15'03"	Twigs ( <u>Salix</u> <sup>a</sup> )	5,410 ± 110	Base of thaw-lake deposit 0.5 m thick. Dates inception of lake and places limit on youngest possible age of underlying lake deposits (USGS-507, 508).

I-10621 (76Ahp26c)	Blow-out in dunes at south end of small thaw lake near Icy Cape (Wainwright B-5 & 6)	70°18'20" 161°43'00"	Wood and charcoal	Less than 185	Collected in lens of wood, charcoal, butchered bone, and chert flakes exposed beneath 7-13 cm aeolian sand and dates an occupation site which proves to be unexpectedly young. Wood identified as spruce ( <u>Picea</u> <sup>C</sup> ) was probably driftwood. Bones include many Rangifer (reindeer or caribou, some juvenile), a calcaneus of <u>Pusa</u> (ringed seal), and the anterior portion of a mandible of <u>Equus</u> (Geological Survey pack horse?).
I-10622 (76Ahp151)	12-m high coastal bluff on Baldwin Peninsula, Kotzebue Sound (Kotzebue C-1)	66°39'45" 162°08'06"	Wood ( <u>Picea</u> <sup>a</sup> )	More than 40,000	From base of thaw-lake deposit 2 m thick and associated with spruce logs up to 25 cm thick with attached roots. Sequence rests on Kotzebuan (middle Pleistocene) marine deposits extending about 10 m above sea level. Site is about 50 km west of present spruce limit. Evidently this complex was deposited in a thaw lake of Sangamon age which developed in and undercut an interglacial spruce woodland.
I-10624 (76Ahp174b)	Barrier bar ca. 3.5 km north of Kivalina. Chukchi Sea coast (Noatak D-6)	67°48'18" 164°43'30"	Wood and charcoal	Less than 185	Dates occupation of abandoned igloo constructed of driftwood and whalebone; a greater age had been expected on basis of lithic material. House dated in order to estimate minimum age of underlying beach ridge and to provide information on rate of coastal progradation.
I-10625 (77Ahp36)	Canning Point (Flaxman Island A-3)	70°04'45" 143°34'30"	Wood ( <u>Salix</u> <sup>a</sup> )	5,360 ± 110	From woody peat layer covered by 1 m of wind-blown sand which accumulated in small pond. Peat is vertical, being deformed by truncated ice wedges older than the sand accumulation which was dated previously as 3,945 ± 115 (I-10, 369--Hopkins and Robinson, 1979) and younger. Radiocarbon results place lower limit on age of lake and of aeolian sand accumulation and record river-bank willow thickets that lived when sea level was lower, shoreline displaced to north, and summer climate was warmer, perhaps because of remoteness of shore.

I-10637 (77Ahp40d)	8-7 m bluff, Flaxman Island (Flaxman Island A-4)	70°10'34.5" 145°56'48"	Detrital peat	4,250 + 170	Together with I-10371 (4,890 + 230 years) and I-10372 (2,375 + 175 years) (Hopkins and Robinson, 1979), these samples date various events recorded in an 8.7 m bluff at the east end of Flaxman Island overlooking Leffingwell Channel. The section is as follows: (This account corrects some misinterpretations given in Hopkins and Robinson, 1979.)
I-10638 (77Ahp40f)	-----Ditto-----	--Ditto---	Detrital peat	2,775 + 125	1.35 m Cliffhead dune--medium sand with interbeds of detrital peat. I-10372 from 0.55 m below top and I-10638 from base.
I-10639 (77Ahp40i)	-----Ditto-----	--Ditto---	Wood ( <u>Salix</u> <sup>a</sup> )	10,080 + 170	3.30 m Thaw-lake deposits (not cliff-head dune as stated in Hopkins and Robinson, 1979) consisting of interbedded silt and detrital peat. Contains Canning Ash at 2.95 m below top. I-10371 collected 10 cm above ash and evidently is redeposited older peat. I-10637 is 5 cm below ash and places maximum limit on age. Sequence cut by ice wedges 2 m wide.
					2.0 m Deposits of older thaw lake--silt with with chunks of peat and scattered pebbles and cobbles. I-10639 from base.
					1.0+ m Frozen medium sand
					1.7 Covered by slumped debris
					Dating of cliff-head dune shows that Leffingwell Channel originated as barren flood plain of Staines River, occupied about 2,800 to 1,800 years ago.
I-10640 (77Ahp43b)	4-m bluff, N side Flaxman Island, 2 km W. of Leffing- well Channel (Flaxman Island A-4)	71°11'13.5" 145°59'09"	Detrital peat with <u>Salix</u> <sup>a</sup>	9,280 + 150	From thaw-lake deposits 2.5 m thick resting on interbedded marine medium and fine sand with erratic boulders of Flaxman Formation. Sample comes from 10-cm woody and peaty zone at base of thaw-lake sequence and is associated with willow stems up to 5 cm diameter, larger than willows now growing along Beaufort Sea coast. Conceivably may sample same lake as that represented by I-10639.

I-10642 (77Ahp99a)	From upper (south- ern) of two gravel pits on Putulagayuk River active in 1977 (Beechey Point B-3)	70°16'45" 148°32'24"	Detrital peat	5,470 ± 110	Dates history of Holocene drainage changes on Sagavanirktok River fan. Wall of gravel pit showed 0.9 m of oxbow sediments (bedded sand and silt) containing pink layer, probably Canning River ash, near base, resting on more than 4 m of downward-coarsening sand and gravel containing detrital wood and peat and representing alluvium of stream much larger than present-day Put River which evidently then carried much of discharge of Sagavanirktok River (Jan Cannon, 1979 Ann. Rept. to OCSEAP). Sample collected 0.9 m below top of Sagavanirktok alluvium.
I-10643 (77Ahp83)	E. bank Putulagayuk River 0.25 km above MP road, near Pumping Sta. No. 1 (Beechey Point B-3)	70°15'51" 148°38'15"	Peaty sand	2,150 ± 160	Collected at base of 0.75 m layer of frost-stirred windblown sand resting on terrace alluvium laid down when Put River carried much of drainage of Sagavanirktok River (see I-10642 above). Establishes minimum age for diversion of Sagavanirktok River and incision of present-day Putulagayuk River.
I-10644 (77Ahp84)	1.5 m terrace on E. bank Putula- gayuk River 0.45 km above BP road.	70°15'57" 148°38'24"	Twigs	7,200 ± 180	From detrital peat a few cm thick forming surface of small 1.5 m gravel terrace inset in Put River channel which here is incised 3 m below broad Sagavanirktok terrace dated by I-10642 and I-10643. Detrital peat contains many twigs and concentrations of <u>Pisidium</u> and <u>Valvata</u> shells <sup>c</sup> , mollusks typical of ponds, not streams. Fauna and unexpectedly great age indicates detrital peat is redeposited from an older thaw-lake deposit.
I-11052 (78ACrII- 66a)	1 km east of Drew Point and a few hundred meters west of USGS-692 (Teshekpuk D-2)	70°15'36" 161°56'30"	Peat	7,750 ± 125	Peat collected by D. L. Carter from basal few centimeters of 2-m peat mass accumulated in ponds of high-center ice-wedge polygons. Wedges are 1.1 m across. Sample dates inception of peat accumulation and ice-wedge growth at this locality and places minimum age of drainage of thaw lake represented by USGS-692.

- a Identified by J. T. Quirk, Forest Products Laboratory  
b Identified by J. Carr, Central Washington State University.  
c Identified by D. M. Hopkins, U.S. Geological Survey.  
d Identified by C. A. Repenning, U.S. Geological Survey.

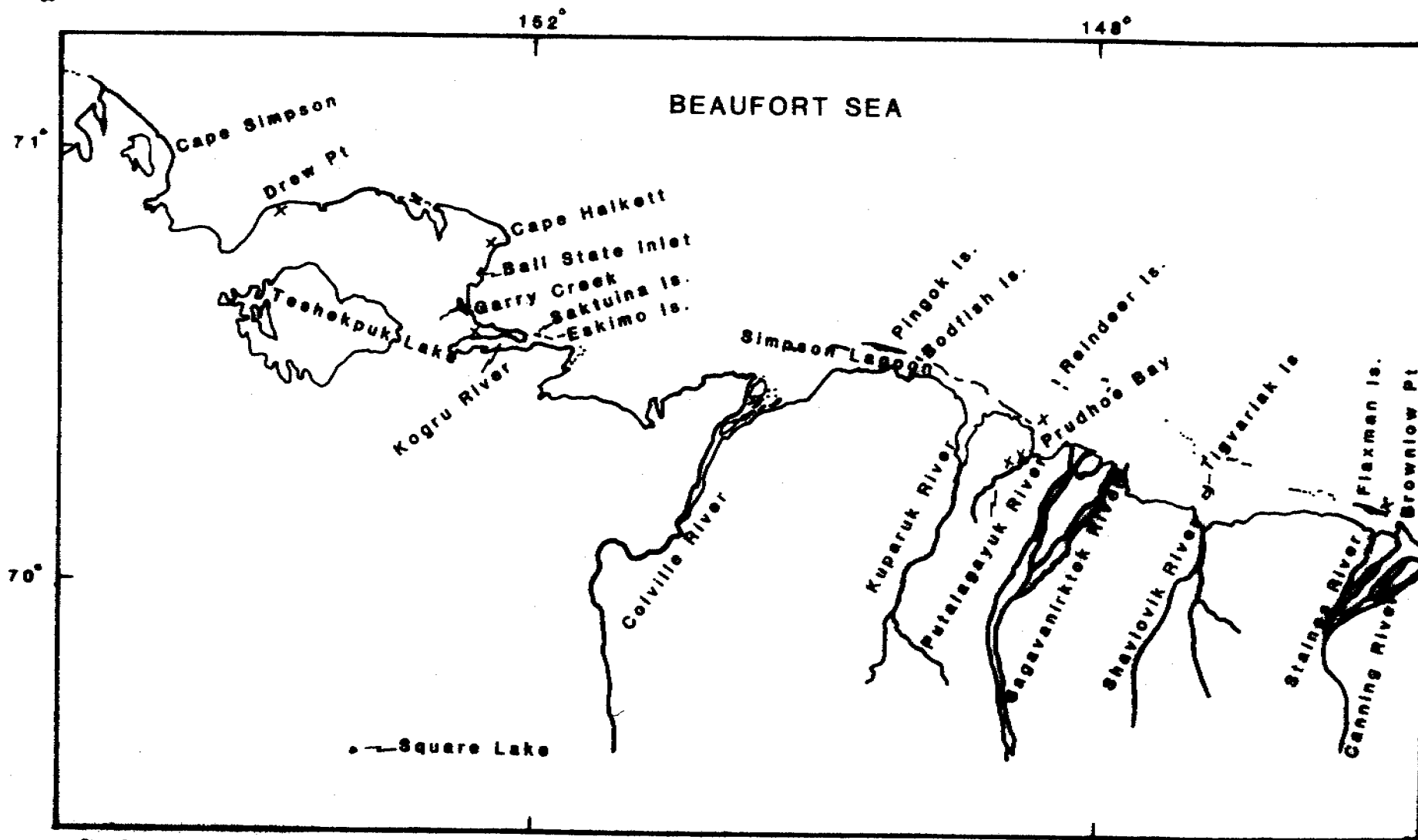


Figure E-1. Location map, central Beaufort Sea coast. x indicates sites of radiocarbon samples referred to in Table 1.

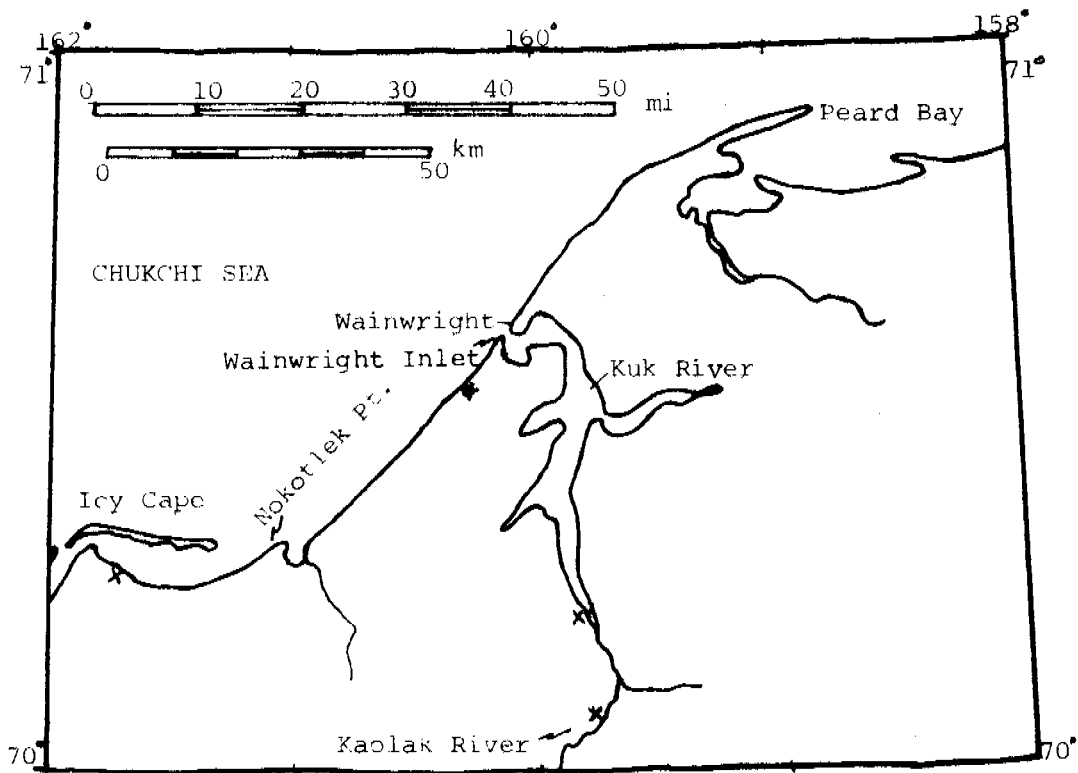


Figure E-2. Location of Wainwright - Kuk River area. \* indicates site of radiocarbon samples referred to in Table 1.

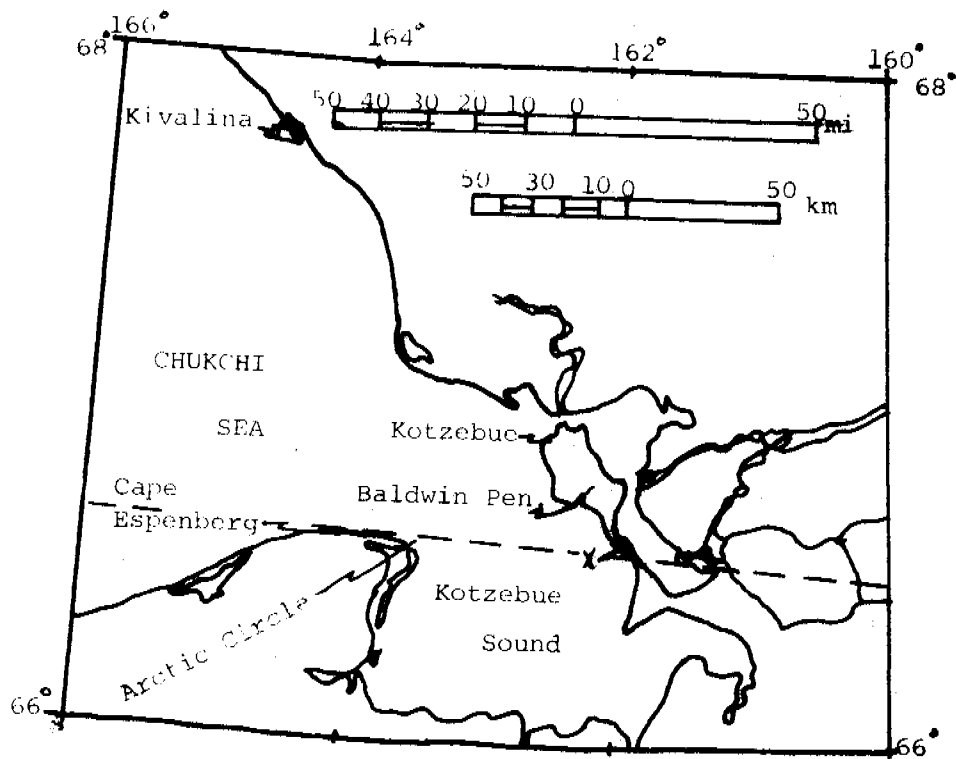


Figure E-3. Kivalina - Kotzebue Sound location map.  
 X indicates site of radiocarbon samples  
 referred to in Table 1.

## APPENDIX F

### OSTRACODES FROM 1977 OFFSHORE BOREHOLES IN THE BEAUFORT SEA

By Elisabeth M. Browsers

This report concerns 85 samples from offshore boreholes PB-5-8 (Fig. F-1), drilled in March-May, 1977. The holes were drilled in shorefast ice over the continental shelf in Prudhoe Bay. Identifications of ostracodes are listed in Tables F-2 through F-7 and interpretations are given below.

Borehole:

PB5

Environment:

The lowest samples in this borehole (8a-8d) indicate nearshore shallow marine conditions, possibly with a brackish influence, as indicated by the presence of *CYTHEROMORPHA MACCHESNEYI*, *HETEROCYPRIDEIS SORBYANA*, and *PARACYPRIDEIS PSEUDOPUNCTILLATA*. As is seen in the foraminifer assemblages, the ostracode species diversity is highest in sample 7d (MF-4329). However, four of these species are non-marine forms that live in freshwater lakes and streams. The non-marine influence indicates deposition closer to a land mass than the previous samples, possibly in an estuary. This interpretation disagrees with the forams - perhaps higher productivity or relatively deep water nearshore might yield these foram assemblages. It is improbable that freshwater ostracodes would be distributed in abundance to an offshore marine habitat. The nearshore marginal marine to marine environment continues to the uppermost sample, 2.75 (MF-4148), with several samples containing occasional non-marine elements (4C, 3C).

Stratigraphic range:

These species range from the Pleistocene to the Recent. @

Climatic zone:

The presence of *PARACYPRIDEIS PSEUDOPUNCTILLATA*, *RABILIMIS SEPTENTRIONALIS*, *CYTHERETTA TESHEKPUKENSIS*, *LOXOCONCHA VENEPIDERMIDEA*, and *CYTHEROPTERON MONTROSIENSE* restrict this to a frigid climatic zone.

PB6

Environment:

The samples in this borehole (Shelby tube to 3h/e) indicate deposition in a shallow, nearshore, marine to marginal marine environment. Sample MF-4156 contains a mixed assemblage of marine species with a non-marine species (*LIMNOCYTHERE* sp. 1). This indicates close proximity to shore.

Stratigraphic range:

These species range from Pleistocene to Recent.

Climatic zone:

The presence of *PARACYPRIDEIS PSEUDOPUNCTILLATA*, *RABILIMIS SEPTENTRIONALIS*, and *CYTHERETTA TESHEKPUKENSIS* restrict this to a frigid climatic zone.



PB7

Environment:

The ostracodes occurring in samples 3a and 6.12-6.5 indicate near-shore marine to marginal marine conditions. The assemblages become more diverse in number of species and individuals up-section. This is probably indicative of more offshore conditions (still neritic), and a more normal marine salinity. Non-marine elements are still contributing rare valves to all of the upper samples. The greatest diversity of species occurs in sample 3.75-5.00, presumably indicating a more stable environment than in previous samples. Above this sample, nearshore marine conditions prevail.

Stratigraphic range:

These species range from Pleistocene to Recent. @

Climatic zone:

Frigid, based on PARACYPRIDEIS PSEUDOPUNCTILLATA, RABILIMIS SEPTENTRIONALIS, CYTHERETTA TESHEKPUKENSIS, and LOXOCONCHA VENEPIDERMOIDEA.

PB8

Environment:

Samples 20.21-21.3 through 190, the lowest samples examined, indicate a shallow nearshore marine assemblage typical of the Quaternary deposits of the Arctic, and similar to the fauna in boreholes PB 5-7. At sample 18c (MF-4225), a faunal change begins with the appearance of KRITHE GLACIALIS, a deeper water, more open ocean form. This change continues in sample 18a (MF-4224), with the additional introduction of RABILIMIS MIRABILIS and ACANTHOCYTHEREIS DUNELMENSIS. Kris believes that the interval below MF-4200, sample 10c, represents the last interglacial, when Atlantic species appeared in Alaskan waters. In the interval covered by samples 18c through 13i, I find four species of Atlantic origin - KRITHE GLACIALIS, CALLISTOCYTHERE cf. C. CLUTHAE, RABILIMIS MIRABILIS, and CYTHEROPTERON PARALATISSIMUM. The presence of these species can be interpreted two ways: a) the species represent the last penetration of Atlantic species into Alaska, possibly marking the last glacial, or b) the migration had already occurred, and these species were living in deeper water, so that this interval may indicate a greater water depth than in previous samples, and thus may not be related to a particular geologic event.

Water depth gradually decreases (or shoreline is getting closer), beginning with sample 15c. RABILIMIS SEPTENTRIONALIS reappears in sample 13g. EUCYTHERIDEA PUNCTILLATA also appears in relatively large numbers at this point. The latter species is probably of Atlantic origin, although it is recorded as circumpolar in distribution by Elofson (1941). Several non-marine species appear occasionally in this interval, especially from samples 10e through 9a. @

I do not detect a great change at MF-4200, as the foraminifers indicated. I pick up a change in sample 10g (MF-4202) with the introduction of *FINMARCHINELLA ANGULATA*. This species is a typical cold water form, ranging from frigid to cold temperate. It occurs twice further up the core. In sample 10a (MF-4199) above, *CYTHEROPTERON* aff. *C. PYRAMIDALE* and *EUCYTHERE DECLIVIS* appear. *FINMARCHINELLA FINMARCHICA* occurs in samples 9d-8d. The genus *FINMARCHINELLA* is probably Pacific in origin, having migrated a circumpolar route to the North Atlantic; at this point (Pleistocene), the species *F. FINMARCHICA* evolved, so that the species is now of Atlantic in origin (see MAR-68-2, 4/9/68, by J. E. Hazel). The presence of *F. FINMARCHICA* at MF-4196 is indicative of a warming of the Arctic, because this species ranges from subfrigid to warm temperate waters of the Atlantic. Its occurrence means that the Arctic warmed up to subfrigid water temperatures at some point prior to the time of deposition of sample MF-4196, allowing the species to cross the Arctic; possibly *CYTHERE DECLIVIS* migrated at the same time.

Above sample 10c, a typical modern Arctic assemblage develops. Three *CYTHEROPTERON* species came in - *C.* aff. *C. PYRAMIDALE*, *C.* aff. *C. RALATISSIMUM* and *C.* aff. *C. ARCTICUM*; these forms of the genus are typically cold water species. At sample 9a (MF-4195), *NORMANICYTHERE* sp. and *N. CONCINELLA* are introduced, and continue to the top of the core. The top of the core indicates a greater water depth than that inferred for the very bottom, and also deeper compared to the other boreholes. The assemblage in sample 1a/1b (MF-4171) is a typical Arctic, normal marine, shallow shelf fauna.

#### Stratigraphic range:

Late Pleistocene to Recent.

*FINMARCHINELLA FINMARCHICA* indicates the last warming of the Arctic Ocean to subfrigid temperatures.

#### Climatic zone:

Primarily frigid for the entire borehole examined for ostracodes. At some point prior to 9d, subfrigid. @

#### Conclusions:

The shallow nearshore marginal marine to marine environment that contains such species as *PARACYPRIDEIS PSEUDOPUNCTILLATA*, *RABILIMIS SEPTENTRIONALIS*, *EUCYTHERIDEIS BRADII* and *HETEROCYPRIDEIS SORBYANA* is essentially the same for PB1, the upper part of PB2, PB3, PB5, PB6, PB7, and the lowest part of PB8.

Most of PB2 and the lower part of PB8 are indicative of deeper normal marine water. This is suggested by the presence of species such as *RABILIMIS MIRABILIS*, *KRITHE GLACIALIS*, and *ACANTHOCYTHEREIS DUNELMENSIS*.

The Middle part of PB8 indicates some temperature changes associated with *FINMARCHINELLA FINMARCHICA*. This species is probably closely related to the last interglacial warming event.

The upper part of PB8 reflects a "typical" Arctic ostracode assemblage - That is, normal marine salinity shallow shelf, frigid water temperatures. This assemblage is not environmentally correlative with any of the other boreholes.

The above interpretations are somewhat preliminary because the geographic and stratigraphic distribution of marine ostracodes from the cold temperate to frigid realms has not been determined with the level of confidence attained for other organisms. However, I believe that an adequate framework for general determinations exists, and this will improve markedly as my ostracode studies progress. @

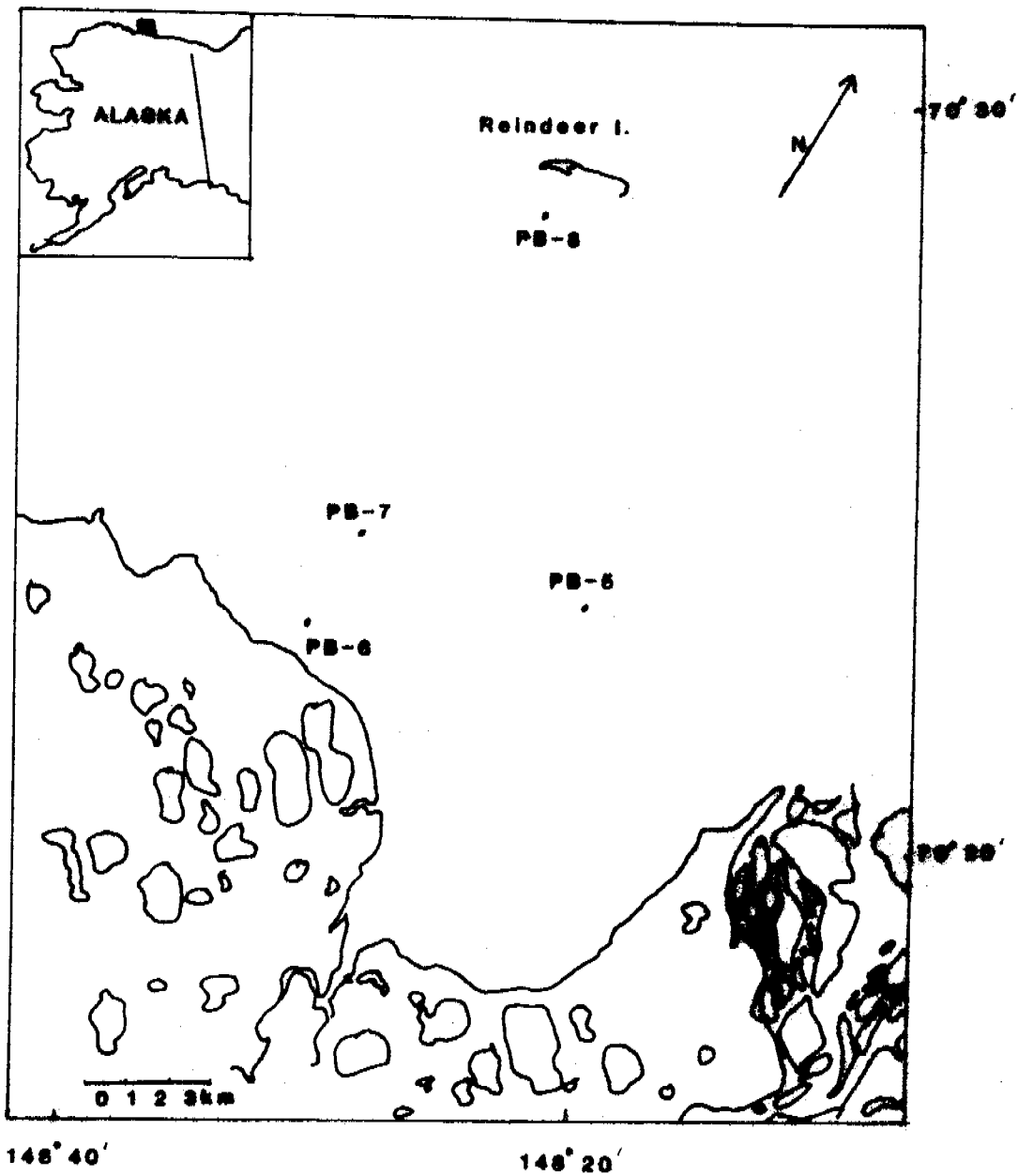


Figure F-1. Map of site locations in Prudhoe Bay, Alaska.

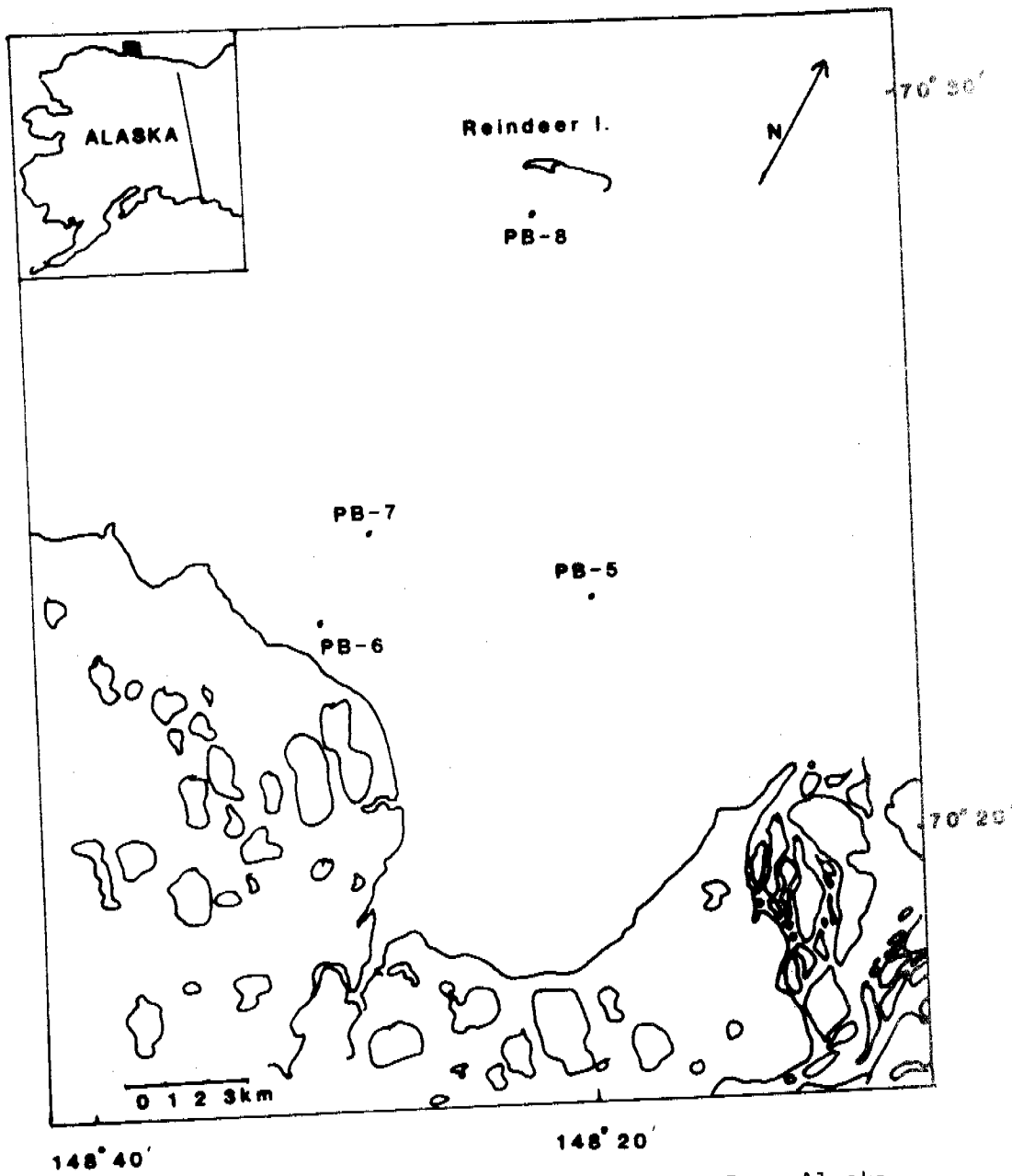


Figure F-1. Map of site locations in Prudhoe Bay, Alaska.

226

	MF 4148	4149	4325	4326	4528	4150	4151	4329	4152	4153	4154
<i>Paracyprideis pseudopunctillata</i>	17		14	21	60			30	27	100	31
<i>Heterocyprideis sorbyana</i>	17	44	13	32	13			09	13		08
<i>Cytheromorpha macchesneyi</i>		44	32	08	07		33	18	07		31
<i>Cytheromorpha</i> sp. A.				04	13			03	07		
<i>Loxoconcha venepidermoidea</i>							33	03			
<i>Cytheropteron montrosiense</i>								03			
<i>Cytheretta teshekpuensis</i>						60		09	07		23
<i>Rabilimis septentrionalis</i>	50	06	36	32	07	33		03	27		08
<i>Pontocythere</i> sp. A.	17			01				03	13		
<i>Eucytheridea bradli</i>		06				07	33				
<i>Eucythere declivis</i>				trace							
Cyprid -genus indet.			02								
<i>Cyprinotus</i> -sp. indet.			02								
<i>Ilyocypris</i> sp.								03			
<i>Cytherissa lacustris</i>								09			
<i>Limnocythere liporeticulata</i>			02								
<i>Limnocythere</i> sp. I.								06			
<i>Candona</i> spp.				01				03			
total %	101	100	101	99+	100	100	99	102	101	100	101
total identifiable	6	16	63	242	15	15	3	33	15	1	13
total present	7	19	58	680	21	24	4	39	4	1	10
diversity	4	4	7	8	5	3	3	13	7	1	5

FIGURE F-2

Borehole Pb-5

		NF	4156	4330	4157	4158	4159
Paracyprideis	pseudopunctillate		04	04			
Heterocyprideis	sorbyana		34	44	50		
Cytheromorpha	macchesneyi		48	28			
Cytheromorpha	sp. A.		07	04			
Cytheretta	teshekpukensis		01				
Rabilimis	septentrionalis		06	20	50		
Eucytheridea	bradii						100
Limnocythere	sp I		01				
	Total %		101	100	100		100
	total identifiable		101	25	2		1
	total present		95	25	2	1	1
	diversity		7	5	2	1	1

↑  
fragment

FIGURE F-3

Borehole Pb-6

228

	MF	4165	4333	4166	4167	4324	4168	4170	4169
Paracyprideis pseudopunctillata	13	08	14	31	30	39	20	100	
Heterocyprideis sorbyana	16	14	14	14	30	14			
Cytheromorpha macchesneyi	27	38	11	12	15	17	40		
Cytheromorpha sp. A	01	12	02	04		06			
Loxococoncha venepidermoidea		02	01						
Loxococoncha sp. A			01						
Roundstonia globulifera			01						
Cytheretta teshekpukensis	03	01	06	01					
Cytheretta edwardsi			Trace						
Rabilimys septentrionalis	34	20	49	35	18	22	20		
Pontocythere sp. A		04		02					
Eucytheridea bradli	04		02						
Eucytheridea punctillata							20		
Eucythere declivis		01	Trace	01					
Ilyocypris sp.				01	04				
Cytherissa lacustris			Trace						
Cytherideid					04				
Limnocythere sp. I	01	01	Trace			01			
Candona sp.	01								
Total %	100	101	101	101	101	99	100	100	
total identifiable	100	125	365	163	27	69	5	1	
total present	95	97	357	126	352	63	3	1	
diversity	9	10	14	9	6	6	4	1	

FIGURE F-4

Borchute Pb-7





## APPENDIX G

### MICROFOSSIL STUDIES OF PELUKIAN AND FLAXMAN DEPOSITS, ALASKAN COAST OF BEAUFORT SEA

By D. M. Hopkins, Kristin McDougall, and  
Elisabeth Browsers

Attached are plots of stratigraphic occurrences of foraminifera and ostracodes in Pleistocene marine deposits exposed along the Beaufort Sea coast (Fig. G-1).

Cape Simpson Section (Table G-1).--The best and most important section is the Cape Simpson section, which appears to consist, at base, of overconsolidated clay and near-beach sand of middle Pleistocene age overlain unconformably by interglacial deposits of Pelukian age overlain in turn by erratic-bearing silty sand of the Flaxman Formation.

This surprisingly high bluff lines the coast in the area of the Cape Simpson oil seeps. The site is tens of kilometers seaward of the Pelukian shoreline, and it is consequently surprising to see Pelukian clays standing so high above present sea level. Dave Carter thinks that the Cape Simpson area is an actively rising anticline and that the Pleistocene deposits here stand several meters above their original positions.

The basal unit in the bluff evidently consists of middle Pleistocene deposits not ordinarily seen above sea level along the Beaufort Sea coast. The condition of microfossil remains and, in one specimen, lack of fossil remains indicates that there is an unrecognized unconformity at the top of this part of the section.

The Pelukian section contains a number of open-water foraminifera species and the character of the fauna reinforces the conviction that this section is uplifted--one would expect that it was originally in relatively deep water far from shore.

The fine silty sand of the Flaxman Formation at the top of the section has a much more impoverished fauna with much fewer individuals. The open-water species and the Atlantic immigrants are lacking. This could be interpreted to mean that the Flaxman Formation was deposited in shallower water,

nearer shore and represents the regressive part of the last interglacial section. The apparent continuation of the Pelukian type of fauna into the base of the muddy sand might be taken to support this, but alternately, it might reflect reworking of Pelukian fossils into basal Flaxman Formation during a later transgression. We must examine the Cape Simpson exposures once again to determine whether or not there is an unconformity between the Pelukian and the Flaxman beds. However, the presence of plant remains throughout the Flaxman Formation suggests that it was deposited during an interglacial, rather than a later interstadial.

Drew Point Section (Table G-2).--I originally misinterpreted this section as representing Flaxman Formation resting unconformably upon Pelukian beds. However, microfossil evidence and radiocarbon-dating shows that the upper part of the sequence is an early Holocene thaw lake containing a few redeposited marine microfossils; the predominance of Limnocythere suggests that the lake was somewhat saline, due, perhaps, to salt spray or, more likely, to interstitial brine in the sediments in which it developed. The lower part of the section seems to be Flaxman Formation, not Pelukian as I had originally assumed.

The Pleistocene marine beds at Drew Point lack the open-water species and, except for Elphidium asklundi, lack the Atlantic immigrants which characterize the Pelukian beds at Cape Simpson. Although erratic boulders are very scarce at Drew Point, it is evident that the marine beds there represent the Flaxman Formation rather than the Pelukian.

The foram data on the Drew Point Section was plotted over a period of weeks and needs to be checked for errors of detail.

Miscellaneous Sections (Table G-3).--Also attached are plots for a series of single grab samples collected from various points along the Beaufort Sea coast. The Kogru River-Saktuina Island samples were collected from peaty silt underlying sand and fine-gravel accumulations that represent ancient interglacial (Pelukian) barrier islands and shoals. The peaty silts contain rich faunas including a few extra-limital species and the Atlantic Elphidium asklundi. However, in keeping with their paleogeographic setting (near the Pelukian shoreline and still nearer to a barrier chain), these deposits lack the open-shelf forams and ostracodes that occur at Pelukian levels in our offshore boreholes and at Cape Simpson.

The Kogru River exposures have also yielded a rich molluscan fauna, including several extra-limital species. The sand and gravel deposits also contain abundant Macoma balthica, which is now almost extinct in

the Beaufort Sea and which lives more or less strictly in lagoons; taken by itself, it suggests lowered salinities, but I must admit that lowered salinities are not consistent with the molluscan fauna nor with the microfaunas reported here.

The samples labeled "Probably Flaxman" came generally from thin deposits of fine pebbly sand exposed at or very near sea level--deposits that I consider to be regressive beach deposits. The few pebbles are exotic types, presumably from Greenland. The microfaunas seem to be consistent with my assumption that these deposits represent the top of the Flaxman Formation.

The samples labeled "Flaxman Formation" came from typical sandy silt and clayey silt with abundant glacially striated exotic dropstones. At Brownlow Point and on Canning Lagoon, these deposits could be seen to be overlain by thin pebbly sand, 30 cm thick--regressive beach deposits such as the sand at Garry and Ball State Inlets.

Exotic microfauna.--The Pelukian microfaunas include several species that have not thus far been encountered in the Beaufort Sea, according to Kris McDougall and Ellie Brouwers. (Some of these have been encountered only in the Pelukian deposits of the offshore boreholes.) There are also one or two rare forms which appear to now be limited to the Pacific Ocean and its marginal seas:

Foraminifers:

<u>Gordiospira arctica</u>	Atlantic endemic--only in boreholes
<u>Scutuloris tegmanis</u>	Atlantic endemic--only in boreholes
<u>Elphidium asklundi</u>	Atlantic endemic--is this species extinct or is it present in Atlantic today?
<u>Elphidium oregonensis</u>	Pacific form--turned up in one collection from Pelukian deposits at Teshekpuk Lake

Ostracodes:

<u>Rabillimis mirabilis</u>	Atlantic endemic
<u>Cluthia cluthae</u>	Atlantic endemic--found only in boreholes
<u>Eucytheridea punctillata</u>	Atlantic endemic--found only in boreholes
<u>Finmarchinella finmarchica</u>	Atlantic endemic--found only in boreholes
<u>Krithe glacialis</u>	Atlantic endemic? Perhaps will be found in Beaufort Sea in future
<u>Cytheropteron paralatissimum</u>	Atlantic endemic? Perhaps will be found in Beaufort Sea in future
<u>Normanicythere concinella</u> = <u>N. leioderma</u> ?	Enters Beaufort Sea and Pacific Ocean in Pelukian for first time?
<u>Microcythera</u> sp.	Southern genus confined to warmer water.

The Pelukian mollusk fauna differs in lacking Atlantic species but in containing large numbers of individuals of several species now reaching northern limits between Peard Bay and Point Barrow or (in the case of Mytilis edulis and Macoma balthica being represented in Beaufort Sea now

by only rare individuals or a few very small relict populations). Also, the mollusk fauna includes one extreme extralimital form--Natica janthostoma, a snail now ranging from northern Honshu to southern Kamchatka but which is very abundant in Pelukian deposits between the Yukon River and the Arctic Circle; it also appears very sparsely in Pelukian deposits further north, including the Ice Cellar at Point Barrow and one collection from Kogru River.

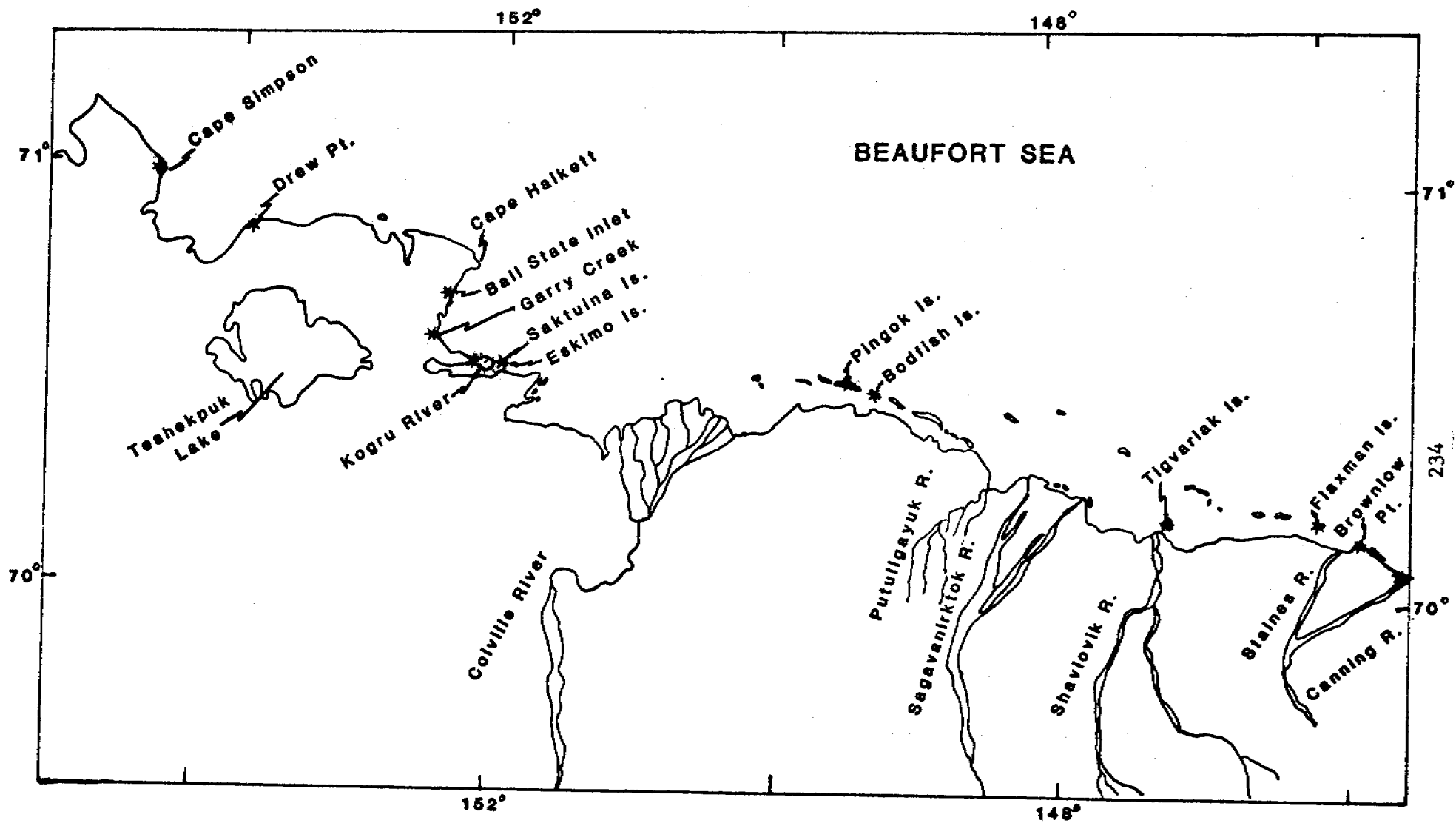


Figure G-1. Locations of 1977 and 1978 microfossil collections along the Beaufort Sea coast.  
 \* may represent more than one sample locality.

TABLE G-1.

CAPE SIMPSON

(78Ahp17)

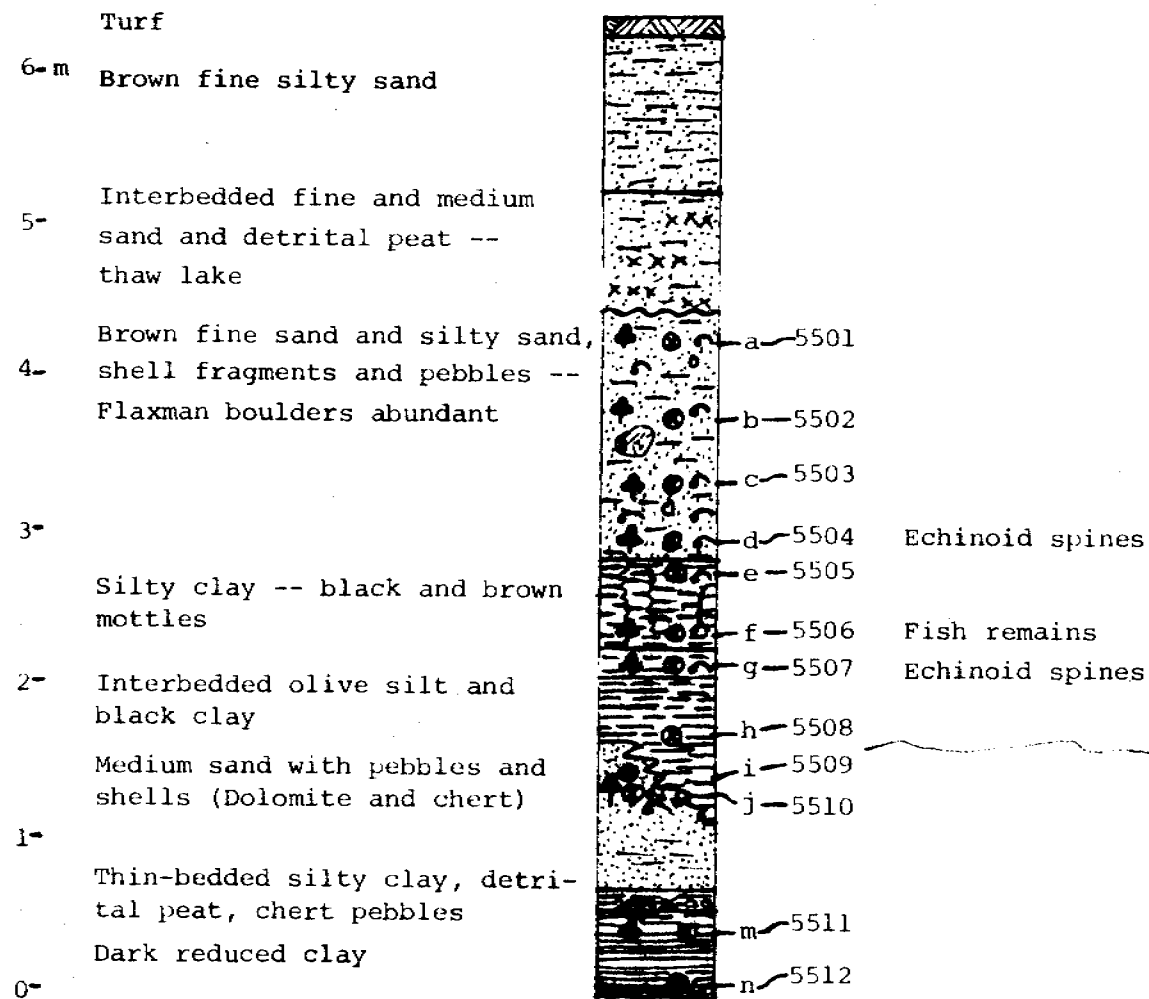
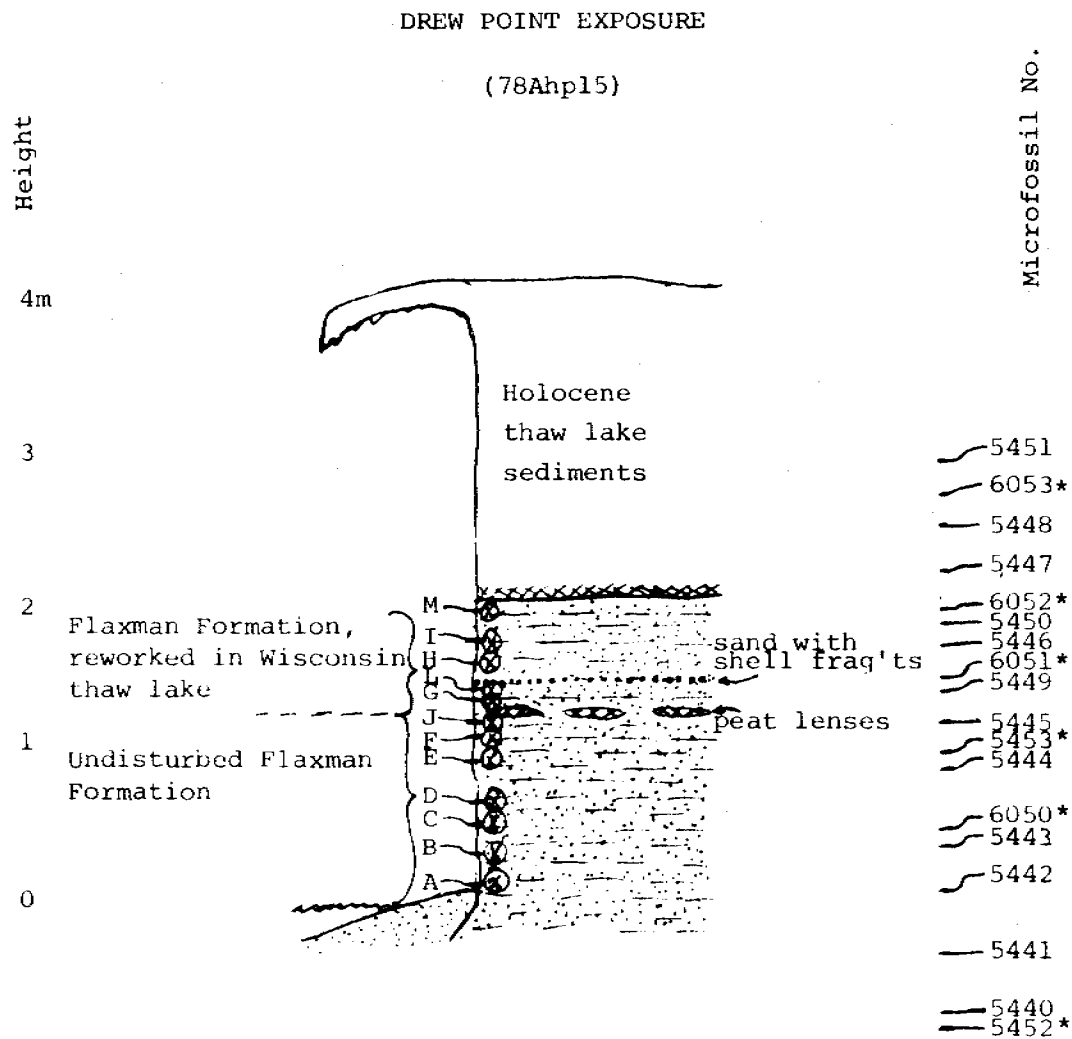




TABLE G-2.

\* Microfossil # 5452 and 5453 are samples Ahp 15Q and R, collected from equivalent exposure 300 m away, and projected into this section. Microfossil # 6050 through 6053 are samples 79ACr 028A<sub>3</sub> through 79ACr 028D<sub>3</sub>, collected by L. D. Carter from this section.





□								
□	X	X X X X X	X X X X X X	X X X X X X X X	X X X X X X X X X	X X X X X X X X X	X	
□	X	X X X X X	X X X X X X	X X X X X X X X X	X X X X X X X X X X	X X X X X X X X X X X	X	
□	X	X X X X X X	X X X X X X X X	X X X X X X X X X X X X	X X X X X X X X X X X X X X	X X X X X X X X X X X X X X X X	X	
□	X	X X X X X X X X	X X X X X X X X X X X	X X X X X X X X X X X X X X	X X X X X X X X X X X X X X X X X X	X X	X	
□	X	X X X X X X X X X X X X	X X X X X X X X X X X X X X	X X X X X X X X X X X X X X X X X X X X	X X	X X	X	

- Buccella frigida
- Elphidiella groenlandica
- Elphidium albiumbilicatum
- E. asklundi
- E. clavatum
- E. excavatum alba
- E. incertum
- E. orbiculare
- Elphidium sp.
- Polymorphina sp.
- Quinqueloculina seminulum

Diversity

○							
○							
○							
○							
○							
○							

- Cytheromorpha macchesneyi
- Heterocyprideis sorbyana
- Paracyprideis pseudopunctillata
- Cytheropteron montrosiense
- Eucytheridea bradii
- Rabilimis septentrionalis
- Candona rectangulata
- Ilyocypris bradyi
- Limnocythere camera
- L. inopinata
- L. platyforma
- L. staplini
- Limnocythere sp. indeterminate
- Prionocypris ? sp. indeterminate

○ = non-marine

□ = deep water or open shelf

7,750 ±  
4-11052

fish  
10 eggs  
900s  
463  
750s  
691

Low abundance, low diversity  
Absence or extremely low numbers and poor preservation suggest thaw lake

FORAMINIFERA INTERPRETATION

MARINE OSTRACODE INTERPRETATION

FRESHWATER OSTRACODE INTERPRETATION

Marginal marine, shallow, nearshore - typical of modern fauna

Non-marine Marginal marine

Estuary or salt marsh, elevated salinities (2 to 15 ppt NaCl), pH 8-9, water shallow, Ilyocypris indicates some current (but washed in ?)



APPENDIX H

EXTINCT AND EXTRA-LIMITAL MOLLUSKS IN PELUKIAN DEPOSITS OF

KOGRO RIVER AND ESKIMO ISLANDS

By D. M. Hopkins and Louie Marinovich

We have compiled all the information available on the living mollusk faunas from the Beaufort Sea (table H<sub>-1</sub>) and compared it with the fossil faunas from the ancient Pelukian barrier chain extending from Dease Inlet eastward to Harrison Bay in order to determine the number and abundance of extra-limital (warm-water) mollusks in the Pelukian faunas of western Beaufort Sea. Our sources for the modern fauna included:

Elizabeth Macpherson, 1971, "The marine mollusks of Canada":

National Museums of Canada Scientific Publication in Biological Oceanography No. 3 (deals only with gastropods).

F. R. Bernard, 1979, "Bivalve mollusks of the western Beaufort Sea":

Nat. History Museum Los Angeles County, v. 313.

F. J. E. Wagner, 1977, "Recent mollusc distribution patterns and paleobathymetry, southeastern Beaufort Sea": Canadian Journal of Earth Sciences, v. 14, p. 2013-2018.

Nettie MacGinitie, 1959, "Marine mollusca of Point Barrow, Alaska":

U.S. National Museum Proc., v. 109, no. 3412, p. 59-208.

Beach collections made in 1978 along the coast and islands of

Beaufort Sea between Barrow and the Canning River by R. E. Nelson and D. M. Hopkins, and identified by L. Marinovich.

The compilation confirms previous observations that the Pelukian fauna of Beaufort Sea contains several (at least 10!) mollusk species that are either not present or very rare there today. Among these, Macoma balthica,

M. lama, Siliqua, and the new species of Polinices are very abundant, and form a significant part of the fauna. Mytilus edulis, Tellina lutea, Macoma sp. cf. M. brota, Mya elegans, and Spisula voyi are rarely encountered and are not numerous in the collections that do contain them. Natica janthostoma is extremely abundant in Pelukian collections from the Yukon Delta to Cape Krusenstern but quite rare further north; we know of only two Pelukian occurrences north of Point Hope--in the Barrow Ice Cellar and at Kogru River. The remaining two forms, Liomesus nux and Acteocina sp., are rare in the Pelukian Beaufort Sea faunas and perhaps are still present though very rare on the Beaufort Sea floor.

Louie Marincovich suspects that the undiagnosed species of Polynices will eventually turn out to be a North Atlantic form. It is interesting to note that several species of foraminifera and ostracoda endemic to the North Atlantic also reached Beaufort Sea during the Pelukian transgression.

Evidence on Seward Peninsula indicates clearly that the Pelukian shoreline was formed during the last (Sangamon, Eem, or Kazantsev) interglacial interval. The presence in Beaufort Sea Pelukian faunas of mollusks now reaching northern limits in Bering or Chukchi Sea and of mollusks, ostracodes, and foraminifers now limited to the North Atlantic Ocean probably indicates that when Pelukian sea level was at its highest (some 7 m above present sea level), shelf waters in Beaufort Sea were probably more effectively warmed during the summer open-season and that the open-water season was longer during Pelukian time than at present.

## Table (H-1)

EXTRA-LIMITAL (WARM-WATER) MOLLUSKS FROM PELUKIAN DEPOSITS  
OF WESTERN BEAUFORT SEA

## GASTROPODS

<u>Natica ganthostoma</u>	Presently limited to northwestern Pacific and southern Kamchatka known only in Anvilian and Pelukian beds in NW Alaska
<u>Polinites</u> n. sp.	Atlantic form? Not found in any modern collections from Beaufort, Chukchi, or Bering Seas, nor in Pacific Ocean
<u>Liomesus ooides</u>	Not reported at Barrow or MacKenzie Bight
<u>Acteocina</u> sp.	Not reported at Barrow or MacKenzie Bight

## PELECYPODS

<u>Mytilus edulis</u>	I found a single valve in litter of 1970 storm surge at Esook (Harrison Bay D-5). Otherwise no reports of its presence in Beaufort Sea
<u>Tellina lutea</u>	Northern limit near Peard Bay
<u>Macoma brota</u>	Northern limit near Barrow
<u>M. lama</u>	Extends eastward to Dease Inlet in Beaufort Sea
<u>M. balthica</u>	Small population in Simpson Lagoon, and reported in a few offshore grab samples. Also early Holocene occurrence in drill core in Stefansson Sound. Nevertheless, this brackish-water mollusk is <u>very</u> rare north of Kasegeluk Lagoon, Chukchi Sea
<u>Mya elegans</u>	Northern limit uncertain but lies somewhere in Chukchi Sea between Icy Cape and Peard Bay
<u>Siliqua patula</u>	Northern limit near Peard Bay
<u>Spisula voyi</u>	Northern limit near Peard Bay

Collections of D. M. Hopkins, D. L. Carter, and R. E. Nelson, 1978-1979.  
Identifications by Louie Marinovich.

	Teshekpuk Lake	Kogru River (North shore)												South shore Kogru River opp. Saktuina Pt.		Saktuina Island		East Eskimo Island			
	M7212	M7215	M7216	M7343	M7344	M7345	M7346	M7405	M7406	M7407	M7415	M7416	M7417	M7418	M7419	M7421	M7422	M7423	M7424	M7425	
<u>Natica ganthostoma</u>												X									
<u>Polinites</u> n. sp.				X	X	X	X	X		X								X			
<u>Liomesus ooides</u>	X																				
<u>Acteocina</u> sp.			X				?														
<u>Mytilus edulis</u>											X	X									
<u>Tellina lutea</u>										X								X			
<u>Macoma brota</u>											cf.	cf.						cf.			
<u>M. lama</u>				X	X	?	X	X	X	X	cf.	X	X					X	X	X	X
<u>M. balthica</u>	X	X	X	X	X		X	X	X	X	X	X	X		X			X	X	X	X
<u>Mya elegans</u>											X										
<u>Siliqua patula</u>		X							X	X	X	X						X			X
<u>Spisula voyi</u>											X								X		

EXTRA-LIMITAL (WARM-WATER) MOLLUSKS FROM PELUKIAN DEPOSITS  
OF WESTERN BEAUFORT SEA

GASTROPODS

<u>Natica janthostoma</u>	Presently limited to northwestern Pacific and southern Kamchatka known only in Anvilian and Pelukian beds in NW Alaska
<u>Polinices</u> n. sp.	Atlantic form? Not found in any modern collections from Beaufort, Chukchi, or Bering Seas, nor in Pacific Ocean
<u>Liomesus ooides</u>	Not reported at Barrow or MacKenzie Bight
<u>Acteocina</u> sp.	Not reported at Barrow or MacKenzie Bight

PELECYPODS

<u>Mytilus edulis</u>	I found a single valve in litter of 1970 storm surge at Esook (Harrison Bay D-5). Otherwise no reports of its presence in Beaufort Sea
<u>Tellina lutea</u>	Northern limit near Peard Bay
<u>Macoma brota</u>	Northern limit near Barrow
<u>M. lama</u>	Extends eastward to Dease Inlet in Beaufort Sea
<u>M. balthica</u>	Small population in Simpson Lagoon, and reported in a few offshore grab samples. Also early Holocene occurrence in drill core in Stefansson Sound. Nevertheless, this brackish-water mollusk is <u>very</u> rare north of Kasegeluk Lagoon, Chukchi Sea
<u>Mya elegans</u>	Northern limit uncertain but lies somewhere in Chukchi Sea between Icy Cape and Peard Bay
<u>Siliqua patula</u>	Northern limit near Peard Bay
<u>Spisula voyi</u>	Northern limit near Peard Bay

Collections of D. M. Hopkins, D. L. Carter, and R. E. Nelson, 1978-1979.  
Identifications by Louie Marinovich.

M7414	East Eskimo Island					X	X			X
M7413		X					X			X
M7412	Saktuina Island						cf.			X
M7411						X				X
M7210	South shore Kogru River opp. Saktuina Pt.					X				X
M7417						X				X
M7416						X				X
M7415		X				X				X
M7407						X				X
M7406		X				X				X
M7405						X				X
M7346		X				X				X
M7345						X				X
M7344		X				X				X
M7343						X				X
M7216						X				X
M7215	Teshekpuk Lake					X				X
M7212						X				X

Kogru River  
(North shore)

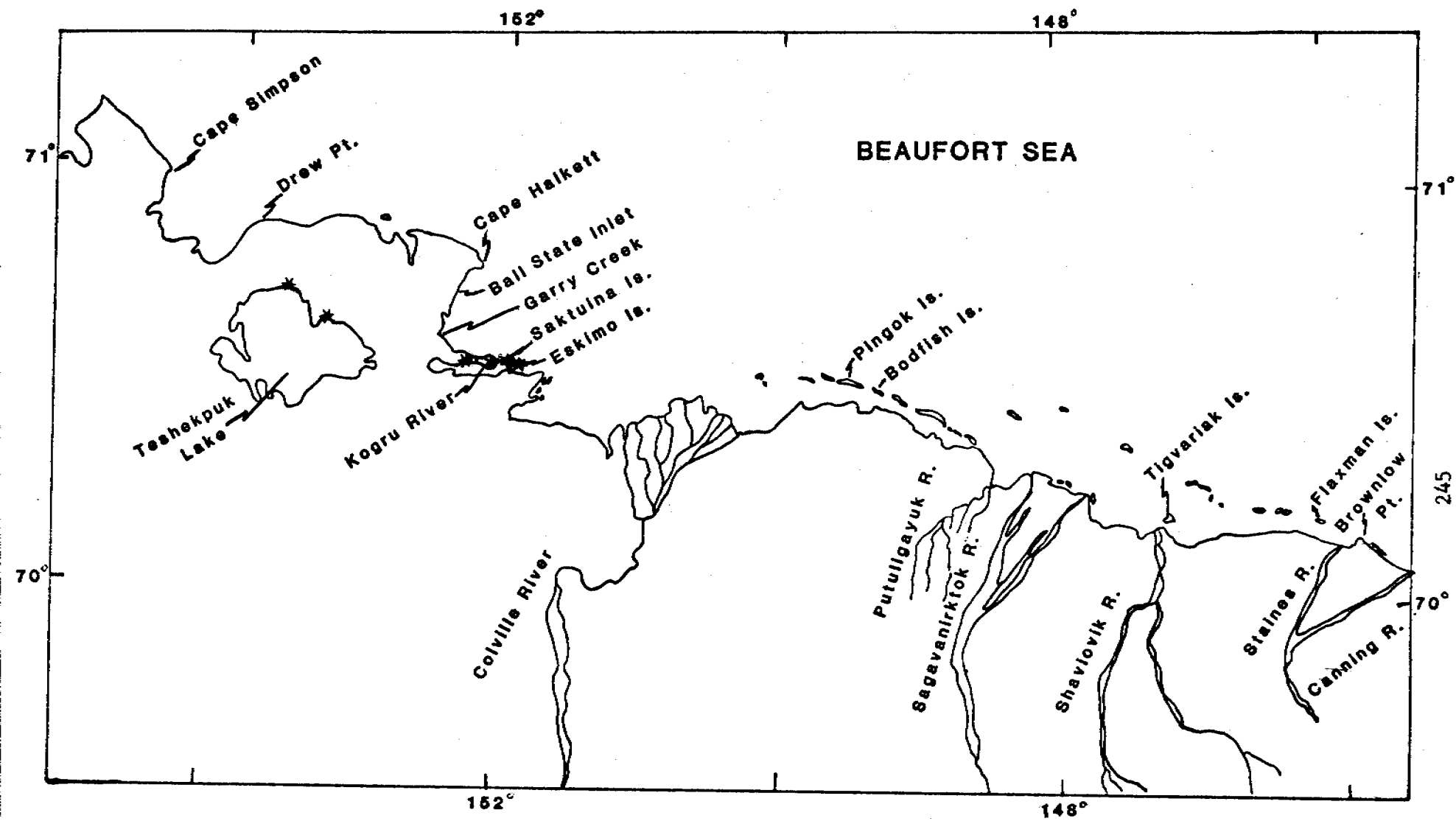


Figure H-1. Location map of collections containing extra-limital mollusks in Pelukian deposits. may represent more than one collection site.



APPENDIX I

IDENTIFIED FOSSILS FROM THE FLAXMAN FORMATION

By J. T. Dutro, Jr.

The area of origin of erratic boulders in the Flaxman Formation remains uncertain. The fossils contained in the occasionally fossiliferous carbonate boulders of the Flaxman Formation may eventually aid in recognition of the Flaxman Formation source area. For that reason, we append two identification reports on early Paleozoic fossils collected in Flaxman Boulders near Brownlow Point.

- (1) Boulder from Flaxman Formation exposed on the beach near Brownlow Point, Alaska. Lat. 70 deg. 09 min. 39 sec. N., Long. 145 deg. 51 min. 51 sec. W.

77ANr 12f

CATENIPORA sp.

Simple rugose coral

These are Upper Ordovician or Silurian in age.

Identification by W. A. Oliver

- (2) 77ANr12F (USGS 10157-SD): Alaska, Flaxman Island A-4 quad.; 70 deg. 09 min. 39 sec. N., 145 deg. 51 min. 51 sec. W.; large dolomite boulder in Flaxman Formation exposed on the beach near Brownlow Point. Collector: Peggy Smith, 1977.

In addition to the corals reported by Oliver (see report dated 11/8/78), this collection contains several other macrofossil fragments, the most striking of which is a large annulate cephalopod about 30 cm long. It is slightly curved and tapers from about 5 cm in diameter near the living chamber to about 2.5 cm at the proximal end. This cephalopod is probably a dawsonoceratid,

according to Rousseau Flower (personal commun., 1/80). This family is essentially limited to the Silurian, although questionable finds have come from latest Ordovician and Middle? Devonian beds. Taken with the occurrence of CATENIPORA reported by Oliver, the best estimate of age is Silurian, although a latest Ordovician age is possible.

The other fossils present in the collection are indeterminate echinoderm ossicles, indeterminate brachiopod fragments and euomphalacean gastropods.

There are Ordovician and Silurian platform sequences in the Arctic in several places, but the nearest is the Katakturuk Formation which crops out in the Sadlerochit Mountains. The precise source of this boulder in the Flaxman Formation is not determinable from these few fossils.

Identification by J. T. Dutro  
U.S. Geological Survey

From:

Pacific Science Congress, XIV (Khabarovsk),  
Abstracts, Additional Volume, p. 15-16 (1979).

THE FLAXMAN FORMATION OF NORTHERN ALASKA:

RECORD OF EARLY WISCONSINAN SHELF GLACIATION IN THE HIGH ARCTIC?

David M. Hopkins

U.S. Geological Survey

Menlo Park, California 94025

The Flaxman Formation (which includes some of the deposits described by R. F. Black, 1964, USGS Prof. Paper 302-C, as the "Skull Cliff unit of the Gubik Formation") is a thin sheet of glaciomarine stony sandy silt that underlies the northernmost part of the Arctic Coastal Plain of Alaska and is also present in patches on the continental shelf of the Beaufort Sea. It rests, probably unconformably, on marine mud of last interglacial (Pelukian) age. Glaciomarine deposits similar to the Flaxman Formation but older than the Pelukian transgression are also present on the Arctic Coastal Plain.

The formation is characterized by glacial dropstones foreign to northern Alaska, including red granite, granulite-facies metamorphic rocks, pyroxenite, diabase, pink quartzite, and abundant dolomite. Discussions with Canadians indicate that the erratics did not come from the Canadian Arctic Islands. They may be derived from Keewatin but are matched better in northern Greenland.

Ridges of pebbly sand cresting near 7 m above mean sea level (MSL) at Point Barrow and Cape Simpson lie seaward of the Pelukian shoreline and may represent the Flaxman shoreline. At Cape Simpson and Drew Point, frozen, ice-rich sandy silt of the Flaxman Formation rests on frozen, ice-poor clayey silt presumably of Pelukian age. The structure of the ice in the clayey silt suggests that it was frozen, then thawed during the Flaxman transgression, then refrozen, in contrast to the overlying Flaxman, which seems to have undergone only one freezing cycle. These relations seem to indicate that the Flaxman transgression was separated from the interglacial Pelukian transgression by a distinct regression.

Offshore boreholes show that the Flaxman Formation is confined on the continental shelf to interfluvial areas between submerged valleys partially backfilled with alluvial gravel and Holocene mud. On the interfluvial areas, the

Flaxman Formation persists as a thin sheet of stony mud or as a lag deposit of scattered boulders or fine sandy gravel resting on stiff, overconsolidated marine clay of Pelukian age.

The age of the Flaxman Formation is not yet definitively established. Detrital peat interbedded in the beach ridges of possible Flaxman age at Barrow has yielded radiocarbon ages ranging from  $25,300 \pm 2300$  (I-1364) to  $>44,000$  years (W-2676). However, detrital peat in gravel filling a submerged valley trenched through Flaxman and Pelukian deposits near Prudhoe Bay is  $42,800 \pm 1440$  years old (USGS-249). The Flaxman Formation is most probably of early Wisconsinan age.

Worldwide sea level has never stood above present MSL since the last interglacial. Consequently, the Flaxman Formation must have been deposited at a time when the coast of northern Alaska was isostatically depressed, perhaps by the weight of continental ice over Arctic Canada. The Flaxman Formation may provide a record of early Wisconsinan glaciation on the high-arctic Canadian and Greenland shelves and subsequent destruction of shelf glaciers by rising sea level during abortive deglaciation more than 42,800 years ago. Ice caps on the Barents and Kara Sea shelves probably existed during this same time interval, rather than during late Wisconsinan/Würmian time, as some have postulated.

## APPENDIX K

### Discrepancy in correlation of transgressive marine deposits of Alaska and the eastern Arctic

D. M. Hopkins and L. D. Carter, U.S. Geological Survey, Menlo Park, CA

Comparison of the results of amino-acid racemization studies of Alaskan and eastern Arctic fossil mollusks reveals a large discrepancy in age assignments of apparently synchronous deposits in the two regions and leads us to believe that the ages of interglacial and interstadial deposits on Baffin and Ellesmere Islands may have been considerably underestimated. Our data base consists of allo/iso-leucine ratios in amino acids extracted from fossil Mya, Hiatella, Cyclocardia, and Macoma balthica shells. The Alaskan samples were collected in the field or selected from older collections by us; analyses were performed by G. H. Miller and J. K. Brigham at INSTAAR. Although results of amino-acid racemization studies have resulted in significant revisions in correlation and age assignments among some of the older Quaternary marine deposits of western and northern Alaska, analyses of shells from Pelukian deposits have been supportive of our intra-Alaskan correlations and not in conflict with the extensive evidence that the Pelukian transgression took place during the last interglacial interval.

The Pelukian transgression is represented by analyzed shells from nine localities ranging from St. Paul, Pribilof Islands (lat. 57°N, mean annual temperature [MAT] +0.4°C) to Barrow (lat. 71°N, MAT -14.6°C). Racemization ratios decrease with MAT from a high of 0.065 for total leucines and 0.25 for the free fraction for a shell from St. Paul, Pribilof Islands, to lows less than 0.02 for total leucines and quantities of free leucines too small to be detected in Pelukian shells from the Arctic coastal plain of northern Alaska (MAT, colder than -10°C). Pelukian shells from northern Alaska cannot, in fact, be distinguished from living shells on the basis of racemization studies.

Radiocarbon dating places Pelukian deposits on the Arctic coastal plain older than 51,000 years. Relationships to moraines on the shores of Seward Peninsula and Kotzebue Sound indicates that the Pelukian transgression is younger than the penultimate glaciation and older than a Wisconsinan glaciation. The consistent altitude of the Pelukian shoreline at  $7 \pm 3$  m throughout the 1,600 km of coastline from the Yukon to the Colville Rivers indicates that Pelukian sea level was higher than now. Lateral continuity with forest beds at Deering, Seward Peninsula, and on the Baldwin Peninsula and presence of extra-limital mollusks at nearly every fossil locality indicates that Pelukian air and sea temperatures were warmer than now. Straightness of a 250-km-long barrier chain and presence of microfauna now endemic to the North Atlantic indicates that Pelukian deposits of northern Alaska formed at a time when the Beaufort Sea and channels between the Canadian Arctic islands were more open than now. For these reasons, we correlate Pelukian deposits with the last interglacial (isotope stage 5e) and not with any subsequent interstade.

Though MATS on Baffin Island are similar to MATS on the northern Alaska Arctic coastal plain, allo/isoleucine ratios reported for shells from deposits on Baffin Island ascribed to the last interglacial or to early Wisconsinan interstades (Miller and others, 1977) are far higher than those in shells from the Pelukian deposits of northern Alaska. Allo/isoleucine ratios reported to us by J. K. Brigham (oral communication, 11/79) in mollusks from deposits of the Cape Broughton interstade, thought to be of mid-Wisconsinan age (Feyling-Hanssen, 1976), are similar to racemization ratios in mollusks from middle Pleistocene deposits in northern Alaska. Even allowing for the possible effects of differences in climatic history that may have resulted from differences in position relative to year-round open seas, it still appears that marine deposits on Baffin Island must be older than has been postulated.

## APPENDIX L

### APPLICATION OF AMINO ACID GEOCHRONOLOGY TO DEPOSITS OF THE ARCTIC COASTAL PLAIN, ALASKA: PRELIMINARY RESULTS AND IMPLICATIONS

J.K. Brigham<sup>1</sup>, D.M. Hopkins<sup>2</sup>, L.D. Carter<sup>2</sup>, G.H. Miller<sup>1</sup>

<sup>1</sup>INSTAAR and the Department of Geological Sciences

<sup>2</sup>U.S. Geological Survey, Menlo Park, Calif.

The Coastal Plain of northern Alaska represents one of the few large geographical areas in the Arctic to have remained free of continental ice throughout the Late Pliocene and Pleistocene. Consequently, eustatic sea level fluctuations which accompanied the glacial episodes throughout this time are recorded across this landscape as major transgressive and regressive sequences. Although some tectonic warping has occurred, the unconsolidated deposits of the Arctic Coastal Plain, the Gubik Formation, comprise one of the most complete records of high sea level stands in Arctic North America. The preliminary analyses of mollusc collections along the Arctic coast from Nome to the Colville River have shown that the epimerization of isoleucine in several species can differentiate major transgressive episodes where the stratigraphy is well documented. Shell analyses from the type localities of the classic transgressive sequences (Hopkins 1967, 1973) at Nome and Kotzebuan illustrate a reasonable progression of alloisoleucine/isoleucine ratios. Even at a mean annual temperature (MAT) of  $-4.8^{\circ}\text{C}$ , shells from the oldest units (estimated at 2.2 my, Hopkins, 1967) have not yet reached a racemic value of 1.30, indicating that the technique can be used as a relative age index into the late Pliocene. At Pt. Barrow (MAT  $-14.6^{\circ}\text{C}$ ) and across the entire Coastal Plain, a more severe thermal history is suggested by the fact that very little protein diagenesis has occurred even in shells of Pelukian age (last interglacial). Because the epimerization of isoleucine is so slow at these temperatures, it may be necessary to examine enantiomeric ratios of other amino acids (such as alanine) which racemize more quickly to gain better resolution between units of different age. At the present time, at least five major shorelines can be documented (Carter, unpubl) east of Pt. Barrow, toward the Colville River, but it remains unclear how these sequences correlate with shorelines at the western end of the Coastal Plain.

Miller (unpubl, 1979) has determined that the chronology of glacial and sea level events along the northeast coast of Baffin Island represents a much greater portion of the Quaternary than was previously recognized. The precise age of the oldest units is unknown; however it appears that the Cape Christian Interglacial

(previously thought to be the last interglacial,  $^{18}\text{O}$  stage 5e) may be as much as 200,000 to 500,000 years old. Despite the greater antiquity of the Baffin deposits, a significant anomaly is apparent between the age assignments of similar amino acid ratios (in areas of similar present MAT) from northern Alaska and Baffin Island. Discrepancies between different regions of the Arctic suggest that the duration of ice cover (basal temperatures  $\leq 0^\circ\text{C}$ ) and marine transgressional episodes (temperatures  $-1^\circ$  to  $+1^\circ\text{C}$ ) play an important role in modifying the thermal history, and hence, the rates of protein diagenesis in these areas (c.f. Miller and Mangarud, 1980). In this light, it is important to emphasize that the chronology of Baffin Island represents a glacioisostatically-induced sea level record whereas the Coastal Plain is marked by global, eustatically-induced events; the thermal history of Baffin shells is probably more complex than those from the Arctic Coastal Plain.



## APPENDIX M

### SUMMARY BIBLIOGRAPHY FOR YEAR ENDING MARCH 1980

- Brigham, J.K., Hopkins, D.M., Carter, L.D., and Miller, G.H., 1980, Application of amino acid geochronology to deposits of the Arctic coastal plain, Alaska; preliminary results and implications: University of Colorado Institute of Arctic Alpine Research, 9th Arctic Workshop, Abstracts, p. 34-35.
- Hartz, R.W., Holden, K., Hopkins, D.M., and Shearer, G., 1979, Location map and summary logs for the Geological Survey's 1979 Beaufort Sea Over-the-Ice drilling program: U.S. Geological Survey Open-File Report 79-1303.
- Hopkins, D.M., 1979, The Flaxman Formation of northern Alaska; record of early Wisconsinan shelf glaciation in the high arctic?: Pacific Science Congress, XIV, (Khabarovsk), Abstract, Additional Volume, p. 15-16.
- \_\_\_\_\_, 1979, Landscape and climate of Beringia during late Pleistocene and Holocene time, in Laughlin, W.S., and Harper, A.B., eds., The first Americans; origins, affinities and adaptations: New York, Gustav Fischer, p. 15-41.
- \_\_\_\_\_, 1979, Short resume of the geology of the Cape Nome-Safety Lagoon area, in Bockstoce, J., The archaeology of Cape Nome, Alaska: University of Pennsylvania, University Museum Monograph 38, p. 79.
- Hopkins, D.M., and Carter, L.D., 1980, Application of amino acid geochronology to deposits of the Arctic coastal plain, Alaska: University of Colorado Institute of Arctic and Alpine Research, 9th Arctic Workshop, Abstracts, p. 12-13.
- Hopkins, D.M., Hartz, R.W., and Robinson, S.W., 1979, Record of a pre-historic storm surge in the Wainwright Inlet-Kuk River area, in Johnson, K.M., and Williams, eds., The United States Geological Survey in Alaska; accomplishments during 1978: U.S. Geological Survey Circular 804-B, p. B29-B31.
- Hopkins, D.M., and Robinson, S.W., 1979, Radiocarbon dates from the Beaufort and Chukchi Sea coasts, in Johnson, K.M., and Williams, J.R., eds., The United States Geological Survey in Alaska; Accomplishments during 1978: U.S. Geological Survey Circular 804-B, p. B44-B47.
- Lee-Wong, F., Vallier, T.L., Hopkins, D.M., and Silberman, M.L., 1979, Preliminary report on the petrography and geochemistry of basalt from the Pribilof Islands and vicinity, southern Bering Sea: U.S. Geological Survey Open-File Report 79-1556, 51 p.
- \_\_\_\_\_, 1979, Petrology of alkali basalt from the Pribilof Islands region, southern Bering Sea: EOS, American Geophysical Union Transactions, v. 60, p. 972.

#### Publications In Press or In Progress

- Herman, Y., and Hopkins, D.M., in press, Arctic Ocean climate in late Cenozoic time and its relation to global events: Science.

Miller, G., and Hopkins, D.M., in press, Degradation of molluscan shell protein by lava-induced heat flow, Pribilof Islands, Alaska: Conference Proceedings, Ed Hare, editor.

Taylor, A., Woo, G.S., Hopkins, D.M., Prager, E.M., and Wilson, A.D., in press, Electron microscopy of mammoth tissues--an overview: Science.

Submitted for Publication

Hopkins, D.M., Matthews, J.V., Schweger, C.E., and Young, S.B., eds., in prep., Paleocology of Beringia: Academic Press (to be published in 1981).

Hopkins, D.M., Smith, P.A., and Matthews, J.V., Jr., Dated wood from Alaska and the Yukon; Implications for forest refugia in Beringia: Quaternary Research.

Porter, Lee, and Hopkins, D.M., Butchered caribou skulls, Pleistocene and Recent, from eastern Beringia: American Antiquity.

The first part of the document discusses the importance of maintaining accurate records of all transactions. It emphasizes that every entry, no matter how small, should be recorded to ensure the integrity of the financial statements. This includes not only sales and purchases but also expenses, income, and transfers.

The second part of the document provides a detailed breakdown of the accounting cycle. It outlines the ten steps involved in the process, from identifying the accounting entity to preparing financial statements. Each step is explained in detail, with examples provided to illustrate the concepts.

The third part of the document discusses the various types of accounts used in accounting. It categorizes them into assets, liabilities, equity, revenue, and expense accounts. It also explains how these accounts are used to record and summarize the financial activities of a business.

The fourth part of the document discusses the importance of the double-entry system. It explains how every transaction is recorded in two accounts, one as a debit and one as a credit, to ensure that the accounting equation remains balanced. This system provides a clear and concise way to track the flow of money in a business.

The fifth part of the document discusses the various methods used to record transactions. It compares the journal method, the ledger method, and the T-account method. It also discusses the advantages and disadvantages of each method and provides examples of how they are used in practice.

The sixth part of the document discusses the importance of the closing process. It explains how the temporary accounts (revenue, expense, and dividend) are closed to the permanent accounts (assets, liabilities, and equity) at the end of each accounting period. This process ensures that the financial statements for the next period start with a clean slate.

The seventh part of the document discusses the various types of financial statements. It explains the purpose and format of the balance sheet, the income statement, the statement of retained earnings, and the statement of cash flows. It also discusses how these statements are used by management and external stakeholders to make informed decisions.

The eighth part of the document discusses the importance of the audit process. It explains how an independent auditor is hired to examine the financial statements and provide an opinion on their accuracy. It also discusses the various types of audits and the role of the auditor in ensuring the reliability of the financial information.

The ninth part of the document discusses the various types of taxes that a business may be required to pay. It explains the difference between income tax, sales tax, and property tax, and provides information on how to calculate and pay these taxes. It also discusses the importance of keeping accurate records to support the tax returns.

The tenth part of the document discusses the various types of insurance that a business should consider. It explains the benefits of liability insurance, property insurance, and life insurance, and provides information on how to choose the right policy for the business. It also discusses the importance of reviewing the policy regularly to ensure it remains up-to-date.

ANNUAL REPORT

Research Unit: 205  
Reporting Period: April, 1979-  
March, 1980

GEOLOGIC PROCESSES AND HAZARDS OF THE BEAUFORT SEA  
SHELF AND COASTAL REGIONS

Peter Barnes

Erk Reimnitz

Pacific-Arctic Branch of Marine Geology  
345 Middlefield Road  
Menlo Park, California 94025

April 1, 1980

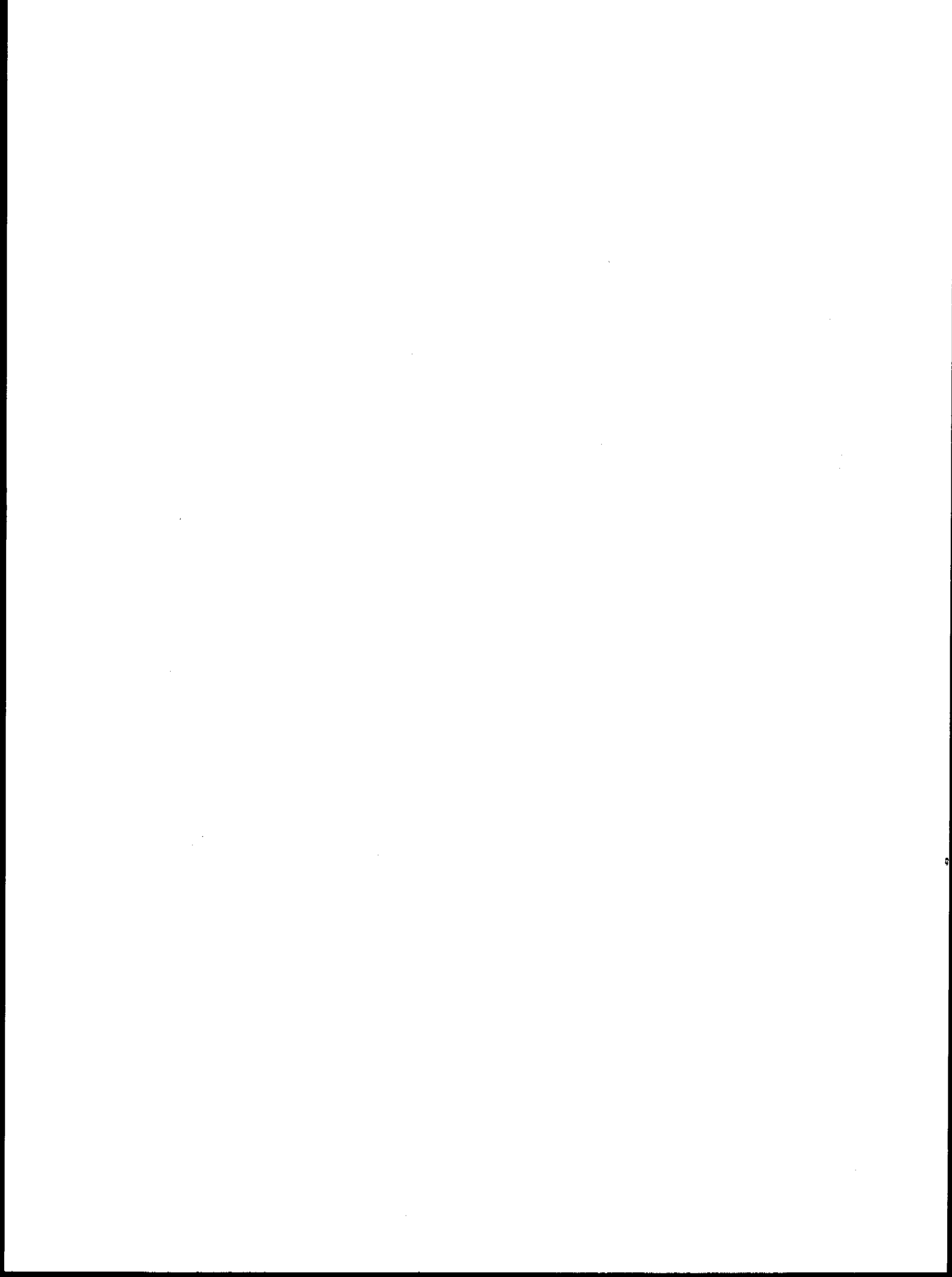


TABLE OF CONTENTS

PAGE

I.	Summary of Objectives, conclusions and implications.....	260
II.	Introduction	
	A. General nature and scope of study.....	262
	B. Specific objectives.....	262
	C. Relevance to problems of petroleum development.....	263
III.	Current state of knowledge.....	263
IV.	Study area.....	268
V.	Sources, methods and rationale of data collection.....	269
VI, VII, and VIII.	- Results, Discussion, Conclusions.....	269
	(as attachments to report)	
	A. New seismic evidence for a widespread occurrence of gas in submarine sediments at shallow depths, Prudhoe Bay, Alaska	
	B. Overconsolidated surficial deposits on the Beaufort Sea shelf	
	C. Bathymetric changes in the vicinity of the West Dock, Prudhoe Bay, Alaska	
	D. Reassessment of ice gouging on the inner shelf of the Beaufort Sea, Alaska	
	E. Break in gouge character related to ice ridges	
	F. Super sea-ice kettles in the arctic nearshore zone - Reindeer Island	
IX.	Needs for further study.....	271
X.	Summary of fourth quarter operations.....	271
XI.	Published Reports.....	272

## I. Summary of objectives, conclusions and implications with respect to OCS oil and gas development.

The present investigation is an expansion and intensification of our earlier studies on the marine geology and modern sedimentary environment off arctic Alaska with emphasis on rates and processes. In particular we have concentrated on phenomena involving ice and its unique influence on the shelf and inshore environment. The marine environment of the arctic shelf poses special problems to offshore development. Faulting, tectonic activity, and sea floor instability are environmentally of lower concern in the Beaufort Sea, when compared to processes and low temperatures involving sea ice. Seven years of study have provided a basic understanding of this unique marine geologic environment. However, many important aspects have yet to be addressed. For example, the major processes involved in ice gouging of the sea floor are reasonably understood, including distribution, densities, gouge trends, rates of gouging, depths of reworking and the variability of gouge formation from year to year. Critical questions remain regarding the interaction of the stamukhi with the continental margin, the distribution and character of gouging in this zone, rates of gouge infilling, and the time of formation of the stamukhi zone. Neither are the effects of the stamukhi zone on oceanographic circulation, sediment disruption and dispersal, and the shelf profile properly understood.

Another area where we have poor understanding involves coastal zone processes. The spring flooding of the sea ice with river water is reasonably well known as a phenomenon but the intensity of the associated processes of transport, scour and ice movement are only poorly understood. Rates of coastal erosion are known to be significant, but the fate of these erosional products, their relationship to river input, and the growth and maintenance of the barrier islands need to be assessed. Inside the 2-m bench where ice rests on the bottom at the end of the winter, a unique sedimentary environment exists where tides and surges set up significant currents. Furthermore, the ice canopy may interact with the seabed causing each to exhibit a unique character.

The past year of field work and subsequent laboratory and office work has resulted in the following observations regarding the arctic nearshore environment.

Preliminary analysis of a series of 60 vibracores taken in the nearshore area between the Sagavanirktok River and the Colville River shows five different environments. Lagoonal and bay sediments are indistinctly laminated sandy silts and clays. Cores in the vicinity of the barrier islands are sands and gravels with an abundance of depositional sedimentary structures. Off-shore shoals are characterized by clean well-laminated sands underlain by finer material on the ridge flanks. Off the Colville delta layered sands, silts and peats are replaced seaward beyond 5 m by disrupted or poorly laminated muds, probably related to strudel and ice gouge reworking. The absence of gravels except in the immediate vicinity of the coastal bluffs and barrier islands is of significance to offshore development.

1. Investigations show snow depth and ice thickness correlate negatively, ice-bottom morphology correlates with a stable snow-ridge morphology, and loci of under-ice oil pockets are readily discernible from the surface. Both ice bottom and snow surface relief varied by about 30 cm on wave lengths of about 10 m. Seasonal variability in snow accumulation and wind patterns are expected to modify these observations.
2. A systematic grid of survey lines, coupled with bottom samples and diving observations, provides a detailed description of the size, configuration, surface characteristics, and geology of the boulder patch in Stefansson Sound and suggests the boulders originated as a shallow water lag deposit.
3. Sea floor morphology changed drastically between 1977 and 1978 from waves and currents associated with 1977 open season storms. The changes suggest a) erosion and deposition are episodic, b) maximum observed gouge incisions may be too shallow, and c) shelf sediments are predominantly deposited in gouge incisions.
4. Detailed observation on a recent ice gouge made after the large wave events of 1977 show extremely rapid rates of gouge infilling and reworking. These observations imply a) age of less than 10 to 20 years for gouges on the inner shelf, b) that acoustic measurements of older gouge incisions give values far below the true depth of incision, and c) that open excavations are likely to infill during a summer like that of 1977.
5. A bathymetric survey along the northeast side of Cross Island shows 7 m water depth where the island once was. This is coupled with diving observations which fail to show exposures of Quaternary Gubik Formation. This suggests that the island originated as a constructional form, similar to true barrier islands.
6. Eolian sand deposits are found on the fast ice downwind of gravelly barrier islands in the arctic. One small island exposure lost over 300 tons of sand in eight months, suggesting a deflation rate of 2 mm per winter. Wind winnowing of island surfaces is effective year round, while sediment supply by waves is effective for only two to three months in the arctic. This suggests wind removal of sand as a possible mechanism to explain their coarseness relative to those of lower latitudes, where sand dominates.
7. Vast quantities of sediment slush under-ice ice up to 5 m thick appear to be associated with the 'boulder patch'. The ice formed random-oriented plates and granules in early October 1978. Although of great significance to sediment transport and biological processes as well as to developmental activities, the mechanisms leading to ice growth, accumulation in observed formations, and the process of sediment inclusion remain unknown.
8. Ice cores obtained from the fast ice in the spring of 1978 show a widely distributed 'dirty' ice horizon up to 1 m thick. Sediment concentrations are an order of magnitude greater than would be expected from simple freezing of shelf sea water. Earlier observations show that 'dirty' ice is not present on the inner shelf every year. The accumulation has significant impact on light transmission and the growth of organisms as well as on the sediment transport regime and the thermal and structural character of the fast ice; yet these mechanisms are unknown.



9. The problem of how the shoals of the stamukhi zone interact with ice to control ice zonation is critical to ice management in the seaward part of the lease area. During the past winter there was no multiyear ice on the shelf during freeze-up. Our observations this spring showed massive ridges composed of first year ice clearly associated with shoals northwest of Prudhoe Bay. We also recovered sediments from the stamukhi ridges containing marine shells suggesting displacement from the nearby sea floor. An enigma exists where first year ice, not nearly thick enough to contact the crests of shoals, focused the major ridge building over these bathymetric features.

## II. Introduction

### A. General nature and scope of study

Arctic continental shelves, where ice is present seasonally for part of the year, comprise 25% of the total world shelf area. Yet the interaction of ice in the regime of sedimentary processes on North American arctic shelves is poorly understood. Investigation of the continental shelf and shores of the Chukchi and Beaufort Seas was initiated in 1970. The primary goal of this program has been to understand both the processes unique to arctic shelves and the role of more conventional processes in temperate latitudes.

### B. Specific objectives

Many questions have been raised on the basis of our past investigations, which apparently hold the key to an understanding of the seasonal cycle in the marine environment. It is these tasks that we address in our current research.

1) Process of ice gouging - in particular the repetitive rates of gouging, rates of sediment infilling, seasonal distribution, and the extent to which it occurs outside the area of our past investigations. The ice bottom interactions in the stamukhi zone where the bulk of oceanic energy is expended on the continent needs special emphasis.

2) Shelf sediment transport regime - including reworking and resuspension of bottom materials by ice and benthos, distribution of river effluents, and ice rafting. The latter aspect has taken a new turn with the recent discovery of slush ice formation in early fall, and fine sediment entrainment with important implications for dispersal of pollutants.

3) The fast-ice zone; its undersurface morphology and its influence on nearshore current circulation, bedforms, sediment transport, permafrost, and on river discharge.

4) An estimation of coastal erosion and its relationship to the formation of offshore islands, submerged shoals, and the stability of the coastal marine environment.

5) Inner shelf oceanography, and its relationship to the sedimentary environment. This includes upwelling in the coastal zone, the dispersal of highly saline (60 ‰) and cold (-5°) water generated in the shallow embayments, lagoons, and river mouths during the winter, and the possibility of anchor ice formation and ice rafting as factors in the sedimentary environment.

6) Outlining the Pleistocene stratigraphy and geologic history of the shelf as an aid to determining a sea level curve for the Beaufort Sea.

7) Delineation of sediment character on the inner shelf from a correlation of available seismic reflection records, samples and drill hole data.

### C. Relevance to problems of petroleum development

The character of the arctic continental shelf and coastal area, with year round and seasonal sea ice and with permafrost, faces the developer with many special problems. The interaction of the arctic shelf with the arctic pack ice takes the form of ice gouging and the formation of a large stamukhi zone each winter.

Oil drilling and production during the next several years will probably not extend into the stamukhi zone seaward of the seasonal fast-ice zone. Of critical concern are the ice gouge and strudel scour effects on structures and pipelines. A similar emphasis has been taken by the Canadian Beaufort Sea Project in their more advanced state of knowledge and readiness to lease their outer continental shelf lands (Milne and Smiley, 1976). Any structure which is to be mated with the ocean floor requires data concerning the strength and character of the ocean floor. Furthermore, foundation materials in the form of gravels will be needed for work pads offshore. In addition, the offshore drilling operation may encounter permafrost and associated gas hydrates which could be substantially altered during the process of pumping hot oil up to the sea floor or along the sea floor in gathering and transportation pipelines potentially causing structural failure and blowouts.

### III. Current state of knowledge

The state of recent knowledge has been excellently summarized in the Arctic Institute of North America's 1974 publication: The Coast and Shelf of the Beaufort Sea. The bulk of background geologic material for the Alaskan Beaufort shelf has been summarized in articles by Reimnitz, Barnes, Naidu, Short, Walker and others, in this same volume. The OCSEAP Beaufort Sea synthesis volume contains a very useful summary of the current state of knowledge. References to more recent material may be found in the OCSEAP synthesis report on winter studies currently being prepared, where recent findings of under-ice slush in Stefansson Sound and their implications are discussed, and also in the Results and Discussion sections below and in the appended reports.

Briefly, results to date have clearly established drifting ice as a major influence on the marine geologic and sedimentologic environment of arctic shelves (best summarized in Reimnitz and Barnes, 1974; Barnes and Reimnitz, 1974; and in the 1976, 1977, 1978, and 1979 Annual Reports). In the 1979 Annual Report the occurrence of slush ice below the fast ice has first been reported, along with speculations on processes of its formation, of sediment entrainment, and implications for sediment transport. A recent interdisciplinary meeting on the subject has pointed out the importance of the phenomenon for the arctic environment, and the need for specific studies.

Major boundaries exist which are related to inner shelf sea ice zonation (Fig. 1). Inside the 2 m contour, ice rests on the bottom at the end of the seasonal growth and generally remains stable and undisturbed through the winter. Seaward from this bottom fast ice, a zone of relatively undisturbed, floating fast ice as much as 2 m thick extends offshore to where it meets the moving ice of the polar pack. At this juncture, shear and pressure ridges develop which are grounded, forming the stamukhi zone. Each of these zones apparently has distinctive sedimentologic, permafrost, morphologic and ice gouge characteristics.

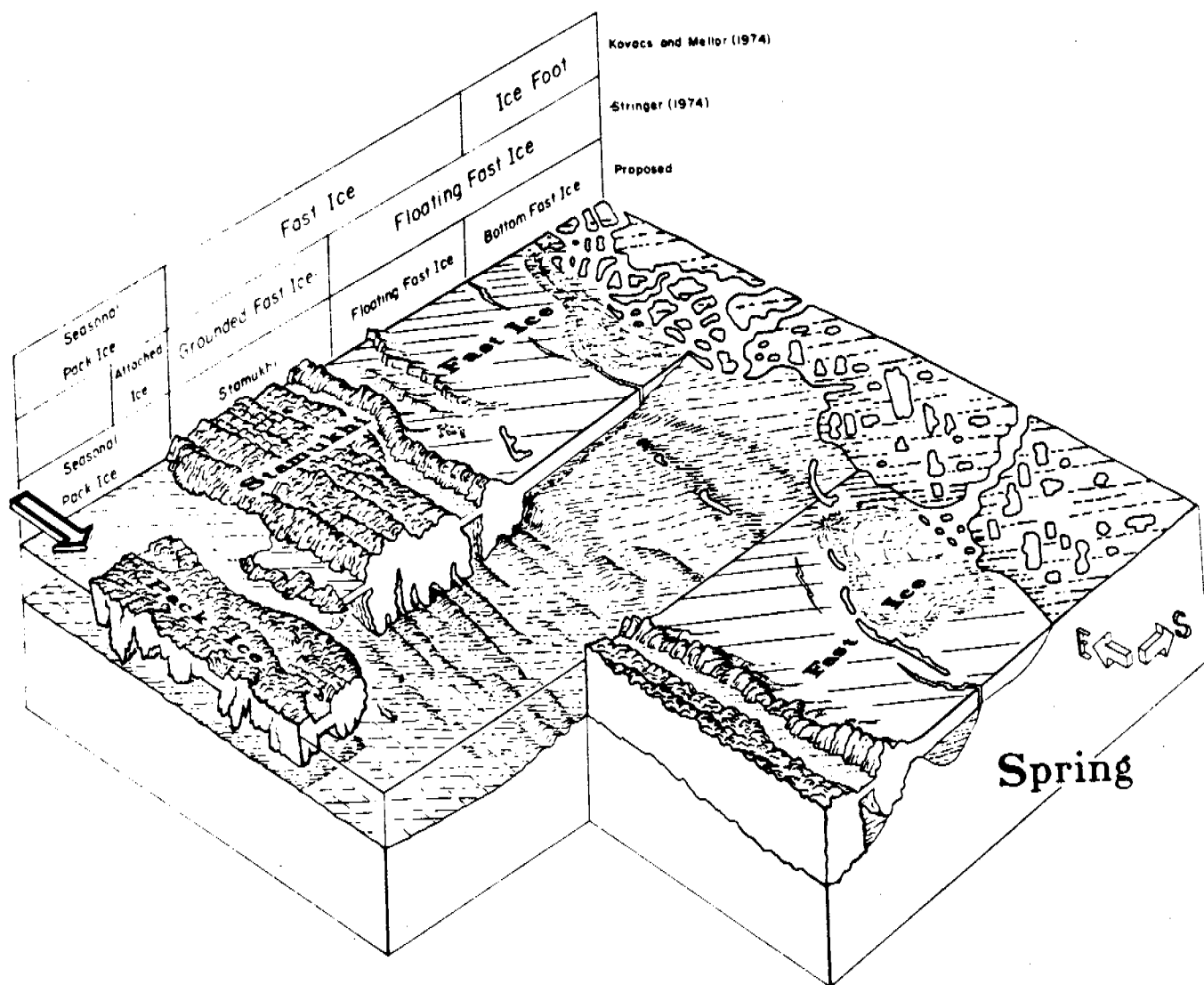


Figure 1. Diagram of an idealized cross-section of the fully developed ice zonation along the Alaskan Beaufort Sea coast at the time of maximum ice growth in spring. Drawing by Tau Rho Alpha.

A rudimentary framework for the processes and related sedimentologic record over the major ice zones can be established (Fig. 2) which relates the relative importance of ice and water as dynamic agents affecting the sea bottom. The major processes involved in each ice zone are:

Bottom fast ice zone:

1) River overflow onto the sea ice and subsequent drainage through strudle holes and cracks causes sea-floor scour depressions and initiates sub-ice sediment transport.

2) Sub-ice tidal and storm surge currents act to maintain and perhaps enlarge tidal channels in lagoons and bays.

3) Storm surges raise sea level as much as 3 m, erode beaches, coastal bluffs, and islands and inundate the coastal plains.

4) Wave action modifies beaches and coasts during the open water season.

5) Ice-push acts on exposed parts of coasts and offshore islands.

6) Ad-freezing of sediments and lowering of sediment temperatures occurs where sea ice is in contact with the bottom.

Floating fast ice zone:

1) Waves and currents result in moderate reworking of the bottom sediments.

2) Ice gouging occurs in exposed areas primarily in winter but to a lesser extent during summer. In years with exceptional storms, gouges on the inner shelf may be obliterated or vastly altered.

3) Bioturbation and sedimentation are most dominant in this zone throughout the year.

4) Fast ice thickness is inversely related to snow depth, forming elongate ice-bottom troughs parallel to the snow ridges formed on the surface by northeast winds (Fig. 3).

5) In some years phenomena apparently involving anchor ice formation concentrate sediments in and beneath the fast-ice canopy.

Stamukhi zone:

1) Ice gouging of bottom reworks sediments to depths in excess of 25 cm in less than 100 years, maximum gouge incisions are probably in excess of 2 m, obliterating sedimentary structures. Resulting sedimentary structures are a discontinuous series of shoestring deposits.

2) Current transport and scour are associated with grounded keels of ice.

3) Control of inner shelf ice character results from coastal configuration and distribution and orientation of submerged shoals. Creation or maintenance of these shoals is probably related to ice-related processes.

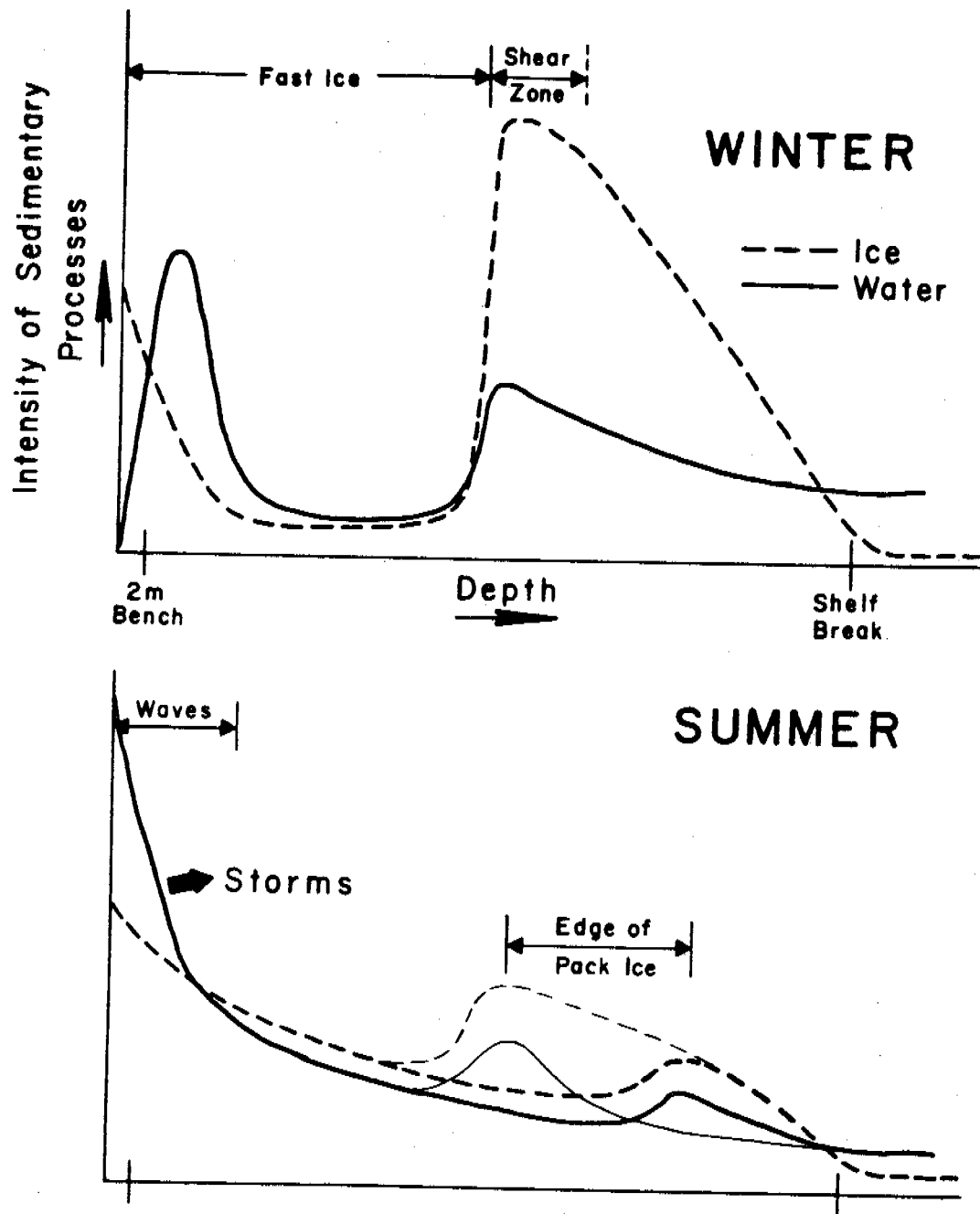


Figure 2. Conceptual model of the relative importance of ice and water as process agents on the bottom sediments of the arctic shelf off northern Alaska.

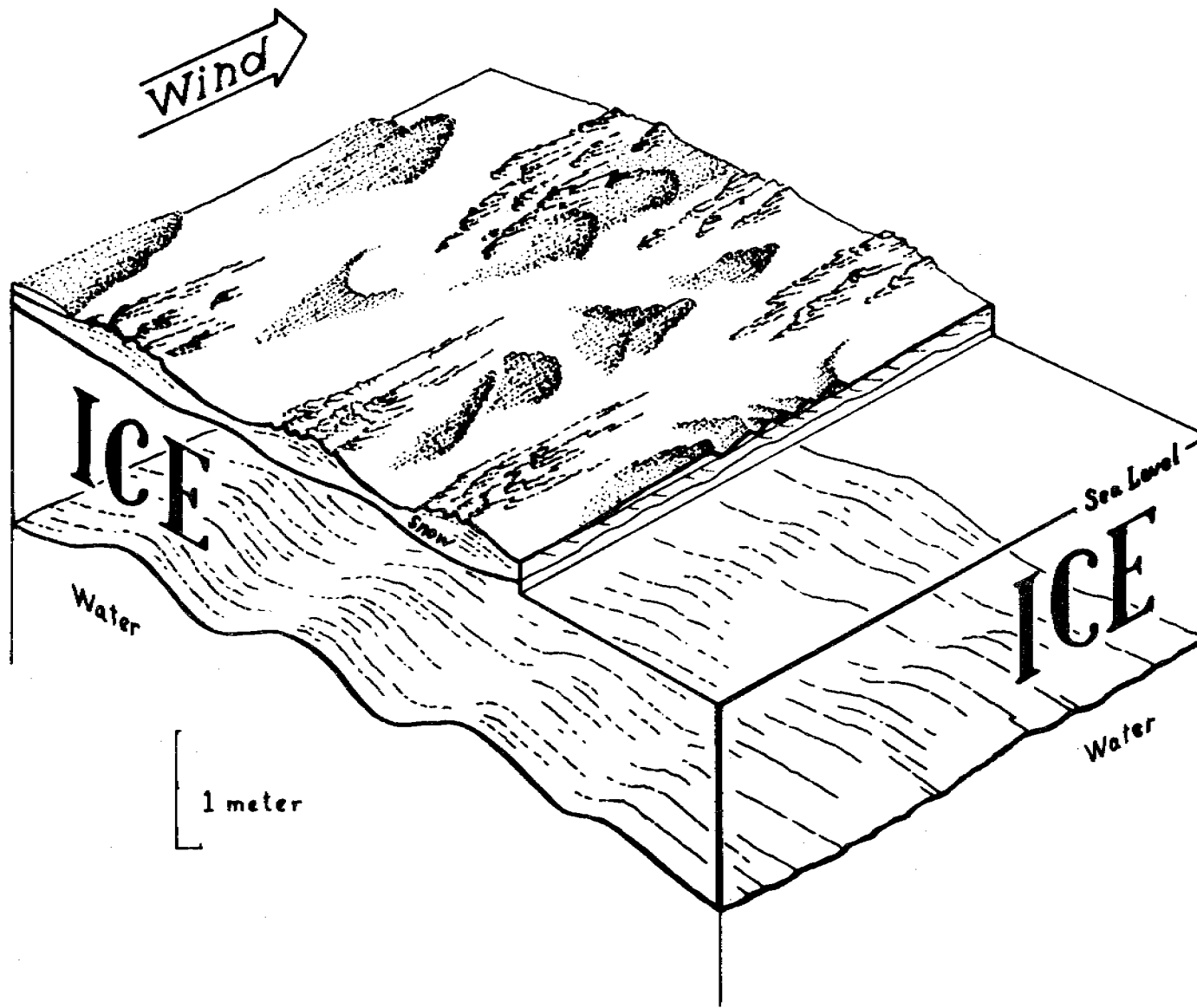


Figure 3. Block diagram by Tau Rho Alpha depicting the relationships between snow patterns and fast-ice morphology.

#### IV. Study Area

The primary study area includes the Beaufort Sea shelf between Barter Island on the east and Point Barrow on the west with emphasis on an inshore segment between Flaxman Island and Cape Halkett. The adjacent land is a broad, flat coastal plain composed mainly of Quaternary deposits of tundra-silts, sands, and gravels. In much of the area, the coast is being eroded by the sea at a rapid rate forming coastal bluffs as much as 6 m high. The line of bluffs is interrupted by low mud flats at the mouths of major rivers. Much of the coast is marked by islands at varying distances from the shore. Most of the islands are less than 3 m in elevation, narrow, and comprised of sand and gravel. Others are capped by tundra and are apparently erosional remnants of the inundated coastal plain. Coast-parallel shoals are also a feature of the inner shelf.

The shelf is generally rather flat and remains shallow for a considerable distance from shore. Off the Colville River the 2-m isobath is up to 12 km from shore. The width of the shelf is variable, ranging from 55 km in the east to 110 km in the west. The shelf break lies at depths of 50 to 70 m. The shallowness of the shelf break and the presence of elevated Pleistocene beach lines suggests a broad regional uplift. The Holocene marine sediments on the inner shelf are generally 5 to 10 m thick and composed of complex textural and compositional character. Ice and oceanographic factors interact to form a compound structural character of ice flow heterogeneity or wave and current-bedded sequences.

The rivers flood in early June, delivering 50 to 80 percent of the yearly runoff in a 2-3 week period. The bulk of sediment input from rivers is associated with this flood. No river gravels presently reach the ocean. Initial flooding seaward of the river delta occurs on top of the unmelted sea ice, although the influx of warmer water eventually leads to ice-free areas off the deltas early in the sea-ice melt season. River drainage basins are located in the Brooks Range and the eastern rivers drain directly into the ocean while the western rivers meander across the broad coastal plain.

Sea ice is a ubiquitous feature in the study area. New ice starts to form in late September and grows to a thickness of 2 m through the winter, welding remnant older ice into more or less solid sheets. Where forces are sufficient, ice fractures and piles into hummocks and ridges. By June, sea-ice melting is well underway and usually sometime in July enough ice has melted so that the protected bays and lagoons are free of ice, and temperate latitude processes of waves and wind-driven currents are active. Ice remains on the shelf in the study area throughout the summer. Its location and concentration depend on the degree of melting and winds. The prevailing northeasterly wind tends to carry drifting summer ice away from the shore while the westerlies pile ice against the coast. Ice commonly remains grounded throughout the summer on many of the shoals on the inner shelf.

Currents and waves are a function of the winds during the open-water season. Waves are generally poorly developed due to the limited fetch which results from the presence of ice during most of the summer. Water circulation is dominated by the prevailing northeasterly winds which generate a westerly flow on the inner shelf. In winter currents under the ice are generally sluggish although restrictions of the tidal prism by ice at tidal inlets and on the broad, shallow, 2-m bench cause significantly higher velocities.

## V. Sources, methods and rationale of data collection

A. Equipment operated routinely from the R/V KARLUK includes bottom sampling and coring gear, water salinity, -temperature, and -turbidity sensors, fathometers, a high and medium resolution seismic system, and a side-scan sonar. Precision navigation is maintained to 3 m accuracy with a range-range system.

Special techniques include (a) repetitive sonar and fathometer surveys of ice gouges, (b) diving observations and bottom photography, (c) measurements of sediment thicknesses within ice gouges by combined use of narrow beam echo sounder, and (d) a near-bottom tow package incorporating sub-bottom profiler and television, (4) nearsurface stratigraphic studies using a vibracorer capable of obtaining 2-m long cores and (f) detailed surveys of bathymetry in river and lagoonal channels and in the vicinity of manmade structures. Coastal observations of rates of bluff erosion and the distribution and elevation of storm surge strand lines was carried out by helicopter. Winter ice observations involve ice coring, diving observations along with modified system of upward-looking fathometer, and side-scan sonar.

B. The past and present status of data and product submission to NOAA-BLM-OCSEAP is given in the table on the following page.

## VI, VII, VIII. Results, Discussion and Conclusions - (As attachments to report)

- A. New seismic evidence for a widespread occurrence of gas in submarine sediments at shallow depths, Prudhoe Bay, Alaska
- B. Overconsolidated surficial deposits on the Beaufort Sea shelf
- C. Bathymetric changes in the vicinity of the West Dock, Prudhoe Bay, Alaska
- D. Reassessment of ice gouging on the inner shelf of the Beaufort Sea, Alaska
- E. Break in gouge character related to ice ridges
- F. Super sea-ice kettles in the arctic nearshore zone - Reindeer Island



RU-205, Barnes and Reimnitz, Product Submission Status, REPORTS TO NOAA-BLM

Data Products	Other Sources of Data (Numbers refer to references, p. 15-18)																								
	Sept. 1980	June 1980	March 1980	Dec. 1979	Sept. 1979	June 1979	March 1979	Dec. 1978	Sept. 1978	June 1978	March 1978	Dec. 1977	Sept. 1977	June 1977	March 1977	Feb. 1977	Dec. 1976	Sept. 1976	June 1976	March 1976	Dec. 1975	Sept. 1975			
<b>NON DIGITAL</b>																									
-core descriptions													6												
-acoustic profiles w/nav.														x				x	x						1B,19,24,25,32
<b>DIGITAL</b>																									
-water temp./sal.																			x	x					13, Lost equipment
-current meter																			x	x	x				Lost equipment
-nephelometer																									
<b>SUMMARY PRODUCTS</b>																									
-Ice gouge maps																									7,9,18,28,31,33,34,37,38
-Evaluation of ice hazards	x	x	x											x	x	x									1A,7,9,10,16,17,26,27,28,30,31,33
-Offshore gravel resources																									2,7,14,18,35
-Holocene marine sediments																									2,7,10,14,16,27,29,33,35
-Bottom currents and processes	x	x	x	x										x	x	x									1A,2,7,10,14,16,34
-Sediment transport regime	x													x	x	x	x	x	x	x	x	x	x	0	2,7,10,11,13,14,18,20,27,33
-Interpretation of stamukhi																									7,8,9,10,14,18,26,27,30,31,33,37
-Coastal erosion and delta progradation																									7,10,11,12,17,18,23
-Boulder patch																									7
-Ice thickness morphology																									3
<b>ADDITIONAL INFORMATION</b>																									
-Sediment distribution and character																									2,7,10,14,29,34,35,37
-Charts																									1B, 2,8,26,27
-Oceanographic observations																									3,10,13,23,36
-Engineering properties																									10,14,29,33
-Chukchi Sea studies																									37,38
-Freshwater resources																									12,17
-Sediment interstitial salt, sea floor temperature																									29
-Diving observations																									2,3,7,10,29,31,33
-Barrier islands																									7,10,11,27,33,35
-River processes																									12
-Storm surges																									23

x- data or information submitted  
 0- work in progress or planned  
 for this period

## IX. Needs for further study

The primary emphasis of future work should include the following: recurrence rates and intensity of ice gouging in the stamukhi zone; rates of sediment reworking and sediment infilling; focused efforts on the problems related to slush ice; determination of the rates of sediment migration along the mainland coast; assessing the character of ice sediment interaction in the vicinity of the 2-m bench, as related to sub-ice current scour, oil entrapment and sediment stability; an evaluation of the engineering character of surficial sediment units on the shelf; and an assessment of the Holocene stratigraphy for clues as to sea level history, gravel sources, and engineering

## X. Summary of 4th Quarter Operations

### A. Ship or laboratory activities

1) Ship or field trip: None

2) Personnel involved in project:

Peter Barnes	Project Chief - Geologist	U.S.G.S.,	Marine	Geology
Erk Reimnitz	Principal Investigator-Geologist	"	"	"
Ed Kempema	Physical Science Technician	"	"	"
Peter Minkler	Physical Science Technician	"	"	"
Robin Ross	Physical Science Technician	"	"	"
Doug Rearic	Physical Science Technician	"	"	"

### 3) Methods

Efforts this quarter have been primarily aimed at data compilation, data reduction, and report writing. Significant project efforts during the quarter were:

- a) description and characterization of old and new ice gouge records over large areas of the shelf
- b) preparation of the annual report
- c) preparation of manuscripts for internal and external publication
- d) preparation and planning for summer field efforts
- e) computer compilation of bathymetry and precision-navigation data of Reindeer and Pingok Islands and of West Dock area
- f) compilation of data and observations on overconsolidated materials
- g) study of seafloor in area of large ice ridges
- h) participation in slush ice meeting and winter studies synthesis
- i) geophysical investigation and mapping of gas-charged sediments

### 4) Data collected or analyzed:

DATA TYPE	Km of record or number of samples analyzed
Side-scan sonar	100 km
Bathymetry profiles	100 km

Published Reports

- 1A. Aagaard, Knut, Atlas, R., Barnes, P.W., Callay, R.J., Craig, P., Harrison, W.D., Pritchard, R.S., Lowry, L., Martin, Seelye, Nummedal, Dag, Schell, D.M., and Wisemann, W.J., 1977, Spills transport and effects of oil: in G.Weller, D. Norton and T. Johnson, (eds.): Beaufort Sea Synthesis Report - Environmental impacts of OCS development in Northern Alaska; Outer Continental Shelf Environmental Assessment Program, Arctic Project - Special Bulletin no. 15, p. 179-187.
- 1B. Barnes, P.W., Reimnitz, Erk, Ross, R., Kempema, E., and Minkler, P., 1980, U.S. Geological Survey marine geologic studies in the Beaufort Sea, Alaska, 1979; data type, location, and records obtained, U.S. Geol. Survey open-file report (number pending), 3 maps.
2. Barnes, P.W., Reimnitz, Erk, and Ross, Robin, 1980, Nearshore surficial sediment textures, Beaufort Sea, Alaska: U.S. Geological Survey Open-File Report 80-196, 41 p.
3. Barnes, P.W., Reimnitz, Erk, Toimil, L.J.,. and Hill, H.R., 1979, Fast-ice thickness and snow depth in relation to oil entrapment potential, Pudhoe Bay, Alaska, in Proceedings of Fifth International Conference on Port and Ocean Engineering under Arctic Conditions at the Norwegian Institute of Technology, August, 1979, p. 1205-1225.
4. Barnes, P.W., and Reimnitz, Erk, 1977, Ice gouge obliteration and sediment redistribution event; 1977-1978, Beaufort Sea, Alaska, U.S. Geological Survey Open-File Report 79-848, 22 p.
5. Barnes, P.W., and Toimil, L.J., 1979, Inner shelf circulation patterns, Beaufort Sea, Alaska: U.S. Geological Survey Miscellaneous Field Studies Map MF-1125.
6. Barnes, P.W., Reimnitz, Erk, Toimil, Larry, Maurer, Douglas, and McDowell, David, 1979, Core descriptions and preliminary observations of vibracores from the Alaskan Beaufort Sea shelf: U.S. Geological Survey Open-File Report 79-351, 71 p.
7. Barnes, P.W., and Hopkins, P.M., (eds.), 1978, Geological Sciences, in Interim Synthesis Report: Beaufort/Chukchi, Gunter Weller, David Norton, Toni Johnson, (eds.), National Oceanic and Atmospheric Administration, Environmental Research Laboratories, Boulder, Colo, p. 101-131.
8. Barnes, P.W., and McDowell, David, 1978, Inner shelf morphology, Beaufort Sea, Alaska: U.S. Geological Survey Open-File Report 78-785, 3 p.
9. Barnes, P.W., McDowell, David, and Reimnitz, Erk, 1978, Ice gouging characteristics: their changing patterns from 1975-1977, Beaufort Sea, Alaska: U.S. Geological Survey Open-File Report 78-730, 40 p.
10. Barnes, P.W., Reimnitz, Erk, Drake, D.E., and Toimil, L.J., 1977, Miscellaneous hydrologic and geologic observations on the inner Beaufort Sea shelf, Alaska: U.S. Geological Survey Open-File Report 77-477, 95 p.
11. Barnes, P.W., Reimnitz, Erk, Smith, Greg, and McDowell, David, 1977, Bathymetric and shoreline changes in northwestern Prudhoe Bay, Alaska: The Northern Engineer, v. 9, n. 2, p. 7-13.

12. Barnes, P.W., and Reimnitz, Erk, 1976, Flooding of sea ice by rivers of northern Alaska; in ERTS-1, A new window on our planet, R.W. Williams, Jr., and W.D. Carter, (eds.): U.S. Geological Survey Professional Paper 929, p. 356-359.
13. Barnes, P.W., and Garlow, R., 1975, Surface Current Observations-Beaufort Sea, 1972: U.S. Geological Survey Open-File Report 75-691, 3 p.
14. Barnes, P.W., and Reimnitz, Erk, 1974, Sedimentary processes on arctic shelves off the northern coast of Alaska, in J.C. Reed and J.E. Sater, (eds.): The Coast and Shelf of the Beaufort Sea, The Arctic Institute of North America, Arlington, Va., p. 439-576.
15. Grantz, A., Barnes, P.W., Dinter, D.A., Lynch, M.B., Reimnitz, Erk, and Scott, E.W., 1980, Geologic framework, hydrocarbon potential, environmental conditions, and anticipated technology for exploration and development of the Beaufort Shelf north of Alaska: U.S. Geological Survey Open-File Report 80-94, 42 p.
16. Grantz, Arthur, Barnes, P.W., Eittreim, S.L., Reimnitz, Erk, Scott, E.W., Smith, R.A., Stewart, George, and Toimil, L.J., 1976, Summary of sediments, structural framework, petroleum potential, environmental conditions, and operational considerations of the United States Beaufort Sea, Alaska area: U.S. Geological Survey Open-File Report 76-830, 32 p.
17. Harden, Deborah, Barnes, P.W., and Reimnitz, Erk, 1977, Distribution and character of naleds in northeast Alaska: Arctic, v. 30, p. 28-40.
18. Hopkins, D.M., Barnes, P.W., Biswas, N.N., Cannon, J.K., Chamberlain, Edwin, Dygas, J., Harrison, W.D., Naidu, S., Nummedal, Dag, Rogers, J.C., Sellmann, P.V., Vigdorichik, Michael, Wiseman, W.J., and Osterkamp, T.E., 1977, Earth Science Studies in G. Weller, D. Norton and T. Johnson (eds); Beaufort Sea synthesis Report - Environmental impacts of OCS development in northern Alaska; Outer Continental Shelf Environmental Assessment Program, Arctic Project - Special Bulletin, n. 15, p. 43-72.
19. Maurer, D.K., Barnes, Peter, and Reimnitz, Erk, 1978, U.S. Geological Survey marine geologic studies in the Beaufort Sea, Alaska, 1977; data type, location, and records obtained: U.S. Geological Survey Open-File Report 78-1066, 3 p.
20. Reimnitz, Erk, Ross, Robin, and Barnes, P.W., 1980, Dinkum Sands: U.S. Geological Survey Open-File Report 80-360, 11 p.
21. Reimnitz, Erk, and Ross, Robin, 1979, Lag deposits of boulders in Stefansson Sound; Beaufort Sea, Alaska: U.S. Geological Survey Open-File Report 79-1205, 26 p.
22. Reimnitz, Erk, and Maurer, D.K., 1979, Eolian sand deflation, a cause for gravel barrier islands in arctic Alaska?: Geology, v. 7, p. 507-510.

23. Reimnitz, Erk, and Maurer, D.K., 1979, Effects of storm surges on the Beaufort Sea coast, northern Alaska: *Arctic*, v. 32, n. 4, p. 331-344.
24. Reimnitz, Erk, Barnes, P.W., and Kempema, Ed, 1979, Marine geologic studies in the Beaufort Sea, Alaska, 1978; data type, location, records obtained, and their availability: U.S. Geological Survey Open-File Report 79-384, 4 p.
25. Reimnitz, Erk, Barnes, P.W., and Mauere, Doug, 1979, U.S.G.S. Marine geologic studies in the Beaufort Sea, Alaska, 1976; data type, location, and records obtained: U.S. Geological Survey Open-File Report 79-566, 3 p.
26. Reimnitz, Erk, and Maurer, D.K., 1978, Stamukhi shoals of the arctic-some observations from the Beaufort Sea: U.S. Geological Survey Open-File Report 78-666, 17 p.
27. Reimnitz, Erk, Toimil, L.J., and Barnes, P.W., 1978, Arctic continental shelf morphology related so sea-ice zonation, Beaufort Sea, Alaska: *Marine Gology*, v. 28, p. 179-210.
28. Reimnitz, Erk, Barnes, P.W., Toimil, L.J., and Melchoir John, 1977, Ice gouge recurrence and rates of sediment reworking, Beaufort Sea, Alaska: *Geology*, v. 5, p. 405-408.
29. Reimnitz, Erk, Maurer, D.K., Barnes, P.W., and Toimil, L.J., 1977, Some physical properties of shelf surface sediments, Beaufort Sea, Alaska: U.S. Geological Survey Open-File Report 77-416, 8 p.
30. Reimnitz, Erk, Toimil, L.J., and Barnes, P.W., 1977, Stamukhi zone processes: Implication for developing the arctic offshore area: Offshore Technology Conference, Houston, Tx., Proceedings v. 3, p. 513-518.
31. Reimnitz, Erk, and Barnes, P.W., 1976, Influence of sea ice on sedimentary processes off northern Alaska, in ERTS-1, A new window on our planet, R.S. Williams, Jr., and W.D. Carter (eds.): U.S. Geological Survey Professional Paper 929, p. 360-362.
32. Reimnitz, Erk, 1976, High-resolution seismic profiles, Beaufort Sea, 1975: U.S. Geological Survey Open-File Report 76-747, 3 plates.
33. Reimnitz, Erk, and Barnes, P.W., 1974, Sea ice as a geologic agent on the Beaufort Sea shelf of Alaska, in J.C. Reed and J. E. Sater (eds.): *The Coast and Shelf of the Beaufort Sea, The Arctic Institute of North America*, Arlington, Va., p. 301-351.
34. Reimnitz, Erk, Barnes, P.W., and Alpha, T.R., 1973, Bottom features and processes related to drifting ice on the arctic shelf, Alaska: U.S. Geological Survey Miscellaneous Field Studies Map MF-532.
35. Rodeick, C.A., 1979, The origin, distributon, and depositional history of gravel deposits on the Beaufort Sea continental shelf, Alaska: U.S. Geological Survey Open-File Report 79-234, 87 p.

36. Toimil, L.J., and Reimnitz, Erk, 1979, A herringbone bedform pattern of possible Taylor-Gürtler type flow origin seen in sonographs: *Sedimentary Geology*, v. 22, p. 219-228.
37. Toimil, L.J., 1978, Ice-gouged microrelief on the floor of the eastern Chukchi Sea, Alaska; a reconnaissance survey: U.S. Geological Survey Open-File Report 78-693, 102 p.
38. Toimil, L.J., and Grantz, Arthur, 1976, Origin of a bergfield at Hanna Shoal, northeastern Chukchi Sea and its influence on the sedimentary environment: *AIDJEX Bulletin*, n. 34, p. 1-42.

Published Reports included in 1980 Annual Report

- Barnes, P.W., Reimnitz, Erk, and Ross, Robin, 1980, Nearshore surficial sediment textures, Beaufort Sea, Alaska: U.S. Geological Survey Open-File Report 80-196, 41 p.
- Barnes, P.W., Reimnitz, Erk, Toimil, L.J., and Hill, H.R., 1979, Fast-ice thickness and snow depth in relation to oil entrapment potential, Pudhoe Bay, Alaska, in *Proceedings of Fifth International Conference on Port and Ocean Engineering under Arctic Conditions at the Norwegian Institute of Technology*, August, 1979, p. 1205-1225.
- Barnes, P.W., and Reimnitz, Erk, 1977, Ice gouge obliteration and sediment redistribution event; 1977-1978, Beaufort Sea, Alaska, U.S. Geological Survey Open-File Report 79-848, 22 p.
- Barnes, P.W., and Toimil, L.J., 1979, Inner shelf circulation patterns, Beaufort Sea, Alaska: U.S. Geological Survey Miscellaneous Field Studies Map MF-1125.
- Grantz, A., Barnes, P.W., Dinter, D.A., Lynch, M.B., Reimnitz, Erk, and Scott, E.W., 1980, Geologic framework, hydrocarbon potential, environmental conditions, and anticipated technology for exploration and development of the Beaufort Shelf north of Alaska: U.S. Geological Survey Open-File Report 80-94, 42 p.
- Reimnitz, Erk, Ross, Robin, and Barnes, P.W., 1980, Dinkum Sands: U.S. Geological Survey Open-File Report 80-360, 11 p.
- Reimnitz, Erk, and Ross, Robin, 1979, Lag deposits of boulders in Stefansson Sound; Beaufort Sea, Alaska: U.S. Geological Survey Open-File Report 79-1205, 26 p.
- Reimnitz, Erk, and Maurer, D.K., 1979, Eolian sand deflation, a cause for gravel barrier islands in arctic Alaska?: *Geology*, v. 7, p. 507-510.
- Reimnitz, Erk, and Maurer, D.K., 1979, Effects of storm surges on the Beaufort Sea coast, northern Alaska: *Arctic*, v. 32, n. 4, p. 331-344.

NEW SEISMIC EVIDENCE FOR A WIDESPREAD OCCURRENCE  
OF GAS IN SUBMARINE SEDIMENTS AT SHALLOW DEPTHS, PRUDHOE BAY, ALASKA

by

Gary Boucher, Erk Reimnitz, and Ed Kempema

## INTRODUCTION

During August, 1979, the authors collected high-resolution seismic data in the vicinity of Prudhoe Bay, Alaska, for analysis by digital seismic techniques. An important preliminary result of that study is the identification of an interface at a depth of 20 to 35 m beneath the seafloor that appears to represent a rather widespread occurrence of free gas in the pore space of the sediment. The gas was identified in a geotechnical borehole which was the subject of a seismic study. We discuss below the extension of the borehole and digital seismic results to other seismic records made in that area, from which we infer that a gas patch of at least 50 km<sup>2</sup> area exists there. We originally conceived the experiment as an attempt to apply vertical seismic reflection techniques, with digital processing, to the mapping and characterization of ice-bonded material in the offshore environment near Prudhoe Bay. In principle, reflection methods, if applicable, would be expected to offer somewhat greater sensitivity and spatial precision than the refraction methods heretofore used to identify ice-bonded material (Hunter et al., 1978, and Rogers and Morack, 1978, e.g.). This experiment is part of a more general study on uses of acoustical techniques to measure physical properties of seafloor sediments in situ.

## EXPERIMENTAL APPROACH

We recorded seismic data continuously on a precision analog tape recorder aboard the R/V KARLUK for later digitization at real-time sampling rates of 4 kHz and 10 kHz. A non-expendable calibrated wide-band sonobuoy was used to obtain refraction/wide-angle reflection profiles for velocity and reflectivity analyses. Although this device performed poorly, some useful data were obtained. Refraction and reflection data were recorded side-by-side on magnetic tape. Several seismic sources were used to take advantage of various characteristics of each: a Uniboom, a Minisparker, and a 5-in<sup>3</sup> air gun. The Uniboom produces a desirably simple and repeatable signal; the Minisparker signal is significantly stronger but less clean and less repeatable; and the 5-in<sup>3</sup> air gun has substantially greater energy content at frequencies between 100 and 500 Hz.

## ANALYSIS

At this preliminary stage, the analysis is limited to consideration of the reflection sequence at one point in the vicinity of a geotechnical bore hole reported by Harding-Lawson Associates (1979). We have directed our analysis toward a particular reflector in the sequence that we believe to represent the upper boundary of a layer containing interstitial gas. The identification of ice-bonded sediments will not be discussed here.

The analog tape records made aboard the R/V KARLUK during seismic profiling (Fig. 1) were digitized in the laboratory. The seismic data were then deconvolved by cross-correlation with a model pulse derived from the direct arrival and spectrum-whitened to produce a wide-band, zero-phase source wavelet. Unambiguous amplitude and phase measurements can be made from the deconvolved data. We then concentrated on a particular seismic reflector, establishing that it represents an interface with a negative reflection coefficient of surprisingly large magnitude. See figures 2 and 3.

#### INFERENCE OF A "GASSY" LAYER

Our inference that this seismic reflector represents a rather widespread accumulation of interstitial gas in the sub-bottom sediments developed as follows. (1) Flammable gas was observed bubbling from the drill string and mud at a nearby geotechnical borehole, causing the drilling effort to be aborted. (2) The reflection coefficient associated with the anomalous reflector is negative and has a magnitude of at least 0.4. Such a large change in acoustic impedance with negative sign is difficult to obtain without invoking the presence of interstitial gas in the sediment, but is entirely consistent with the presence of gas. (3) Having made the identification of this characteristic seismic reflection, we traced its occurrence on a number of conventional high-resolution seismic records from the surrounding area, obtained from several years of seismic profiling. The identification of the "gassy" reflector on the conventional graphic records was made on the basis of its strength (bearing in mind that much records are made under the influence of automatic gain control), its apparent negative polarity (sometimes ambiguous), its continuity over extended profile distances, and its restriction to a narrow range of sub-bottom depth. This same reflector is characterized as 'weak' over a considerable area on the basis of its appearance on portions of some profiles. The locally diminished reflection amplitude may be a result of a change in the "gassy" reflector, or it may result from a change in the properties of the overlying sediments. Figure 4 shows the extent of the layer we interpret as gas.

#### DISCUSSION

One characteristic feature of the "gassy" reflector is its abrupt, unexplained termination in many areas (Fig. 1). Where such terminations occur, we show the boundary of the gas patch as a solid line in figure 4. Where the reflector gradually diminishes in strength, we omitted such lines. The area underlain by the strong gas reflector is about 16 km x 3 km, elongated in the east-west direction, and located landward of a line connecting Dinkum Sands and Narwhal Island.

Assuming a sound velocity of 1440 m/sec., the depth to the reflector was measured from the records. It varies from 22 to 34 m (true depths would be about 20% greater). A few representative determinations are shown by the large numbers in Figure 4. On the basis of other drill holes in the vicinity (Harding and Lawson Associates, 1979) the anomalous reflector may frequently be associated with a change from a stiff, fine-grained, clay-silt-fine sand marine accumulation to a thick underlying accumulation of sandy gravel or gravelly sand, presumably of non-marine origin. It is reasonable to conclude that the fine, compact material may form a seal for gas trapped in the coarser material beneath.



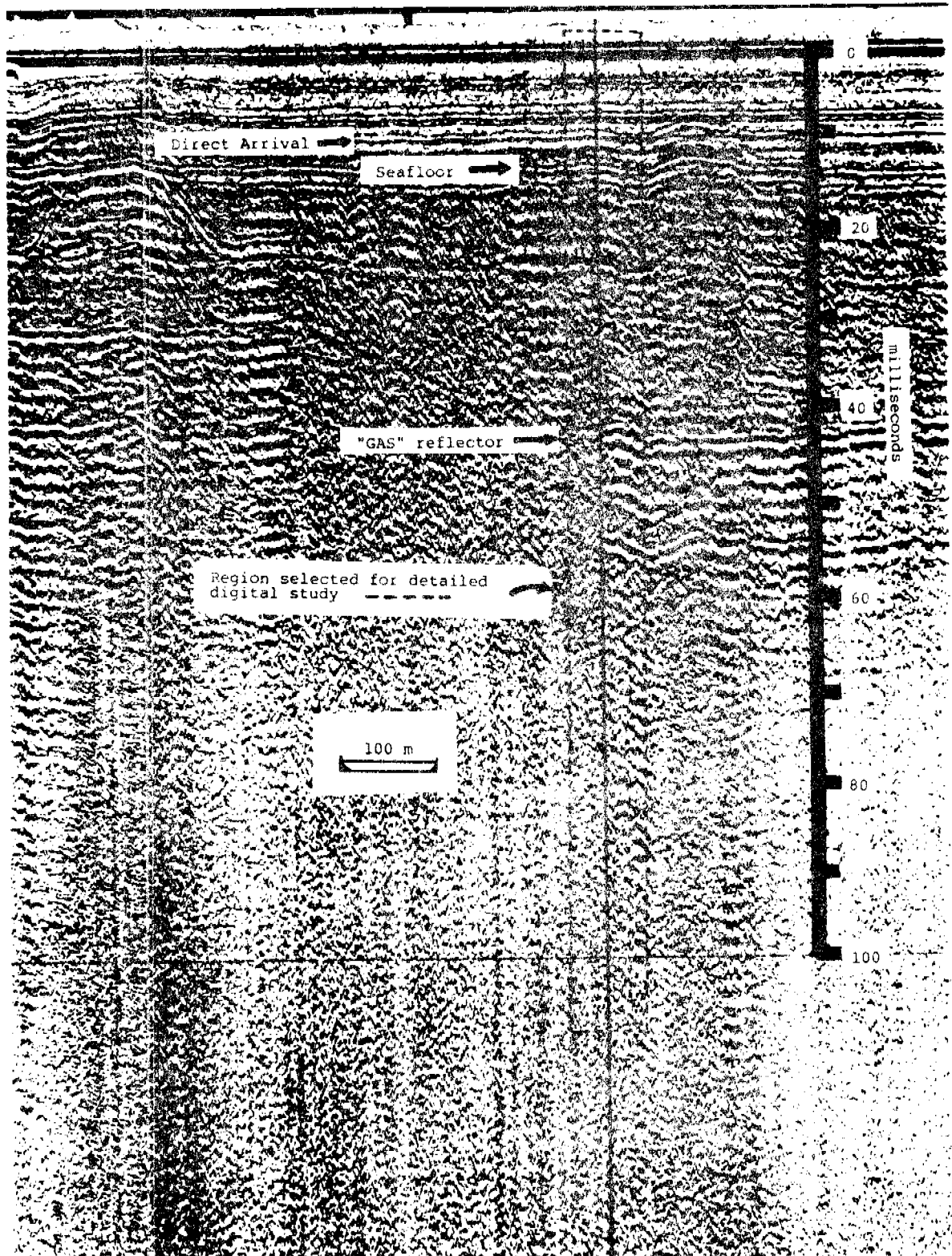


Fig. 1. Section of shipboard seismic record made with the Uniboom source, indicating by the dashed box the small portion of the record where a detailed digital analysis was made. The "gas" reflector is indicated, and is highly visible, despite the poor quality of the record. The seafloor multiple of the "gas" reflector can be seen about 12 milliseconds below the primary reflector.

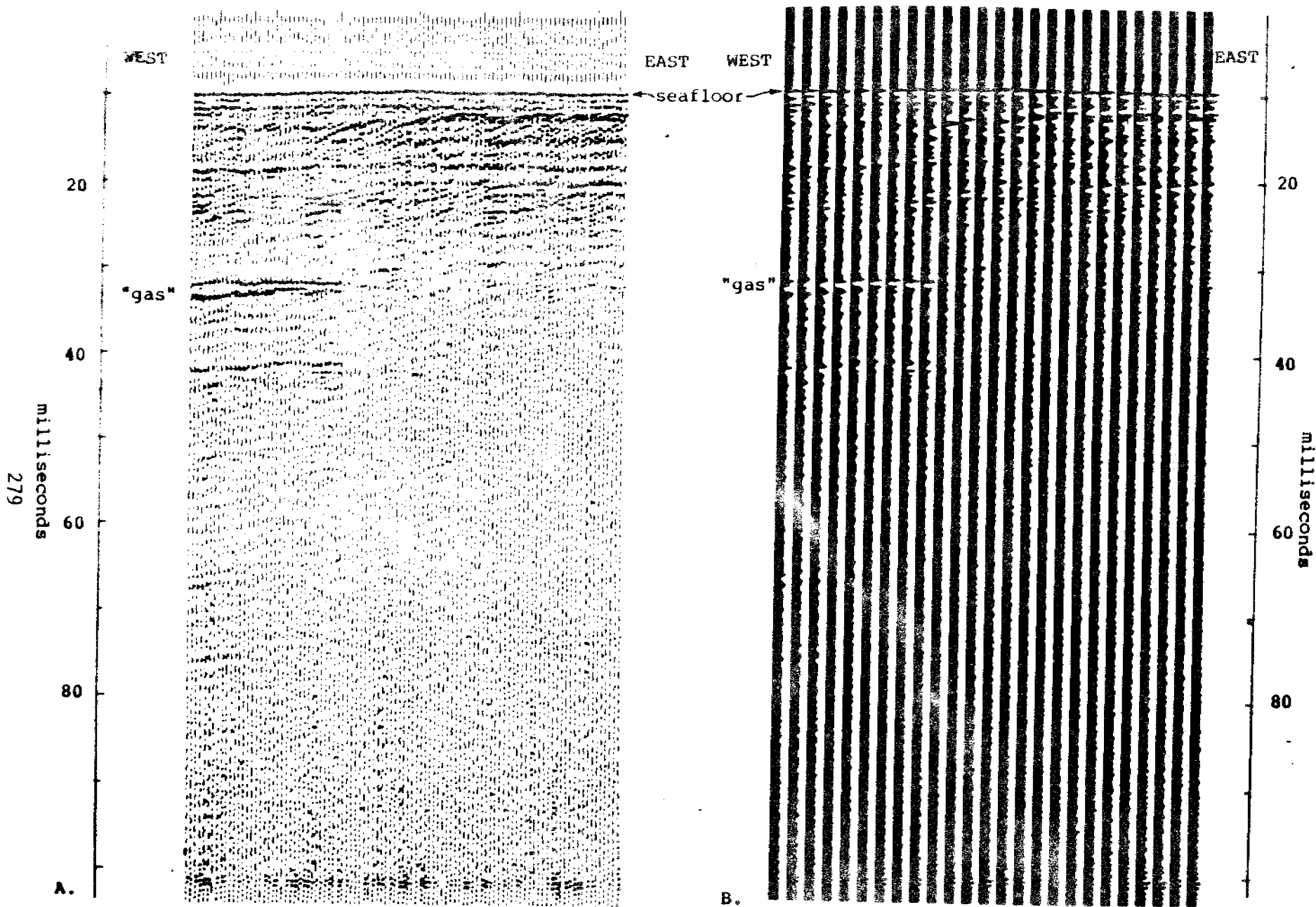


Figure 2. Two presentations of deconvolved data from the area boxed in figure 1. A. is the clipped wiggle-trace section, corresponding to a normal seismic reflection section. B. is the same data subjected to 5-fold vertical stacking, unclipped and showing the negative as well as the positive sides of the waveform in order to emphasize the "gas" reflector.

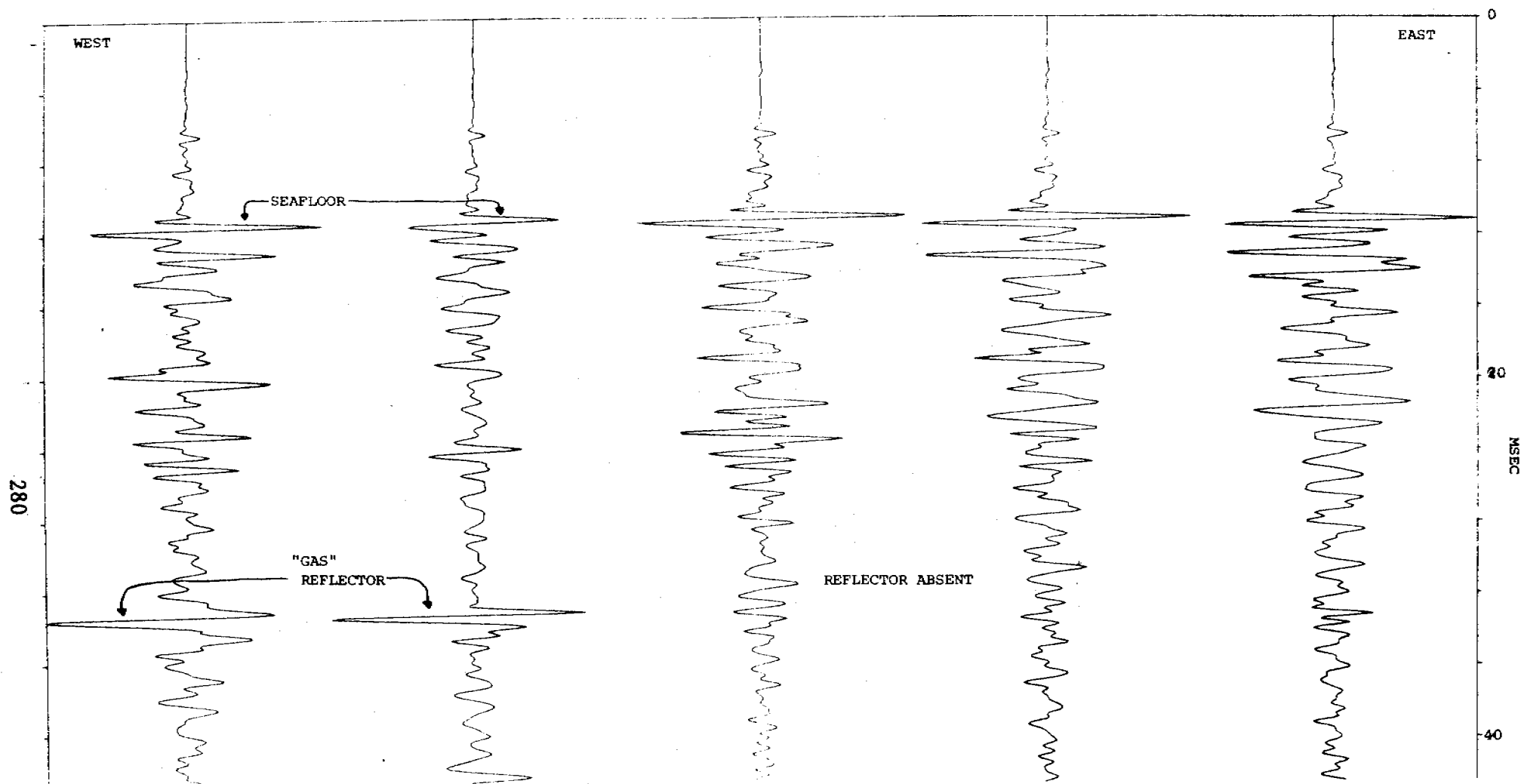


Figure 3. Large-scale wiggle trace presentation of the same data as in figure 2, but subjected to 20-fold vertical stacking to reduce random noise. The large amplitude downward spike representing the "gas" reflector clearly shows the negative polarity and great strength of this reflector. The traces were normalized to the maximum amplitude on the record. A zero-phase wavelet deconvolution has been performed. The direct arrival and a reflection, probably from the hull of the boat, can be seen ahead of the seafloor reflection. The amplitude of the "gas" reflection is somewhat degraded on the bottom trace because the reflector is not quite flat in that section of the data.

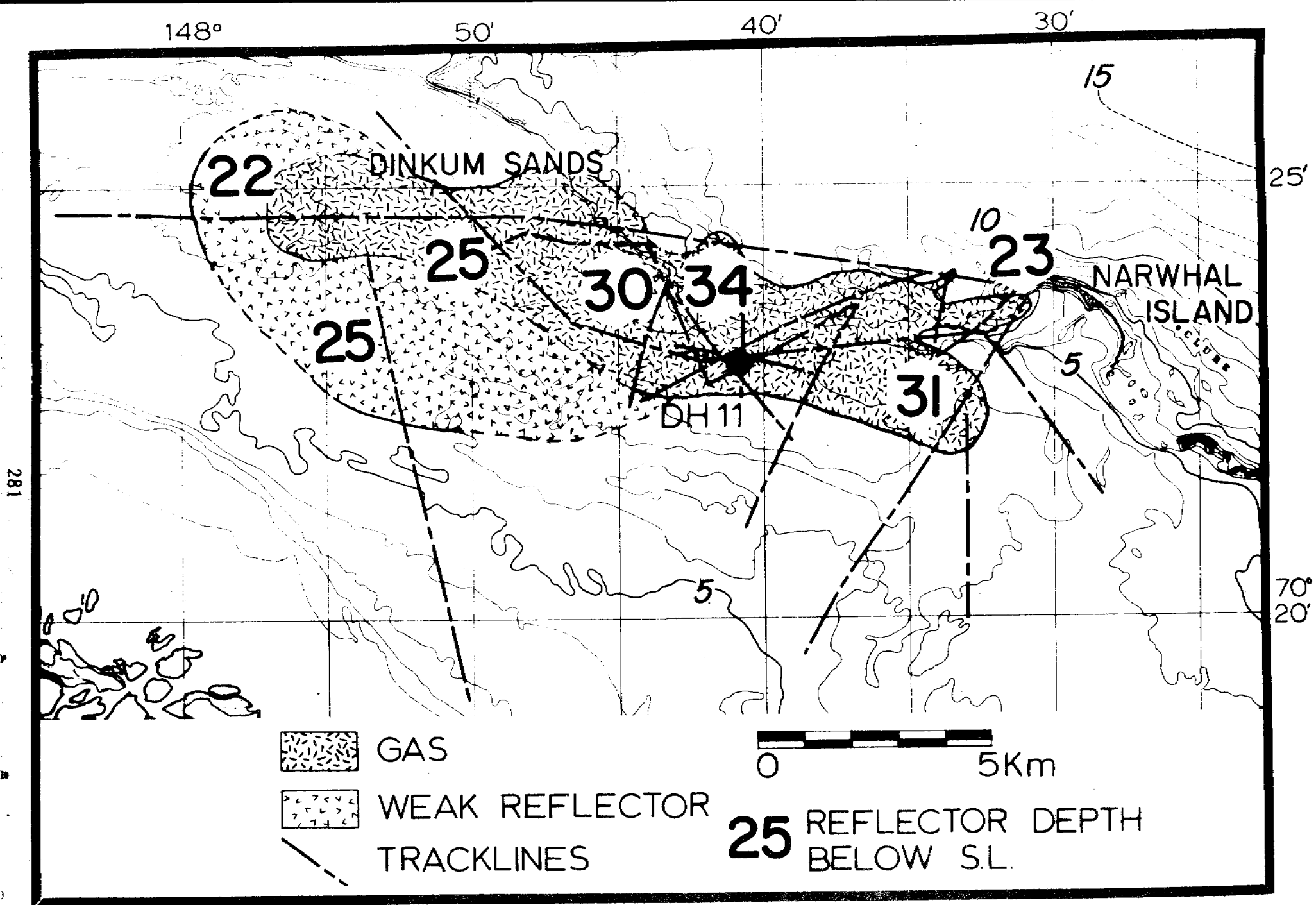


Figure 4. The extent of the gas-charged reflector in Stefansson Sound. The reflector was first identified by seismic signal analysis and then mapped by comparing the section of analyzed record with conventional records from the area. The indicated depth of the reflector is based on reflection time assuming a sound velocity of 1440 m/sec.

## CAUTIONARY REMARKS

We must point out that other interpretations of the anomalous reflecting layer may be possible, and further that the presence of interstitial gas in the sediments at locations far removed from either the drill hole or the detailed seismic analysis is not conclusively proved. One may seek to account for the negative sign and magnitude of the reflection coefficient of the anomalous layer without invoking the presence of gas. One possibility is an interface between high-velocity ice-bonded sediments above, and unfrozen sediments beneath. However, unless the velocity in the frozen material is unreasonably large, nearly 5000 m/sec., it is not possible to achieve a reflection coefficient large enough to explain the observations. Hence the presence of interstitial gas remains the simplest explanation consistent with the observations.

## VII. CONCLUSION

Our identification of the gas-bearing layer is conclusively proven only in the vicinity of the drill-hole data and the detailed quantitative seismic analysis. But we feel that our interpretation of the gas-rich sediment horizon extending over an area covering at least 50 km<sup>2</sup> will prove to be reliable. Similar-appearing strong reflectors with the characteristic abrupt terminations are a widespread phenomenon on the Beaufort Sea shelf. The occurrence of this previously unexplained phenomenon has added serious uncertainties, and even resulted in misinterpretations of regional shelf stratigraphy based on seismic reflection data. Thus in the initial attempt at mapping the thickness of the Holocene marine sediments on the shelf by seismic techniques (Reimnitz, et al., 1972), the strong anomalous reflector investigated in the present study was interpreted as representing the base of a section of modern marine sediments over 20 m thick. Reimnitz and Ross (1979) in their mapping of the Boulder Patch have shown that much of the area here shown to be underlain by gas-rich sediments coincides with areas where the Gubic Formation crops out and Holocene sediments are lacking entirely.

The presence of free gas in sediments is potentially hazardous in drilling operations and construction activities, as shown by the drillers' abortion of hole 11 when gas was encountered. Thus areas characterized by strong negative reflectors on high resolution seismic records should be approached with the necessary precautionary measures by developers.

Other work on the ice-bonded sediments and other characteristics of the bottom sediments in this region will follow.

## REFERENCES CITED

- Harding and Lawson Associates, 1979, U.S.G.S. Geotechnical Investigation, Beaufort Sea, 1979. Volumes 1, 2, and 3.
- Hunter, J. A., Neave, K. G., MacAulay, H. A., and Hobson, G. D., (1978), Interpretation of sub-seabottom permafrost in the Beaufort Sea by seismic methods. Part I. Seismic refraction methods, in National Research Council of Canada: Proceedings of the third international conference on permafrost, 1978, vol. 1, p. 514-520.
- Rogers, J. C., and Morack, J. L. (1978) Geophysical investigation of offshore permafrost, Prudhoe Bay, Alaska, Interpretation of sub-seabottom permafrost in the Beaufort Sea by seismic methods. Part I. Seismic refraction methods, in National Research Council of Canada: Proceedings of the third international conference on permafrost, 1978, p. 560-566.
- Reimnitz, Erk and Robin Ross, 1979, Lag deposits of boulders in Stefansson Sound, Beaufort Sea Alaska: U.S. Geological Survey Open File Report 79-1205, 26 p.
- Reimnitz, E., Wolf, S. C. and Rodeick, C. A. 1972, Preliminary interpretation of seismic profiles in the Prudhoe Bay area, Beaufort Sea, Alaska. U.S. Geological Survey open file report 548, 11 pp.

## Attachment B

### Overconsolidated surficial deposits on the Beaufort Sea shelf

by Erk Reimnitz, Edward Kempema, Robin Ross, and Peter Minkler

#### INTRODUCTION

Silty clay, which is apparently overconsolidated, has been reported in connection with studies of ice-gouging processes on the surface of the Beaufort Sea shelf (Reimnitz et al., 1973; Reimnitz and Barnes, 1974). Slabs of this concrete-like material are ripped off to form highly angular ledges and blocky outcrops. Overconsolidation is a term used to describe consolidated sedimentary material which is more highly consolidated than is normal for the existing overburden. Our interpretations of the stiff silty clay are based on the appearance of bottom deposits as seen in photographs, direct observation of the sea bottom, and on our operation of hand-held shear vanes which go off-scale in measurements of such material. In more recent work we therefore prefer to use the terms stiff or very stiff to describe this apparently abnormal material. Laboratory measurements of soil engineering properties of sediments were made from a borehole sample taken where we had noted outcrops of stiff silty clays. These measurements show that the materials are actually "highly overconsolidated" (Chamberlain, et al., 1978).

The mechanisms which cause overconsolidation of sediments are of considerable scientific interest. An understanding of these mechanisms would help to shed light on the geologic history of the shelf and coastline. Chamberlain et al. (1978) showed that freezing and thawing cycles lead to overconsolidation, and speculated that freezing of the marine sediments during transgression of a barrier island across the borehole site may be responsible for overconsolidation encountered there.

At this time in the offshore development of the lease sale area a knowledge of the distribution of such overconsolidated materials is of extreme interest to the developer. Such materials overlying sand and gravel needed for island construction offshore could make mining these deposits extremely difficult and perhaps impractical. The shape and overall appearance of the overconsolidated silty clay outcrops on the seafloor and their relation to nearby migrating deposits of granular surface materials indicate very violent water movement which occurs sporadically, and should serve as a warning to developers.

#### METHODS AND OBSERVATIONS

For these reasons we have compiled all available direct observations on abnormally firm surficial deposits in the study area (Fig. 1) Our listing includes brief notes representing excerpts from field observations with simple numbers keying the observations to station locations on a map (Fig. 2). This report also includes more detailed information from several typical outcrop areas, with fathograms, sonographs, and underwater photographs.

Most of the initial observations of stiff silty clay were made during routine sampling and diving operations. Patterns soon became apparent. Where sub-bottom reflectors on high-resolution seismic records crop out, indicating

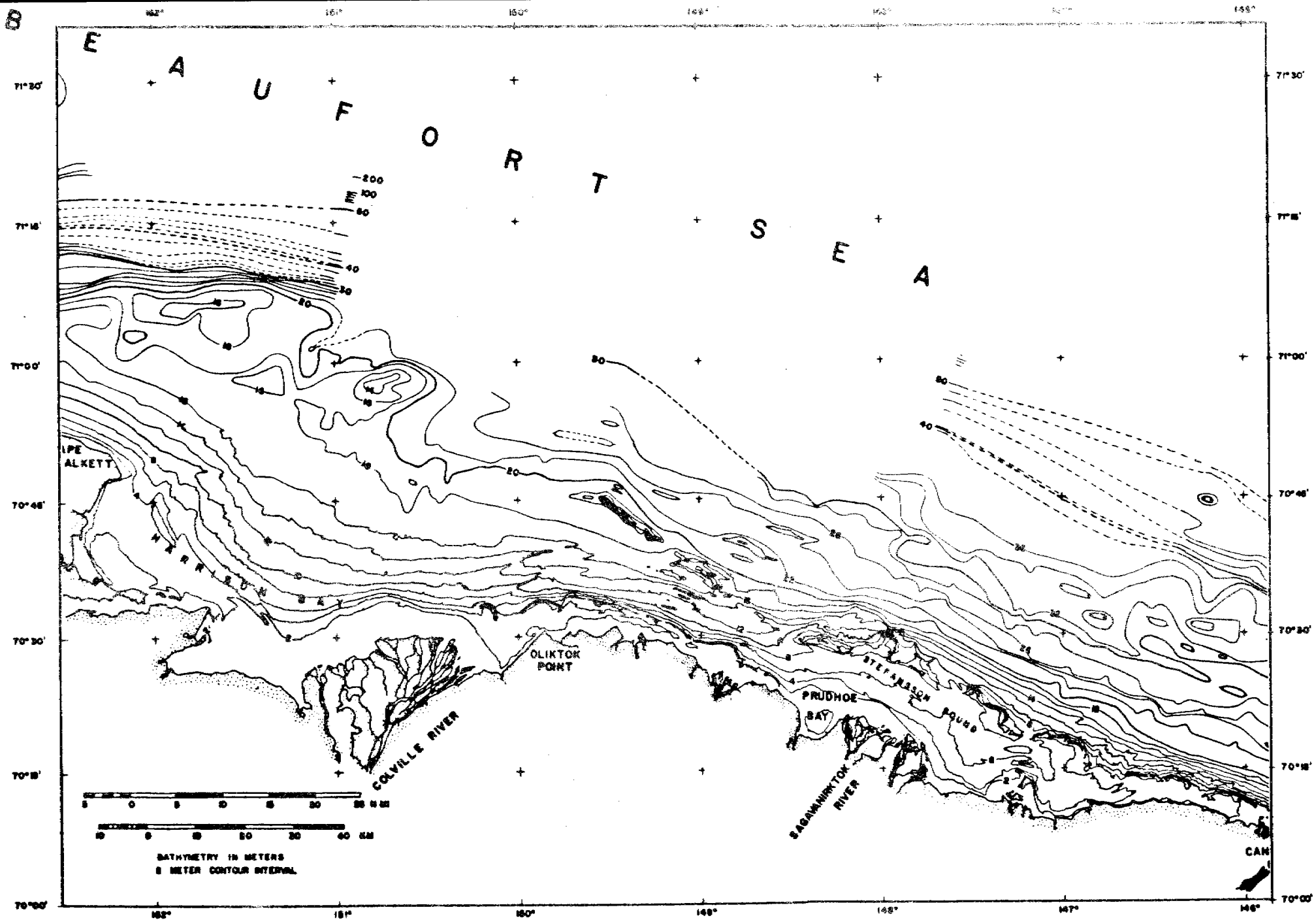


Figure 1. Bathymetric map of study area.  
Depth in meters (Barnes and McDowell, 1978).



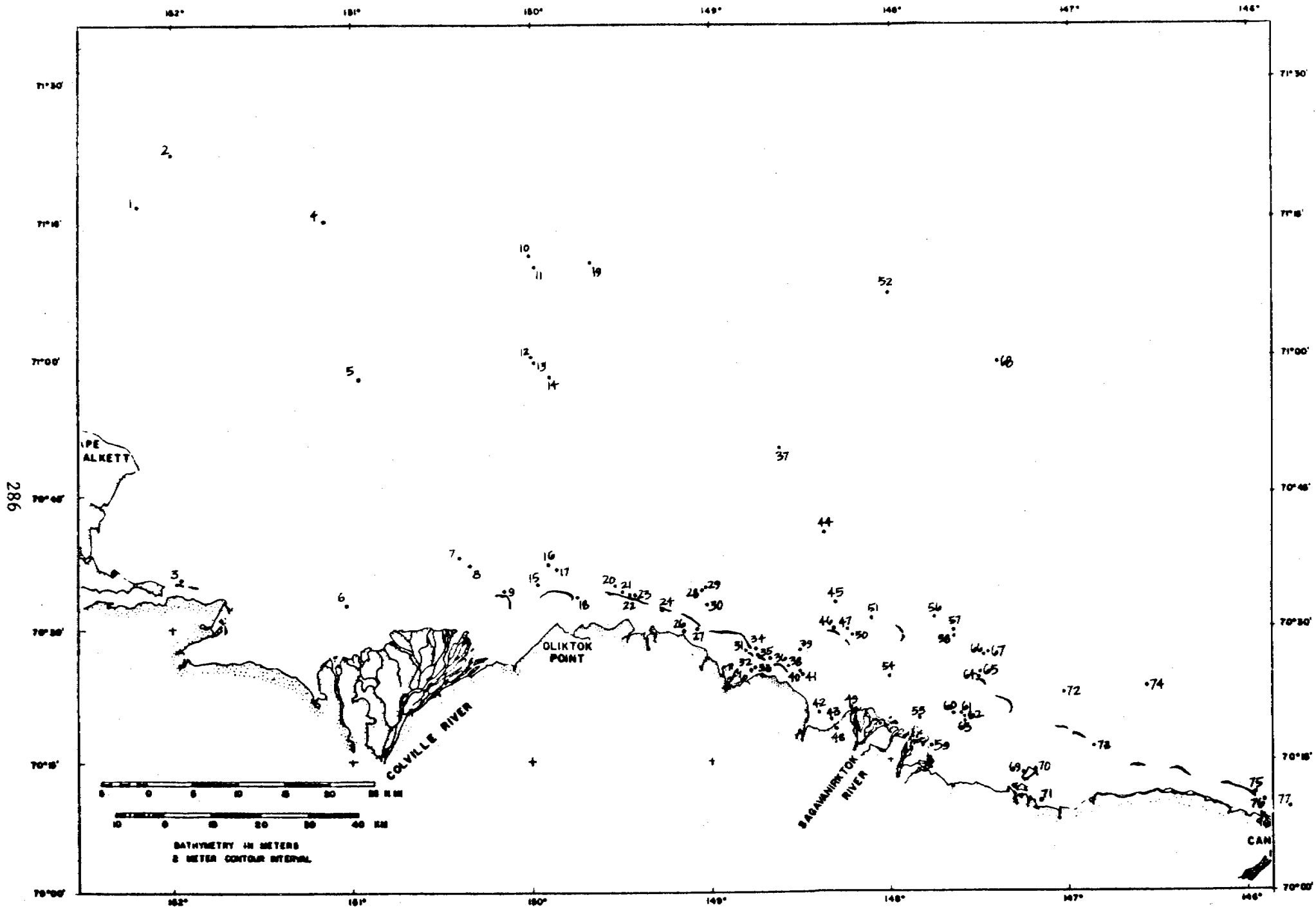


Figure 2. Locations where stiff silty clay and similar overconsolidated materials occur. Numbers increase from west to east, and correspond with those used in the text.

"windows" in the cover of Holocene marine sediments, stiff silty clay can almost certainly be found near the surface. On sonographs such outcrops commonly appear as highly irregular small-scale relief patterns. Where bodies of sand are migrating across jagged-relief surfaces of stiff silty clay, the sand generally is impenetrable to seismic signals and the sub-bottom reflector is lost. But here the topographic depressions between smooth sand bodies characteristically reveal highly irregular surfaces, indicating the presence of the hard substrate. A number of stiff silty clay sites recently investigated were selected on the basis of such geophysical data. However, many occurrences of stiff silty clay cannot be predicted from geophysical data. Thus the shallow water site near Thetis Island, where our experimental seafloor furrowing equipment suffered extensive damage from such outcrops, was not anticipated.

List of sites and notes on overconsolidated materials

The following compilation is arranged in order from west to east, and numbered accordingly. A few additional observation sites located outside of figures 1 and 2 are listed at the end with map coordinates.

1. 72ABP 67      Subsurface stiff mud matrix with fine-to-medium-grained sandy texture--no pebbles (grab).
2. 72ABP 66      Hard clay (core).
3. 72AER 97      Dark grey stiff silty clay (grab).
4. 71ABP 73      Stiff, grey, gravelly clay (grab).
5. APB            Stiff clay with sand pockets (70°58.8'N, 150°58.0'W).
6. V-21          Very firm, slightly clayey silt at 170 cm (vibracore).
7. DS-78-39      Firm mud on gouge floor and also below soft material adjacent to gouge (dive).
8. DS-78-36      Stiff silty clay exposed in new gouge (dive).
9.                Plowing experiment off Thetis Island near beach caused heavy damage to the plow after pulling forces exceeded 5000 lbs. The very small grappling hook used in dragging for the plow from an outboard-powered skiff became hung up on jagged relief features. These features were interpreted as outcrops of overconsolidated silty clay (observation: E.R., 8/23/76).
10. 72ABP 50b     Stiff black/grey, fine-grained mud with organic material (grab).
11. 72ABP 45c     Stiff mud with clay lumps and layers of tundra grass (like a layering of peat). Numerous worm burrows. Mud is fine to very fine grit sand (grab).
12. ABP           Very stiff, fine-grained sandy mud (71°00.0'N, 150°00.0'W).
13. 71ABP 78      Stiff, grey, sandy clay (grab).
14. 71ABP 79      Stiff, muddy clay (grab).
15. 71AER 14      Grey silty clay, very stiff at bottom of 20-cm-long core.
16. DS-78-37      Very stiff black silty clay forming jagged ledges, mounds, and angular blocks where recently disrupted by ice gouging process, but perfectly rounded to polished shapes of outcrops and mud balls were equally common. The stiff silty clay here underlies an actively migrating sandwave field, and is polished in the process by moving sand. Nearly impenetrable with an entrenching tool (dive).
17. 72AER 212b    Stiff sandy mud below 5 cm of soft ooze and 15 cm of gravel (dive and anchor flukes).
18.                Closed circuit television showed outcrops of stiff, silty clay on floor of Spy Island tidal channel. (observation: E.R., 8/26/76).
19. 72ABP 45b     Very fine, stiff mud with small lumps of clay and worm burrows (grab).
20. DS-79-51      Overconsolidated, thinly bedded silty clay, cropping out in troughs between sand waves, and forming jagged to current-polished relief forms up to 50 cm high and 1 m in diameter--also mud balls of 10-cm size (dive, photos, sonographs).

21. DS-78-42 Very stiff dark grey to black silty clay exposed in jagged knolls up to 30 cm high (dive).
22. 72AER 127 Angular slab of well-consolidated dark grey to brown mottled silt at 6-m depth (dive).
23. 72AER 122 Well consolidated black silty clay, laminated in shore-parallel trough at 9-m depth (grab). Observed by divers to form ledges and angular chunks up to 50 cm high (dive).
24. Stiff, cohesive pebbly mud, at least 30 cm thick, in swash zone on lagoon side of Bodfish Island (observation: E.R., 8/29/72).
26. Patches of firm silty clay along swash zone (observation: E.R., 8/5/79).
27. Overconsolidated silty clay forming ledges in swash zone and varying to firm, black silty clay with odor of  $H_2S$ . Patchy distribution along beach (observation: E.R., 7/18/79).
28. 72AER 174 Highly consolidated silty clay landward of Loon Shoal (grab).
29. 72AER 183 Irregular jagged outcrops of stiff, old sandy mud with burrows, outer 2 cm oxidized. Protruding from sandy bottom (dive).
30. V-46 Stiff mud with rounded pebbles at 65 cm (vibracore).
31. 72AER 93 Rather stiff grey, clayey silt from vertical walls of tidal channel between Long Island and Channel Island (grab).
32. Stiff, cohesive, laminated to cross-laminated silty clay with sandy and organic-rich laminae, forming vertical cliff in upper part of strudel scour (dive: E.R. 8/24/72).
33. 72AER 161 Highly consolidated sediments from walls of channels.
34. 72AER 128 Slab of highly consolidated black silt apparently covered by thin gravel (anchor flukes).
35. 72AER 154 Highly consolidated silt from bottom of 1.2-m deep strudel scour (dive).
36. 72AER 97 Dark grey stiff silty clay (grab).
37. DCS-7 Stiff silty clay (photos).
38. Sta 7 Cobbles and pebbles overlying frozen sediment or stiff silty clay (Pers. commun., Woodward and Clyde 1979).
39. DS-76-6 Very firm muddy sand (shear strength  $9.52 \text{ KN/M}^2$ ) (dive).
40. DS-72 Very stiff greasy sediments below thin cover of soft mud "probably the overconsolidated silty clay" (dive: E.R. 8/30/72).
41. 72AER 188 Black, consolidated sandy mud, bedded, from upper vertical walls of strudel scour.
42. 71AER 18 Dark grey, very stiff silty clay (core).
43. 71AER 16 Dark grey stiff silty clay (core).
44. 71ABP 69 Very stiff grey clay with trace of sand. Penetrated only 2 cm (grab).
45. 72AER 165 Outcrops of consolidated sandy silty clay, forming ledges, observed over a distance of about 100 m with nearly 3 m of relief. Some burrows in outcrops (dive).
46. 72AER 129 Angular slab of highly consolidated silty clay, faintly layered with few fibers of organic matter (dive).
47. DS-79-50 Overconsolidated silty clay, with up to 0.5-m high jagged to current-polished relief forms, ledges and mudballs, occurring over extensive areas. Large sand bodies are traveling across jagged surface without leaving any trace of sand in crevices (dive, photos).
48. Stiff, silty clay, forming ledges in swash zone (observation: E.R., 9/12/78).
49. Consolidated brown to grayish brown mud forming ledges in swash zone at Heald Point (observation: Rodeick, 7/17/73).
50. 71AER 26 Overconsolidated silty clay with up to 2-m relief; small-scale angular relief forms: cracks, crevices, gullies in irregular pattern cropping out in an extensive area with bodies of migrating sand at 8-m depth (dive).
51. V-43 Very stiff, slightly sandy, clayey silt at 170 cm (vibracore).
52. 71ABP 29 Stiff greenish-grey mud (grab).
54. V-29 Extremely stiff silty clay in bottom of vibracore.
55. DS-76-8 Very firm mud below thin sand layer, too strong for shear vane measurement (dive).
56. 72AER 138 Highly consolidated dark grey clayey silt on small knoll (grab).
57. V-35 Probably firm, pebbly mud at two spots near 18 m, where vibracorer did not penetrate (observation: E.R., 8/23/77).

58. V-36 Same as V-35.
59. Stiff, cohesive clay beds in upper beach at toe of solifluction lobes, interbedded with beach material of sandy gravel at Pt. Brower. Possibly a result of sorting during solifluction and overconsolidation by freeze-thaw?
60. KDDS-3 Clay overlain by thin layer of mud and scattered patches of cobbles and boulders. Bottom not penetrated more than a few cm. Abundant marine life in rock patches (dive: Ken Dunton, 8/3,4,5/80).
61. KDDS-11 Hard impenetrable clay overlain by thin (1 cm) layer of soft mud. Pebbles and cobbles scattered with attached kelp, boulders rare (dive: Ken Dunton, 8/7/79).
62. KDDS-1 Mud and hard clay with cobbles and boulders in scattered patches; much silt, some pebbles. Abundant marine life in rock patches (dive: Ken Dunton, 7/23,24,25,79).
63. KDDS-11 Rocky, cobbles and boulders common, underlain by penetrable gravel-mud or impenetrable clay. Kelp and invertebrate life abundant (dive: Ken Dunton, 8/7,17,18,19,20/79).
64. 72AER 145 Highly consolidated black silt below pebbly sand (anchor flukes).
65. DS-76-17 Angular blocks of overconsolidated silty clay on surface and outcrops of same material; very similar to that seen on Reindeer and Argo Islands (dive).
66. V-32 Very firm pebbly mud collected during attempt to vibracore at 18-m depth north of Narwhal Island. No penetration (observation: E.R., 8/22/77)
67. V-33 Same as V-32.
68. 71ABP 28 Stiff, gravelly clay (grab).
69. Overconsolidated silty clay in swash zone on northwest side of Tigvariak Island below beach material (observation: E.R., 7/76).
70. DS-76-11 Slightly sandy, very firm mud, in which shear vane went off scale at the surface (over 9.52 KN/M<sup>2</sup>).
71. DS-76-11 Slightly sandy, very firm mud in which shear vane went off scale at the surface (over 9.52 KN/M<sup>2</sup>).
72. DS-79-54 Very firm sandy to pebbly mud in slightly undulating relief along stamukhi zone boundary, but resistant to ice gouging (dive, photos, sonographs).
73. DS-79-49 Overconsolidated silty clay partly covered by sand, cobbles and boulders, forming jagged to current-polished knolls and fluted forms with parallel alignment in places. Nearly impenetrable by entrenching tool (dive, photos).
74. 71ABP 13 Stiff grey mud with abundant pebbles to 1.5 cm. One 6-cm cobble (grab).
75. Highly consolidated silty clay at sea level below beach material on north side of Flaxman Island, containing abundant shallow-water foraminifera, organic material and possibly volcanic ash (unnumbered sample E.R., 8/20/73).
76. DS-76-4 Grey, cohesive, bedded stiff mud forming ledges along flanks and in floor of 10-m deep tidal channel (dive).
77. AJT 25 Hard clay with few pebbles (grab).
- 
- 72ABP 10 70°20.5'N - Very stiff mud at 40 cm depth (core).  
144°36'W
- 72ABP 12 70°08.4'N - Hard mud at 60-cm depth (core).  
145°29'W
- 71ABP 80 70°55.7'N - Stiff sandy clay (grab).  
149°23'W
- 71ABP 90 71°07.5'N - Stiff clay without pebbles (grab).  
153°00'W
- 71ABP 95 71°32.2'N - Stiff clay at 15-30 cm (core).  
156°04'W

#### Five study sites presenting more detailed information

1. Testline 2. - This site is in an aeriually restricted field of sand waves on a testline we have re-surveyed annually since 1973 for the purpose of monitoring rates of ice gouging. The sandwave field is seen in every one of those surveys at the same spot, changing only in the detailed configuration of waves. Thus the sand waves are actively moving. Figure 3 is a sonograph of the sand waves recorded during the summer of 1979. The sinusoidal dark bands with mottled appearance are troughs between the light sand bodies which show a rather smooth surface and do not return much of the outgoing sonar signal. The waves trend roughly north/south. In 1978, the year in which we noted the formation of sediment waves where gouges used to be (Barnes and Reimnitz, 1979), we made a dive at this site (station 16 in Fig. 2). A fathometer profile recorded prior to the dive at right angles to the wave crests is shown in figure 4.

The very stiff silty clay occurred in troughs between the sand waves. Beds of the material which were recently raked by ice keels formed vertical ledges 20 to 30 cm high, often highly angular and sharp, but commonly rounded off and polished by current activity, leading to undercutting at the base. A few well-rounded mud balls and some fluted surfaces were observed, together with windrows of clam shells, sticks, and other land-plant debris recently eroded from the substrate as evidenced by the fact that necks were still attached. All signs, including lack of evidence of bioerosion of outcrops, indicate that recent extremely strong current activity has polished the stiff silty clay. The overconsolidated material can be broken off from ledges along conchoidal fracture planes, and is too hard and brittle to permit formation of ice gouges.

2. Pingok Island. - A number of dives in the Pingok Island area, dating back to 1972, provided information on the distribution of stiff silty clay (station numbers 20, 21, 11, and 23). Closely spaced bathymetric surveys were made over several seasons in order to monitor changes in the sea bottom. One of these was made in 1979 along tracklines shown in figure 5. The bathymetry is contoured at 0.5-m intervals (Fig. 6). The topography consists of one major shore-parallel bar, from which other bars branch off at nearly right angles in the seaward direction. Short (1973) reported that the shore-parallel bars in this area are migrating westward at an average rate of 70 m/yr..

Many of our bathymetric profiles, in particular those shore-parallel over the seaward appendages of the main bar, clearly show jagged relief in the troughs between the sand bodies (Fig. 7). Ice in the nearshore regions generally ground on bars; the bars are gouged by ice whereas the troughs are protected. The rough relief in the troughs therefore is not caused by ice gouging. A dive was made in 1979 specifically to study the jagged relief in the troughs between the sandwaves shown in figure 7. The dive traverse included parts of two adjacent sandwaves. Along this traverse we found jagged relief in the form of vertical ledges, angular, steep-sided humps, and current-polished knolls carved from very stiff silty clay. As at the testline 2 site, rounded, polished features were present; a striking phenomenon, since physical disruption of such material by ice creates angular features. A small, presumably rather recently formed ledge is shown in a photograph (Fig. 8). Such ledges expose horizontally-bedded, very stiff silty clay,

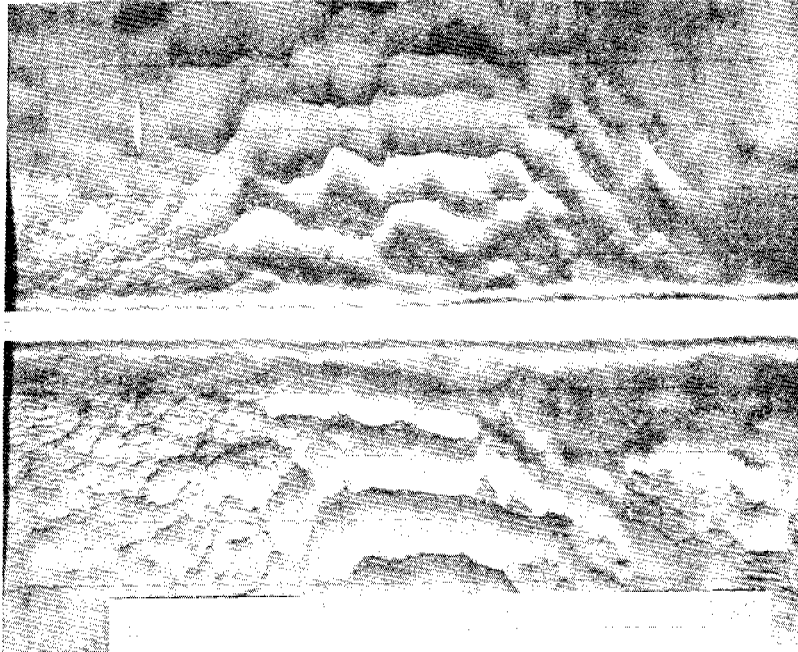


Figure 3. Side-scan sonar record of sandwave field exposing stiff silty clay in troughs. The jagged relief of silty clay is occasionally covered by a transient layer.

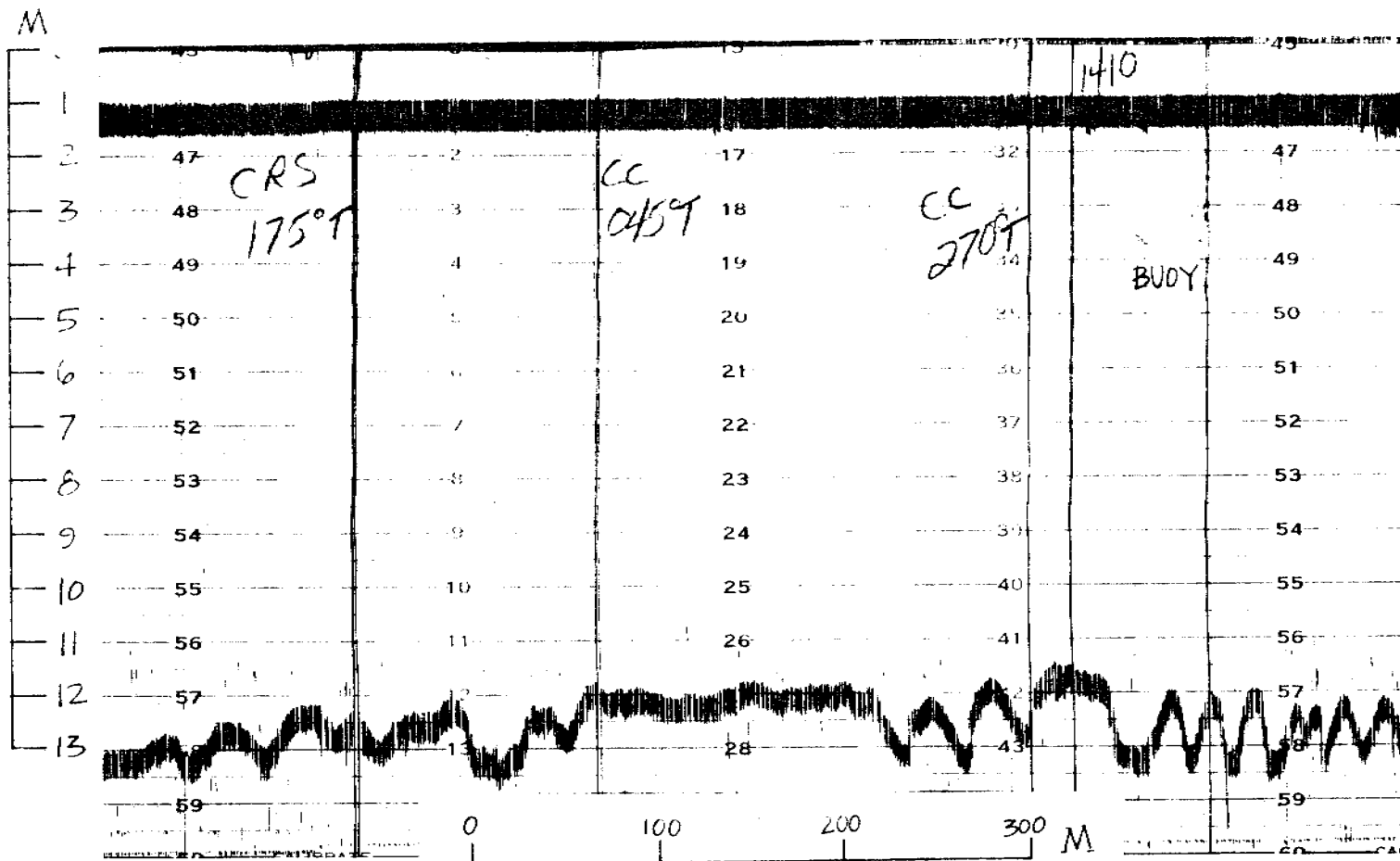


Figure 4. Fathometer record of sand waves on stiff silty clay, at a right angle to figure 3, and covering part of the traverse studied by diving (between buoys).

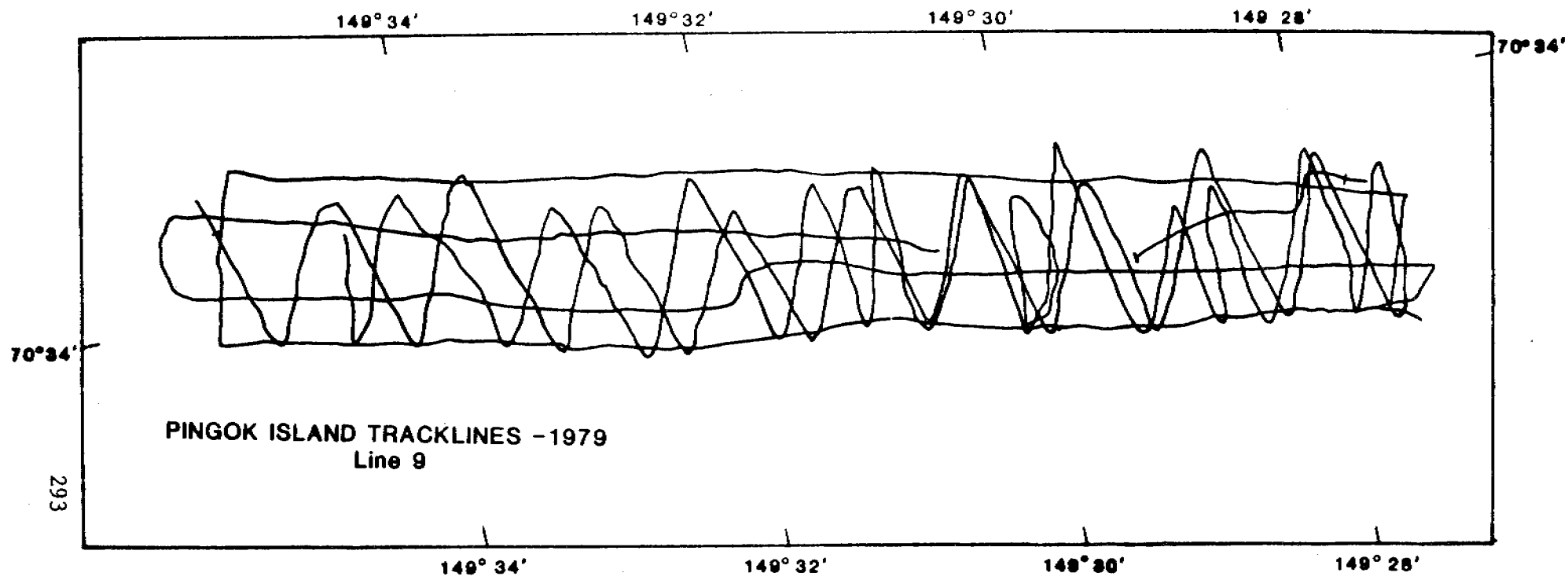


Figure 5. Trackline coverage of Pingok Island nearshore bathymetric survey in 1979. Position control is by range-range navigation accurate to +5 m.



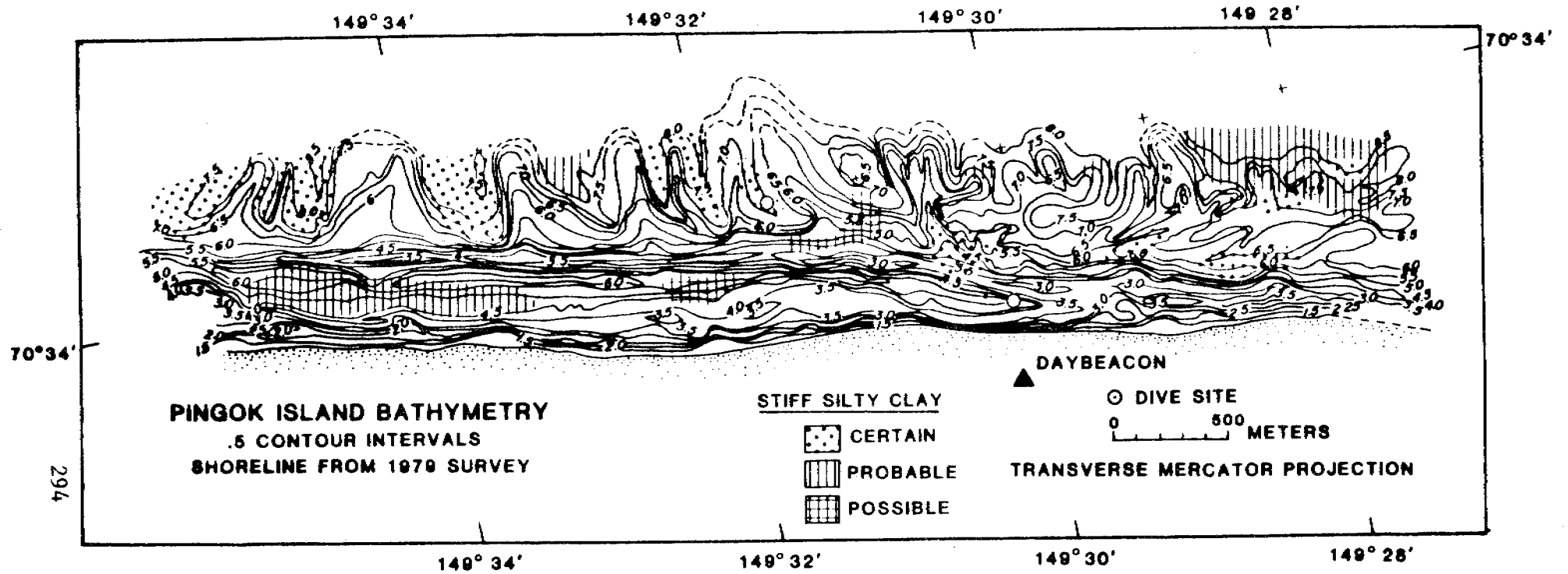


Figure 6. Bathymetry of Pingok Island nearshore area, contoured at 0.5 m interval. Also shown are locations of two dive sites at which stiff silty clay was observed, and an interpretation of stiff silty clay distribution showing a general correlation between the clay and troughs.

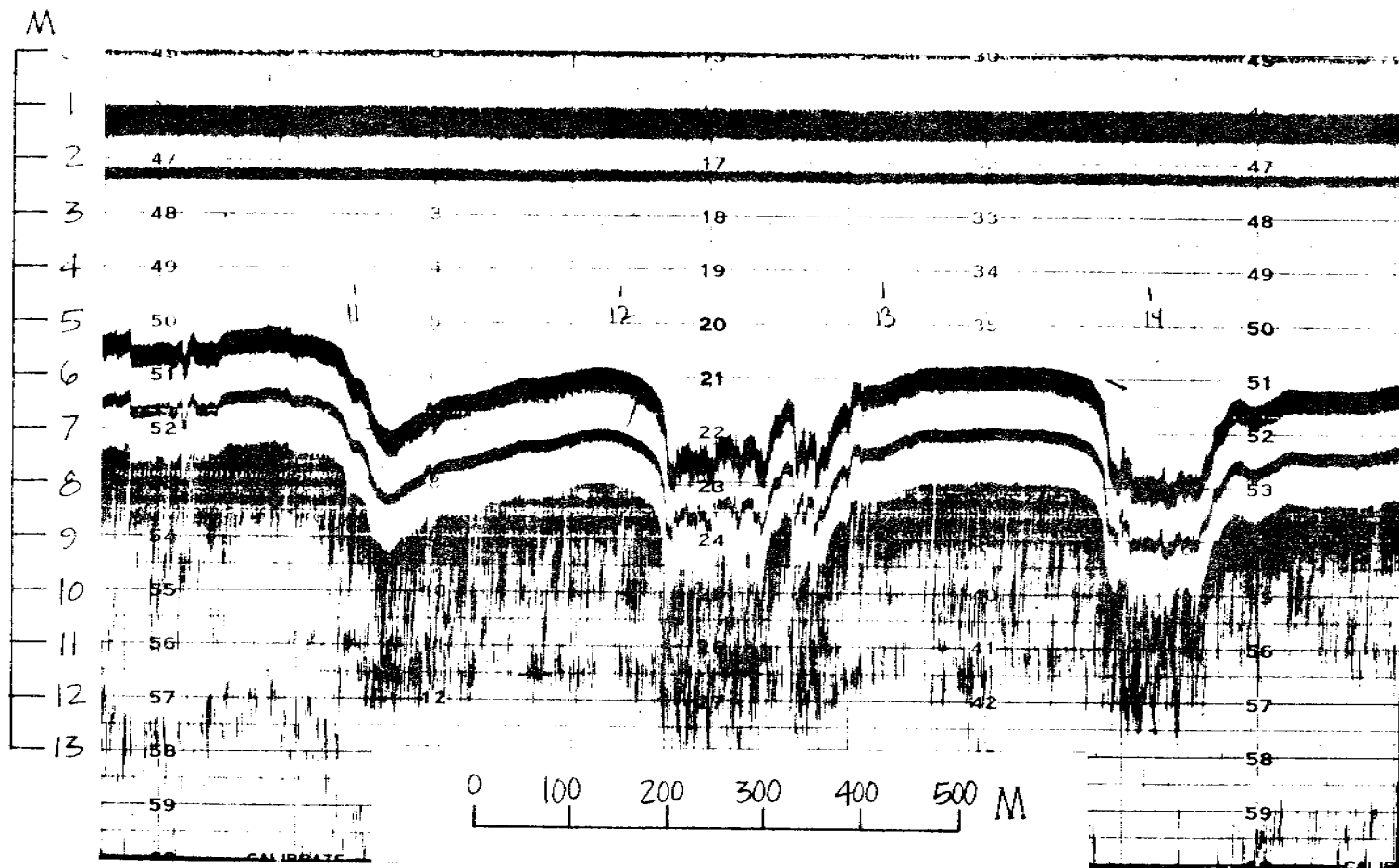


Figure 7. Bathogram parallel to shore, crossing sandwaves which branch off seaward of the shore-parallel bar. Ice is commonly stranded on bar crests, resulting in rough relief. At the time of the survey a jagged relief, recording many ancient ice gouge events on stiff silty clay, is seen in the ice-sheltered troughs.

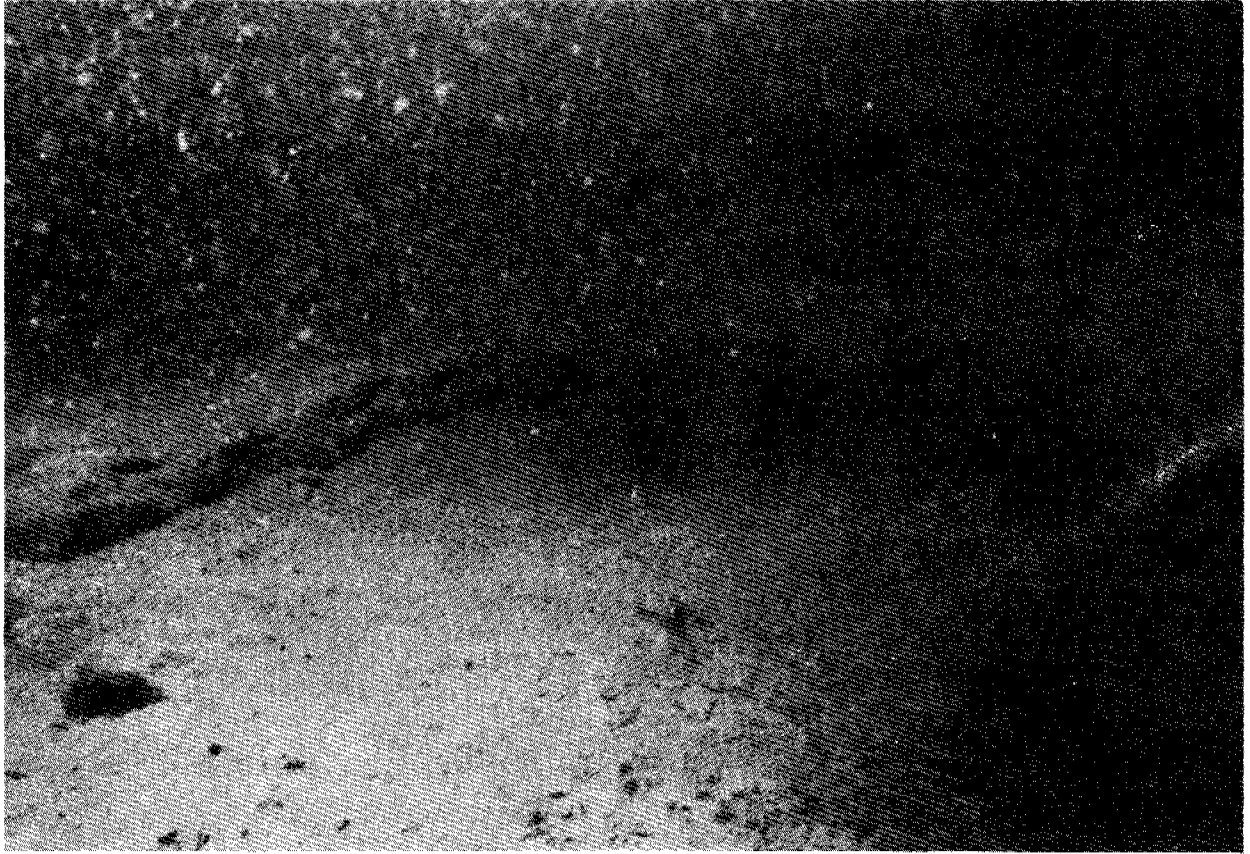


Figure 8. Bottom photograph of a 15-cm high ledge in extremely stiff silty clay cropping out in the troughs between sand waves.

occasionally containing fibrous organic material along bed planes. There is a notable lack of evidence of bioerosion and burrowing in the outcrops.

We compiled a map of stiff silty clay in the survey area using the diving observations combined with fathograms of the jagged relief. Differing degrees of certainty of our interpretation are indicated by different patterns (Fig. 6). The results show a seaward-sloping, jagged surface of overconsolidated materials, ranging from 4.5 m to more than 8.5 m in depth. The major littoral bedforms are moving across this surface. Two shore-parallel bathymetric profiles gathered along the same track in both 1978 and 1979 (Fig. 9) suggest that during this time period little, if any, migration occurred. However, some of the jagged relief in the troughs had been covered by new sediment.

3. Reindeer-Argo Islands. - On the seaward side of Reindeer and Argo Islands and roughly straddling the area between the 6-m and 10-m isobath, lies a zone of overconsolidated silty clay which crops out either in isolated irregular knolls and ledges or as patches of jagged relief up to 2 m high and 100 m or more wide. This zone extends at least from the west tip of Reindeer Island, in an extensive patch 9 km long, towards Cross Island. We have observed these outcrops in numerous dives as well as on underwater television. This zone is also seen on side-scan sonar and fathometer recordings. A typical patch of overconsolidated silty clay was studied in 1979 and is described below.

A sonograph (Fig. 10) shows mottled dark patterns, occurring locally in the form of semi-parallel short linear reflectors. These dark patterns surround a light-colored smooth patch of seafloor which trends obliquely across the sonograph taken along an easterly course. The accompanying fathogram (Fig. 11) shows jagged relief of up to 500 cm in the mottled areas on the sonograph. Very smooth rounded bottom lies between the regions of jagged relief and represents bodies of sand.

On a 120-m-long diving traverse over the jagged bottom area we found thinly bedded very stiff silty clay, so firm that it was nearly impossible to collect a sample with an entrenching tool. This silty clay formed sharp ledges (Fig. 12) which occasionally flanked irregular, flat-bottomed gullies from 10 cm to 20 cm deep where bedded material was exposed. Some of the relief consisted of small jagged piles with angular features. However, much of the relief had been rounded off in varying amounts by currents and ranged from slightly rounded to highly rounded and polished (Fig. 13). Between irregular gullies and ledges there were several regions as much as 10 m across in which solid silty clay formed a smooth to slightly undulating surface. The depressions contained small, temporary accumulations of brown kelp (Fig. 12) and several contained pebbles. In view of the proximity of sand bodies, the complete lack of sand accumulations in even narrow cracks is astonishing.

4. Eighteen-meter Bench. - An anomalous break-in-slope associated with a drastic change in ice gouge density at a depth of about 18 m, which in some years coincides with the inner boundary of the stamukhi zone, has been discussed in several publications (Reimnitz and Barnes, 1974; Reimnitz, et al., 1978), and is again discussed in Attachment D of this report. Four attempts to obtain vibracores, here listed as stations 57, 58, 66, and 67, failed to penetrate. This pronounced feature, occurring in several variations but most commonly as in figure 14, extends along the stamukhi zone over a

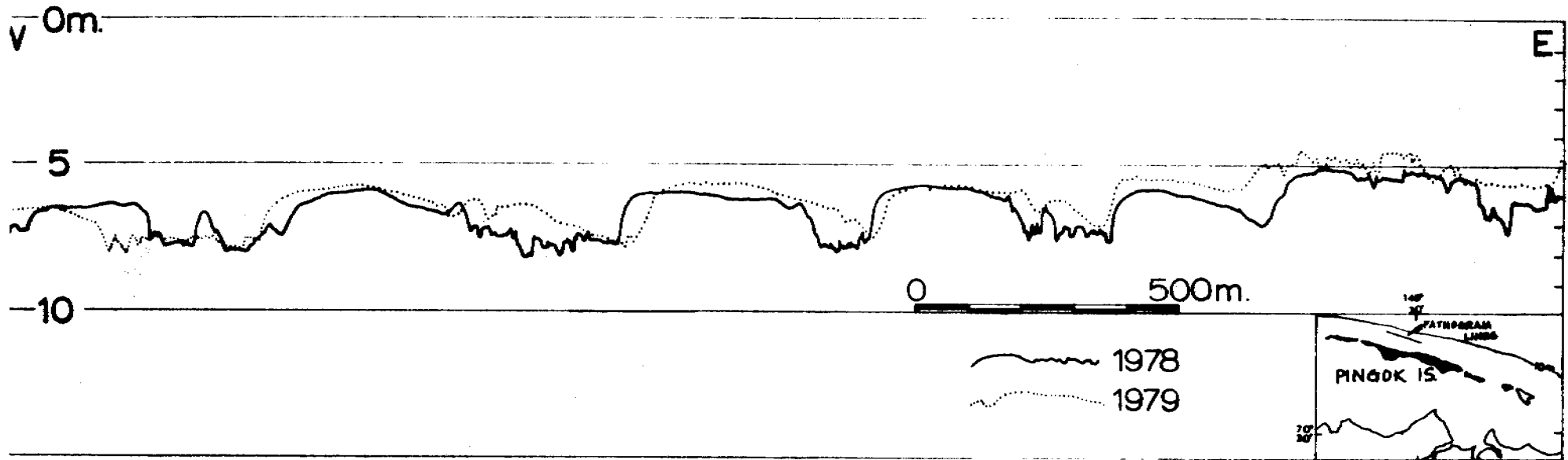


Figure 9. Comparative fathograms along identical shore-parallel tracks, from 1978 to 1979, recording little change in the positions of sandwaves; slight infilling in troughs is also seen.

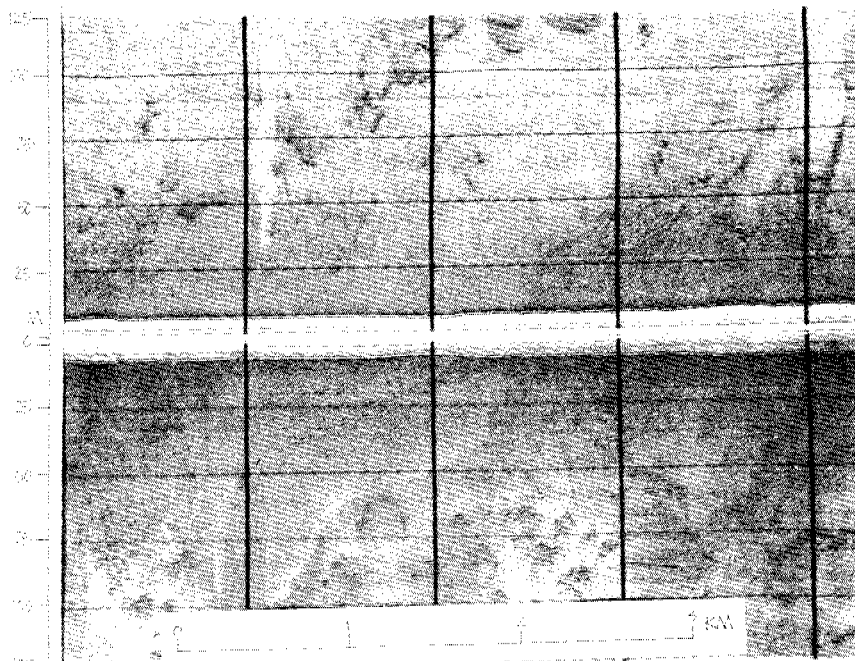


Figure 10. Sonograph of dark mottled bottom representing a jagged relief in stiff silty clay surrounding lighter grey homogenous patch representing a thin body of sand at station 47. Linear reflectors in stiff silty clay areas are semi-parallel ledges.

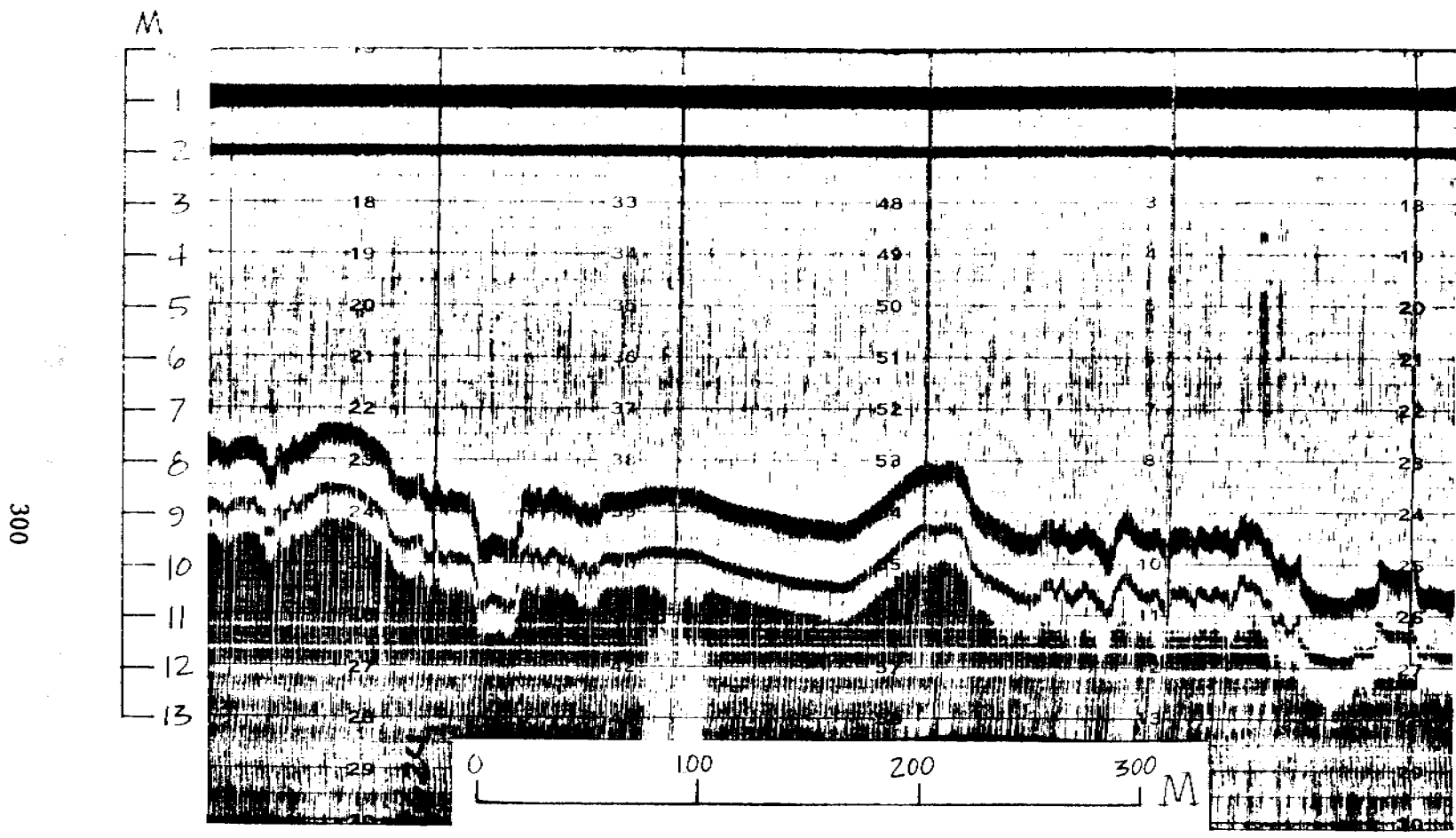


Figure 11. Bathogram along diving traverse at station 47, where jagged relief is carved from stiff silty clay.



Figure 12. 10-cm-high ledge and angular blocks of stiff silty clay to right of ledge, along with brown kelp and a crab.



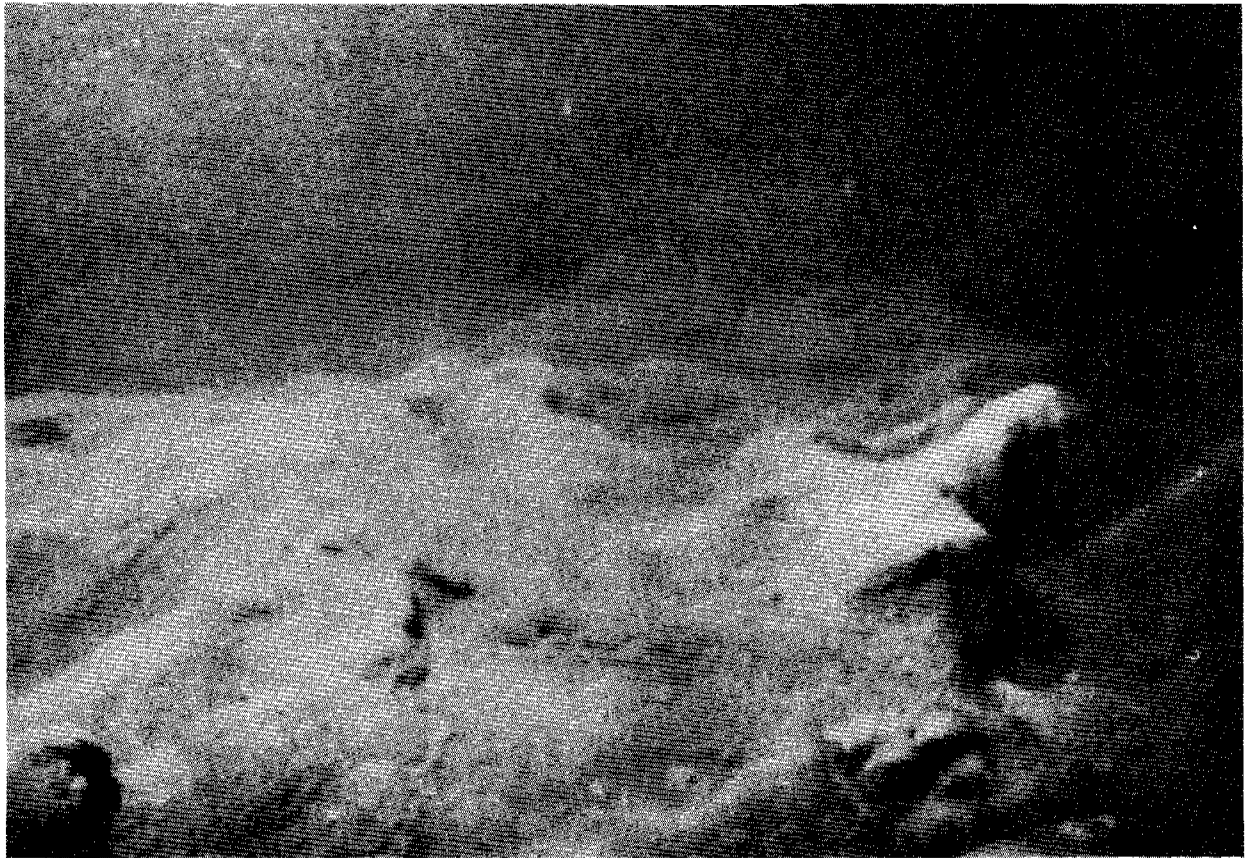


Figure 13. Stiff silty clay as in figure 12 at station 47, being transformed by wave and current action into sub-rounded shapes. All covered by about 1 cm of ooze.

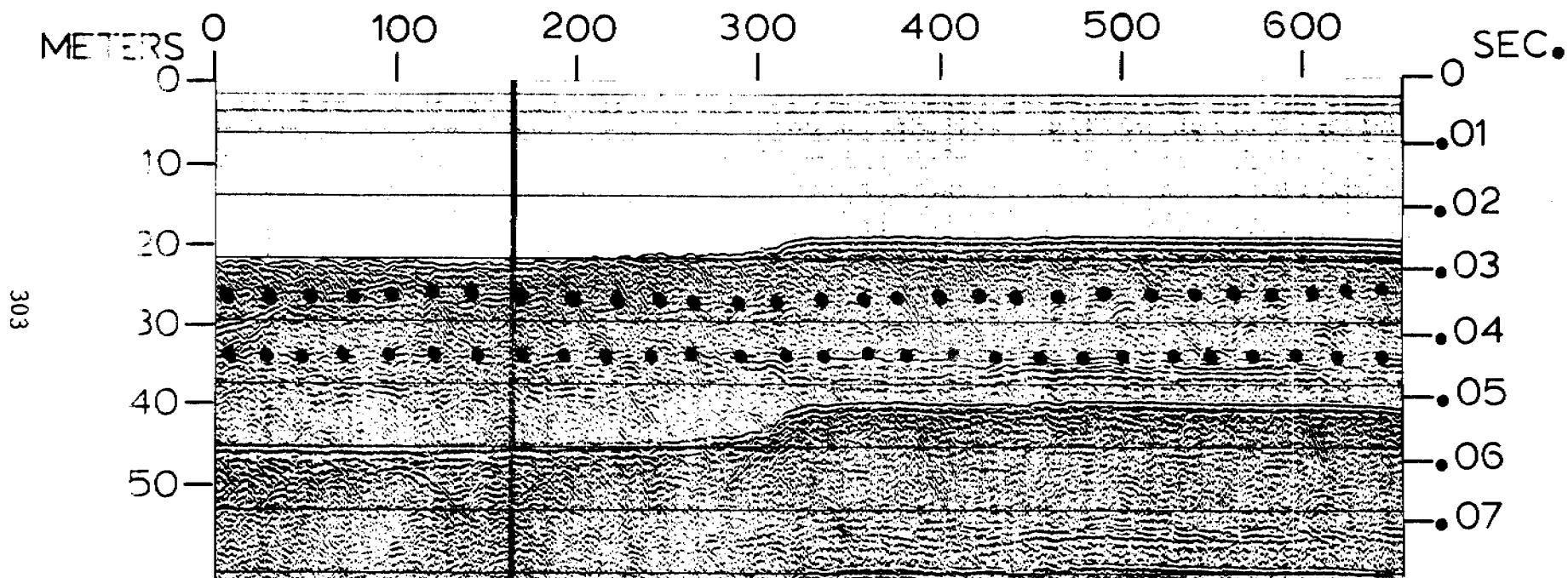


Figure 14. Seismic record from the open shelf at a depth of 20 to 22 m across a slight break in the slope. This break separates intensively gouged bottoms from smooth bottoms. Dotted lines mark two horizontal subbottom reflectors that are intermittently traceable along the survey track. The strong reflector at 42 to 45 m is a multiple of the seafloor echo. (From Reimnitz and Barnes, 1974).

distance of at least 100 km. Several dives were made at station 72, one on top of the bench and two in the highly gouged terrain seaward of the break.

On top of the bench we traversed very firm pebbly to sandy mud, with barely noticeable undulating relief over distances of tens of meters and several minor ice gouges. Pebbles commonly had hydroids and other sessile organisms attached to them, suggesting relative protection from ice gouging. The overconsolidated material here is abnormal in that it contained an abundance of pebbles. The grain size of the materials was similar to that which we encountered on our other two dive traverses seaward of the break in slope where large gouges are abundant. But the sediments were generally soft, pebbles had no trace of marine growth, and all evidence pointed to frequent churning by ice, as shown in figures 15 and 16. A few large chunks of firm material broken by angular fractures were seen cropping out.

5. Belvedere Island. - Using side-scan sonar, we crossed several extensive patches of what appeared to be stiff silty clay east of Belvedere Island in 1973 (Fig. 17). The mottled dark areas were ranked as "funny bottom," until we made a dive in 1979. The station is labeled 73 here. The bottom along the diving traverse within the "funny bottom" area was largely covered by thin, medium to coarse sand formed into ripples. From this sand cover cobbles and boulders up to 1 m in diameter protruded from a bed of extremely stiff silty clay (Fig. 18). The cement-like material formed irregular, 10 to 20 cm high, commonly elongated, rounded knolls. In patches these knolls were aligned as seen in figure 18, but the alignment varied from one patch to another. We saw a few open burrows extending down into the silty clay and several minor ice scratches, perhaps similar to those which produced the oblique lineation in the outcrop areas in figure 17. The boulders held a growth of brown kelp similar to the boulder in the patch at Stefansson Sound, but other organisms such as soft corals and anemones were lacking. Some boulders had been recently overturned by ice, as shown by kelp attached to the underside, but the large ones were held firmly in place by the silty clay. Drifting ice had carved scratches as much as 1 cm deep into the tops of the boulders. Some of the relief in figure 18 may have been caused by dislodged boulders.

6. Leffingwell Entrance. - A small study, made of the tidal channel east of Flaxman Island, has been reported (Reimnitz and Toimil, 1977). Of importance to the present report is the fact that bedded firm clay forms the ledges along the steep flanks of the channel from a depth of 4 m to the floor at 10 m (Fig. 19). A picture of the clay in the channel floor is reproduced in figure 20.

#### C<sup>14</sup>-ages and Foraminiferal studies

Very few sample analyses that may help to identify the depositional environment and processes of consolidation have been done on the overconsolidated materials listed here. Foraminiferal studies of stiff silty clay from stations 41 and 75 (Ron Echols, written communication) suggest shallow marine environments of about 2 and 4 meters, respectively. A "whole-sample" C<sup>14</sup> age for station 41 is 4,360  $\pm$  95 yrs BP. In a strudel scour nearby (station 32) a tundra bed below the overconsolidated material is dated 4,118  $\pm$  189 yrs BP. At both of these stations the overconsolidated material is less than 0.5 m thick. Off Pingok Island (station 23) where a sloping surface of

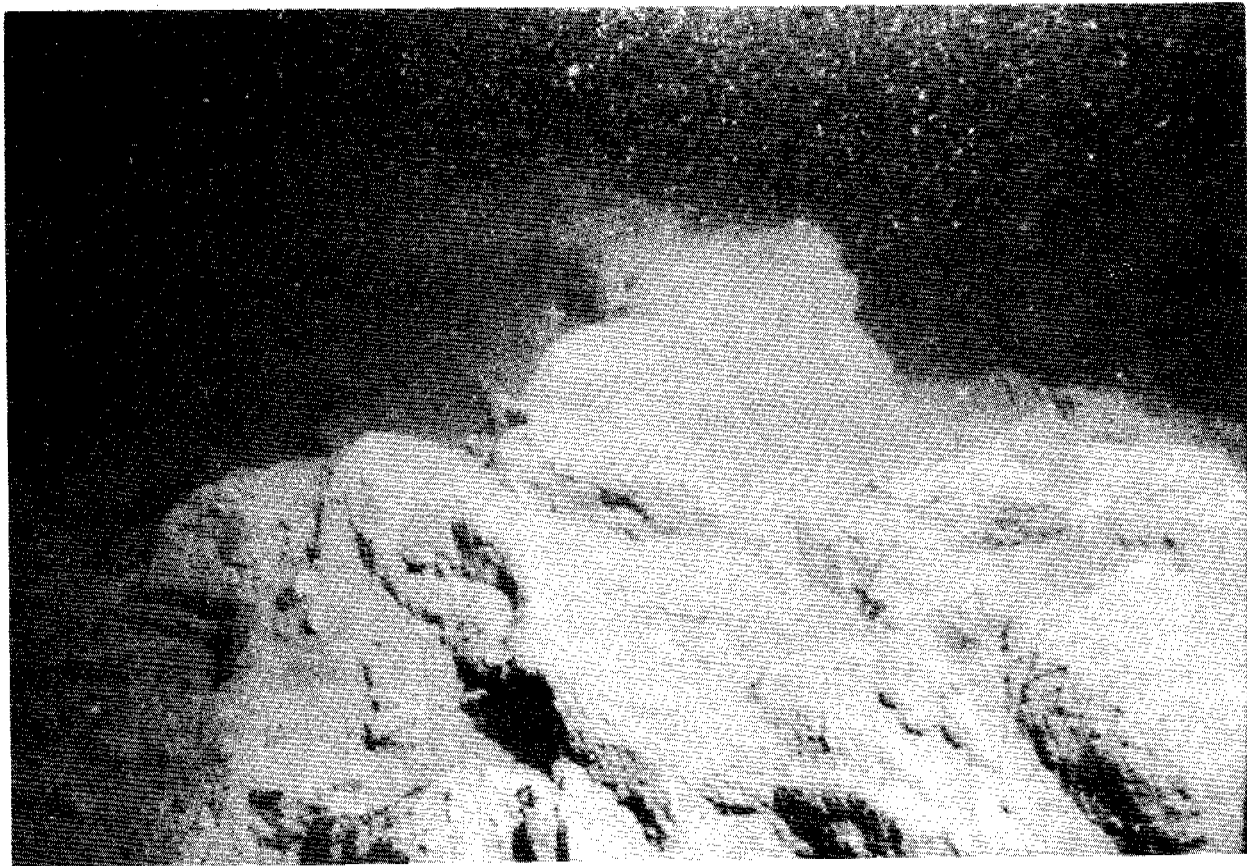


Figure 15. Soft, sandy, pebbly mud at station 72, intensely churned by ice gouging, along seaward side of 18-m bench shown in figure 14. This material contains a few large chunks of very firm pebbly mud.

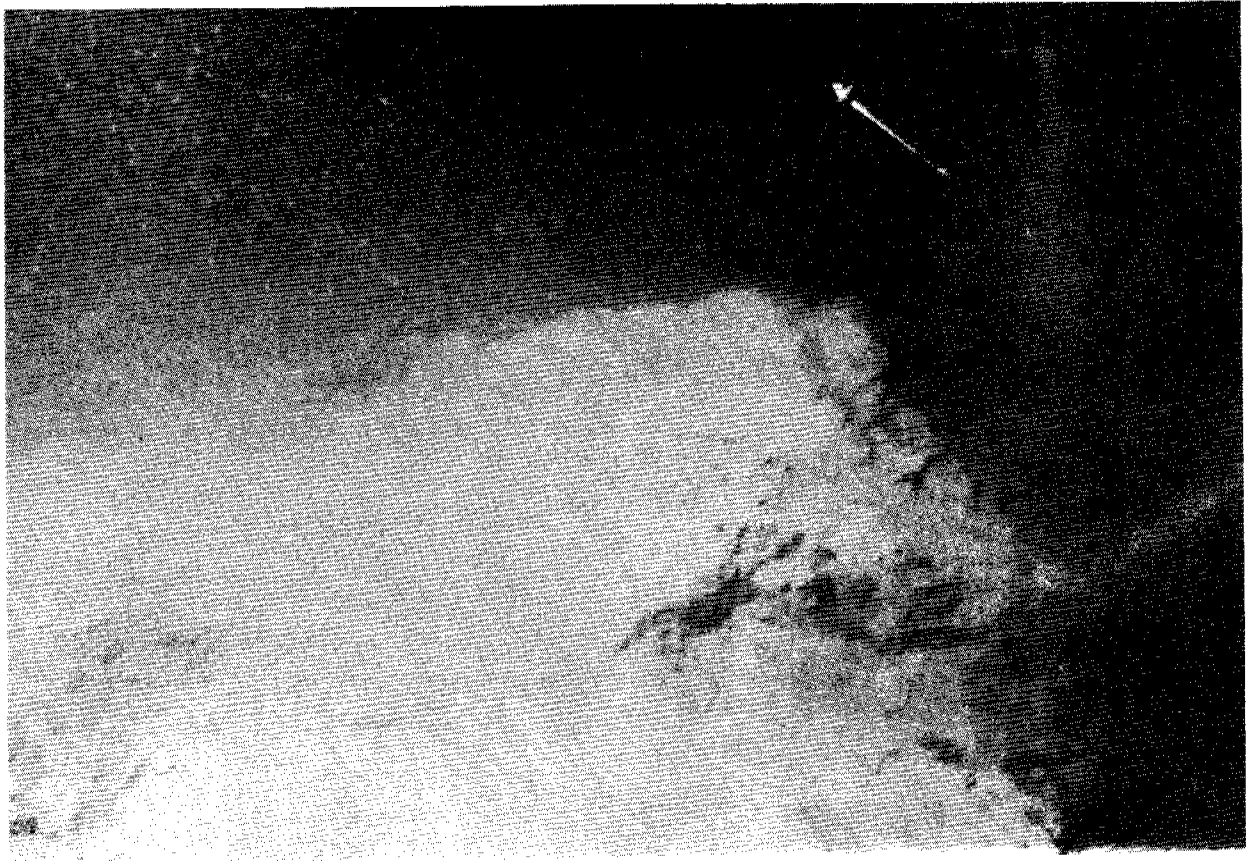


Figure 16. Bottom photo of same place as figure 15, showing diver-held shear-vane and parallel grooves in soft mud produced by plastic deformation under sliding ice.

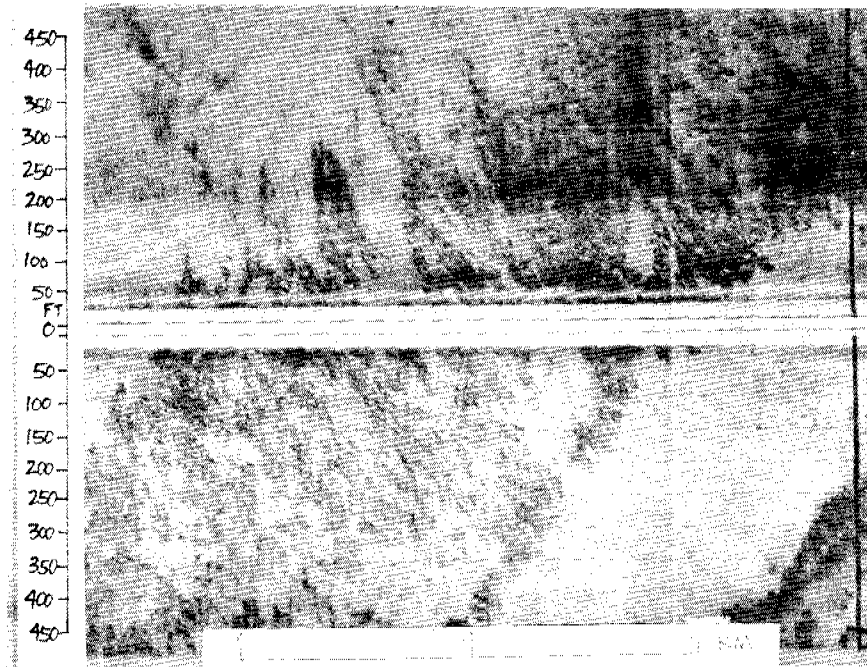


Figure 17. Sonograph near station 73, showing dark mottled areas with faint lineation oblique to ship's track, and light grey homogenous bottom. The former represents boulders and jagged relief in stiff silty clay (see photograph in figure 18) with ice-scratches, and the latter represents thin sand cover.

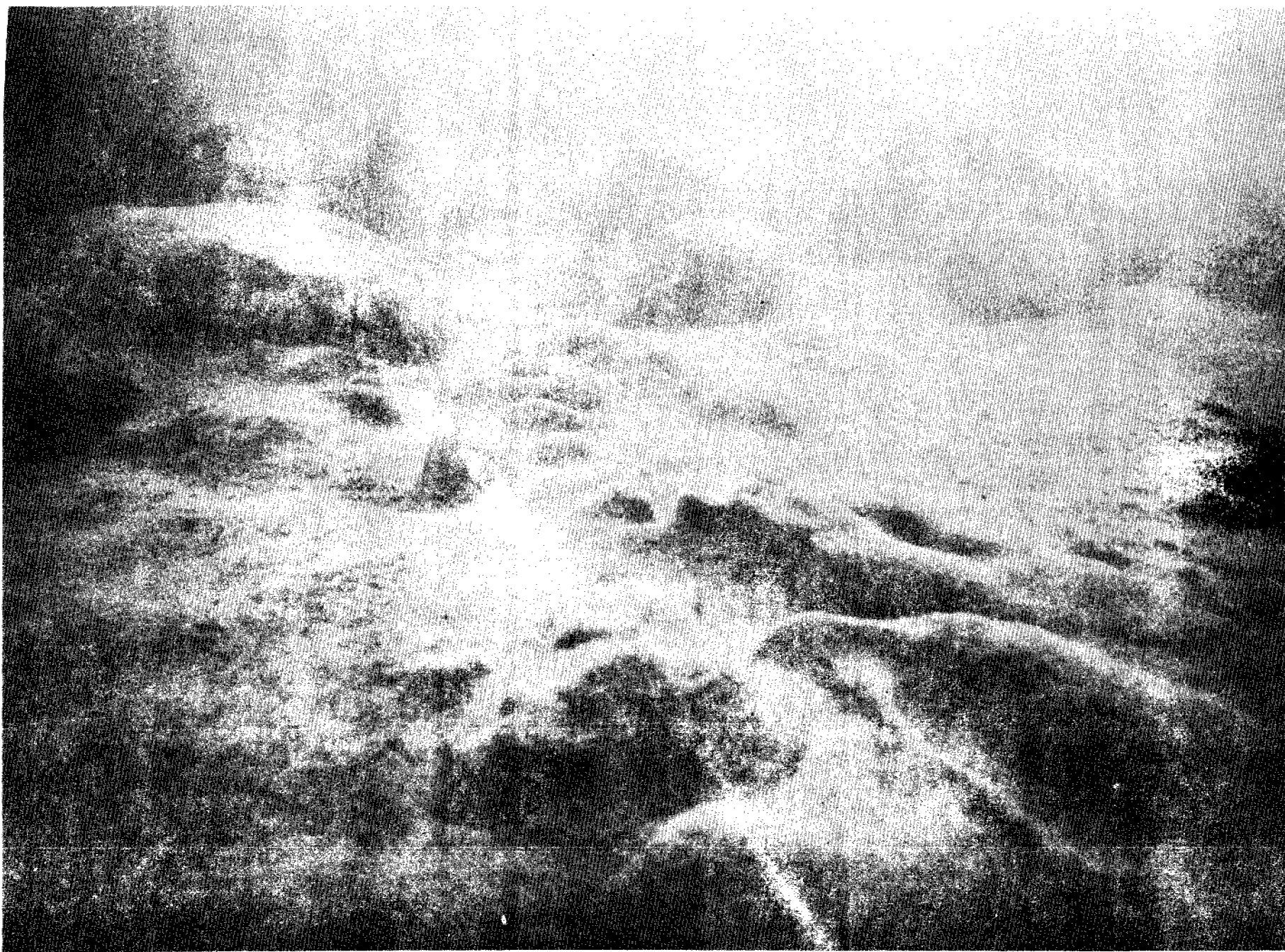


Figure 18. Bottom photo of current-polished relief features in extremely stiff silty clay, extending from lower right to central background. Boulders with kelp in background. A thin ooze covers entire bottom and kelp.

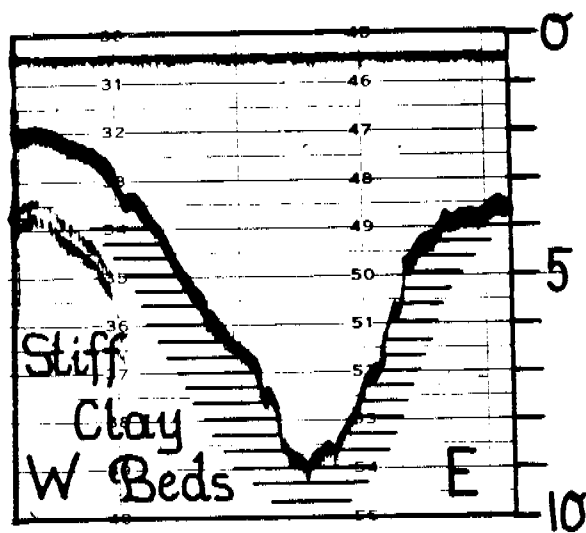


Figure 19. Bathogram across Leffingwell Channel exposing stiff bedded clay in lower 5 m of walls and on floor. (Station 76).

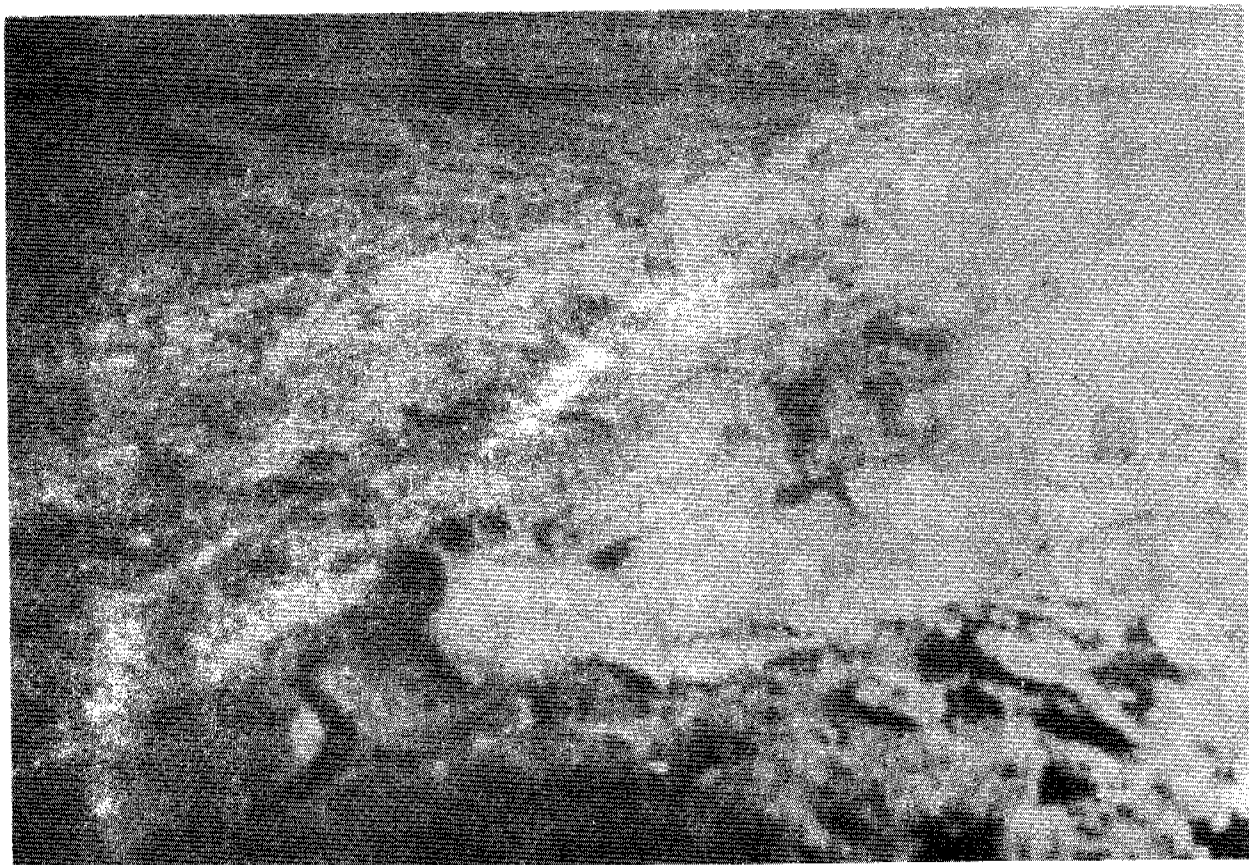


Figure 20. Photograph of Leffingwell Channel floor--stiff bedded clay under sand-starved crescent-shaped ripples at station 76.



overconsolidated material crops out over extensive regions, overlying shell materials of marine mollusks have been dated 3,466  $\pm$ 292 yrs. BP. Whole-sample dates for overconsolidated materials at stations 29 and 46 are 11,810  $\pm$ 280 yrs and 11,890  $\pm$ 200 yrs BP respectively.

#### DISCUSSION AND CONCLUSIONS

The compilation of observations on overconsolidated materials on the shelf surface in the Beaufort Sea shows that such deposits occur in various textural types and settings and range from modern thin, discontinuous layers in the swash zone to thick-bedded sections of Pleistocene marine sediments exposed in the walls of tidal channels. The regional distribution is widespread and irregular, reflecting the density pattern of sampling stations and observation sites. From an extensive trackline net of high-resolution seismic surveys and a series of permafrost borings on the shallow shelf, a number of nearsurface geologic units have been identified. The observed pattern of surficial overconsolidated materials seems to transgress facies changes and geologic boundaries. Overconsolidation of sediments is apparently a phenomenon typical for arctic marine conditions which has frustrated a number of marine geologists employing standard coring techniques in surface sediment studies (Reimnitz and Barnes, 1974). Until vibrocoring techniques were employed, 50 cm of penetration had been the maximum in the study area.

Eight stations are listed here where overconsolidated cohesive sediments occur on beaches or in the swash zone. Because of ice-bonding of sediments in overlying solifluction lobes and coastal bluffs of Quaternary sediments, we have not been able to establish by digging whether the overconsolidated materials are outcrops of the Gubic Formation. In some places the material in the swash zone almost certainly represents the toe of solifluction lobes extending seaward from coastal bluffs, suggesting some process of sediment sorting during solifluction and interaction with waves. Here the overconsolidation must be the result of alternate thawing and freezing discussed by Chamberlain et al. (1978). Because of the thin and discontinuous nature of overconsolidated silty clay in shallow water we believe that some of this material is part of the transgressive sequence, interbedded and interfingering with beach materials. This theory, however, has not been proven.

Freezing of sediments during passage of a migrating barrier island was postulated by Chamberlain et al. (1978) and may explain overconsolidation in some areas but certainly not in others, as for example off Pingok Island (stations 20 through 23). Pingok Island represents a remnant of the coastal plain consisting of Quaternary deposits. Some of our diving observations suggest that sediment squeezing during the process of ice gouging, when plastic deformation, rather than simple plowing action is involved (see figure 16), may result in overconsolidation (Reimnitz and Maurer, 1977). However, observations made along the edge of the 18-m bench (station 72) suggest just the opposite. Here texturally identical materials in the terrain of intense gouging are soft, and extremely firm where not gouged, landward of the break in slope. Thus the overconsolidated materials on the Beaufort Sea shelf so far only raise questions that cannot be answered.

The details of shape and appearance of jagged relief initially carved into stiff silty clay by ice disruption suggest extremely strong current-

smoothing and polishing. The smoothed forms combined with our knowledge that ice disruption of the seafloor occurs on average once every 50 to 100 years (Barnes et al., 1978) and that burrowing organisms are also active, suggest that the current erosion is a periodic event to be expected during the life of the oil field.

## REFERENCES

- Barnes, Peter, Reimnitz, Erk, and Drake, David, 1977, Geologic processes and hazards of the Beaufort Sea shelf and coastal regions, in: Environmental Assessment of the Alaskan Continental Shelf, Quarterly Reports, April-June, v. 2, p. 449-569.
- Barnes, Peter, Reimnitz, and Drake, David, 1977, Marine environmental problems in the ice-covered Beaufort Sea shelf and coastal regions, in: Environmental Assessment of the Alaskan Continental Shelf, Annual Reports, March, v. 17, p. 1-229.
- Barnes, P.W., and McDowell, David, 1978, Inner shelf morphology, Beaufort Sea, Alaska, U.S. Geological Survey Open-File Report 78-785, 3 p.
- Barnes, P.W., McDowell, David, and Reimnitz, Erk, 1978, Ice gouging characteristics: their changing patterns from 1975-1977, Beaufort Sea, Alaska, U.S. Geological Survey Open-File Report 78-730, 42 p.
- Barnes, Peter, and Reimnitz, Erk, 1979, Ice gouge obliteration and sediment redistribution event; 1977-1978, Beaufort Sea, Alaska, U.S. Geological Survey Open-File Report 79-848, 22 p.
- Chamberlain, E.J., Sellman, P.V., Blouin, S.E., Hopkins, D.M., and Lewellen, R.I., 1978, Engineering properties of subsea permafrost in the Prudhoe Bay region of the Beaufort Sea, Third International Conference on Permafrost, Edmonton, Alberta, Canada, p. 629-635.
- Dunton, Kenneth, and Schonberg, Susan, 1979, An arctic kelp community in Stefansson Sound, Alaska: A survey of the flora and fauna, in: Broad, A.C., Annual Report of the Environmental Assessment of Selected Habitats in the Beaufort and Chukchi Littoral System, Western Washington University, p. 3-1 to 3-49.
- Reimnitz, Erk, Barnes, Peter, and Alpha, Tau Rho, 1973, Bottom features and processes related to drifting ice on the Arctic Shelf, Alaska, U.S. Geological Survey Map F-532.
- Reimnitz, Erk, and Barnes, P.W., 1974, Sea-ice as a geologic agent on the Beaufort Sea shelf of Alaska: in: Reed, J.C., and Sater, J.E., (eds.), The Coast and Shelf of the Beaufort Sea, Arctic Institute of North America, Arlington, Va., p. 301-353.
- Reimnitz, Erk, Maurer, Douglas, Barnes, Peter, and Toimil, Lawrence, 1977, Some physical properties of shelf surface sediments, Beaufort Sea, Alaska, U.S. Geological Survey Open-File Report 77-416, 8 p.
- Reimnitz, Erk, Toimil, L.J., and Barnes, Peter, 1978, Arctic continental shelf morphology related to sea-ice zonation, Beaufort Sea, Alaska, Marine Geology, v. 28, p. 179-210.
- Shott, A.D.,<sup>1978</sup> Beach dynamics and nearshore morphology of the Alaskan Arctic Coast, PhD dissertation submitted to the Louisiana State University Agricultural and Mechanical College, 139 p.

## Attachment C

Bathymetric changes in the vicinity of the West Dock,  
Prudhoe Bay, Alaska.

by Peter Barnes and Peter Minkler

### INTRODUCTION

The marine environment in the vicinity of the causeway, which constitutes most of the West Dock facility at Prudhoe Bay has been the subject of considerable discussion with regard to the impact that such a feature may have on the environment. In part this discussion has been generated by the need to know what the immediate effects on the environment are as a result of the building of that structure and in part because knowledge is needed in anticipation of construction of additional structures similar to the causeway if the petroleum industry decides to locate production activities offshore.

In an effort to assess the morphologic changes, bathymetric surveys of the area adjacent to the West Dock were conducted in 1976 and 1979. Additional bathymetry from U.S. Coast and Geodetic Survey data of 1950 was compared to the 1976 data in a report by Barnes et al., 1977. This comparison resulted in the conclusion that the bathymetry was essentially unchanged since the 1950 survey except to the east and northeast of the causeway extension where local scour appears to have developed, perhaps in response to propwash from extensive tug and barge traffic.

In this report we assess these two extensive earlier surveys (1950, 1976) with a more areal restricted survey taken in the summer of 1979. As the data were obtained only one season after the building of the causeway, a more recent survey would show new changes not developed by the earlier survey.

### METHODS AND OBSERVATIONS

A close grid of tracklines were run on the west side of the West Dock on August 30, 1979 and on the east side of the dock on September 18, 1979 (Fig. 1). Using tide data from the West Dock tidal station (Preliminary data from NOAA tide station 949-7649, Prudhoe Bay, Alaska), the data for August 30 and September 18 were adjusted to mean lower low water (MLLW) at the time of the survey. This data is about 0.4 ft below mean sea level. The 1950 data from the U.S. Coast and Geodetic Survey are also adjusted to MLLW. The 1976 survey was not adjusted for tides but tidal information indicates the 1976 data is 0.4 ft. above MLLW. Thus the data on the 1950 and 1979 bathymetry are within 0.1 ft. while the data for the 1976 survey is 0.4 ft. higher, thus indicating slightly deeper water.

Observations based on the 1976 survey led to the conclusion that there were inconsequential changes since the 1950 survey with the exception of the northeast-facing segment of the causeway where scour was indicated, possibly related to tug and barge activity (Figs. 2 and 3).

An industry study concluded that sediment accumulation was probable at the base of the eastern side of the dock where it intercepts the longshore transport. Furthermore, Stump Island would not be affected by the presence of the causeway. No mention is made in this study of the potential effects of the causeway on sedimentation around the causeway except for the coast, the dock, and the leeward islands.

The 1979 survey (Fig. 4) indicates that measureable shoaling has occurred in most areas surrounding the dock. West of the dock depths are two or more feet shallower than measurements taken in 1950 and 1976. On the eastern side of the causeway the water is approximately 1 ft. shallower than in the earlier surveys except in the area immediately adjacent to the causeway where a channel has been maintained. The channel may be maintained as a result of longshore erosion of the bottom sediments at the base of the causeway slope or by scour action of tug and barge activity. This shoaling can be seen by comparing figures 2, 3, and 4.

In the vicinity of the dock head, at the most seaward extent of the causeway, a shoal exists to the east of the causeway which was also present in the 1976 survey. Gravel placement activities associated with causeway construction are believed to be responsible for initiating the formation of this feature. There also appear to be two to three feet of shoaling seaward of the terminus of the causeway. Tugs hold barges against the terminus, pushing the barges against the end of the dock; the resulting propwash (and sediments) moving seaward could cause formation of the shoal.

#### DISCUSSION AND CONCLUSIONS

The West Dock and causeway appear to have formed an effective break in the sediment transport regime, causing an increase in sedimentation in association with this feature. Sedimentation is most pronounced on the west side, although there is some shoaling on the east side as well. Shoals are built up approximately 0.5 ft. per year on the west side of the causeway and at about half that rate on the east side.

The increased sedimentation rates in the bight southwest of the causeway are a result of decreased wave and current activity. This "backwater" would allow sediment to be more readily deposited than if the area were unprotected. The prevailing light to moderate open water, wind, and waves are from the northeast, resulting in coastal circulation to the west. Thus the causeway acts to almost completely block wave and current activity from the dominant direction.

Future plans to extend the existing causeway and to build new causeways should take account of the fact that sedimentation will be enhanced, at least in the immediate vicinity of such structures. Because of prevalent northeasterly winds and observed stormy conditions over the past several years, breaks in the causeway might reduce the siltation rate. We would estimate that breaks on the order of 5 to 10 percent of the causeway length

might significantly affect the siltation rate. This estimate is based on the approximate ratio of openings in the barrier island chain encompassing Simpson Lagoon where sedimentation rates are known to be low and thus the island chain must be reasonably well flushed.

#### REFERENCES

Barnes, Peter, Reimnitz, Erk, Smith, Greg, and McDowell, David, 1977,  
Bathymetric and shoreline changes in northwestern Prudhoe Bay, Alaska:  
The Northern Engineer, v. 9, n. 2, p. 7-13.

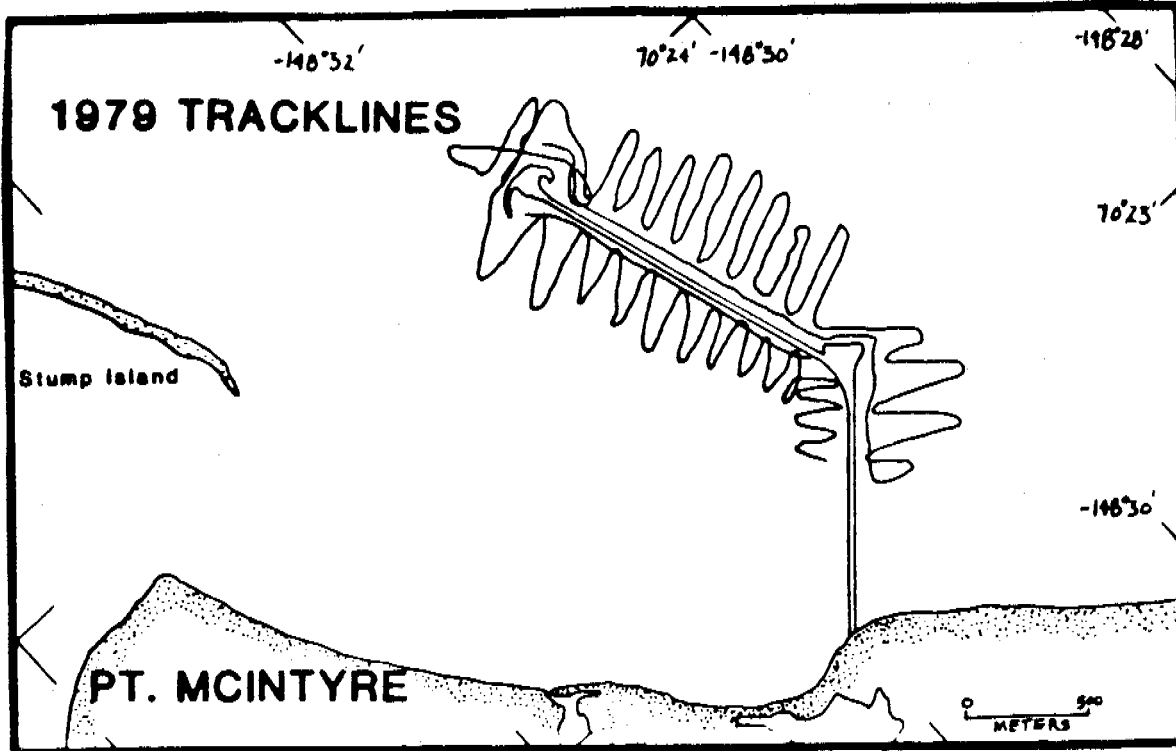


Figure 1

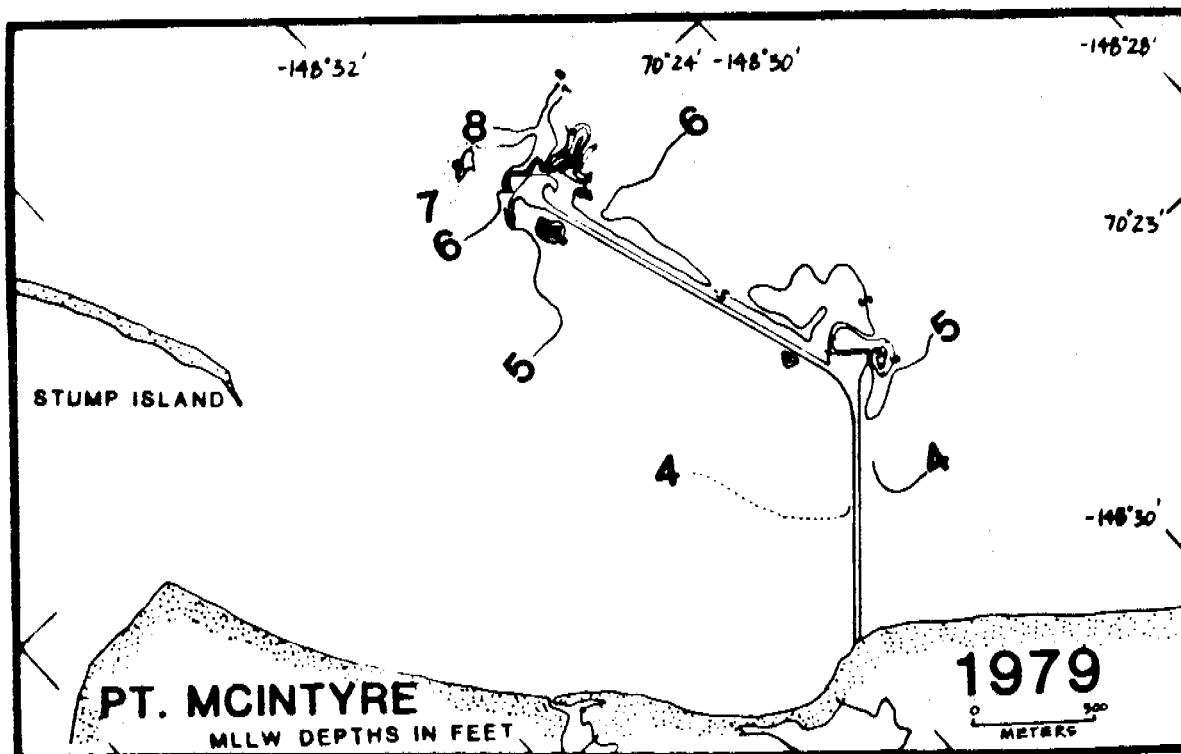


Figure 4

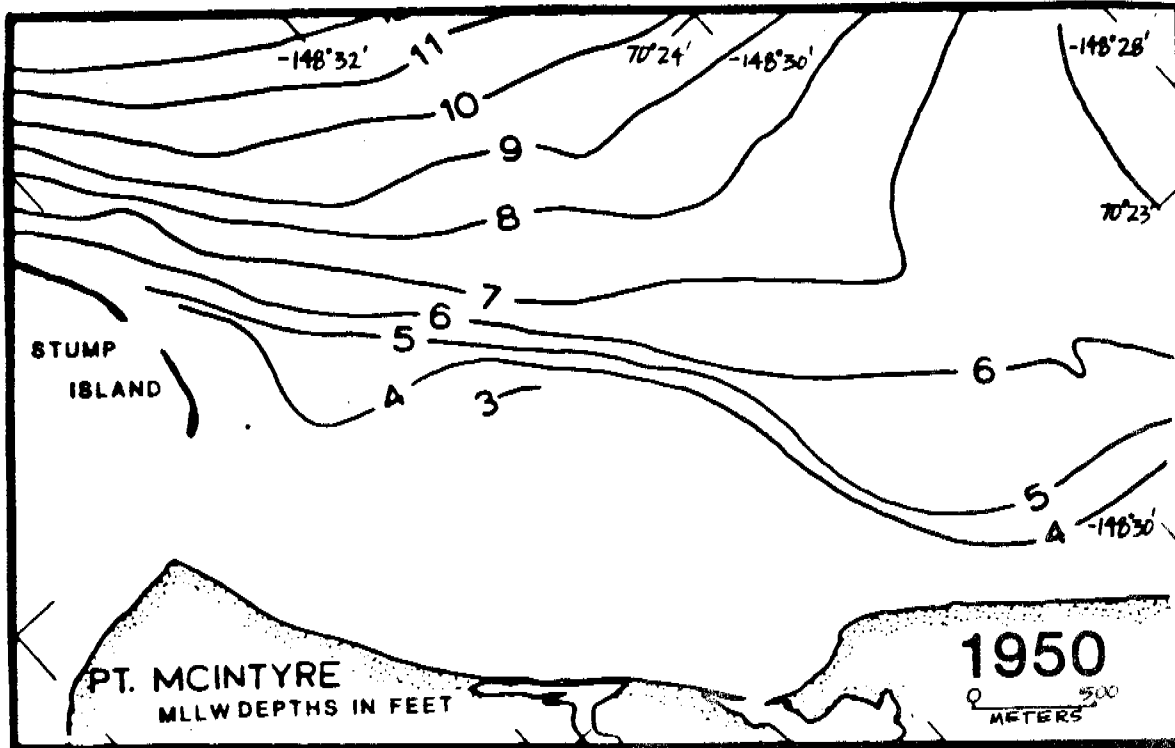


Figure 2

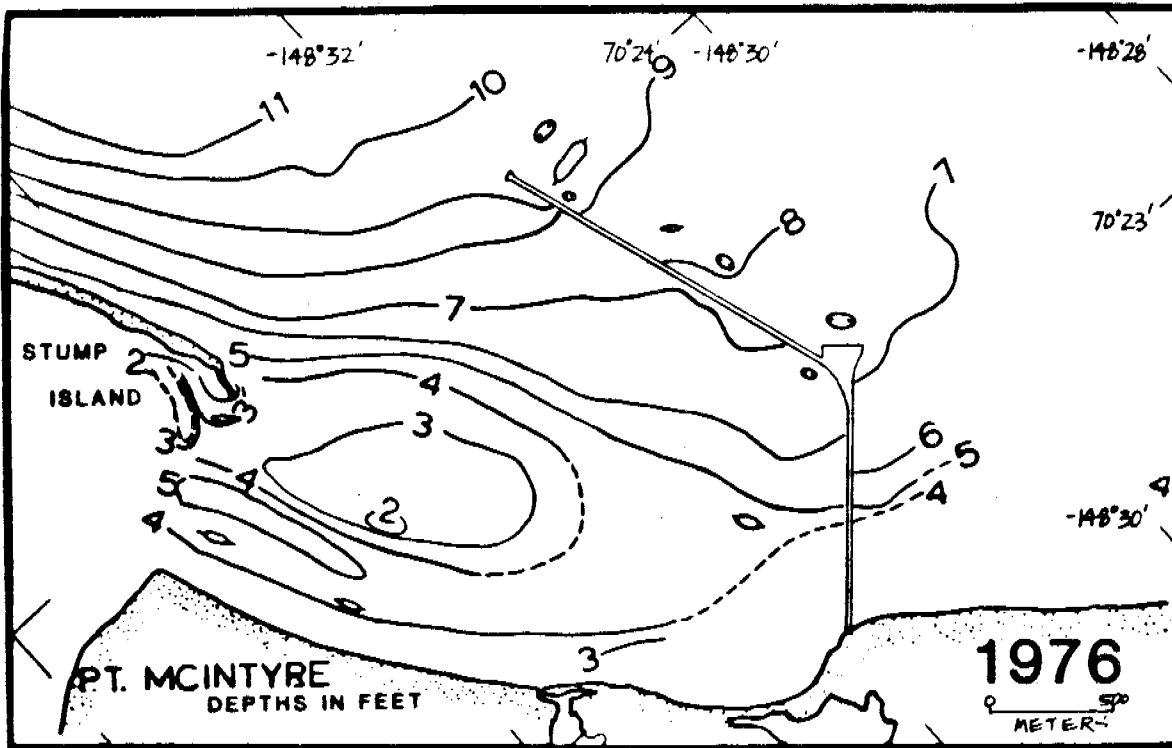


Figure 3



## Attachment D

### Reassessment of ice gouging on the inner shelf of the Beaufort Sea, Alaska -

#### A Progress Report

by Douglas Rearic and Peter Barnes

### INTRODUCTION

Interaction of ice with the seabed on high-latitude shelves is an important geologic process (Reimnitz and Barnes, 1974; Lewis, 1978). Ice incising the seafloor as ice gouges threatens seafloor and subseafloor structures such as pipelines. Initial compilation of seabed and ice zonation data suggests a causal relationship exists between the character and intensity of ice gouging and the formation of pressure ridges on the inner Beaufort Sea shelf (Reimnitz and others, 1978). Data gathered since earlier studies suggests that ice gouge zonation can be better defined when compilations of the new data are included.

Since 1972 we have been recording morphologic data on the ice-gouged continental shelf of the Beaufort Sea using side-scan sonar and bathymetric profiling. Seven years of data from the R/V Loon, R/V Karluk, and USCG Ice Breaker Glacier have produced many records of the inner and central shelf ice-gouge features. In January, 1979 we began a correlation and analysis of these records to redefine and reassess ice gouging in the north slope lease area. The primary objective has been to assemble quantitative data on ice-gouge characteristics and processes and to analyze this data for characteristic trends in ice-gouge processes. We present here a summary of the work that has been completed, some preliminary results, and projected plans.

### DATA COLLECTION METHODS

Fifty tracklines covering 1500 kilometers of the lagoon, bay and shelf environments of the Beaufort Sea, including the lease area, were chosen so that the data coverage would be evenly distributed from Cape Halkett to western Camden Bay and offshore to the 35-m isobath (Figure 1). The trackline navigation was plotted in 1-km segments at our field chart scales of 1:80,000 and 1:50,000 (Figure 2). The sonographs and fathograms recorded along the tracklines were also divided into 1-km segments and correlated segment for segment with the plotted navigation. A data sheet was then developed to organize the data and descriptions obtained from our records (Figure 3). Once this had been accomplished the records were studied in detail, quantifying the gouge characteristics in each segment.

The gouge character was quantified using the techniques outlined in Barnes, et al. (1978). All ice-gouge incisions that were observed on the sonographs were counted and recorded for each segment. The average gouge orientation was measured and then oriented to true north. The maximum incision width was also measured on the sonograph. Gouge incision depths were

measured from the fathogram in 20-cm increments and the maximum incision depth was also recorded for each segment. Maximum ridge heights bounding the gouges were measured. Other gouge and seafloor features observed and/or measured included: multiple-incision gouges, tick marks (Reimnitz et al., 1973), strudel scours (Reimnitz et al., 1974), sediment waves and ripples, shoals, 7 kHz subbottom return, 'funnybottom' outcrops (Barnes et al., 1977), boulders (Reimnitz and Ross, 1979), and areas containing a dramatic change in ice-gouge characteristics (Reimnitz and Barnes, 1974)

Interpretation of the records requires subjective judgements in most all cases. To minimize this factor, all the counting and measuring was performed by one individual so that the subjective error would be consistent. The interpretation of the records to produce quantified data (Figure 3) is now approximately 80 percent complete and preliminary analyses are underway. Present emphasis will be on mid-shelf records from Glacier whose poor navigation and bathymetry produce an inferior data set.

#### ANALYSIS OF DATA

Below are listed projected results of the present analysis of records.

##### Computer Analysis

The data will be computer filed to permit the use of pre-existing programs for statistical calculations and contour mapping. In addition to satisfying our immediate needs, theoretical models relating ice zonation, ice gouges, and various seafloor features may be created.

##### Detailed Contour Mapping

The combination of large chart scale and small segment counting size will allow detailed contour mapping of such features as gouge density, maximum incision depths, and gouge orientation (Reimnitz and Barnes, 1974; Barnes et al., 1978).). A small portion of one of the six navigation plotting sheets generated during the project has been reproduced as Figure 2. Contouring at this scale will maximize coverage of the inner shelf area and provide information about processes.

##### Statistical Investigations

More than 50,000 gouges have been counted, measured, and oriented, thus providing a strong basis upon which to develop a statistical model of ice-gouge character in the Beaufort Sea. W.F. Weeks of the U.S. Army's CRREL (Cold Regions Research and Engineering Laboratories) has initiated a detailed analysis of the gouge depth data. Preliminary results from this work appear in the Annual Report for RU-88.

##### Morphologic Observations

Detailed observations of bedforms and their relation to the ice regime, to each other, and to the wave and current regime will be made from the records. These observations serve as a basis to explore the relationship between sediment waves, sediment ripples, and shoals in different hydrologic and ice environments on the shelf. The effect of shoals on the gouge process is presently under study.

## THE 18-METER BENCH - A MORPHOLOGICAL BOUNDARY

Observations based on data compiled to date are given here. For the purpose of this report we are calling this feature the 18-meter bench although we recognize that it does not always occur at 18 m nor as a bench. Characteristics of the bench are complementary to other attachments to this report (Stiff Clay, Attachment B, and The Break in Gouge Density and Ridging, Attachment E). A marked change in seabed character exists seaward of the barrier islands at an average depth of 20 m (Figure 4). This feature has been identified previously and described in literature as a boundary or change in ice-gouge character (Reimnitz and Barnes, 1974), sediments (Reimnitz and Barnes, 1974), and ice zonation (Reimnitz et al., 1978). At 31 crossings of this boundary marked changes in seafloor morphology, sea-ice morphology, and ice-gouge character have been consistently noted. Boundary determinations were made using sonar and bathymetric records together with LANDSAT photographs of the shelf (approximate scale: 1:1,000,000).

The seafloor boundary area investigated consists of a shoal and bench complex parallel to the coast extending at least from Eastern Harrison Bay to western Camden Bay. The present western end of the boundary is described as a shoal area with relief of three to four meters that extends from Stamukhi Shoal (north of Oliktok Point) to a point approximately 17 km north of Reindeer Island. At this point the boundary becomes a bench and slope break with water depth increasing 2 to 4 meters seaward of this feature (Figure 5A). The bench runs from Reindeer Island to Flaxman Island. Five km north of Flaxman Island the boundary is again marked by a system of shoals that continues into Camden Bay.

Some of the shoal crossings show an onshore/offshore increase in water depth on the shoal flanks similar to the slope break area. On boundary crossings near the shoal systems the bench has a slight upward bulge at the crest suggesting that a shoal might be in the process of building or disintegrating. One such crossing of the bench occurred approximately 18 km northeast of Reindeer Island (Figure 5B).

Under repetitive ice grounding the shoal might be subject to grinding down of the crests. However, resurveys of arctic shoal areas show they are maintaining their morphological character despite intensive ice interaction (Reimnitz and Maurer, 1978). This suggests there may be a constructive process involved that replenishes crest sediments. Perhaps that process may relate to the bench and shoal processes reported here.

The stamukhi zone is hypothesized to develop where rotating polar-pack ice contacts the seaward extension of the headlands (Reimnitz et al., 1978). Ice ridging occurs at these points and then a shearing of the ice between two points of contact. As the headlands are somewhat stable, the stamukhi zone should occur in roughly the same location year after year. The shear movement of ice along the stamukhi zone and along the bench may preferentially displace sediments laterally rather than onshore and account for the lack of shoal development along the benchlike boundary between major promontories. In contrast, ice keel motion at promontories may have a larger onshore component which might be responsible for development of the shoals. Thus, shoals associated with the gouge character change boundary might be expected at major promontories such as Oliktok, Cross Island, Flaxman Island and Barter Island

while between these points a bench character to the boundary might be expected.

Sediments inside the boundary on the bench are compacted gravelly muds, while seaward of the boundary the same sediments are less compact, at least in the upper 50 cm (Barnes et al., 1979). Statistical analysis of the boundary indicates an average increase in gouge density of 75 gouges per kilometer and an average increase in maximum incision depth of 0.5 m seaward of the bench and shoal complex. Gouge density increases towards the boundary until a maximum density is reached in the boundary segment. Succeeding offshore segments decrease in density but do not fall to the lower densities found inshore (Figure 3). Maximum incision depth seaward of the boundary was generally greater than 1 m but inshore incision depths were consistently less than 1 m. Deflection in orientation averages  $27^{\circ}$ , offshore and inshore of the boundary. However, this change may be insignificant as the orientation shift occurs clockwise and counterclockwise and is highly dependent on the bathymetry of the area. Deflections in orientation may be local in character and therefore may not conform to statistical averages calculated for the entire shelf.

An ice-gouge character change coexists with this seafloor bathymetric boundary (Figures 3, 6, and 7). The change in character of the gouges is related to seafloor morphology. Where the seafloor boundary is represented by a bench the character of gouges changes on the seaward slope of the bench. In the area of shoals the character of the gouges changes inshore of the shoal at a distance that appears to be related to height and width of the shoal (Figure 4). This is consistent with present theory which considers ice gouging to be an upslope process. In the bench environment the upslope direction is toward shore only where the shoal environment is upslope in the offshore as well as the onshore direction (Figure 8).

Studies of LANDSAT Satellite imagery indicate a correlation between the major inner ice ridge of the stamukhi zone (Reimnitz et al., 1978) and other morphological boundaries (Figure 9). Because of the scale used, exact points cannot be plotted to correlate with sonar and bathymetry records. However, visual observations show a good correlation between boundaries and indicate that boundary-associated ice features are continuous to the east of the project area.

#### CONCLUSIONS AND FUTURE RELATED PROJECTS

Special attention has been paid to gouge morphology. All gouge forms observed on the records have been previously identified and reported and no new information regarding gouge morphology has been added (Reimnitz et al., 1973).

Seven years of morphologic data gathered on the seabed provide a basis for assessment of the character of ice gouging on the inner shelf. Critical data were gathered in the last two years due to favorable ice conditions, thus providing a more complete data base.

A seabed morphologic boundary, apparently associated with the inner edge of the stamukhi zone, has been defined on all track lines crossing this boundary. Topographically the boundary takes the form of either a shoal or a 2-4-m-high bench which parallels the shore and the offshore islands. The

shoal and bench forms grade laterally into one another. A causal relationship exists between the sea-ice and seabed boundary. Apparently the grounding of the inner ridges of the stamukhi zone act to maintain and perhaps to generate the topographic bench and shoals associated with the boundary.

Future projects may relate to subjects presently under study. The USCG Ice Breaker Glacier collected sonar and seismic records of portions of the outer shelf of the Beaufort Sea in 1972. Correlation of these records with our present work would expand our knowledge of ice gouging in deeper areas of the shelf.

Precisely re-navigated "test" lines annually surveyed (ice conditions permitting), also provide valuable information, since most of our measurements do not contain a time parameter. These data are primarily used to increase our understanding of rates of shelf processes in the Beaufort Sea. Two additional test lines, taken off Karluk and Flaxman Islands, have been added.

Based on results of our data analysis, we believe we now have a data collection technique which enables us to present quantitative ice gouge data in a consistent form. This consistency will allow us to integrate new ice-gouge data as it is acquired and will lead to better understanding of this dynamic geologic process.

#### REFERENCES

- Barnes, P.W., McDowell, David, and Reimnitz, Erk, 1978, Ice gouging characteristics: their changing patterns from 1975-1977, Beaufort Sea, Alaska, U.S. Geological Survey Open-File Report 78-730, 40 p.
- Barnes, P.W., Reimnitz, Erk, and Drake, D.E., 1977, Marine environmental problems in the ice-covered Beaufort Sea shelf and coastal regions: Annual Report to National Oceanic and Atmospheric Administration, Environmental Assessment of the Alaskan Continental Shelf; Principal Investigators' Reports, April 1977. 16 p.  
Attachment: J. Funnybottom diving observations - Summer, 1976, 21 p.
- Barnes, P.W., Reimnitz, Erk, Toimil, Larry, Maurer, Douglas, and McDowell, David, 1979, Core descriptions and preliminary observations of vibracores from the Alaskan Beaufort Sea shelf, U.S. Geological Survey Open-File Report 79-351, 71 p.
- Lewis, C.F.M., 1978, The frequency and magnitude of drift-ice groundings from ice-scour tracks in the Canadian Beaufort Sea. POAC 77 Proceedings, v. 1, p. 568-79.
- Reimnitz, Erk, and Barnes, P.W., 1974, Sea ice as a geologic agent on the Beaufort Sea shelf of Alaska: in: Reed, J.C., and Sater, J.E., (eds.), The Coast and Shelf of the Beaufort Sea, Arctic Institute of North America, Arlington, Va., p.
- Reimnitz, Erk, and Barnes, P.W., and Alpha, T.R., 1973, Bottom features and processes related to drifting ice on the arctic shelf, Alaska: U.S. Geological Surveyb Miscellaneous Field Studies Map MF-532.

Reimnitz, Erk, and Maurer, D.K., 1978, Stamukhi shoals of the arctic--some observations from the Beaufort Sea, U.S. Geological Survey Open-File Report 78-666, 17 p.

Reimnitz, Erk, Rodeick, C.A., and Wolf, S.C., 1974, Strudel scour: a unique arctic marine geologic phenomenon, Journal of Sedimentary Petrology, v. 44, n.2, p. 409-420.

Reimnitz, Erk, and Ross, C.R., 1979, Lag deposits of boulders in Steffanson Sound, Beaufort Sea, Alaska, U.S. Geological Survey Open-File Report 79-1205.

Reimnitz, Erk, Toimil, L.J., and Barnes, Peter, 1978, Arctic continental shelf morphology related to sea-ice zonation, Beaufort Sea, Alaska, Marine Geology, v. 28, p. 179-210.

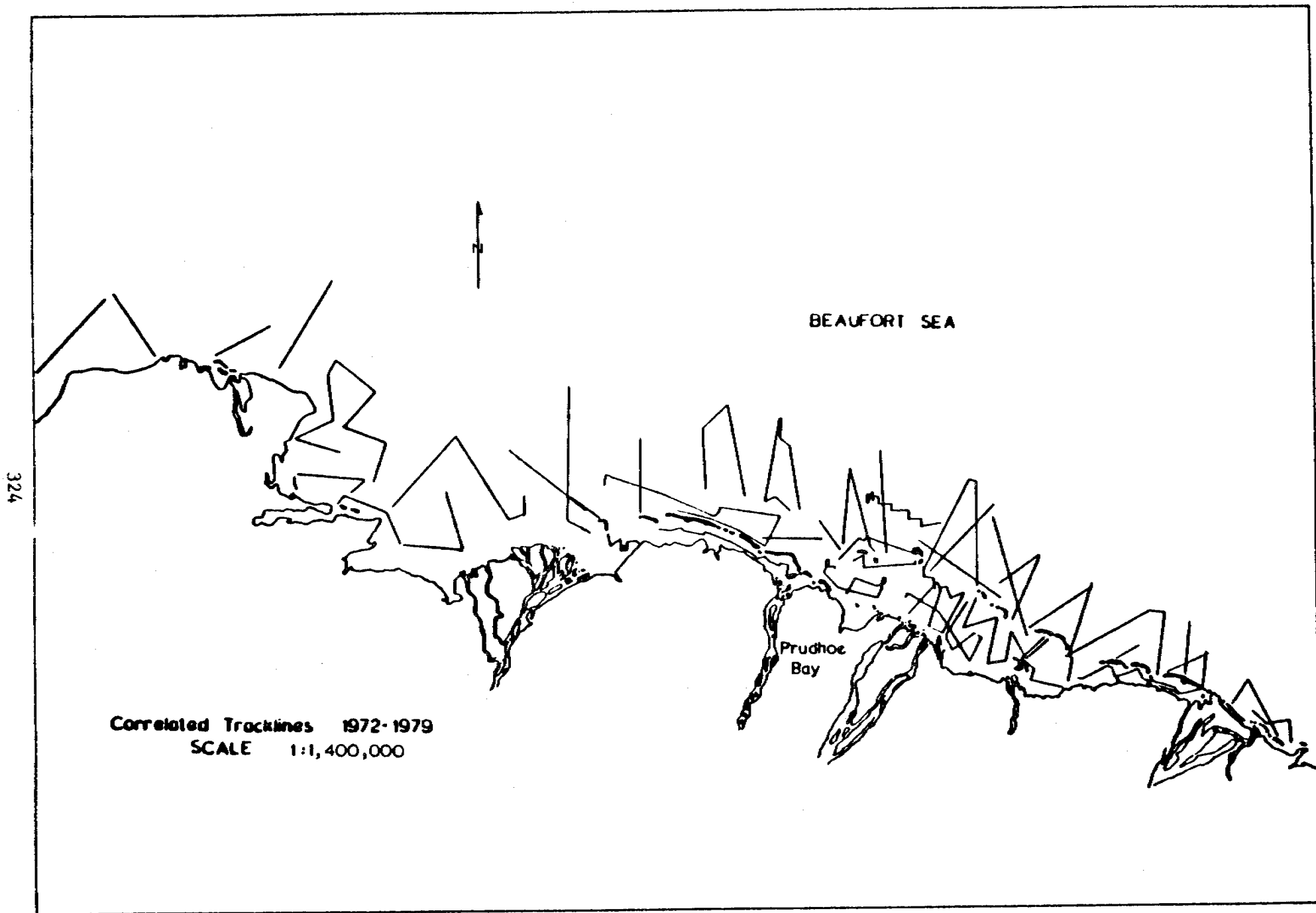


Figure 1. Correlated trackline coverage of the Beaufort Sea inner shelf.

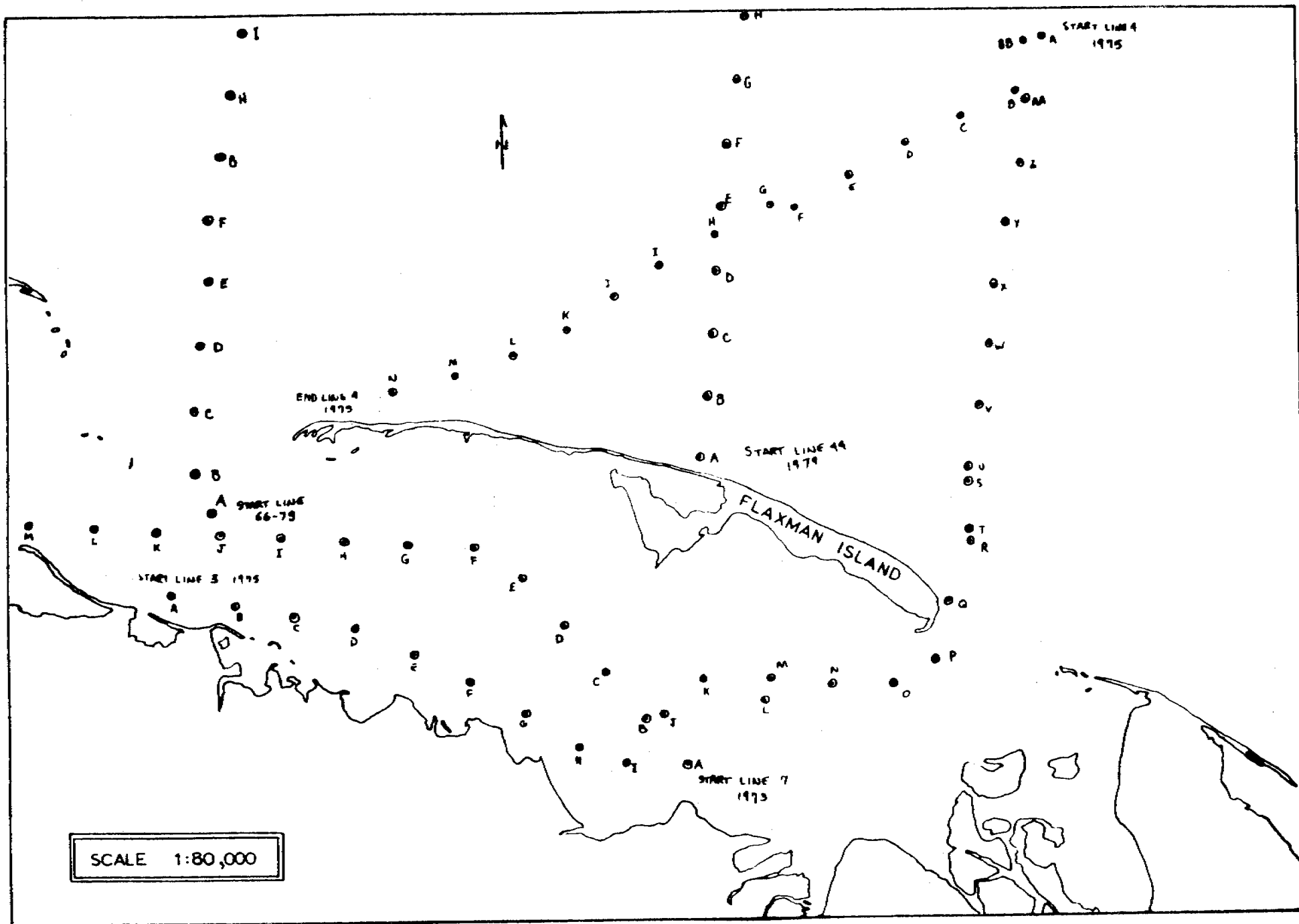


Figure 2. A small portion of navigation plotting sheet 1. - Flaxman Island. Segment points are plotted at one kilometer intervals along the trackline.



STATION		ICE GOUGE DATA RECORD															SEGMENT SCALE		VESSEL		REMARKS					
92																	1 1695		KARLUK							
DATE																	1.1524		4.0							
263																										
SEGMENT	KM	START TIME	START BIRTH	DIRECTION	WIND	TEMP	PRESS	HGT	DENSITY	CORRECTION	T	INCISION DEPTH DISTRIBUTION METERS											M	M	REMARKS	
												1	2	3	4	5	6	7	8	9	10	11				12
AB 1	11.0	11.8	9.5	35L	90	086	-	L	74	100	98	33	11	0	0	0	0	.3	11	.3	0	-	-	-	125	-20CM SWELL - DEPTHS ARE CORRECTED FOR SWELL. SWELLING IS FEINT RETURN DUE TO ORIENTATION.
BC 2	112.0	11.7	5.3		80	076	-	L	58	97	56	47	11	1	0	0	0	.4	5	.3	0	-	-	-	18.3	SMALL SWELL - THE TROUGH BETWEEN TRENCHES ARE OBSERVABLE SWELLING AND MAY BE FILLED WITH RECENT SEDIMENTS.
CD 3	1132.5	13.0	6.2		-	-	-	0	0	0	0	0	0	0	0	0	0	1.2	0	1.2	0	-	-	-	19.8	3 REVER SWELL AT 1440
DE 4	1142.0	13.5	7.2		130	126	-	L	5	108	5.4	5	1	0	0	0	0	.2	3	1.2	0	-	-	-	-	
EF 5	1150.6	15.0	8.2		115	141	-	L	5	120	6.4	5	1	0	0	0	0	.2	5	.2	0	-	-	-	22.0	
FG 6	1500.0	17.7	9.3		90	116	-	L	56	97	54	51	4	1	0	0	0	.5	12	.3	0	-	-	-	23.2	
GH 7	1506.6	20.5	10.3		100	076	-	L	110	97	106	97	11	2	0	0	0	.4	40	.5	1	2	25	031	2.8	
HI 8	1520.8	21.9	11.4		110	106	-	L	74	98	72	57	12	5	0	0	0	.4	12	.3	0	-	-	-	27.4	
IJ 9	1531.2	22.3	12.5		115	111	-	L	108	97	106	83	14	8	2	1	0	.8	18	.4	1	8	43	116	28.7	
JK 10	1541.0	23.1	13.6		120	116	-	L	96	98	94	73	21	2	0	0	0	.5	9	.4	0	-	-	-	-	
KL 11	1551.0	22.4	14.7		125	121	-	L	96	104	79	45	18	13	0	0	0	.5	6	.4	0	-	-	-	27.2	
LM 12	1601.8	22.1	15.8		115	111	096	L	127	99	125	100	17	9	0	1	0	.8	21	.9	3	4	22	131	28.2	
MN 13	1612.0	21.8	16.9		100	096	-	L	111	97	139	114	25	5	0	0	0	.5	10	.8	2	3	37	021	29.1	THE MARKS (2) WERE: 086" T 3: 100M
NO 14	1622.8	20.5	18.0		120	116	066	M	239	98	234	167	25	30	12	5	0	.9	20	1.0	6	12	58	126	27.5	4.5 METER BOWLS - VERY HIGH DENSITY BOWLS TO SEAWARD OF BRANCH. BRANCH IS AT POINT N.
OP 15	1631.2	23.0	19.1		125	121	076	L	165	104	171	96	22	20	16	9	2	1.2	10	1.2	6	4	32	126	-	HIGH DENSITY OF BOWLS CAUSE DIFFICULTY IN OBSERVING SWELL GOUGES AND POINTS. HIGHER GOUGES THROUGH OUT SWELL BOWLS.
PO 16	165.2	24.1	20.2		125	121	116	L	162	104	168	60	35	31	17	13	6	1.5	14	1.4	4	3	23	116	-	

Figure 3. Data sheet - page 1. of line 92-77. Note gouge character change at point N. See figures 6 and 7.

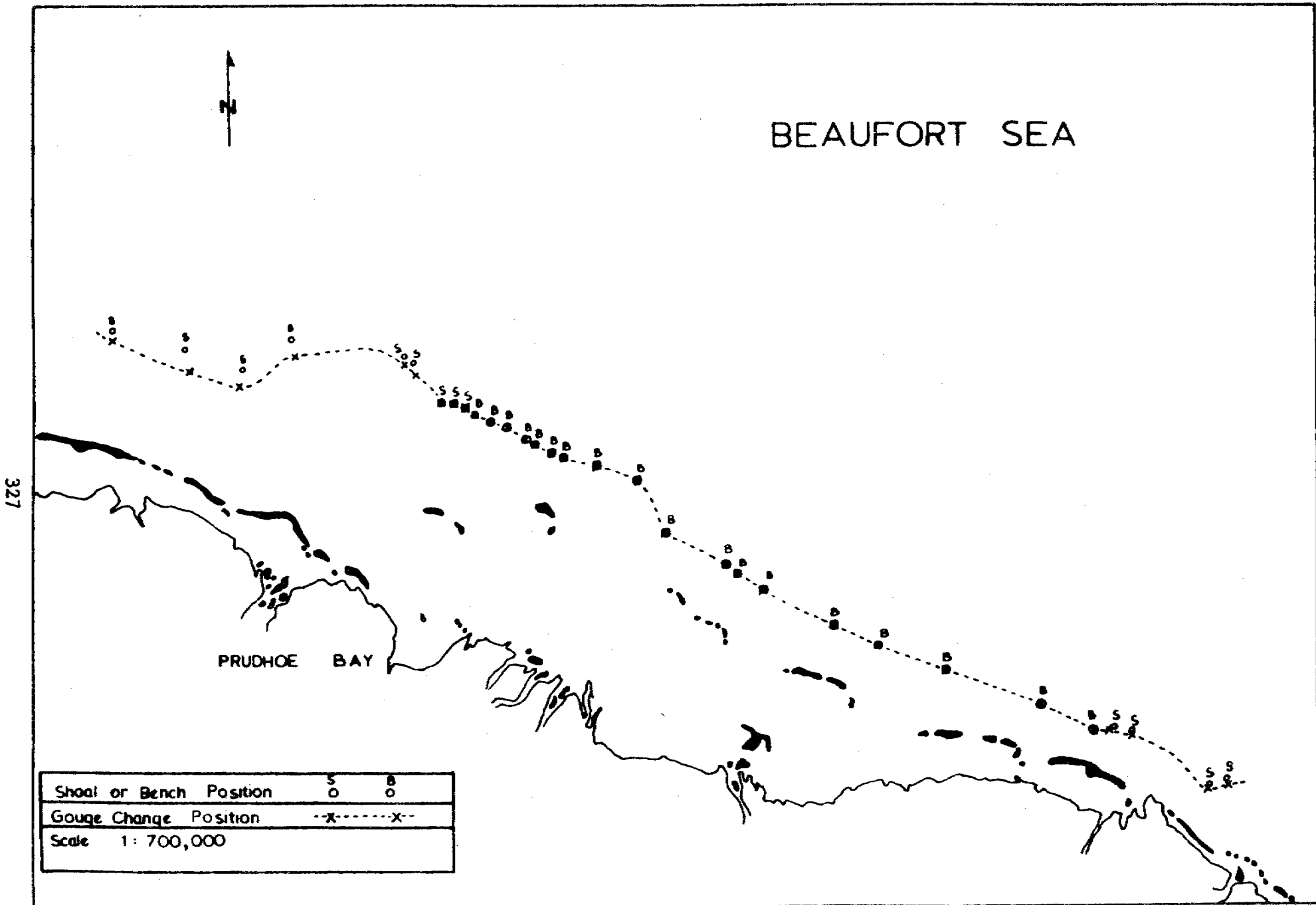
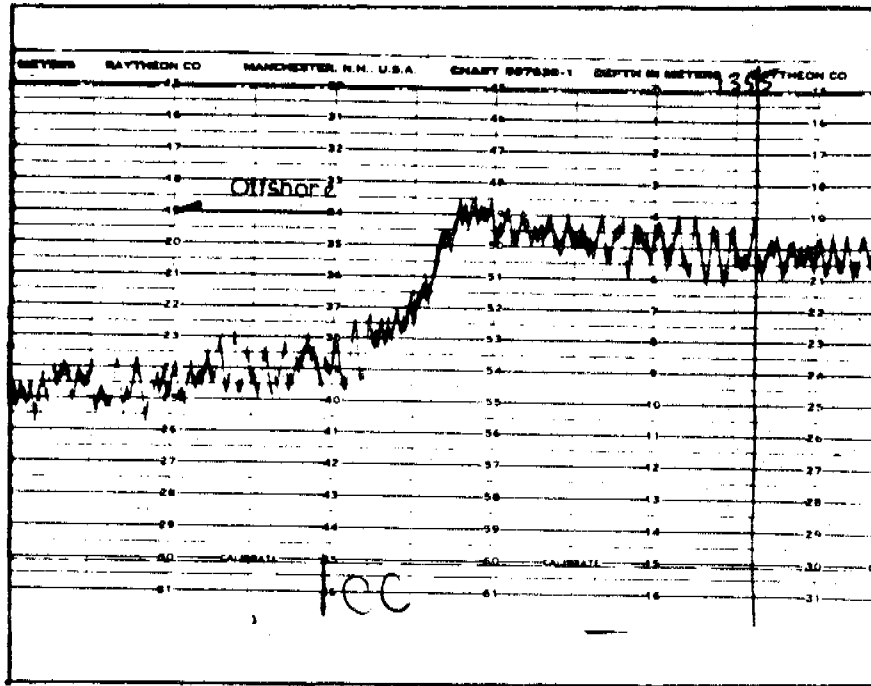
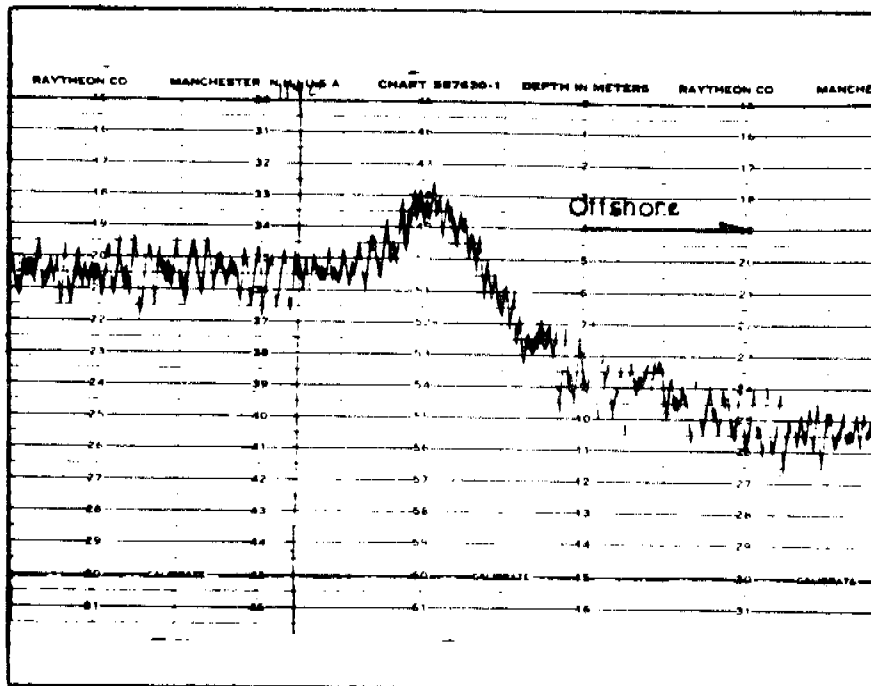


Figure 4. The 18 meter morphology boundary. The shoal position is its seaward extent.



A. BATHYGRAM OF BENCH



B. BATHYGRAM OF BENCH AND SHOAL

Figure 5. Bench morphology between Reindeer and Cross Islands.

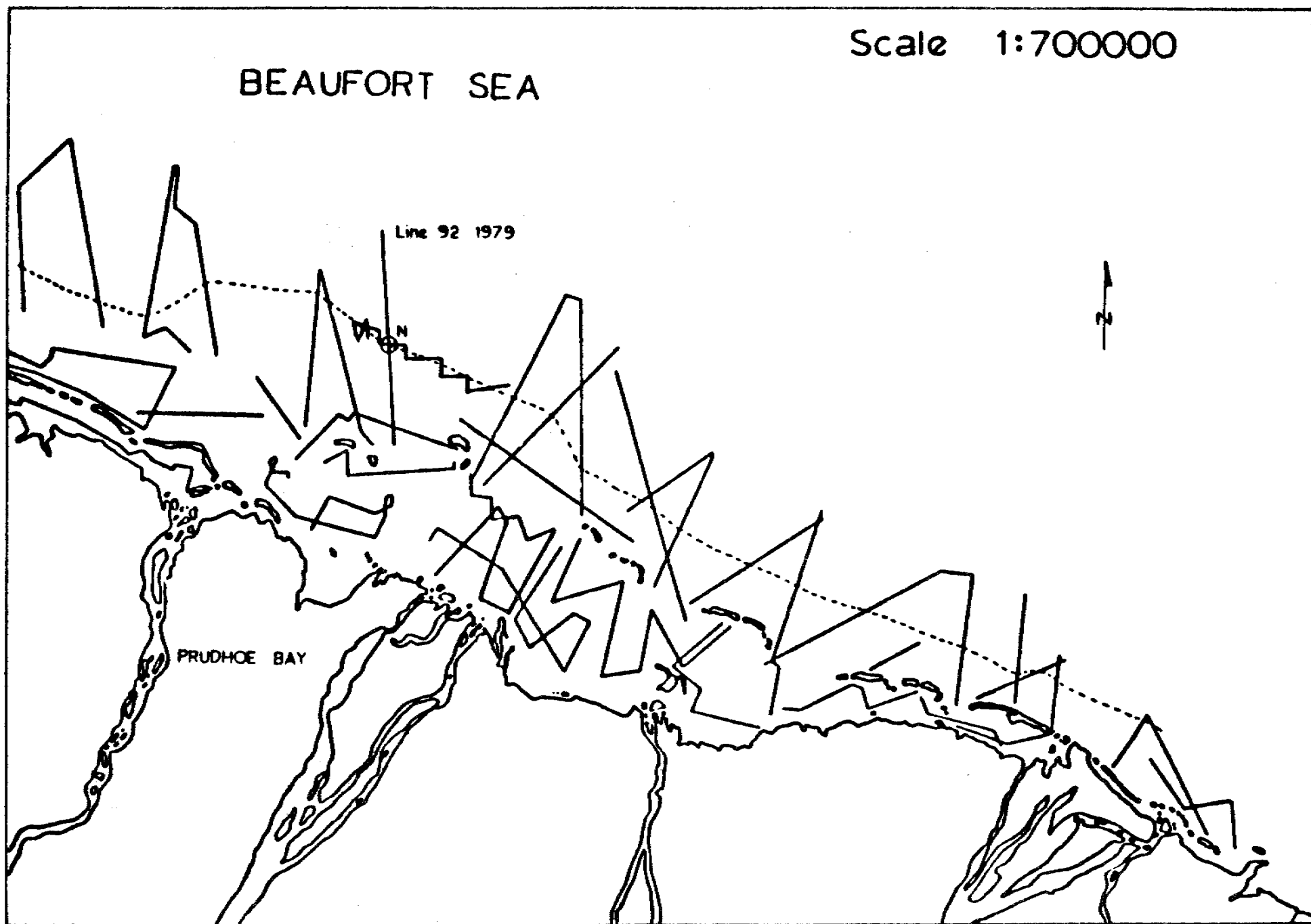
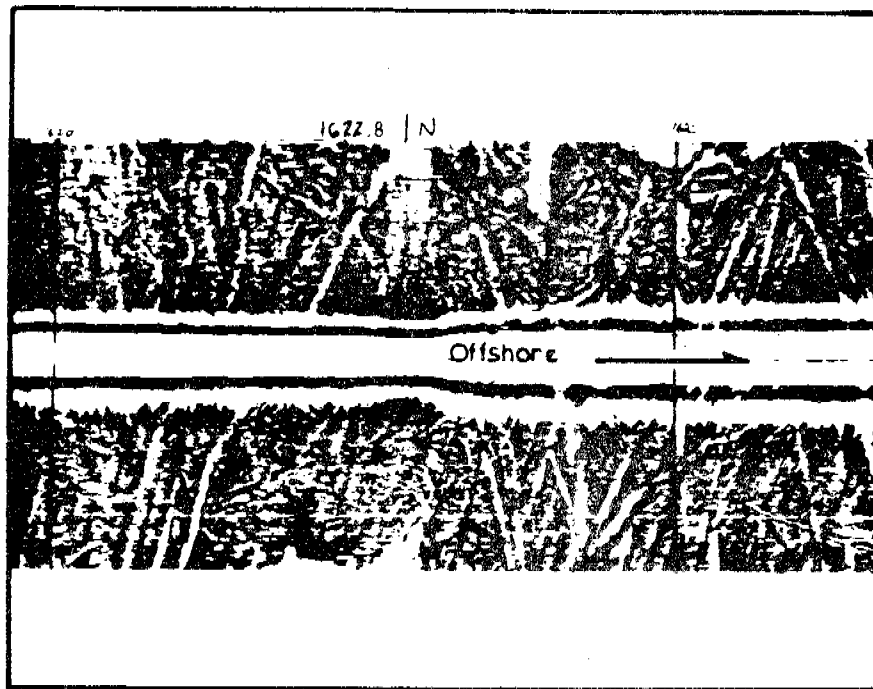
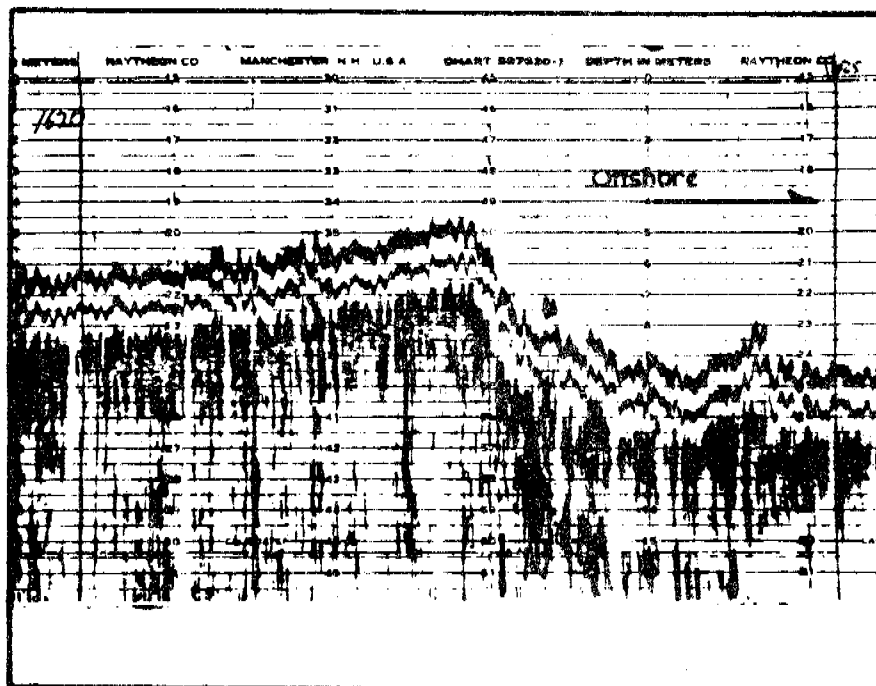


Figure 7. Ice young morphology boundary and related trackline coverage (see figures 5 and 7, point 7).



A. SONOTRAPH



B. BATHOGRAM

Figure 7. Sea floor and gouge morphology boundary - Line 02-70, point w.  
See figures 3 and 6, point N.

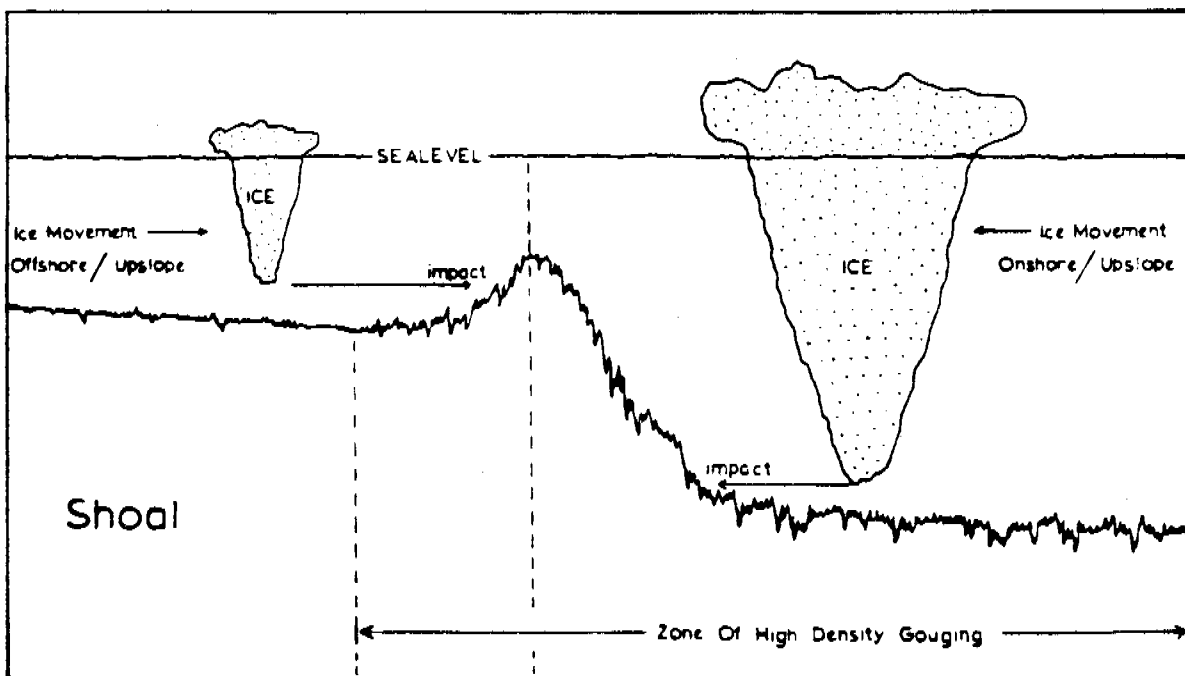
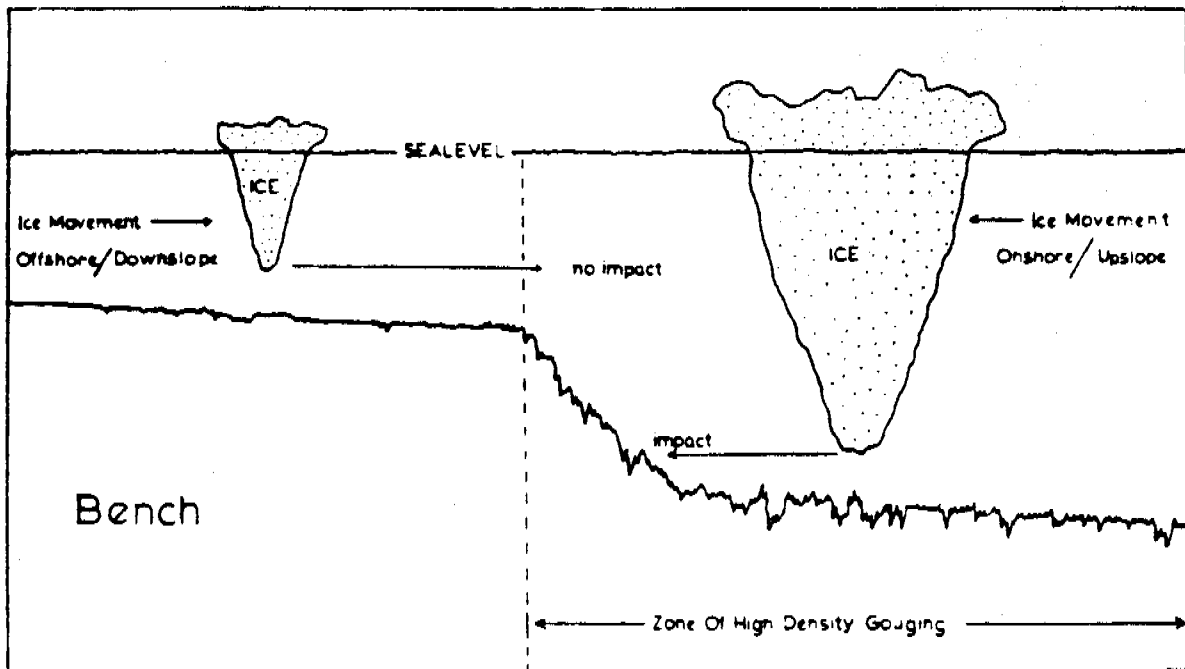
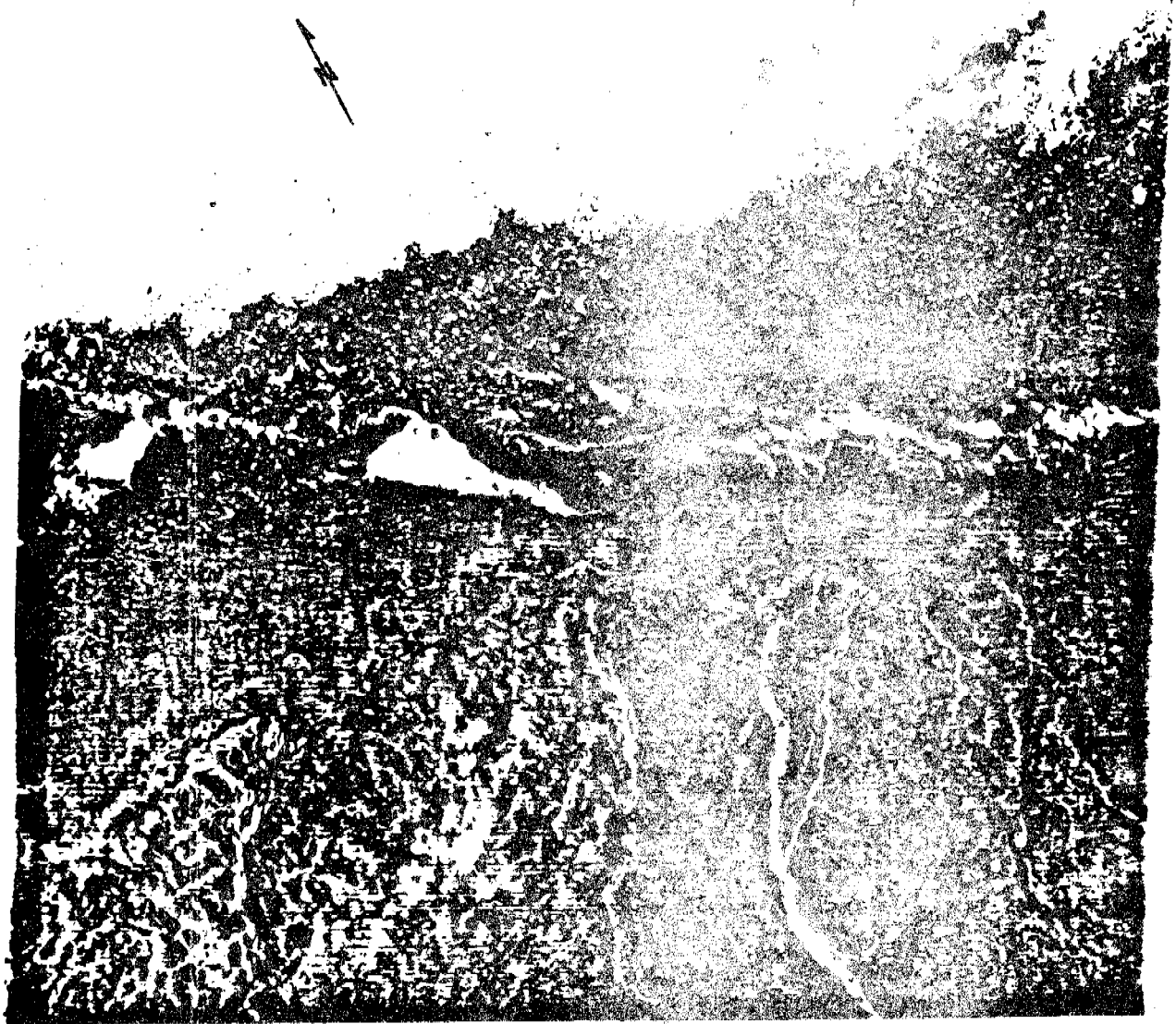


Figure 8. Ice gouge character change position as it relates to a bench and a shoal environment.

00038



PRUDHOE BAY

Figure 9. Landsat photograph of sea ice grounded on the 18 meter morphology boundary; Sept. 06, 1974.

## Attachment E

Break in gouge character related to ice ridges.

by Peter Barnes, Robin Ross, and Erk Reimnitz

### ABSTRACT

During the summer of 1979 a series of three precisely navigated side-scan sonar and bathymetry lines were run along well-located ice ridges observed in the spring of the same year. No obvious set of gouges lead up to the location of the ridge nor were gouges associated with the existing remnants of the ice ridges observed in summer. However, the innermost ice ridge of the stamukhi zone appears to correlate with a marked change in gouge character and to an abrupt change in bottom slope. The gouge orientation is essentially similar on both sides of the change. Diver observations coupled with vibracore sample data indicate that there is a decrease in the compactness of the surficial gravelly mud sediments on the seaward side of the slope and gouge change. Although the sediment textures are similar, there is a significant change in seabed character associated with the stamukhi zone. The cause and effect relationship between the ice zonation and the seabed character is well established; however the mechanisms for the abrupt nature of the break are unsure.

### INTRODUCTION

Previous studies have indicated or suggested a change of seabed and ice-gouge character associated with the stamukhi zone. Reimnitz and Barnes (1974) noted a small break in slope and an associated change in sediment character (Barnes and Reimnitz, 1974). The change in sediment character also correlates with a change in sedimentary structures (Barnes and Reimnitz, 1974). A change in ice-gouge character has been alluded to but never clearly associated with ice zonation (Brooks, 1974; Barnes et al., 1978).

During the summer of 1979 we became aware of the existence of data on the location of the ridges of the stamukhi zone (Reimnitz et al., 1978) in an area to the north of Narwhal Island (Fig. 1). These data, gathered from aerial photography, were kindly provided by researchers of the Shell Development Company of Houston, Texas. During the latter half of the summer season in 1979 exceptionally open-water conditions prevailed in the area of the ice-ridge data. Utilizing a precision navigation system, the remnant grounded ice features and seabed were studied in the vicinity of the stamukhi ridges previously located in the spring. This report is a preliminary interpretation of the relationships that were observed between spring ice ridges, grounded ridge remnants, seabed topography, and ice-gouge character.

### METHODS

Locations of the innermost shear ridge of the stamukhi zone and several other ridges seaward, along with major rubble piles, were located utilizing aerial photography. The accuracy of these locations is unknown but believed to be within 50 m. These positions were transferred to a UTM projection at a scale of 1:20,000 with a precision of  $\pm 20$  m. Summer navigation aboard the R/V KARLUK utilized a range-range navigation instrument accurate to 3 m and giving



positional accuracy to better than 10 m. Judging by the location of a major rubble field reported on by Hanson and Metzner (1979), whose position is unlikely to have changed from spring to summer, due to being heavily grounded, our summer positions were within 20 m of the ridges located in the spring aerial photography.

In addition to the navigational data, the following information was gathered. The location of many but not all grounded ice remnants was determined from shipboard navigation and a hand-held range finder. Bathymetry was obtained using a fathometer with a resolution of 20 cm, while seabed morphology was studied using a side-scan sonar on a 250-m-scan width. The particulars of these systems are given in Reimnitz and Barnes, 1974 and Barnes et al., 1978.

The seabed character was analyzed utilizing the sonographs and fathograms and the techniques outlined in Barnes et al., 1978., Data include maximum incision depth, orientaton, and bathymetry.

#### OBSERVATIONS-COMMENTS

Grounded ice remnants:

As shown in figure 2, summer observations of grounded ice along trackline 81 indicated that ridge remnants were still present for 5-10 percent of ridge length. This would suggest that a minimum of 5-10 percent of the spring ridge was also, considering the extensive melting and movement in the early part of summer, in contact with the bottom. Most of the remnants observed along this trackline extended less than 3 m above sea level, which suggests that in water depths of 18 to 20 m these remnants were not heavily grounded at the time of observation. We do not have information on the height of this ridge prior to the melt season.

These are the first observations we are aware of that strongly indicate that winter ridges are grounded and suggest that a minimal percentage of the ridges are resting on the seabed in winter. This data also documents the persistence of these grounded features well into the open-water season. Open water existed on the shelf outside of the 20 to 22-m contour at the time of the survey.

Bathymetry:

Maximum incision depths for ice gouges were taken from fathograms for 250-m segments of the three tracklines surveyed. The maximum observed gouge incision was 1.4 m. The most striking observation regarding these data is the abrupt change in maximum incision depths as one proceeds seaward along the tracklines. Associated with the increase in incision depths is a break in the bottom slope, which in this area takes the form of a steepening of the slope at about 18 m down to about 20 m. Elsewhere along this break the slope has been observed to be lesser and greater and often associated with a minor shoal (see Attachment D to this report).

Ice-gouge morphology (sonographs):

The general character of ice-gouge morphology was examined on the sonographs and found to be clearly different; undergoing a marked change associated with the change in bathymetry. Gouges become much crisper,

clearer, and more numerous on the seaward side of the observed bathymetric boundary. This change is illustrated in the sonographs illustrated in figure 3.

The orientations of the dominant gouge trend were determined for 250-m segments on either side of the boundary, using techniques given in Barnes et al. (1978). The trends in both areas are essentially the same--the largest portion of the gouges is parallel to the trend of the coastline and the bathymetric contours. There is an inconclusive suggestion that the gouges inshore of the break in slope are oriented more east-west and the gouges on the seaward side oriented more north-south. These relationships are summarized in figure 4.

#### Sediment character:

Vibracores taken across this boundary indicate an extremely tough seabed. Of four attempts to vibracore in 1978, only one sample was recovered and that was from the seaward side of the boundary (Barnes et al., 1979). The successful core recovered 50 cm of a poorly sorted mixture of gravel- to clay-sized material which was noted to be very highly compacted. Two attempts to vibracore in 1979 were also unsuccessful in penetrating or recovering cores.

Diver observations confirm and amplify the coring observations. Two dives were made by one of the authors (E.R.), one inside and one seaward of the boundary in the general area of this study. The dive on the higher inshore part of the bench revealed a smooth undulating surface of compacted muddy gravels with clasts to at least 10-cm diameter. There was no evidence of any recent ice gouging. Furthermore, hydroids and other seabed critters were common. On the seaward side of the bench the seabed was obviously more recently disrupted although the gravelly muds indicate that the sediments on both sides of the boundary are the same. Softer reworked sediments were encountered on the seaward side, although blocks, slabs, and outcrops of highly consolidated material were common.

The ice distribution observed during the period of these dives presented an enigma as high concentrations of grounded ice features including ridges tens of meters long occurred inshore of the bench, while seaward of the bench was essentially clear of ice.

#### DISCUSSION

The principal question to be discussed is whether the seabed morphology is related to the observed sea-ice ridging. The observations are suggestive but inconclusive at present.

Reimnitz et al. (1978) proposed an ice zonation of the inner Beaufort Sea shelf that includes an accretionary grounded ridge system, called the *stamukhi* zone, whose inner boundary occurs at the approximate position of the observed change in seabed character. Thus the inner ridges observed in the spring of 1979 and those grounded ridge remnants noted during the present survey represent parts of the *stamukhi* zone. If the location of the *stamukhi* zone were reasonably repetitive over tens or hundreds of years, as is suggested by the controlling mechanisms (Reimnitz et al., 1978), the seabed under this zone should be more intensely reworked due to the abundance of ridges and grounded features associated with this zone. If this were the case then the reworked

and deeply scoured and eroded area seaward of the break in slope would represent an area where repetitive ice keels of the stamukhi zone had bulldozed, resuspended, and reworked sediments to a greater extent than in the area onshore from this zone.

The 1979 observations are inconclusive with regard to the above hypothesis. Indeed, the major ridging, as outlined in the aerial photographic survey, is oriented approximately parallel to the break in slope-gouge character, but in reality cuts obliquely across the boundary from north to south (Figs. 1 and 2). Similarly, the grounded ridge fragments noted in summer also cut across this boundary (Fig. 2). This would suggest that the boundary should be less pronounced than observed as the inner edge of the stamukhi is not clearly associated with the seabed boundary. The location of the grounded ice ridge fragments further suggests modern ice gouging should be clearly present inside of this boundary. Neither the sonographs nor the diving observations suggest a gradational boundary nor well-defined modern gouges. Furthermore the summer distribution of grounded ridge features--at least in 1979--was clearly dominated by grounded features inside of this boundary, whereas the hypothesis would be better served if the major grounded features were further seaward, as in the case of the stamukhi at Stamukhi Shoal (Reimnitz and Maurer, 1978).

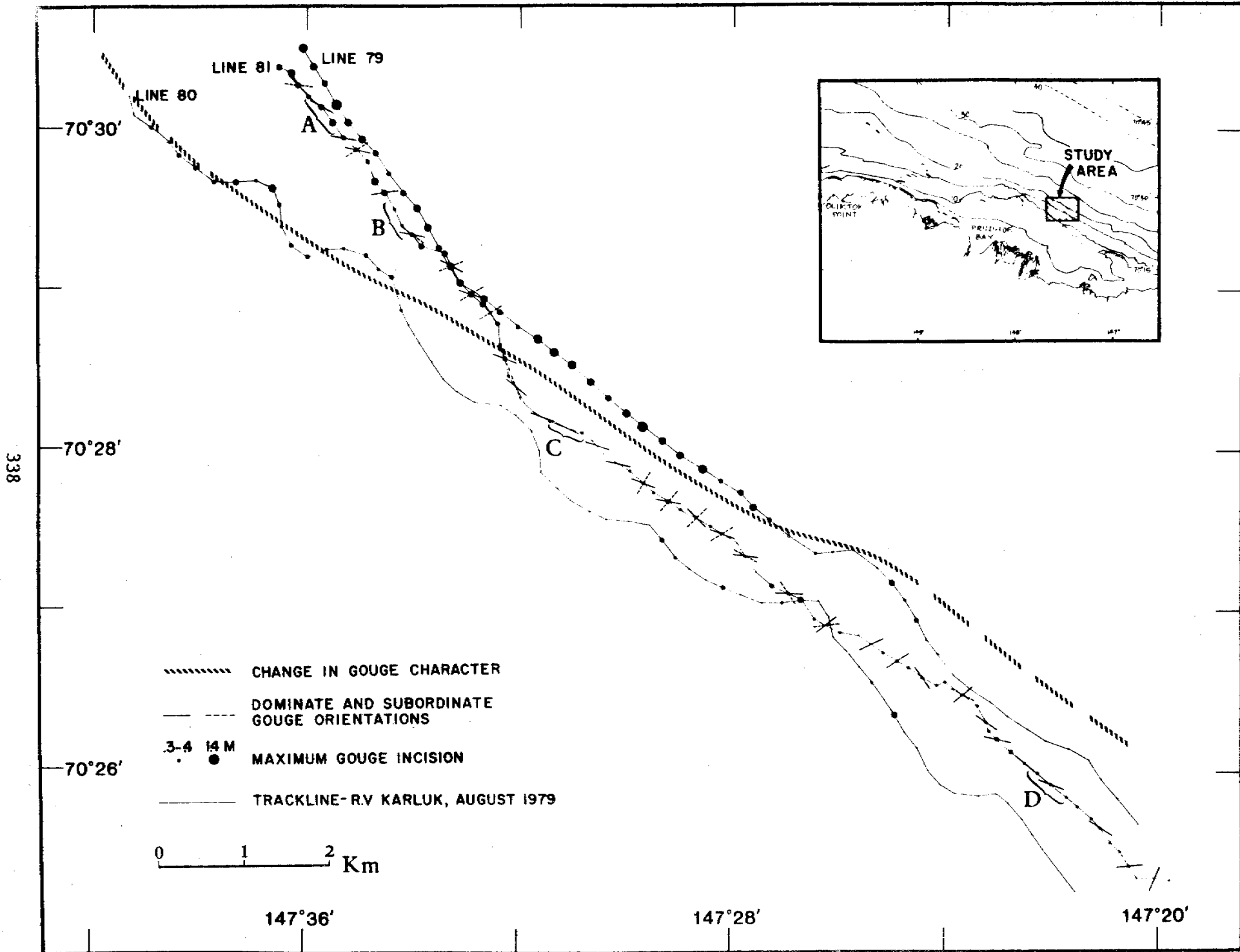
#### CONCLUSIONS

- 1) A series of ice ridges grounded during the winter and spring of 1979 north of Narwhal Island. Five to ten percent of these ridges were encountered as grounded remnants in August 1979, suggesting a minimal value for the amount of the ridge grounded in winter.
- 2) The ridging appears to be associated with a marked change in seabed topography and ice-gouge morphology. A 1- to 3-m-high break in slope separates an onshore area of subdued and shallow gouge incisions in a compact gravelly mud from an offshore area of crisp, deeply incised gouges cut into soft to compact gravelly muds. Gouges in both areas are essentially coast-parallel.
- 3) An explanation using a direct association of the ridging with the abrupt change in seabed character is hindered by observations of seabed character, the location of the 1979 ridges cutting across the boundary, and the summer 1979 distribution of grounded ice features.
- 4) The similarity of seabed sediments, the orientation of the gouges as well as the intensity of the gouges on the seaward side of the boundary strongly suggest that slope break and seabed character are the result of ice gouging. The boundary also appears to be clearly related to the location of the stamukhi zone. However, the factors causing the boundary to be abrupt and well-defined remain an enigma.

FIGURES 1 AND 2

Figure 1. Ice gouge character along lines 79, 80, and 81. Maximum gouge incisions are taken from fathograms. Dominant and subordinate gouge orientations were measured on the sonograph from trackline 81. The change in gouge character was determined from both sonographs and fathograms. Photographs from sections of the sonograph from Line 81 are represented by letters and are shown in figure 3.

Figure 2. Map of same area as figure 1. Grounded ice remnants were located in August, 1979. These compare with ice ridges drawn using data obtained from Shell Development Company. Depth contours were determined from 1979 fathograms.



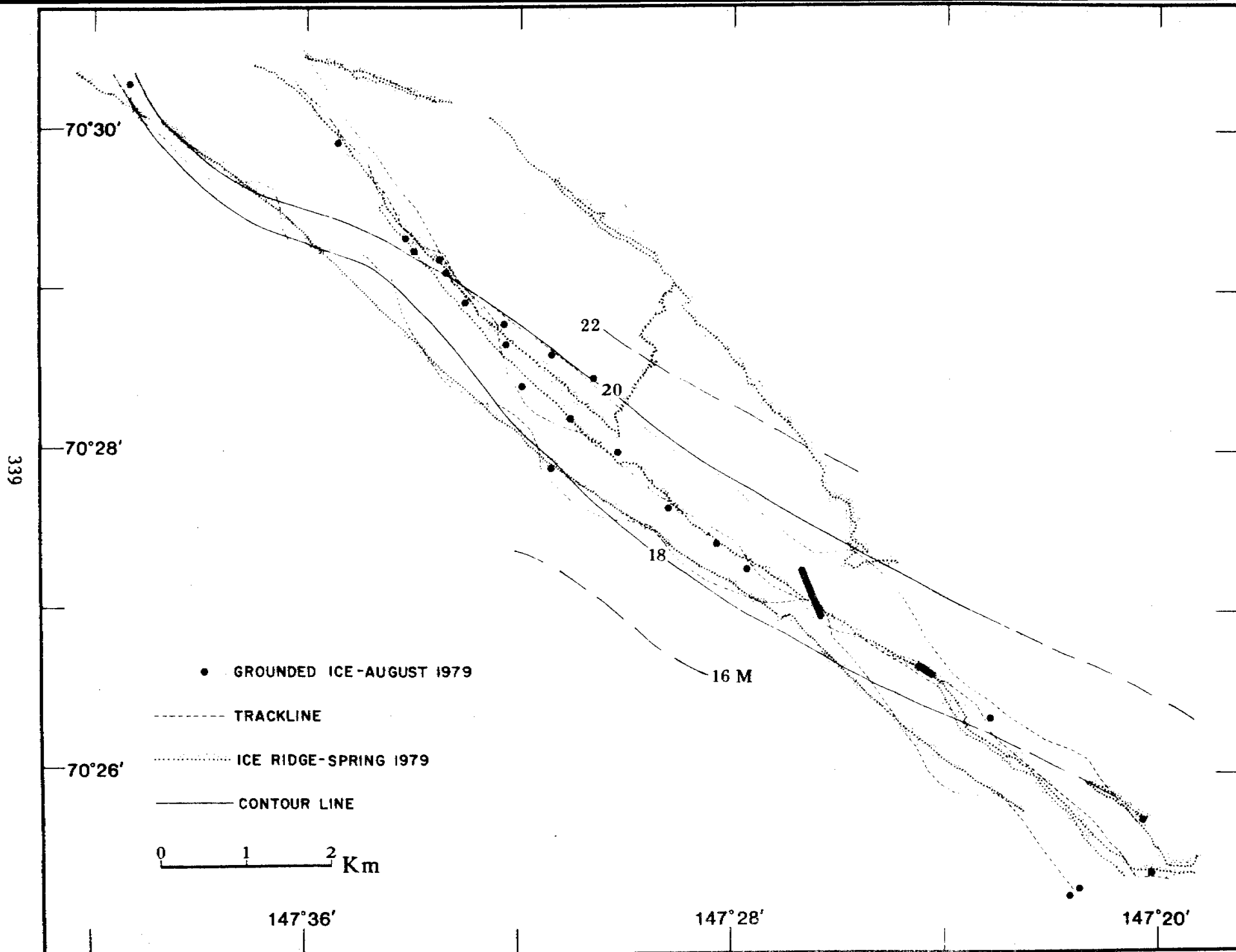


Figure 2.

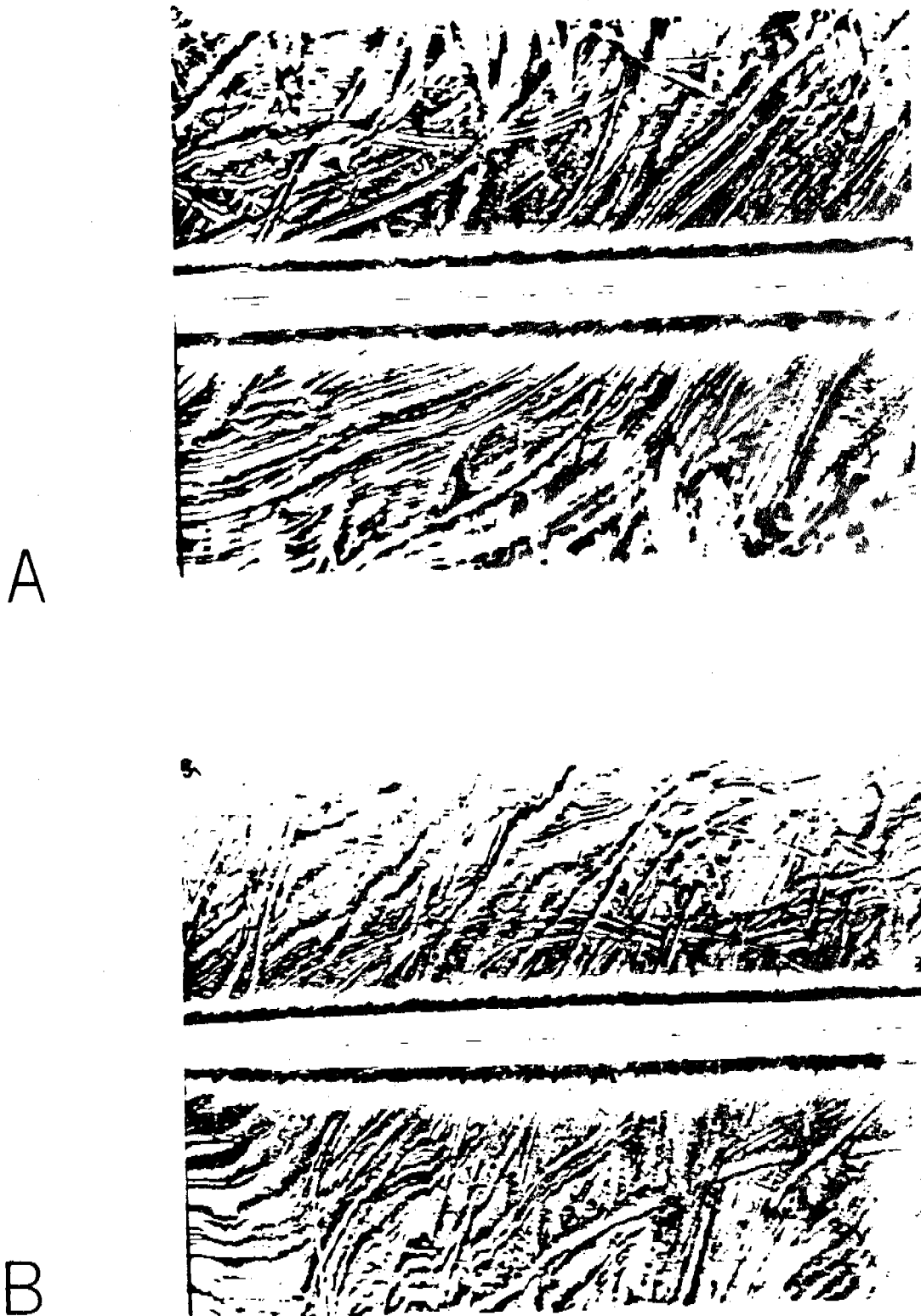
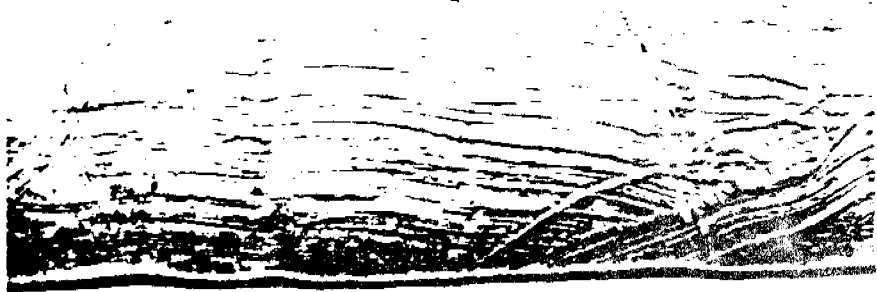
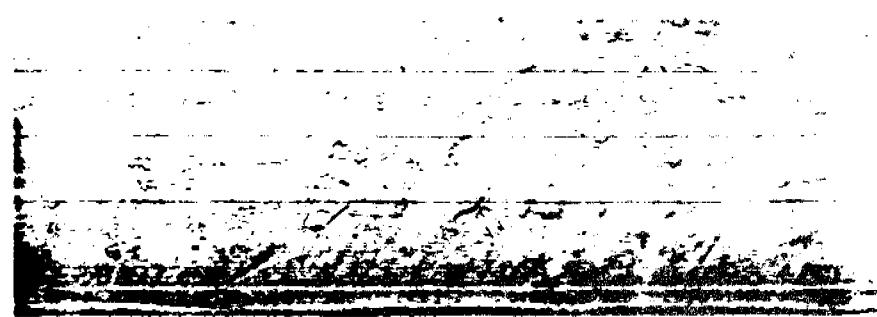


Figure 3. Sonographs of seabed morphology along trackline 81. A and B are taken of the seabed seaward of the boundary. C and D illustrate the subdued seabed character typical of the bench area inshore from the boundary.



C



D

Figure 3.



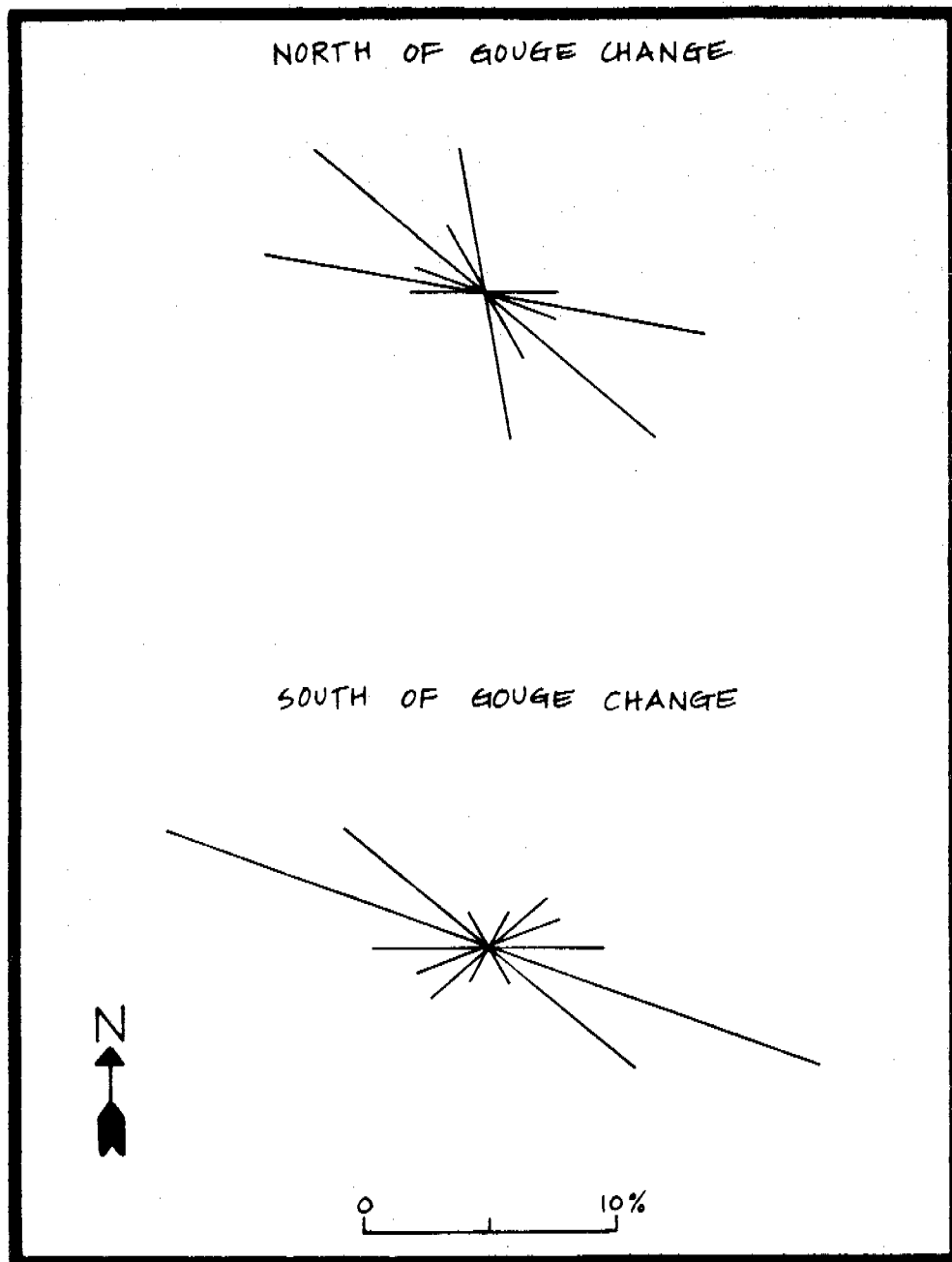


Figure 4. Dominant orientations of gouges measured north and south of the change in gouge character. Bar shows the percent of the total number of gouge orientations in  $30^{\circ}$  segments.

#### REFERENCES

- Barnes, P.W., and Reimnitz, Erk, 1974, Sedimentary processes on arctic shelves off the northern coast of Alaska, in: Reed, J.C., and Sater, J.E., (eds.), The Coast and Shelf of the Beaufort Sea, Arctic Institute of North America, Arlington, Va., p. 439-576.
- Barnes, P.W., McDowell, David, and Reimnitz, Erk, 1978, Ice gouging characteristics: their changing patterns from 1975-1977, Beaufort Sea, Alaska, U.S. Geological Survey Open-File Report 78-730, 40 p.
- Barnes, P.W., Reimnitz, Erk, Toimil, Larry, Maurer, Douglas, and McDowell, David, 1979, Core descriptions and preliminary observations of vibracores from the Alaskan Beaufort Sea shelf, U.S. Geological Survey Open-File Report 79-351, 71 p.
- Brooks, L.D., 1974, Ice scour on northern continental shelf of Alaska, in: Reed, J.C., and Sater, J.E., (eds.), The Coast and Shelf of the Beaufort Sea, Arctic Institute of North America, Arlington, Va., p. 355-366.
- Hanson, Arnold and Metzner, Ronald, 1979, Forty-meter ice pile in the proposed Beaufort Sea lease area, Abs. Alaska Science Congress, 1979.
- Reimnitz, Erk, and Barnes, P.W., 1974, Sea ice as a geologic agent on the Beaufort Sea shelf of Alaska: in: Reed, J.C., and Sater, J.E., (eds.), The Coast and Shelf of the Beaufort Sea, Arctic Institute of North America, Arlington, Va., p. 355-366.
- Reimnitz, Erk, and Maurer, D.K., 1978, Stamukhi shoals of the arctic--some observations from the Beaufort Sea, U.S. Geological Survey Open-File Report 78-666, 17 p.
- Reimnitz, Erk, Toimil, L.J., and Barnes, Peter, 1978, Arctic continental shelf morphology related to sea-ice zonation, Beaufort Sea, Alaska, Marine Geology, v. 28, p. 179-210.

## Attachment F

### Super sea-ice kettles in the arctic nearshore zone - Reindeer Island

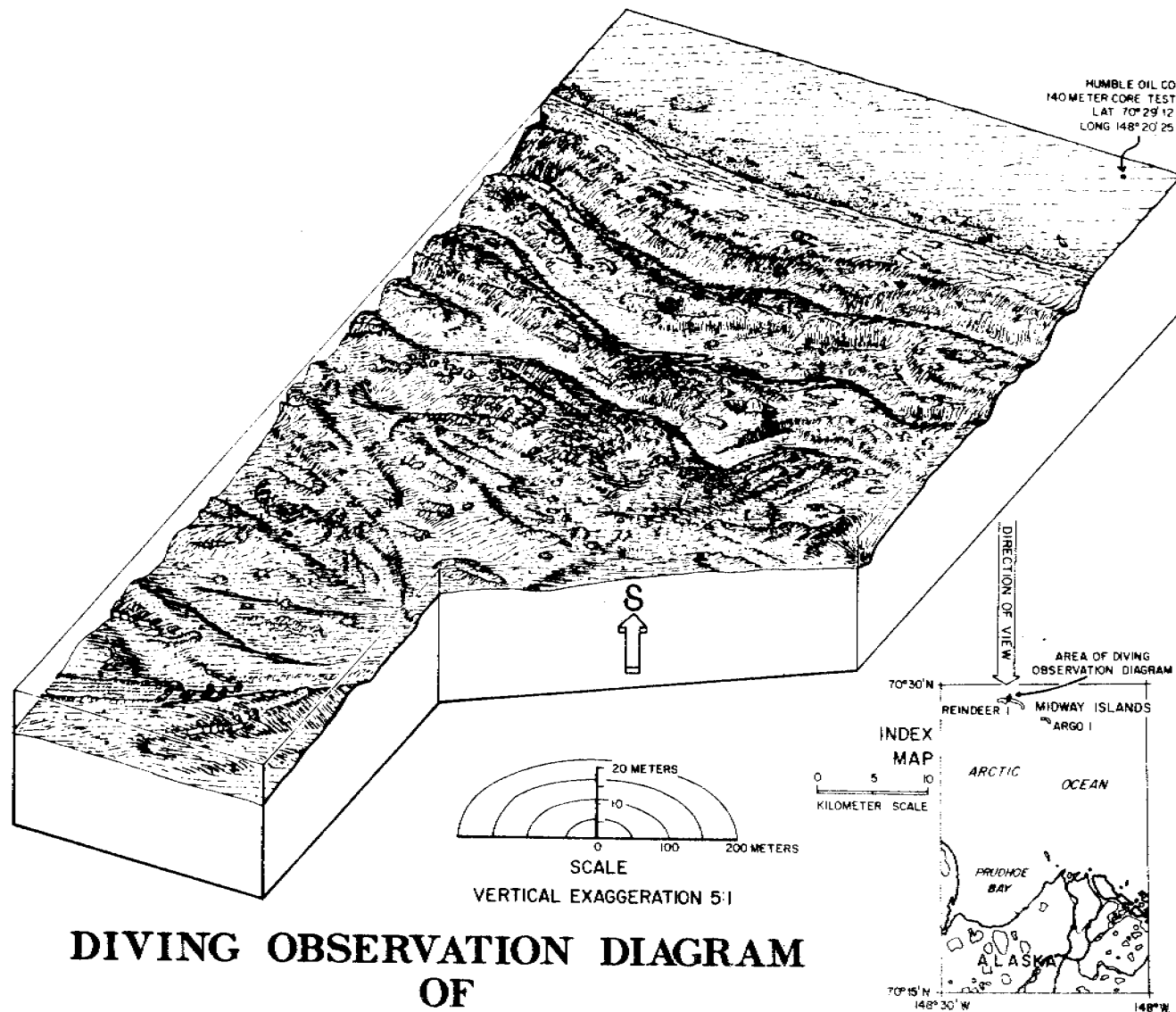
by Erk Reimnitz and Ed Kempema

#### INTRODUCTION

Broad, undulating, non-linear relief forms of the arctic nearshore environment have presented problems in drawing depth contours for coastal charts. The origin of these relief forms, which differ greatly from typical ice-gouged relief, has remained obscure for many years (Reimnitz et al., 1972). Recently, detailed, repetitive bathymetric surveys using accurate navigational controls have been used in a small area off Reindeer Island to delineate major closed depressions and isolated knolls. These detailed surveys reveal major changes in relief over a period of three years. We can now be certain that the major bedforms are produced by current- and wave-erosion and deposition around grounded ice during high-energy events in the nearshore zone. The findings presented here will be of importance to design of pipelines connecting offshore wells with onshore transportation systems, where similar environments must be crossed.

#### METHODS

Our first bathymetric survey of the Reindeer Island nearshore area was made in 1972. That survey was run on previously established shore ranges at 100-m line spacing, referenced to a test-well casing on the island. The fathometer used provided resolution of 0.25 to 0.5 m depth changes. The distances from shore were established by radar ranges to the baseline on the island. The bathymetric survey was correlated with eight diving traverses made during the same summer. The methods of study and results of the study were presented in detail by Reimnitz and Barnes (1974). A physiographic diving observation diagram made by Tau Rho Alpha summarizes the findings and is presented here as figure 1. The next bathymetric survey was run in 1976, when we used a Del Norte Trisponder navigation system giving ranges accurate to  $\pm 5$  m. The ranges were recorded on magnetic tape. The shore stations are located at the Reindeer Island well head (used previously) and on the Cross Island Racon tower. Depths were recorded with a precision survey fathometer with resolution of 10 to 20 cm. The ranges and depths were digitized and computer-plotted. A printout of tracklines surveyed is shown in figure 2. The third survey of the Reindeer Island area was made in 1979. Essentially the same methods and equipment were used as in the second survey. Part of the navigation data were recorded at 10-sec intervals on magnetic tape and plotted by computer. Water depths were entered manually on this plot. Several additional survey lines run later in the season through the same area were also plotted manually (on UTM-grid) from paper printout of ranges. Water depths were entered manually on this plot. The depths at line crossings from the two surveys, run about four weeks apart, match precisely and we are confident of the accuracy of these data. A copy of the 1979 trackline coverage is shown in figure 3.



## DIVING OBSERVATION DIAGRAM OF REINDEER ISLAND

BY

TAU RHO ALPHA ERK REIMNITZ CRAIG RODEICK ANDREW D. OESTERLE

Figure 1. Diving observation diagram of an area north of Reindeer Island. Bathymetry is based on closely spaced sounding lines surveyed in 1972. Smaller bottom features are generalized from numerous diving traverses. (From Reimnitz and Barnes, 1974).

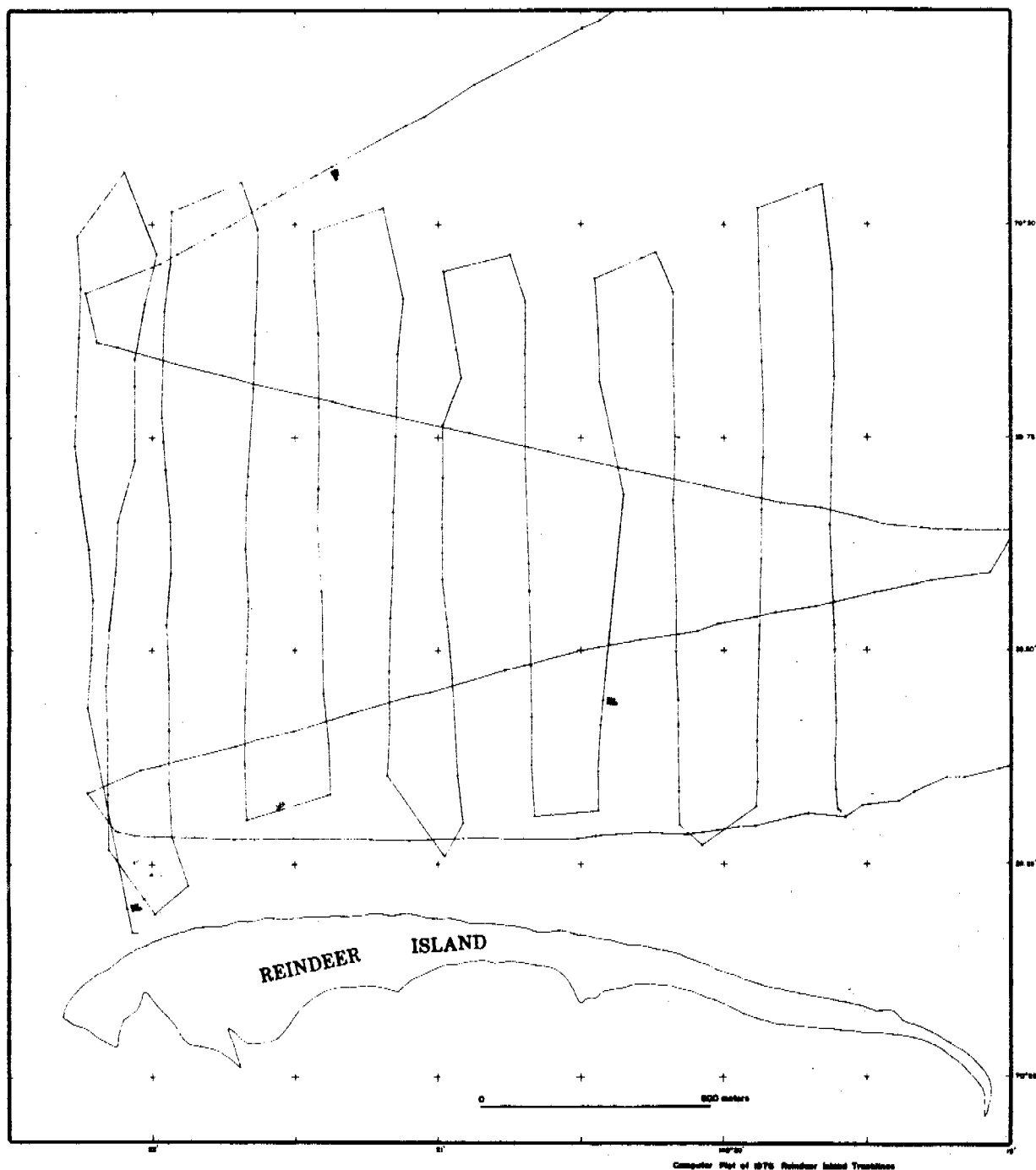


Figure 2. Bathymetric survey tracklines of 1976. Shoreline as surveyed in 1978.

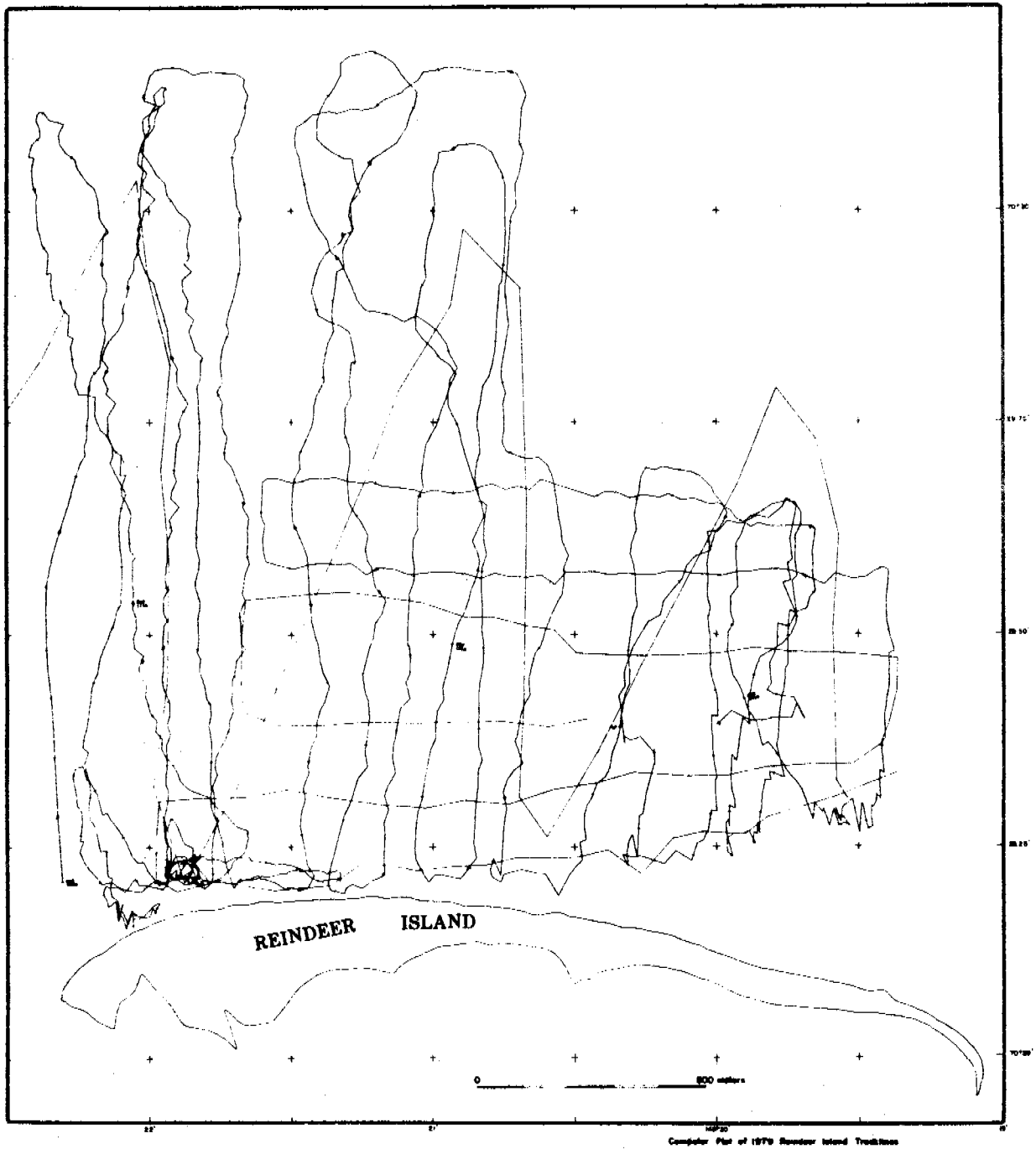


Figure 3. Bathymetric survey tracklines of 1979. Blank area in upper right due to dense pack ice. Shoreline as surveyed in 1978.

## RESULTS

The water depths measured in the last two precision surveys are contoured at 0.5 m intervals (Figs. 4 and 5). The 1972 bathymetry depicted in figure 1, while internally coherent, cannot be accurately matched to the two recent surveys, because of differences in survey techniques. However, figures 4 and 5 can be matched accurately and discrepancies in water depth and morphology represent changes that occurred during the three-year period between surveys. The greater complexity of bottom relief in 1979 is due to a denser survey net.

A well-developed set of shore-parallel bars, depicted in the 1972 interpretation of 1972 survey data (Fig. 1), was not present during surveys in 1976 and 1979. We confess trying to push our artistic license in contouring in order to show parallel bars, because the grounded ice in the area generally aligns parallel to the beach. This alignment is shown in an aerial photograph of Reindeer Island (Fig. 6) taken in late September 1976, after the bathymetric survey had been completed. The area is instead characterized by an irregular and complex pattern of closed depressions and isolated knolls with relief of 2 to 3.5 m.

In comparisons of figures 4 and 5, considerable changes are evident. As an aid to understanding the changes, figure 7 focuses on two small sectors, A and B, (see figures 4 and 5), which are shown side by side with tracklines at the scale of original work sheets. Sectors A and B both show semi-circular "pot holes" in 1976 that cannot be found again in 1979, while a new depression of about 2.5 m depth was formed in the western part of sector A. The overall bottom morphology in 1976 appears to be dominated by isolated knolls, whereas pot-holes dominate the area in 1979.

## INTERPRETATION AND CONCLUSIONS

Sandy nearshore environments not dominated by the presence of ice are generally characterized by seaward sloping bottoms with or without slope reversals at longshore bars and have little relief in shore-parallel profiles. Isobaths are therefore parallel to the shoreline. In arctic seas similarly shaped bottoms are also found nearshore (i.e. Short et al., 1974, and Attachment B of this report). However, the type of seafloor dominated by large-scale potholes and mounds, as observed in our surveys off Reindeer Island, is equally common. Where survey tracklines are widely spaced such areas can be contoured only by drawing wiggly lines. The repetitive detailed studies off Reindeer Island allow an interpretation of the origin of these bedform patterns.

The nearshore bedforms undergo drastic changes over periods of only three open-water seasons and therefore are highly active seafloor features. These certainly are not produced by any process of ice-gouging or bulldozing as discussed by Reimnitz et al. (1972) and Reimnitz and Barnes (1974). A process of sediment adfreeze to longterm grounded ice floes followed by rip-out of bottom material on the scale of the large potholes resulting when floes are dislodged has ever been documented. Such a process probably can be ruled out entirely as a possible mechanism. Based on our observations and other published reports, all large volumes of sediment on floating ice can be explained in other ways. These considerations eliminate direct action of ice

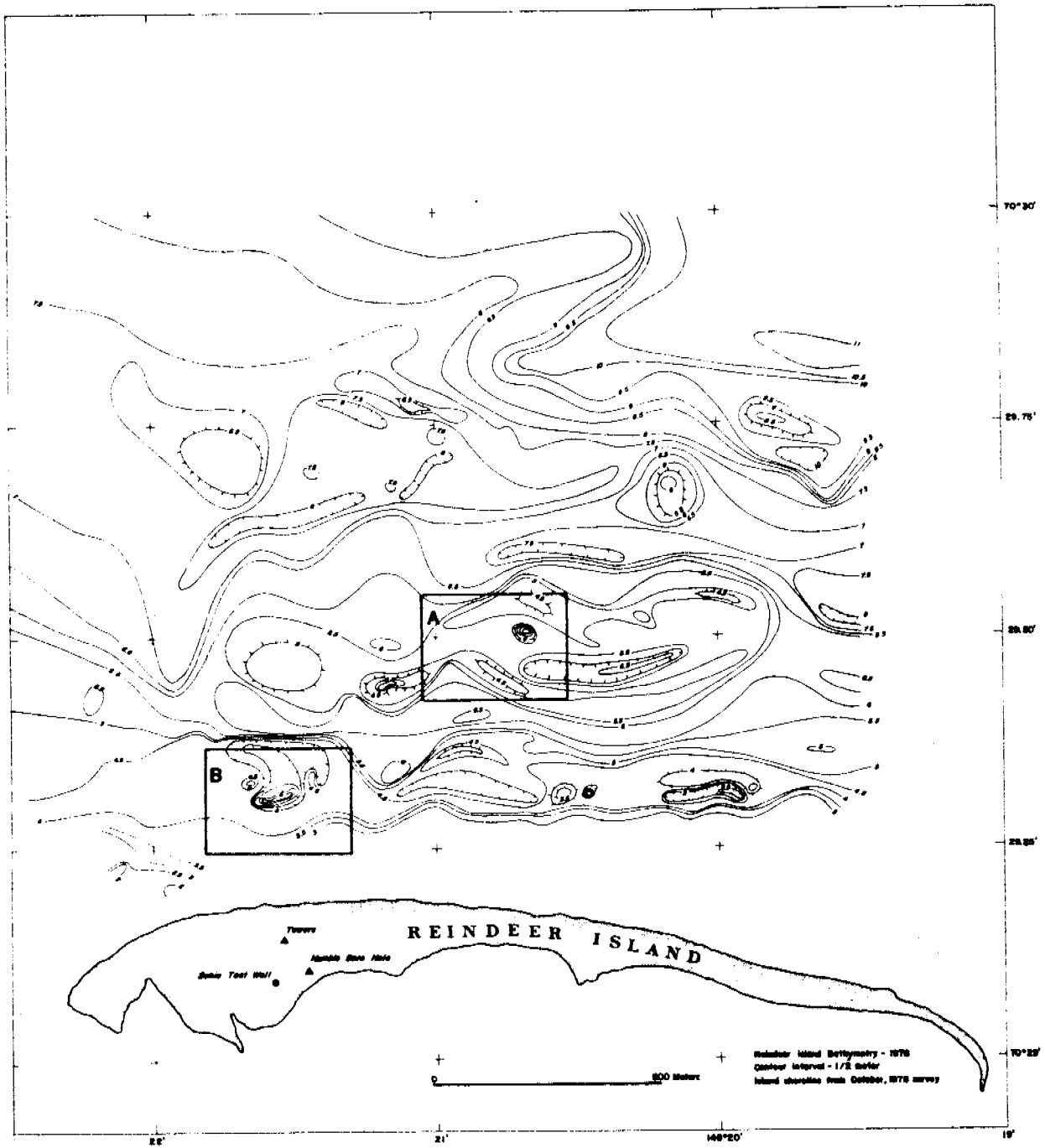


Figure 4.



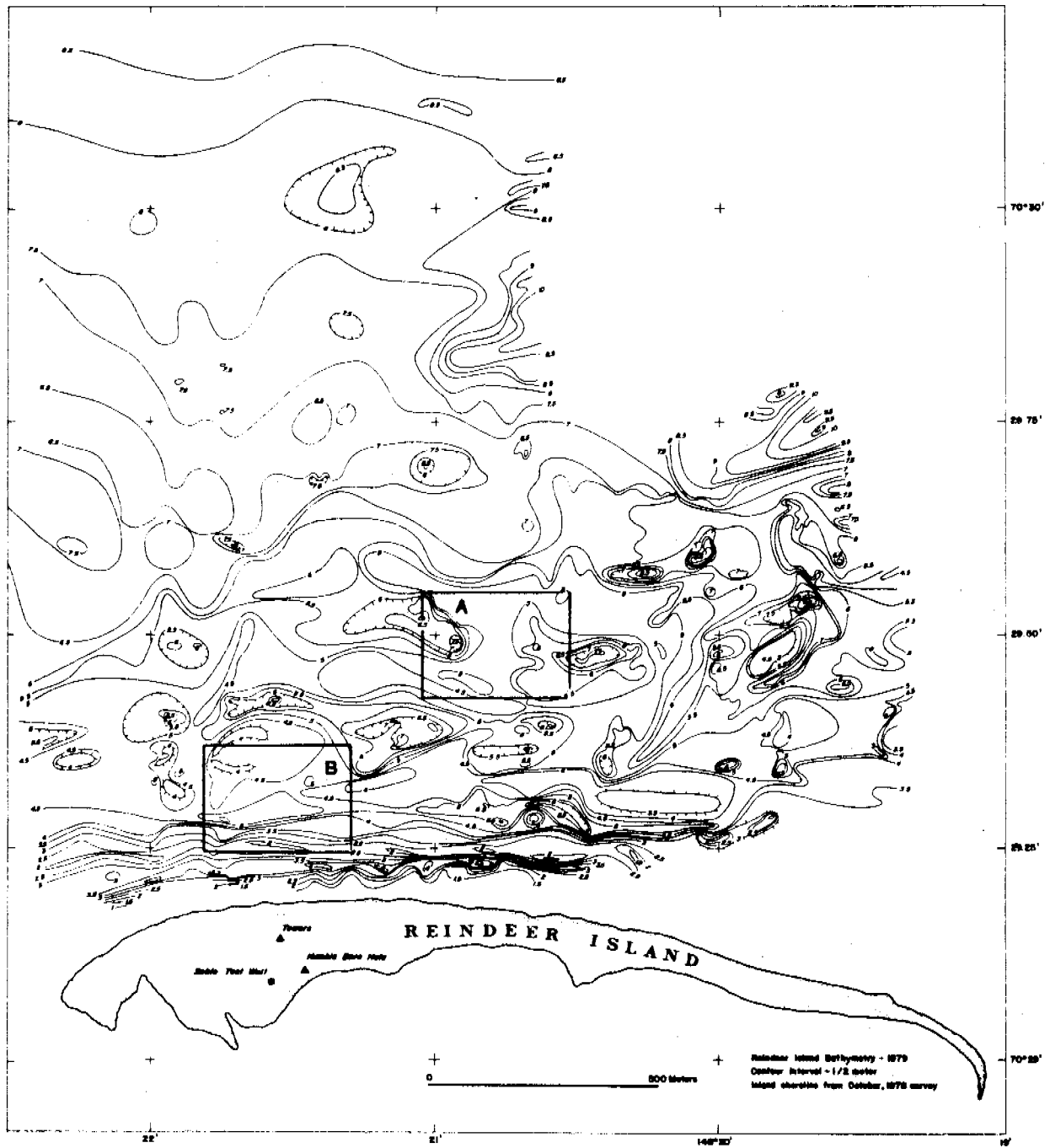
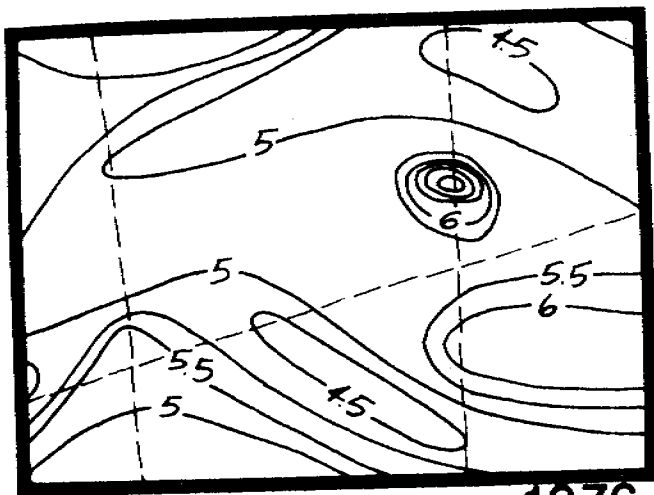


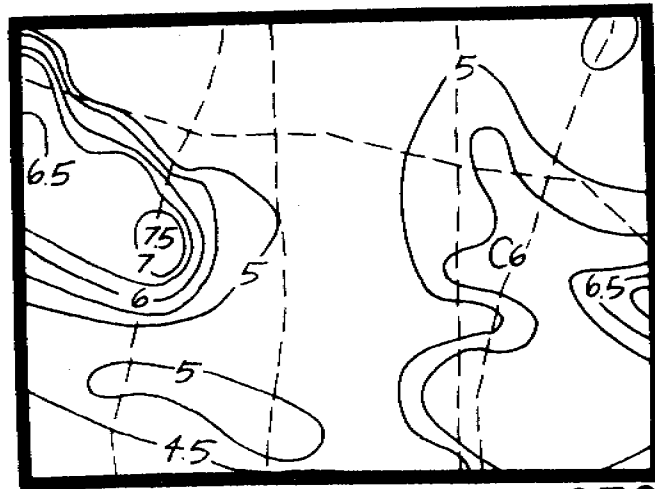
Figure 5.



Figure 6. Oblique aerial photograph of Reindeer Island taken in late September 1976 looking westward. The second, best developed line of ground ice suggests a continuous shore-parallel bar not actually present.

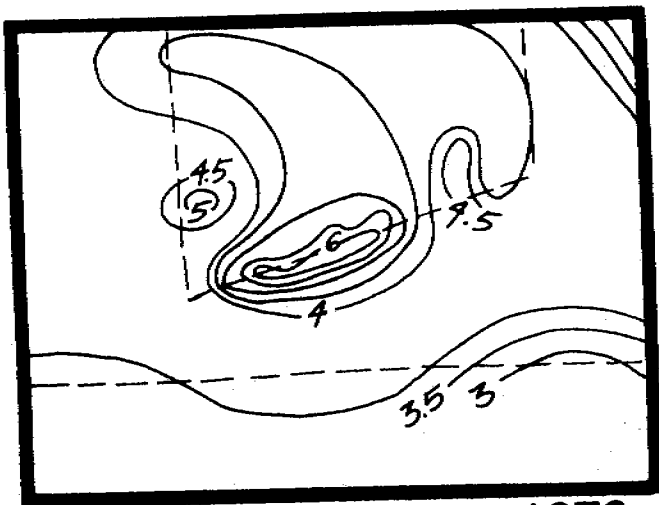


1976

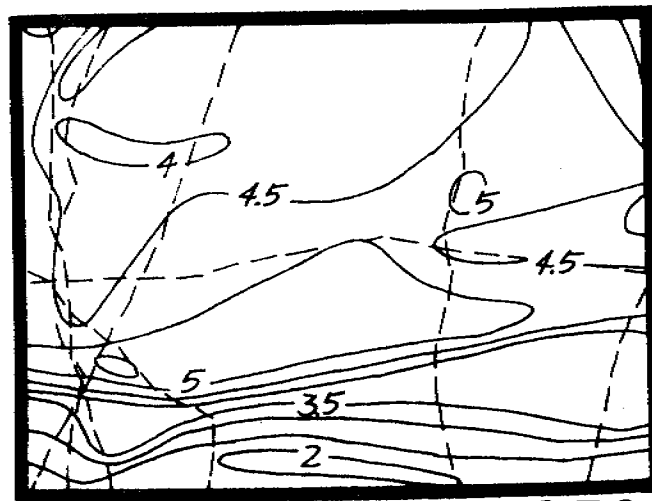


1979

A



1976



1979

B

Figure 7. Comparison of identical sectors of seafloor with relief as mapped in 1976 and 1979. For locations refer to figures 4 and 5. Tracklines are presented by dashed lines. Major changes are evident.

as a cause and therefore suggest that hydraulic processes of the relatively open-water season (July through September) are a probable cause. There is no known littoral process of true open-water conditions that focuses on isolated spots long enough to create scour depressions of the size mapped off Reindeer Island. For this reason, and because the bedform pattern is restricted to arctic nearshore regions, we postulate an interaction of hydraulic processes with grounded floes in the littoral zone as a cause for this bedform pattern. Focusing of hydraulic processes around ice/seafloor contact regions and resulting small-scale bedforms have been previously discussed, mainly on the basis of diving observations around grounded ice (Reimnitz et al., 1972, 1973; Reimnitz and Barnes, 1974). Related to this is the fact that side-scan sonar studies of a large number of individual grounded floes in summer failed to show gouges leading to such floes. Summer hydraulic processes apparently soon eliminate any traces of how a grounded floe became stuck in the mud.

The large potholes in the nearshore region therefore seem to be large counterparts to sea-ice kettles seen on beaches. Figure 8 is an aerial photograph of the pockmarked foreshore of nearby Cross Island. These pockmarks were produced during storms in the previous fall and recently vacated by melting of growlers. The water's edge describes on a small scale the crenulated pattern of isobaths seen on a much larger scale offshore, where grounded ice of bergy-bit size and larger interacts with wave and current regime.

This study may not be the first one to document the presence of large sea-ice kettles in the nearshore regions of the Arctic. Hume and Schalk (1967) and Schalk and Hume (1961) in their nearshore studies off Barrow describe "holes" which formed where ice had grounded temporarily during storms. However, their soundings were not dense enough to reveal the full complexity of the seafloor.

The large sea-ice kettles in the nearshore zone may be partially the result of vertical movement of bergy bits in a seaway. This movement produces pulsating flows that transport sand away from the point of ice impact. Processes of cut and fill will have to be considered in the construction of pipelines through the littoral zone.



Figure 8. Sea-ice kettles along foreshore of Cross Island prior to open-water season. With an offshore increase in water depth and size of ice, sea-ice kettles also increase in size.

#### REFERENCES

- Hume, J.D., and Schalk, M., 1967, Shoreline processes near Barrow, Alaska , A comparison of the normal and the catastrophic: *Arctic*, v. 20, n. 2, p. 86-103.
- Reimnitz, Erk, Barnes, P.W., Forgatsch, T.C., and Rodeick, C.A., 1972, Influence of grounding ice on the Arctic shelf of Alaska: *Marine Geology*, v. 13, p. 323-334.
- Reimnitz, Erk, and Barnes, P.W., 1974, Sea ice as a geologic agent on the Beaufort Sea shelf of Alaska: in: Reed, J.C., and Sater, J.E., (eds.), *The Coast and Shelf of the Beaufort Sea*, Arctic Institute of North America, Arlington, Va., p. 301-351,
- Reimnitz, Erk, Barnes, P.W., and Alpha, T.R., 1973, Bottom features and processes related to drifting ice on the arctic shelf, Alaska: U.S. Geological Survey Miscellaneous Field Studies Map MF-532.
- Schalk, M., and Hume, J.D., 1961, Review of shoreline investigations 1954-1959, Point Barrow, Alaska, in *The First National Coastal and Shallow Water Research Conference*, Baltimore, Tallahassee, Los Angeles, October, 1961, Proceedings: The National Science Foundation and the Office of Naval Research, p. 91-94.
- Short, A.D., Coleman, J.M., and Wright, L.D., 1974, Beach dynamics and nearshore morphology of the Beaufort Sea Coast, Alaska: in: Reed, J.C., and Sater, J.E., (eds.), *The Coast and Shelf of the Beaufort Sea*, Arctic Institute of North America, Arlington, Va., p. 477-488.

The first part of the document discusses the importance of maintaining accurate records of all transactions. It emphasizes that every entry, no matter how small, should be recorded to ensure the integrity of the financial statements. This includes not only sales and purchases but also expenses and income. The document further explains that proper record-keeping is essential for identifying trends, managing cash flow, and complying with tax regulations. It also notes that clear records can help in resolving any disputes or audits that may arise.

In the second part, the author provides a detailed overview of the accounting cycle. This cycle consists of eight steps: identifying the accounting entity, choosing the accounting method, analyzing transactions, recording transactions in the journal, posting to the ledger, preparing a trial balance, adjusting entries, and preparing financial statements. Each step is explained in detail, with examples provided to illustrate the process. The author stresses that following these steps in order is crucial for producing accurate and reliable financial information.

The third section focuses on the classification of assets and liabilities. It discusses how to distinguish between current and long-term assets and liabilities, and how to properly value them. The author provides guidelines for recognizing and measuring these items, ensuring that they are reported at their fair market value. This section is particularly important for understanding the balance sheet and how it reflects the company's financial position at a given time.

Finally, the document concludes with a summary of the key points discussed. It reiterates the importance of accuracy, consistency, and transparency in financial reporting. The author encourages readers to stay up-to-date on changes in accounting standards and regulations to ensure their records remain current and compliant. The overall message is that diligent financial record-keeping is the foundation of a successful business.

UNITED STATES DEPARTMENT OF THE INTERIOR  
GEOLOGICAL SURVEY  
345 Middlefield Road, M/S 77  
Menlo Park, California 94025

EASTERN GULF OF ALASKA SEISMICITY:  
ANNUAL REPORT TO THE NATIONAL OCEANIC AND  
ATMOSPHERIC ADMINISTRATION  
FOR APRIL 1, 1979 THROUGH MARCH 31, 1980

By

John C. Lahr, Christopher D. Stephens and John Rogers

This study was supported by the Bureau of Land Management through interagency agreement with the National Oceanic and Atmospheric Administration, under which a multi-year program responding to needs of petroleum development of the Alaskan continental shelf is managed by the Outer Continental Shelf Environmental Assessment Program Office.

Open-file Report

80-459

This report is preliminary and has not been edited or reviewed for conformity with Geological Survey standards and nomenclature. Any use of trade names and trademarks in this publication is for descriptive purposes only and does not constitute endorsement by the Geological Survey.



ANNUAL REPORT

Title: Earthquake Activity and Ground Shaking  
in and along the Eastern Gulf of Alaska

Report by: John C. Lahr and Christopher D. Stephens and John Rogers

Principal Investigators: John C. Lahr, Christopher D. Stephens

Office of Earthquake Studies

U.S. Geological Survey

Menlo Park, California 94025

Research Unit: 210

Reporting Period: April 1, 1979 through March 31, 1980

Number of Pages: 37

31 March 1980

CONTENTS

PAGE

I. Summary of objectives, conclusions and implications with respect to OCS oil and gas development .....	360
II. Introduction .....	361
III. Current state of knowledge .....	362
IV. Study area .....	364
V. Methods and rationale of data collected .....	364
VI., VII. and VIII. Results, discussion and conclusions .....	365
IX. Needs for further study .....	385
X. Summary of October 1979-March 1980 operations .....	387
XI. Auxiliary Material .....	391

I. Summary of objectives, conclusions, and implications with respect to OCS oil and gas development.

The objective of this research is to analyze the earthquake activity in the Northeast Gulf of Alaska (NEGOA) and adjacent onshore areas in order to develop a better model for the current tectonic framework. This information is critical to the establishment of criteria for the safe development of oil and gas. A great earthquake ( $M > 8$ ) associated with low-angle oblique underthrusting of the sea floor beneath the continental shelf could be accompanied by strong ground shaking throughout much of the eastern Gulf of Alaska, possibly from Cross Sound to Kayak Island (Page, 1975) and could trigger tsunamis, seiches, and submarine slumping, any of which could be hazardous to offshore and coastal structures (Meyers, 1976).

During the past year particular emphasis has been placed on developing a kinematic model to represent the regional tectonic framework applicable to the NEGOA. This has involved study of the seismic data collected during the past 5 years as well as review of the historic seismic record and geologic constraints. The tectonic model developed, although still tentative, reflects our current state of knowledge.

In the proposed model, the portion of the North American plate bordering the Gulf of Alaska is divided into two sub-blocks, which are partially coupled to the Pacific plate. Based on the model, future earthquakes will be most frequent along the north dipping thrust faults of the Pamplona zone, between Icy Bay and the Aleutian megathrust. Earthquakes should also be expected, although less frequently, on the thrust contact between the Pacific plate and the Yakutat block. This hypothesized thrust boundary underlies the offshore region south of Yakutat at shallow depth and dips gently to the north or northwest.

A rough estimate of the level of seismic activity and the largest expected event has been made for each of the four principal source regions effecting the NEGOA. For example, the return period for events greater than or equal 7.3 on the thrust zone underlying the Yakutat block is estimated to be 180 years. These estimates should be subjected to further review and compared with those derived by other methods before being used in further calculations. The final step in generating parameters useful to design engineers has not been taken. This would involve generating estimates of the probability of a given level of shaking as a function of exposure time and site location.

The level of seismic activity during the past tens of years has been lower than would be expected if the rate of seismicity were constant and given by the return periods calculated. This discrepancy could be interpreted as an indication that a large percentage of the regional plate convergence takes place aseismically. Given the temporal fluctuations in seismicity observed elsewhere in the world, the sequence of magnitude 8 events that occurred at the turn of the century, and the recent magnitude 7.3 ( $M_S$ ) St. Elias earthquake, we conclude that the recent low level of activity is well below the average to be expected.

## II. Introduction

### A. General nature and scope of study.

The purpose of this research is to investigate the earthquake potential in the NEGOA and adjacent onshore areas. This will be accomplished by assessing the historical seismic record as well as by collecting new and more detailed information on both the distribution of current seismicity and the nature of strong ground motion resulting from large earthquakes.

## B. Specific Objectives.

1. Record the locations and magnitudes of all significant earthquakes within the NEGOA area.
2. Prepare focal mechanism solutions to aid in interpreting the tectonic processes active in the region.
3. Identify both offshore and onshore faults that are capable of generating earthquakes.
4. Assess the nature of strong ground shaking associated with large earthquakes in the NEGOA.
5. Compile and evaluate frequency vs. magnitude relationships for seismic activity within and adjacent to the study areas.
6. Evaluate the observed seismicity in close cooperation with OCSEAP Research Units 16 and 251 towards development of an earthquake prediction capability in the NEGOA.

## C. Relevance to problem of petroleum development.

It is crucial that the seismic potential in the NEGOA be carefully analyzed and that the results be incorporated into the plans for future petroleum development. This information should be considered in the selection of tracts for lease sales, in choosing the localities for land-based operations, and in setting minimum design specifications for both coastal and offshore structures.

## III. Current state of knowledge

The eastern Gulf of Alaska and the adjacent onshore areas are undergoing compressional deformation caused by north-northwestward migration of the Pacific plate with respect to the North American plate (Figure 1). Direct evidence for continued convergent motion comes from studies of large earthquakes along portions of the Pacific-North American plate boundary adjacent to the eastern Gulf of Alaska.

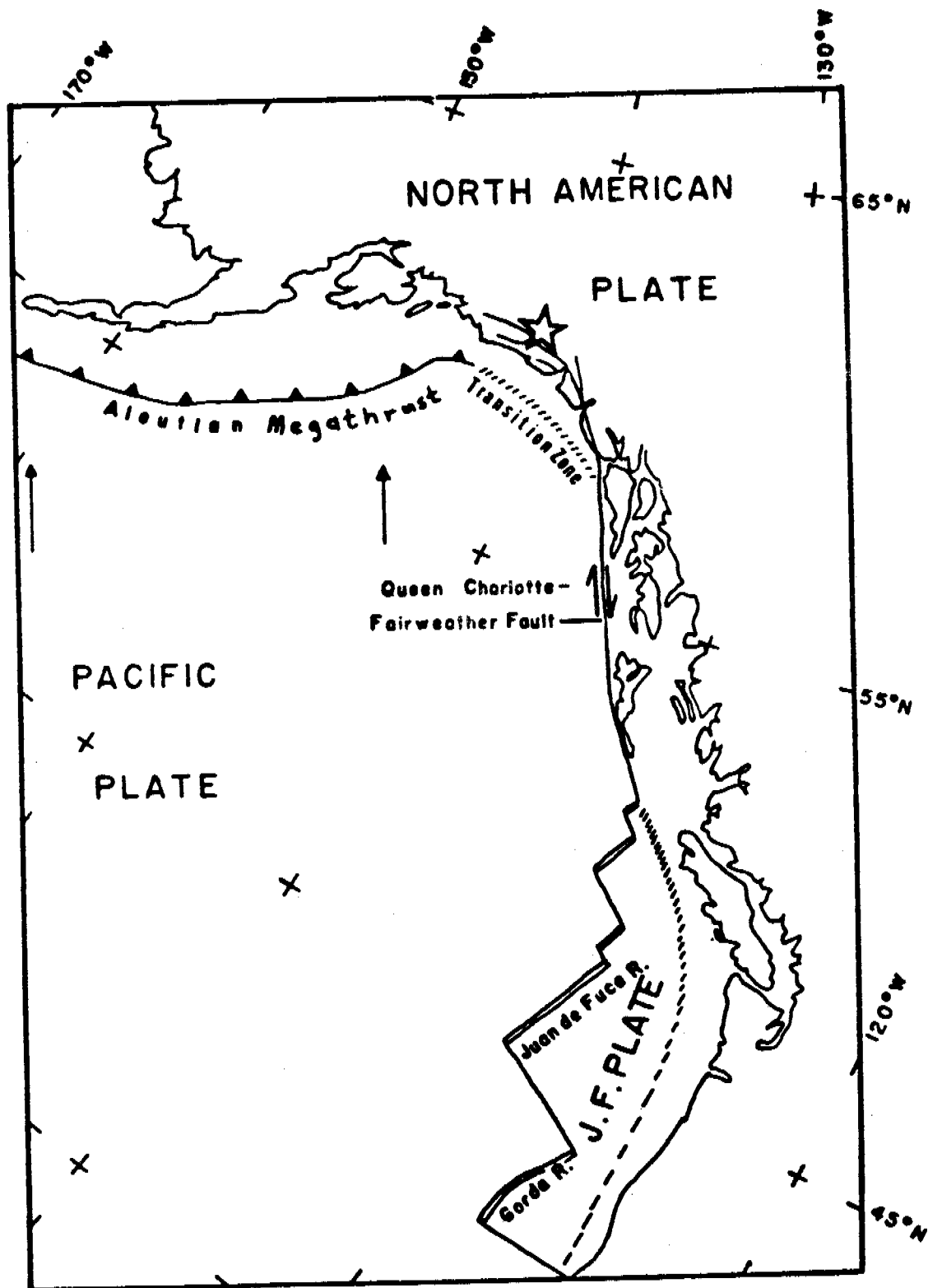


Figure 1. Current motion of Pacific plate with respect to North American plate. Juan de Fuca (J.F.) plate also shown. Star indicates epicenter of the earthquake of 28 February, 1979.

The 1958 earthquake on the Fairweather fault in southeast Alaska was accompanied by right lateral slip of as much as 6.5 m (Tocher, 1960). The 1964 Alaska earthquake resulted from dip slip motion of about 12 m (Hastie and Savage, 1970) on a fault plane dipping northwestward beneath the continent from the Aleutian Trench and extending from eastern Prince William Sound to southern Kodiak Island. In the intervening region between these earthquakes, from approximately Yakutat Bay to Kayak Island, the precise manner in which this convergent motion is accommodated is not known. The model which is presented here for accommodating the regional convergence is based on work in progress by Lahr and Plafker and has been reported on previously (Lahr et al., 1979A).

#### IV. Study Area.

This project is concerned with the seismicity within and adjacent to the eastern Gulf of Alaska continental shelf area. This is the southern coastal and adjacent continental shelf region of Alaska between Montague Island and Cross Sound.

#### V. Methods and rationale of data collection.

The short-period seismograph stations installed along the eastern Gulf of Alaska under the Outer Continental Shelf Environmental Assessment Program as well as the other stations operated by the USGS in southern Alaska are shown in Figure 1 of Chapter X. Single-component stations record the vertical component of the ground motion, while three-component stations have instruments to measure north-south and east-west motion as well. Data from these instruments are used to determine the parameters of earthquakes as small as magnitude 1. The parameters of interest are epicenter, depth, magnitude, and focal mechanism. These data are required to further our understanding of the regional tectonics and to identify active faults.

A network of strong motion instruments is also operated. These devices are designed to trigger during large earthquakes and give high-quality records of large ground motions which are necessary for engineering design purposes.

VI., VII. and VIII. Results, Discussion and Conclusions.

The next four sections on kinematic model, plate motions, comparison with observations, and implications for seismic hazards are excerpts from Lahr and Plafker (1980).

PROPOSED KINEMATIC MODEL FOR PACIFIC-NORTH AMERICAN INTERACTION

A working model has been developed for the Holocene Pacific-North American plate interaction along the Gulf of Alaska. In this model deformation within the North American plate is concentrated mainly on the boundaries of two blocks. First, these boundaries will be described, then the motions within the model will be given and finally the model will be compared with the available data on displacement rates. The tectonic setting and major boundaries are illustrated in Fig. 2. The Yakutat block (YB), which has been described by Plafker and others (1978), is bounded by the Transition zone (TZ), the Fairweather fault (F), and the Pamplona zone (PZ) which passes through Icy Bay (I). North and east of the Yakutat block is the Wrangell block (WB). The Wrangell block is bounded on the northeast by the Denali (D), Totschunda (T), Duke River (DR), Dalton (DA), and Chatham Strait (C) faults, and on the south by the Aleutian megathrust (AM), the Pamplona zone (PZ), and the Fairweather fault, including its offshore continuation (F). The northwestern boundary of the Wrangell block is speculative; it is tentatively assumed to diverge southward from the Denali fault, through Cook Inlet (CI), around Kodiak Island (KO) and back to the Aleutian megathrust.

The extent and configuration of the Pacific plate underlying Alaska can be inferred, at least partly, from the distribution of subcrustal earthquakes that make up the Benioff zone. These events occur within the underthrust



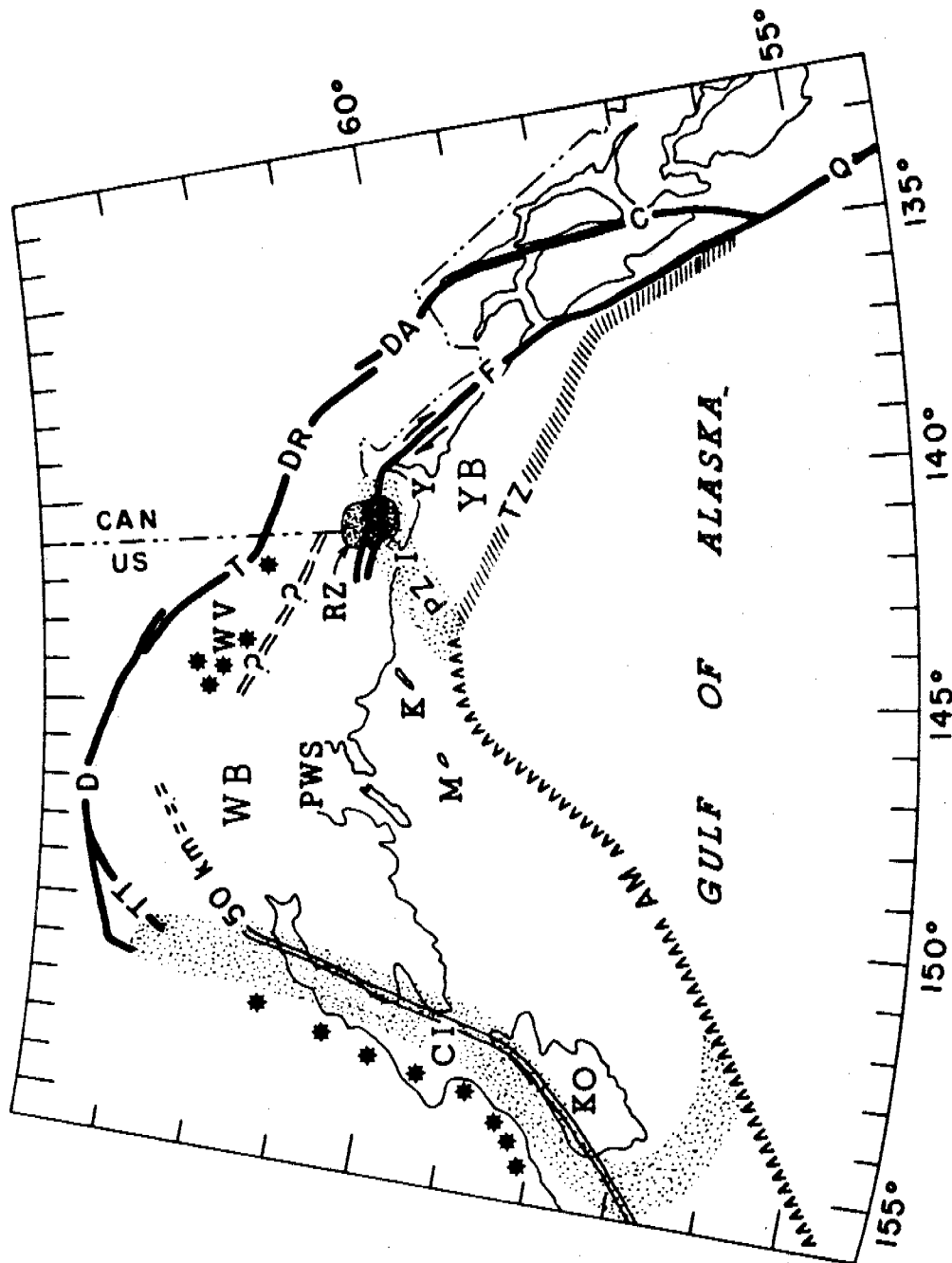


Fig. 2 Map of southern Alaska and western Canada emphasizing the principal regional tectonic features. Faults after (Clague, 1979; Beikman, 1978). KO, Kodiak Island; M, Middleton Island; K, Kayak Island; CI, Cook Inlet; PWS, Prince William Sound; I, Icy Bay; Y, Yakutat Bay; WV, Wrangell volcanics; RZ, rupture zone of 28 February 1979 earthquake; AM, Aleutian megathrust; TZ, Transition zone; Q, Queen Charlotte Islands fault; C, Chatham Strait fault; DA, Dalton fault; DR, Duke River fault; T, Totschunda fault; D, Denali fault; TT, Talkeetna fault; F, Fairweather fault; PZ, Pamplona zone; double line, 50 km isobath of Benioff zone, queried where inferred; WB, Wrangell block; YB, Yakutat Block.

oceanic plate near its upper surface. The 50-km isobath of earthquake foci shown in Fig. 2 northwest of the Aleutian megathrust (AM) represents an active Benioff zone (Lahr, 1975). Further east, however, northwest of the Transition zone (TZ), no earthquakes as deep as 50 km have been observed, and a Benioff zone is not defined here.

The continuity of the Pacific plate below the Gulf of Alaska and the hundreds of kilometers of convergence indicated by the Benioff zone northwest of Prince William Sound imply that a similar amount of convergence has taken place in the zone between Prince William Sound and the Queen Charlotte Islands fault. The queried 50-km isobath in Fig. 2 indicates a plausible position for the underthrust Pacific plate based on two assumptions: the first is that the andesitic Wrangell volcanic rocks (WV), (Deininger, 1972; MacKevett, 1978) are situated approximately above the 100-km isobath of the Benioff zone as is typical for andesitic volcanoes associated with an underthrust plate; the second is that the dip of the plate between 50 and 100 km depth is similar to that observed elsewhere along the Aleutian arc (Davies and House, 1979). The Wrangell volcanoes have not been highly eruptive for about 3 my, however, and may no longer be aligned above the Benioff zone. In any case it seems likely that the Pacific plate extends at shallow depths below much of the Yakutat and Wrangell blocks, a configuration that should be conducive to significant coupling between those blocks and the Pacific plate.

## PLATE MOTIONS IN MODEL

Motions in the kinematic model presented in this paper are relative to the stable parts of the North American plate, in particular the interior of Alaska. First the velocities in the preferred model will be given and then they will be compared with the available data on relative rates of motion. The Pacific plate is rotating clockwise about a pole in eastern Canada, and is moving northwestward at 6.5 cm/yr along the Queen Charlotte Islands fault. The velocity increases to the southwest as distance from the pole of rotation increases. The Yakutat block is moving parallel to the Pacific plate but with a slightly lower relative velocity ( $\sim 6$  cm/yr). Motion of the Wrangell block is taken to be counterclockwise rotation about an axis near Kodiak Island, such that its northeastern edge moves in a right-lateral sense relative to the North American plate with a velocity of approximately 1 cm/yr. The relative rates of motion are indicated in Fig. 3.

## COMPARISON OF MODEL WITH OBSERVATIONS

This kinematic model is in reasonable agreement with historical seismicity and known rates of relative plate movement, where data are available. Historical large earthquakes along the Queen Charlotte Islands (Q) and the Fairweather (F) faults with dextral strike-slip motion support the viewpoint that these are principal plate boundaries (Tobin and Sykes, 1968; Gawthrop and others, 1973).

The rate of relative motion across the Fairweather fault has probably averaged roughly 5.8 cm/yr in a right-lateral sense for the past thousand years (Plafker and others, 1978), in reasonable agreement with the value of 5 cm/yr predicted by the model.

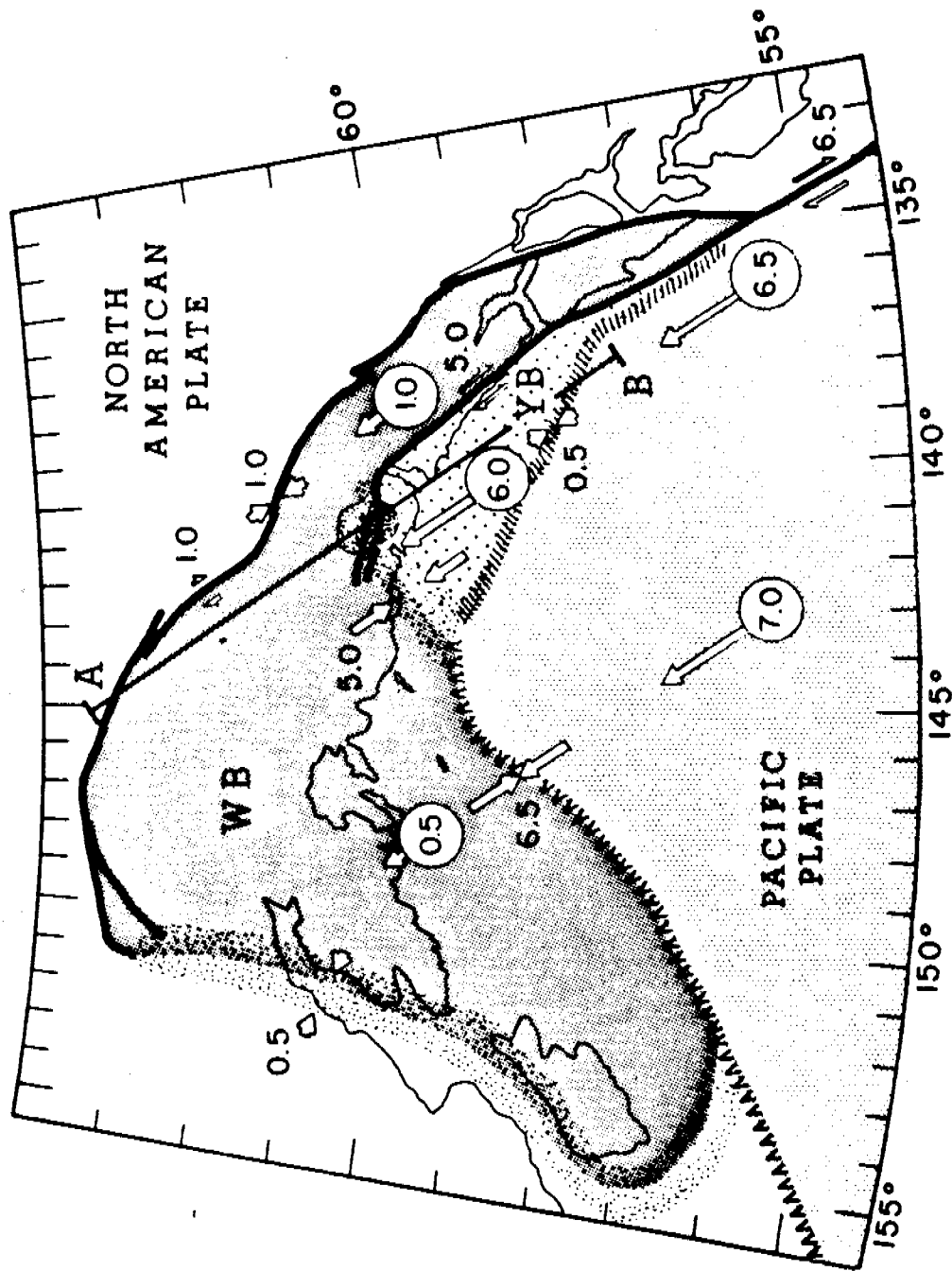


Fig. 3 Proposed model for present crustal deformation along the Pacific-North American plate boundary in southern and southeast Alaska. Circled numbers give rate of motion (cm/yr) of Pacific plate, Yakutat block and Wrangell block with respect to North American plate. Numbers next to paired vectors give rate of motion across indicated zone. Dotted bands enclose surface outcrops of major zones of deformation and faulting. A-B location of cross section of Fig. 3; WB, Wrangell block; YB, Yakutat block.

The Yakutat block may have a more northerly direction of motion than that given by the model. Convergence across the Fairweather fault is suggested by young uplift, folding and faulting along the coast in the Lituya Bay Area (Plafker and others, 1978) and uplift in the Yakutat Bay area that is best explained by movement on inferred northeast-to-north-dipping thrust faults (Thatcher and Plafker, 1977). Since the conclusions of this paper are not effected by the exact orientation of the Yakutat block motion, the simplest assumption of motion parallel to the Pacific plate motion has been used. The model rates for the Yakutat block and Pacific plate were set to give some convergence across the Transition zone (TZ), in agreement with data from the 6.7 ( $M_s$ ) earthquake which occurred along the continental margin southwest of Cross Sound. The rupture zone of this earthquake, as delineated by aftershocks, was 60 km long by 15 km wide, and the focal mechanism is compatible with oblique thrust faulting (Gawthrop and others, 1973).

The Pamplona zone, which constitutes the northwestern boundary of the Yakutat block, is a broad zone of late Cenozoic onshore and offshore folds and thrust faults which dip to the northwest or north (Plafker and others, 1978; Thatcher and Plafker, 1977). Seismic activity has been recorded along both offshore and onshore portions of this zone (Page, 1975; Stephens and others, 1979).

The Denali (D) and Totschunda (T) faults of Fig. 1 have undergone 1 to 2 cm/yr average dextral displacement during the Holocene (Richter and Matson, 1971; Plafker and others, 1977; Stout and others, 1973) although some parts may not have moved during the past 1,500 to 2,000 years (Plafker and others, 1977). The Duke River (DR), Dalton (DA), and Chatham Strait (C) faults do not prove Holocene displacements, and in some places there is geomorphic evidence to support the viewpoint that they could not have moved more than one or two meters in the past few hundred years (Clague, 1979). However, because seismic

activity has been noted in the vicinity of these faults (Clague, 1979), they are considered the most likely southern continuation of the Denali-Totschunda system. Dextral motion of more than a total of 0.5 km is precluded on a direct connection between the Totschunda and Denali faults by geologic data (Plafker and others, 1978). Thus, if the Fairweather fault has short circuited across the Saint Elias Mountains to connect with the Totschunda fault, this newly established break cannot be more than 25,000 to 50,000 years old.

Counterclockwise rotation of the Wrangell block (WB) would produce convergence on its northwestern edge which would be greatest towards the north, along the zone of unnamed faults (TT) that diverge from the Denali fault and trend southwestward parallel to the Alaska Range, between the Chulitna River and Tonzona/Tatina Rivers (Reed and Nelson, 1977). West of these faults, which are mostly thrust faults, there is no evidence that the Denali fault has been active in Quaternary time (Plafker and others, 1977). Rotation of the Wrangell block, as proposed here, is consistent with the change in strike between the Denali (D), Totschunda (T), and Chatham Strait (C) faults. The western boundary of the Wrangell block is hypothetical/ The convergent motion across this boundary may be accommodated by a broad zone of folding.

The Pacific-North American relative motion assumed in this model is roughly 10% higher than the average found for the past 3 my by global plate-motion reconstruction (Minster and Jordan, 1978). The higher rate allows a closer fit to the observed displacement rate on the Fairweather fault and is not an unreasonable deviation since only the Holocene epoch is of concern here.

IMPLICATIONS OF PROPOSED KINEMATIC MODEL FOR  
EASTERN GULF OF ALASKA SEISMIC HAZARDS

Lease sale 55 is located south of Yakutat Bay on the Yakutat block. This region will be subjected to ground shaking from five distinguishable seismic source regions.

1) Underthrusting of the Pacific plate below the Wrangell block northwest of the Aleutian megathrust. The 1964 Alaska earthquake ( $9.2 M_w$ ,  $8.4 M_s$ ) was of this type and ruptured from about Kayak Island to southern Kodiak Island.

2) Underthrusting of the Yakutat block and the Pacific plate below the Wrangell block. This source region extends approximately 200 km northwest from the Pamplona zone. The February 1979 St. Elias earthquake ( $7.3 M_s$ ) noted on Figs. 2 and 3 was of this type.

3) Faulting along the northeast boundary of the Yakutat block. Typical of this would be the 1958 earthquake ( $8.2 M$ ,  $7.9 M$ ) which involved dextral strike-slip on the Fairweather fault. Also included would be the Yakutat Bay earthquake ( $8.4 M_s$ ) of 10 September 1899 which involved complex thrust faulting with as much as 14 m of vertical displacement (Thatcher and Plafker, 1977).

4) Underthrusting of the Pacific plate below the Yakutat block. Although no historic great earthquake of this type is known to have occurred, it would not be prudent to exclude the possibility of one occurring in the future.

5) Earthquakes of smaller magnitude, up to perhaps 6.5 or 7.0, could probably occur with finite probability anywhere within the Yakutat and Wrangell blocks. Although the largest earthquakes would probably fall in categories 1 through 4 and account for nearly all of the convergent motion, smaller events that may occur very near the engineering structure in question must also be taken into account. Fig. 4 shows the known seismic activity in the region south of Yakutat between 1900 and 1979. The USGS seismic network

# EVENTS SOUTH OF YAKUTAT BAY 1900 - JAN 1979

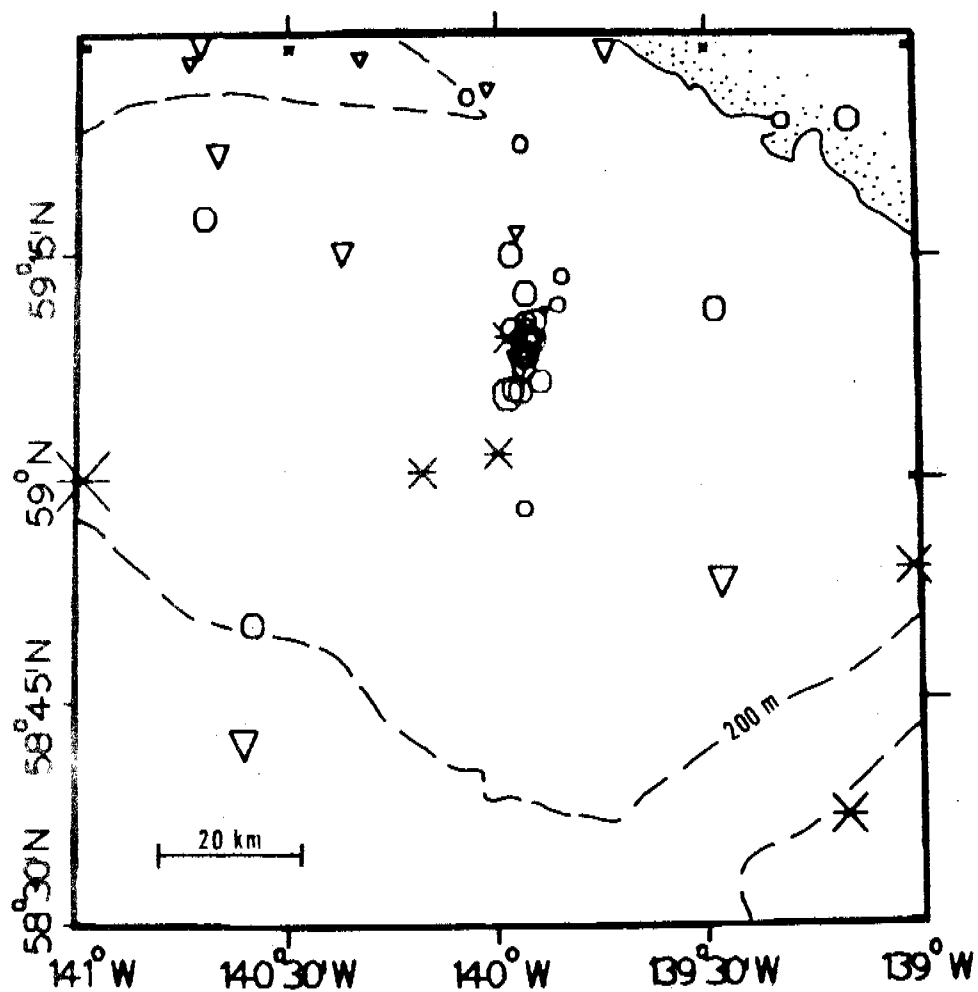


Figure 4. Map showing earthquake epicenters from NGSDC (x's) and USGS (circles - better control; triangles - poorer control) scaled by magnitude. Most of the events occurred in a cluster near the center of the figure. The apparent north-south trend of this cluster may be due to location error.



was installed to the north in the summer of 1974. The 46 events located by the USGS network since that time are indicated by circles (better epicentral control) and triangles (poorer control) on Fig. 4. The symbols are scaled by magnitude, which ranges from less than 1.0 to 3.8. Also shown, as X's, are the events from The National Geophysical and Solar Terrestrial Data Center (NGSDC) earthquake-data file for 1900 through July 1978. This file contains 15 events in the region. The earliest and largest being a magnitude 7 ( $M_S$ ) in 1908 while the three most recent have magnitudes 4.1, 4.2 and 4.4 (Palmer magnitude) and occurred in early 1974. Due to lack of depth control for these events, it is not certain whether they occurred on secondary structures within the Yakutat block or on the interface between the Wrangell block and the Pacific plate (source region 4).

## ESTIMATED RECURRENCE INTERVALS

We have thus far identified the plate boundaries in the southern Alaska region that are expected to be seismically active and estimated the rate of relative displacement across each. The next step is to estimate for each region the average number of earthquakes per unit time within each magnitude interval, up to the size of the largest expected earthquake in the region.

One approach to estimating the frequency versus magnitude distribution is to use the historic record of seismicity. This has several disadvantages. First, if the rate of occurrence of small earthquakes measured over a short interval of time is extrapolated to large events, the implicit assumption is that the rate for small events does not fluctuate greatly with time. Temporal fluctuations in seismicity are known to occur, however, and are documented in the Middle East (Ambraseys, 1975), eastern China (York, et al., 1976) and California (Eaton, in press). Therefore, the statistical parameters determined from a large number of small earthquakes cannot necessarily be extrapolated to small numbers of large earthquakes. Second, the historic record of large events ( $M > 7$ ) in southern Alaska goes back only about 80 years, so the record is too short to be used as a reliable basis for the long term rate of occurrence of large events.

An alternate method of estimating recurrence time, based on the on slip rate and maximum seismic moment for a source region, has been suggested by Molnar (1979). This method equates the rate of relative motion across a fault zone with the long term average rate of slip from earthquakes. As a result of many uncertainties which enter into these calculations, Molnar (1979) estimates the derived recurrence intervals may be in error by as much as a factor of 3 to 5. We feel these errors are still smaller than those generated by using the historic seismic record alone.

Molnar applies this method to the composite Pacific and Indian ocean subduction zones and gets good agreement with the observed record of great earthquakes during the past 50 years. Following Molnar (1979), it will be assumed that the distribution of earthquake moments in each of four principal source regions identified above can be described by the relationship

$N(M_0) = \alpha M_0^{-\beta}$ , where  $N(M_0)$  is the number of events per year with seismic moment greater than or equal to  $M_0$ , and  $\alpha$  and  $\beta$  are constants. If  $M_{0mx}$  is the largest moment for a region,  $A$  is the fault area of the entire region,  $v$  is the long term slip rate,  $\mu$  is the average shear modulus, and  $\beta$  is 2/3 then

$$N(M_0) = \frac{\mu A v}{3(M_{0mx})^{2/3}} (M_0)^{-2/3} \quad (\text{Molnar, 1979}).$$

$\beta$  is defined to be  $b/c$  where  $b$  is the coefficient in the magnitude distribution equation ( $\log(N) = a - bM$ ) and  $c$  is the coefficient in the magnitude-moment relationship ( $M = (\log M_0)/c + d$ ). A  $\beta$  value of 2/3 is based on  $c = 1.5$  and  $b = 1.0$ . The recurrence interval for events with moments greater than or equal to  $M_0$  but not greater than  $M_{0mx}$  is  $T(M_0) = N(M_0)^{-1}$

$$T(M_0) = \frac{3(M_{0mx})^{2/3}}{\mu A v} (M_0)^{2/3} \quad \text{yr} \quad (1)$$

Region 1. Underthrusting of the Pacific Plate below the Wrangell block between Kayak Island and southern Kodiak Island.

For this region the 1964 Alaska earthquake is taken as the largest event. From Kanamori and Anderson (1975):

$$M_0 = M_{0mx} = 8.2 \times 10^{29} \text{ dyne cm}$$

$$A = 1.3 \times 10^{15} \text{ cm}^2$$

The values estimated for the remaining parameters are:

$$\mu = 7 \times 10^{11} \text{ dyne cm}^{-2}$$

$$v = 6.5 \text{ cm yr}^{-1}$$

The recurrence relationship becomes:

$$T(M_0) = 4.7 \times 10^{-18} M_0^{2/3} \text{ yr}$$

This gives the following recurrence times:

<u>Region 1</u>		
<u>Magnitude <math>M_w</math></u>	<u><math>M_0</math> (dyne cm)</u>	<u>Recurrence Interval (yr)</u>
~ 9.2	~ $8.2 \times 10^{29}$	420
≥ 8.6	≥ $10^{29}$	100
≥ 8.0	≥ $10^{28}$	22
≥ 7.3	≥ $10^{27}$	4.7

The magnitudes above are based on the following moment-magnitude relationship:

$$M_w = (\log M_0)/1.5 - 10.7 \quad (\text{Kanamori, 1977})$$

Observed number ≥ 7.3 during past 40 years: 1\*

Expected number ≥ 7.3 during 40 year interval: 8.5

\* The 1964 Alaska earthquake with  $M_w = 9.2$ .

Region 2. Underthrusting of the Yakutat block and the Pacific plate below the Wrangell block.

We will assume a source region of 250 x 200 km<sup>2</sup> and the kinematic model underthrust rate of 5.0 cm yr<sup>-1</sup>. The maximum displacement is estimated from

$$u_{\max} = \frac{3\Delta\sigma w}{4\mu} \quad (\text{Molnar, 1979}) \quad (2)$$

Assuming the stress drop,  $\Delta\sigma$ , is 30 bars ( $3 \times 10^7$  dyne cm<sup>-2</sup>), typical of the largest events (Kanamori and Anderson, 1975);  $\mu = 7 \times 10^{11}$  dyne cm<sup>-1</sup>; and  $w$ , the down dip length, is 200 km, then

$$u_{\max} = 6.4 \text{ m and} \\ \text{Momx} = \mu A u_{\max} = 2.3 \times 10^{29} \text{ dyne cm} \quad (3)$$

The recurrence time relationship for this region is then:

$$T(\text{Mo}) = \frac{(3)(2.3 \times 10^{29})^{1/3}}{(7 \times 10^{11})(3 \times 10^7)(5)} (\text{Mo})^{2/3}$$

$$T(\text{Mo}) = 1.0 \times 10^{-17} (\text{Mo})^{2/3} \text{ yr}$$

Using this equation, the following table is derived:

<u>Region 2</u>		
<u>Magnitude <math>M_w</math></u>	<u>Mo (dyne cm)</u>	<u>Recurrence Interval (yr)</u>
~ 8.9	~ $2.3 \times 10^{29}$	380
≥ 8.0	≥ $10^{28}$	46
≥ 7.3	≥ $10^{27}$	10

Observed number ≥ 7.3 during past 40 years: 1\*

Expected number ≥ 7.3 during 40 year interval: 3.3

\*The February 1979 St. Elias earthquake with  $M_s = 7.3$ .

Region 3. Faulting along the northeast boundary of the Yakutat block.

This faulting will be taken to be strike slip although, as mentioned previously, the northern end includes complex thrusting as well. The largest events in this region will be assumed to have an average of 4 m of strike slip motion on a 350 x 20 km portion of the Fairweather fault.

The estimated maximum moment is

$$M_{\text{omx}} = \mu A u_{\text{max}} = (3.3 \times 10^{11})(7 \times 10^{13})(400) = 9.2 \times 10^{27} \text{ dyne cm}$$

The recurrence interval equation, using the kinematic model's 5 cm yr slip rate, is then

$$T(\text{Mo}) = \frac{(3)(9.2 \times 10^{27})^{1/3}}{(3.3 \times 10^{11})(7 \times 10^{13})(5)} (\text{Mo})^{2/3}$$

$$T(\text{Mo}) = 5.5 \times 10^{-17} (\text{Mo})^{2/3} \text{ yr}$$

The following table gives recurrence intervals and rates of occurrence for events in a few size categories.

<u>Region 3</u>		
<u>Magnitude <math>M_w</math></u>	<u><math>M_0</math> (dyne cm)</u>	<u>Recurrence Interval (yr)</u>
~ 7.9	~ $9.2 \times 10^{27}$	240
≥ 7.3	≥ $10^{27}$	55
≥ 6.6	≥ $10^{26}$	12

Observed number ≥ 7.3 during past 40 years: 1\*

Expected number ≥ 7.3 during 40 year interval: 0.73.

\* The 1958 Fairweather earthquake with  $M_s = 7.9$ .

Region 4. Underthrusting of the Pacific plate below the Yakutat block.

The maximum fault area for this zone is the triangular region with area approximately  $\frac{1}{2}$  (150 x 300) km . The maximum displacement can be estimated from

$$u_{\max} = \frac{3\Delta\sigma w}{4\mu}$$

If, as in the case of region 2, we assume an effective downdip length of 200 km, the maximum displacement would be approximately 6.4 m and

$$M_{\text{omx}} = \mu A u_{\max} = 10^{27} \text{ dyne cm.}$$

Using the kinematic model underthrust rate of 0.5 cm yr<sup>-1</sup>, the recurrence relationship becomes:

$$T(M_0) = \frac{(3)(10^{29})^{1/3}}{(7 \times 10^{11})(2.25 \times 10^{14})(0.5)} (M_0)^{2/3}$$

$$T(M_0) = 1.8 \times 10^{-16} (M_0)^{2/3} \text{ yr}$$

This gives the following recurrence times:

Region 4

Magnitude $M_w$	$M_0$ (dyne cm)	Recurrence Interval (yr)
~ 8.6	~ $10^{29}$	3800
≥ 8.0	≥ $10^{28}$	830
≥ 7.3	≥ $10^{27}$	180
≥ 6.6	≥ $10^{26}$	39

Observed number ≥ 6.6 during past 40 years: 1\*

Expected number ≥ 6.6 during 40 year interval: 1.

\* The Cross Sound earthquake of 1973 with  $M_s = 6.7$ .

The uncertainties in the calculated recurrence intervals should not be disregarded. One assumption inherent in the calculations was that all of the slip takes place seismically, as opposed to a slow creep process. If aseismic slip does take place, then the earthquake recurrence intervals would be proportionately greater.

SENSITIVITY OF CALCULATED RECURRENCE INTERVALS  
TO MODEL CHANGES

For Region 2, which involves underthrusting of the Yakutat block and the Pacific plate below the Wrangell block, the effects of changing the model parameters will be explored. The recurrence time interval,  $T$  (Mo), as estimated in equation 1, has the following dependence on fault length ( $L$ ), downdip width ( $w$ ), shear modulus ( $\mu$ ), and maximum moment ( $M_{omx}$ ):

$$T(\text{Mo}) \propto (Lwv\mu)^{-1} M_{omx}^{1/3}$$

The upper limit of moment,  $M_{omx}$ , when estimated from equations 2 and 3, has the following dependence on  $L$ ,  $w$  and stress drop ( $\Delta\sigma$ ):

$$M_{omx} \propto Lw^2\Delta\sigma.$$

If, for example, the downdip width were actually 100 rather than 200 km, then  $M_{omx}$  would be reduced by a factor of 4 to  $5.6 \times 10^{28}$ , or equivalently the largest events would be reduced from  $8.9 M_w$  to  $8.5 M_w$ . The recurrence intervals would be increased by  $2 \times (\frac{1}{2})^{1/3} = 1.26$ . Thus, the effect of reducing the width of the zone by a factor of two is to increase the recurrence intervals by only 25% while reducing the maximum event by 0.4 units of  $M_w$ . The summary table for this region would become:

Region 2

<u>Magnitude <math>M_w</math></u>	<u><math>M_o</math> (dyne cm)</u>	<u>Recurrence Interval (yr)</u>
~ 8.5	~ $5.6 \times 10^{28}$	190
≥ 8.0	≥ $10^{28}$	60
≥ 7.3	≥ $10^{27}$	13



PREVIOUS RECURRENCE ESTIMATES FOR THE OUTER CONTINENTAL SHELF  
OF THE EASTERN GULF OF ALASKA

Thenhaus and others (1979) have calculated recurrence rates for the Yakutat block (zone 13 in their report) which has almost the same boundaries as Region 4. Based on the past observed seismicity they obtain a b value of 0.6 and the following annual rates of occurrence:

<u>Magnitude</u>	<u>Annual Rate (yr<sup>-1</sup>)</u>
8.2-8.8	.00124
7.6-8.2	.00280
7.0-7.6	.00637
6.4-7.0	.0146
5.8-6.4	.0335
5.2-5.8	.0768
4.6-5.2	.176
4.0-4.6	.403

Their estimate for the magnitude of the earthquake is 8.8. These numbers reflect corrected values, and differ from those published in the draft EIS of BLM (1979) (Paul Thenhaus, personal communication, 1980).

The following table compares Thenhaus' results with those for Region 4 based on the recurrence equation calculated previously. This assumes their magnitudes are equivalent to  $M_w$ .

<u>Magnitude <math>M_w</math></u>	<u><math>M_o</math> (dyne cm)</u>	1.8 x 10 <sup>-16</sup> (M <sub>o</sub> ) <sup>2/3</sup> Region 4	Recurrence Interval (yr) Thenhaus and others Zone 13
≥ 8.2	≥ 2.2 x 10 <sup>28</sup>	1430	806
≥ 7.6	≥ 2.8 x 10 <sup>27</sup>	360	248
≥ 7.0	≥ 3.5 x 10 <sup>26</sup>	90	96
≥ 6.4	≥ 4.5 x 10 <sup>25</sup>	23	40

In this study a b value of 1.0 is assumed while Thenhaus et al. uses 0.6. This accounts for the fact that the estimates agree for  $M \geq 7$ , while Thenhaus and others' recurrence times for the largest events are significantly shorter than ours. Considering the complications, errors and biases (Utsu, 1971) which can enter into calculated b values, we do not feel it is possible to regionalize them in a significant way on the basis of historic seismic data. In addition, Thenhaus and others (1979) remove aftershocks from consideration in their recurrence estimates. If this modification were made to Molnar's method the recurrence estimates would be increased. A model for aftershock occurrence would have to be developed to quantitatively remove their effect. Considering the differences in method and the errors inherent in both methods, the results are remarkably similar.

## COMPARISON OF SEISMIC RECORD WITH RECURRENCE ESTIMATES

Utsu (1971) has pointed out many of the complexities of the Gutenberg-Richter  $\log N(M)$  versus  $M$  linear relationship. Although the relation appears to be valid for large sets of data, its use in small regions and extrapolation above or below the observed data may be risky. There are many complications, such as: bias in the magnitude calculations which may change the slope of the distribution; aftershock sequences and the variation in their sizes and upper magnitude limits with region, depth, and size of the main shock; and variation in the upper bound magnitude with region and depth.

Keeping these problems in mind, the seismicity in the  $140 \times 140 \text{ km}^2$  area including the 1979 St. Elias earthquake and its aftershocks was reviewed as a sample portion of Region 2. During the 20 year interval from 1958 to 1978 6 events occurred with magnitudes greater than or equal 5.0. During the 5 year interval, 1974-1979 there were 7 events with magnitudes greater than or equal 4.0. These numbers would translate into recurrence intervals of 3.3 years for  $M \geq 5$  and 0.71 year for  $M \geq 4$ . Assuming a  $b$  value of 1, the 3.3 yr recurrence time for magnitude 5 and above would give a .33 yr recurrence time for 4 and above. We will assume that the shorter recurrence interval determined from the 20 yr sample is closer to the true distribution. Extrapolating this recurrence time up to magnitude 7.3 and greater yields 658 years. Assuming this portion of Region 2 is typical of all of Region 2, the recurrence time for the entire Region 2 for magnitudes greater than or equal 7.3 is 258 yrs. This recurrence time is roughly a 20 times greater than that calculated previously for Region 2.

The Pacific-North American plate boundary between Yakutat Bay and Kayak Island has been identified as a seismic gap on the basis of its long period of relative quiescence for large events as compared with adjoining regions (Tobin and Sykes, 1968; Kelleher, 1970; Sykes, 1971). Although large events ( $M > 7$ ) were used in identifying this region as a seismic gap, Sykes (1971) points out that the level of both moderate activity and microearthquakes may be low as well. Davies and House (1979) propose an episodic behavior for earthquake activity with four periods: (1) preseismic, (2) seismic, (3) postseismic, and (4) interseismic. The interseismic period of tens or hundreds of years would produce a "seismic gap" with relatively little seismic activity occurring.

Although it is possible that the recurrence intervals calculated by Molnar's (1979) method are an order of magnitude too short, it would be most prudent at this time to assume that Region 2, which is within the identified seismic gap, has been in a period of lower than average seismicity during the past tens of years and that this condition may not continue long into the future.

#### IX. Needs for further study

Toward the goal of developing improved seismic exposure maps for the NEGOA region, considerable additional research is needed. It would be beneficial to develop an integrated model for the adjoining Gulf of Alaska OCSEAP regions based upon data from all of the principal investigators involved. Various approaches should be explored in setting the level of seismicity and the size of the largest events expected for each region. Data from other regions in the world with a similar tectonic setting but longer historic record should be sought, as this data may help overcome the problem of Alaska's short historic record. Additional geologic work that might lead to a better estimate of the frequency of great earthquakes in Alaska is highly desirable. One example of this would be the study of marine terraces.

Once the source regions and moment distributions have been agreed upon, they may be used as the input to statistical programs that generate the return times for given levels of acceleration or velocity at a grid of points. These values may then be contoured and used in seismic hazard planning.

Careful thought should be given to the possibility of including the record of past events in the estimates of future ground motions. As the seismic gap hypothesis gains credence it becomes tempting to enhance the probability of strong ground shaking in regions of seismic gaps and reduce the probability elsewhere. In the light of the nonuniform temporal distributions observed, such as occasional clusters of large events, however, the gap hypothesis should not be given undue emphasis.

The fifth category of earthquakes, events on subsidiary structures, has not been addressed yet in terms of the moment-rate calculations.

X. Summary of October 1979-March 1980 Operations.

a. Field Work in Alaska

Alcan

The new USGS seismic station at Alcan was visited in November 1979. This site is recorded on a helicorder located at the U.S. Border Station on the Alaska Highway. Due to problems of high background seismic noise and poor WWV radio reception (needed for timing) the site was moved to a quieter location and a better antenna was installed.

Valdez

While Alascom was grading snow from the road at the Valdez Earth Station, the USGS data cable was cut. This resulted in an outage for seismic stations FID, GLC and VZW. In addition, carrier drift was occurring at the 3 component local site. Both of these problems were rectified during a December trip to Valdez. The signal was routed through a spare wire pair coming from the local seismic station. (It was not possible to locate the broken cable due to snow). To correct carrier drift problems, all three "202" VCO's were replaced with three new A1VCO's. To accommodate the new A1VCO electronics a new 34 inch diameter culvert replaced the smaller original culvert. The A1VCO's operate off of 3 sets of 3 air cell batteries. It is expected that they will run many years before the batteries need to be changed (as opposed to the "202" VCO 2-year battery change interval).

Finally, a new model filter bridge was installed inside the Earth Station at a more convenient location. This filter bridge will allow Alascom technicians to closely monitor seismic carrier activity.

Yakutat

Due to a severe lightning storm, all USGS equipment for receiving the 6 seismic station were destroyed. (The lightning also destroyed a NOAA weather

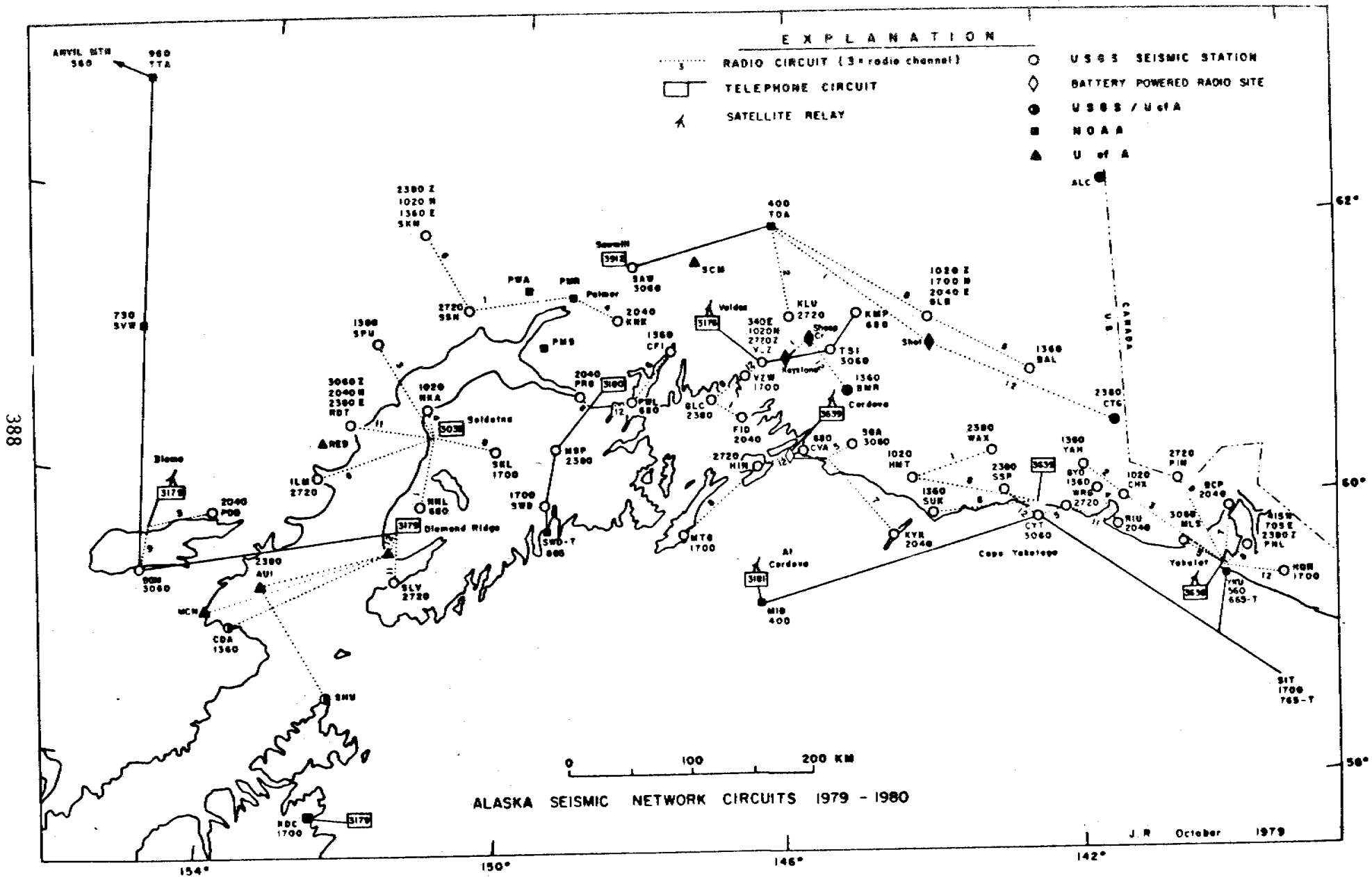


Figure 1

Three new seismic stations, darkened circles, and three new radio-relay sites, darkened diamonds.

radio transmitter and a Coast Guard Remote Radio installation). All the equipment was replaced during a December trip and all stations came back on the air except for YAH.

#### Cordova

During the December trip to Yakutat, a stop was made in Cordova to correct the problem with SGA and KYK (both were off the air). Currently an FAA technician is installing new USGS equipment at the Flight Service Center (the old USGS location is being torn down). The new location will have GE radios and a new model filter bridge. This should allow us to work closely with the FAA technician on future station problems, thus avoiding special trips to Cordova for routine problems.

#### b. Electronic Work in California

##### AIVCO

Work is proceeding on this years' production run of AIVCO's. Currently, the enclosures are being assembled and two circuit boards are going through initial screening.

The old version of the calibrator will be replaced in all new AIVCO's with the EPROM based version. This will allow programming of the calibration cycle plus field selection of one of four different cycles. This new board is presently being manufactured.

##### AIVCO Calibration Decoder

A new lighter weight calibration decoder with an LCD display has been designed and built. The unit will run several months from one 9-v transistor battery and be more compact. This should help reduce the weight of equipment carried on helicopters.

##### Seismic Chart Recorder

Work has started on the design of a new lightweight precision chart recorder. This unit will be taken on helicopters to record on-site calibrations.



### Filter Bridge

A meter-speaker card for the new USGS filter bridge has been designed and built. This card allows technicians to monitor composite carrier output on a meter (calibrated in decibels) while listening to the carrier quality on a speaker. This will aid non-USGS technicians in tracing carrier noise problems and setting levels without special test instruments. Installation of the card in each filter bridge will take place by October 1, 1980.

### c. Other Work

#### Open-File Report

The Open-File Report by Rogers and others (1980) on the A1VCO is complete. The report is 130 pages long and contains full documentation on all circuit boards, wiring and test procedures. The report is currently being distributed to interested individuals and organizations.

#### Calibrator Analysis

A Fortran program to analyze digitized calibrations has been written. It has been tested out on calibration data from HQN (located near Yakutat) with reasonable results. Further testing on other data is planned. When completed, the program will be documented in an open-file report.

#### VHF Radio Permits

The entire VHF radio network used to telemeter seismic data has been documented for use in applying for permanent radio operating permits from IRIG. IRIG is currently reviewing our request which involves 70 sites. We are presently operating under temporary permits, but due to increasing radio interference problems it was felt that permanent status would help avert problems as well as give us some legal standing for portions of the VHF spectrum.

## XI. Auxiliary Material

### A. REFERENCES

- Ambraseys, N., 1975, Studies in historical seismicity and tectonics, in Geodynamics Today: A Review of the Earth's Dynamic Processes, The Royal Society of London, p. 7-16.
- Beikman, H., 1978, Preliminary geologic map of Alaska: U.S. Geological Survey Map, 1:2,500,000.
- Bureau of Land Management, Draft Environmental Impact Statement for the Outer Continental Shelf of the Northeastern Gulf of Alaska, lease sale 55.
- Clague, J., 1979, The Denali fault system in southwest Yukon Territory--a geologic hazard:: in Current Research, Part A, Geological Survey of Canada, Paper 79-1A, p. 169-178.
- Davies, J., and House, L., 1979, Aleutian subduction zone seismicity, volcano-trench separation and their relation to great thrust-type earthquakes: Journal of Geophysical Research, v. 84, p. 4583-4591.
- Deininger, J., 1972, Petrology of the Wrangell volcanics near Nabesna, Alaska: University of Alaska, M. S., Geology, 66 p.
- Eaton, J. P., 1979, Temporal variations in the pattern of seismicity in central California: (abs.): International Symposium on Earthquake Prediction, Proceedings, Paris, France, April 1979 (in press). Gawthrop, W., Page, R., Reichle, M., and Jones, A., 1973, The southeast Alaska earthquake of July 1973: EOS Transactions of the American Geophysical Union, v. 54, p. 1136.
- Hasegawa, H. S., in preparation, Fault parameters of the St. Elias, Alaska earthquake of 28 February, 1979, Earth Physics Branch, Department of Energy, Mines and Resources, Ottawa, Canada.
- Hastie, L. M. and Savage, J. C., 1970. A dislocation model for the 1964 Alaska earthquake: Bull. Seism. Soc. Am., 60, 1389.
- Kanamori, H., and Anderson, D. L., 1975, Theoretical basis of some empirical relations in seismology, Bulletin of the Seismological Society of America, v. 65, p. 1073-1096.

A. REFERENCES (continued)

- Kanamori, H., 1977, The energy release in great earthquakes: Journal of Geophysical Research, v. 82, p. 2981-2987.
- Kolleher, J., 1970, Space-time seismicity of the Alaskan-Aleutian seismic zone: Journal of Geophysical Research, v. 75, p. 5745-5746.
- Lahr, J. C., 1975, Detailed seismic investigation of Pacific-North American interaction in southern Alaska, Ph.D. Thesis: Columbia University, p. 67-79.
- Lahr, J. C., Plafker, George, 1980, Holocene Pacific-North American plate interaction in southern Alaska: Implications for the Yakataga seismic gap, (submitted to Geology).
- Lahr, J. C., Horner, R. B., Stephens, C. D., Fogleman, K. A., and Plafker, George, 1979, Aftershocks of the Saint Elias Mountains, Alaska, earthquake of 28 February 1979, Earthquake Notes, Eastern Section, Seismological Society of America, v. 49, p. 69.
- MacKevett, E. M., Jr., 1978, Geologic map of the McCarthy Quadrangle, Alaska: U.S. Geol. Survey Miscellaneous Geological Investigations Map I-1032.
- Neyers, H., 1976. A historical summary of earthquake epicenters in and near Alaska: NOAA Technical Memorandum EDS NGSDC-1.
- Minster, J., and Jordan T., 1978, Present-day plate motions: Journal of Geophysical Research, v. 83, 5331-5354.
- Molnar, Peter, 1979, Earthquake recurrence intervals and plate tectonics, Bulletin of the Seismological Society of America, v. 69, p. 115-133.
- Page, R. A., 1975. Evaluation of seismicity and earthquake shaking at offshore sites: in Offshore Technology Conference, 7th, Houston, Texas, Proc., v. 3.
- Plafker, G., Hudson, T., Bruns, T., and Ruben, M., 1978, Late Quaternary offsets along the Fairweather fault and crustal plate interactions in southern Alaska: Canadian Journal of Earth Sciences, v. 15, p. 805-816.

A. REFERENCES (continued)

- Plafker, G., Hudson, T., and Richter, D., 1977, Preliminary observations on late Cenozoic displacements along the Totschunda and Denali fault systems: in Blean, K., ed., The United States Geological Survey in Alaska: Accomplishments during 1976, U.S. Geological Survey Circular 751-B, p. B67.
- Reed, B. L. and Nelson, S. W., 1977, Geologic map of the Talkeetna Quadrangle Alaska: U.S. Geological Survey Miscellaneous Field Studies Map MF-870-A.
- Richter, D. H. and Matson, N. A., 1971. Quaternary faulting in the eastern Alaska range: Geol. Soc. Am. Bull., 82, 1529-1540
- Stephens, C., Lahr, J., Fogleman, K., Allan, M., and Helton, M., 1979, Catalog of earthquakes in southern Alaska, January-March 1978: U.S. Geological Survey Open-File Report 79-718, 31 p.
- Stout, J., Brady, J., Weber, F., and Page, R., 1973, Evidence for Quaternary movement on the McKinley strand of the Denali fault in the Delta River area, Alaska: Geological Society of America Bulletin, v. 84, p. 939-948.
- Sykes, L., 1971, Aftershock zones of great earthquakes, seismicity gaps, and earthquake prediction for Alaska and the Aleutians: Journal of Geophysical Research, v. 76, p. 8021-8041.
- Thatcher, W. and Plafker, G., 1977, The 1899 Yakutat Bay, Alaska earthquake: IASPEI/IAVCEI Assembly Abstracts with Programs, p. 54.
- Thenhaus, P. C., Ziony, J. I., Dimenbt, W. H., Hopper, M. G., Perkins, P. M., Hanson, S. L., Algermissen, S. T., 1979, Probablistic estimates of maximum seismic acceleration in rock in Alaska and the adjacent outer continental shelf, Interagency Report to the Bureau of Land Management, U.S. Geological Survey.
- Tobin, D., and Sykes, L., 1968, Seismicity and tectonics of the northeast Pacific ocean: Journal of Geophysical Research, v. 73, p. 3821-3845.

REFERENCES (continued)

- Tocher, D., 1960, The Alaska earthquake of July 10, 1958: Movement on the Fairweather fault and field investigations of southern epicentral region: Bulletin of the Seismological Society of America, v. 50, p. 267-292.
- Utsu, T., 1974, Aftershocks and earthquakes statistics (III), Journal of the Faculty of Science, Hokkaido University, Ser. VII, Geophysics, Vol. III, P. 378-441.
- York, J. P., Cardwell, Richard, Ni, James, 1976, Seismicity and quaternary faulting in China, Bulletin of the Seismological Society of America, v. 66, p. 1983-2001.
8. PAPERS IN PREPARATION OR PRINT.
- Lahr, J. C., Plafker, George, Stephens, C. D., Fogleman, K. A., and Blackford, M. E., 1979, Interim Report on the St. Elias, Alaska Earthquake of 28 February 1979, U.S. Geological Survey Open-File Report 79-670, 23. p. Also in: Earthquake Engineering Research Institute Newsletter, v. 13, no. 4, p. 54-76.
- Lahr, J. C., Horner, R. B., Stephens, C. D., Fogleman, K. A., and Plafker, George, 1979, Aftershocks of the Saint Elias Mountains, Alaska, earthquake of 28 February 1979, Earthquake Notes, Eastern Section, Seismological Society of America, v. 49, no. 4, p. 69.
- Gawthrop, W., Page, R., Reichle, M., and Jones, A., 1973, The southeast Alaska earthquake of July 1973: EOS Transactions of the American Geophysical Union, v. 54, p. 1136.
- Hasegawa, Henry, Stephens, C. D., and Lahr, J. C., 1979, Fault parameters of the St. Elias earthquake of 28 February 1979, Earthquake Notes, Eastern Section, Seismological Society of America, v. 49, no. 4, p. 69.

B. PAPERS IN PREPARATION OR PRINT (continued)

- Stephens, C. D., Horner, R. B., Lahr, J. C., and Fogleman, K. A.,  
1979, The St. Elias, Alaska earthquake of 28 February 1979:  
Aftershocks and regional seismicity, EOS, v. 60, p. 738.
- Stephens, C., D., and Lahr, J. C., 1979, Seismicity in southern and  
southeastern Alaska, in: The United States Geological Survey in Alaska:  
Accomplishments during 1978, U.S. Geological Survey Circular 804B,  
p. 104-106.
- Lahr, J. C., Stephens, C. D., Hasegawa, Henry and Boatwright, John,  
1979, Alaskan seismic gap only partially filled by 28 February 1979  
earthquake, Science, in press.
- Fogleman, K. A., Stephens, C. D., and Lahr, J. C., 1979, Seismicity  
before and after the St. Elias, Alaska earthquake of 28 February  
1979, EOS, in press.
- Lahr, J. C., HYPOELLIPSE/MULTICS: A computer program for determining  
local earthquake hypocentral parameters, magnitude, and first motion  
pattern, U.S. Geological Survey Open-File Report 80-59, 31 p.
- Lahr, J. C., Fogleman, K. A., Stephens, C. D., Helton, S. M.,  
Archdeacon, Richard, Allan, M. A., 1979, Catalog of earthquakes in  
southern Alaska, September-December 1978: U.S. Geological Survey  
Open-File Report (in prep.).
- Rogers, J. A., Maslak, Sam, Lahr, J. C., 1980, A seismic electronic  
system with automatic calibration and crystal reference: U.S.  
Geological Survey Open-File Report 80-324, 130 p.
- Lahr, J. C., Plafker, George, 1980, Holocene Pacific-North American plate  
interaction in southern Alaska: Implications for the Yakataga  
seismic gap, (submitted to Geology).

...the first of these is the fact that the ...

...the second of these is the fact that the ...

...the third of these is the fact that the ...

...the fourth of these is the fact that the ...

...the fifth of these is the fact that the ...

...the sixth of these is the fact that the ...

...the seventh of these is the fact that the ...

...the eighth of these is the fact that the ...

Combined Quarterly Report

July - September 1979

October - December 1979

January - March 1980

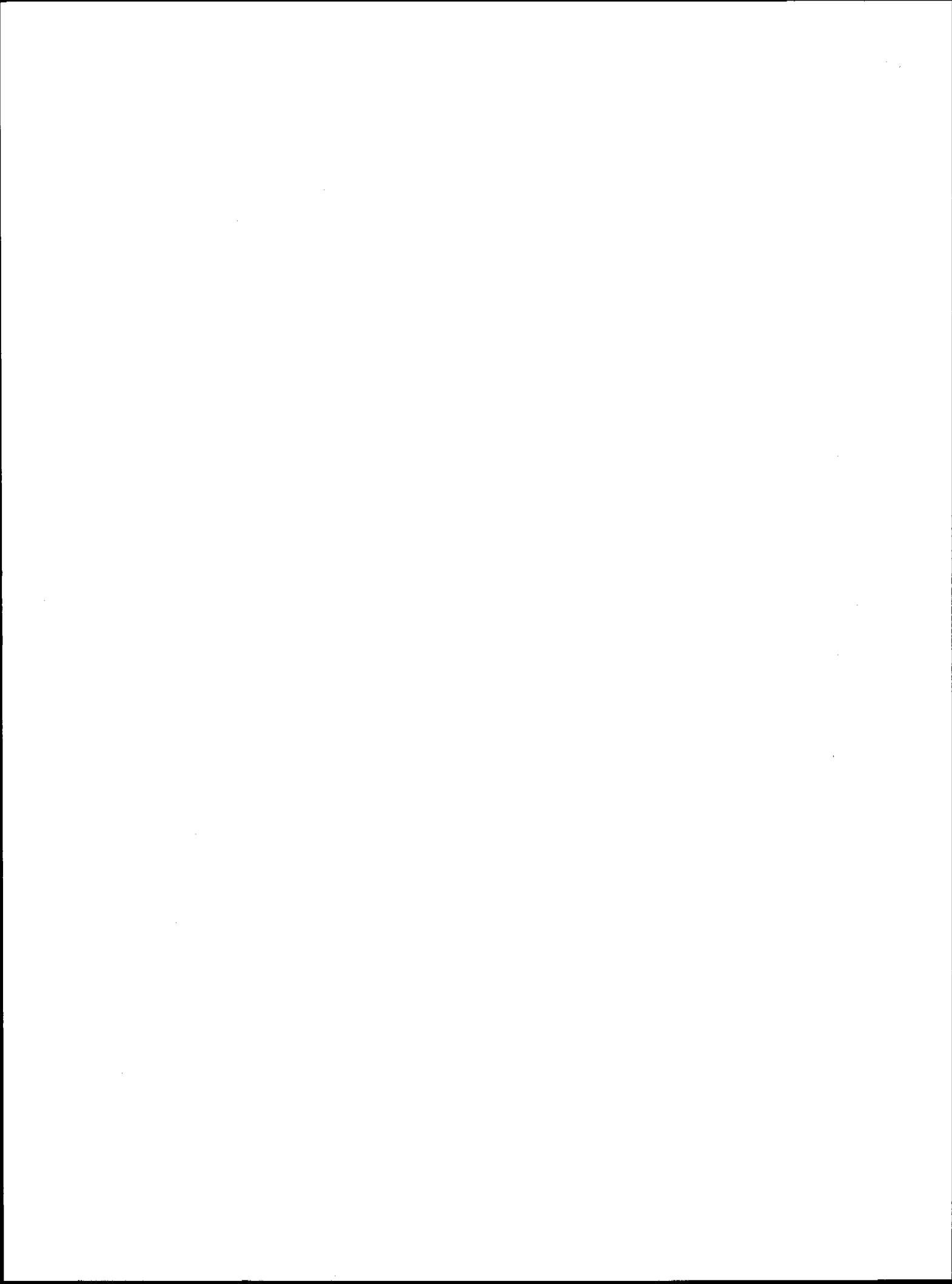
Research Unit #212

EROSION, DEPOSITION, FAULTING, AND INSTABILITY  
OF SHELF SEDIMENTS: EASTERN GULF OF ALASKA

Bruce F. Molnia  
U.S. Geological Survey

May 15, 1980





## Quarterly Report - RU 212

I. This quarterly report is a compilation of results for the time periods July-September 1979, October-December 1979, and January-March 1980. I am including the three previous quarters because I have not previously had the time to coherently synthesize the activities of this fiscal year and the end of last year. Also, I feel that I should tie together the results of the past field season before I begin this summer's studies. Lastly, since no April Annual Report will be submitted (a summary report is to be prepared in August), this is an excellent opportunity to report all progress to date.

II. Task Objectives - This research unit addresses tasks and subtasks C-2, C-3, C-4, C-8, and D-7.

### III. Field or Laboratory Activities

A. Ship and Field Trip Schedule - during the period covered by this report, two cruises partly sponsored by NOAA-BLM, were conducted. The first was from 30 July to 13 August 1979, on the DISCOVERER and the second was from 23 September to 15 October 1979, on the R.V. SEA SOUNDER.

#### B. Scientific Party

DISCOVERER		
1. Bruce F. Molnia	USGS	Chief Scientist
2. Paul R. Carlson	USGS	Party Chief
3. Mark Wheeler	USGS	Watch Stander
4. Tom Atwood	USGS	"
5. Andy Alden	USGS	"
6. William Levy	USGS	"
7. Rod Combellick	N.O.A.A.	N.O.A.A. Office Rep.
8. Chris Olson	USGS	Watch Stander
9. Dorothy Carmichael	USGS	"
10. Edith Stanley	USGS	"
11. Robin Ross	USGS	"

B. Scientific Party (cont;d)

R.V. SEA SOUNDER

1.	Vernon Pilgrim	USGS	Ship Captain
2.	Scott Conrad	"	Chief Engineer
3.	Paul Bates	"	Chief Mate
4.	Bruce Molnia	"	Chief Scientist
5.	Paul Carlson	"	Chief Scientist
6.	John Rapp	"	Geochemist
7.	Jim Nicholson	"	Electronics Tech.
8.	Mike Boyle	"	Electronics Tech.
9.	Keven OToole	"	Mechanical Tech.
10.	John Erickson	"	Mechanical Tech.
11.	Chris Olson	"	Watch Stander
12.	Denree Smith	"	Watch Stander
13.	Ken Johnson	"	Watch Stander
14.	Mark Yeats	"	Watch Stander
15.	Nancy Hardin	"	Watch Stander
16.	Ken Bayer	"	Watch Stander
17.	Jed Tooke	"	Navigator
18.	Tom Atwood	"	Navigator
19.	Edie Stanley	"	Navigator

C. Methods

DISCOVERER - The DISCOVERER cruise consisted of sediment sampling and 3.5 kHz echo sounder profile collection.

R.V. SEA SOUNDER - The SEA SOUNDER cruise collected sediment samples, plus used the following geophysical systems: single channel sparker (1488 km), Uniboom (1842 km), side scan sonar (561.6 km) 3.5 kHz echo sounder (3599.4 km) and 12 kHz echo sounder (3420 km).

D. Sample Locations - two reports are appended at the end of this report that summarize all sample locations.

E. Data Collected

DISCOVERER

1. 406 samples

SEA SOUNDER

1. 55 samples
2. --
3. 3483.3 km (1880.9 nautical miles).

IV. Results - Analyses of hazards and bottom conditions in and adjacent to lease area 55 are continuing. A detailed item by item summary of each contract data product will be included in the August Summary Report. In December 1979, a special set of graphics was prepared for BLM, to be used in the Final E.I.S. for lease sale 55. A copy of the printed BLM geology graphic, plus the data overlay sent to BLM is included in the Appendix of this original report. Copies of this report will not have the graphic or overlay included. Most of the January to March quarter was spent preparing for the May-June 1980 DISCOVERER cruise and processing samples and records collected on the 1979 DISCOVERER and SEA SOUNDER cruises.

V. Results (Preliminary Interpretation)-no data included.

VI. Auxiliary Material.

A. Bibliography of papers published that have been supported by N.O.A.A.-BLM -

Carlson, P. R., and Molnia, B. F., 1980, Seafloor geologic hazards in OCS lease area 55, eastern Gulf of Alaska: Proceedings 1980 Offshore Technology Conference, paper 3914, 12 p.

Carlson, P. R., Molnia, B. F., and Levy, W. P., 1980, Continuous acoustic profiles and sedimentological data from R.V. SEA SOUNDER cruise (S-1-76), Eastern Gulf of Alaska: U.S. Geol. Survey open-file report 80-65.

Molnia, B. F., 1979, Origin of gas pockmarks and craters: Geol. Soc. of America, Abstracts with programs, v. 11, p. 481-482.

Molnia, B. F., 1980, Depositional environment of clay minerals from the northeast Gulf of Alaska, Am. Assoc. Petroleum Geol. Bull., in press.

Molnia, B. F., 1980, Sediment distribution and transport in the northeast Gulf of Alaska: Twenty-Sixth International Geological Congress, Abstracts, in press.

VI. A. Bibliography, etc. (cont'd)

- Molnia, B. F., and Carlson, P. R., 1980, Quaternary sedimentary facies on the continental shelf of the northeast Gulf of Alaska: in Colburn, I., Field, M., Ingle, J., and Douglas, R. (eds.), Quaternary depositional environments of the Pacific coast: SEPM Symposium Volume, p. 157-168.
- Molnia, B. F., and Carlson, P. R., 1980, Quaternary sedimentary facies on the continental shelf on the northeast Gulf of Alaska: Am. Assoc. Petroleum Geol. Bull., v. 54, p. 446-447.
- Molnia, B. F., Levy, W. P., and Carlson, P. R., 1980, Map showing Holocene sedimentation rates in the northeastern Gulf of Alaska: U.S. Geol. Survey Misc. Field Studies Map MF-1170, 1 sheet.
- Quinterno, Paula, Carlson, P. R., and Molnia, B. F., 1979, Distribution of benthic Foraminifera in the Gulf of Alaska: Geol. Soc. of America, Abstracts with programs, v. 11, p. 500.
- Sangrey, D. A., Bouma, A. H., Hampton, M. A., Carlson, P. R., Molnia, B. F., Clukey, E. C., Nelson, C. H., and Olsen, H. W., 1979, Geotechnical engineering characteristics of the outer continental shelf lease areas in Alaska: Proceedings 1979 Port & Ocean Engineering under Arctic Conditions Conference, p. 963-976.
- Quinterno, Paula, Carlson, P. R., and Molnia, B. F., 1980, Benthic foraminifers from the eastern Gulf of Alaska: in Colburn, I., Field, M., Ingle, J., and Douglas, R. (eds.), Quaternary depositional environments of the Pacific coast: SEPM Symposium Volume, p. 13-22.
- Quinterno, Paula, Carlson, P. R., and Molnia, B. F., 1980, Benthic foraminifers from the eastern Gulf of Alaska: Am. Assoc. Pet. Geol. Bull., v. 64, p. 447-448.

VII. Problems Encountered - none.

VIII. Estimate of Funds Expended - All funds for FY 79 have been expended. FY 80 funds for large equipment (~ \$125,000) and salaries and supplies (~ \$100,000) are being spent according to schedule. X-ray film has cost us about \$6,000 more than originally budgeted.



U.S. DEPARTMENT OF COMMERCE  
National Oceanic and Atmospheric Administration  
NATIONAL OCEAN SURVEY

DATE: 13 August 1979

TO: Commanding Officer: NOAA Ship DISCOVERER

FROM: Bruce F. Molnia, U.S.G.S.

SUBJ: Chief Scientist Cruise Report  
RP-4-DI-79A, LEG VII, USGS DC2-79EG  
30 July - 13 August 1979

Objective

Our goal was to collect a sufficiently large number of samples to characterize the nature of the sea floor in and adjacent to lease area 55, the eastern Gulf of Alaska from west of Yakutat to Cross Sound. A preliminary estimate that 225 samples would be the minimum necessary to adequately cover the area led to the selection of 225 sampling sites. These sites plus an additional number of near shore locales selected during the cruise were the targets for the cruise.

Results

All of the 225 pre-selected sampling sites except for five in water depths too great for the ship's winch were sampled. In addition another 45 locations in the near shore and a second additional group in Glacier Bay were also sampled. A grand total of 406 sediment and water samples were collected. These included samples collected with gravity and dart cores, Shipek and Van Veen grabs, and the Sutar Van Veen grab. The attached list summarizes the position, type, depth, and important characteristics of the sediment sampled.

Problems Encountered

Problems encountered revolved around the logistics of coring from the fantail of the DISCOVERER. Many attempts were made until a satisfactory working method could be developed. Equipment loss was 50% related to the difficulties of coring from the fantail area. The geometry of the stern limited the length of core that could be attempted and caused us to abandon plans to attempt to recover cores longer than three meters in length. This in fact, helped to increase the total number of samples collected as less time was necessary to process samples between stations. I would suggest that modifications be made to permit horizontal core deployment and thus lengthen the maximum core recoverable by the DISCOVERER.



General

With one very minor exception, the entire crew went out of their way to help us achieve the successful sampling program that characterizes this cruise. If modifications were made in the design of the coring area I would have no objections to using the DISCOVERER for future cruises.



## DC2-79EG SAMPLE POSITION &amp; DEPTH RECORD

SAMPLE #	LATITUDE (N)	LONGITUDE (W)	DEPTH (M)	LENGTH OF CORE			COMMENTS
				SECT. 1	SECT. 2	SECT. 3	
GR 1000	59 27.4'	148 21.9'		0-17 cm	-	-	test core
GR 1001	59 25.1'	143 14.7'	1370	0-82 cm	-	-	
GR 1002	59 33.2'	143 16.6'	544	0-100 cm	100-197 cm		
GR 1003	59 34.5'	143 16.4'	260	0-51 cm	-	-	
GR 1004	59 27.4'	141 25.9'	172	0-88 cm	88-177 cm	-	
GR 1005	59 27.6'	141 25.9'	172				GEOTECH/295 cm
GR 1006	59 24.7'	141 20.8'	245				bagged
GR 1007	59 24.7'	141 21.0'	245	0-20 cm	-	-	
907 GR 1008	59 21.8'	141 15.0'	322	0-63 cm	-	-	
SH 1009	59 42.0'	140 54.3'	30				bagged
SH 1010	59 39.0'	141 00.1'	66				bagged
SH 1011	59 37.5'	140 58.2'	93				bagged
GR 1012	59 37.6'	140 58.9'	90	0-63 cm			
GR 1013	59 37.9'	141 00.6'	83				GEOTECH/163 cm
GR 1014	59 36.7'	140 59.5'	115	0-56 cm	56-155 cm	-	
GR 1015	59 35.5'	141 01.5'	140	0-84 cm	84-184 cm	-	
GR 1016	59 35.7'	141 01.7'	133				GEOTECH/185 cm
GR 1017	59 34.0'	141 02.8'	190	0-97 cm	97-197 cm	-	
GR 1018	59 30.7'	141 07.4'	261				GEOTECH/195 cm

SAMPLE #	LATITUDE		LONGITUDE		DEPTH (M)	LENGTH OF CORE			COMMENTS
	(N)		(W)			SECT. 1	SECT. 2	SECT. 3	
GR 1019	59	31.1'	141	05.9'	257	0-79 cm	79-179 cm	179-279 cm	
GR 1020	59	26.9'	141	05.6'	310	0-53 cm	-	-	
GR 1021	59	14.4'	141	20.2'	346	0-85 cm	85-185 cm	-	
GR 1022	59	10.5'	141	23.5'	351	0-87 cm	87-188.5 cm	-	
GR 1023	59	14.8'	141	47.2'	206				bagged
GR 1024	59	14.8'	141	47.2'	206				bagged
SH 1025	59	11.2'	141	40.8'	208				bagged
SH 1026	59	09.0'	141	35.3'	285				bagged
SH 1027	59	09.2'	141	35.6'	278				bagged
407 SH 1028	59	06.5'	141	27.5'	348				bagged
GR 1029	59	06.5'	141	27.5'	348	0-37 cm	-	-	
SH 1030	59	03.9'	141	21.1'	281				bagged
SH 1031	59	03.1'	141	09.5'	216				bagged
GR 1032	59	03.2'	141	09.4'	216				bagged
SH 1033	59	01.7'	140	59.1'	183				bagged
SH 1034	59	04.9'	141	34.0'	475				bagged
SH 1035	59	02.0'	141	39.1'	965				bagged
GR 1036	59	02.0'	141	39.1'	965	0-150 cm	-	-	
GR 1037	58	56.6'	141	43.7'	1882				bagged
GR 1038	58	51.1'	141	46.5'	2930	0-47 cm	47-147 cm	-	
GR 1039	58	49.3'	140	53.2'	213				10 cm/bagged

## DC2-79EG SAMPLE POSITION &amp; DEPTH RECORD, p. 3

SAMPLE #	LATITUDE (N)	LONGITUDE (W)	DEPTH (M)	LENGTH OF CORE			COMMENTS
				SECT. 1	SECT. 2	SECT. 3	
GR 1040	58 53.4'	140 48.0'	190				cc + 5 cm/bagged
SH 1041	58 57.9'	140 43.0'	183				bagged
GR 1042	58 57.9'	140 43.3'	183				cc/bagged
SH 1043	59 08.6'	140 51.0'	167				bagged
GR 1044	59 08.6'	140 51.0'	167	0-26 cm	-	-	
SH 1045	59 13.3'	140 56.4'	173				bagged
GR 1046	59 13.3'	140 56.4'	173				cc/bagged
SH 1047	59 18.0'	141 05.9'	181				bagged
SH 1048	59 14.5'	140 41.6'	143				bagged
804 GR 1049	59 14.5'	140 41.6'	143	0-14 cm	-	-	
SH 1050	59 19.0'	140 32.4'	132				bagged
GR 1051	59 19.2'	140 32.5'	132	0-43 cm	-	-	
SH 1052	59 24.4'	140 33.6'	140				bagged
GR 1053	59 24.5'	140 33.6'	141	0-31 cm	-	-	
SH 1054	59 27.2'	140 57.2'	303				bagged
GR 1055	59 27.2'	140 56.9'	303				cc/bagged
SH 1056	59 28.0'	140 47.9'	298				bagged
SH 1057	59 28.0'	140 47.8'	298				bagged/+ outside barrel GR 1058
GR 1058	59 28.0'	140 47.7'	298	0-54 cm	-	-	
SH 1059	59 28.1'	140 34.3'	272				bagged
				2-67 cm	67-152 cm	-	0-3 cm bagged separately

SAMPLE #	LATITUDE		LONGITUDE		DEPTH (M)	LENGTH OF CORE			COMMENTS
	(N)		(W)			SECT. 1	SECT. 2	SECT. 3	
SH 1061	59	32.8'	140	35.7'	250				bagged
GR 1062	59	32.8'	140	35.9'	249				cc/bagged
SH 1063	59	35.8'	140	35.8'	193				bagged
GR 1064	59	36.1'	140	36.2'	193				cc/bagged
GR 1065	59	36.2'	140	36.6'	193				cc/bagged
BC 1066	59	36.2'	140	37.4'	193				10-15 cm/bagged (benthos corer)
SH 1067	59	38.1'	140	36.2'	117				bagged
GR 1068	59	38.1'	140	36.3'	117				cc + 20 cm/bagged separately
SH 1069	59	40.3'	140	37.1'	37				bagged
604 SH 1070	59	34.5'	140	05.6'	22				bagged/pebbles & shells
SH 1071	59	31.5'	140	13.2'	173				bagged/foram sample
GR 1072	59	31.5'	140	13.2'	173	0-82 cm	82-182 cm	-	
GR 1073	59	27.9'	140	18.2'	241	0-86 cm	86-185 cm	-	
GR 1074	59	27.9'	140	18.0'	241				GEOTECH/298 cm
GR 1075	59	24.8'	140	23.4'	188	0-15 cm	-	-	
GR 1076	59	25.0'	140	07.3'	210				GEOTECH/
GR 1077	59	24.9'	140	07.2'	208	0-140 cm	140-285 cm	-	
SH 1078	59	29.3'	140	51.8'	65				bagged
GR 1079	59	29.3'	140	52.0'	70	0-60 cm	60-160 cm	-	
GR 1080	59	26.4'	139	56.9'	163				GEOTECH/177 cm
GR 1081	59	26.3'	139	56.9'	163	0-104 cm	104-203 cm	203-297 cm	

SAMPLE #	LATITUDE		LONGITUDE		DEPTH (M)	LENGTH OF CORE			COMMENTS
	(N)		(W)			SECT. 1	SECT. 2	SECT. 3	
SH 1082	59	23.5'	140	03.5'	179				bagged
GR 1083	59	23.5'	140	03.6'	180				GEOTECH/196 cm
GR 1084	59	23.3'	140	03.9'	178	0-72 cm	72-168 cm	-	
GR 1085	59	21.1'	140	07.8'	162				GEOTECH/189 cm
GR 1086	59	21.0'	140	07.9'	162	0-107 cm	107-206 cm	-	
SH 1087	59	16.1'	140	14.8'	122				bagged
SH 1088	59	10.3'	140	23.5'	131				bagged
GR 1089	59	10.3'	140	23.1'	131				10-12 cm/bagged
SH 1090	59	03.8'	140	33.4'	146				bagged
014 SH 1091	58	53.5'	140	28.3'	181				bagged
SH 1092	58	58.2'	140	18.0'	163				bagged
SH 1093	59	02.6'	140	10.8'	134				bagged
GR 1094	59	02.7'	140	10.9'	135	0-31 cm	-	-	
SH 1095	58	45.8'	140	12.3'	183				bagged
SH 1096	58	49.7'	140	05.2'	175				bagged
GR 1097	58	49.7'	140	05.1'	173				cc/bagged
SH 1098	58	54.3'	139	56.5'	157				bagged
GR 1099	58	54.5'	139	56.3'	157	0-16 cm	-	-	
SH 1100	58	57.9	139	50.3	128				bagged
GR 1101	58	00.0'	139	50.5'	124	0-37 cm	-	-	
SH 1102	59	01.9'	139	44.9'	120				bagged

SAMPLE #	LATITUDE		LONGITUDE		DEPTH (M)	LENGTH OF CORE			COMMENTS
	(N)		(W)			SECT, 1	SECT, 2	SECT, 3	
GR 1103	59 01.9'		139 45.1'		119	0-20 cm	-	-	
SH 1104	59 07.8'		140 02.9'		117				bagged
GR 1105	59 07.8'		140 03.0'		117	0-10 cm	-	-	
SH 1106	59 10.3'		139 56.1'		115				bagged
GR 1107	59 10.4'		139 56.1'		116	0-33 cm	-	-	
SH 1108	59 14.2'		139 49.3'		145				bagged
GR 1109	59 14.2'		139 49.3'		145	0-71 cm	71-171 cm	-	
GR 1110	59 14.2'		139 49.3'		145				GEOTECH/173 cm
GR 1111	59 20.6'		139 54.4'		182				bagged
411 GR 1112	59 20.6'		139 54.4'		182	0-48 cm	-	-	
GR 1113	59 20.8'		139 54.4'		182				bagged
GR 1114	59 25.9'		139 46.5'		105				GEOTECH/194 cm
GR 1115	59 25.9'		139 46.3'		105	0-32 cm	32-132 cm	132-232 cm	
VV 1116	59 25.8'		139 43.7'		78	0-20 cm/A	0-20 cm/B		2 bags; core A subsampled
VV 1117	59 23.8'		139 36.8'		76	0-21.5 cm/A	0-21 cm/B		2 bags; core A subsampled
VV 1118	59 19.9'		139 23.9'		33				1 bag
VV 1119	59 20.0'		139 23.5'		30				1 bag
VV 1120	59 18.4'		139 21.5'		48	0-15 cm/A	0-12.5/B		1 bag; core A subsampled
VV 1121	59 17.4'		139 18.3'		42				1 bag
VV 1122	59 16.9'		139 16.1'		38				1 bag
VV 1123	59 16.1'		139 13.5'		36	0-13 cm/A	0-16 cm/B		1 bag; core B subsampled

SAMPLE #	LATITUDE		LONGITUDE		DEPTH (M)	LENGTH OF CORE			COMMENTS
	(N)		(W)			SECT. 1	SECT. 2	SECT. 3	
VV 1124	59	13.3'	139	07.9'	52				1 bag
VV 1125	59	13.4'	139	07.8'	52				1 bag
VV 1126	59	11.2'	139	00.3'	53				1 bag
VV 1127	59	08.2'	138	50.6'	45				1 bag
VV 1128	59	05.5'	138	42.5'	60	0-27 cm/A	0-21 cm/B		core A subsampled; mollusk smpl
VV 1129	59	03.6'	138	30.3'	82	0-21 cm/A	0-19 cm/B		1 bag; core B subsampled; mollusk
VV 1130	59	02.7'	138	28.9'	92	?/A	0-20 cm/B		1 bag; core B subsampled; mollusk
VV 1131	59	01.9'	138	25.2'	57	0-20 cm			1 bag; core subsampled; mollusk
VV 1132	59	01.0'	138	28.7'	80	0-18 cm			1 bag; core subsampled
VV 1133	59	02.4'	138	32.6'	112	0-19.5 cm			1 bag; core subsampled
VV 1134	59	03.8'	138	35.4'	99	0-18.5 cm			1 bag; core subsampled
GR 1135	59	02.3'	138	31.9'	110	0-41 cm	-	-	
GR 1136	59	01.2'	138	34.1'	130				GEOTECH/
GR 1137	59	01.2'	138	33.8'	129	0-56 cm	56-134 cm	-	
GR 1138	58	59.9'	138	36.1'	140	0-55 cm	-	-	
GR 1139	58	58.7'	138	38.2'	152				GEOTECH/
GR 1140	58	58.7'	138	38.0'	152	0-71 cm	-	-	
GR 1141	58	55.9'	138	42.2'	170	0-76 cm	-	-	
GR 1142	58	55.0'	138	44.2'	164				cc/bagged
SH 1143	58	54.9'	138	44.2'	163				bagged
SH 1144	58	52.5'	138	48.4'	195				bagged

412

SAMPLE #	LATITUDE (N)	LONGITUDE (W)	DEPTH (M)	LENGTH OF CORE			COMMENTS
				SECT. 1	SECT. 2	SECT. 3	
GR 1145	58 52.5'	138 48.5'	197				cc/bagged
SH 1146	58 51.1'	138 53.4'	210				bagged
GR 1147	58 51.1'	138 53.4'	210	0-71 cm	71-166 cm	-	
GR 1148	58 49.1'	138 58.6'	214				GEOTECH/
GR 1149	58 47.0'	139 04.0'	220	0-95 cm	95-175 cm	175-272 cm	
GR 1150	58 44.3'	139 08.6'	232				GEOTECH/
GR 1151	58 42.2'	139 12.1'	242				bagged
GR 1152	58 42.2'	139 12.2'	242				bagged
GR 1153	58 39.9'	139 16.7'	246				bagged
GR 1154	58 39.7'	139 16.8'	246	0-25 cm	-	-	
GR 1155	58 37.6'	139 21.0'	250				bagged
SH 1156	58 37.6'	139 20.9'	250				bagged
SH 1157	58 35.5'	139 25.4'	240				bagged
SH 1158	58 34.0'	139 31.2'	255				bagged
GR 1159	58 34.1'	139 31.0'	255				bagged
GR 1160	58 31.7'	139 35.9'	259	0-21 cm	-	-	
SH 1161	58 29.3'	139 41.0'	252				bagged
GR 1162	58 29.2'	139 41.1'	252	0-43 cm	-	-	
SH 1163	58 28.0'	139 46.2'	219				bagged
GR 1164	58 37.1'	140 05.3'	210				cc/bagged
SH 1165	58 37.2'	140 05.0'	210				bagged



## DC2-79EG SAMPLE POSITION &amp; DEPTH RECORD, p. 9

SAMPLE #	LATITUDE		LONGITUDE		DEPTH	LENGTH OF CORE			COMMENTS
	(N)		(W)			SECT. 1	SECT. 2	SECT. 3	
SH 1166	58	37.6'	140	24.1'	727				bagged
GR 1167	58	37.5'	140	23.9'	770	0-38 cm	-	-	
GR 1168	58	37.2'	140	24.3'	864				GEOTECH/42 cm
SH 1169	58	42.0'	140	18.2'	197				bagged
GR 1170	58	42.1'	140	17.9'	197	0-21 cm	-	-	
SH 1171	58	41.5'	139	55.5'	182				bagged
GR 1172	58	41.7'	139	55.2'	185				cc/bagged
SH 1173	58	45.3'	139	49.2'	175				bagged
GR 1174	58	45.4'	139	49.0'	177				10 cm/bagged
GR 1175	58	52.2'	139	38.6'	145	0-25 cm	-	-	
SH 1176	58	56.6'	139	28.6'	118				bagged
GR 1177	58	56.6'	139	28.3'	118				cc/bagged
SH 1178	59	05.1'	139	37.1'	123				bagged
GR 1179	59	05.1'	139	36.9'	123				GEOTECH/81 cm
GR 1180	59	05.2'	139	36.5'	125	0-62 cm	62-162 cm	-	
SH 1181	59	09.3'	139	29.7'	127				bagged
GR 1182	59	09.4'	139	29.6'	127				GEOTECH/184 cm
SH 1183	59	11.7'	139	26.8'	126				bagged
GR 1184	59	11.8'	139	26.6'	110				GEOTECH/189 cm
SH 1185	59	13.4'	139	23.3'	102				bagged

SAMPLE #	LATITUDE (N)	LONGITUDE (W)	DEPTH	LENGTH OF CORE			COMMENTS
				SECT. 1	SECT. 2	SECT. 3	
GR 1186	59 05.1'	139 23.3'	102	0-80 cm	80-230 cm	-	
SH 1187	59 09.1'	139 00.7'	56				bagged
SH 1188	59 04.4'	139 11.5'	92				bagged
GR 1189	59 04.3'	139 11.5'	92				GEOTECH/193 cm
GR 1190	59 04.2'	139 11.6'	92	0-125 cm	125-223 cm	-	
SH 1191	58 54.0'	139 11.0'	112				bagged
SH 1192	58 51.1'	139 03.4'	161				bagged
GR 1193.1	58 51.1'	139 03.3'	161	0-36 cm	-	-	
SH 1194	58 46.9'	138 55.7'	221				bagged
VV 1195	58 44.4'	138 52.3'	139				1 bag
SH 1196	58 41.9'	138 48.8'	112				bagged
SH 1197	58 39.0'	138 39.6'	103				bagged
SH 1198	58 43.9'	138 30.5'	130				bagged
GR 1199	58 43.9'	138 30.4'	131	0-62 cm	-	-	
GR 1200	58 44.0'	138 30.2'	131	0-45 cm	-	-	
SH 1201	58 48.9'	138 22.8'	79				bagged
SH 1202	58 51.6'	138 17.2'	66				bagged
SH 1203	58 57.9'	138 09.8'	33				bagged
SH 1204	58 50.8'	138 00.0'	23				bagged
SH 1205	58 52.3'	138 04.4'	33				bagged
SH 1206	58 50.9'	138 07.2'	56				bagged

417

## D C2-79EG SAMPLE POSITION &amp; DEPTH RECORD, p. 11

SAMPLE #	LATITUDE		LONGITUDE		DEPTH (M)	LENGTH OF CORE			COMMENTS
	(N)		(W)			SECT. 1	SECT. 2	SECT. 3	
SH 1207	58	49.3'	138	02.1'	38				bagged
SH 1208	58	47.8'	137	59.5'	36				bagged
SH 1209	58	43.6'	138	06.5'	95				bagged
GR 1210	58	43.6'	138	06.4'	94	0-105 cm	-	-	
GR 1211	58	43.6'	138	06.1'	94				GEOTECH/104 cm
SH 1212	58	40.4'	138	12.5'	90				bagged
SH 1213	58	35.9'	138	18.1'	136				bagged
GR 1214	58	35.9'	138	17.9'	136	0-39 cm	-	-	
SH 1215	58	32.0'	138	24.0'	119				bagged
917 GR 1216	58	32.0'	138	23.9'	119	0-21.5 cm	-	-	
SH 1217	58	27.9'	138	31.2'	121				bagged
GR 1218	58	27.9'	138	31.1	122				10 cm/bagged
SH 1219	58	34.5'	138	46.4'	107				bagged
SH 1220	58	28.6'	138	55.9'	93				bagged
SH 1221	58	29.3'	139	14.5'	129				bagged
SH 1222	58	29.3'	139	14.4'	129				bagged
SH 1223	58	32.9'	139	21.1'	161				bagged
SH 1224	58	23.0'	139	05.2'	73				reefal material/bagged
SH 1225	58	23.0'	139	05.2'	75				reefal material/bagged
SH 1226	58	20.4'	139	11.7'	107				bagged
GR 1227	58	20.4'	139	11.7'	107				bagged

SAMPLE #	LATITUDE	LONGITUDE	DEPTH	LENGTH OF CORE			COMMENTS
				SECT. 1	SECT. 2	SECT. 3	
	(N)	(W)	(M)				
SH 1228	58 17.6'	139 16.1'	340				small bag
SH 1229	58 17.6'	139 16.2'	345				small bag
SH 1230	58 15.4'	139 14.5'	1206				bagged
GR 1231	58 15.5'	139 14.5'	1148	0-15 cm	-	-	
SH 1232	58 08.0'	138 51.1'	897				bagged
GR 1233	58 08.4'	138 51.2'	710				bagged
SH 1234	58 13.2'	138 58.9'	212				bagged
GR 1235	58 13.4'	138 58.7'	205				17 cm/bagged
SH 1236	58 16.9'	138 52.7'	130				bagged
417 DC 1237	58 20.9'	138 44.4'	76				4 cm Dart Core/bagged
(SH 1237	58 20.8'	138 44.6'					SH = foram sample)
SH 1238	58 22.0'	138 13.3'	128				bagged
SH 1239	58 32.3'	138 00.4'	134				bagged
GR 1240	58 32.3'	138 00.3'	134				GEOTECH/173 cm
GR 1241	58 32.3'	138 00.1'	132	0-82 cm	82-178 cm	-	
GR 1242	58 26.0'	137 47.3'	167				GEOTECH/199 cm
GR 1243	58 26.0'	137 47.3'	167	0-110 cm	110-189 cm	-	
GR 1244	58 21.3'	137 28.6'	197				GEOTECH/96 cm
GR 1245	58 21.3'	137 28.2'	197	0-99 cm	-	-	
GR 1246	58 24.7'	137 23.8'	173	0-22 cm	-	-	
GR 1247	58 24.9'	137 23.8'	172				cc/bagged
GR 1248	58 25.0'	137 23.9'	171				cc/bagged

SAMPLE #	LATITUDE		LONGITUDE		DEPTH (M)	LENGTH OF CORE			COMMENTS
	(N)		(W)			SECT. 1	SECT. 2	SECT. 3	
SH 1249	58	29.8'	137	42.2'	170				bagged
GR 1250	58	29.4'	137	42.3'	167	0-42 cm	-	-	
SH 1251	58	38.6'	137	53.2'	78				bagged
SH 1252	58	30.6'	137	53.2'	78				bagged
SH 1253	58	39.4'	137	46.4	33				bagged
VV 1254	58	39.4'	137	46.3'	32	0-12 cm/A	0-8.5/B		1 bag; core A subsampled
VV 1255	58	34.7'	137	41.2'	63	0-14 cm	0-12 cm		1 bag; core A subsampled
VV 1256	58	33.2'	137	37.2'	85	0-14 cm	0-10 cm		core A subsampled
VV 1257	58	32.4'	137	38.2'	124	0-21 cm	0-22 cm		1 bag; core A subsampled
VV 1258	58	31.3'	137	31.3'	72	0-17 cm	0-16.5 cm		1 bag; core A subsampled
VV 1259	58	28.3'	137	27.0'	102	0-23 cm	0-21 cm		1 bag; core A subsampled
VV 1260	58	27.8'	137	23.9'	85	0-21 cm	0-20 cm		1 bag; core A subsampled
VV 1261	58	26.8'	137	20.6'	80	0-21 cm	0-22 cm		1 bag; core A subsampled
VV 1262	58	27.1'	137	19.4'	42	0-11 cm	0-16.5 cm		1 bag; core B subsampled
VV 1263	58	24.9'	137	15.3'	113	0-22.5 cm	0-20.5 cm		core B subsampled
VV 1264	58	23.0'	137	11.5'	130	0-21 cm	0-20 cm		1 bag; core A subsampled
VV 1265	58	36.4'	137	43.6'	42				1 bag

SAMPLES 1266/601 - 1285/621 collected with Van Veen aboard Monark:

1266/601 58 25.2' 137 09.7' 15

1267/602 58 25.5' 137 11.0' 13

1268/603 58 26.5' 137 13.7' 17

off Finger Glacier

SAMPLE #	LATITUDE	LONGITUDE	DEPTH	LENGTH OF CORE			COMMENTS
				SECT. 1	SECT. 2	SECT. 3	
	(N)	(W)	(M)				
1269/604	58 27.1'	137 15.9'	17				east side, La Perouse Glacier
1270/605	58 27.5'	137 16.9'	16				middle, La Perouse Glacier
1271/606	58 27.7'	137 17.7'	12				middle, La Perouse Glacier
1272/607	58 27.9'	137 18.0'	7				near runoff stream
1273/608	58 28.7'	137 18.2'	11				west side, La Perouse Glacier
1274/609	58 29.2'	137 21.9'	9				the "Tit"
1275/610	58 30.4'	137 24.4'	9				Doglet Stream
1276/611	58 31.1'	137 26.0'	11				
1277/612	58 32.3'	137 28.2'	8				
419 1278/613	58 33.1'	137 29.9'	10				Topsy Creek reef
1279/614	58 33.3'	137 31.2'	10				west of Topsy Creek
1280/615	58 34.5'	137 33.8'	14				off Chablis Creek
1281/616	58 36.0'	137 36.8'	13				cove east of Lituya Bay
1282/617	58 36.1'	137 38.7'	15				off Lituya moraine
1283/618	58 38.0'	137 35.0'	beach				south shore, Cenotaph Island
1284/620	58 37.2'	137 38.4'	5				Anchor Cove
1285/621	58 38.1'	137 40.7'	16				west of Lituya Bay entrance
SH 1286	58 22.5'	137 52.6'	165				bagged
GR 1287	58 22.7'	137 52.5'	165	0-28 cm	-	-	
SH 1288	58 20.0'	137 58.4'	135				bagged

SAMPLE #	LATITUDE		LONGITUDE		DEPTH (M)	LENGTH OF CORE			COMMENTS
	(N)		(W)			SECT. 1	SECT. 2	SECT. 3	
SH 1289	58	15.9'	138	06.8'	133				bagged
GR 1290	58	16.0'	138	06.8'	133	0-20 cm	-	-	
SH 1291	58	12.5'	138	13.7'	150				bagged
GR 1292	58	12.6'	138	13.8'	150				33 cm/bagged
SH 1293	58	11.5'	138	16.2'	135				bagged
SH 1294	58	11.0'	138	18.0'	144				bagged/small sample
SH 1295	58	11.1'	138	18.1'	144				bagged
SH 1296	58	07.3'	138	24.9'	172				bagged
GR 1297	57	56.7'	138	03.3'	1212	0-94 cm	94-192 cm	-	
GR 1298	58	00.7'	138	01.3'	178	0-23 cm	-	-	
SH 1299	58	02.8'	137	56.9'	173				bagged
SH 1300	58	04.8'	137	52.5'	165				bagged
SH 1301	58	11.0'	137	44.4'	159				bagged/small sample
SH 1302	58	17.2'	137	35.6'	174				bagged
GR 1303	58	17.2'	137	35.6'	174				cc + short core/bagged
GR 1304	58	17.3'	137	35.8'	174	0-66 cm	-	-	
SH 1305	58	19.1'	137	16.4'	184				bagged
GR 1306	58	19.1'	137	16.4'	184	0-68 cm	68-168 cm	-	
GR 1307	58	19.1'	137	16.3'	184				GEOTECH/155 cm
SH 1308	58	20.0'	137	01.3'	159				bagged

SAMPLE #	LATITUDE		LONGITUDE		DEPTH (M)	LENGTH OF CORE			COMMENTS
	(N)		(W)			SECT. 1	SECT. 2	SECT. 3	
GR 1309	58	20.0'	137	01.3'	159	0-58 cm	-	-	
GR 1310	58	20.1'	137	01.3'	158				GEOTECH/34 cm
SH 1311	58	22.0'	136	58.7'	80				bagged
GR 1312	58	22.0'	136	58.5'	78				26 cm/bagged
SH 1313	58	18.0'	136	54.1'	110				bagged
GR 1314	58	18.0'	136	54.0'	110	0-78 cm	78-156 cm	-	
SH 1315	58	16.1'	137	00.4'	177				bagged
GR 1316	58	16.0'	137	00.5'	163				40 cm/bagged
421 GR 1317	58	16.0'	137	00.4'	167	0-82 cm	-	-	
SH 1318	58	15.8'	137	01.8'	155				bagged
SH 1319	58	14.1'	136	47.8'	95				bagged
GR 1320	58	14.1'	136	47.7'	95	0-81 cm	-	-	
SH 1321	58	16.1'	136	52.9'	92				bagged
GR 1322	58	16.1'	136	52.9'	95				GEOTECH/192 cm
GR 1323	58	16.2'	136	53.0'	93				GEOTECH/290 cm
GR 1324	58	16.2'	136	52.8'	93	0-123 cm	123-223 cm	223-320 cm	

SAMPLES 1325/622 - 1334/631 collected with Van Veen aboard Monark:

1325/622	58	23.75'	137	03.70'	21				Kaknau Creek
1326/623	58	24.38'	137	0.36'	4.5				west end, Palma Bay beach
1327/624	58	24.15'	136	58.74'	4.5				stream west of De Langle Mt.



SAMPLE #	LATITUDE		LONGITUDE		DEPTH	LENGTH OF CORE			COMMENTS
						SECT. 1	SECT. 2	SECT. 3	
	(N)		(W)		(M)				
1328/625	58	23.65'	136	54.80'	6.5				Boussole Bay
1329/626	58	23.0'	136	53.8'	7				Astrolabe Bay
1330/627	58	22.08'	136	51.60'	beach				Thistle Cove beach
1331/628	58	22.20'	136	51.54'	beach				Thistle Cove beach
1332/629	58	22.03'	136	52.0'	2.5				Thistle Cove
1333/630	58	21.68'	136	50.8'	3.7				Dixon River mouth, Dixon Harbor
1334/631	58	20.98'	136	48.48'	0.1				Torch Bay
GR 1335	58	10.9'	136	53.5'	175				GEOTECH/147 cm
422 GR 1336	58	10.6'	136	53.1'	178	0-118 cm	-	-	
GR 1337	58	08.9'	136	58.0'	199	0-22 cm	-	-	
GR 1338	58	06.4'	137	04.1'	211				GEOTECH/187 cm
GR 1339	58	06.3'	137	03.9'	222	0-137 cm	137-237 cm	237-337 cm	
SH 1340	58	03.0'	137	11.7'	137				bagged
SH 1341	58	13.1'	137	11.0'	117				bagged
SH 1342	58	14.8'	137	05.4'	107				bagged
SH 1343	58	16.6'	137	09.2'	157				bagged
GR 1344	58	16.6'	137	09.2'	158	0-30 cm	-	-	
SH 1345	58	12.7'	137	15.7'	122				bagged
GR 1346	58	12.7'	137	15.8'	123	0-23 cm	-	-	
SH 1347	58	09.0'	137	22.3'	128				bagged

SAMPLE #	LATITUDE (N)	LONGITUDE (W)	DEPTH (M)	LENGTH OF CORE			COMMENTS
				SECT. 1	SECT. 2	SECT. 3	
GR 1388	58 54.7'	136 58.5'	373	0-61 cm	-	-	Sta. G.B. 4/150 lb wt.
SH 1389	58 52.0'	137 04.6'	344				Sta. G.B. 3
SAMPLES 1390/632 - 1398/641 collected aboard <u>Monark</u> :							
1390/632	58 54.0'	136 55.8'					Lamplug Glacier
1391/633	58 53.3'	137 01.4'					Johns Hopkins/1st glacier, S.E. side
1392/634	58 52.5'	137 02.3'					J.H./2nd glacier, Kashoto?
1393/636	58 50.1'	137 06.3'					J.H./S. side Gilman Gl., on delta
1394/637	58 51.6'	137 06.2'					J.H./muddy waterfall, dirty gl., Tyeen?
423 1395/638	58 51.7'	137 04.5'					J.H./stream across from Hoonah Gl.
1396/639	58 53.2'	137 04.1'					J.H./across from Kashoto Gl.
1397/640	58 53.8'	137 03.7'					J.H./stream, N. side Toyatte Gl.
1398/641	58 55.2'	137 02.1'					J.H./Topeka Gl. stream, N. side of delta
SM 1399	58 53.4'	136 48.8'	374				Sta. G.B. 6
GR 1400	58 53.3'	136 48.4'	358	0-29 cm	-	-	Sta. G.B. 6
SH 1401	58 51.6'	136 34.8'	424				Sta. G.B. 7
SH 1402	58 50.1'	136 30.5'	430				Sta. G.B. 10
SH 1403	58 48.1'	136 26.0'	431				Sta. G.B. 11
SH 1404	58 42.3'	136 13.2'	243				Sta. G.B. 12
SH 1405	58 39.9'	136 09.5'	324				Sta. G.B. 13
SH 1406	58 36.1'	136 02.8'	190				Sta. G.B. 16

311-79 AS STATION POSITIONS & DEPTH - VIDRACORES

STA	LATITUDE N	LONGITUDE W	DEPTH M	SECT. 1 CM	CORE LENGTH			COMMENTS	
					SECT. 2 CM	SECT. 3 CM	SECT. 4 CM		
VIDR 1	59 06.00	138 42.36	56	bagged				mud	
VIDR 2	59 06.00	138 42.17	51	10 - 50	60 - 100	110 - 155			
VIDR 3	59 16.33	139 12.29	35	bagged cc				sand	
VIDR 4	59 17.20	139 15.20	35	bagged				sand	
VIDR 5	59 17.49	139 16.10	36	0 - 60	+ 1 bag			sand	
VIDR 6	59 17.74	139 17.31	39	0 - 20	30 - 50	60 - 95	+ cc	sand & clay	
VIDR 7	59 10.04	139 56.17	116	0 - 29	+ 1 bag (cc)			pebbly, sandy mud	
VIDR 8	59 03.94	139 01.41	122	0 - 29	+ 2 lg bags from frame, 1 lg pebble, cc"			"	
VIDR 9	59 03.50	138 24.65	35	bagged					
VIDR 10	59 03.62	138 24.63	36	bagged				sand	
424 VIDR 11	59 03.53	138 25.32	42	10 - 27	+ bagged top, cc				
VIDR 12	59 03.55	138 25.21	42	0 - 22	+ cc				
VIDR 13	59 02.34	138 24.86	59	10 - 28	+ cc				
VIDR 14	59 02.21	138 25.50	60	10 - 50	60 - 92	+ cc			
VIDR 15	59 03.30	138 28.44	85	"0 - 50"	60 - 100	110 - 142	+ bagged top, cc		
VIDR 16	59 05.05	138 30.97	47	10 - 50	60 - 100	110 - 168			
VIDR 17	59 06.05	138 41.34	50	10 - 50	60 - 100	110 - 162	+ bagged top, cc		
VIDR 18	59 05.98	138 41.51	45	10 - 50	60 - 100	110 - 125	+ cc		
VIDR 19	59 05.70	138 41.75	62	10 - 50	60 - 100	110 - 167	+ bagged top, cc		
VIDR 20	59 05.81	138 42.01	52	10 - 50	60 - 100	110 - 153	+ cc		
VIDR 21	59 02.45	138 25.38	55	10 - 50	60 - 100	110 - 136			
VIDR 22	59 02.22	138 25.56	58	entire core frozen for gas analysis					
VIDR 26	59 17.27	139 16.03	38	10 - 50	60 - 79	+ cc			

STATION	DATE	TIME	ELEVATION M	DEPTH M	SECT.				COMMENTS	
					1 CM	2 CM	3 CM	4 CM		
22V 27	59	17.15	139	16.16	41	0 - 39	+ cc			
22V 28	59	17.62	139	13.26	28	bagged			sand	
22V 29	59	02.05	139	25.65	51	0 - 27	+ cc			
22V 30	58	59.04	139	43.51	150	10 - 50	60 - 100	110 - 150		
22V 31	58	52.10	139	34.15	100	0 - 35	(20 cm core + 13 cm with cc)		pebbly sandy mud over clay	
22V 32	59	42.90	139	13.20	130	bagged			pebbles, mud	
22V 33	58	25.00	136	00.05	64	bagged			pebbles, shell	
22V 34	58	22.50	135	58.69	70	bagged			pebbles, shell	
22V 35	59	03.90	136	12.70	260	0 - 150	150 - 301	+ cc	top overflow	
22V 36	59	03.25	136	12.62	265	0 - 135	135 - 205	205 - 433	433 - 578	top overflow
425 22V 37	59	03.97	136	12.53	260	0 - 131	131 - 201	201 - 431	431 - 501	
						SECT. 5/ 596 - 736	SECT. 6/ 736 - 898			
22V 38	59	03.80	136	12.49	260	0 - 31.5	31.5 - 102.5	102.5 - 332.5	362.5 - 513.5	
						(top 30 cm of SECT. 4 bagged)				
						SECT. 5/ 588.5 - 642.5	SECT. 6/ 642.5 - 792.5			
22V 39	59	03.26	136	12.62	270	0 - 89	89 - 238	238 - 388	394.5 - 538	
22V 40	59	03.83	136	12.99	210	0 - 63	63 - 213			
22V 41	59	02.05	136	09.62	245	7 - 134				
22V 42	58	59.28	136	07.26	245	0 - 151	151 - 301			
22V 43	58	59.23	136	07.63	245	0 - 138	138 - 288	288 - 438	438 - 588	
22V 44	58	55.76	136	08.65	305	bagged				
22V 45	58	55.79	136	08.74	303	0 - 59				
T.V. 46	59	55.69	136	04.30	66	bagged (gravelly sandy mud from T.V. sled)				
22V 47	59	30.72	136	05.42	310	0 - 108	108 - 258			
22V 48	58	50.77	136	05.30	230	0 - 33	33 - 103	103 - 332	332 - 423	

S11-79 EG STATION POSITIONS & DEPTH - GRAVITY CORES

STA #	LATITUDE N	LONGITUDE W	DEPTH M	SECT. 1 CM	SECT. 2 CM	SECT. 3 CM	SECT. 4 CM	COMMENTS
GRAV 49	58 53.70	137 02.40	370	bagged (2 bags)				
GRAV 50	58 53.80	137 02.24	370	0 - 117	117 - 267	267 - 417	+ cc	
GRAV 51	58 54.48	136 58.51	380	0 - 90	90 - 240	240 - 390		
GRAV 52	58 50.62	136 31.78	428	bagged				
GRAV 53	58 52.47	136 31.40	230	bagged (3 bags)				
GRAV 54	58 54.92	136 33.06	150	0 - 42	42 - 192	+ cc		
GRAV 55	58 54.58	136 32.28	165	0 - 135				
GRAV 56	58 56.17	136 37.98	185	0 - 91				
GRAV 57	58 59.32	136 56.74	335	bagged				
GRAV 58	58 59.32	136 56.74	340	bagged				
426 GRAV 59	58 58.75	136 54.01	228	bagged cc				
GRAV 60	58 58.75	136 53.56	44	0 - 28				
BP4SU79E S 2	58 30.9	139 39.9	262	0 - 110				Surveyor core
BP4SU79E S 7	58 46.5	139 32.6	161	0 - 48				Leg 5
BP4SU79E S17	59 02.5	138 50.7	111	0 - 117				"

S11-79 EG WATER SAMPLES:

WS-1	59 07.6	138 39.0		off Dry Bay				
WS-4	59 07.6	138 39.0		off Dry Bay				concentrated
WS-5	59 10.8	138 13.3		Alsek River (pebble beach)				
WS-6	59 14.15	138 13.0		Alsek River				
WS-6/ALSEK 2 - bagged coarse sand & pebbles								
WS-7	59 10.9	138 25.8						
WS-7/ALSEK 1 - bagged coarse sand & pebbles								
WS-8	59 11.3	138 18.7		pebble & cobble beach				
WS-9	59 12.7	138 11.2		on the lake				
WS-9/ALSEK 4 - bagged fine sand & silt								
CLEAR CREEK	59 02.0	138 12.6		bagged sand				

ANNUAL REPORT

Contract #: 03-5-022-55  
Research Unit #: 251  
Task Order #: C1  
Reporting Period: 04/01/79-12/31/79  
Number of Pages: 47

SEISMIC AND VOLCANIC RISK STUDIES  
WESTERN GULF OF ALASKA

H. Pulpan  
J. Kienle

Geophysical Institute  
University of Alaska  
Fairbanks, Alaska

May 13, 1980

TABLE OF CONTENTS

PAGE

I.	SUMMARY . . . . .	427
II.	INTRODUCTION . . . . .	9
III.	CURRENT STATE OF KNOWLEDGE . . . . .	7
IV.	STUDY AREA . . . . .	11
V.	SOURCES, METHODS, AND RATIONALE OF DATA COLLECTION . . . . .	115
VI-VII.	RESULTS AND DISCUSSION . . . . .	152
VIII.	CONCLUSIONS . . . . .	177
IX.	NEED FOR FURTHER STUDY . . . . .	177
X.	SUMMARY OF FOURTH QUARTER OPERATIONS . . . . .	177
XI.	REFERENCES . . . . .	177
APPENDIX:	LAHARS IN CRESCENT RIVER VALLEY, LOWER COOK INLET, ALASKA . . . . .	177

## I. SUMMARY

This report presents the status and the most recent results of an ongoing study which concerns itself with the assessment of the seismic and volcanic hazards associated with petroleum-related developments on a portion of the Alaskan Outer Continental Shelf.

We delineate the major seismic source zones of a region that includes the potential lease areas of lower Cook Inlet, the Kodiak Island Shelf, Shelikof Strait and Bristol Bay. This delineation is based upon historic earthquake data and data derived from a high-gain, telemetered seismic network whose operation is part of the program. Recent seismic activity in the southwestern portion of the study area is discussed in the light of the possible extent of the future rupture zone of a great earthquake ( $M \geq 7.8$ ) that might originate within the Shumagin seismic gap. Focal mechanism studies of selected earthquakes are interpreted in terms of the basic seismo-tectonic processes in the area. We also report on the development of a seismic event detection system, and the routine operation of the seismic network.

The volcanological hazards aspects of the program has reached a major milestone with the publication of a preliminary report on the volcanic hazards of Augustine volcano. Recent results of volcanic hazards related field work are discussed, particularly lahars of Redoubt Volcano in the Crescent River Valley of lower Cook Inlet.



## II. INTRODUCTION

### General Nature and Scope of Study

The present study attempts to develop, for a particular region of the Alaskan Outer Continental Shelf, the technical and scientific basis for decisions related to the impact of seismic and volcanic activity upon the environment as it affects petroleum development. It is a data gathering program in its attempt to obtain pertinent data from a large and remote area at a resolution not previously possible. It is also a scientific program in its attempt to obtain, partly based upon the data, a better understanding of the processes underlying these activities, and it is a technical program in its attempt to quantify, based upon the best understanding gained, the associated risk. The study is one of several such studies, which together cover a major portion of a seismic-tectonic regime, unique for the United States.

### Specific Objectives

The specific objectives over the past years have been (1) to monitor the seismic activity of lower Cook Inlet, Shelikof Strait, and the offshore areas near Kodiak Island and the Alaska Peninsula (The latter between Kodiak Island and the Semidi Islands); (2) to delineate, based upon the seismicity data, potential seismic source areas such as faults; (3) to monitor the seismic activity of some Cook Inlet volcanoes (especially Augustine Island) and to relate this activity to their eruption potential; and (4) to evaluate volcanic hazards of Augustine Island. During the past year we have added to the specific objectives to (1) obtain ground motion records associated with larger earthquakes (strong

motion records), to (2) study in detail (in conjunction with RU 579) the seismic activity in an area off Kodiak Island, (3) to extend the coverage of the seismic network into the Bristol Bay lease area, and (4) expand the volcanic hazard studies to include the Katmai-Shelikof Strait region.

#### Relevance to Problems of Petroleum Development

Petroleum development will require the erection of large temporary and permanent structures. With respect to aseismic design, knowledge of the space-time behavior of large earthquakes, the attenuation of strong ground motion with distance, and the modification of strong ground motion by surficial soil layers is of paramount importance.

Prediction of the space-time behavior requires understanding of the fundamental seismotectonic processes and the largest possible record of seismic activity. Attenuation of strong ground motion with distance, and its modification by soils requires the accumulation of actual strong ground-motion recordings under a variety of conditions.

With respect to volcanic hazards, the type and reach of potentially hazardous phenomena such as, ash flows, glowing clouds (nuées ardentes), ashfalls, toxic fumes, is of consequence. This requires the identification of volcanoes likely to erupt and the determination of the probable eruptive style.

### III. CURRENT STATE OF KNOWLEDGE

#### A. Basic Tectonic Setting

The tectonics of the Gulf of Alaska area is dominated by the interaction between the North American and Pacific plates. Along the Queen Charlotte-Fairweather faults, the two plates are slipping past one

another along a right lateral transform fault system. Along the Aleutian island arc and the Aleutian-Alaska Range, up to Mt. McKinley, the oceanic Pacific plate is underthrusting the North American plate. The Aleutian trench axis marks the initial down bending of the oceanic plate, and the active volcanic arc approximately traces the 100 km depth contour of the subducted plate. The transition zone between these two distinct tectonic regimes lies between the Denali fault and the Gulf of Alaska and contains a complicated system of thrust and strike slip faults. Recently Lahr and Plafker (1980) have proposed a model where this transition zone is divided into two sub-blocks which are partially coupled to the Pacific plate.

#### B. Faults

In our study area, three major fault systems have been mapped--the Castle Mountain fault, the Bruin Bay fault and the Border Ranges fault; in addition, a major unnamed thrust fault separates the Mesozoic and the Cenozoic in southern Kodiak. The trace of the Castle Mountain fault cuts the grain of the arc system at an oblique angle of 20 degrees and transects the volcano line just south of Mt. Spurr volcano. The relative motion along this fault is right lateral strike slip. Fairly recent displacements have occurred along the Castle Mountain fault as indicated by offset Pleistocene glacial deposits and lineations (Evans et al., 1972). Both, the Bruin Bay and the Border Ranges faults are thrusts that follow essentially the trend of the arc structure. However, neither of these faults show any evidence of recent displacement--the Border Ranges fault has been inactive since late Mesozoic-early Tertiary time and the Bruin Bay fault is not off-setting any strata younger than 25 million years (Magoon et al., 1976).

With regard to the offshore areas, seismic reflection surveys indicate little recent surface faulting in the lower Cook Inlet (Magoon et al., 1979). A few small faults have been observed north of the Augustine-Seldovia arch. Normal faults associated with horst and graben tectonics are common near Augustine Island. Surface faulting of the seafloor is indicated in Shelikof Strait between Cape Douglas and Shyak Island (Magoon et al., 1979).

A major zone of faults trends approximately  $N90^{\circ}-50^{\circ}W$  along and offshore of Kodiak Island, with individual faults offsetting the seafloor a maximum of about 10 m (Hampton et al., 1979). This faulted zone could be contiguous with faults to the northeast, off Montague Island, which were active during the 1964 Alaska earthquake (Malloy and Merrill, 1972). A series of major faults is also associated with the shelf break off Kodiak Island.

### C. Seismicity and Seismic Source Zones

The most dominant source of earthquakes in our study area is the Benioff zone, which consists of a shallow, gently-dipping thrust portion and a more steeply-dipping portion that reaches a maximum depth of about 200 km behind the volcanic arc. The potential lease areas of Cook Inlet and Shelikof Strait lie above the steeper-dipping portion while those of Kodiak Island are located above the shallow thrust zones. Within the confines of the seismic network, these zones have been fairly well delineated.

In the Kodiak shelf area, between  $152^{\circ}W$  and  $154^{\circ}W$ , the shallow thrust zone appears especially active (Pulpan and Kienle, 1979). This highly active zone also contains large sediment slides and relatively

strong structural deformation (Hampton et al., 1979). The concentration of seismic activity ends where slides also end and structural deformation decreases significantly. This supports the idea of tectonic segmentation into relatively more or less active zones. Correlation between the seismicity and individually mapped shallow faults has not been established yet.

In lower Cook Inlet a zone of high seismic activity exists below Illiamna volcano. This activity is associated with the deeper portion of the Benioff zone.

Aside from the intense seismicity in the shallow thrust zone, shallow seismicity (hypocentral depth less than 50 km) is diffuse and not preferentially associated with major fault systems. Some shallow seismic clusters do, however, correlate with some volcanoes in Cook Inlet and on the Alaska Peninsula. A persistent linear trend of seismic activity occurs on Kodiak Island near Deadman Bay.

#### D. Volcanology

Calc-alkaline volcanism along the Aleutian arc is the result of plate convergence between the North American and Pacific plates. Nineteen volcanoes form the eastern Aleutian arc from the upper Alaska Peninsula to Cook Inlet. Of these, eight have erupted in this century and another six have active fumarole fields. The 1912 Katmai eruption was one of the largest eruptions in the world in this century. So far we have only considered two of the most active Cook Inlet volcanoes, Augustine and Redoubt.

Augustine Volcano: We have now a reasonable understanding of (1) its eruptive history, (2) its geology and geochemistry, (3) its internal structure, (4) its recent (past 9 years) seismicity and eruptive style.

The principal hazards of Augustine Island are glowing avalanche-nuée ardente eruptions, mudflows, bomb and ash falls, poisonous gases, acid rains and tsunamis. Of these, the most serious hazard to offshore oil and gas development are glowing avalanches and nuées ardentes. Ballistic studies indicate that the ejection range of large bombs is mainly restricted to the Island itself. Ash from the 1976 eruption spread all over southern Alaska, as far north as Anchorage and Talkeetna, and as far east as Sitka, 1100 km away. The ash dispersal is strongly dependent on the prevailing wind directions. Near the island ash falls can be heavy accompanied by acid rains and clouds of noxious fumes. It is clear that no place on the Island itself is safe to erect permanent or semi-permanent structures. The 1883 eruption produced tsunamis that crossed the entire lower Cook Inlet.

Redoubt Volcano: Unlike Augustine Volcano, the much higher peak of Redoubt (10,197 feet) is covered by glaciers which adds hazards due to floods and massive mudflows. For example, during the January 1966 eruptions, excessive meltwater may have accumulated in the summit crater (1 x 1.6 km in size, at an elevation of 8,000 to 8,500 feet) and then drained catastrophically. The outburst of water and ice from the crater apparently caused the Drift River to break up in mid-winter. Two separate flash floods reached the mouth of the Drift River the first of which carried large ice blocks. Such flooding may pose a serious threat to the Drift River Tanker Terminal, which was constructed after the 1966 floods.

Another flood hazard arises from the fact that the glacier that descends from the summit crater due north, the North Glacier, could dam up the Drift River. If an advance occurs, the river could get dammed creating a lake that could drain catastrophically.

Last year, extensive lahar deposits (minimum volume of 170 million m<sup>3</sup>) were discovered in the Crescent River Valley. They practically fill the entire valley and were erupted 3,635 years B.P. A preprint of a paper by Riehle et al. (1980) discussing these deposits is given in Appendix 1. The new discovery of such extensive lahar deposits emphasizes the great potential of Redoubt to produce massive lahars in the valleys radiating from it. Little is known about the geology of Mt. Redoubt, which has never been mapped in detail. Historic eruptions occurred in 1778, 1819, 1902, 1933 and 1965-68 with eruption intervals ranging from 31 to 83 years.

#### IV. STUDY AREA

Over the past years the main target areas for the study were Cook Inlet and the shelf area off Kodiak Island. Recently, the potential lease areas of Shelikof Strait and Bristol Bay have been included into this program. The active seismic zone off Kodiak Island has received special consideration through a cooperative program with RU 579. The volcanic hazards portion of the program which originally was primarily concerned with Augustine Island has now extended to include Redoubt, Mt. Douglas and some other Alaska Peninsula volcanoes.

#### V. SOURCES, METHODS AND RATIONALE OF DATA COLLECTION

##### A. High Gain Network

The major effort in data collection concerns the operation of a regional, high-gain, telemetered seismic network. Data from this

network permit the delineation of the seismic source zones (Benioff zone segmentation, faults, seismic gap boundaries), the study of short-term space-time behavior of seismicity, the determination of the mode of tectonic deformation (from fault plane solutions) and the study of seismicity patterns associated with volcanic activity. Figure 1 shows the latest layout of this system, including the new installation planned for installation in Bristol Bay. The network consists of 28 short-period, vertical component seismographs.

One of the major technical changes affected during this past year was the design, testing and installation of a seismic event detection and recording system. The field installation occurred in King Salmon. There are several reasons that lead to the development of this system. Under the present system, the extension of the network into Bristol Bay would have required the lease of an additional telephone line between Dillingham and Homer (at a cost of approximately \$14,000 per year). By placing a recording system in King Salmon a line between Dillingham and King Salmon only is required. Also, the present mode of continuous recording on Develocorders is both expensive in materials and maintenance; the digital recording of "useful" information only, as controlled by the event detector, will permit faster and less labor-intensive routine data processing.

No major technical changes have been made, but we have continued our effort to make the system even more resistive to the harsh environment and technically more reliable. Minor changes included the installation of a repeater station between Blue Mountain (BMT) and King Salmon and the installation of a parallel VHF link between these sites, to make this important link more reliable. Environmentally more protective



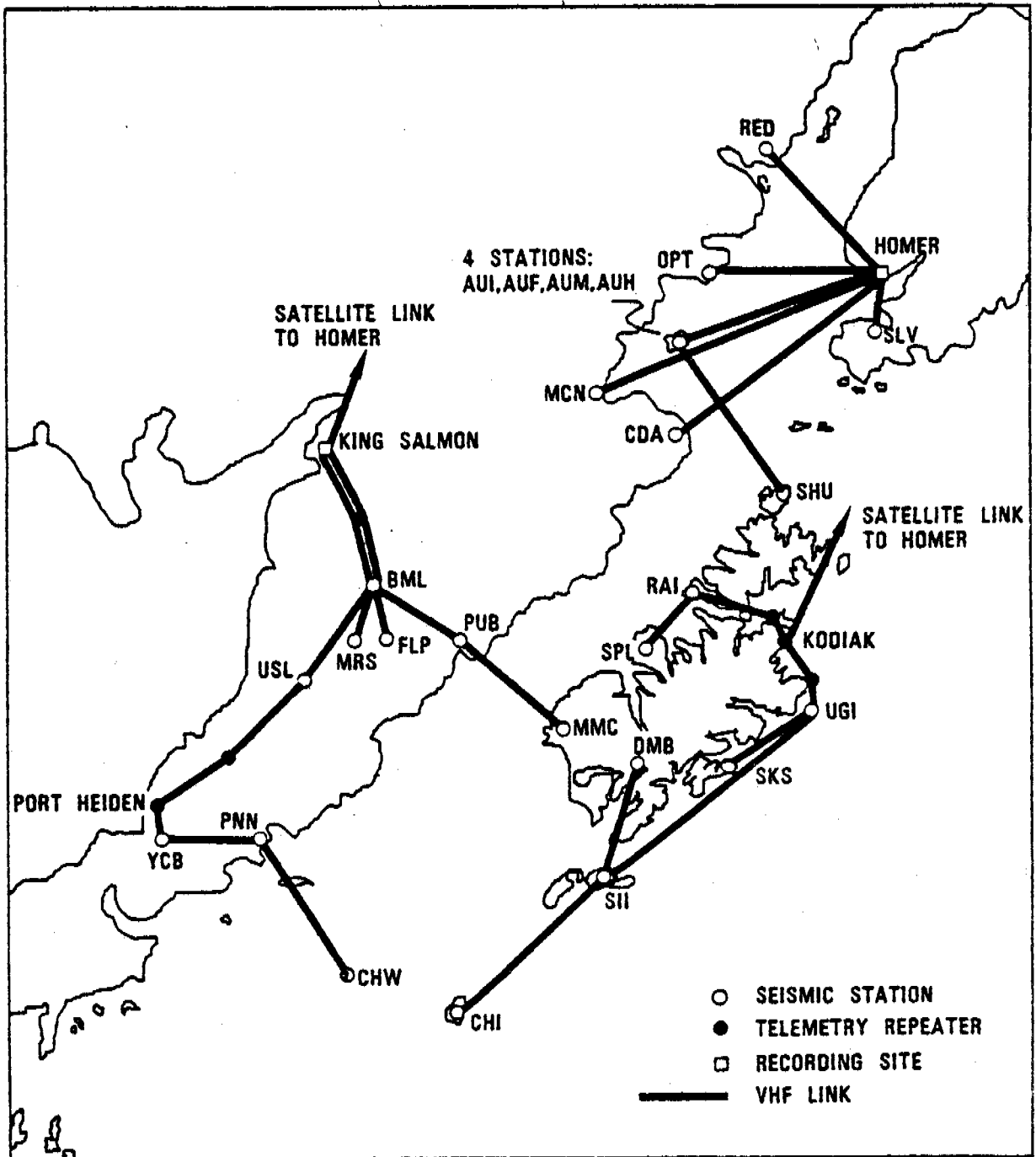


Fig. 1 - Present configuration of the seismic networks in Cook Inlet, on Kodiak and on the Alaska Peninsula.

housings for the electronic equipment were installed throughout the system. On the whole, the system has performed well during the past year.

For some of the studies conducted during this year, we have used seismic data from adjoining networks and from the Worldwide Standard Seismograph System.

#### B. Strong-motion Accelerographs

Over the recent years, we have begun to install strong-motion accelerographs at certain locations of the high-gain network. We are presently operating Kinematics SMA-1 instruments at (see Figure 1) PNN, BMT, and SII and the instruments developed by the University of Texas at UGI, SKS, and CHI. The purpose of these instruments is to obtain strong ground motion records associated with larger earthquakes ( $M > 6$ ) in order to eventually obtain a representative relationship between the attenuation of this ground motion with distance.

#### C. Volcanological Field Work

Volcanological-glaciological field work, was carried out last year on Augustine and Redoubt Volcanoes in Cook Inlet.

Augustine Volcano: In June 1979, J. Kienle and S. Swanson spent 13 days on the Augustine Island to study historic and prehistoric flows and tephra on the north and east side of Augustine Island, to collect samples for geochemical analysis and to find  $C^{14}$  datable organic material.

Redoubt Volcano: During last year's (1979) field season, the volcano was visited by a joint State of Alaska, Geological and Geophysical Surveys' field party (J. Riehle and K. Emmel) and University of Alaska

(J. Kienle, S. Swanson, P. MacKeith and D. Solie) from August 4 to 11. New vertical aerial photo coverage now covering all of Redoubt Volcano was obtained last year.

We resurveyed the 15 stakes on the North Glacier terminus from the 2 baseline bench marks, established in 1978, collected a suite of rocks on the lower flanks of the volcano and conducted reconnaissance mapping of lahars in the upper Drift River and Crescent River valleys (Appendix 1).

## VI-VII. RESULTS AND DISCUSSION

### A. Seismicity

Figures 2 through 11 are quarterly epicenter maps for the first three periods of 1979. In general, the seismicity pattern during these periods supports the conclusion reached over the past years with regards to the predominant seismic source zones of the area: the Benioff zone is the most dominant feature, the highest rate of activity occurring at intermediate depth below the Mt. Iliamna areas of Cook Inlet; a generally diffuse shallow (hypocentral depth less than 50 km) seismicity that does not generally correlate with faults, but occasionally clusters near certain volcanoes; continued shallow seismicity with a more or less linear trend near and north of Deadman Bay on Kodiak Island. Somewhat unusual is the increased seismicity to the southwest of Kodiak Island (Figure 12). Two moderate size earthquakes occurred in that area: a magnitude 5.9 ( $M_b$ ) on February 13, 1979, and a magnitude 6.5 ( $M_b$ ) on May 20, 1979. The first of these we placed at 55 km depth and 55.22°N and 155.92°W. In locating this event, we also used the arrival time at LDGO's station at Sand Point (SDN). A joint solution using additional

data from the LDGO network, and using the structural model adopted by LDGO, places the event at 50-km depth and about 55.2°N and 157.0°W (Davies and Jacob, 1979). The occurrence and location of this event is of interest with respect to its relationship with the Shumagin gap. Most of the seismic energy accumulated as consequence of the convergence of the North-American and Pacific plates along the Aleutian-Alaskan arc system is released during great ( $M > 7.8$ ) earthquakes (Kanamori, 1977). The aftershock zones of these great earthquakes have fairly sharp boundaries indicating that portion of the system over which accumulated energy has been released. Areas left between recent aftershock zones, the seismic gaps, thus appear to be the most likely sites for the next great earthquakes. The Shumagin Island area is presently considered to be part of such a seismic gap. Its eastern boundary is generally considered to be the western margin of the aftershock zone associated with the 1938 magnitude 8.3 ( $M_S$ ) earthquake. The aftershock zone of that event is not well defined (Sykes, 1971). Its eastern boundary appears to coincide with the western boundary of the rupture area of the 1964 great Alaska earthquake. This boundary coincides with a transverse boundary perpendicular to the arc through Wide Bay which has seismic, volcanic and geological expressions (Pulpan and Kienle, 1979). Such termination of aftershock zones of the Alaska-Aleutian plate boundary by transverse boundaries, has been observed by others (Mogi, 1969; Sykes, 1971; Pulpan and Kienle, 1979). The western boundary of the 1938 event is probably limited by the location of the main shock (55.5°N, 158.4°W) or one of the better located aftershocks (55.1°N, 158.8°W) (Davies, personal communication). The above margin implies a length of somewhat more than 300 km for the rupture length of the 1938 event. Such a

length is consistent with the seismic moment derived by Kanamori (1977) for this event.

If we accept the above limits for the 1938 rupture zone, the February 17, 1979 event would be located within it. It is also aligned with three other moderate sized events of magnitude 5.4 and above, which Davies and Jacob (1979) interpret as part of a "Mogi doughnut", i.e., the perimeter of a highly stressed zone, that is seismically active as opposed to its interior, and which has been observed to outline the rupture area of a future large earthquake (Mogi, 1969). Thus, the February 13, 1979 event indicates the possibility of the rupture surface of a future great earthquake in the Shumagin seismic gap to extend through the aftershock zone of the 1938 event.

The cluster of events near Chirikof Island on Figure 12, is associated with the February 13, 1979 event. It presents a mislocation of those aftershocks for which no readings from LDGO's Sand Point (SDN) station was available. It is indicative of the problems associated with the attempt to locate events outside the network with poor azimuthal control. Those events that were originally located using SDN were also located without that station. Figure 13 shows the rather erratic change in the location, though there is a general tendency for the location to be pulled towards the closest station (CHI, on Chirikof Island).

Another moderate size earthquake occurred on May 20, 1979 within the block defined by the aftershock zone of the 1938 event. We located this magnitude 6.5 ( $M_B$ ) event at  $56.60^\circ\text{N}$  and  $157.07^\circ\text{W}$ , i.e., arcward from the shallow thrust zone where the subducted plate bends, attaining its steeper dip. The USGS's preliminary determination of epicenter (PDE) service, using depth phases, located this event at 72 km, which we

believe to be more correct than our own hypocentral depth of 30 km, as this event is also located at the perimeter of our network.

#### B. Source Mechanism Studies

Focal mechanism (fault plane) solutions of earthquakes provide information on the nature of the stress system associated with them. If a statistically representative sample both in time and space can be obtained, it will greatly contribute to the understanding of the mechanical behavior of the system. We have obtained a few such solutions based upon data from both the regional network and the World Wide Standard Seismograph Network (WWSSN).

Figures 14 through 17 show, for different data sets, the first motion distribution, on a stereographic projection of the lower focal hemisphere, for the magnitude 6.5 ( $M_B$ ) earthquake of April 12, 1978 off Kodiak Island. The regional data set (Figure 14) does not permit any solution due to the restricted azimuthal distribution of readings, which is a consequence of the event lying outside the network. First motion polarities obtained from WWSSN long-period stations permit the definition of only one of the two solution planes (Figure 15). This is a steeply-dipping plane which strikes in a direction parallel to the strike of the trench-arc system in this area. The data set based upon the first motion directions from USGS's Earthquake Data Report (EDR) from worldwide short-period stations, also defines just one steeply-dipping plane (Figure 16). Combination of all three data sets (Figure 17) permits the construction of both planes of the solution, the shallow-dipping plane being, however, not very well constrained (shown dashed in the Figure). Based upon the distribution of the aftershocks, which also define a

gently dipping plane (Figure 18), we interpret the latter to be fault plane and the steeply-dipping, well constrained plane as the auxiliary plane of the solution. Thus the April 12, 1978 event represents shallow angle underthrusting between the two converging plates. Similar solutions have been found by Stauder and Bollinger (1966) for the larger aftershocks in this area of the 1964 Alaska Earthquake.

Figures 19 through 22 represent solutions for some intermediate depth events in the lower Cook Inlet area. Parameters of the solutions are given in Table 2. In none of these solutions does either the fault plane or the auxiliary plane (the ambiguity as to which is first and which is the latter is inherent in the method) align itself with the steeply-dipping seismic zone for which these events are representative (see Figure 23 and Table 2). However, in three of the four events the tension axis of the inferred stress system (denoted as T on the figures) aligns itself along the down-dip direction of the seismic zone. The seismicity data indicate that the dip of the seismic zone is approximately 45 degrees at depths below 70 km and that it strikes about N30°E. Thus, for perfect down-dip alignment of the T-axis, the latter should have an azimuth of 300 degrees and a plunge of 45°. Table 1 indicates this alignment for three of the events, though the plunge of the T-axis for the November 27, 1978 event is somewhat steep. The solution for the December 18, 1978 event does not fit the pattern of the other events at all. Here, both tension and compression (denoted P in the figure) axis align themselves more or less along the strike of the seismic zone. It remains to be seen as we complete further solutions how representative this type of solution really is.

Down-dip extension at intermediate depth has been found by Isacks and Molnar (1971) to be predominant in subduction zones which are characterized either by gaps in the seismicity as a function of depth or by absence of deep earthquakes. The latter is the case for the Aleutian-Alaska system. Thus down-dip extension at intermediate depth can be interpreted as indicative of gravitational sinking of the subducting lithosphere. More recent studies indicate that in some descending slabs both down-dip compressional and down-dip extensional events do occur (Hasegawa et al., 1978; Engdahl, 1978). This co-existence of the two types of events is observed in areas where two distinct parallel dipping zones of seismicity have been discerned. Engdahl and Scholz (1977) interpret this as unbending of the slab which produces compressional and tensional stresses in the upper and lower portions of the slab, respectively, the parallel zones of seismicity representing the two stress regimes. Our data do not show down-dip compressional events and no double seismic zone. The first could be due to the small number of mechanism solutions obtained so far, the latter could conceivably be a consequence of hypocenter mislocation due to an improperly assumed crustal velocity structure and the two-dimensionality of that structure which does not take into account the presence of the high-velocity subducting plate. Engdahl et al. (1977) have shown that this lack also has some influence upon the orientation of the stress axes derived in fault plane solutions.

C. Augustine Volcano

A preliminary report on the volcanic hazards of Augustine Volcano has been submitted separately.



Table 1. Fault plane solution parameters

Month	Day	Year	Latitude (Deg)	Longitude (Deg)	Depth (km)	Pole 1		Pole 2		B		P		T	
						Trend (Deg)	Plunge (Deg)	Trend (Deg)	Plunge (Deg)	Trend (Deg)	Plunge (Deg)	Trend (Deg)	Plunge (Deg)	Trend (Deg)	Plunge (Deg)
April	12	1978	56.33	-152.55	30	319	20	136	80	228	01	320	66	137	24
November	27	1977	60.29	-153.49	196	233	38	338	20	90	46	192	12	292	40
February	17	1978	59.29	-152.36	77	143	03	235	50	51	40	176	35	288	31
December	27	1977	58.33	-155.06	116	325	29	158	60	60	06	150	15	310	74
December	18	1977	59.96	-152.99	137	01	62	211	26	114	10	19	20	234	68

#### D. Redoubt Volcano

##### Petrology

During the 1979 field season a helicopter supported sampling program was conducted on Redoubt Volcano. Extremely rugged terrain limited landings on the volcano to one on a glacier on the south side near the 1500 m contour and a second landing near the 1800 m contour. All other sampling during 1979 was done near the flanks of the volcano. However, these samples together with previous sample collections taken from the base and summit of Redoubt Volcano offer a fairly complete picture of the lavas.

Tholeiitic basalt and andesite are the dominate lava-types at Redoubt Volcano. Hornblende is a common accessory mineral in both the andesites and basalts. The andesites commonly contain both hypersthene and a clinopyroxene. Basalts and andesites commonly form lava flows on Redoubt Volcano. Lava flows are often interlayered with mudflow deposits.

Chemistry of the Redoubt basalts and andesites are distinct. Table 1 gives the whole rock chemical composition of samples from Redoubt Volcano. Basalts fall in the compositional range 54-56 weight per cent silica, while andesites have a silica content in the range 59-60 per cent silica. More silica-rich lavas characteristic of explosive eruptions, have not been identified from Redoubt Volcano. Mudflows and airfall tephra represent the most significant hazard from Redoubt Volcano.

##### Lahars in Crescent River Valley

Appendix 1 is a self contained discussion of this subject.

Table 2. Whole rock chemical analyses of  
ejecta from Redoubt Volcano

	1	2	3	4	5	6	7	8	9
SiO <sub>2</sub>	54.01	54.91	56.29	59.18	60.46	60.40	59.46	59.92	59.72
TiO <sub>2</sub>	0.74	0.62	0.65	0.59	0.56	0.54	0.74	0.65	0.68
Al <sub>2</sub> O <sub>3</sub>	18.31	18.79	17.95	18.25	18.16	18.20	18.10	17.83	18.20
Fe <sub>2</sub> O <sub>3</sub>	-	-	-	-	-	-	2.75	3.01	3.63
FeO	8.56*	8.26*	7.73*	6.49*	6.14*	5.81*	2.91	3.13	2.13
MnO	0.16	0.16	0.15	0.14	0.15	0.15	0.14	0.15	0.14
MgO	4.59	4.06	3.92	2.89	2.51	2.34	2.60	2.59	2.24
CaO	9.73	8.48	8.89	6.96	6.80	6.82	7.14	6.70	6.95
Na <sub>2</sub> O	3.24	3.49	4.86	3.96	4.19	4.08	3.94	3.99	4.16
K <sub>2</sub> O	0.98	0.71	1.05	1.47	1.40	1.41	1.58	1.61	1.73
P <sub>2</sub> O <sub>5</sub>	0.18	0.18	0.19	0.25	0.23	0.22	0.20	0.20	0.21
Total	100.50	99.66	101.68	100.18	100.60	99.97	99.56	99.78	99.79

\*Total Fe as FeO

- (1)&(3) Basalt from the 1500 m elevation on the south side of Redoubt Volcano.
- (2) Basalt from near the north base of Redoubt Volcano.
- (4) Andesite from 1800 m elevation on the north side of Redoubt Volcano.
- (5) Ash deposited on deck of ship in Cook Inlet during 1902 eruption:  
Analyzed by G. G. Cunningham.
- (6) Andesite from summit dome of Redoubt Volcano: collected by J. Kienle:  
Analyzed by G. G. Cunningham.
- (7)&(8) Andesite block erupted by Redoubt Volcano in February, 1966, collected  
by R. B. Forbes: Analyzed by H. Haramura.
- (9) Andesitic pumice erupted by Redoubt Volcano in February, 1966, collected  
by R. B. Forbes: Analyzed by H. Haramura.

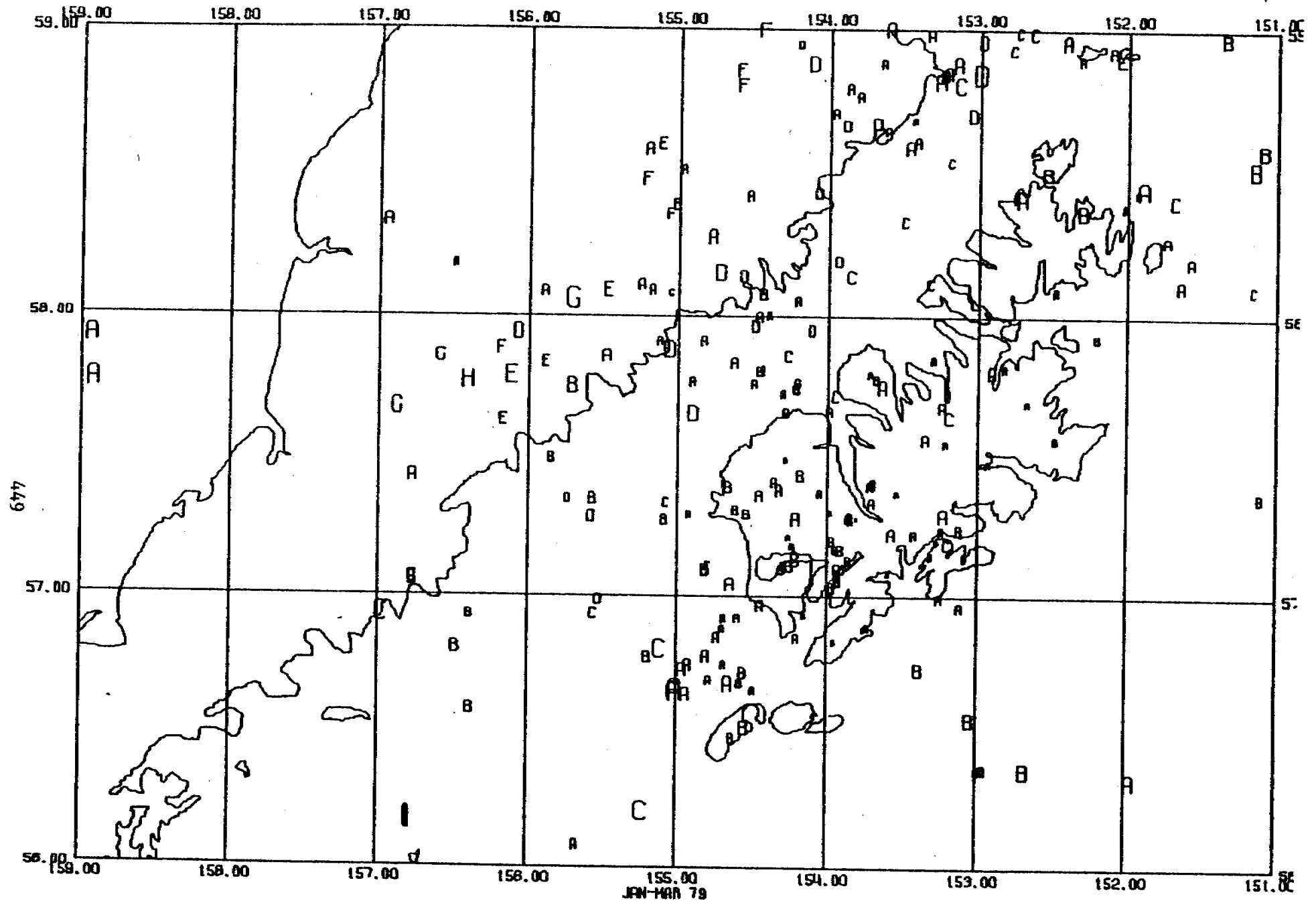


Fig. 2 - Epicenter map, Kodiak-Alaska Peninsula, January-March 1979, all locatable events.

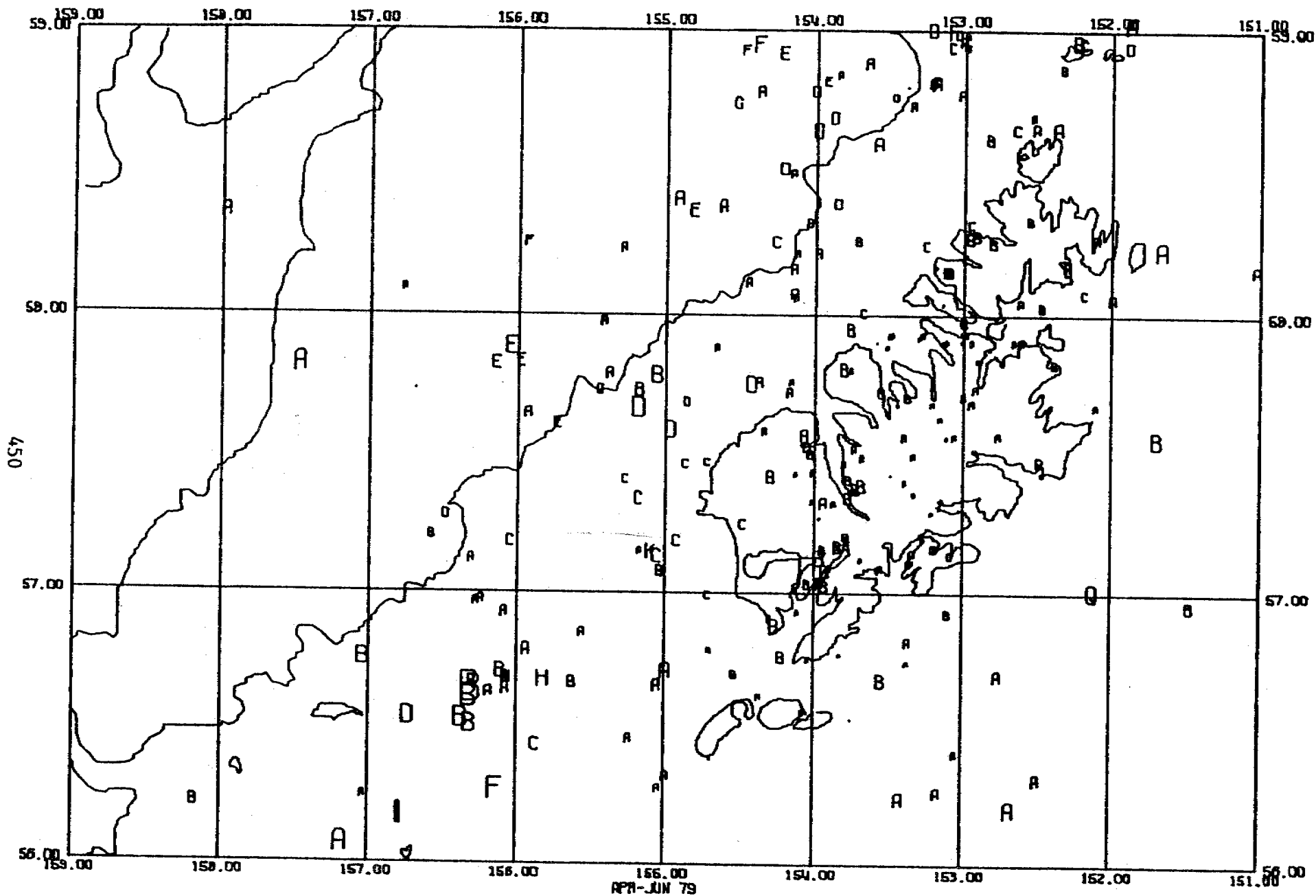


Fig. 3 - Epicenter map, Kodiak-Alaska Peninsula, April-June 1979, all locatable events.

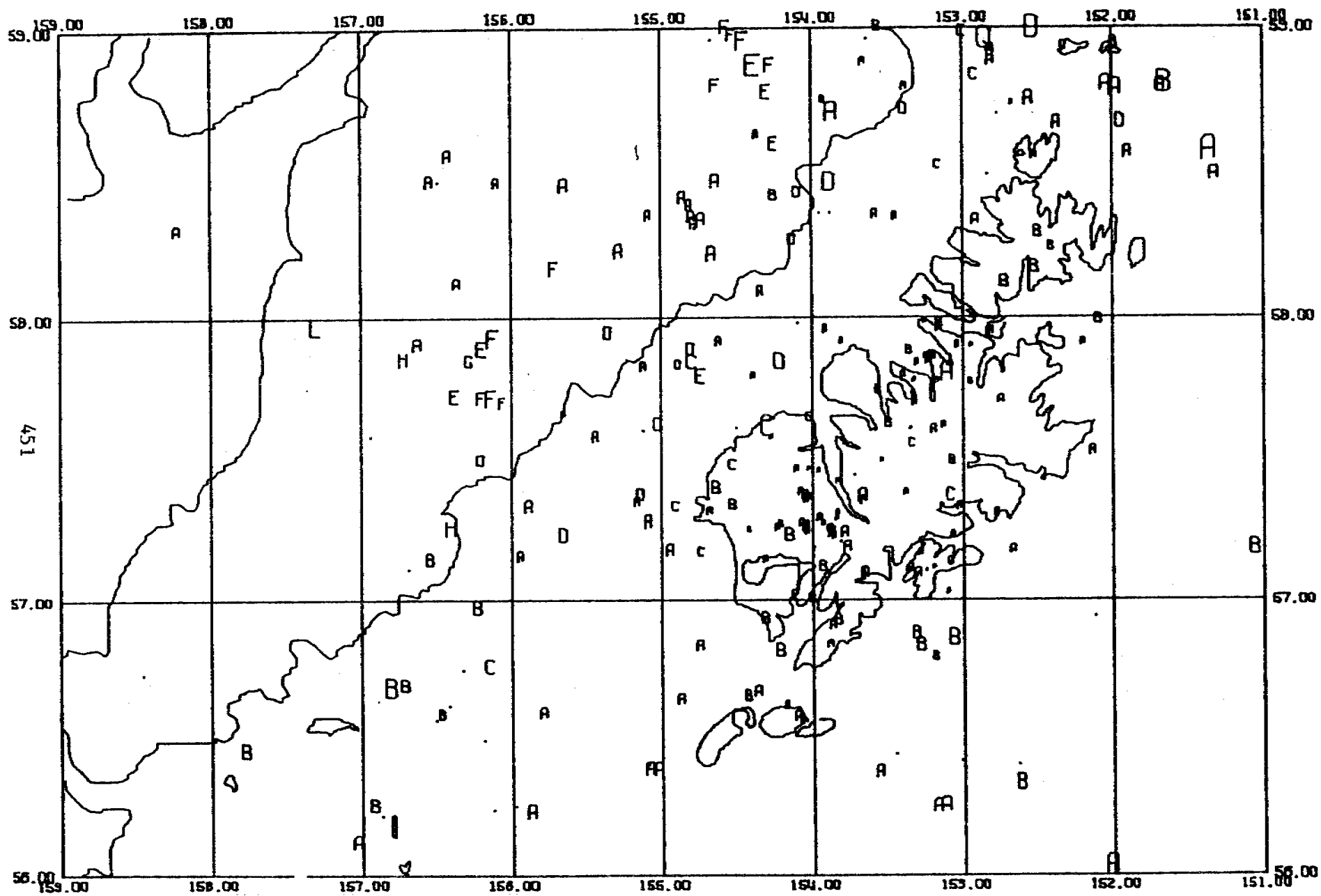


Fig. 4 - Epicenter map, Kodiak-Alaska Peninsula, July-September 1979, all locatable events.

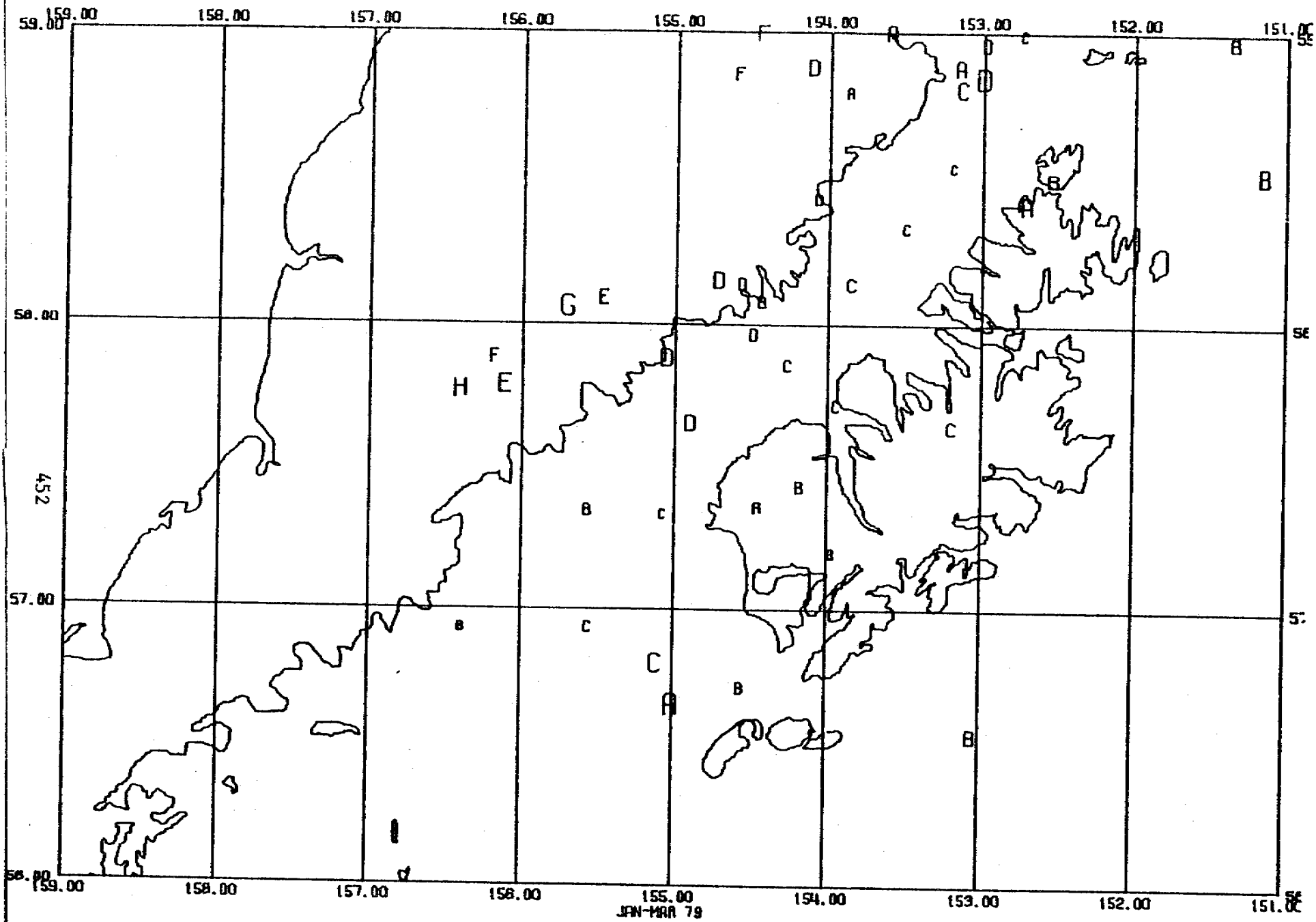


Fig. 5 - Epicenter map, Kodiak-Alaska Peninsula, January-March 1979, class 1 events.

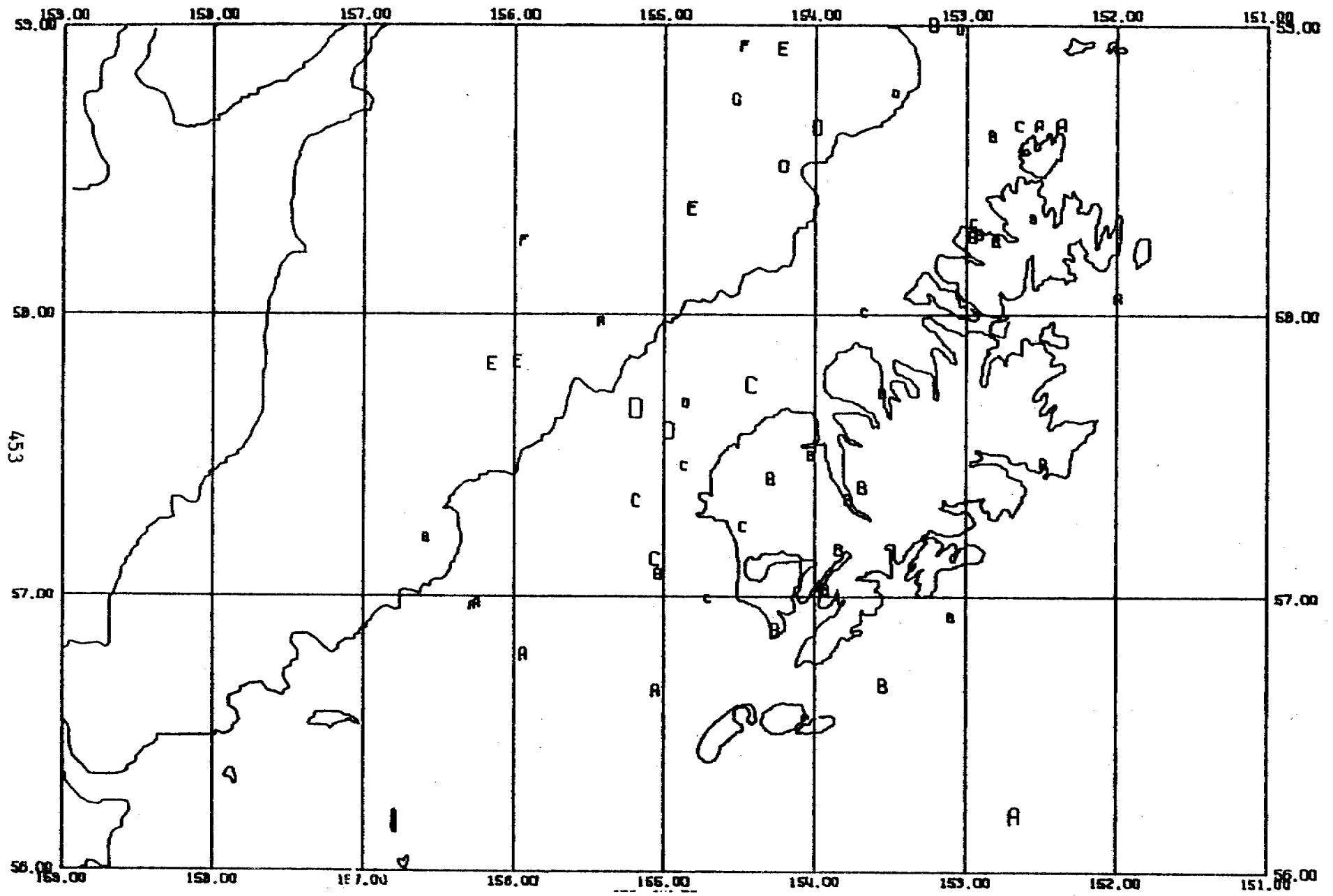
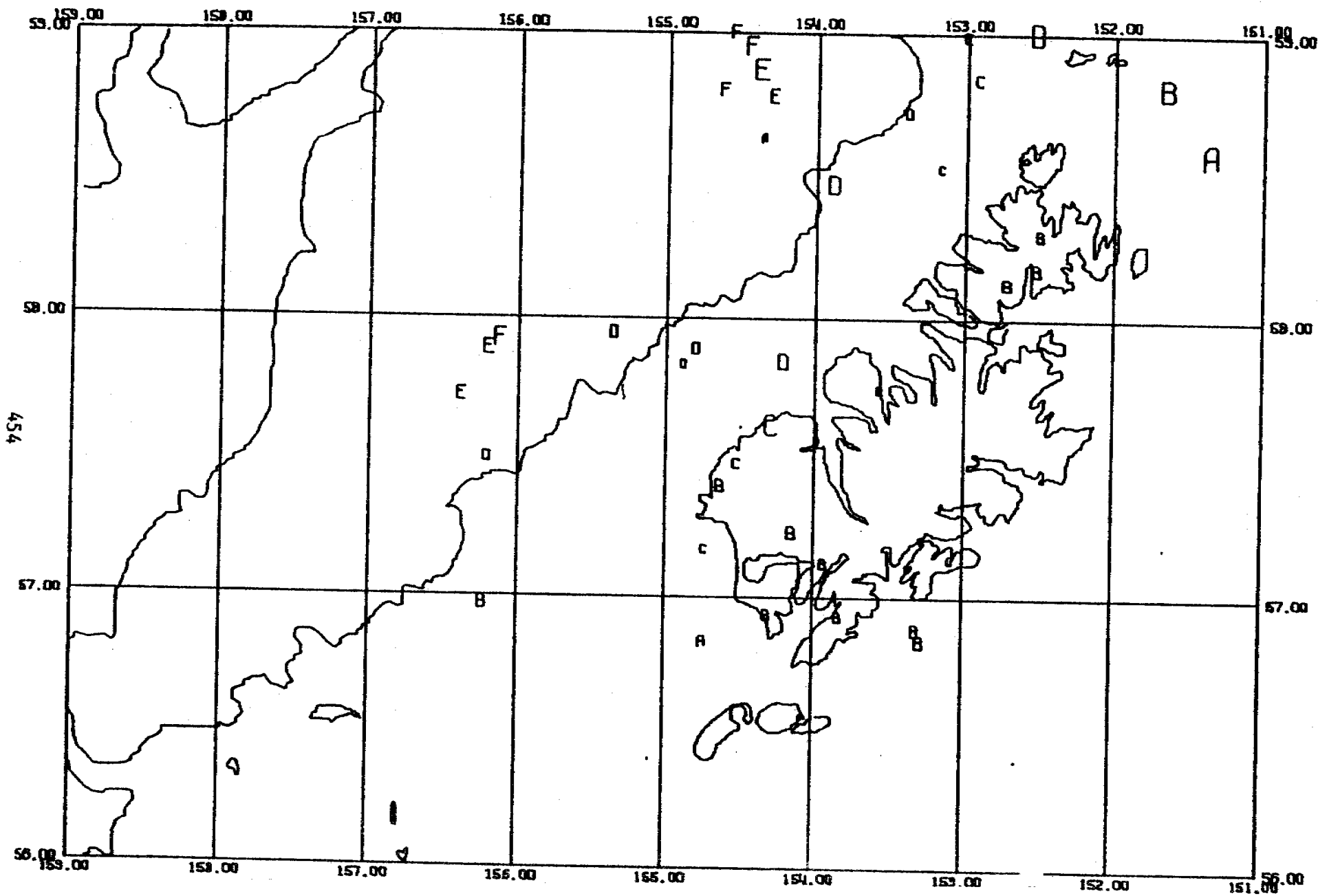


Fig. 6 - Epicenter map, Kodiak-Alaska Peninsula, April-June 1979, class 1 events.





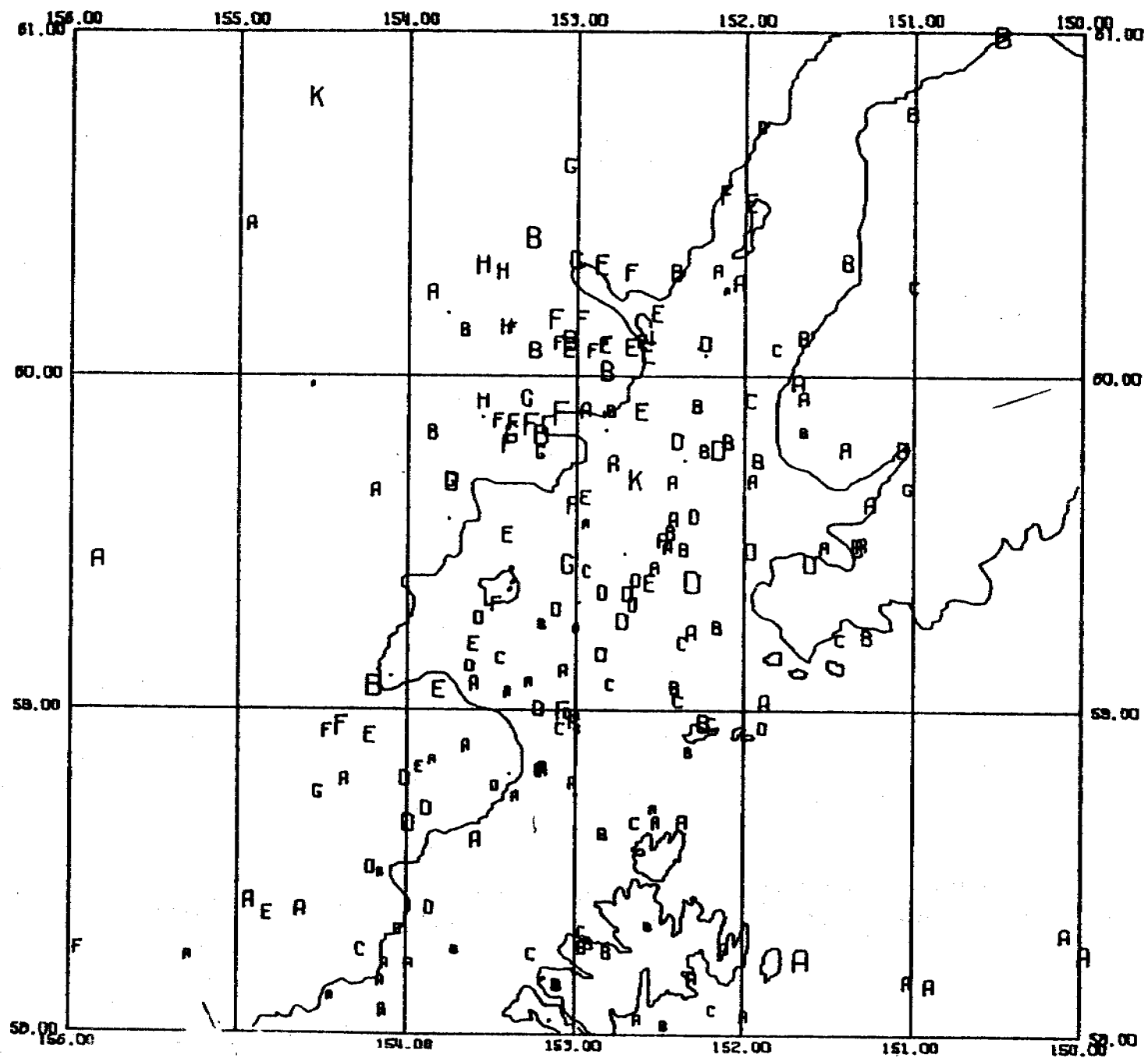


Fig. 8 - Epicenter map, Lower Cook Inlet, April-June 1979, all locatable events.

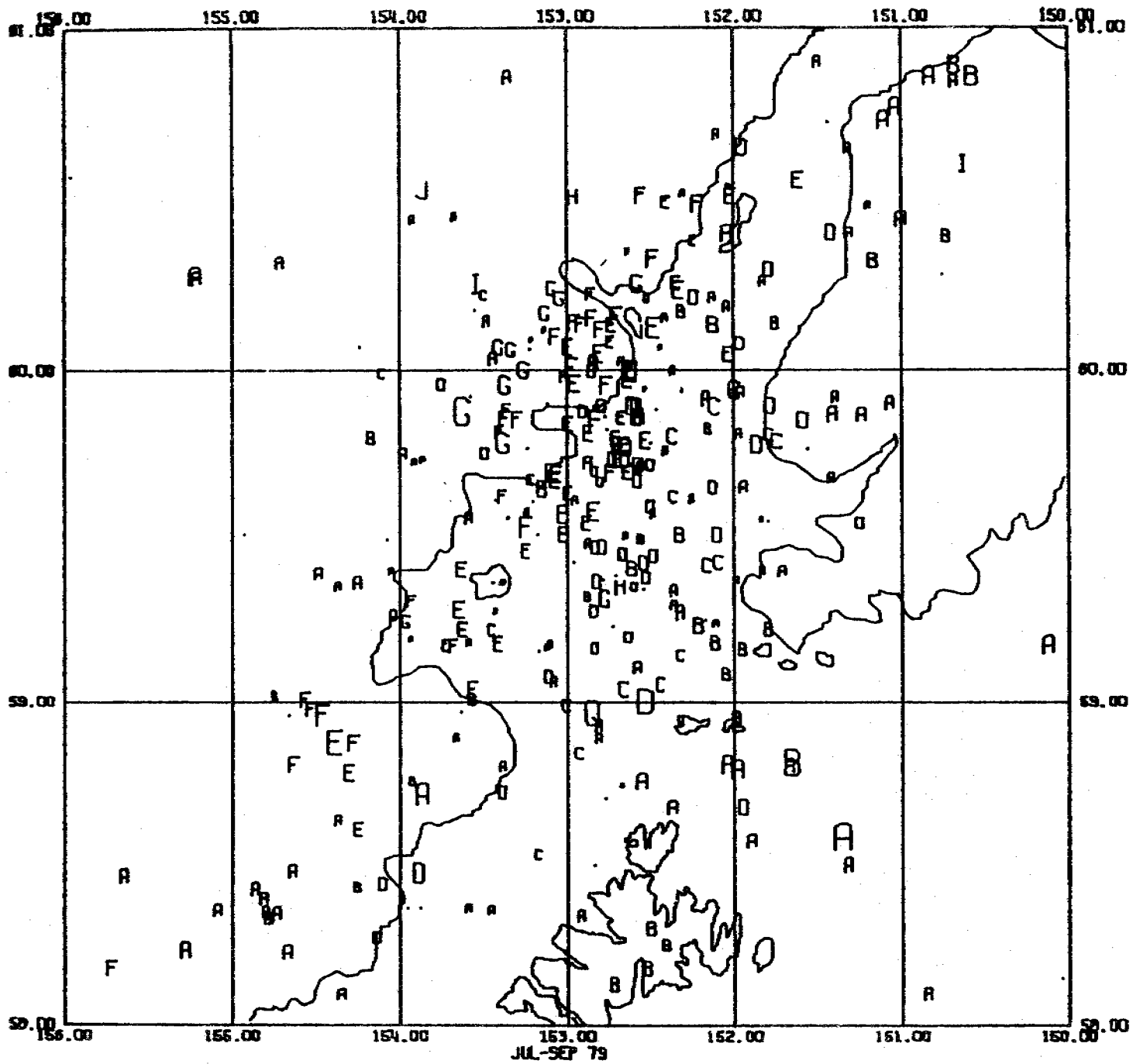


Fig. 9 - Epicenter map, Lower Cook Inlet, July-September 1979, all locatable events.

457

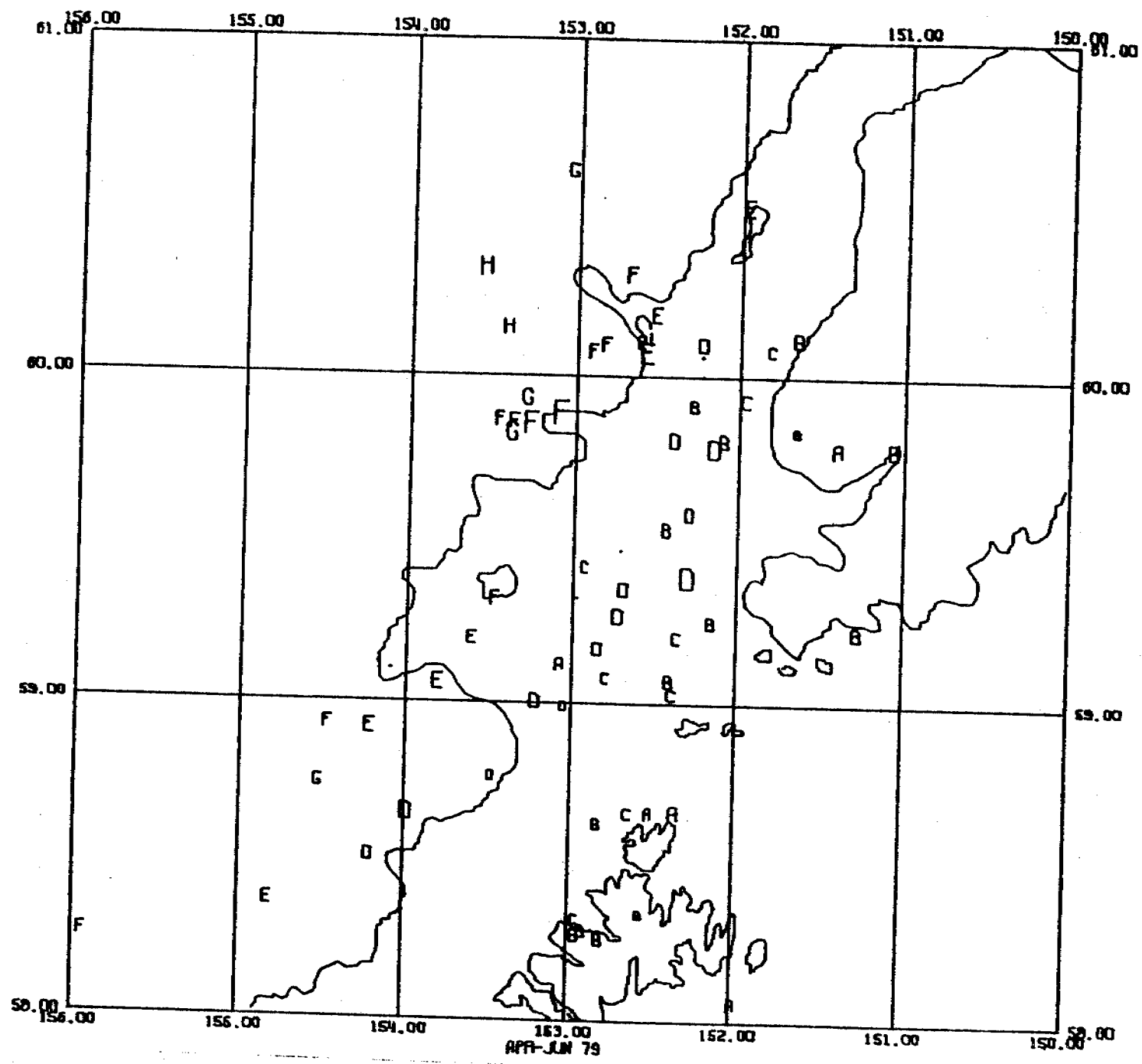


Fig. 10 - Epicenter map, Lower Cook Inlet, April-June 1979, class 1 events.

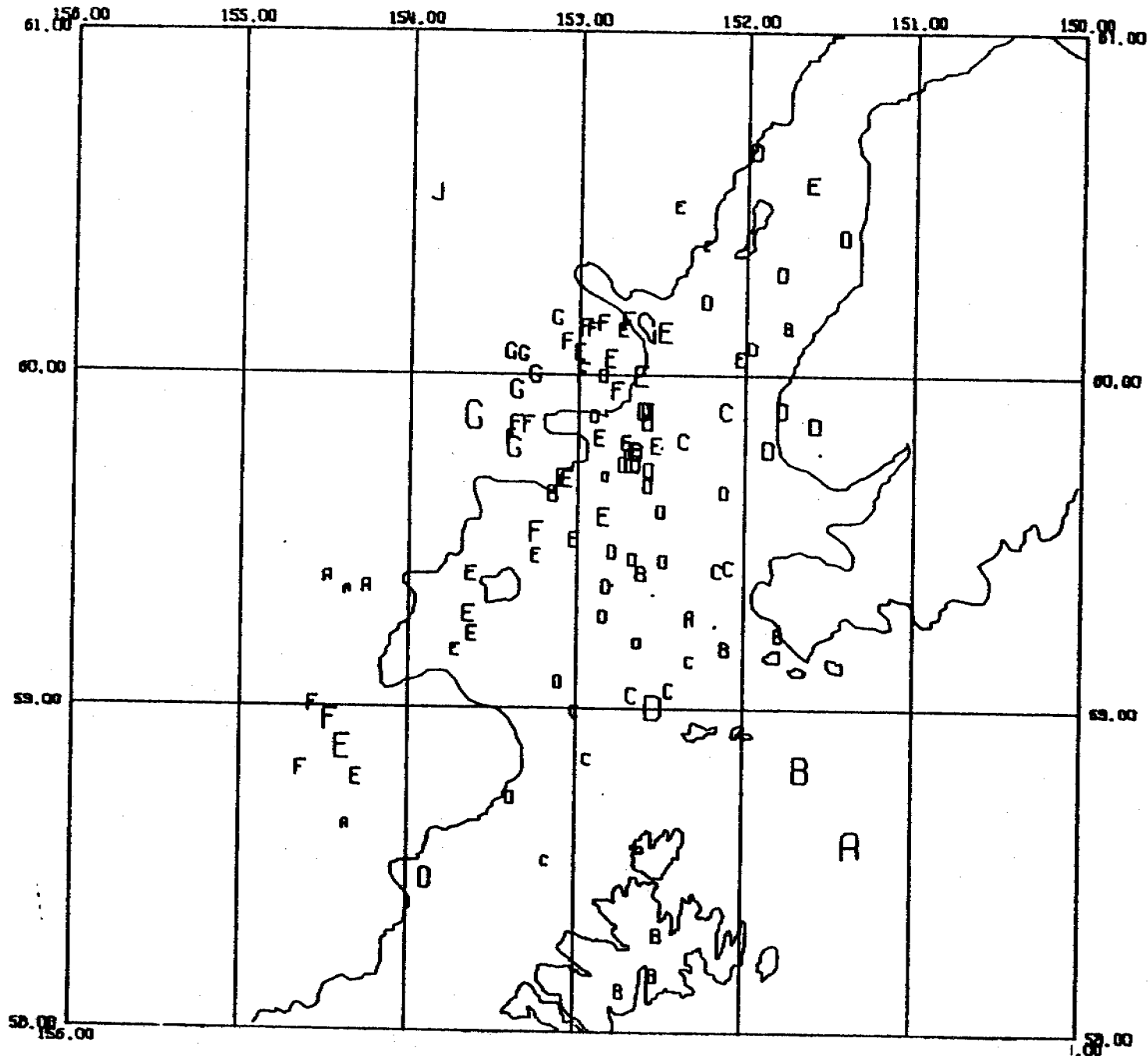


Fig. 11 - Epicenter map, Lower Cook Inlet, July-September 1979, class 1 events.

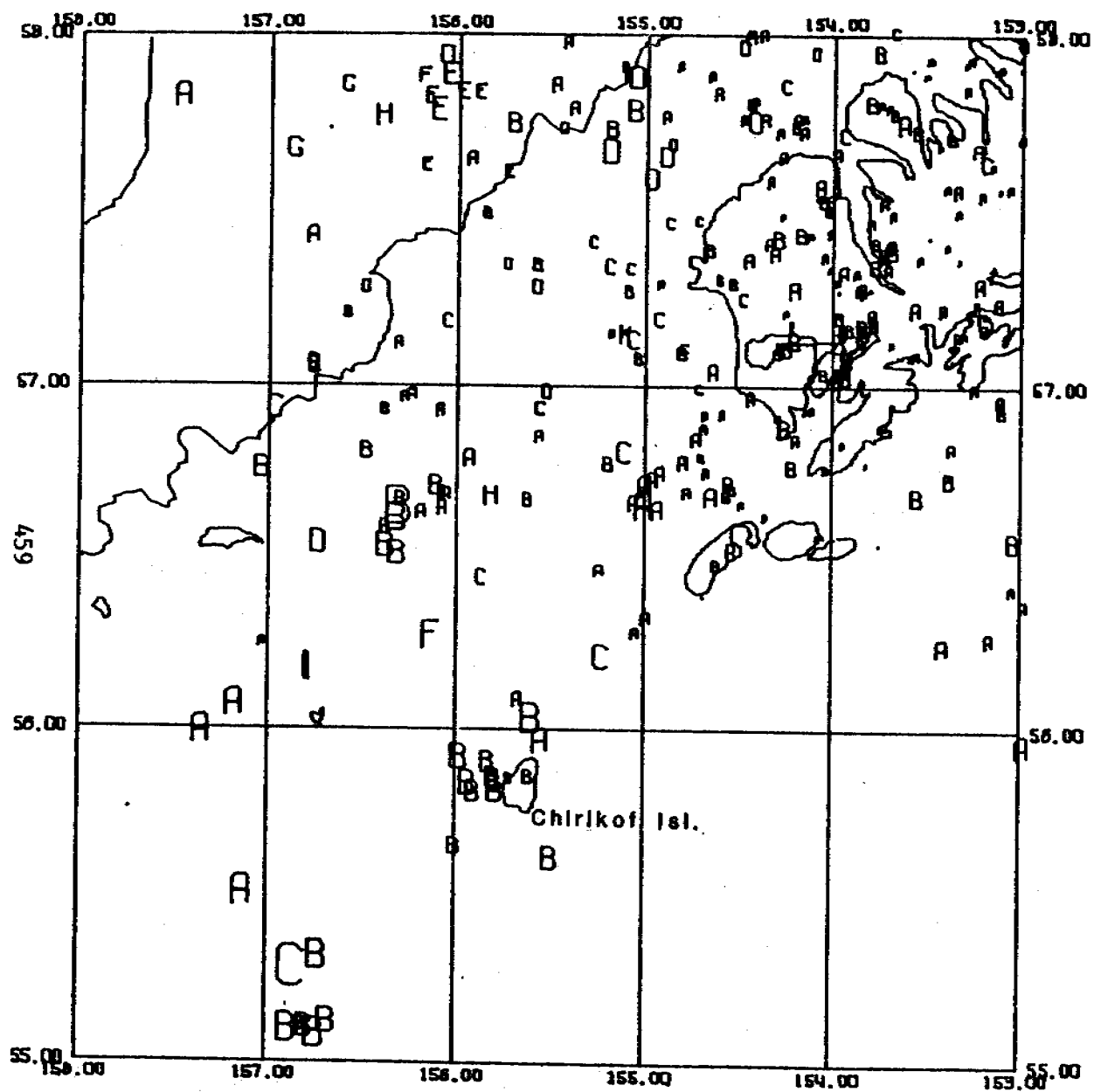


Fig. 12 - Epicenter map, southwest of Kodiak Island, January-June 1979, all locatable events.

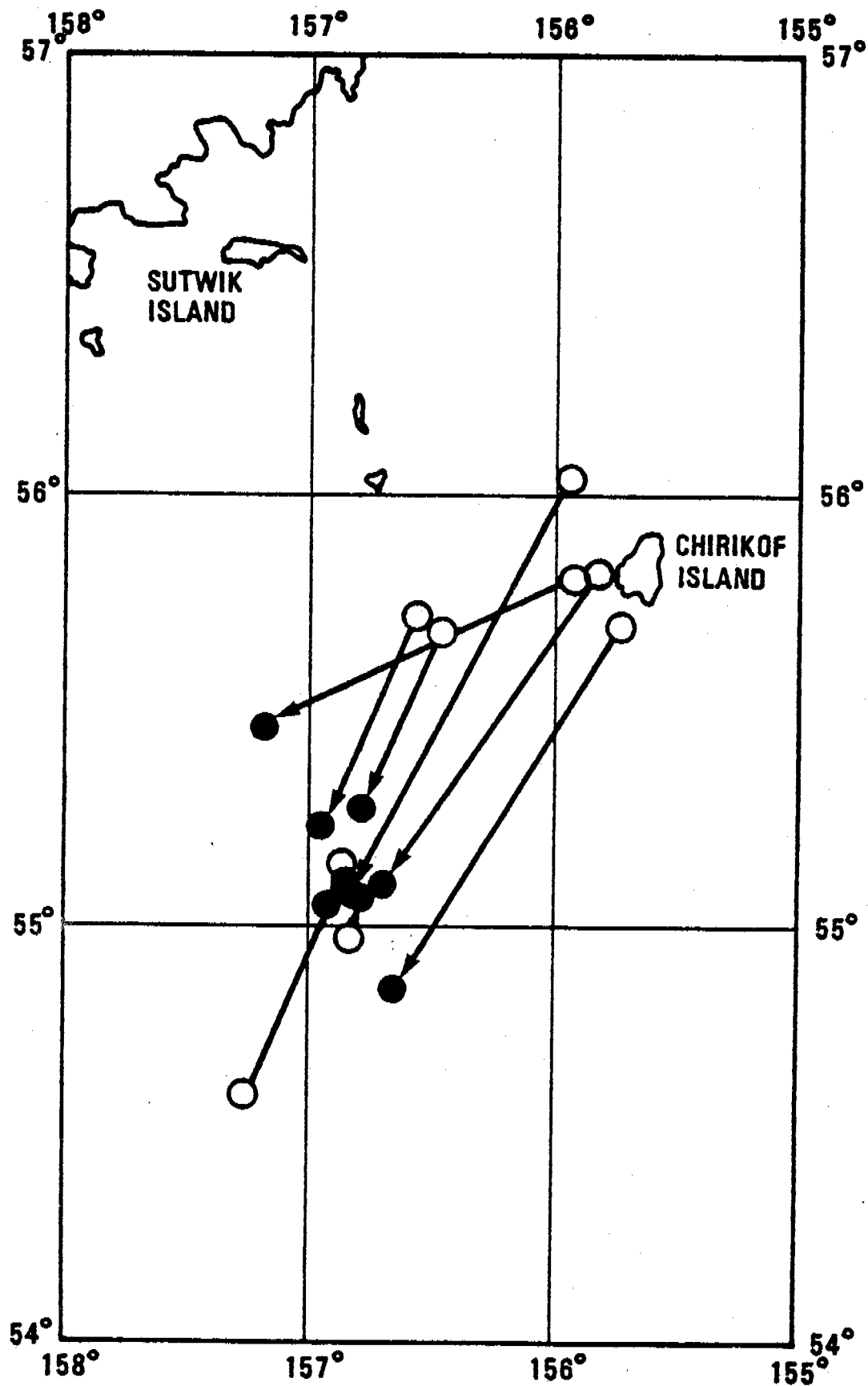


Fig. 13 - Selected Feb. 1979 earthquakes in the Semidi Island region southwest of Kodiak Island showing epicentral shift (arrows) due to station selection for location. Open circles are epicenters based on using data from the network shown in Figure 1. Closed circles are epicenters based on also using arrival times from Sand Point, 200 km west of the epicenters.

APRIL/12/19 03:42:03  
-152.56 56.34 M= 6.5 DEPTH= 30.00

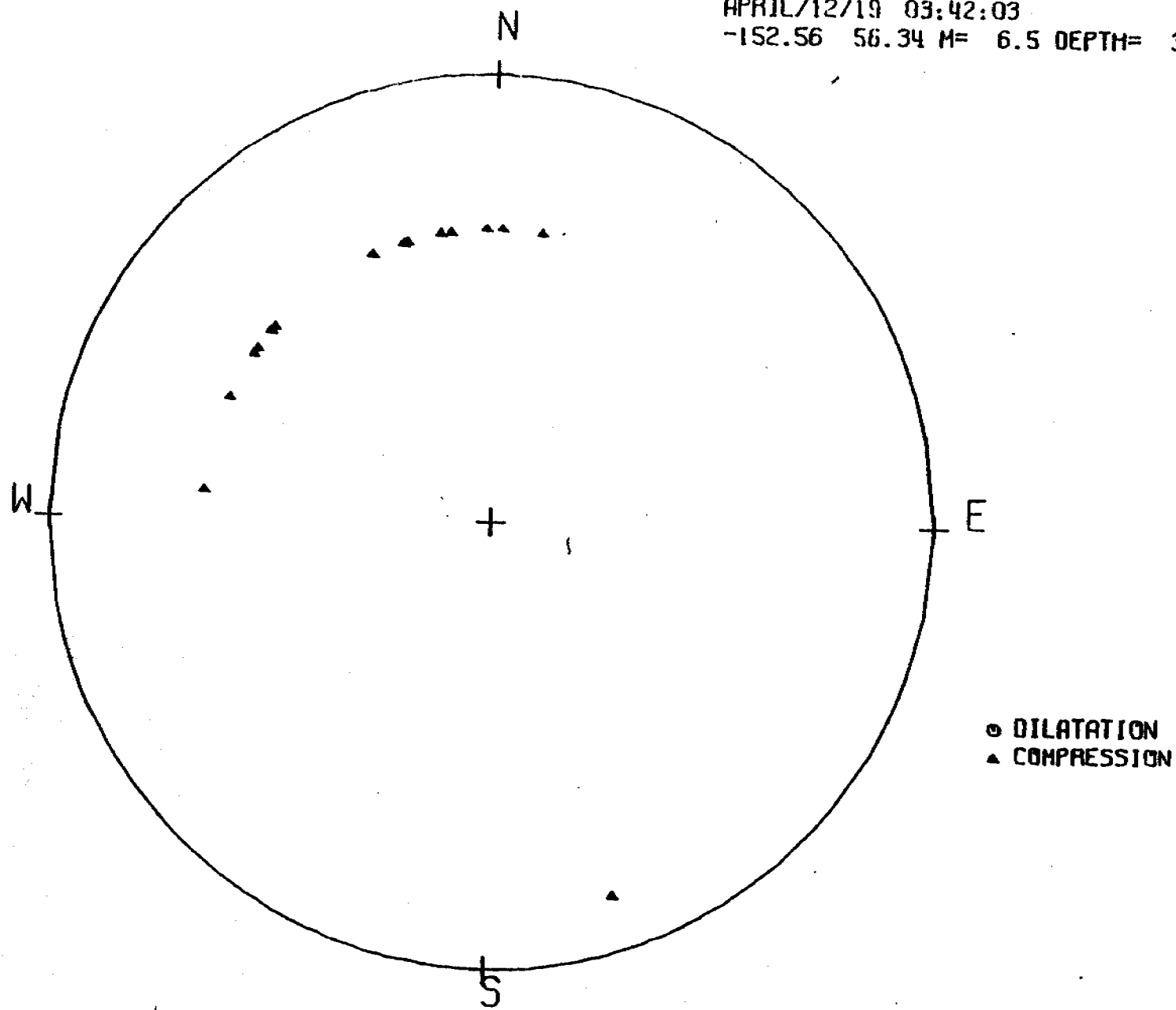
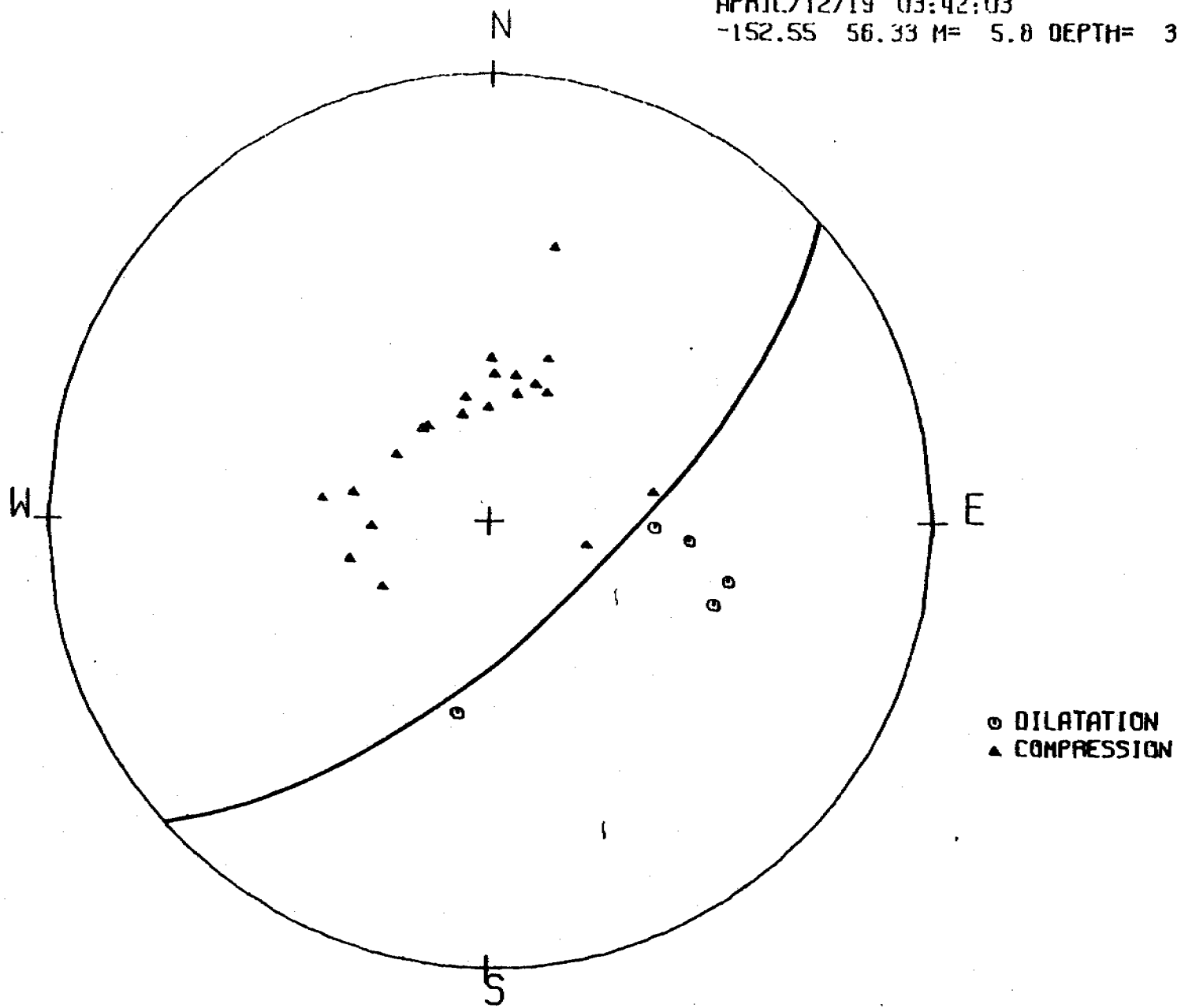


Fig. 14 - First motion distribution from regional data for April 12, 1978 earthquake. Lower focal hemisphere.



WSSN LP STATION  
APRIL/12/19 03:42:03  
-152.55 56.33 M= 5.0 DEPTH= 30.00



462

Fig. 15 - First motion distribution from WSSN long period data for April 12, 1978 earthquake. Lower focal hemisphere.

APRIL/12/78 03:42:03  
-152.56 56.34 M= 6.5 DEPTH= 30.00

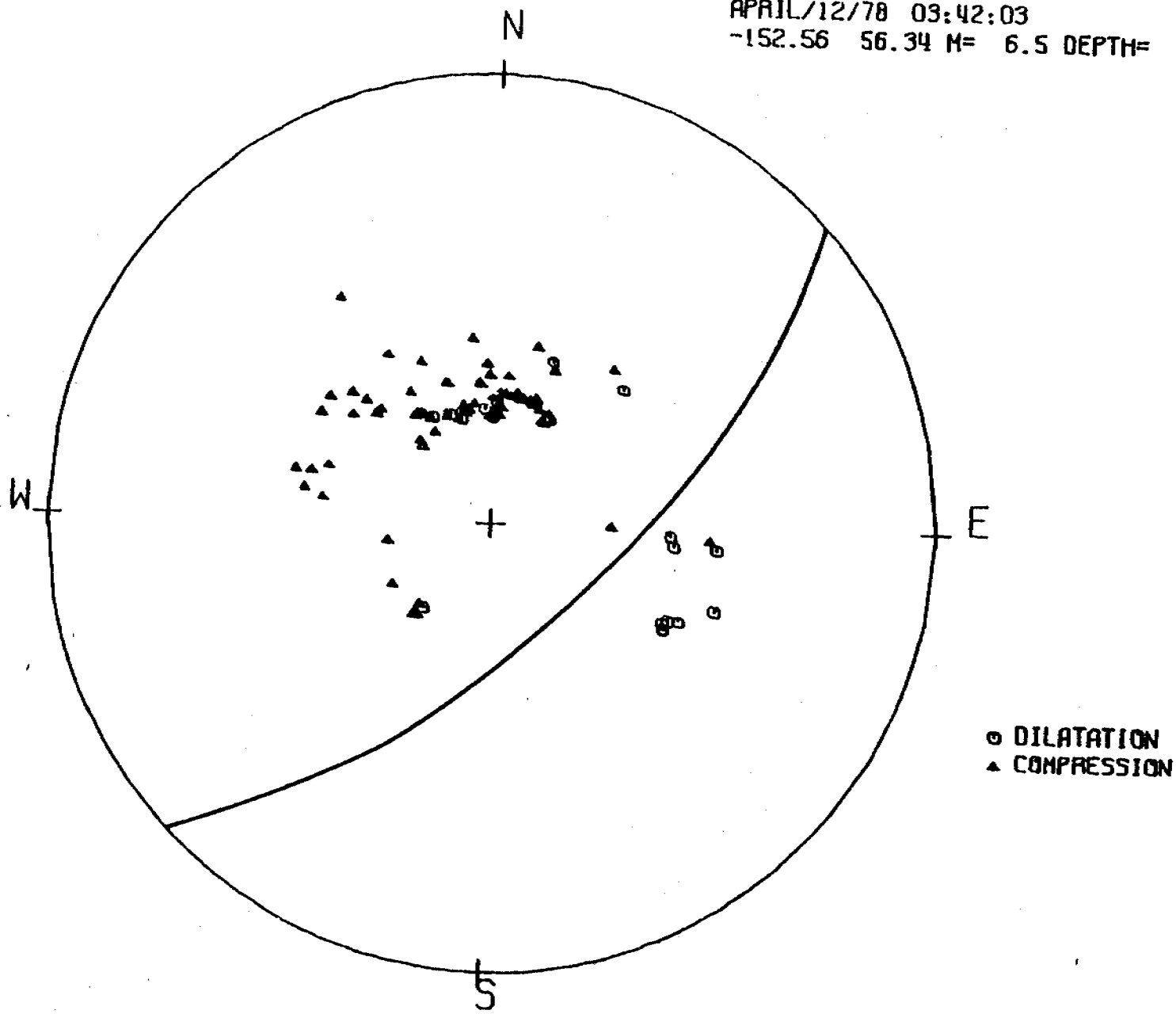
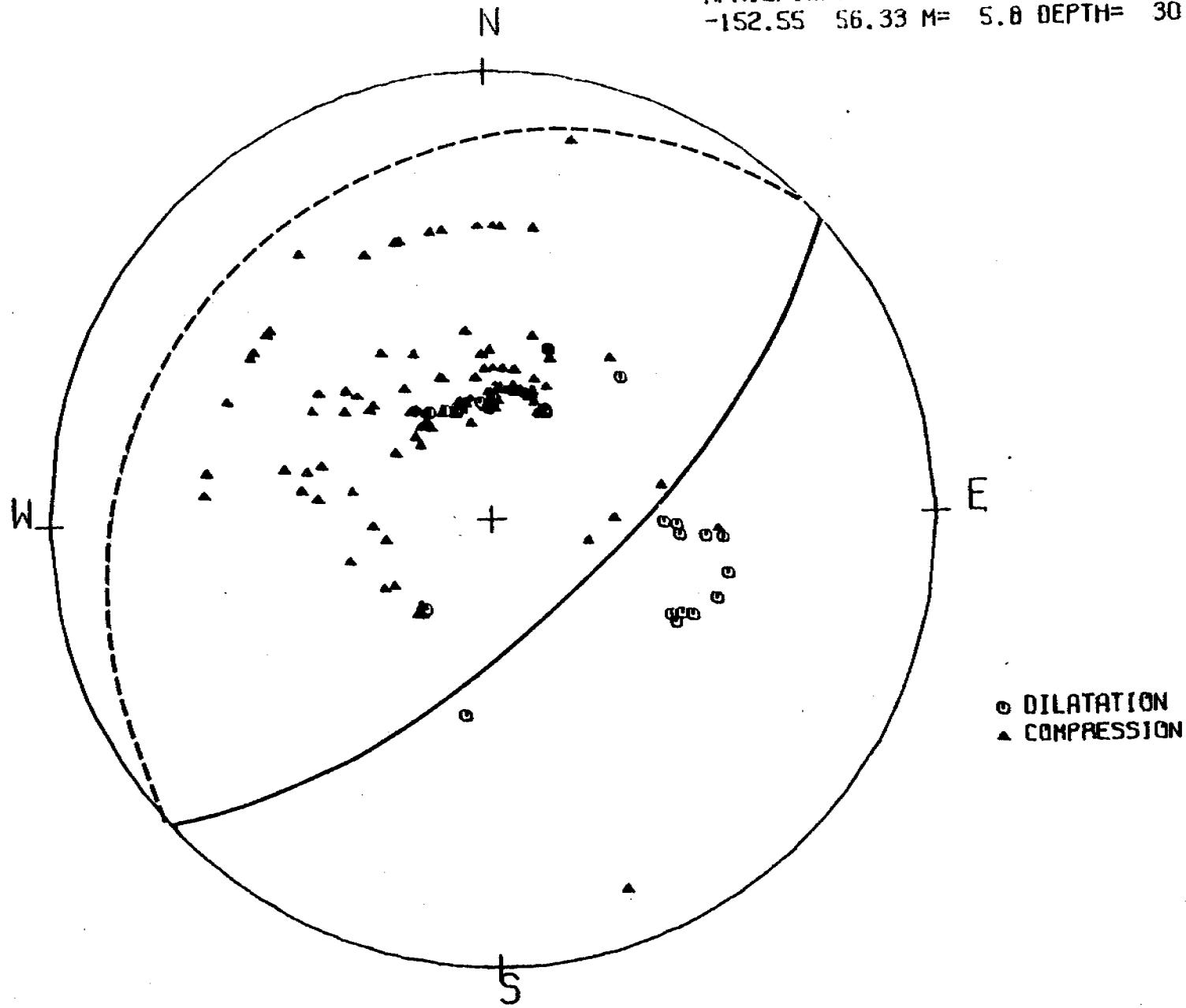


Fig. 16 - First motion distribution from Earthquake Data Report (EDR) listings of impulsive arrivals for April 12, 1978 earthquake. Lower focal hemisphere.

HWSSN LP, ALL SP  
APRIL/12/19 03:42:03  
-152.55 56.33 M= 5.8 DEPTH= 30.00



464

Fig. 17 - First motion distribution, combined data set for April 12, 1978 earthquake. Lower focal hemisphere. Assumed fault plane is dashed since it is poorly constrained.

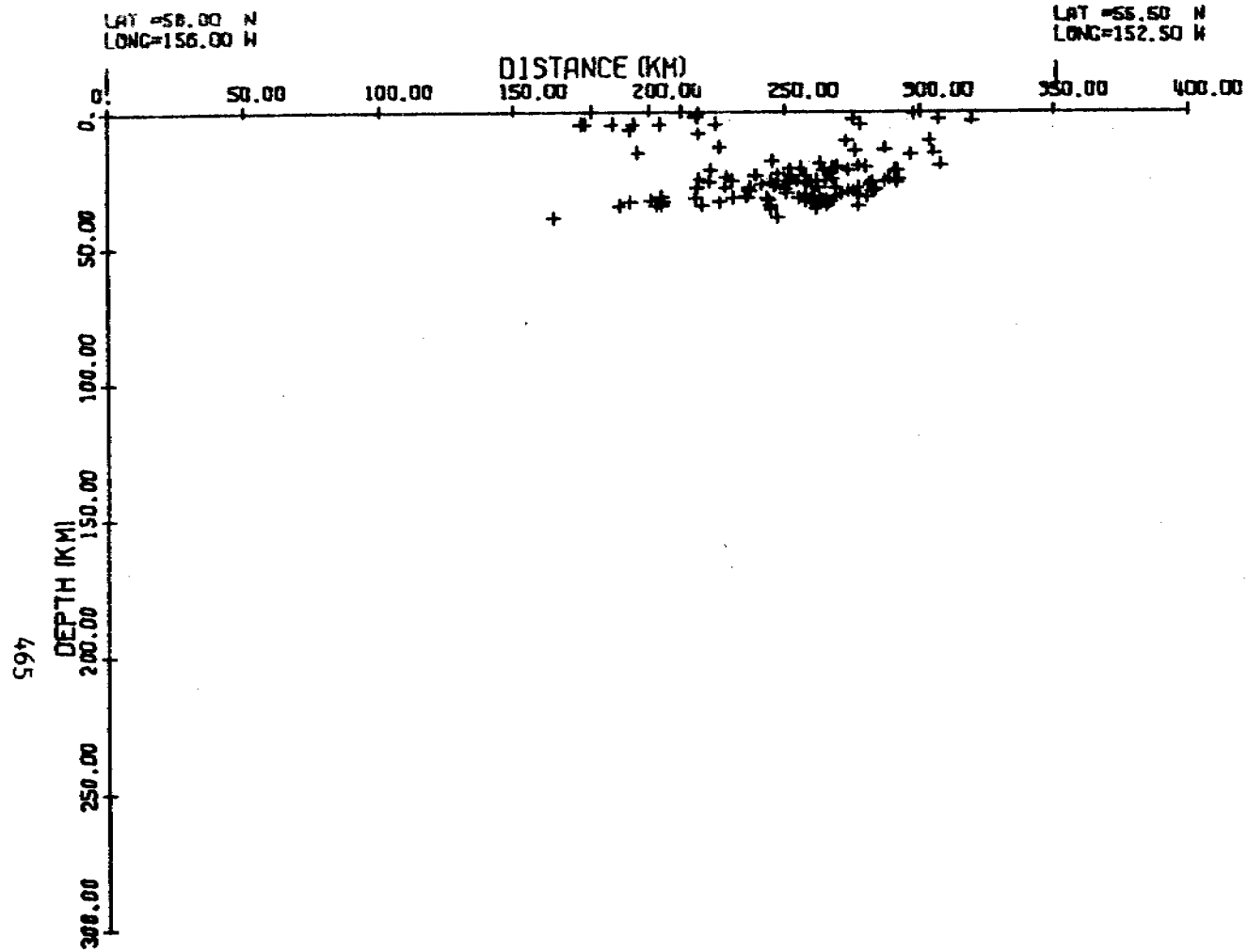
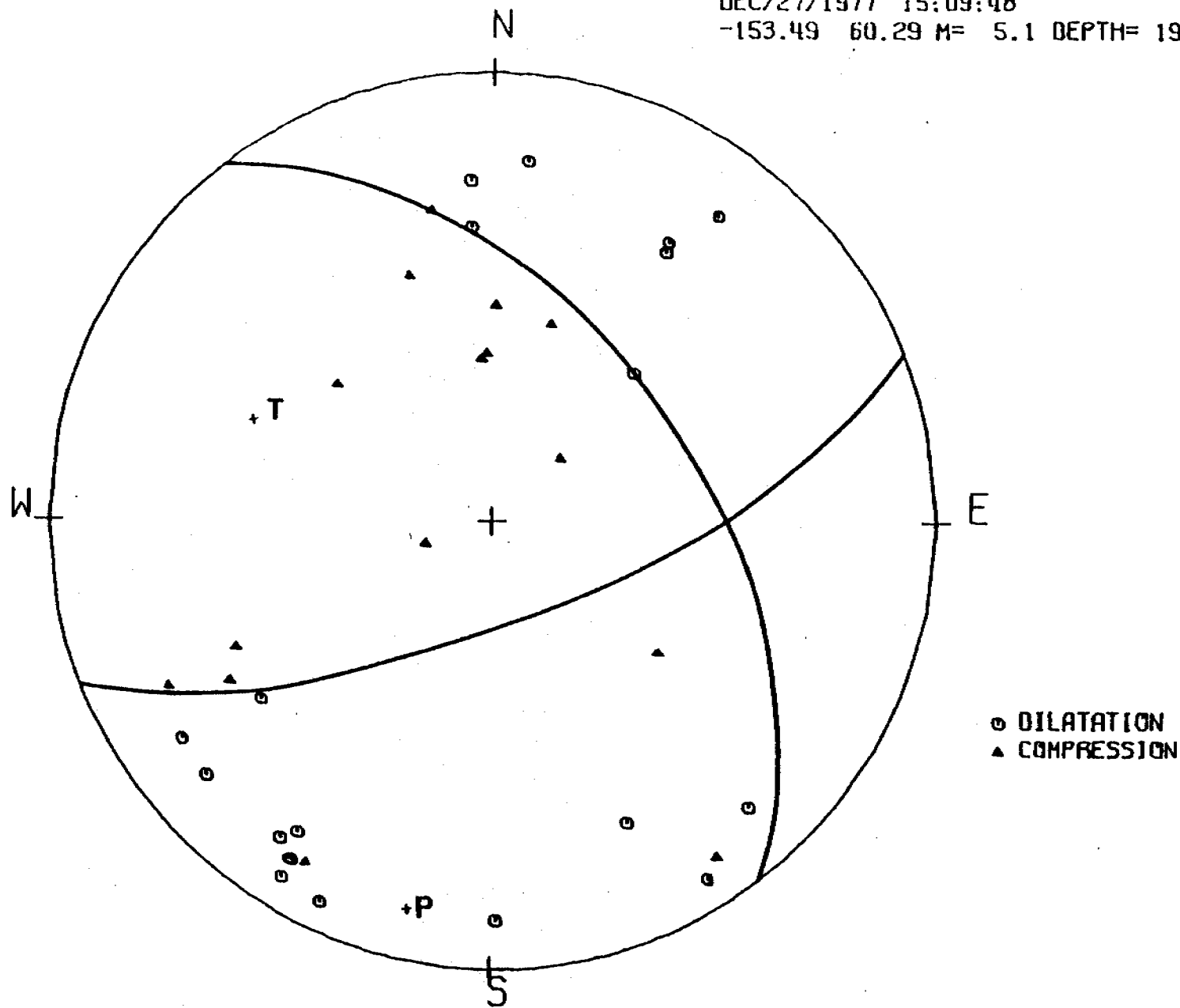


Fig. 18 - Projection of the aftershocks of the April 12, 1978 earthquake off Kodiak Island onto a vertical plane, perpendicular to the arc structure.

REGIONAL SP  
DEC/27/1977 15:09:48  
-153.49 60.29 M= 5.1 DEPTH= 196.00



466

Fig. 19 - Fault plane solution for December 27, 1977 earthquake.  
Lower focal hemisphere.

REGIONAL DATA  
NOV/27/1977 15:05:07  
-155.06 50.33 M= 4.5 DEPTH= 116.00

467

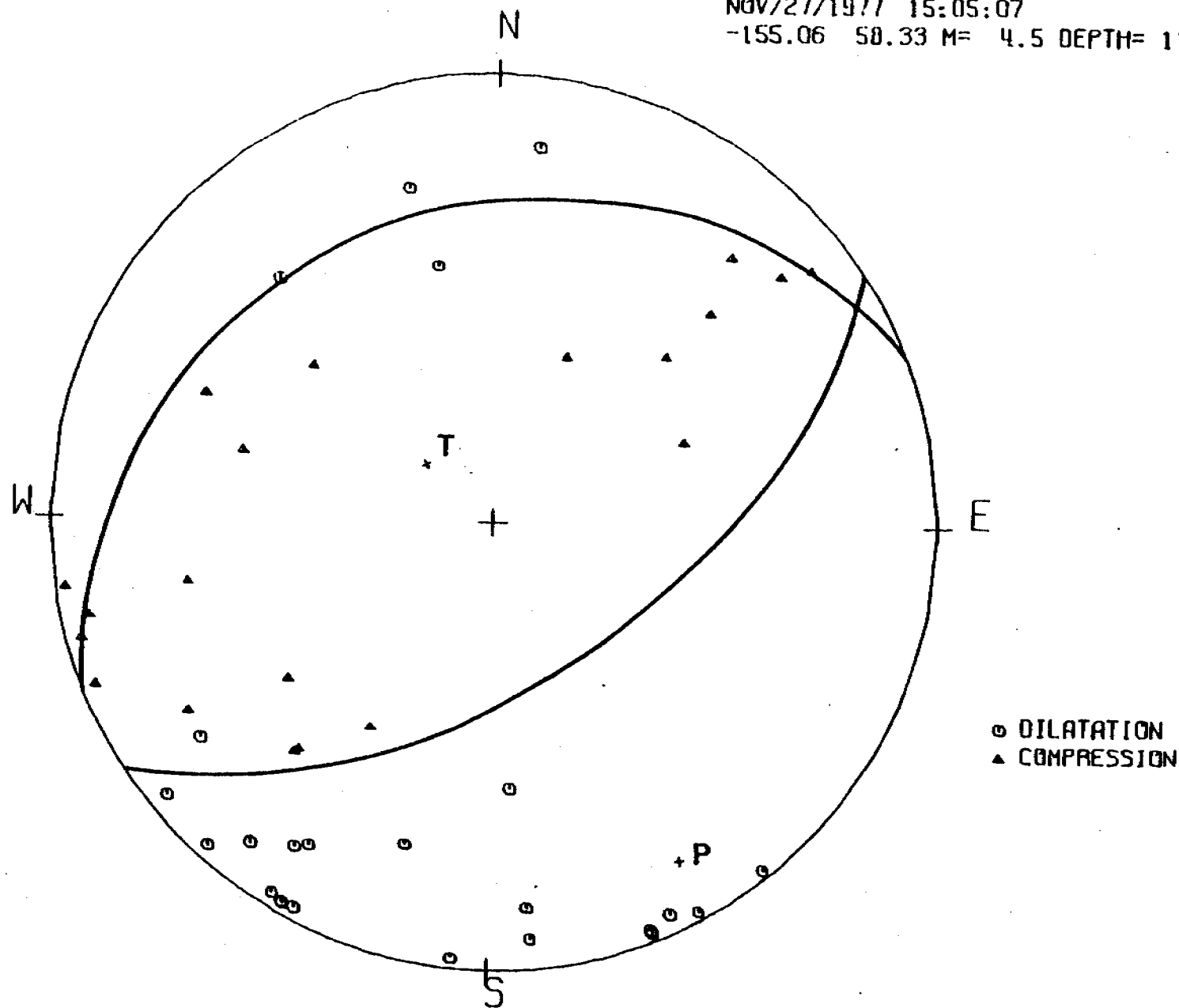


Fig. 20 - Fault plane solution for November 27, 1978 earthquake.  
Lower focal hemisphere.

REGIONAL SP  
FEB/12/1978 08:56:39  
-152.36 59.29 M= 5.2 DEPTH= 77.00

468

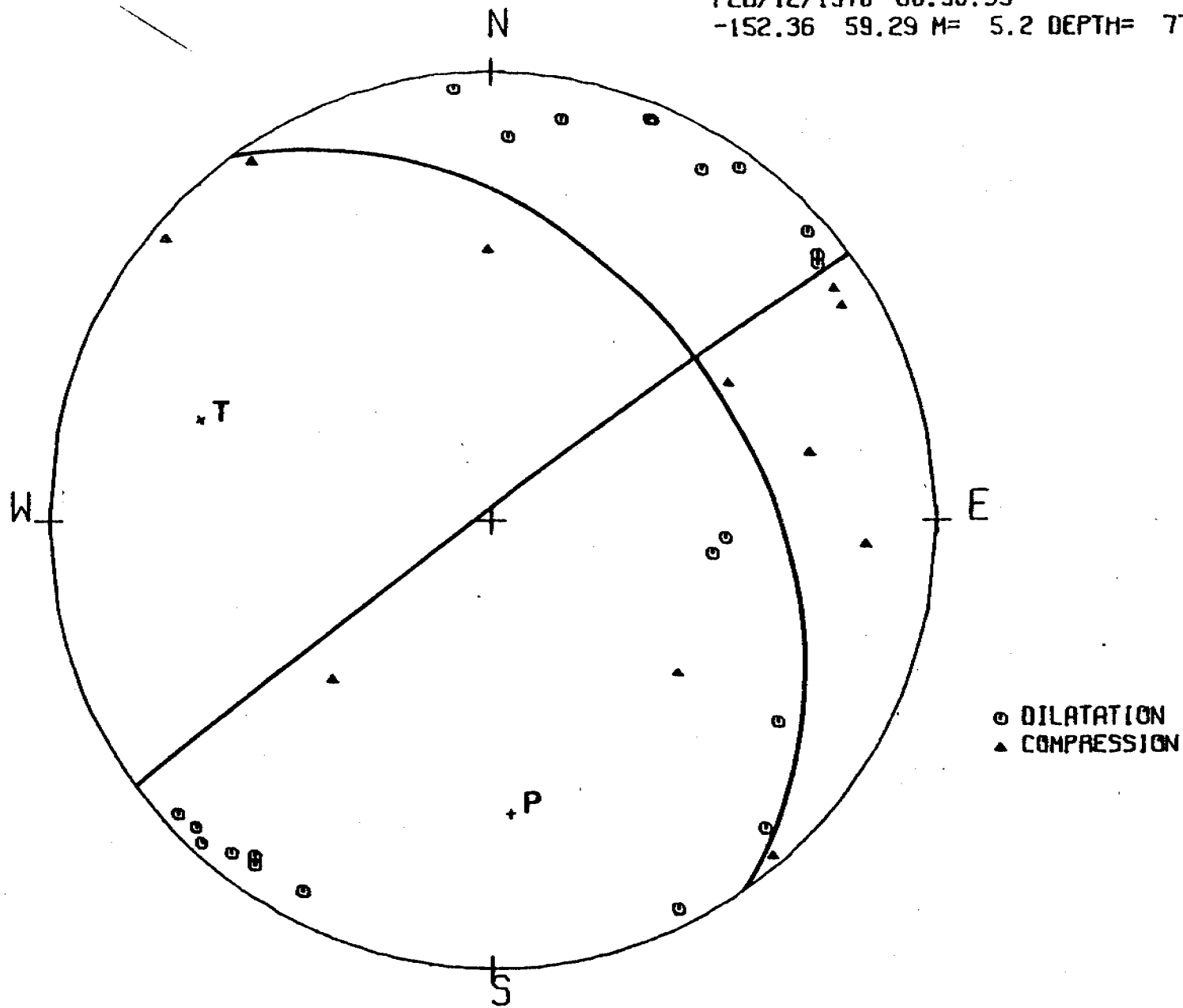


Fig. 21 - Fault plane solution for February 12, 1978 earthquake.  
Lower focal hemisphere.

REGIONAL DATA  
DEC/18/1977 05:07:17  
-152.99 59.96 M= 4.7 DEPTH= 137.00

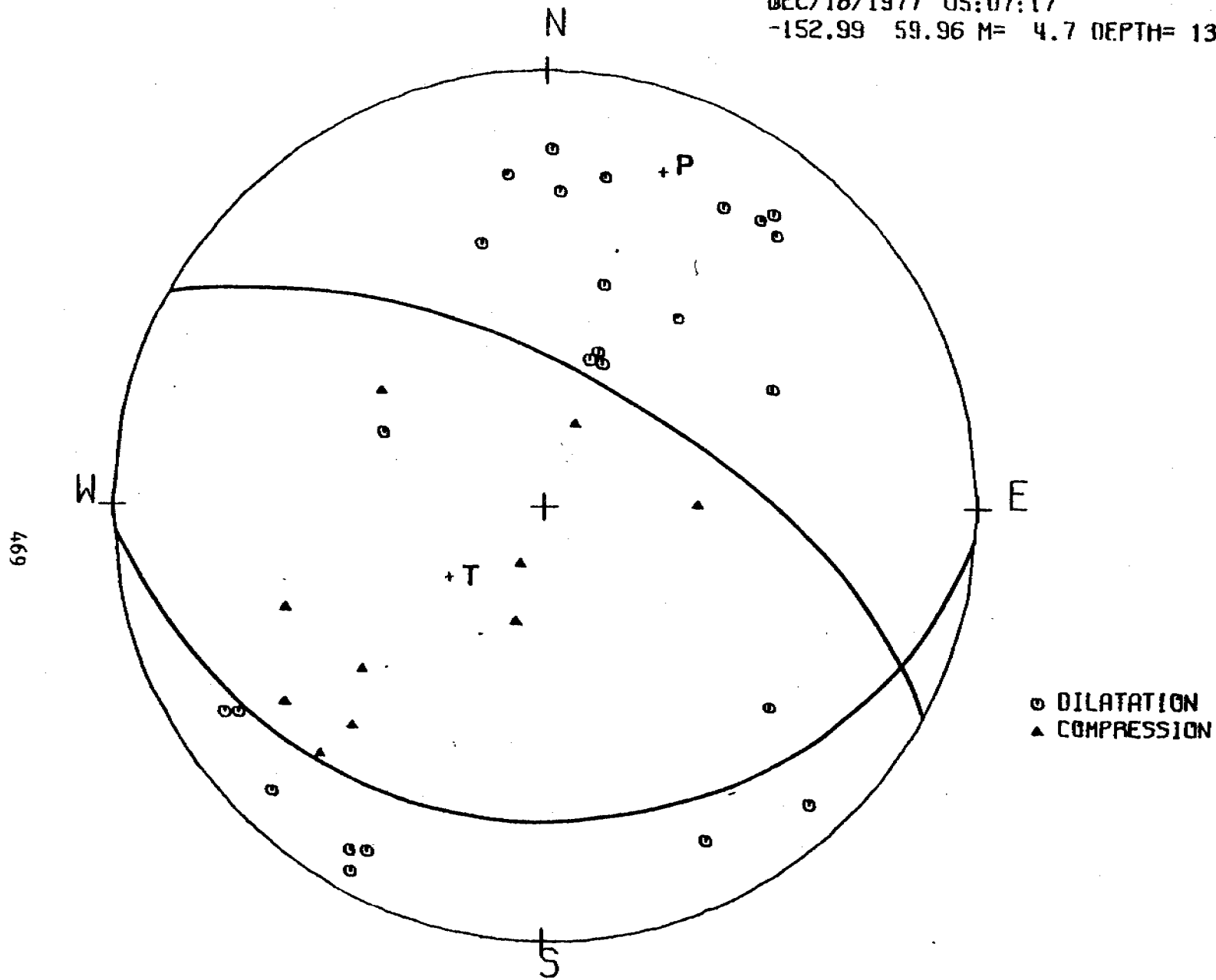


Fig. 22 - Fault plane solution for December 18, 1977 earthquake. Lower focal hemisphere.



470

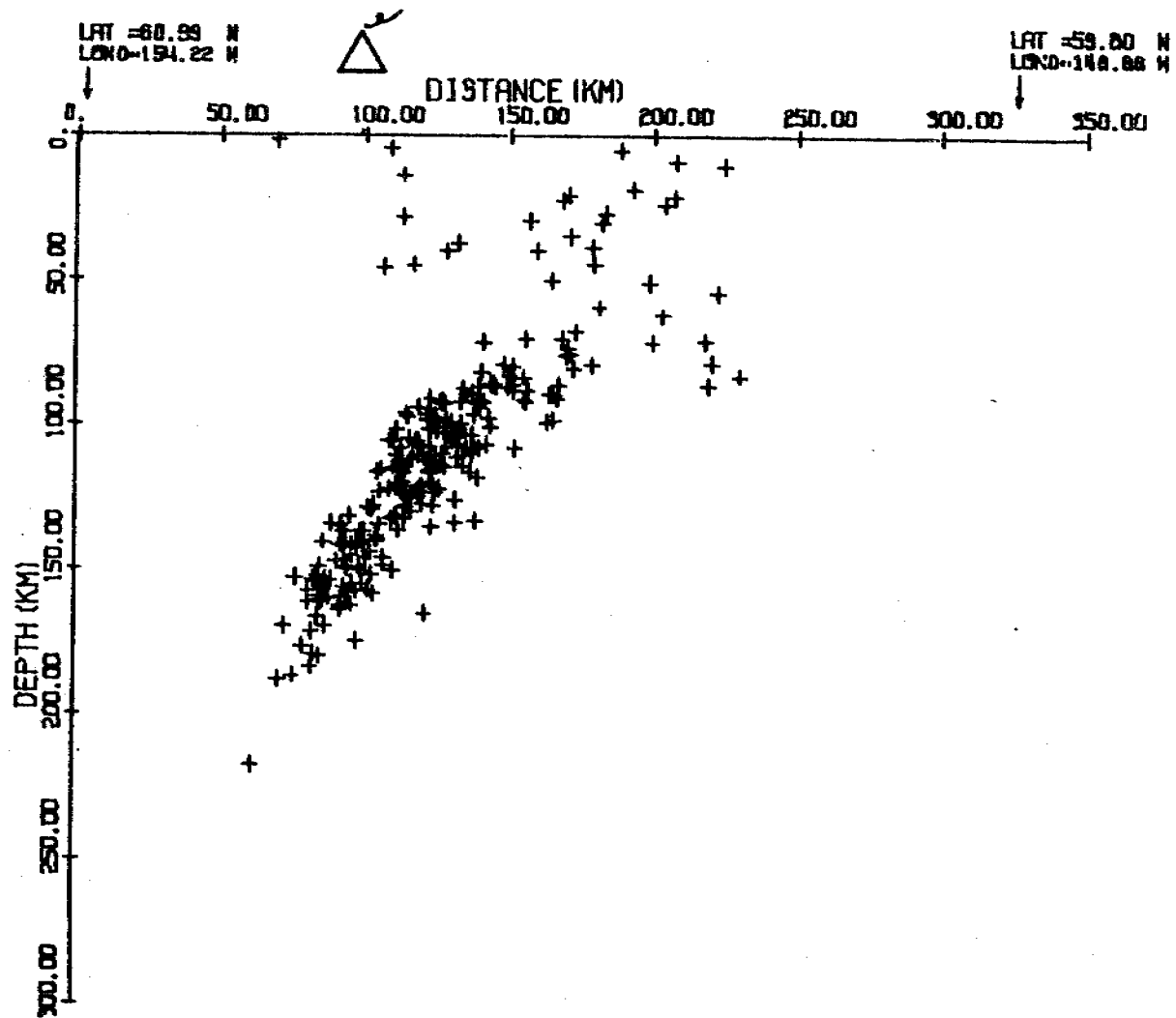


Fig. 23 - Bentoff zone in Lower Cook Inlet based upon the best located events.

## VIII. CONCLUSIONS

The greatest seismic risk is associated with the shallow seismic thrust zone of the subducting Pacific plate. On the Kodiak shelf suggested lease areas overly this thrust zone. However, the Kodiak portion of this zone falls within the rupture zone of the 1964 Great Alaska Earthquake and the probability for a great earthquake ( $M > 7.8$ ) to occur within a certain time period there, appears lower than in the shallow thrust zone near the Shumagin Islands to the southwest where a seismic gap has been identified. This seismic gap is located between the western margin of the aftershock zone of the 1938 magnitude 8.3 earthquake and the eastern margin of the aftershock zone of the 1946 magnitude 7.4 earthquake. A recent moderate size event within the aftershock zone of the 1938 event appears to be the continuation of a seismicity pattern observed within the Shumagin gap, that might be interpreted as the indicator of the perimeter of the rupture area of the next great earthquake. This and the seismicity pattern observed over the past years indicate the possibility that the rupture area of a future great earthquake in the Shumagin gap might extend beyond the gap boundaries and possibly all the way to the western margin of the 1964 aftershock zone.

Fault plane solutions obtained for events in the study area indicate that the earthquake activity along the Kodiak shelf is primarily associated with underthrusting. A small sample of intermediate depth events in the lower Cook Inlet area indicates that earthquake activity is in response to gravitational sinking of the subducting slab.

Seismic activity outside the shallow thrust zone continues to show a lack of correlation with known faults, although a linear trend of shallow seismicity on Kodiak Island near Deadman Bay continues to be active. This trend does, however, not correlate with any known or inferred geological structure.

Augustine volcano with its very active recent eruptive history presents perhaps the greatest volcanic risk within the lower Cook Inlet and Shelikof Strait lease areas. Based on its eruptive history in this century Augustine can be expected to erupt again within the lifetime of potential petroleum development in lower Cook Inlet. Having monitored the volcano for 9 years through its last major eruptive cycle in 1976, we now have learned what eruption precursors to expect before a major eruption, thus enhancing our chances of perhaps predicting the next one through careful geophysical monitoring.

IX. NEED FOR FURTHER STUDY

X. SUMMARY OF FOURTH QUARTER OPERATIONS (January-March 1980)

Routine data analysis was completed for the time period April 1 through September 31, 1979. Hypocenter parameters and epicenter maps for this time were submitted to the NOAA/OCSEAP data management. Work on earthquake fault plane solutions continued and detailed analysis of the data from the joint experiment with RU 579 was begun.

Final testing of the event detection system was completed at the Fairbanks laboratory and the system installed in King Salmon in April. A maintenance trip was made to the recording site in Homer. A trip was required to Kodiak to repair equipment at the Cape Chiniak repeater site.

## XI. REFERENCES

- Davies, J. N., and K. Jacob, A Seismotectonic Analysis of the Seismic and Volcanic Hazards in the Pribilof Islands-Eastern Aleutian Island Region of the Bering Sea, Environmental Association of the Alaskan Continental Shelf, Annual Rept. of Principal Investigators for the Year Ending March 1979, IX, 2-92, 1979.
- Engdahl, E. R., and C. H. Scholz, A Double Benioff Zone Beneath the Central Aleutians: An Unbending of the Lithosphere, Geophys. Res. Lett., 4(10), 473-476, 1977.
- Engdahl, E. R., N. H. Sleep, and Ming-Te Lin, Plate Effects in North Pacific Subduction Zones, Tectonophysics, 37, 95-116, 1977.
- Evans, C. D., F. H. Buck, R. T. Buffler, S. G. Fisk, R. B. Forbes, and W. B. Parker, The Cook Inlet--An Environmental Background Study of Available Knowledge, Prepared by the University of Alaska, Resource and Science Service Center, Alaska Sea Grant Program, Anchorage, Alaska, for the Alaska District Corps of Engineers, Anchorage, Alaska, 446 pp. 1972.
- Hampton, M. A., A. M. Bouma, R. Von Huene, and H. Pulpan, Geo-Environmental Assessment of the Kodiak Shelf, Proc. Offshore Tech. Conf., April 30-May 3, 1979, 1, Houston, Texas, 365-376. 1979.
- Isacks, B., and P. Molnar, Distribution of Stresses in the Descending Lithosphere from Global Survey of Focal Mechanism Solutions of Mantle Earthquakes, Rev. Geophys. Space Phys., 9, 103-174, 1971.
- Kanamori, H., The Energy Release in Great Earthquakes, J. of Geophys. Res., 82, 2981-2988, 1977.
- Lahr, J. C., and G. Plafker, Holocene Pacific-North American Plate Interaction in Southern Alaska: Implications for the Yakataga Seismic Gap, preprint, submitted to Geology, 1980.
- Magoon, L. B., W. L. Adkison, F. B. Chmelik, G. L. Dolton, M. A. Fisher, M. A. Hampton, E. G. Sable, and R. A. Smith, Hydrocarbon Potential, Geologic Hazards, and Infrastructure for Exploration and Development of the Lower Cook Inlet, Alaska, U.S. Geol. Survey, Open File Report 76-449, 124 pp., 1976.
- Magoon, L. B., A. H. Bouma, M. A. Fisher, M. A. Hampton, E. W. Scott, and C. L. Wilson, Resource Report for Proposed OCS Sale No. 60 Lower Cook Inlet-Shelikof Strait, Alaska, U.S. Geol. Survey, Open-File Report 79-600, 38 pp., 1979.

- Malloy, R. J., and G. F. Merrill, Vertical Crustal Movement on the Sea Floor, The Great Alaska Earthquake of 1964, Oceanography and Coastal Engineering, National Research Council, National Academy of Sciences, Washington, D.C., 252-265, 1972.
- Mogi, K., Some Features of Recent Seismic Activity In and Near Japan: Activity Before and After Great Earthquakes, Bull. Earthquake Res. Inst. Tokyo Univ., 47, 395-417, 1969.
- Pulpan, H., and J. Kienle, Western Gulf of Alaska Seismic Risk, Proc. Offshore Tech. Conf., April 30-May 3, 1979, 4, Houston, Texas, 2209-2219, 1979.
- Stauder, W., and G. A. Bollinger, The S-Wave Project for Focal Mechanism Studies: The Alaska Earthquake Sequence of 1964, Scient. Report, 124 pp., 1966.
- Sykes, L. R., Aftershock Zones of Great Earthquakes, Seismicity Gaps, and Earthquake Prediction for Alaska and the Aleutians, J. Geoph. Res., 76, 8021-8041, 1971.

A P P E N D I X

LAHARS IN CRESCENT RIVER VALLEY,  
LOWER COOK INLET,  
ALASKA

James R. Riehle<sup>1</sup>

Juergen Kienle<sup>2</sup>

Karen S. Emmel<sup>1</sup>

(1) State of Alaska  
Department of Natural Resources  
Division of Geological and Geophysical Surveys  
Anchorage, Alaska 99501

(2) Geophysical Institute  
University of Alaska  
Fairbanks, Alaska 99701

## ABSTRACT

Previously unrecognized lahars (deposits of volcanic mudflows) are described from the Crescent River valley, west side of lower Cook Inlet. The lahars extend from glacier valleys on the southwest flank of Redoubt Volcano to the shores of Cook Inlet, a distance of more than 25 km (16 mi). A single radiocarbon analysis of a large block of wood implies an age of 3635 years before present for the lowest exposed lahar in sea cliffs. Triggering of the lahars may have been by events similar to those resulting in mudflows and flooding of Drift River during eruptions of Redoubt Volcano in 1966. Thus, although it has been several thousand years since lahars reached the coast in Crescent River valley, there is a small but real possibility of such events occurring again.

## INTRODUCTION

"Lahar" is a flowing mixture of rock debris and water that originates on the flanks of a volcano; it also refers to the resulting deposits (Crandall, 1971, p. 3, following van Bemmelen, 1949). Many lahars also qualify as mudflows or debris flows. Sharp and Nobles (1953) used "debris flow" to mean the deposits of a rapid flowage of loose soil and rock debris mixed with water. Varnes (1958) restricted "mudflow" to moving debris containing 50% or more of sand sized and finer material. Poor sorting of mudflow materials results in high density and high transport competency, but it is essential that there be a fluid phase (clay-water mixture) with sufficient strength and density to support the smaller granular constituents (Rodine, 1974). Each size range of granular constituents in turn supports the next larger size range.



During flow, mudflows are more than 80% by weight sediment; so-called "hyperconcentrated flows" are intermediate between normal streamflow (less than 40% sediment) and mudflows (Beverage and Culbertson, 1964). Lahar deposits may range from truly nonsorted deposits to deposits more characteristic of water-laid sediments.

Lahars may originate in many ways. Some have originated directly through volcanic activity, such as eruptions through a crater lake, direct eruption or ejection of mud through volcanic vents, avalanching of hot volcanic rock debris, and meltwater lahars, generated by eruption of hot ash and blocks onto snow, by extrusion of lava into snow, or by subglacial volcanic heating. Other lahars have been only indirectly related to volcanic activity. Failures of crater walls, for example, may occur at times other than during an eruption. Blankets of ash and pumice, common on flanks of active volcanoes, are prone to sliding when saturated during heavy precipitation. Areas of volcanic rock may be weakened by alteration, such as around fumaroles and hot springs; on steep slopes, the weakened rock may fall by landsliding and form lahars. Some volcanic landslides have dammed rivers; the dams have later failed, leading to floods and associated lahars. Among the most spectacular floods are those caused by volcanic heating of glaciers in Iceland. Termed "jökulhlaups", the floods are the result of sudden release of meltwater stored in subglacial or englacial reservoirs.

For a more complete description of historic lahars and their effects we refer to Crandall, 1971; MacDonald, 1972; Williams and McBirney, 1979.

## DESCRIPTION AND INFERRED ORIGIN OF THE DEPOSITS

### A) Setting

Redoubt Volcano is an active, andesitic stratovolcano located 175 km west-southwest of Anchorage and 20 km inland from the west shore of Cook Inlet (Fig. 1). Since the discovery of the volcano in 1778 by Captain Cook (Beaglehole, 1967), 4 periods of activity have been recorded between 1778 and 1933 (Coats, 1950). While the 1778, 1812, and 1933 events were apparently minor, with only "smoke"<sup>1</sup> being reported, in the literature the 1902 activity was an important eruption, which spread ash about 200 km to the northeast to the towns of Knik, Hope and Sunrise.<sup>2</sup> The most recent activity occurred during the period 1965-1968. During these years vulcanian ash eruption clouds reached heights of up to 13,500 meters (45,000 feet) (Wilson and others, 1966; Wilson and Forbes, 1969). On January 25 and February 9, 1966, two flash floods with fronts of 4.5 to 6 m (15 to 20 feet) occurred on the Drift River (see Fig. 1), the first flood carrying ice blocks of considerable size (described as big as a "D-7 cat"); the second flood was apparently ice-free.<sup>3</sup> The flooding was probably caused by a sudden outbreak of meltwater from the summit crater and was associated with one or more lahars which passed down the north flank of the volcano onto the Drift River floodplain (Post and Mayo, 1971; Miller, 1973).

<sup>1</sup> Smoke is a word frequently used in historic records, and refers to steam or steam and ash clods.

<sup>2</sup> Accounts in the newspaper "The Alaskan", various articles in March, 1902.

<sup>3</sup> The January 25, 1966 flood was reported in the Fairbanks Daily News Miner, January 26 edition, entitled "Volcanic Action puts 22 on Run", referring to a seismological crew which had to be rescued from the mouth of the Drift River, near the present tanker terminal. The second flood was mentioned by Mr. Frentley, Atlantic Oil Co., Anchorage in a 1966 telephone conversation with Dr. R. B. Forbes, Geophysical Institute of the University of Alaska.

The 1966 lahars occurred in the same location as older lahars which have constructed a large cross-valley fan adjacent to an unnamed glacier on the Drift River floodplain. All the lahars have apparently come from the summit crater, which is breached to the north, and followed the glacial trough down to the valley. Snow and glacial ice are probably the sources of the water involved in the lahars (Post and Mayo, 1971).

#### B) Extent and Surface Morphology

The inferred extent of the Crescent River lahars, based on photo-interpretation, is shown in Figure 1. A stereo photopair of the area east of Crescent Lake is shown in Figure 2. There, as well as adjacent to Cook Inlet, the surface morphology of the deposits is that of an alluvial fan. Note in Figure 2 the relict radial channels and the apparent absence of throughgoing active surface drainage.

The deposits are probably thickest in the areas of the fans, east of Crescent Lake and adjacent to Cook Inlet, and thinner in the narrow linear valley areas (see Crandall, 1971, p. 7). The total area inferred to be underlain by lahars is about  $87 \text{ km}^2$  ( $34 \text{ mi}^2$ ). Using a conservative figure of 2 m for an average thickness, a minimum estimate of the volume is 170 million ( $1.7 \times 10^8$ )  $\text{m}^3$ . This volume estimate may be in error by an order of magnitude, but it serves to emphasize the enormous size of the deposit.

Photointerpretation suggests a source of the lahars at the head of one, and possibly all, of four tributary valleys which drain from the summit region of Redoubt Volcano southwest to the North Fork of Crescent River. Three of these four valleys contain glaciers at their heads.

The original seaward extent of the lahars is unknown. Large blocks of fresh andesite, similar to blocks contained in the lahars, at least where exposed in sea cliffs, occur offshore in the intertidal zone at Crescent River. We have not mapped the seaward extent of such blocks, but it seems certain that the original extent of the lahars has been reduced by marine erosion.

An interesting geomorphic feature in Figure 2 is a series of low mounds along the banks of Crescent River. Similar mounds have been reported from Mt. Rainier lahars by Crandall (1971), who summarizes descriptions of lahatic mounds from elsewhere: Such mounds are of two types of origin. One type consists of a mound of large blocks of rock, commonly veneered by fine lahar material. The blocks are probably deposited in an initial rush of the lahar, and the finer material subsequently drains away downvalley such that the surface adjacent to the blocks is lowered. The other type of mound is the result of extrusion of lahatic material under hydrostatic pressure. At the top of one of the Crescent River mounds we observed 45 cm of alternating layers of light ash and dark, organic-rich ash atop lahar deposit which we exposed to a total depth of 75 cm. Although we found no large blocks, the deposit could be a lahar veneer. The Crescent River mounds are from 15 to 60 m across and are up to 10 or 15 m high. Of the mounds described by Crandall, the block-cored mounds are up to 120 m across and up to 30 m high. The extrusion mounds, however, are up to 800 m across and up to 200 m high. Comparing the sizes of the Crescent River mounds, we prefer a rock-pile origin.

#### C) Internal Characteristics of the Deposits

We have examined the lahars only along sea cliffs bordering Cook Inlet, where exposures are up to 10 m high. Massive, nonsorted diamicton,

comprising deposits of at least 2 individual lahars, forms the cliff (Fig. 3). We have not traced the contact of the 2 lahars laterally, therefore we don't know if more than 2 lahars are present in sea cliffs between Polly Creek and Squarehead Cove. Stratified fluvial sediments make up only a minor part of the material exposed in the sea cliffs. Up to a meter of fluvial sediments are exposed beneath the lowermost lahar at most locations; there may be other lahars at depth. Where stratified deposits occur between or atop exposed lahar deposits, the stratified deposits comprise thin sheets or lenses rather than cut-and-fill channel deposits. Such deposits may have formed during the final stages of lahar activity when some flushing of fines by internal drainage occurred.

The lahars resemble glacial till in their massive, nonsorted aspect. As noted by Crandall (1971, p. 5), "many lahars closely resemble till, and the distinction between the two sometimes is not possible in the field". We have noted an upward decrease in the mean size of cobble and larger clasts within individual lahars, and a crude point count suggests that the abundance of pebble and larger clasts decreases from about 40% at the bottom to about 20% at the top. Crandall (1971, p. 6) indicates that where such vertical gradation occurs, it can help in distinguishing lahar from till.

The largest clasts are about 1 m maximum in dimension, while the majority of coarse clasts are less than about 0.75 m. The clasts consist of predominantly fresh, porphyritic andesite. A few clasts are equigranular, dioritic rocks of the Aleutian Range batholith (Detterman and others, 1976) on which Redoubt Volcano is constructed. X-ray diffraction analyses of fines from two lahar samples indicate mainly plagioclase and hornblende with very little clay or chlorite. Thus, the

material comprising the lahars appears to come from fresh flows and volcanic ash. We have no data to indicate that hydrothermal alteration products are present in significant amounts.

The size distributions of 2 samples of the fine portion of a lahar are shown in Figure 4, with distributions of samples of Mt. Rainier lahars and of glacial till for comparison. Bull (1964) used sorting coefficient, phi standard deviation, and phi quartile deviation to classify alluvial fan deposits into waterlaid, mudflow, and intermediate categories. Our lahar analyses fall in Bull's mudflow category by all three parameters, and the sand-sized and finer fraction is greater than 50% (at least at the top of the lahar). Thus, our samples are true mudflows.

Midway between Polly Creek and Crescent River we saw a tilted block of stratified sand and gravel (Fig. 5). The steep dip of bedding and the absence of an obvious channel cut in the surface of the lahar suggest that the block is an accidental inclusion of pre-lahar fluvial sediments. A sand dike in the block suggests that the block may have suffered brittle failure while the enclosing lahar was still fluid. Such gentle treatment of large objects trapped in mudflows is not uncommon, and indicates that flow is dominantly laminar rather than turbulent (Johnson, 1970, p. 442).

Airfall ash layers commonly occur immediately beneath the upper and lower lahars. Near Crescent River, for example, 1 cm of medium to coarse, sand-sized ash underlies the lahar deposits; beneath the ash is up to 1 m of laterally discontinuous, stratified sand and gravel, which in turn overlies another lahar. Ash layers at the base of lahars have been reported from elsewhere and simply indicate the inability of mudflows to erode during passage (Crandall, 1971, p. 8).

We have no data bearing specifically on the temperatures of emplacement. The colors of the lahars are purple-grey and red-brown. At one locality, between an ash layer at the base of the lower lahar and above cross-bedded fluvial sediments, is 6 cm of red-brown sand and silt. The red-brown color may be due to heating by the lower lahar, or it may be primary. Wood fragments in the lower, purple-grey lahar have a thin black rind which may be carbon arising from post-depositional oxidation or from heat during emplacement. In a really hot lahar (400°C or hotter) the matrix and clasts should have a consistent direction of remanent magnetization but we did not test this for the Crescent River lahars.

#### AGE OF LAHARS

We have a single radiocarbon analysis of a large woody fragment from the lower lahar, collected from a sea cliff exposure about 6 km east of the Crescent River. The wood had a carbon rind a few mm thick but did not appear to be internally carbonized. The radiocarbon age is 3635 years before present.<sup>4</sup> At the sample locality the upper lahar rests directly on the lower with no intervening ash, organic material, or fluvial deposits. The two lahars apparently followed each other closely in time.

Near to the sample locality, the upper lahar is overlain by the soil profile shown in Figure 6. Six distinct layers of airfall ejecta are identified, most of them occurring in the lower part of the section. Although we have no data bearing on rates of peat accumulation at the site, the presence of more than 40 cm of peat and organic soil above the upper lahar seems grossly consistent with an apparent age of 3600 years.

<sup>4</sup> Analyses by Geochron Laboratories, Cambridge, Mass. Lab No. GX5771. Age  $3605 \pm 145$  C-14 years A.D. 1950. C-14 half-life: 5570 years; other C-14 age determinations of Crescent River lahar wood samples and soils are being made but are not yet available at the time of writing.

## SPECULATIVE ORIGIN OF THE LAHARS

Based on the available data, we speculate on a possible scenario for the mode of origin of the Crescent River lahars. At least two lahars are documented; each was preceded by deposition of airfall ash. At one locality, the thin basal ash layer occurs atop fluvial deposits; this suggests that an ash eruption closely preceded emplacement of the lahar. Thus, the lahars may have been triggered by eruptive activity. The fractured block of fluvial sediments (Fig. 5) may have been frozen at the time of transport; such a possibility helps to explain its apparent brittle behavior. If so, conditions may have been similar to those at the time of flooding on the Drift River in the winter of 1966. Eruptive activity in the winter of 1966 led to melting of snow and ice; in the case of the Crescent River lahars, heat may have been provided by airfall ejecta, lava, subglacial heating or all three. It would be important to confirm or deny the presence and lithologies of large blocks in the mounds near Crescent Lake. Very large blocks would require a rock slide or fall for their origin, which could be related to specific areas and processes in the summit area of the volcano.

## POTENTIAL HAZARDS OF LAHARS

Numerous examples of death and destruction by lahars are available in the literature (e.g., reviews by Crandall, 1971; MacDonald, 1972; Williams and McBirney, 1979). A primary purpose of this paper is to document a potential hazard for planners of future development. To this end we will briefly note that destructiveness of lahars is in part due to rapidity of movement, so that there is little time for advance warning. Velocities of very fluid lahars on steep slopes are as much as 80 or 100 km/hour (50 to 60 mph); generally velocities on lower slopes, where estimated by observers, have been less. Another characteristic of



lahars contributing to their destructive nature is that they tend to concentrate in valleys, where they can move to great distances from the volcano. Among the largest known lahars are ones from Mt. Rainier which have travelled more than 100 km! The Crescent River lahars, while large, are hardly comparable to such giants.

Finally, the surface elevation of a lahar during passage is commonly greater than the surface elevation of the resulting deposit. For example, the block-cored mounds discussed previously are believed to originate by lowering of the lahar surface after deposition of the blocks. Thus, a minimum estimate of the surface elevation during passage is the present elevation of the top of lahar material on the mounds. Detailed inspections along the valley walls might reveal the "high water mark" of the Crescent River lahars; presumably the height of this mark above the present surface of the lahar deposits decreases where the lahars debouched from narrow valleys onto fans. For development planning, we stress that the present average thickness of individual lahar deposits exposed in sea cliffs (1 to 2 m) underestimates by an unknown amount the depth of the lahars during passage.

#### ACKNOWLEDGEMENTS

A preliminary survey of the lahar deposits was carried out in June, 1978, as part of a field project to assess geologic processes and resources of the coastal zone. Other members of the 1978 field party were M. Howland and C. Price (D.G.G.S.) and B. Molnia (U.S.G.S.). We thank these workers for their contributions and discussions in the field. The sample of wood submitted for radiocarbon analysis was found by Howland and Emmel. The 1979 field party was supported by the BLM through an interagency agreement with NOAA, under which a multi-year program responding

to the needs of petroleum development of the Alaskan Continental Shelf  
is managed by the OCSEAP office (Contract No. 03-5-022-55, Task 2).

## REFERENCES CITED

- Beaglehole, J. C., (Editor), 1967. The journals of Captain James Cook on his voyages of Discovery, III. The voyage of the Resolution and Discovery 1776-1780: Cambridge University Press, Cambridge, p. 370.
- Bull, W. B., 1964. Alluvial fans and near-surface subsidence in western Fresno County, California: U.S. Geological Survey Professional Paper 437-A, 71 pp.
- Coats, R. R., 1950. Volcanic activity in the Aleutian arc: U.S. Geological Survey Bulletin 974-B, p. 35-49.
- Crandall, D. R., 1971. Postglacial lahars from Mount Rainier Volcano, Washington: U.S. Geological Survey Professional Paper 677, 75 p.
- Detterman, R. L., Hudson, T., Plafker, G., Tysdal, R. G., and J. M. Hoare, 1965. Reconnaissance geologic map along Bruin Bay and Lake Clark faults in Kenai and Tyonek quadrangles, Alaska: U.S. Geological Survey Open-File Report 76-477, 4 pp.
- Flint, R. F., 1957. Glacial and Pleistocene geology: John Wiley and Sons, Inc., 553 pp.
- Johnson, A. M., 1970. Physical processes in geology: Freeman Cooper and Co., 577 pp.
- MacDonald, G. A., 1972. Volcanoes: Prentice Hall, 510 pp.
- Miller, T. P., 1973. Evaluation of Redoubt Volcano for designation as a Registered Natural Landmark: unpublished report on file at Branch of Alaskan Geology, U.S. Geological Survey, Anchorage.
- Post, Austin, and L. R. Mayo, 1971. Glacier dammed lakes and outburst floods in Alaska: U.S. Geological Survey Hydrologic Investigations Atlas HA-455.
- Rodine, J. D., 1975. Analysis of the mobilization of debris flows: Ph.D. dissertation, Stanford University, 225 pp.

- Sharp, R. P., and L. H. Nobles, 1953. Mudflow of 1941 at Wrightwood, southern California: Geological Society of America Bulletin, v. 64, p. 547-560.
- Varnes, D. J., 1958. Landslide types and processes, Ch. 3 in Eckel, E. B., ed., Landslides and engineering practise: National Research Council, Highway Research Board Special Report 29, p. 20-47.
- Williams, Howel, and A. R. McBirney, 1979. Volcanology: Freeman Cooper and Co., 397 pp.
- Wilson, C. R., and R. B. Forbes, 1969. Infrasonic waves from Alaskan volcanic eruptions: Journal of Geophysical Research, v. 74, p. 4511-4522.
- Wilson, C. R., Nichparenko, S., and R. B. Forbes, 1966. Evidence for two sound channels in the polar atmosphere from infrasonic observations of the eruption of an Alaskan volcano: Nature, v. 211, p. 163-165.

## FIGURE CAPTIONS

- Figure 1. Photointerpretation map, showing inferred extent of lahars in Crescent River valley. (Base map is U.S.G.S. Kenai quadrangle, 1958 edition).
- Figure 2. Stereo photo pair showing the fan morphology of the lahar deposits north of the Lake Fork of Crescent River. Note the low mounds along the north bank of the North Fork (between arrows). The possible origin of these mounds is discussed in the text.
- Figure 3. Lahar deposits exposed in sea cliffs about 6 km northeast of the outlet of Crescent River. The base of the lowest exposed lahar (1) and the contact between the lower and upper lahars (2) are marked. Stratified fluvial sediments underlie the lahars, separated from them by the soil horizon marked (1). Insert shows variation in sizes of representative clasts from the bottom and top of the lower exposed lahar. (Field notebook for scale).
- Figure 4. Cumulative curves of the size distribution of two samples of matrix from Crescent River lahars. Shaded portion is the area covered by curves of eight samples of the Osceola Mudflow, Mt. Rainier (Crandall, 1971, Fig. 11). Dashed lines are the average curves for multiple samples of each of two different continental till sheets (Flint, 1957, Fig. 7-5).
- However, Crandall (1971, Fig. 3) reports size distribution of some till deposits from near Mt. Rainier which are similar to size distributions of the Osceola Mudflow. Therefore, size distributions of the Crescent River lahars provide permissive evidence that the deposits could be mudflow deposits, but the distributions do not serve to unequivocally distinguish till from lahar.
- Figure 5. Block of stratified sand and gravel enclosed in lahar material, in sea cliffs about 4 km northeast of the outlet of Crescent River. A sand dike (d) is marked. The view of this sea cliff exposure is horizontal, so that the steeply inclined bedding is readily apparent. We interpret the block as fluvial sediments which were incorporated in the lahar and transported to this site. The total exposed width of the block is about 2 m. (Photograph by M. Howland, A.D.G.G.S.)
- Figure 6. Stratigraphic succession in soil profile overlying upper lahar near radiocarbon sample locality.



Figure 1. Photointerpretation map, showing inferred extent of lahars in Crescent River valley. (Base map is U.S.G.S. Kenai quadrangle, 1958 edition).

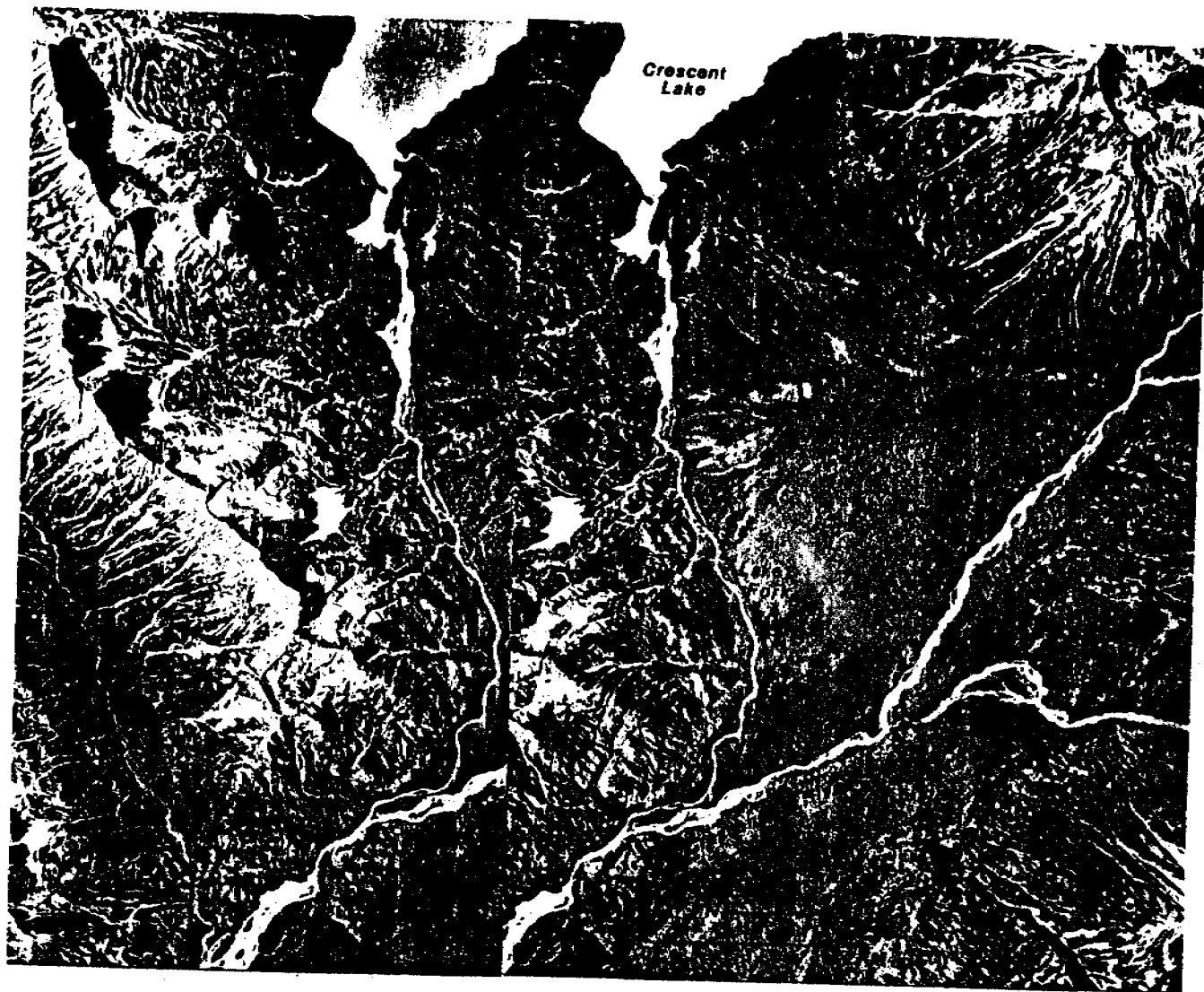


Figure 2. Stereo photo pair showing the fan morphology of the lahar deposits north of the Lake Fork of Crescent River. Note the low mounds along the north bank of the North Fork (between arrows). The possible origin of these mounds is discussed in the text.

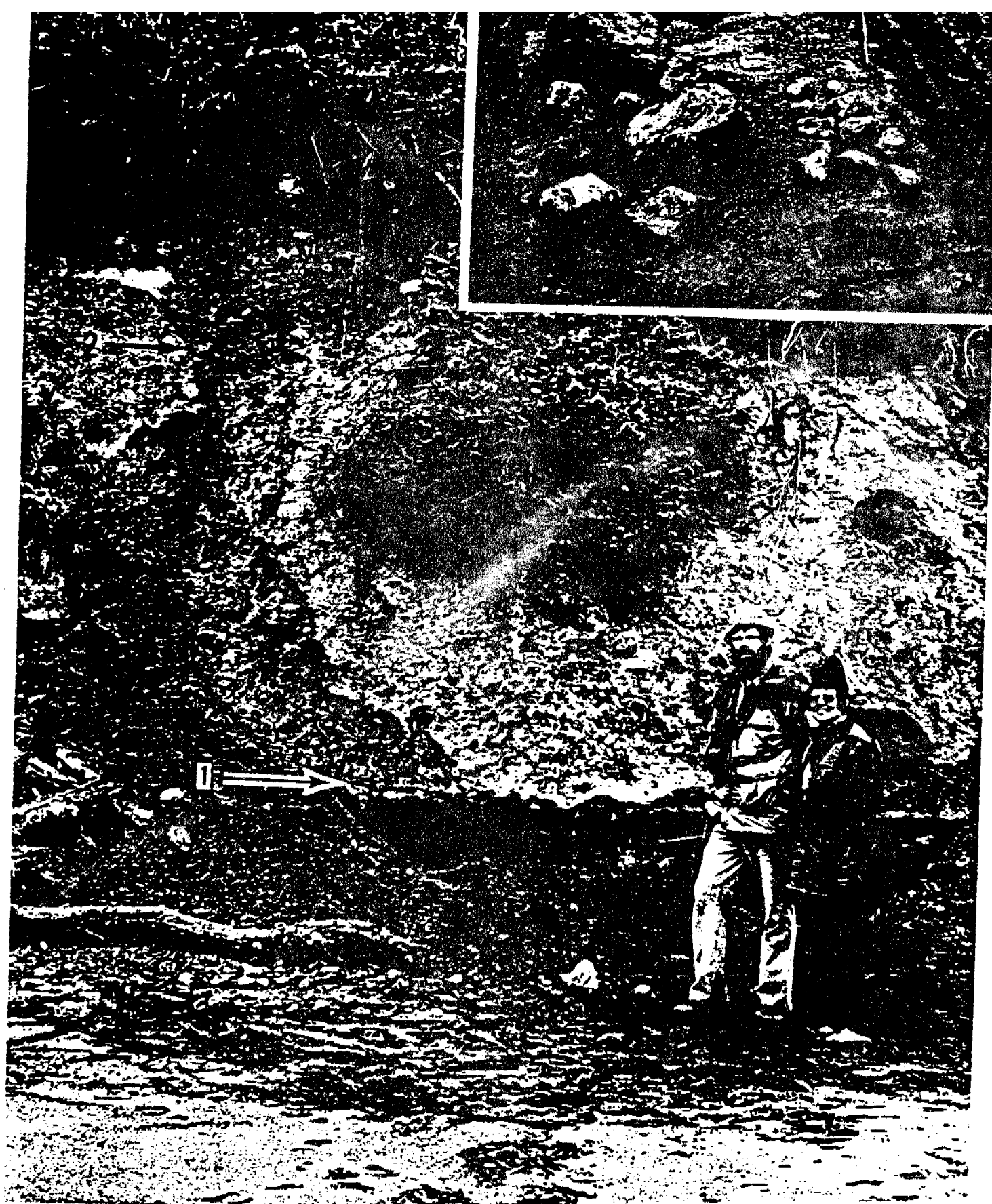


Figure 3. Lahar deposits exposed in sea cliffs about 6 km northeast of the outlet of Crescent River. The base of the lowest exposed lahar (1) and the contact between the lower and upper lahars (2) are marked. Stratified fluvial sediments underlie the lahars, separated from them by the soil horizon marked (1). Insert shows variation in sizes of representative clasts



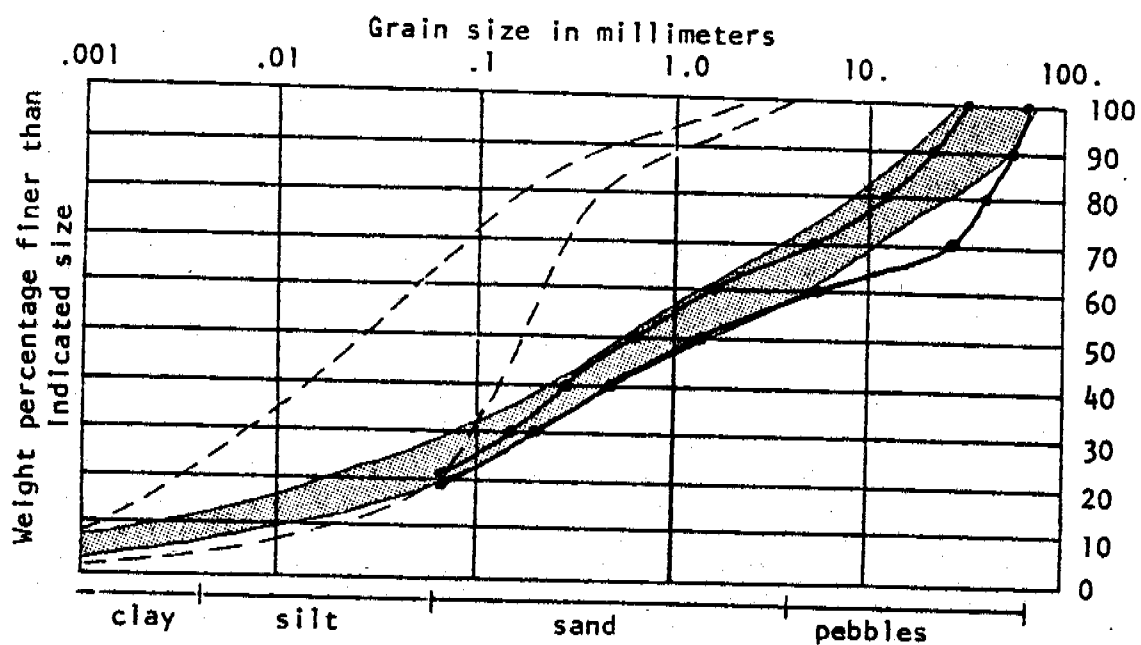


Figure 4. Cumulative curves of the size distribution of two samples of matrix from Crescent River lahars. Shaded portion is the area covered by curves of eight samples of the Osceola Mudflow, Mt. Rainier (Crandall, 1971, Fig. 11). Dashed lines are the average curves for multiple samples of each of two different continental till sheets (Flint, 1957, Fig. 7-5).

However, Crandall (1971, Fig. 3) reports size distribution of some till deposits from near Mt. Rainier which are similar to size distributions of the Osceola Mudflow. Therefore, size distributions of the Crescent River lahars provide permissive evidence that the deposits could be mudflow deposits, but the distributions do not serve to unequivocally distinguish till from lahar.



Figure 5. Block of stratified sand and gravel enclosed in lahar material, in sea cliffs about 4 km northeast of the outlet of Crescent River. A sand dike (d) is marked. The view of this sea cliff exposure is horizontal, so that the steeply inclined bedding is readily apparent. We interpret the block as fluvial sediments which were incorporated in the lahar and transported to this site. The total exposed width of the block is about 2 m. (Photograph by M. Howland, A.D.G.G.S.)

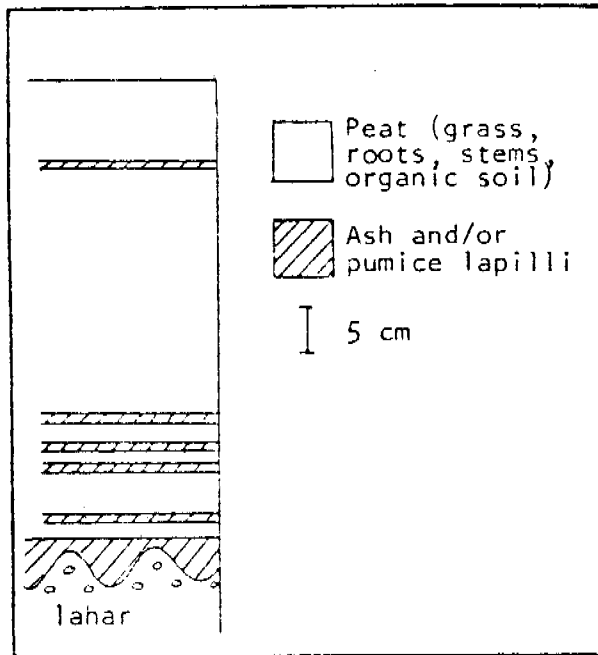


Figure 6. Stratigraphic succession in soil profile overlying upper lahar near radiocarbon sample locality.

ANNUAL REPORT

Contract Number: 03-5-022-55  
Research Unit Numbers: 253, 244, 256  
OCSEAP Task Numbers: D8 and D9  
Reporting Period: April 1, 1979 to  
March 31, 1980

SUBSEA PERMAFROST:  
PROBING, THERMAL REGIME AND DATA ANALYSIS

T.E. Osterkamp  
W.D. Harrison

Geophysical Institute  
University of Alaska  
Fairbanks, Alaska 99701

April 1, 1980

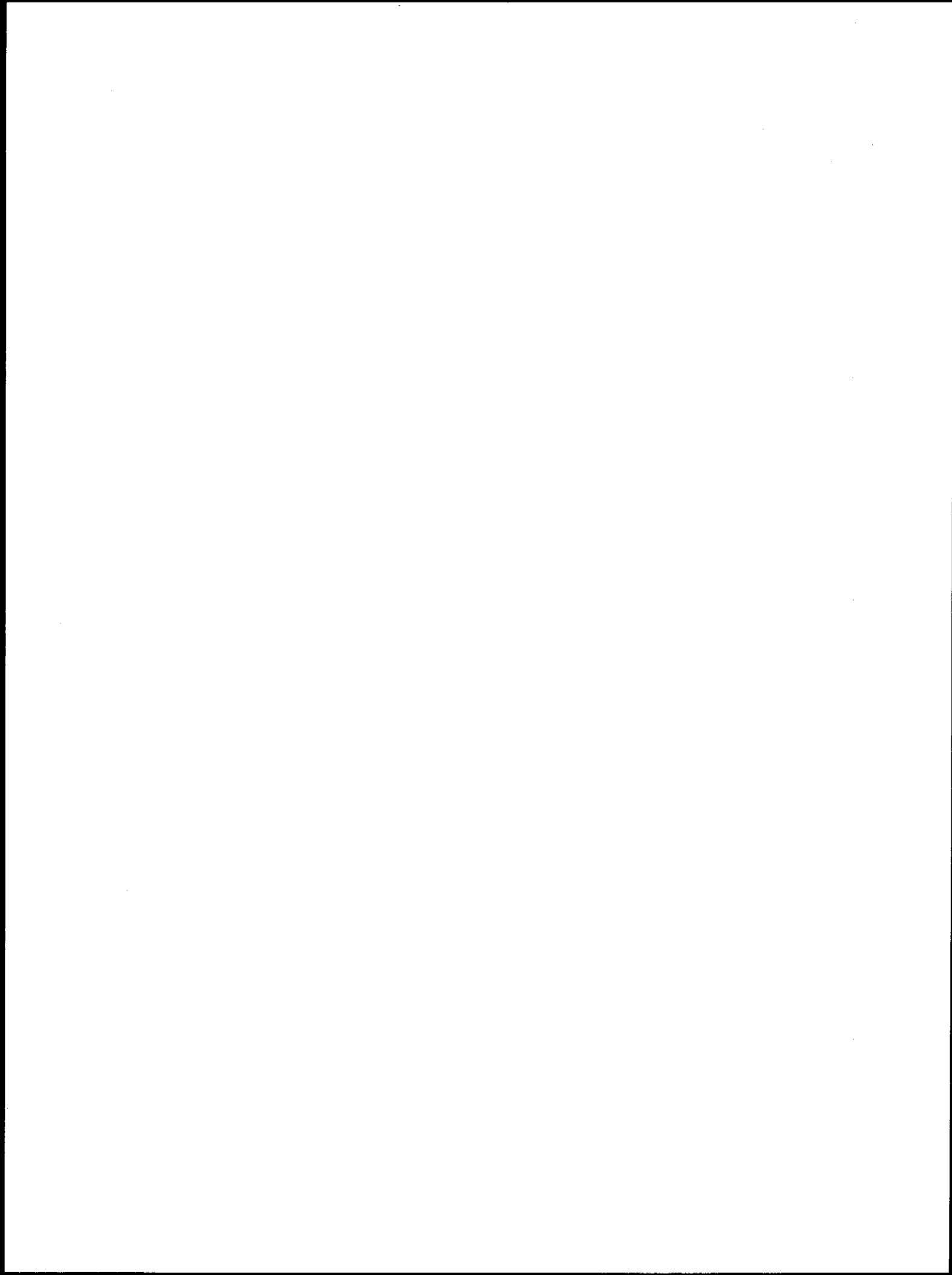
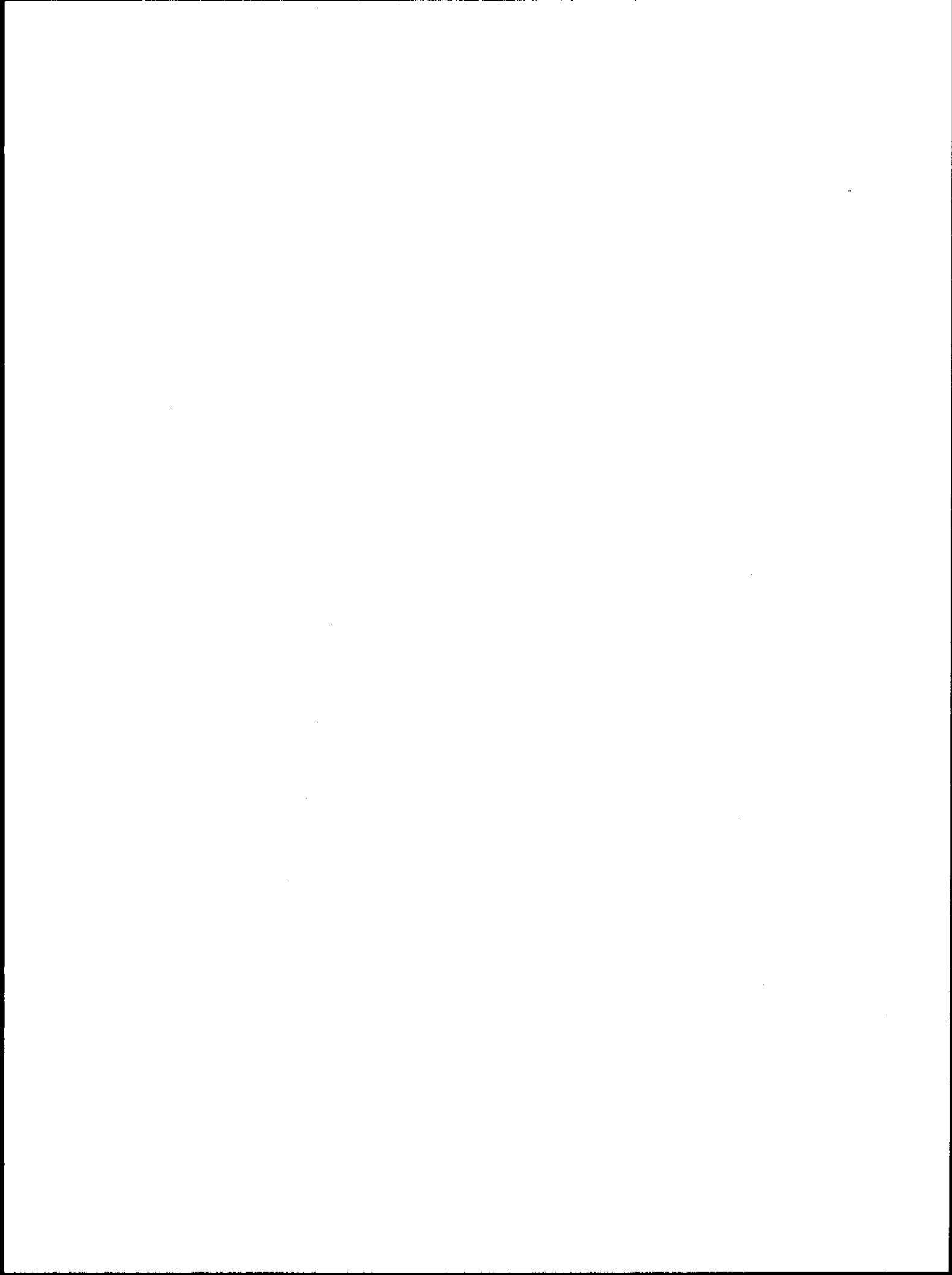


## TABLE OF CONTENTS

	Page
I. SUMMARY OF OBJECTIVES, CONCLUSIONS AND IMPLICATIONS	501
II. INTRODUCTION	501
A. General Nature and Scope of Study	501
B. Specific Objectives	501
C. Relevance to Problems of Petroleum Development	502
III. CURRENT STATE OF KNOWLEDGE	504
IV. STUDY AREA	506
V. METHODS AND RATIONALE OF DATA COLLECTION	507
VI. RESULTS AND DISCUSSION	511
VII.	
VIII. SUMMARY AND CONCLUSIONS	524
IX. REFERENCES, FIGURES AND TABLES	526
X. ACKNOWLEDGEMENTS	570
APPENDICES	571
Appendix A - Subsea permafrost temperature data; 1979 field season.	
Appendix B - Subsea Permafrost - Summary of the Results of Probing, Thermal, Chemical, and Hydrological Measurements and Analyses for RU253, 255 and 256, 1975-1979.	
Appendix C - Sediment-Laden Sea Ice: The Role of Frazil and Anchor Ice in its Formation and Development, by T.E. Osterkamp and J.P. Gosink.	
Appendix D - Ice coverage and temperature data in the Chukchi Sea used to assess the presence and distribution of subsea permafrost.	



## I. SUMMARY OF OBJECTIVES, CONCLUSIONS AND IMPLICATIONS WITH RESPECT TO OCS DEVELOPMENT

The objectives of this study are to determine the distribution and properties of subsea permafrost in Alaskan waters, in cooperation with other OCSEAP investigators. Besides direct measurements, our program includes an effort to understand the basic physical processes responsible for the subsea permafrost regime, as a basis for predictive models.

The detailed conclusions of our work in the Beaufort Sea Lease Sale area for 1979 are summarized in Section VIII and an executive summary (1975-1979) is given in Appendix B. The work on sediment-laden sea ice and the role of frazil and anchor ice in its formation and development by Osterkamp and Gosink is reported in Appendix C. Ice coverage and temperature data used to assess the presence and distribution of subsea permafrost in the Chukchi Sea are given in Appendix D. By now it should be evident from these and other OCS studies in Alaskan waters that ice-bearing subsea permafrost is widespread and may exist near the sea bed both near and very far from shore. The latter observation would not have been predicted three years ago. Compared to onshore permafrost, subsea permafrost is more complex because it is usually in a transient state, and because salt becomes a new, important and unpredictable variable. The subsea permafrost is also much more easily disturbed because of the salt, and because it is warmer. The permafrost-related development problems are therefore probably more serious offshore than onshore. A curious similarity is that excavation of materials may not be feasible offshore at some locations because of shallow ice-bonding.

## II. INTRODUCTION

### A. General Nature and Scope of Study

This work is part of the OCSEAP study of the distribution and properties of permafrost beneath the seas adjacent to Alaska. The study involves coordination of the efforts of a number of investigators (RU 204, 271, 253, 255, 256, 473, 103, 407) and synthesis of the results of both field and laboratory research.

### B. Specific Objectives

The specific objectives of our particular project are:

1. To investigate the properties and distribution of subsea permafrost in OCS lease sale areas through a drilling, jetting and probing program and associated interpretation and laboratory analysis.
2. To investigate boundary conditions at the sea bed relevant to the subsea permafrost regime.
3. To study heat and salt transport processes in subsea permafrost, in order to develop models to describe and predict properties and



distribution. This work is supported by National Science Foundation although some preliminary results are used here.

4. To extend the area of subsea permafrost field studies using simple probing techniques to determine temperature and salinity profiles, depth to any ice-bonded boundary, hydraulic conductivity, soil types, thermal properties and possible other properties.

### C. Relevance to Problems of Petroleum Development

(Much of this section was prepared in cooperation with other research units on subsea permafrost.)

Experience obtained in the terrestrial environment has indicated the necessity for careful consideration of permafrost during development activities. Both the National Academy of Sciences review of subsea permafrost problems and Canadian studies suggest that the consequences of errors in planning or design of facilities are potentially greater offshore than on land in terms of loss of human life, environmental damage, and costs.

The primary problem in any new activity in this environment will be lack of data on:

1. The horizontal and vertical distribution of subsea permafrost and the properties of this complex material.

The importance of this information is indicated below in relation to various development activities. This is based on a compilation of data from several sources (Hunter and others, 1976; Osterkamp and Harrison, 1976A; 1976B; OSCEAP reports of Sellmann and others, 1977 (RU 105) and the National Academy of Sciences Report, 1976.

2. Differential thaw subsidence and reduced bearing strength due to thawing of ice-rich permafrost.

(a) Thaw subsidence around well bores causing high down-drag loads on the well casing.

(b) Differential settlement associated with hot pipelines, silos in the sea bed, and pile and gravity structures causing instability.

(c) Differential strain across the phase boundary between bonded and unbonded permafrost.

3. Frost Heaving

(a) Well bore casing collapse due to freeze-back

(b) Pipelines - differential movement

(c) Gravity structures including gravel islands - local heaving causing foundation instability

- (d) Pile structures - differential stress in pile founded structures
4. Seismic data interpretation - Data can be misinterpreted and can lead to improper design of offshore production and distribution facilities. Also, special care needs to be taken in the interpretation of seismic exploration data.
5. Excavation - (dredging, tunneling, trenching)
- (a) Increased strength of material associated with bonded sediment
  - (b) Over-consolidated sediment can influence excavation rates and approach
  - (c) Thaw can be induced in deeper sediment by removal of material at the sea bed
  - (d) Highly concentrated and mobile brines can be found in the sediment
  - (e) Insufficient data on engineering properties for design of excavation equipment and facilities
6. Gas Hydrates
- (a) Blowouts - can result from gas hydrate decomposition during drilling operations
  - (b) Fire danger
  - (c) Misinterpretation of seismic data
7. Corrosion - Fluids (brines) with concentrations several times normal sea water are common in shallow water (< 2 m).

To develop proper precautions against these potential problems, we must obviously develop a better understanding of the horizontal and vertical distribution of subsea permafrost and the processes that control this distribution. This is no easy task in view of the  $>2 \times 10^3$  km coastline subject to potential subsea permafrost problems. It should be emphasized that with the exception of some shallow data obtained three years ago in the Chukchi Sea (Osterkamp and Harrison, 1978) drilling data exist only near Barrow, Harrison Bay and in the Beaufort Sea Lease Sale area in the Beaufort Sea of Alaska and that extrapolations to other areas must be highly speculative. The 1979 U.S.G.S. offshore drilling program represents a substantial increase in the subsea permafrost data base in the Beaufort Sea Lease Sale Area although much of these data remain to be analyzed.

The exact precautions to take in preventing the above problems (2-7) cannot be specified at present due to a lack of data and the obvious site specific nature of these problems. However, precautions will probably involve:

- (a) An adequate casing seal to drill safely through permafrost
- (b) A drilling program designed to minimize the thermal disturbance to permafrost and gas hydrates.
- (c) An adequate casing seal to control hydrate decomposition and other high pressure fluids from greater depths
- (d) Adequate assurance of the structural stability and integrity of silos and other structures
- (e) Protection against casing collapse should the well be suspended over a season

For the present the concerns are for the safety of exploratory drilling, but the eventual objective is not only to find, but to produce hydrocarbons. At that stage, permafrost and gas hydrate conditions will be even more important since hot fluids in the well are unavoidable. Thus, it is very important to maximize the derived downhole information at the initial stage of exploratory drilling.

Because of the great variability of offshore conditions, extensive site investigation programs will be necessary at each drill site prior to the actual drilling of the well. Without such site specific information it may be difficult to assure a safe drilling program. A partial list of potential accidents is as follows:

- (a) Ruptured well casings
- (b) Ruptured pipelines
- (c) Damage to the drilling structures
- (d) Damage to the production structures
- (e) Casing collapse
- (f) Corrosion and resulting weakening of metals in structures, pipelines, etc.
- (g) Blowouts
- (h) Fires on rigs

These potential accidents could result in the loss of human life, environmental damage and considerable cost to industry in correcting the problems.

### III. CURRENT STATE OF KNOWLEDGE

Regional details concerning the areal distribution and thickness of subsea permafrost in the Beaufort Sea are poorly known. Several studies have established its existence and local properties (Hunter and others, 1976; Osterkamp and Harrison, 1976A; Lewellen, 1976; Rogers et al.,

1975; and the OCSEAP reports of Rogers and Morack (RU 271); Sellman et al., (RU 105); Hopkins et al., (RU 204) and Osterkamp and Harrison (RU 253, 255 and 256). The 1979 U.S.G.S. offshore drilling program in the Beaufort Sea Lease Sale Area has added significantly to the data base although much of the analysis of this data remains to be done. The above studies have been restricted to 3 areas in the Beaufort Sea although it appears that subsea permafrost is present along the entire coastline from the Bering Straits to the Mackenzie Delta; a distance of  $> 2.3 \times 10^3$  km. These 3 sites are Elson Lagoon, Beaufort Sea Lease Sale Area and the Mackenzie Delta. Two shallow holes were drilled in the Chukchi Sea near Barrow (Lachenbruch et al., 1962; Osterkamp and Harrison, 1978). Some additional work of a reconnaissance nature has been done in Harrison Bay and in the Chukchi Sea near Kotzebue (Osterkamp and Harrison, 1978). Even though the sites cover a very limited area they are situated in distinctly different geological and marine settings.

Some data are available from direct observations that can help establish some ideas of subsea permafrost limits. The data from the drilling programs supported by NOAA at Prudhoe Bay and the Navy Program at Barrow indicate that permafrost (as defined by temperatures colder than  $0^{\circ}$  C throughout the year) is present in every hole from near the sea bed to depths at least as great as 80 meters, which is the maximum depth of the exploratory holes. However, seismic data indicate the absence of continuous ice-bonding in some of these holes (Rogers and others, 1975). One additional industry hole at Prudhoe Bay on Reindeer Island suggests bonded permafrost exists in two zones from 0 to 20 m and 90 to 125 m from the surface, although this hole was never thermally logged. Borehole temperature data available prior to 1977 are given by Lewellen, 1976; Osterkamp and Harrison, 1976A, 1977; Lachenbruch and Marshall, 1977 and the OCSEAP reports of Sellman and others. These data indicate permafrost is present 17 km from shore as seen in hole PB-2 at Prudhoe Bay and 11 km at Barrow at B-2. Recent OCS reports of Rogers and Morack describe seismic studies indicating widespread distribution of bonded permafrost in the proposed Beaufort Sea Lease Sale Area, and most surprisingly, bonded permafrost as little as 5 m below the sea bed outside the Barrier Islands.

Considerable data on the extent and distribution of subsea permafrost have been obtained by Canadian government and industry studies in the Mackenzie River region. Drilling and thermal data have confirmed the presence of permafrost and information of the upper limit of the bonded permafrost was obtained based on a study of industry seismic investigations (Hunter et al., 1976). Additional information concerning ice-bearing permafrost, can be inferred from the thermal data shown earlier. Most of these records have negative thermal gradients, a suggestion of ice-bearing permafrost at depth.

The studies conducted by Osterkamp and Harrison (1976A) and by Sellman and others (OCSEAP reports) near Prudhoe Bay across the land/sea transition established the depth to bonded permafrost along this single line in some detail out to the 2 meter water depth and less detail beyond. These studies, and those of Lewellen (1973) and Osterkamp and Harrison (OCS reports) near Barrow, indicate that bonded permafrost is found at a shallow depth beneath the sea bed in 2 m of water or less,

where the sea ice annually freezes to the sea bed. There is also considerable evidence for a seasonally active layer beneath the sea bed in this region. From Pt. Barrow to Herschel Island the area from the beach to the 2 m water depth is about 3400 km<sup>2</sup>. In this zone the limited data indicate that bonded permafrost will be near the surface, probably within 20 meters. This may not apply to areas near major river deltas where the environment is anticipated to be modified by warmer waters during periods of discharge.

Permafrost distribution in areas other than the shallow water environments is implied from results of the drilling and seismic efforts mentioned above, from analysis of climatic and sea level history data, as well as from negative bottom water temperatures which suggest permafrost can exist on most of the Beaufort Sea shelf.

Recent seismic studies (RU 271) have shown that the top of the ice-bonded permafrost may be quite variable with relief of several tens of meters over short distances and may be near the sea bed at sites far offshore.

Thawing at the sea bed in the presence of negative sea bed temperature has been found by Lewellen (1973), Osterkamp and Harrison (1976A) and CRREL-USGS (RU 105) drilling programs. This has been attributed to the infiltration of salts into the sea bed. The distribution of these salts in the thawed sediments has been determined by Osterkamp and Harrison (1976A) (RU 253) and by CRREL (RU 105) (Iskandar, Osterkamp and Harrison, 1978) Page and Iskandar (1978), Page (1978).

Preliminary studies of seismic, sea bed temperatures and other data imply that ice-bonded subsea permafrost is probably absent in most of the southern Chukchi Sea in the deeper waters although it may still survive in shallow nearshore waters (OCSEAP 1976 fourth quarterly report of Harrison, Dalley and Osterkamp, 1976).

A map showing the location of boreholes and other data gathered during the OCSEAP, Sea Grant, NSF and USGS funded studies in the Lease Sale Area is shown in Figure 1. Sellman et al., (RU 105) are presently analyzing industry seismic data in the Lease Sale Area. This research when coupled with other seismic research (RU 271), geological research (RU 204 and 473), probing, drilling (RU 105, 253, 255, 256) and interpretation of the results offers the possibility of constructing a regional map of the upper ~ 100 m of subsea permafrost in the Lease Sale Area. Unfortunately, very little is known about the base of subsea permafrost (or equivalently its thickness) although it may be possible to obtain some information from industry boreholes on Reindeer and Flaxman Islands and from audio-frequency magnetic-telluric measurements of permafrost thickness on Flaxman and Cottle Islands (Heacock, Osterkamp and Akasofu, unpublished research).

#### IV. STUDY AREA

Our efforts during the 1979 field season were concentrated entirely in the Beaufort Sea Lease Sale Area. Holes were drilled along 4 lines at Flaxman Island, Point Brower-Jeanette Island, Reindeer Island and Long Island and some additional research was done along our study line at the West Dock. The location of these holes is shown in Figure 2.

## V. METHODS AND RATIONALE OF DATA COLLECTION

The basic approach is to make direct observations of temperature, pore water salinities and subsea soil conditions in holes made with lightweight driving or rotary-jetting equipment. The techniques do not permit the acquisition of the detailed data that can be obtained with a drill rig, particularly since soil samples are not taken, but they do have the advantages of speed and lightweight. Thus, data can be obtained rapidly and cheaply over a wide area. In the driving technique, a portable motorized cathead and tripod and 64 kg drop hammer, are used to drive drill rod with attached probes into the sea bed. The depth capability depends upon soil type and is optimum for the relatively coarse conditions typical of Prudhoe Bay. There we have achieved a depth of 26 m, which was determined by our available supply of drill rod. Our rotary-jetting apparatus was completely redesigned this past summer to make it lighter, safer and easier to operate. In the rotary-jetting method a 3/4 inch steel water pipe drill string with a bit and a one-way valve at the bottom of the string is rotated and jetted into the sea bed using a small gasoline powered pump and drill. This design is the result of 4 years of field experience. The depth capability depends on soil type and is optimum for fine-grained soil conditions. At Barrow and Prudhoe Bay we have achieved depths in excess of 30 m below the sea bed. The type of data that can be obtained with the driving and rotary-jetting techniques is briefly described in the following paragraphs.

We have used several variations of the above techniques. For example, when the sidewalls of a hole are stable the pipe string can be "washed" down without rotation. During this past season, we experimented with placing pipe in the sea bed using a portable gasoline powered driver similar to those used for breaking concrete. The initial results were mixed, however, it now appears that we can place pipe or tubing in the sea bed to depths of 10-20 m depending on soil types.

Soil Conditions: Information about subsea soil conditions can be obtained from both the rotary-jetting and driving techniques, although soil samples are not taken. The experience of the driller, as in any type of drilling, is extremely important, and drilling in known material has been a factor in building up our experience. In rotary-jetting, the "feel" and sound of the drill are different in clay, silt, sand and gravel. Compact clays feel like hard rubber when the string is dropped onto the bottom of the hole; bonded materials feel more like concrete and usually drill very slowly. Unbonded silt and silty sands usually drill rapidly, as long as the hole walls do not cave, which may happen if too much sand is present. The grains of sand and gravel can be felt when raising and lowering the string off the bottom, and by the roughness of the drilling. Gravels are extremely hard to drill by rotary-jetting, due to loss of circulation, caving, and the difficulties of flushing larger soil particles from the hole. Direct identification of soil type is possible when soil cuttings are washed to the surface, as occurs on land or where the sea ice is frozen to the sea bed. Wood, shells, etc. may be recovered this way, although one must realize that they may not always come from the bottom of the hole but may be washed out of the walls of the borehole.

The driving technique works best in the soils that are the most difficult to jet, sands and gravels, which can often be identified by the rapid driving progress. On some occasions clay can be identified when it comes up stuck on the drill rod. By and large, soil identification is less positive than with the rotary-jetting technique. Both techniques can detect the presence of firmly ice-bonded sediments, which can be penetrated by the jetting technique.

Temperatures: Both techniques are well suited to provide access holes for temperature measurements. In the rotary-jetting technique the pipe is left in the hole. To prevent freezing, the pipe is normally run with a check valve at the bottom, and upon hole completion a non-freezing fluid is pumped through it. In the driving technique temperatures can be measured inside the drill rod, which has to be left in place until the temperature measurements are completed. In 1978 a new technique was developed, wherein a continuous length of 12.7 mm O.D. tubing is run inside the drill rod, and attached to a suitable driving point at the bottom. When the hole is completed the drill rod is removed, and the point and tubing remain behind, providing access for temperature measurement. This frees the drill rod, and the equipment needed to remove it, for immediate use elsewhere while temperatures are equilibrating. The undisturbed or "equilibrium" temperatures usually can be accurately estimated after a few days, depending upon the time spent in drilling and other factors, particularly any loss of drilling fluid. Some of the problems are discussed later. Temperature is logged inside the pipe or tubing with a single thermistor on a cable. Information about the approach to temperature equilibrium, accuracy and thermistor calibration are given by Osterkamp and Harrison (1976A).

Soil Interstitial Water Salinity: Salinity is important in determining the presence or absence of ice, and in giving clues to the past history of the soil. Therefore considerable effort has been devoted to developing techniques for determining the interstitial water salinity using the driving equipment. NSF support has been used for this phase of the work. The water is admitted into plastic tubing run inside the drill rod through a porous metal filter at the bottom, and sampled inside the tubing with a special bailer. The tubing can be cleared and closed at its lower end before the rod is driven to the new sampling depth. It is therefore not necessary to pull the drill pipe between samples.

The method has an interesting limitation if the freezing temperature of the free interstitial water is higher than the in situ temperature. Liquid will still be collected, but it will not be representative of the soil bulk H<sub>2</sub>O salinity, because the solid phase fraction of the H<sub>2</sub>O in the soil is not collected. There is an added complication in fine grained soils, because some of the collected water may freeze in the probe as soon as it is removed from soil phase until equilibrium with ice at the in situ temperature is reached. Only this liquid would be sampled by our bailer. Therefore, when the measured freezing temperature of the collected liquid is equal to the in situ temperature, one can only conclude that the soil bulk H<sub>2</sub>O freezing temperature is higher than or equal to the in situ temperature, and that ice may be present in the soil under these conditions.

Hydraulic Conductivity: The saturated hydraulic conductivity (essentially the permeability) of the soil is calculated from the rate at which water from the soil enters the filter, which is determined with a water level sensor. The exact calculation is extremely difficult for some of the geometrically complicated shielded filters that we have used, but we have been able to derive a simple and reasonably accurate approximate method.

Thermal Properties and the Detection of Ice: Past experience in the interpretation of temperature profiles in fine-grained subsea permafrost and in warm, saturated, fine-grained subaerial permafrost (Osterkamp, unpublished research) has shown that it can be difficult or impossible to detect the position or presence of ice-bearing permafrost soils from temperature profiles alone. The difficulties appear to be associated with the presence of unfrozen pore fluids which lead to a variable ice-content or ice-bonding at temperatures near, but less than, the equilibrium freezing point of the pore fluids. Our drilling methods in subsea permafrost have the same difficulties since they depend on a certain degree of ice bonding to detect the presence of the ice. Also, since we do not take soil samples at depth it is desirable to have a technique to determine soil properties in situ, particularly thermal conductivity. These considerations led us to design a borehole heating experiment for the purpose of detecting the position of ice-bearing permafrost and to determine the thermal conductivity of subsea permafrost soils in situ. In addition, we hoped to obtain the pore fluid salinity from the freezing-point-depression as determined from temperature profiles measured immediately after heating the borehole.

In practice, the borehole heating experiment is similar to the probe method for measuring the thermal conductivity of materials (Bullard, 1954; Lachenbruch, 1957, Carslaw and Jaeger, 1959). The "probe" in our borehole heating experiment was either 1/2" O.D. plastic tubing (3/32" wall) or 3/4" schedule 40 black iron water pipe installed in our boreholes for temperature logging purposes. The tubing was filled with anti-freeze and the pipe with a mixture of anti-freeze and sea water. A 5 kW generator was used to heat a length of 2-conductor cable which was placed inside the tubing or pipe in the borehole while heating it. Current and voltage were monitored periodically during the time of heating, which varied from 15 to 120 minutes. The boreholes were logged just prior to the time of heating and at selected times after heating, usually over a time period of a few days or less. Prior to heating, the boreholes were generally within a few hundredths °C of equilibrium. The heat dissipated in the boreholes was relatively small. Where ice-bonded permafrost was present it was probably sufficient to melt the ice in the sidewall of the borehole to a depth on the order of 1 cm.

It should be possible to determine the position of ice-bearing permafrost in the borehole by comparing temperature profiles measured before and just after heating the borehole. With ice present in the soil, the latent heat required to melt it should constrain the temperature curve during the period of heating. Comparison to an adjacent depth not containing ice should show a strong temperature difference across the ice-bearing boundary. Examples of this behavior in the REINC and FLAXB holes are given below.



In principle, it should be possible to obtain the freezing-point-depression of the pore fluids from temperature profiles after the borehole has been heated. However, in practice, it appears that the complexity introduced by the presence of pore fluids in the permafrost and the intrusion of sea water into the thawed annulus around the borehole during drilling may prevent us from making a reliable determination. Much more work is required on this aspect of the method.

The *in situ* determination of the thermal conductivity of unbonded (non-ice-bearing) subsea permafrost follows the same procedure as used in standard probe measurements. For a continuous linear heat source of constant strength in an infinite homogenous medium the temperature disturbance at a time  $t$  is (Lachenbruch, 1957)

$$\Delta T = \frac{P}{4\pi K} \ln \frac{t}{t-s} \quad (1)$$

where  $s$  is the period of heating and  $P$  is the power dissipated per unit length which can be calculated from the current and voltage measurements and the length of the heating wire. Equation 1 neglects the finite size and thermal characteristics of the borehole (pipe, water, tubing, fluid, loose soil particles), and effects associated with the proximity of the measured depth to the sea bed or hole bottom, or with layers of varying thermal properties. It is possible to evaluate the associated errors and/or to modify Eq. 1 to take them into account (Lachenbruch, 1957; Carslaw and Jaeger, 1959). The usual approach is to graph  $\Delta T$  vs.  $\ln \frac{t}{t-s}$  and to select the straight line portion of the curve which has a slope of  $P/4\pi K$  and thus determines  $K$ . Examples of this approach to determine  $K$  are given in Sec. VI and VII. An error analysis shows that the total error in these determinations of  $K$  appears to be about  $0.3-0.5 \text{ W } (^\circ\text{C-m})^{-1}$ . This appears to be dominated by the error in power determination which could amount to 25% in some cases.

Subsea permafrost is relic and usually near its melting point. It may contain salts in unfrozen pore fluids along with solid ice. Application of heat to this warm, possibly salty, ice-bearing permafrost may melt ice. The associated latent heat effect may make it difficult or impossible to determine  $K$  by this method. Ideally, the temperature rise to determine  $K$  by heating the borehole should be held to a very small value to minimize the latent heat effect.

The analysis of these borehole heating data appears to be relatively straightforward in some of the holes and very complex in others. Detection of the presence of ice-bearing permafrost seems possible provided the boreholes are logged immediately after heating. Determination of  $K$  appears to be a more complex matter especially in ice-bearing permafrost. Unfortunately, these two measurements are also somewhat at odds since substantial heating seems to be desirable to detect the presence of ice-bearing permafrost while very small heating is desirable to minimize latent heat effects when trying to determine  $K$ . Interpretation of these results is continuing and we also plan to carry out borehole heating experiments during the 1980 field season to gain additional experience with the method.

## VI. and VII. RESULTS AND DISCUSSION

### A. Flaxman Island Area - Drilling, Lithology, Temperature Data and Borehole Heating Experiment

Three holes, A, B and C, were drilled about on a true N-S line passing through Leffingwell's cabin on Flaxman Island during May 1979. Their general location is shown on the map in Figure 2 and additional information on their location, site characteristics and drilling is shown in Table 1. Hole A was drilled in the lagoon south of Flaxman Island to test Hopkin's hypothesis on the existence of a paleo-river valley of the Staines River between Flaxman Island and the coast. Several additional holes were to be drilled nearer the coast but an unusually early overflow of water on the ice from the Staines River prevented us from completing the work. Holes B and C were drilled seaward of Flaxman Island to obtain information on the subsea permafrost regime, specifically, sediment types, temperatures, presence of ice-bonded permafrost, etc. A fourth hole, D, was drilled on the spit bounding a lagoon on the north shore of Flaxman Island during September, 1979, in line with the other holes. The purpose of this hole was to determine the subsurface conditions on this part of Flaxman Island, which consists of a low-lying gravelly bar with scattered large boulders. This setting contrasts with the eastern portion of the island which is a tundra remnant.

#### 1. Hole A

Hole A (designated FLAXA) was drilled from the smooth, fast-ice sheet with our rotary-jetting rig at a site 893 m south of Leffingwell's cabin. The lithology determined during drilling is shown in Figure 3. The sea bed was hard, somewhat sandy and may have been partially frozen. It was underlain by hard clay to a depth of  $\approx 9.4$  m which graded into sand to  $\approx 11$  m where gravel was encountered for the rest of the hole ( $\approx 13.4$  m). This lithology (i.e.  $\approx 9.4$  m of hard clay) suggests that a paleo-river valley does not exist at the site of hole A. However, it does not rule out the existence of such a valley between this site and the coast, a distance of about 3 km.

Since only 2 temperature logs were made (Figure 4) we did not attempt to obtain an extrapolated temperature profile. The profile of May 26 is probably within a few hundredths  $^{\circ}\text{C}$  of equilibrium above the 9 m depth but not below it where the thermal disturbance during drilling suggests that sea water was forced into the formation. Sea bed temperature, between  $-2.2$  and  $-2.3^{\circ}\text{C}$ , suggests higher than normal salinity ( $>40\text{‰}$ ) under the ice cover at the time of drilling. This higher salinity might be expected since there was only about  $1/2$  m of water between the bottom of the ice cover and the sea bed. The mean annual sea bed temperature (MASBT) is near  $-1.0^{\circ}\text{C}$ . There is a change in slope of the May 26th profile at the 9.3 m depth which appears to be related to the change in lithology from clay to sand and gravel.

#### 2. Hole B.

Hole B (designated FLAXB) was drilled with our rotary-jetting rig from a smooth pan of ice 165 m offshore from Flaxman Island on the N-S line noted above. This hole was in 3.2 m of water just inshore from the

first grounded pressure ridge. The lithology is shown in Figure 3. There was about 5 cm of soft mud at the sea bed underlain by  $\approx 4$  m of very hard, sandy clay followed by hard clay to the total depth reached (17.2 m). Ice-bonded permafrost was not positively identified during drilling although the bottom of the hole always felt hard and no caving occurred. The sea bed temperature was about  $-1.85^{\circ}\text{C}$  on May 15th which corresponds to a sea water salinity of  $\approx 33.8\text{‰}$  assuming equilibrium conditions under the ice. It does not seem likely that the sea bed was frozen unless the pore water was relatively fresh although this is a possibility as noted below.

The extrapolated temperature profile is shown in Figure 5. The approach to thermal equilibrium after drilling, as determined from graphs of temperature versus reciprocal elapsed time since drilling, was fairly linear except for distinct changes in slope near the 4.15 m, 8.15 m and 15.15 m depths. There was a change in soil type (Figure 3) near the 4 m depth and, in addition, the borehole heating experiment suggests the presence of ice-bearing permafrost below the 4-5 m depth. The temperature at this depth is near  $-2.1^{\circ}\text{C}$ . The changes at the 15.15 m depth and below may have been associated with the presence of anti-freeze or possibly with a change in ice content or soil type. Interpretation of the temperature profile in Figure 5 suggests a change of temperature gradient near the 8 1/2 m depth from  $\approx 0.235^{\circ}\text{C m}^{-1}$  to  $\approx 0.181^{\circ}\text{C m}^{-1}$  which is consistent with the change that would be produced in going from unfrozen to frozen clay soil. However, the borehole heating experiment suggests that a change in soil type or in the ice content of frozen soil would be a more plausible explanation.

The MASBT is  $\approx -1.0^{\circ}\text{C}$  which is slightly colder than the value for a similar water depth near the West Dock at Prudhoe Bay. The temperature gradients noted above are relatively large and the temperatures quite cold; much like nearshore conditions. This suggests that Flaxman Island may have been over the site of hole B in recent times, say within the last few centuries.

Hole B (or FLAXB) was one of the four in which the borehole heating technique described in Section V was tried, in this case 16 days after hole completion. Figure 6 shows 1 temperature profile (B5) measured immediately after heating this borehole for 90 minutes and 4 additional profiles measured over the next 2 days. The small temperature increase below 4 or 5 m after heating indicates the presence of ice, which buffers the temperature response by the latent heat of melting much as an ice bath would do. The situation is less clear above 4 or 5 m, where the presence of ice may be "patchy". The situation is also not entirely clear near the bottom of the hole, where the 15.15, 16.15 and 16.61 m points behave somewhat differently from those above. This was also noticed in the pre-heating temperature data, as discussed above.

Figure 7 shows the approach to equilibrium, based on the above 4 temperature profiles and the B4 profile which was measured just prior to heating the borehole (see Section V for method). The thermal conductivities were determined from the slopes of the lines shown in Figure 7 using Eq. 1 (Section V) and are given in Table 2 for the 5 to 15 m depths. These values are typical of frozen fine-grained soils. When the B5 temperature profile was included in Figure 7 the curve connecting any given depth generally became very non-linear possibly due to the finite size of the borehole and/or latent heat effects.

### 3. Hole C

Hole C (designated FLAXC) was drilled from a large sea ice floe incorporated into a field of very rough ice just outside of the first grounded pressure ridge 684 m from shore. The lithology in Figure 3 shows that the sea bed was sand down to 0.8 m with very hard sediments from 0.8 - 4 m which seemed to be a silt or clay containing sand and gravel. The sediments were softer from 4 m to about 18 or 19 m where there was an increase in hardness. Below 14 m the lithology may be in error by 1.6 m because of a possible error in counting the number of pipe sections on the drill string. At 20.2 m, hard ice-bonded permafrost was encountered in a silty clay although we believe that the sediments may have been ice-bearing for several meters above this depth. The sediments remained ice-bonded to the 28 m depth reached in this hole.

The logging pipe that was used in this hole froze shut at the 15 m depth soon after drilling but thawed to 17 1/2 m at the time of the last temperature logging (May 29). Figure 8 shows the temperature profile obtained at this time down to the 17 1/2 m depth. This profile is nearly identical to the extrapolated profile but extends 2 1/2 m deeper. The sea bed temperature was  $\approx -1.84^{\circ}\text{C}$  which corresponds to a water salinity of  $\approx 33.6\text{‰}$  under the ice for equilibrium conditions. The MASBT is near  $-1.30^{\circ}\text{C}$ . The temperature at the top of the hard ice-bonded permafrost was near  $-2.5^{\circ}\text{C}$  which is quite cold. Considering our experience in Hole B (FLAX B) it seems likely that ice-bearing permafrost exists at some shallower depth. There is a slight change in the temperature gradient near the 14 m depth (Figure 8) and an increase in hardness was noted at about 18 or 19 m. Unfortunately, there is no additional information to help decide on the possible presence of ice-bearing or ice-bonded permafrost.

### 4. Hole D

Hole D was drilled about 3 m from the water edge on the south side of the spit. The lithology consists of about 4 m of gravelly sand, 3 m of very hard sediments which were probably ice-bonded clay,  $\approx 5$  m of unfrozen sandy clay and 1.8 m of harder clay (Figure 3). The hole was terminated at 13.8 m, apparently on a rock. This hole was not logged for temperature but we plan to do so during our 1980 field season.

### 5. General comments

A layer of very hard sediments near the sea bed was found in the Flaxman Island area. This sediment appeared to be silt or clay with sand, sandy clay, or sandy silt. The U.S.G.S. drilling program found similar hard sediments from the 1-5 m depth in their boring number 18. They determined that this hard layer was a hard, saturated gray silt, with numerous seams and pockets of gray, black, dense, fine-grained silty sand with small micaceous particles, about 2 m thick lying over a very stiff, saturated gray silty clay which became less stiff below the 5 m depth. Their boring number 18 was located  $< 2$  km ENE from our hole C in 11.3 m of water. This suggests that these very hard sediments found near the sea bed may be a general feature of the Flaxman Island area.

## B. Jeanette Island Line - Drilling, Lithology and Temperature Data

Three holes, A, B and C were drilled with our rotary-jetting rig and completed with 3/4" schedule 40 black iron pipe on a line passing through Point Brower and Jeanette Island. Their general location is shown on the map in Figure 2 and additional information on their location, site characteristics and drilling is shown in Table 1. These 3 holes were drilled to determine the sediment types, temperature, presence of ice-bonded permafrost etc. on a line that transected the "boulder patch".

### 1. Hole C

Hole C (JEANC or Pt. Brower hole) was drilled from the smooth fast ice sheet in about 3.4 m of water about 1.6 km offshore from Pt. Brower on a line through Jeanette Island. Figure 9 shows the lithology determined during drilling. The sea bed was soft, but not sticky, possibly silt, and the first 5 1/2 m were very easy drilling, suggesting the sediments may have been somewhat unconsolidated. A very distinct transition to what was thought to be ice-bonded permafrost occurred at 5 1/2 m in the fine-grained soil and a transition to what may have been ice-bonded silt occurred at 12.2 m. Ice-bonded clay or silt was thought to exist from 5 1/2 m to 16.2 m where a very hard layer was found. This layer was a few cm in thickness and was thought to be solid ice. Below 16 1/2 m, the sediments graded into ice-bonded gravel which continued to the bottom of the hole at 21.9 m. Unfortunately, the hole was flooded soon after drilling by an unusually early overflow of water on the ice from the Sagavanirktok River break-up. However, by May 26 this overflow had refrozen enough to support the 205 helicopter which allowed us to obtain 2 temperature logs of the hole.

Figure 10 shows the temperature profile on June 9, 1979. The temperature in the pipe = 0.7 m above the sea bed was  $-0.06^{\circ}\text{C}$  which suggests that fresh water from the Sagavanirktok River break-up was present under the ice at this time. The same result is true for May 26. This fresh water probably produced an increase in sea bed temperature of about  $1.8^{\circ}\text{C}$  or more when it forced the sea water from under the ice at this site. There was a very complex return to equilibrium; however, it appears from extrapolation of temperatures at selected depths that the equilibrium temperature profile below the 7 m depth is several hundredths  $^{\circ}\text{C}$  warmer than the June 9 profile. The MASBT is difficult to determine in the presence of a phase boundary so near the sea bed but appears to be near  $-1.0^{\circ}\text{C}$ . The thermal gradient is about  $0.04^{\circ}\text{C m}^{-1}$ .

Comparison of the 2 temperature profiles suggests that water may have been forced into the sediments from the sea bed to the 3 m depth. The return to equilibrium was toward colder temperatures above the 7 m depth but toward warmer temperatures below the 7 m depth. There is also a distinct change in gradient near the 12 m depth where a possible change in lithology was noted. Considering both the drilling and temperature data it seems likely that ice-bonded permafrost occurs near the 6 m depth. If this interpretation is correct, the phase boundary temperature is about  $-1.3^{\circ}\text{C}$ , which is the warmest one we have measured.

## 2. Hole B

Hole B (designated JEANB) was drilled from the smooth fast-ice cover at a site estimated to be about 1.2 km N of Dive Site #11 on a line from Point Brower to Jeanette Island. The lithology is shown in Figure 9. A sandy sea bed was found with sand down to about 2 m grading into silty clay which continued to the 10 m depth and finally into a hard clay from 10 m to the 15.4 m depth reached.

Three temperature profiles were used to construct the extrapolated temperature profile shown in Figure 11. The temperature on the sea bed measured by a probe placed there through a hole in the ice was  $-1.832^{\circ}\text{C}$  which corresponds to a sea water salinity = 33.4‰ for equilibrium conditions. Extrapolation of the temperature profile in the pipe between 2 measured points spanning the sea bed gave  $-1.845^{\circ}\text{C}$  at this time. This difference of a few hundredths  $^{\circ}\text{C}$  is typical. The depth of maximum temperature was about 7 m. The MASBT was  $-1.1^{\circ}\text{C}$  and the thermal gradient about  $0.040^{\circ}\text{C m}^{-1}$ . There does not appear to be any evidence for ice-bearing permafrost to the depth drilled although the temperature gradient implies that ice-bonded permafrost is present at shallow depth.

## 3. Hole A

Hole A (designated JEANA) was drilled from a flow incorporated in rough ice along the line noted above at a distance estimated to be  $\approx 1$  km seaward of Jeanette Island. The lithology is shown in Figure 9. The sea bed was sand to a depth of 0.1 - 0.2 m changing to clay or possibly clayey silt to 13.7 m; harder clay continued to 22 m where it graded into a very hard clay by 22 1/2 m which remained to the bottom of the hole at 30 m. The first hard clay found at 13.7 m is thought to be the ice-bonded permafrost table.

Five temperature logs in hole A were used to construct the extrapolated temperature profile shown in Figure 12. This profile is probably within  $0.01^{\circ}\text{C}$  of the equilibrium profile except for 14-18 m where it may be off by several times as much. The sea bed temperature was  $-1.83^{\circ}\text{C}$  corresponding to a sea water salinity of  $\approx 33.4$ ‰ for equilibrium conditions. Depth of maximum temperature was about 8 m. The MASBT is near  $-1.4^{\circ}\text{C}$ . The change in thermal gradient at 13.8 m is interpreted to be the ice-bonded permafrost table which is within 0.1 m of the depth noted during drilling. The temperature there is  $-1.61^{\circ}\text{C}$ .

## 4. General comments

The probable existence of ice-bonded permafrost in fine-grained soils at a depth of 5 1/2 m in hole C which is  $\approx 1.6$  km offshore from Point Brower contrasts with what has been found in a different environment at the West Dock where the ice-bonded permafrost is  $\approx 5$ -6 times as deep for the same distance offshore. If the very hard layer in hole C at 16.2 m was ice, as we believe, then this is the first observation we have of such a thick ice layer in the sediments. This observation is reinforced by that of the U.S.G.S. in their boring number 13 which is located  $\approx 5$  1/2 km offshore and almost on our drill line. They found a

layer of massive ice containing clay soils about 0.6 m thick at the 10 - 10.6 m depth. This ice was just under the ice-bonded permafrost boundary at 9.8 m and will produce a thaw settlement of  $\approx 1/2$  m when it thaws. Unfortunately no temperature data are available from this hole since ice movement destroyed the pipe before it could be logged. We did not encounter ice-bonded permafrost in hole B which is  $\approx 11 1/2$  km west of U.S.G.S. boring 20. The ice-bonded permafrost table in hole A is more than twice as deep as that in boring 20. However, the temperatures there are nearly identical ( $\approx -1.6^\circ\text{C}$ ).

### C. Long Island Area - Drilling, Lithology and Temperature Data

Four holes, A, B, C, and D were drilled with our rotary-jet rig and completed with 3/4" black iron pipe on a line N 25°E seaward from Long Island during May, 1979. Their general location is shown on the map in Figure 2 and additional information on their location, site characteristics and drilling is shown in Table 1. The rationale for these holes was to test Hopkin's hypothesis on the existence of a paleo-river valley of the Sagavanirktok River seaward of Long Island.

#### 1. Hole A

Hole A (designated LONGISA) was drilled in 3.6 m of water at a site  $\approx 315$  m offshore from the island. The lithology is shown in Figure 13. Hard clay was found to a depth of  $\approx 5$  m, clay or silt to a depth of  $\approx 7$  m grading into gravel which continued to the total depth reached, 13.3 m. Figure 14 shows the last temperature profile obtained in this hole 13 days after it was drilled. It is estimated that this profile is within  $0.1^\circ\text{C}$  of equilibrium except possibly for the bottom point. Sea bed temperature was  $\approx -1.90^\circ\text{C}$  which corresponds to a sea water salinity of  $\approx 34.6\text{‰}$  for equilibrium conditions. At the time of the last logging the sea bed temperature increased to  $-1.50^\circ\text{C}$ , probably due to fresher water under the ice from the Kuparuk River which was breaking-up and flowing over the ice on Simpson Lagoon at that time. The MASBT is  $\approx -1.2^\circ\text{C}$  although this value is not as reliable as most of our other holes since hole A was so shallow.

#### 2. Hole B

Hole B (designated LONGISB) was drilled in 5.8 m of water at a site  $\approx 600$  m offshore from the island. The lithology consisted of clay to 7 m and then gravel to the bottom of the hole at 12.8 m (Figure 13). Only one temperature profile was obtained in this hole, 23 days after drilling, since the pipe froze shut and could not be thawed until late in the season. This temperature profile is shown in Figure 15 and is estimated to be within  $0.1^\circ\text{C}$  of equilibrium. The sea bed temperature at the time of this logging was  $-1.80^\circ\text{C}$  which corresponds to a sea water salinity of  $\approx 32.9\text{‰}$  for equilibrium conditions. This salinity is near normal and suggests that little, if any, fresh water from the Kuparuk River reached the site at this time. A crude estimate of the MASBT in this shallow hole is  $-1.2^\circ\text{C}$ .

### 3. Hole C

Hole C (designated LONGISC) was drilled in 9.7 m of water at a site  $\approx 1.8$  km offshore from the island. The lithology shown in Figure 13 was clay down to about 5-6 m underlain by gravel to the bottom of the hole at  $\approx 11.0$  m. Three temperature profiles were used to obtain the extrapolated temperature profile in Figure 16. The temperature at the sea bed was  $\approx 1.89^{\circ}\text{C}$  corresponding to a sea water salinity of  $\approx 34.5\text{‰}$  for equilibrium conditions. A rough estimate of the MASBT in this shallow hole is about  $-1.4^{\circ}\text{C}$ .

### 4. Hole D

Hole D (designated LONGISD) was drilled in 14.0 m of water at a site estimated to be  $\approx 3.2$  km offshore from the island. The lithology (Figure 13) consisted of a layer of clay about 2 m in thickness grading into gravel to the total depth reached,  $\approx 7$  m. Only one temperature profile, shown in Figure 17, was obtained 7 days after drilling. The sea bed temperature was  $\approx -1.85^{\circ}\text{C}$  at that time which corresponds to a sea water salinity of  $\approx 33.6\text{‰}$ . A rough estimate of the MASBT in this very shallow hole would be  $-1\ 1/2^{\circ}\text{C}$ .

### 5. General comments

Holes A, B, C and D have a lithology consisting of a layer of clay, decreasing in thickness seaward, over gravel. These lithologies and those obtained in the U.S.G.S. borings 3 and 5 may be sufficient to ascertain whether or not a paleo-river valley of the Saganavirktok River passes through this area.

#### D. Reindeer Island Area - Drilling, Lithology, Temperature Data and Borehole Heating Experiment

Three holes, A, B, and C were drilled north of Reindeer Island during May, 1979. The rotary jetting rig was used and holes were completed with 3/4" black iron pipe. Their general location is shown on the map in Figure 2 and additional information on their location, site characteristics and drilling is given in Table 1. These holes were drilled to obtain information on the subsea permafrost regime adjacent to a barrier island and to supplement information we obtained in a hole farther offshore, in deeper water, during the 1978 field season. All the holes were drilled from floes of smooth ice incorporated into the rough ice north of Reindeer Island. A fourth hole, D, was drilled during September, 1979 on the shoreward side of the island.

#### 1. Hole A

Hole A (designated REINA) was drilled on the offshore side of the island in 3.75 m of water at a site about 352 m from the USGS Reindeer Island tower. The lithology determined during drilling is shown in Figure 18. There was silt or silty clay down to about 7 m with a harder clay down to about 15.8 m where hard frozen clay was found. The borehole heating experiment, discussed below, also suggests the presence of ice-bonded permafrost below 16 m. Under this permafrost table, which appeared to be sharply defined, there was a meter of frozen clay, a meter of frozen gravel, another meter of frozen clay and then frozen gravel to the total depth reached at 23.5 m.



Four temperature logs were obtained prior to heating this hole. However, its return to equilibrium after drilling was complex, probably due to changing soil types and ice present in the soil below the 16 m depth. The temperature profile shown in Figure 19 was the fourth profile measured 19 days after drilling. It is estimated that this profile was within several hundredths °C of equilibrium. The change in lithology at 7 m and the permafrost table at 16 m can be seen on the temperature profile. Temperature at the ice-bearing permafrost table is about -1.62°C. The temperature at the sea bed was -1.87°C which would correspond to a water salinity of  $\approx 34.1\text{‰}$  for equilibrium conditions. The MASBT is near -0.8°C.

The borehole heating experiment was also carried out in this hole 21 days after drilling. Figure 20 shows 4 post-heating temperature profiles (A5, 6, 7 and 8). Unfortunately the first profile after heating was not measured until the next day so that it is difficult to determine the depth to ice-bearing permafrost from the large latent heat effects associated with the presence of ice, as was possible in FLAXB. Judging from the smaller residual heating effects it appears that ice was present below  $\approx 16$  m in the hole which agrees with the 15.7 m depth determined during drilling, and with the interpretation of the pre-heating temperature data discussed previously. The return to equilibrium is shown in Figure 21. While some depths in Figure 21 show a nearly linear return to equilibrium, most do not, probably in some cases because freezing of the pore fluid was still taking place after the initial disturbance due to drilling. Analysis of these data must await further development of the method.

## 2. Hole B

Hole B (designated REINB) was drilled on the offshore side of the island in 5.4 m of water at a site 744 m from the USGS Reindeer Island tower. The lithology determined during drilling is shown in Figure 18 and is very similar to that of hole A. The depth below the sea bed to the ice-bearing permafrost table (16 m) is also the same as in hole A, although the water is deeper (Table 1). An extrapolated temperature profile is shown in Figure 22. The sea bed temperature was  $\approx -1.87^\circ\text{C}$  which corresponds to a sea water salinity of  $\approx 34.1\text{‰}$  for equilibrium conditions. The MASBT is near -1.2°C. Distinct changes in the extrapolated temperature profile can be seen near the 7, 11 and 16 m depths. The change at 7 m appears to be associated with the change in lithology from silt to clay sediments. The change at 11 m could be due to ice-bearing sediments at that level and below to the 16 m depth where hard, ice-bonded permafrost was found. The temperature at the ice-bonded permafrost table (16 m) was about -1.65°C.

## 3. Hole C

Hole C (designated REINC) was drilled at a site about 2 1/2 km offshore of Reindeer Island in 11.5 m of water. The sea bed was clay (Figure 18) which continued down to 10.7 m where a hard ice-bonded permafrost table was encountered. Ice-bonded gravel was found just under this table to the bottom of the hole at  $\approx 16$  m. A second hole drilled near this hole also encountered ice-bonded permafrost at 10.7 m. The temperature profile shown in Figure 23 was measured 25 days after

drilling. Above the 11 m depth the temperatures in Figure 23 are probably within a few hundredths °C of their equilibrium values. Below 11 m the return to equilibrium was very complex but with little or no temperature change with time or depth. The sharp break in slope in Figure 23 in the vicinity of 13 m suggests that something significant occurs there. The approach to equilibrium is also most complex in this region. The effect does not seem to be due to the presence of the ice-bearing permafrost table, which is several m higher, as determined from the drilling and borehole heating experiments. There is another reason why this is probably not a phase boundary; if it were the thaw rate implied by the large break in temperature gradient would imply a thaw rate on the order of  $0.01 \text{ m a}^{-1}$ , which seems much too large given the immersion history of this site. The most obvious explanation seems to be that the temperatures in Figure 23 are far from equilibrium. The slow approach to equilibrium is probably due to a transition to a very ice-rich lithology, or at least to one in which the ice is very accessible near the borehole wall, and has to be melted or frozen before equilibrium can be approached. The sea bed temperature was  $-1.83^\circ\text{C}$ , which corresponds to a salinity of  $\approx 33.4\text{‰}$  for equilibrium conditions. The MASBT is  $\approx -1 \frac{1}{2}^\circ\text{C}$  and the temperature at the ice-bonded permafrost boundary  $\approx -1.7^\circ\text{C}$ .

The borehole heating experiment was also carried out in hole C, 25 days after drilling. Figure 24 shows 1 temperature profile measured 4 1/2 hours after heating and 3 subsequent profiles measured over the next 2 days. Ice-bearing permafrost appears to be present at depths below 10-11 m. Figure 25 illustrates the return to equilibrium after heating the borehole. This return appears to be very complex, but a marked flattening of the curves below about 11 m seems to be due to buffering of the thermal response by ice. The most linear behavior occurs in the vicinity of 7 m and corresponds to a thermal conductivity of about  $1.9 \pm 30\% \text{ W/m-deg}$ . A complete analysis must await further development of the method.

#### 4. Hole D

Hole D was drilled on Reindeer Island with our rotary-jet rig on August 31, 1979. This hole is  $\approx 300 \text{ m}$ ,  $\text{N}250^\circ\text{E}$  from the USGS tower and  $\approx 4 \text{ m}$  from the shoreline. The lithology is shown in Figure 18. We expect to measure the temperature profiles during the 1980 field season.

#### 5. General Remarks

Boring #4 of the U.S.G.S. 1979 offshore drilling program was  $\approx 1.2 \text{ km}$  NW of our hole C. The lithology in that hole was somewhat similar to our Reindeer Island line except for the presence of 3-4 m of sand at the sea bed. They encountered ice-bonded permafrost at  $\approx 12.3 \text{ m}$  where the temperature was  $\approx -1.73^\circ\text{C}$  which is near that found in holes A, B, and C. The MASBT was  $\approx -1 \frac{1}{2}^\circ\text{C}$ , about the same as in hole C.

#### E. Prudhoe Bay West Dock Area - Drilling, Lithology, Temperature and Electrical Conductivity Data and Borehole Heating Experiment

Several holes were driven near the West Dock at Prudhoe Bay along the study line defined in 1975 bearing  $\text{N}31^\circ\text{E}$  from North Prudhoe Bay

State #1 (NPBS#1) well. Their general location is shown on the map in Figure 2 and additional information on their location, site characteristics and drilling is shown in Table 1. Holes A and B (also designated as holes 700 and 689, their distances from shore in meters) were placed to obtain temperature data. They were driven and finished with plastic tubing. Holes B and C (also designated as holes 701 and 687) nearby were used to obtain profiles of soil interstitial water conductivity and hydraulic conductivity. Shallow soil samples were obtained from hole E (837). An interstitial water velocity experiment was carried out at holes F, G, H, I.

### 1. Hole A (hole 700)

Hole A (designated Dock A) was driven in  $\approx 1.8$  m of water where the sea ice cover was in contact with the bottom but not frozen to it. The blow count data are shown in Figure 26. Two temperature logs were used to construct the extrapolated temperature profile in Figure 27. The sea bed temperature was  $-2.95^{\circ}\text{C}$  which corresponds to a sea water salinity of  $\approx 56\text{‰}$ . Evidently there was little circulation of sea water under the ice, although erratic tidal uplift of the ice occurred. (See section F.2. below). The MASBT is  $\approx -0.7$  and the temperature gradient  $\approx 0.068^{\circ}\text{C m}^{-1}$ . The ice-bonded permafrost boundary was not reached in this hole.

The possibility exists that the sea bed was partially frozen (i.e., ice-bearing). DOCK A was logged twice (A1 and A2 temperature profiles) and then heated to the 2.39 m depth for a period of 10 minutes on May 19th to obtain some idea of its response to heating. A value of  $K \approx 1.9\text{W } (^{\circ}\text{C-m})^{-1}$  was found for the 1.39 m depth. It was logged again on the morning of May 20th at a few selected depths (A3 logging at depths of 1.39, 2.39, 3.39, 7.39, 12.39, and 17.39 m), heated immediately after logging for 15 minutes and then logged three times during the day (Figure 28, A4, A5 and A6 temperature profiles). The A2 and A3 temperature logs are almost identical (within  $0.002^{\circ}\text{C}$ ) except for the 1.39, 2.39 and 3.39 m depths so that the choice of A2 or A3 as the pre-heating temperature profile probably does not have much effect on the determination of K values except at shallow depths. The pre-heating profile was chosen to be A2, except for the 1.39, 2.39 and 3.39 m depths where the A3 profile was used. Table 3 gives the K values determined using Eq. 1 and a graph of temperature vs.  $\ln(t/t-s)$  as shown in Figure 29. The return to equilibrium after heating was nearly linear as demonstrated by the line drawn through temperatures for each depth. Examination of the lines for all depths shows that the A4 logging was usually warmer by a few hundredths  $^{\circ}\text{C}$  than a straight line through the A2, 5 and 6 logging values would indicate. Accordingly, straight lines were drawn visually from the A2 values through A5 and 6 values with slightly less weight given to A4 values. The 0.39 m depth was not included in Table 3 because the approach to equilibrium was not linear perhaps due to its proximity to the sea bed. The conductivity values in Table 3 are similar to those we have estimated previously by other methods for this site. It should be noted that the errors in these preliminary measurements may be large as discussed above.

## 2. Hole B (hole 689)

Hole B (designated DOCKB) was driven in  $\approx 1.8$  m of water at a site  $\approx 11$  m shoreward from Hole A. The blow count data (Figure 30) suggest that the sea bed may be partially frozen to a depth of  $\approx 1$  m. Three temperature logs were used to construct the extrapolated temperature profile shown in Figure 31. The sea bed temperature was  $\approx -2.90^\circ\text{C}$  corresponding to a salinity of  $\approx 55\text{‰}$  for equilibrium conditions, much the same as for hole A. The MASBT is  $\approx -0.7^\circ\text{C}$  and the temperature gradient is  $0.071^\circ\text{C m}^{-1}$ . Hole B is a few hundredths  $^\circ\text{C}$  colder than hole A over the 14-18 m depths. An extremely sharp ice-bounded permafrost boundary was encountered at 24.3 m, where the temperature is  $-2.425^\circ\text{C}$ .

## 3. Holes C (701) and D (687)

In holes 687 and 701 near the Prudhoe Bay West Dock an electrical conductivity profile of interstitial water was obtained through the thawed layer. The sampling probes described in Section V were used for the task. The electrical conductivity of the samples was measured to estimated precision and accuracy of better than 1/2%. The results are given in Table 4 and in Figure 32.

The errors associated with sampling and sample handling seem to be slightly larger in some cases than would be indicated by the precision of the conductivity measurement, judging by the results from those depths from which two samples were obtained (Figure 31). Where gradients are large another factor that must be considered is the finite size of the probe, which samples over a length of 0.1 m. Also, because of the driving tip, the center of this sampling length cannot be brought any closer than about 0.1 m from an impenetrable boundary.

The general features of the two profiles are similar. The shallow data show large conductivity values and gradient. This is due to seasonal partial freezing in the sea bed which concentrates the salt in the remaining liquid water. Since the probe samples only the liquid water, the bulk  $\text{H}_2\text{O}$  conductivity is not determined by this method when ice is present. Below 1 or 2 m to 24.5 m depth, temperature measurements indicate that no ice is present, so the bulk  $\text{H}_2\text{O}$  conductivity is determined.

Considering that the zero of conductivity is suppressed in Figure 31, there is not a great deal of variation with depth (below the layer of seasonal freezing), although a roughly 5% increase from top to bottom is evident. The finer scale variations superimposed on this seem to be real because, with the exception of the data at 18.2 m depth, they tend to occur in both holes. The most noteworthy feature is the extremely sharp gradient near the bottom of the thawed layer. It is likely that this gradient is actually much larger, and that what is seen in Figure 31 has been smeared out by the finite dimensions of the probe, as noted above. These sharp gradients exist just above the beginning of ice-bounded permafrost, which the blow count data obtained during sampling (Figures 26 and 29) indicate to be extremely well-defined mechanically. The ice-bounded permafrost is 0.1 to 0.2 m deeper in hole 687 than in hole 701.

#### 4. Hydraulic conductivity

The rate of inflow into the probe when obtaining the interstitial water samples discussed above was used to estimate hydraulic conductivity. The results are given in Table 5. There is a fairly large scatter in the data, much of which must be due to a true variability and anisotropy of the property (compare Table VI, 1976 report). But some of it must be due to the measurement method or the failure of the concept of a pressure independent hydraulic conductivity; an erratic inflow not obeying Darcy's law was observed in many cases. The resulting error in the estimated hydraulic conductivity can amount to an order of magnitude in a few cases; hole 701, 5.88 m depth for example. However, the sampling program was designed to obtain the fastest possible interstitial water sampling rate, and no measurements such as outflow rates from the probe were made that might have improved the hydraulic conductivity data.

#### F. Heat and Mass Transport Mechanisms Near the West Dock

##### 1. Interstitial water salinity

The most noticeable feature in the soil interstitial water conductivity profiles discussed briefly above is the sharp gradient just above the beginning of hard ice-bonded permafrost (Figure 32). We feel that this sharp conductivity gradient at the ice-bonded or "phase" boundary is a thin (0.1 or 0.2 m) boundary layer, above which the salt transport regime is convective (transport by moving interstitial water). Adjacent to the phase boundary, the salt transport must be diffusive (transport by molecular diffusion). Part or all of the remaining boundary layer may be diffusive, however the possibility of motion of the pore fluid cannot be ruled out. The observation is critical because it seems to verify our interpretation of the physics that determines the rapid thaw rate near the West Dock, (Harrison and Osterkamp, 1978). The basic idea is that in order to melt relatively fresh ice at the negative temperatures prevailing beneath the Beaufort Sea, salt must be transported into it from the overlying sea water through the thawed layer. Molecular diffusion is the obvious way of doing this, but the process requires a large salinity gradient, with the high salinity, and therefore high density, at the top of the thawed layer. It can be shown that if the thawed layer is thick enough and sufficiently permeable, this situation becomes gravitationally unstable, and the interstitial water starts to move, or convect. The process is sustained by the thawing itself because the transformation of relatively fresh ice to salty water acts as a salt sink. Convection results in much more rapid salt transport than diffusion, and therefore greatly accelerated thawing. The convective transport regime cannot prevail all the way down to the phase boundary, because the ice-bonded permafrost is impermeable (Osterkamp and Harrison, 1976), and the interstitial water velocity perpendicular to it must therefore be zero. Diffusion therefore must take over the salt transport close to the boundary, and it requires a large salinity gradient to sustain the several centimeters per year thaw rate that probably exists near hole 687 and 701. It seems to be this large gradient that we have finally observed. Because of the experimental difficulties noted above, the actual gradient is probably larger than indicated in Figure 32.

## 2. Interstitial water velocity experiment

If, as it appears, convective motion of the soil interstitial water is a key factor in the development of the thawed layer at the West Dock, the motion may have another observable consequence, the associated pressure gradients in the soil that drive it.

Pressure measurements were made in an array of 4 holes (F, G, H and I) located about 10 m east of hole 687. The holes had depths from 5.8 to 10.4 m beneath the sea bed, and a maximum horizontal spread of about 3.8 m, and were arranged so that pressure gradients in all three directions could be sensed. Each hole was a driven probe with a filter on the bottom to admit the water. Pressure gradients were studied by comparing water levels after they had stabilized. The main factor limiting the sensitivity was the sometimes erratic response to tidal and artificially induced changes. Two probes in addition to the four failed to respond to small changes at all, and data from them were discarded. It was concluded that any real pressure differences in excess of hydrostatic were less than 0.05 or 0.1 m (head units), and the gradient less than 0.03 m/m. Using Darcy's law, a value of  $4 \text{ m a}^{-1}$  for the hydraulic conductivity, and a value of 0.4 for the porosity, a corresponding order of magnitude upper limit on the velocity of  $0.3 \text{ m a}^{-1}$  is obtained. This is the same order of magnitude for the velocity that we have estimated by indirect methods. It may be possible to improve the sensitivity of the method.

Although we feel that the motion is driven primarily by gravity because of density gradients, rather than by external forces such as waves or tides, the tides and the response of the sea ice to them at this site are of interest. Normally the 1.85 m thick ice was grounded, but on one and probably on two occasions during the mainly daytime period of observations from May 29 to June 1, the ice was floated with respect to the driven probes. Maximum observed uplift was about 0.10 m.

## G. Chukchi Sea

Our 1977 Annual Report contained a part called "Delineation of most probably areas for subsea permafrost in the Chukchi Sea from existing data". An important part of this work was the compilation of sea bed temperature data, which together with sea level history data and crude thermal models, was used to investigate the possible existence of permafrost at present beneath the Chukchi Sea. This permafrost would have survived from Bering land bridge times when the Chukchi Sea was emergent. The acquisition of new data, planned 1980 field studies, and the better understanding of rate controlling mechanisms gained from our Beaufort Sea studies, make it worthwhile to update this work. This is a major undertaking and so far only the mean monthly sea bed temperatures and ice cover data have been updated (Tables 6 and 7). The updated reference list for all the temperature data used is given in Table 8. These data will be the basis of a new estimate of mean annual bottom temperature distribution in the Chukchi Sea.

## VIII. SUMMARY AND CONCLUSIONS

Portable drilling and probing methods were used in subsea permafrost studies in the Beaufort Sea lease sale area. As in previous years data on the thermal, chemical and hydrologic regimes of the subsea permafrost were obtained as well as some selected properties (e.g. thermal and hydraulic conductivities). A new technique was tested for in situ measurement of thermal conductivity and the detection of ice, with promising results. Some experiments on the physics of mass transport processes were carried out. On a regional basis some of the results are as follows:

### A. Flaxman Island Area:

Four holes were drilled in the Flaxman Island area in mostly fine-grained sediments. Hard sediments were found near the sea bed in most cases. A hole about 0.9 km inshore of the island suggests that there is no paleo-river valley at that site. Ice was identified in the other three holes, one of which was on the spit to the north side of the island. The other two holes were offshore of the spit. A steep temperature gradient in the one, 165 m to the north of the spit, suggests that the island occupied that site fairly recently. A borehole heating experiment was used to detect ice and to obtain thermal conductivity values for fine-grained, ice-bonded subsea permafrost sediments in this hole.

### B. Jeanette Island Area

Three holes were drilled along a line between Pt. Brower and Jeanette Island in mostly fine-grained sediments. In a hole 1.6 km from Pt. Brower, hard sediments were encountered only 5.6 m below the sea bed, and are tentatively identified with ice-bonding, although the temperature at this boundary ( $-1.3^{\circ}\text{C}$ ) is higher than at any phase boundary we have identified previously. Evidence for segregated ice was also found. In a hole near Dive Site #11 no ice was found to the 15 m depth reached, although it almost certainly exists deeper. An ice-bonded permafrost layer was found at 15 m depth in a hole about 1 km offshore of Jeanette Island. The existence of segregated ice in the Pt. Brower hole and a nearby USGS hole suggests thaw settlement will occur when this ice melts.

### C. Long Island Area

Four holes were drilled on the seaward side of Long Island in sediments consisting of a layer of clay, decreasing in thickness seaward, overlying gravel. Ice-bearing permafrost was not identified; the holes were shallow and temperature data sparse.

### D. Reindeer Island Area

Three holes were drilled at distances of up to 2 1/2 km seaward of Reindeer Island in sediments that consisted mostly of clay overlying gravel. An ice-bearing permafrost boundary was found in all holes at 10 to 16 m. The difficulty of obtaining equilibrium temperatures under

some ice-bearing conditions, even with a month of temperature data, is demonstrated in one hole. The borehole heating experiment was tried in 2 of these holes to determine the ice-bearing permafrost boundary and thermal conductivity of the sediments.

#### E. Prudhoe Bay West Dock

Temperature, interstitial water electrical conductivity, hydraulic conductivity and thermal conductivity profiles were obtained through the 24 m thick thawed layer at two sites about 14 m apart near the West Dock, in relatively coarse-grained sediments. The major features in the electrical conductivity profiles were the same in both holes. Particularly interesting is a fraction of a meter thick layer of high electrical conductivity (salinity) gradient at the bottom of the thawed layer, which we tentatively interpret as a diffusive boundary layer, marking the transition from a convective salt transport regime to a diffusive one at the impermeable ice-bonded boundary. From a pressure gradient experiment an upper limit on the order of 0.3 m/year was estimated for the soil interstitial water velocity responsible for the convective salt transport regime.

#### F. Chukchi Sea

An update of the seabed temperature distribution data in the Chukchi Sea was carried out, as the basis for an improved estimate of potential permafrost occurrence there.



## IX. REFERENCES

- Black, R. F., 1964. Gubik Formation of Quaternary Age in Northern Alaska, U.S.G.S Professional Paper 302-C, p. 59-91.
- Bullard, E., 1954. Heat flow through the flow of the Atlantic Ocean, Proc. Royal Society, A, Vol. 222, p. 403-429.
- Carslaw, H. S. and Jaeger, J. C., 1959. Conduction of heat in solids, Oxford University Press, New York, NY.
- Doherty and Kester, 1974. Freezing Point of Sea Water, J. Marine Research, Vol. 32 (2), p. 285-300.
- Harrison, W. D., 1972. Temperature of a temperate glacier, J. of Glaciology, Vol. 11, No. 61, p. 15-19.
- Harrison, W. D., P. D. Dalley and T. E. Osterkamp, 1977. Permafrost beneath the Chukchi Sea-preliminary report, In OCSEAP Annual Report, by T. E. Osterkamp and W. D. Harrison, 1977, Appendix II.
- Harrison, W. D., and T. E. Osterkamp, 1978. Heat and Mass Transport Processes in Subsea Permafrost I: An Analysis of Molecular Diffusion and its Consequences, J. Geophys. Res., Vol. 83, No. C9, p. 4707-4712, and Appendix II, this report.
- Hopkins, D. M., 1976-1979. Annual OCSEAP Reports, Arctic Project Office, University of Alaska, Fairbanks, Ak, 99701.
- Hunter and others, 1976. The Occurrence of Permafrost and Frozen Sub-Seabottom Materials in the Southern Beaufort Sea, by J. A. M. Hunter, A. S. Judge, H. A. MacAuley, R. L. Good, R. M. Gagne, and R. A. Burns, Beaufort Sea Project Technical Report #22, Department of the Environment, Victoria, B. C., Canada.
- Iskandar, I. K., T. E. Osterkamp and W. D. Harrison, 1978. Chemistry of Interstitial Water from the Subsea Permafrost, Prudhoe Bay, Alaska, Proceedings of the Third International Conference on Permafrost, p. 92-98. National Research Council of Canada, Ottawa, Ontario, Canada K1A 0R6.
- Lachenbruch, A. H., 1957. A probe for measurement of thermal conductivity of frozen soils in place, Trans. American Geophysical Union, Vol. 38, No. 5, p. 691-697, October, 1957.
- Lachenbruch, and others, 1962. Temperatures in Permafrost, by A. H. Lachenbruch, M. C. Brewer, G. W. Greene and B. V. Marshall, in "Temperature-its Measurement and Control in Science and Industry", Vol. 3, Part 1, p. 791-803, Reinhold Publishing Corp., New York.
- Lachenbruch, A. H. and Marshall, B. V., 1977. Subsea Temperatures and a Simple Tentative Model for Offshore Permafrost at Prudhoe Bay, Alaska, U.S.G.S. Open File Report 77-395.
- Lewellen, R. I., 1973. The Occurrence and Characteristics of Nearshore Permafrost, North Alaska. Permafrost: The North American Contribution to the Second International Conference, National Academy of Sciences, Washington, D.C.

- Lewellen, R. I., 1974. Offshore Permafrost of Beaufort Sea, Alaska, in "The Coast and Shelf of the Beaufort Sea", Proceedings of a symposium on Beaufort Sea Coast and Shelf Research, J. C. Reed and J. E. Sater, Editors, Arctic Institute of North America.
- Lewellen, R. I., 1976. Subsea Permafrost Techniques, Symposium on research techniques in coastal environments, Louisiana State University, Baton Rouge, Louisiana.
- National Academy of Sciences, 1976. Problems and Priorities in Offshore Permafrost Research, Committee on Permafrost, Polar Research Board, Assembly of Mathematical and Physical Sciences, National Academy of Sciences. Available from Polar Research Board, 2101 Constitution Avenue, N.W., Washington D.C. 20418.
- Osterkamp, T. E., A conceptual model of offshore permafrost, Rept. No. UAG-234, Geophysical Institute, University of Alaska, Fairbanks, Ak. 99708.
- Osterkamp, T. E., and W. D. Harrison, 1976A. Subsea Permafrost at Prudhoe Bay, Alaska: Drilling report, University of Alaska, Geophysical Institute Report, UAG R-245, Sea Grant Report 76-5.
- Osterkamp, T. E., and W. Harrison, 1976B. Subsea Permafrost: Its Implications for Offshore Resource Development, The Northern Engineer, Vol. 8, No. 1, p. 31-35.
- Osterkamp, T. E., and W. D. Harrison, 1977. Subsea Permafrost Regime at Prudhoe Bay, Alaska, U.S.A., Journal of Glaciology, Vol. 19, No. 81, p. 627-637.
- Osterkamp, T. E., and W. D. Harrison, 1977. Offshore Permafrost-Drilling, Boundary Conditions, Properties, Processes and Models. Delineation of Most Probable Areas for Subsea Permafrost in the Chukchi Sea from Existing Data. Subsea permafrost: Probing, Thermal Regime and Data Analysis. OCSEAP 1977 Annual Report.
- Osterkamp, T. E., and W. D. Harrison, 1978. Subsea Permafrost: Probing, thermal regime and data analysis, OCSEAP 1978 Annual Report.
- Page, F. W., 1978. Geochemistry of Subsea Permafrost at Prudhoe Bay, Alaska, Masters of Arts Thesis, Dartmouth College, Hanover, N.H.
- Page, F. W., and I. K. Iskandar, 1978. Geochemistry of Subsea Permafrost at Prudhoe Bay, Alaska. U. S. Army Cold Regions Research and Engineering Laboratory, Hanover, N.H. Special Report 78-14.
- Reimnitz, E., and P. W. Barnes, 1974. Sea Ice as a Geologic Agent on the Beaufort Sea Shelf of Alaska. Proceedings of a Symposium on Beaufort Sea Coast and Shelf Research, Edited by J. C. Reed and J. E. Sater, Arctic Institute of North America.
- Rogers, J. C. and others, 1975. Nearshore Permafrost Studies in the Vicinity of Point Barrow, Alaska, University of Alaska, Geophysical Institute Report UAG R-237, Sea Grant Report 75-6.

- Rogers, J. C., and J. L. Morack, 1977. Beaufort Seacoast Permafrost Studies, OCSEAP 1977 Annual Report.
- Rogers, J. C., and J. L. Morack, 1978. Beaufort Seacoast Permafrost Studies, OCSEAP 1978 Annual Report.
- Rogers, J. C., and J. L. Morack, 1979. Beaufort Seacoast Permafrost Studies, OCSEAP Quarterly Report, January 1, 1979.
- Sellman, P. V., et al., 1977-1979. Annual OCSEAP Reports, Arctic Project Office, University of Alaska, Fairbanks, Ak. 99701.
- USGS., 1979. Geotechnical Investigation, Beaufort Sea, Harding-Lawson Associates, Anchorage, Ak, July, 1979.

## LIST OF FIGURES

- Figure 1. Location map for boreholes in the Beaufort Sea Lease Sale area made by the OCSEAP, Sea Grant, NSF and USGS drilling programs.
- Figure 2: Location map for boreholes made during the 1979 field season by RU .
- Figure 3. Lithology of Flaxman Island holes A, B and C, and D as determined by rotary-jet drilling.
- Figure 4. Measured temperature profiles for Flaxman Island hole A (FLAXA).
- Figure 5. Extrapolated temperature profile for Flaxman Island hole B (FLAXB).
- Figure 6. Measured temperature profiles in Flaxman Island hole B (FLAXB) after the hole was heated for a period of 90 minutes.
- Figure 7. Graph of the  $\ln (t/t-s)$  vs. temperature (see Equation 1) for Flaxman Island hole B (FLAXB) which demonstrates the approach to equilibrium after heating the borehole for 90 minutes.
- Figure 8. Measured temperature profile in Flaxman Island hole C (FLAXC) on May 29, 1979, 17 days after drilling.
- Figure 9. Lithology of the Jeanette Island holes A, B and C as determined by rotary-jet drilling.
- Figure 10. Measured temperature profile in Jeanette Island hole C (JEANC) on June 9, 1979, 37 days after drilling.
- Figure 11. Extrapolated temperature profile for Jeanette Island hole B (JEANB).
- Figure 12. Extrapolated temperature profile for Jeanette Island hole A (JEANA).
- Figure 13. Lithology of Long Island holes A, B, C and D as determined by rotary-jet drilling.
- Figure 14. Measured temperature profile in Long Island hole A (LONGISA) on May 30, 1979, 13 days after drilling.
- Figure 15. Measured temperature profile in Long Island hole B (LONGISB) on June 10, 1979, 23 days after drilling.
- Figure 16. Extrapolated temperature profile for Long Island hole C (LONGISC).

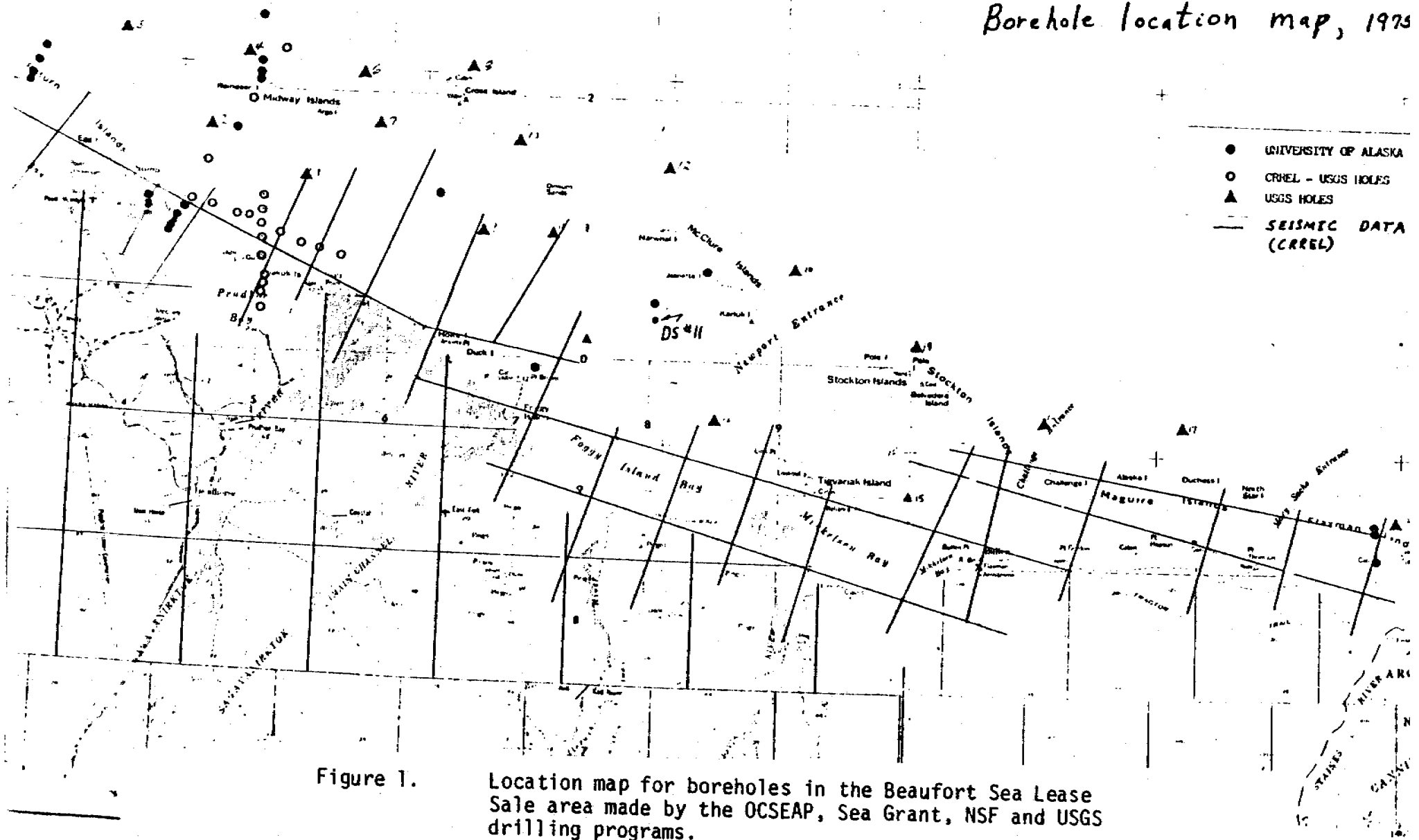
- Figure 17. Measured temperature profile in Long Island hole D (LONGISD) on May 27, 1979, 7 days after drilling.
- Figure 18. Lithology of the Reindeer Island holes A, B, C and D as determined by rotary-jet drilling.
- Figure 19. Measured temperature profile in Reindeer Island hole A (REINA) on May 24, 1979, 19 days after drilling.
- Figure 20. Measured temperature profiles in Reindeer Island hole A (REINA) after the hole was heated for a period of 76 minutes.
- Figure 21. Graph of the  $\ln (t/t-s)$  vs. temperature (see Equation 1) for Reindeer Island hole A (REINA) which demonstrates the approach to equilibrium for selected depths after heating the borehole for 76 minutes.
- Figure 22. Extrapolated temperature profile for Reindeer Island hole B (REINB).
- Figure 23. Measured temperature profile in Reindeer Island hole C (REINC) on May 29, 1979, 25 days after drilling.
- Figure 24. Measured temperature profiles in Reindeer Island hole C (REINC) after the hole was heated for a period of 120 minutes.
- Figure 25. Graph of the  $\ln (t/t-s)$  vs. temperature (see Equation 1) for Reindeer Island hole C (REINC) which demonstrates the return to equilibrium for selected depths after heating the borehole for 120 minutes.
- Figure 26. Blow count profile for West Dock hole A (DOCKA).
- Figure 27. Extrapolated temperature profile for West Dock hole A (DOCKA).
- Figure 28. Measured temperature profiles in West Dock hole A (DOCKA) after the hole was heated for a period of 15 minutes.
- Figure 29. Graph of the  $\ln (t/t-s)$  vs. temperature (see Equation 1) for West Dock hole A (DOCKA) which demonstrates the approach to equilibrium after heating the borehole for 15 minutes.
- Figure 30. Blow count profile for West Dock hole B (DOCKB).
- Figure 31. Extrapolated temperature profile for West Dock hole B (DOCKB).
- Figure 32. Electrical conductivity profiles of interstitial pore water samples from West Dock holes C (701) and D (687).

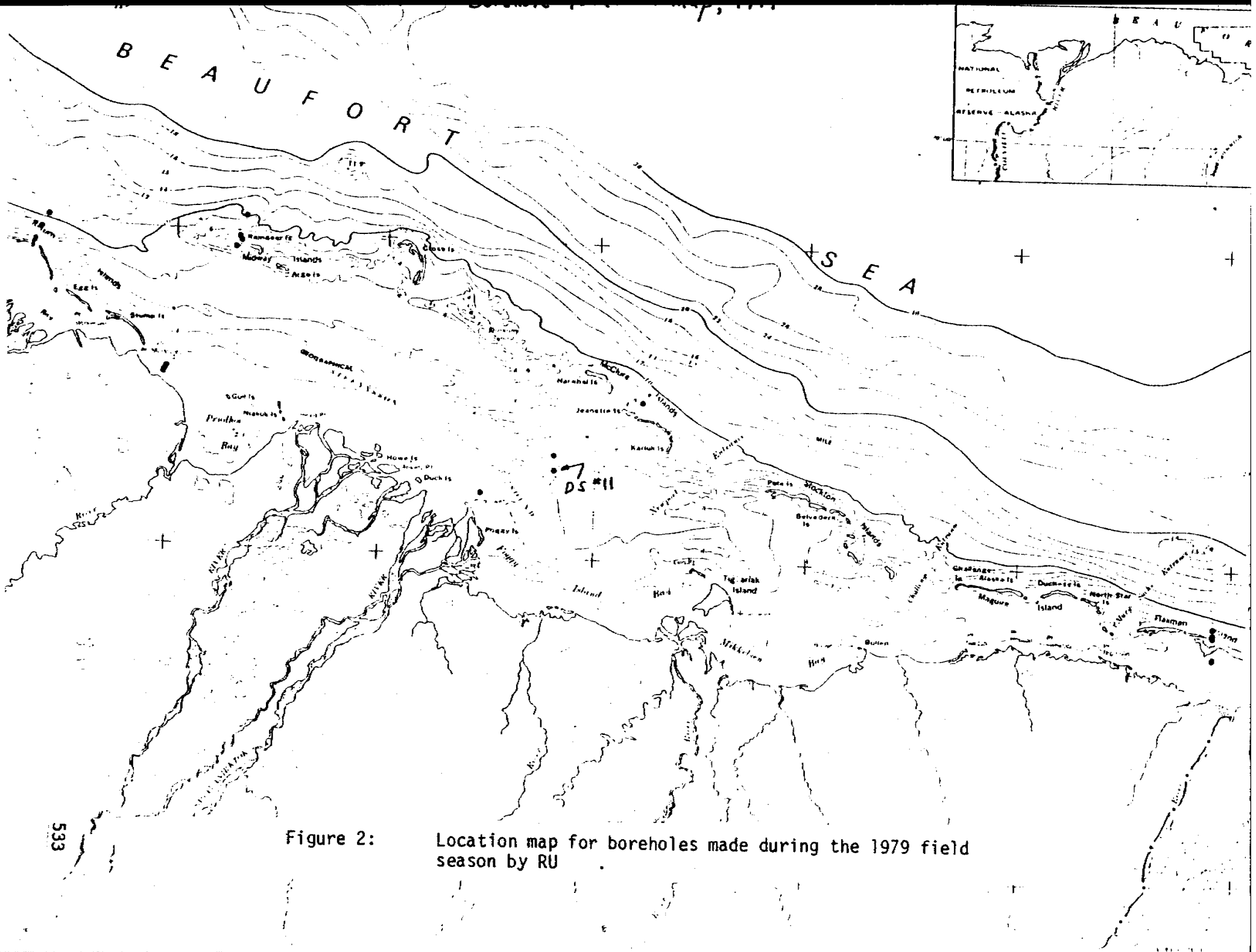
## TABLES

- Table 1. General information on boreholes drilled during the 1979 field season.
- Table 2. Thermal conductivity values for Flaxman Island hole B (FLAXB) (5-15 m depths) as determined from the borehole heating experiment.
- Table 3. Thermal conductivity values for West Dock hole A (DOCKA) as determined from the borehole heating experiment.
- Table 4. Electrical conductivities of interstitial pore water samples from West Dock holes C (701) and D (687).
- Table 5. Hydraulic conductivity values obtained during the process of sampling the interstitial pore water in West Dock holes C (701) and D (687).

E A U F O R T S E A

## Borehole location map, 1973







- Drill Hole Logs

- Flaxman Island Line

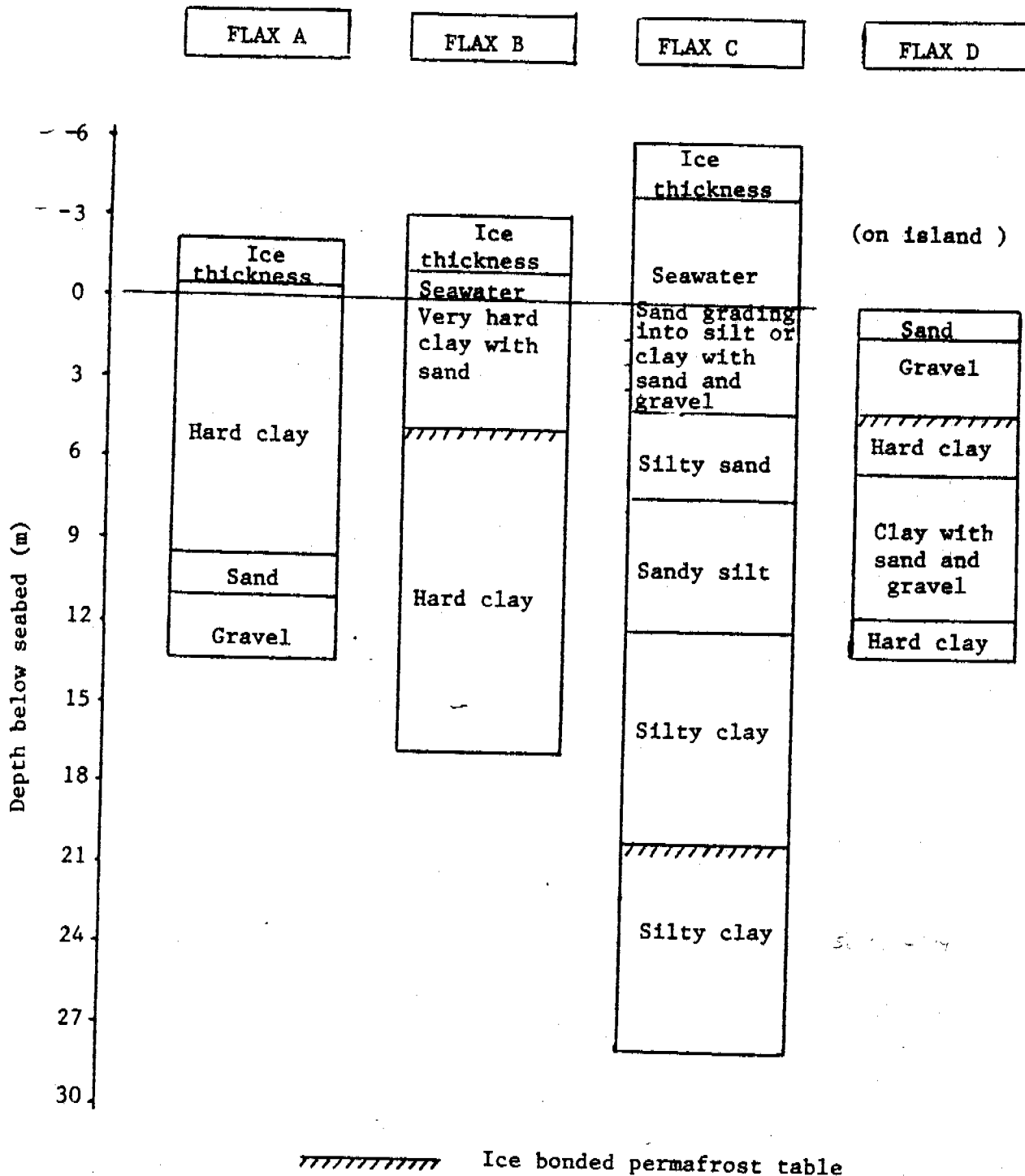
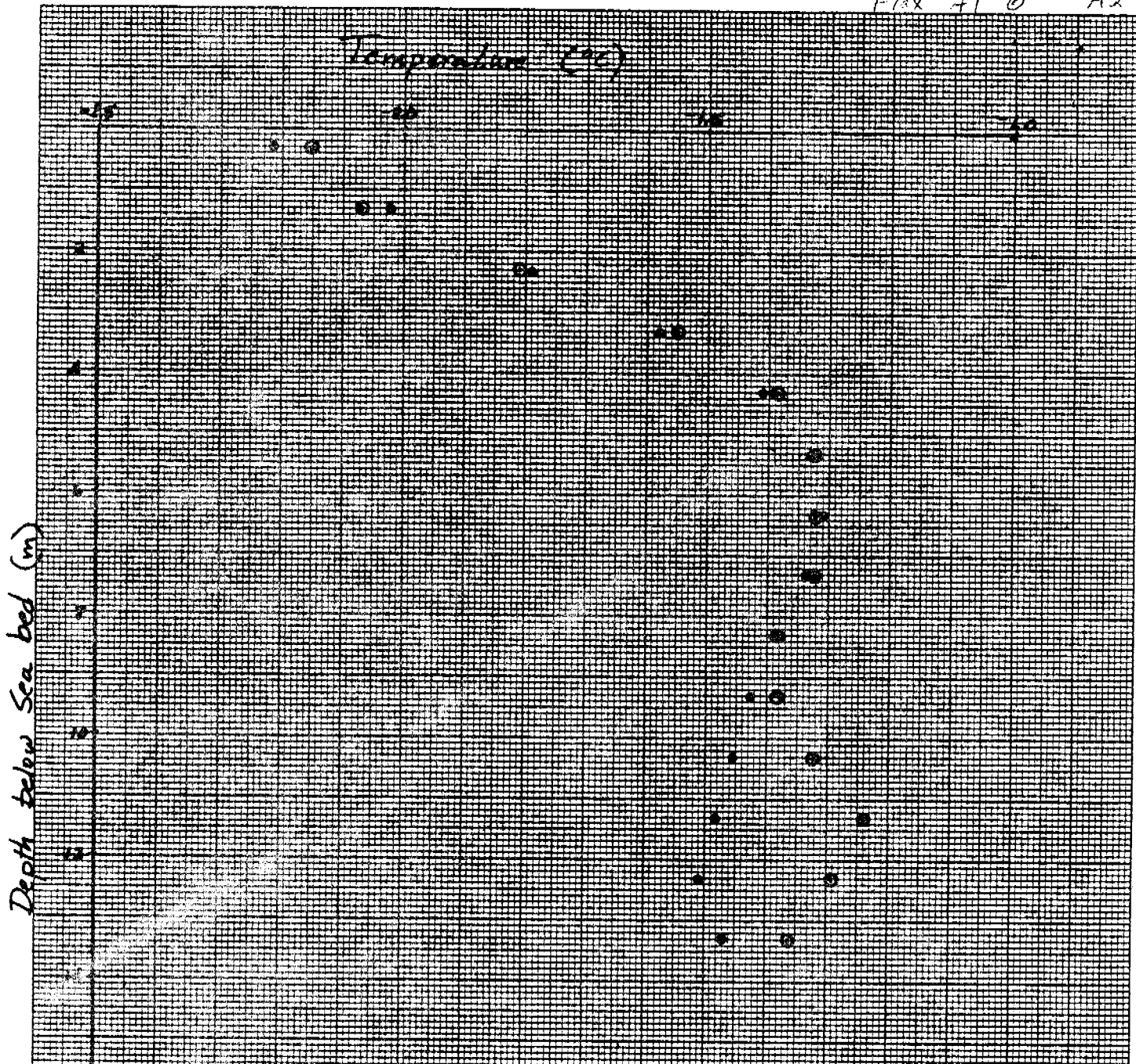


Figure 3. Lithology of Flaxman Island holes A, B and C, and D as determined by rotary-jet drilling.



Temperature Profiles  
 Flaxman Island  
 Hole - FLAX A  
 o May 13, 1959 12:15  
 . May 26, 1959 12:00

Figure 4. Measured temperature profiles for Flaxman Island hole A (FLAXA).

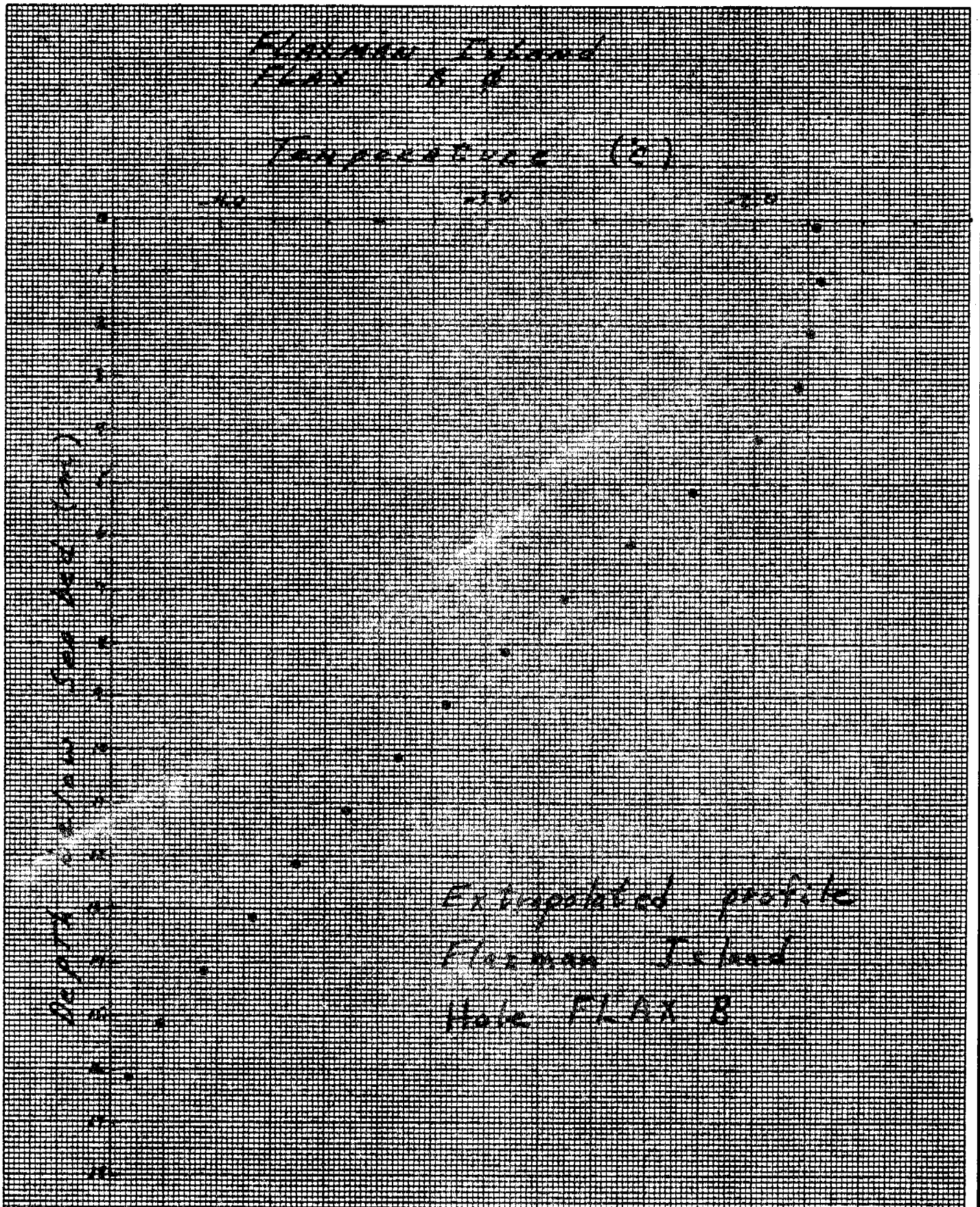


Figure 5. Extrapolated temperature profile for Flaxman Island hole B (FLAXB).

FLAXMAN ISLAND  
79-2

790520 16:39:00 HOLE FLAXB  
CABLE LAN NEW BRIDGE

TEMPERATURE (°C)

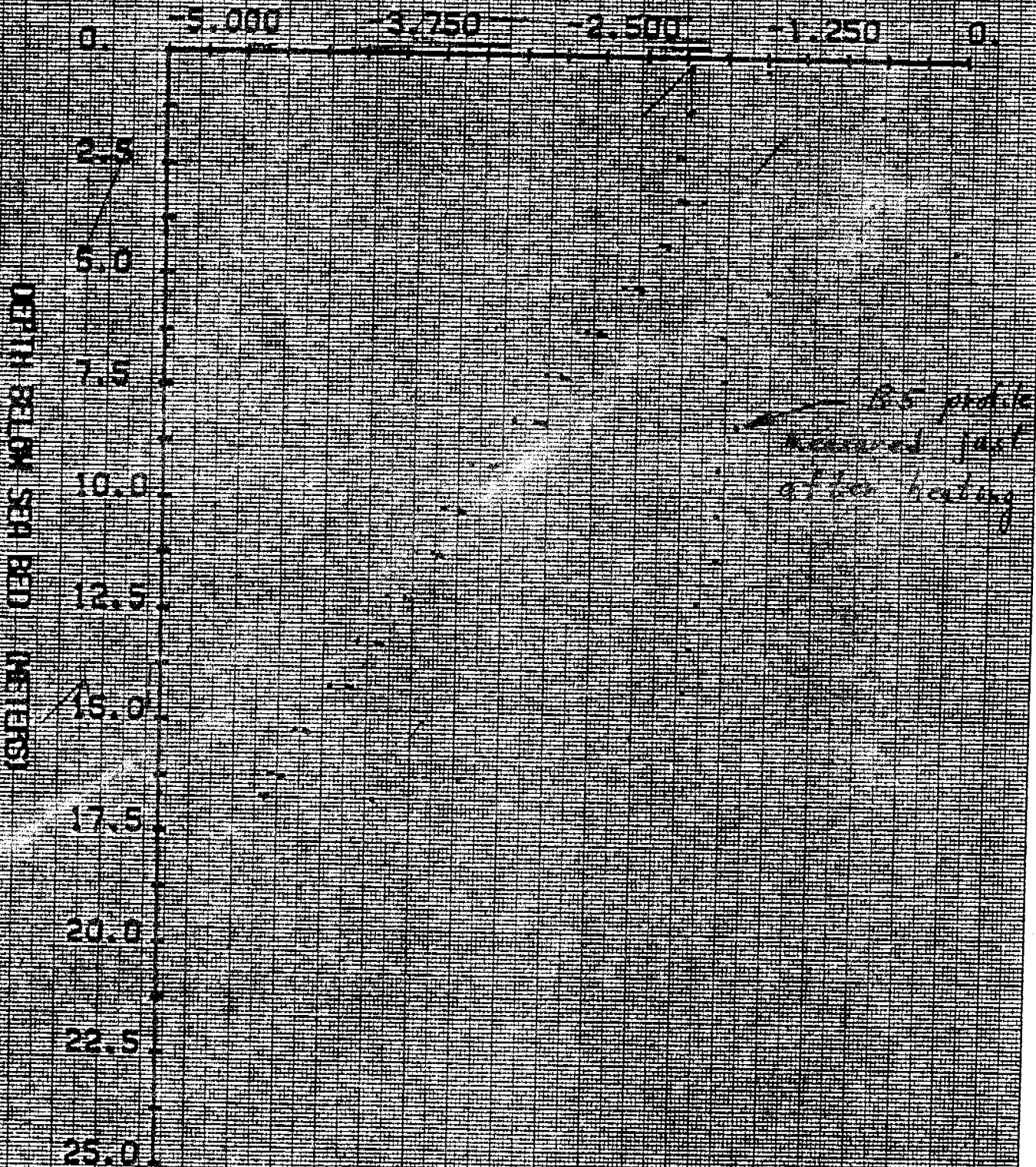


Figure 6. Measured temperature profiles in Flaxman Island hole B (FLAXB) after the hole was heated for a period of 90 minutes.

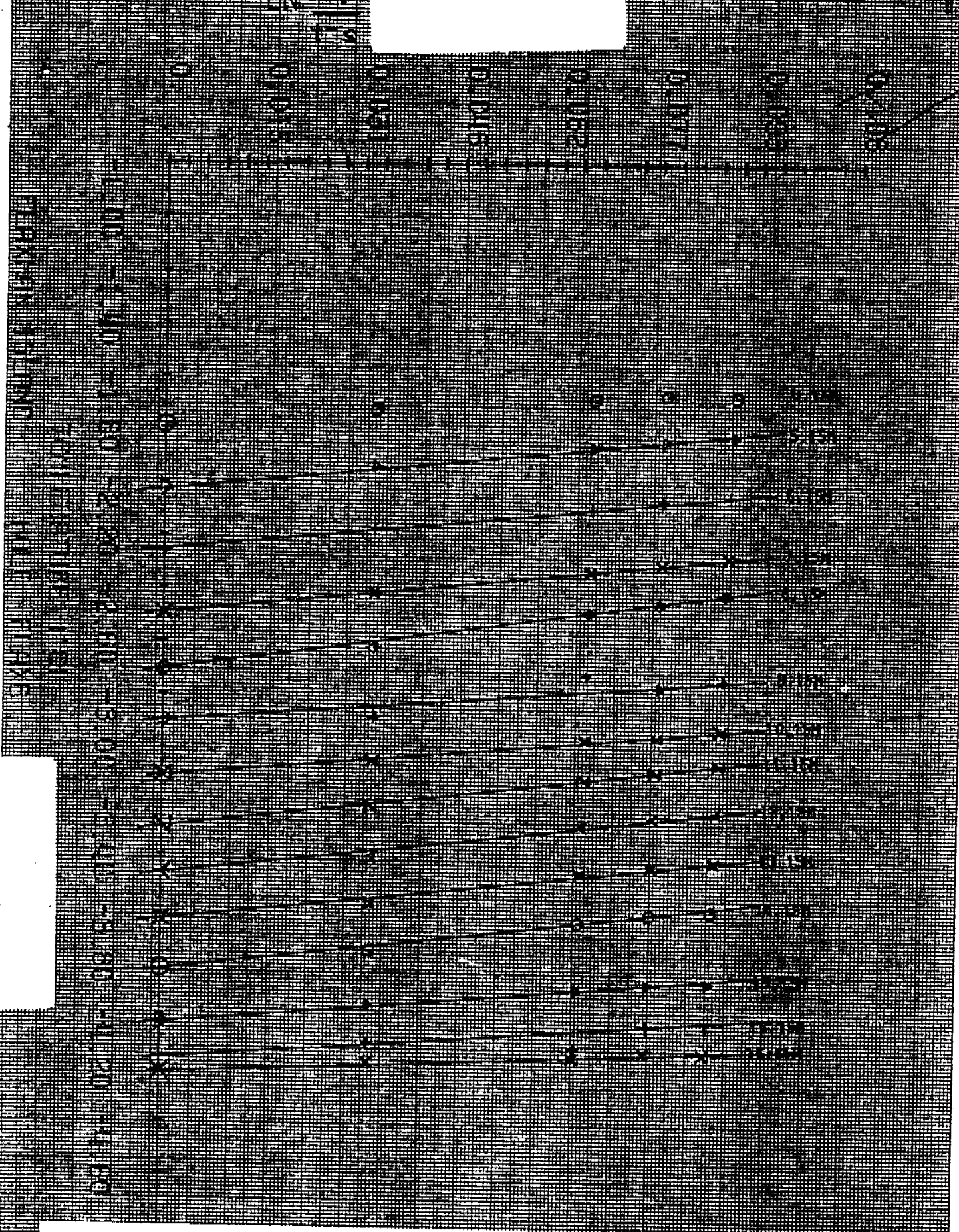


Figure 7. Graph of the  $\ln(t/t-s)$  vs. temperature (see Equation 1) for Flaxman Island hole B (FLAXB) which demonstrates the approach to equilibrium after heating the borehole for 90 minutes.

Flax C4

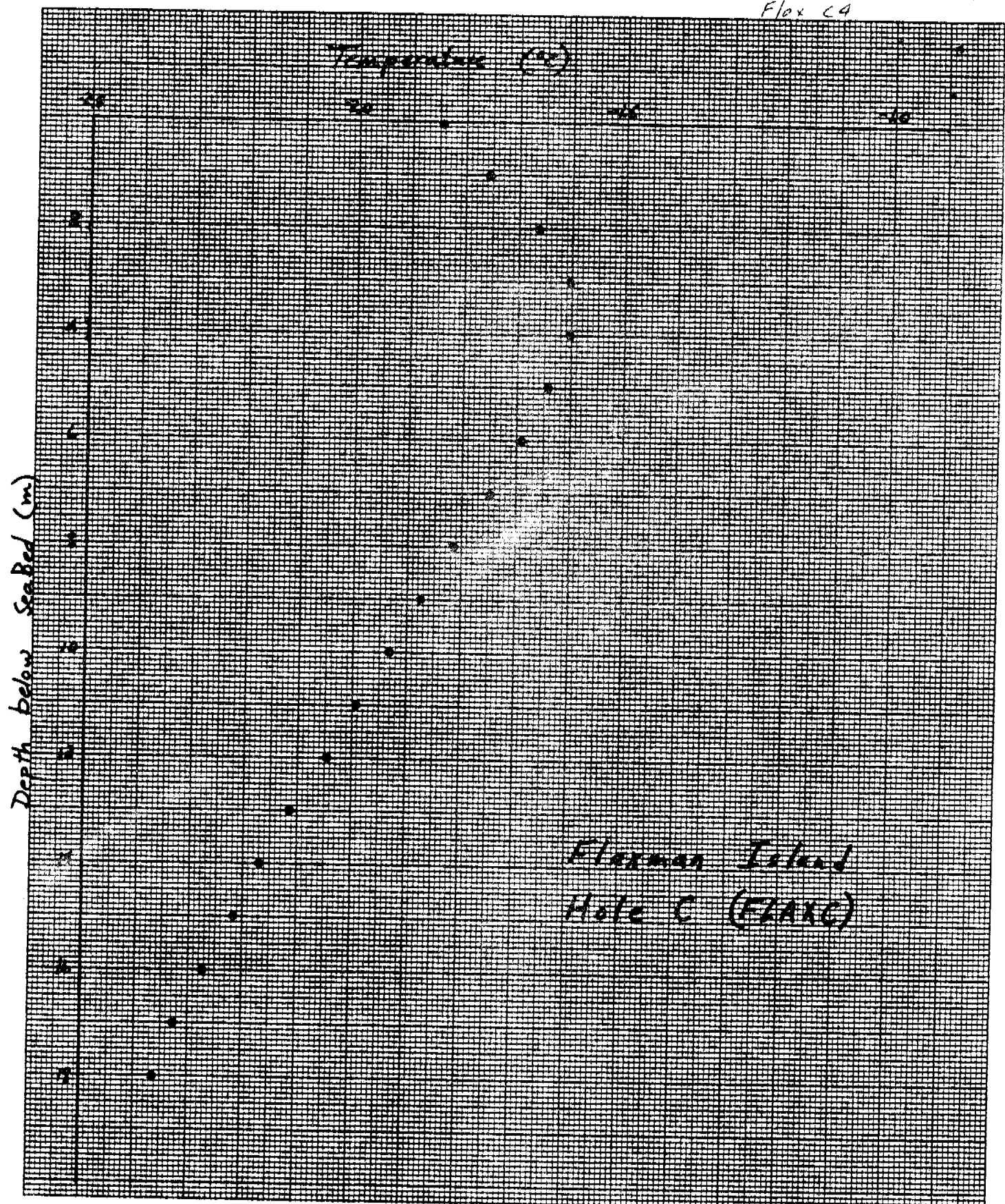


Figure 8. Measured temperature profile in Flaxman Island hole C (FLAXC) on May 29, 1979, 17 days after drilling.

Drill Hole Logs

Jeanette Island Line

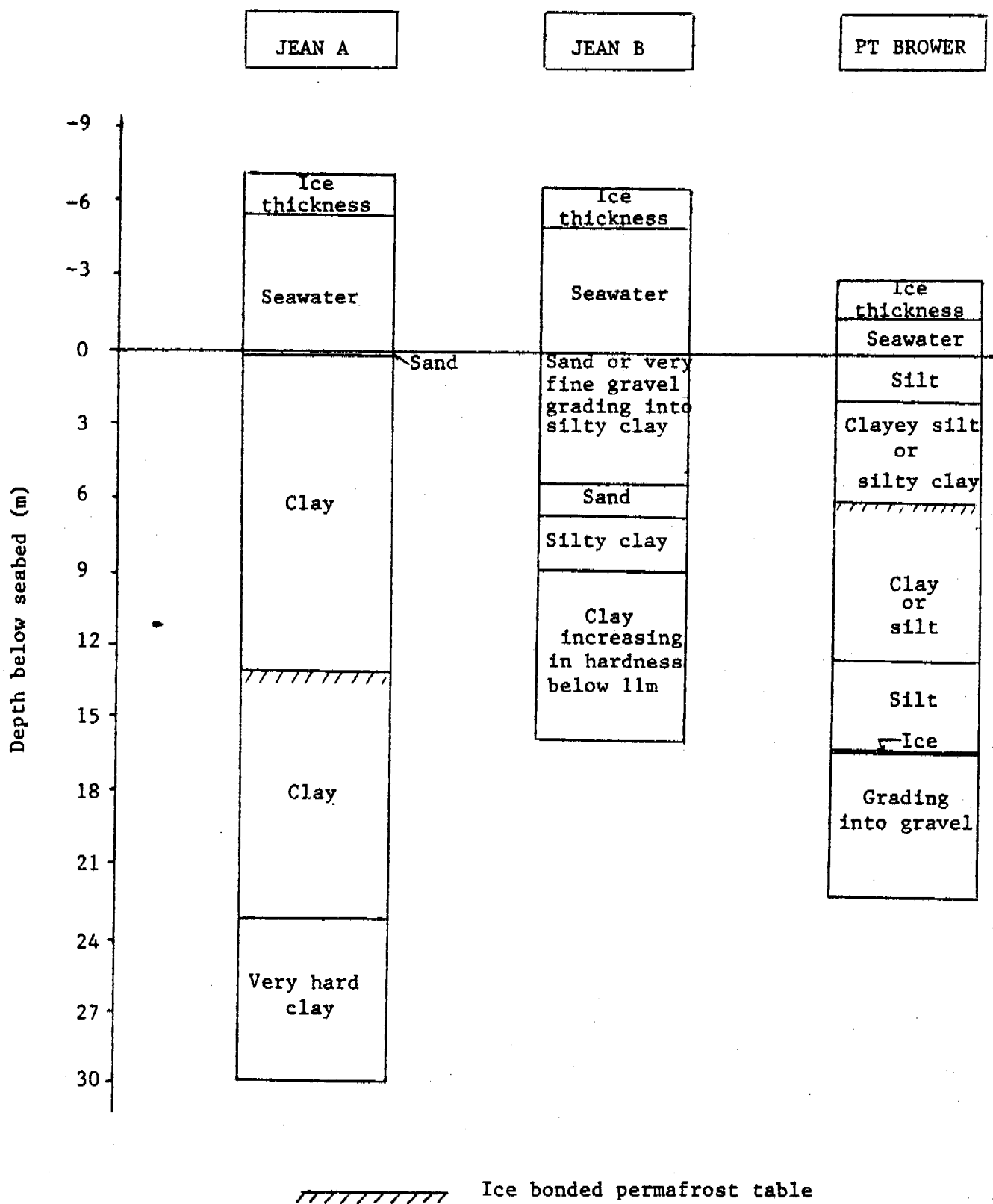


Figure 9. Lithology of the Jeanette Island holes A, B and C as determined by rotary-jet drilling.

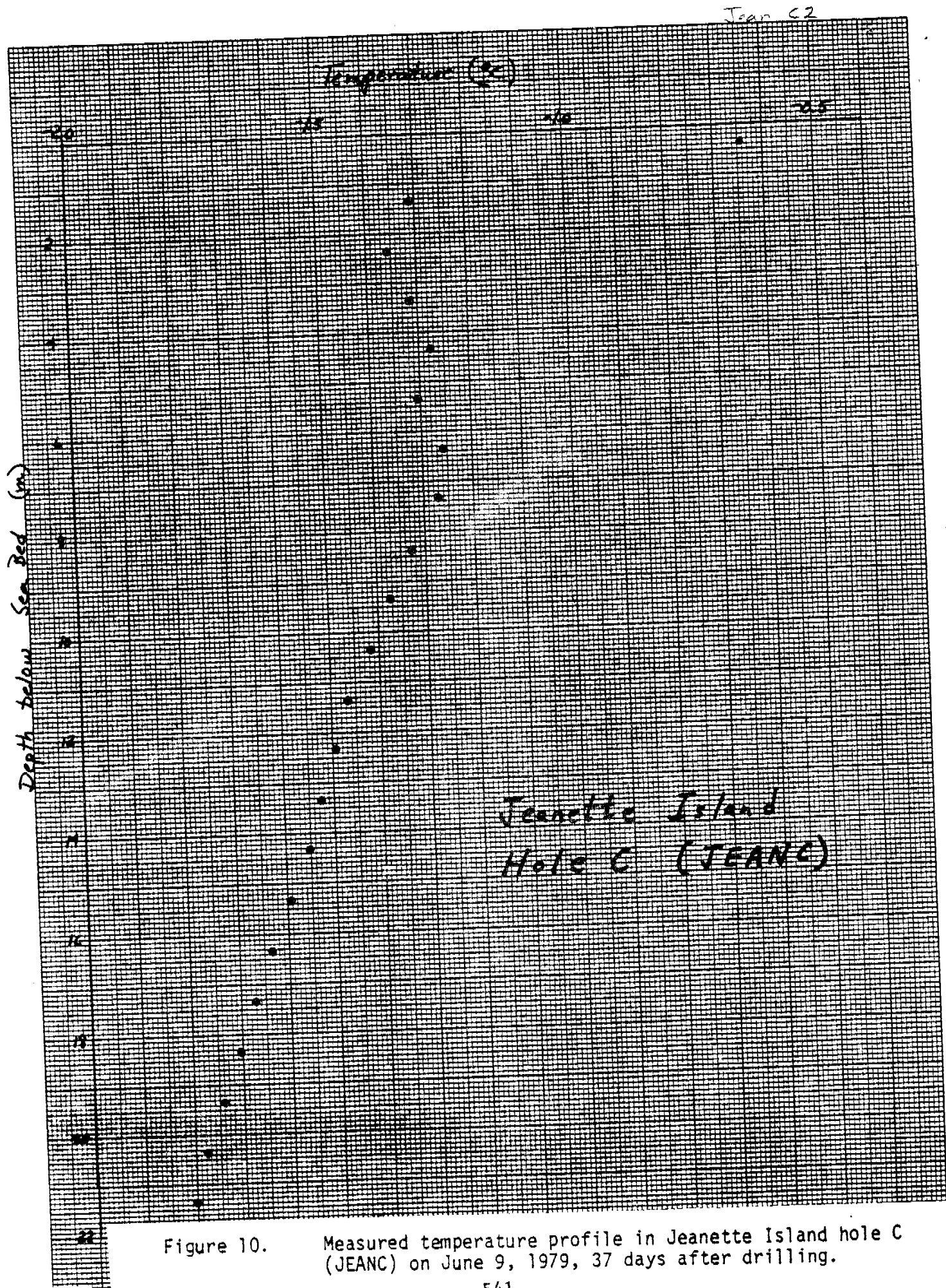


Figure 10. Measured temperature profile in Jeanette Island hole C (JEANC) on June 9, 1979, 37 days after drilling.



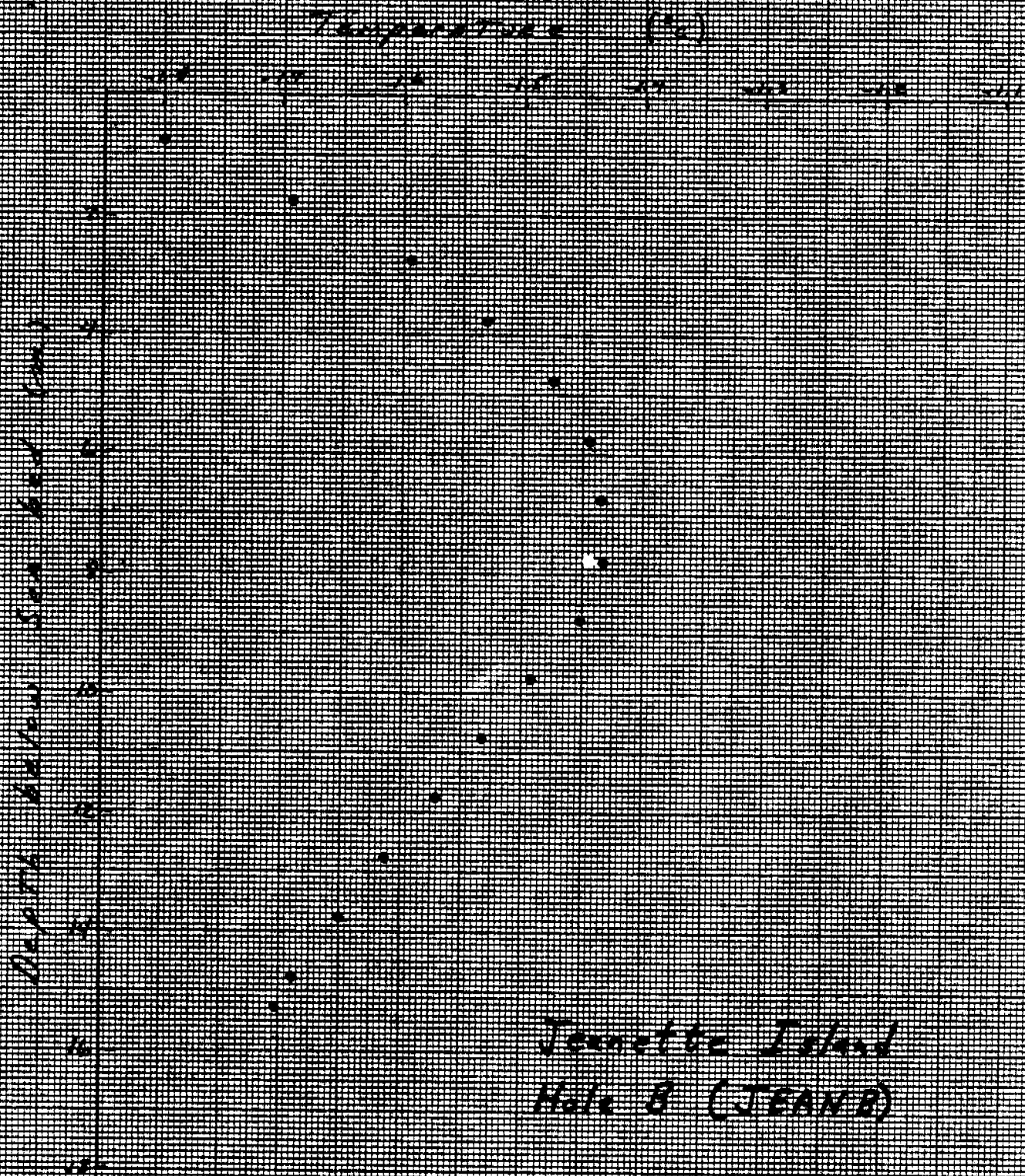


Figure 11. Extrapolated temperature profile for Jeanette Island hole B (JEANB).

46 1513

NEOPHEL & ESSER CO. MADE IN U.S.A.

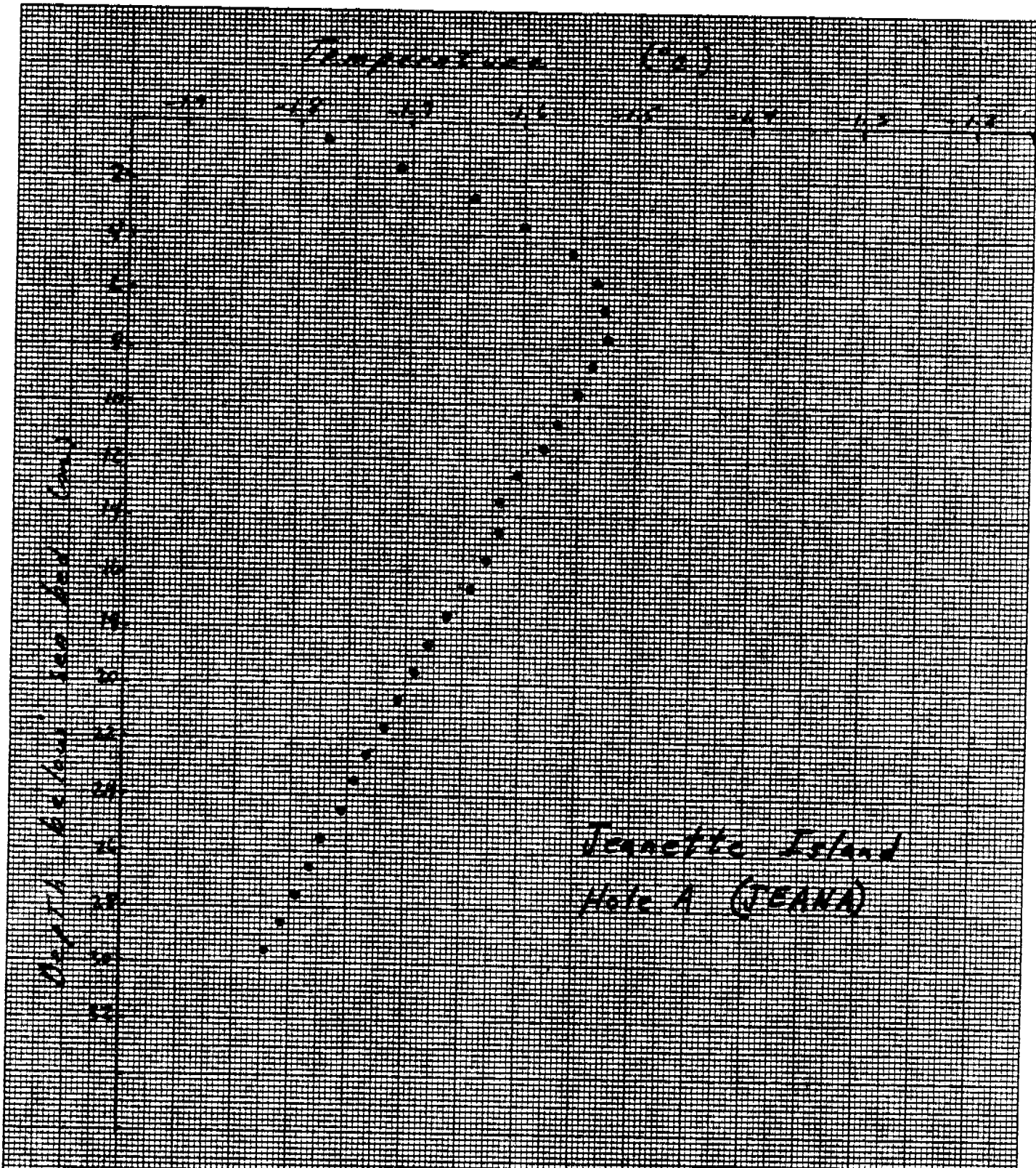


Figure 12. Extrapolated temperature profile for Jeanette Island hole A (JEANA).

Drill Hole Logs  
Long Island Line

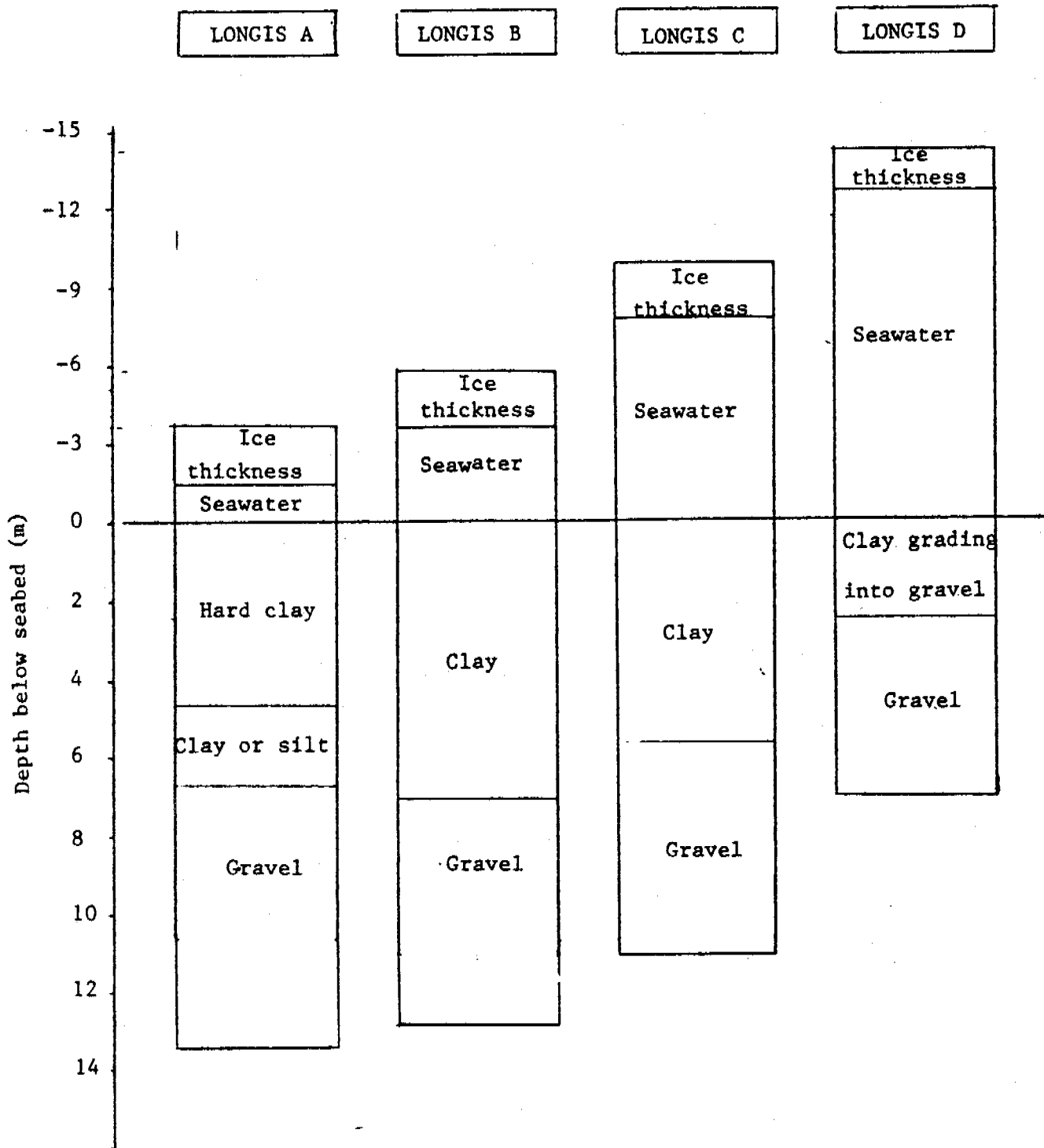


Figure 13. Lithology of Long Island holes A, B, C and D as determined by rotary-jet drilling.

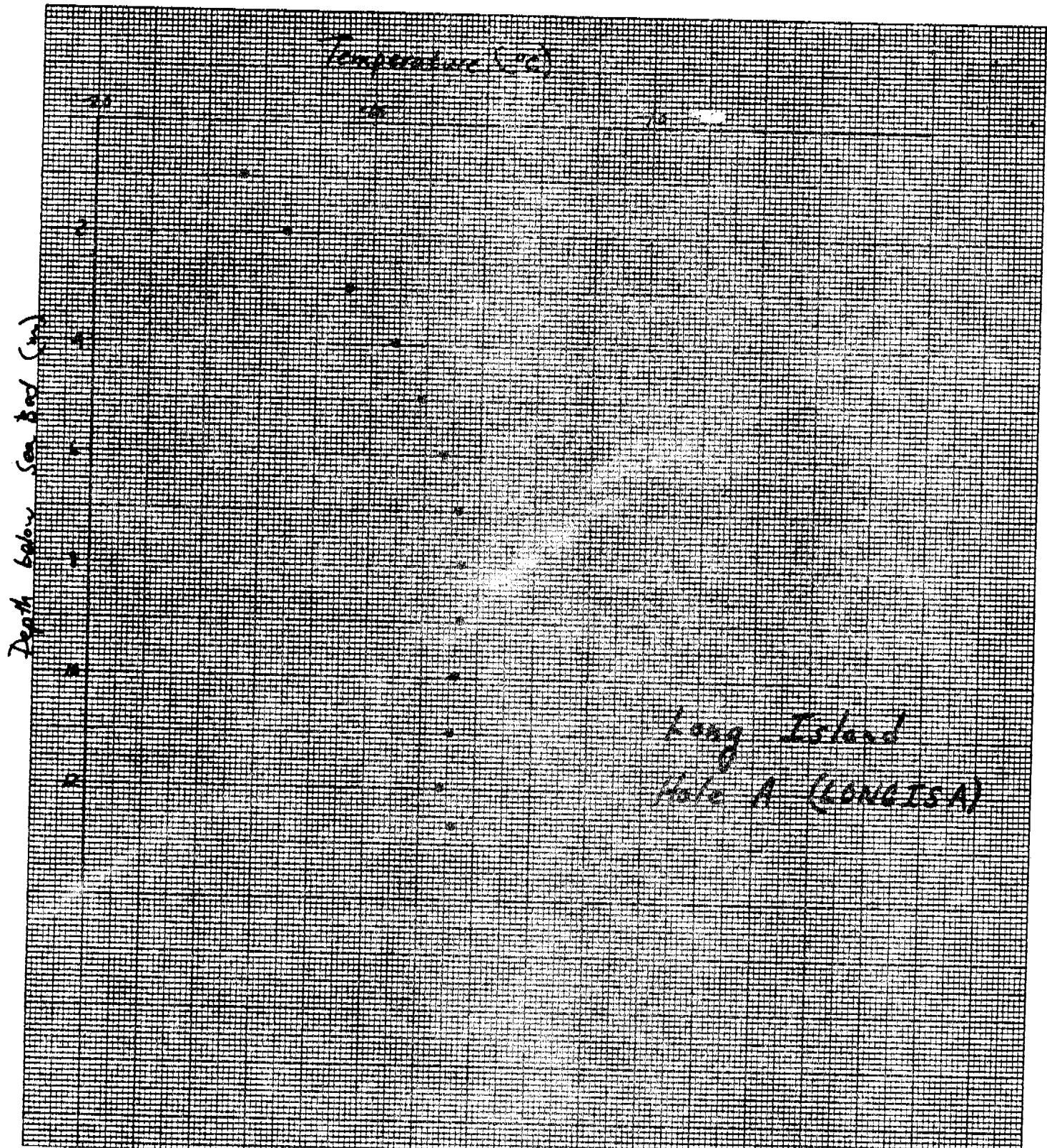


Figure 14. Measured temperature profile in Long Island hole A (LONGISA) on May 30, 1979, 13 days after drilling.

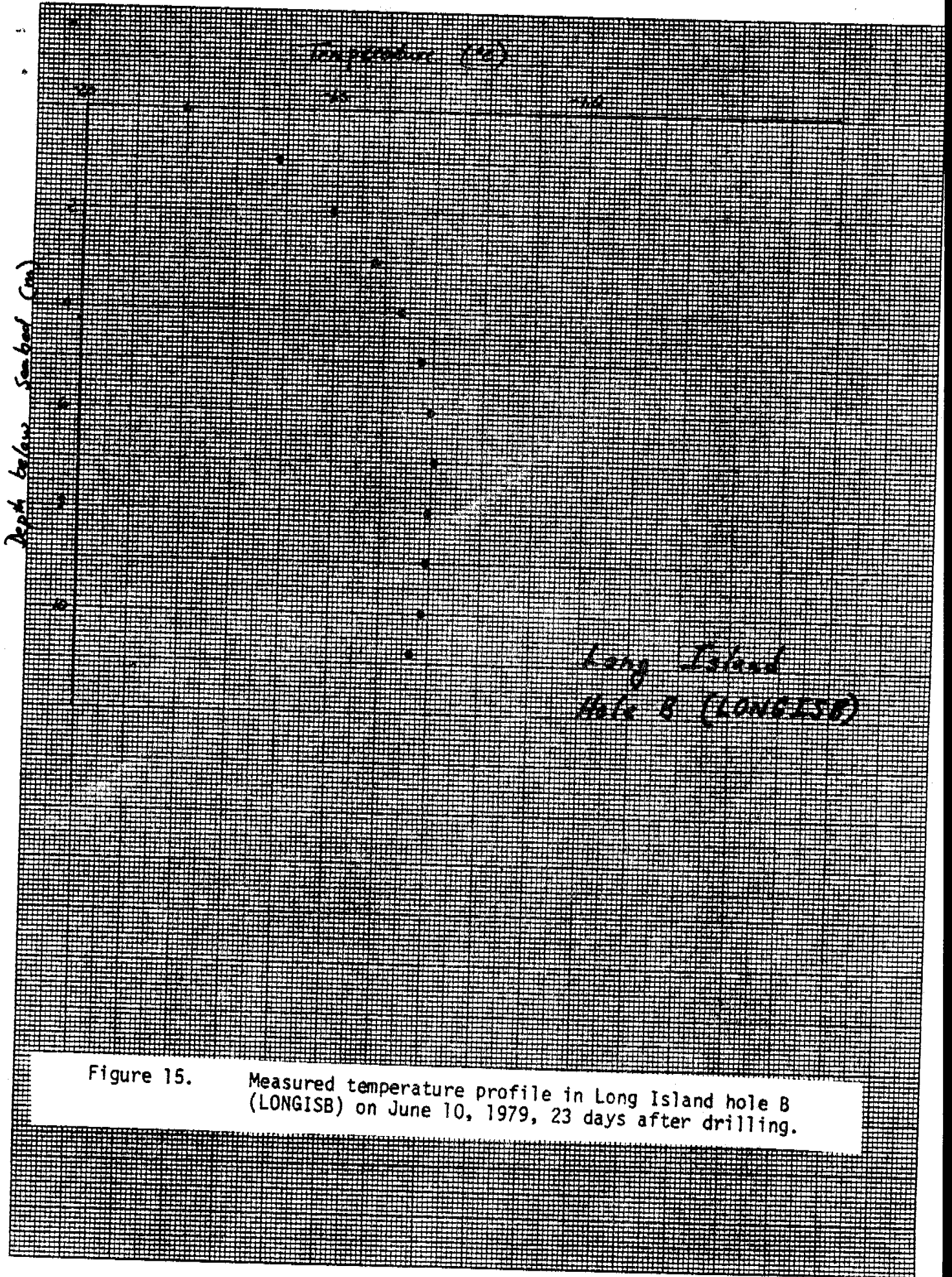
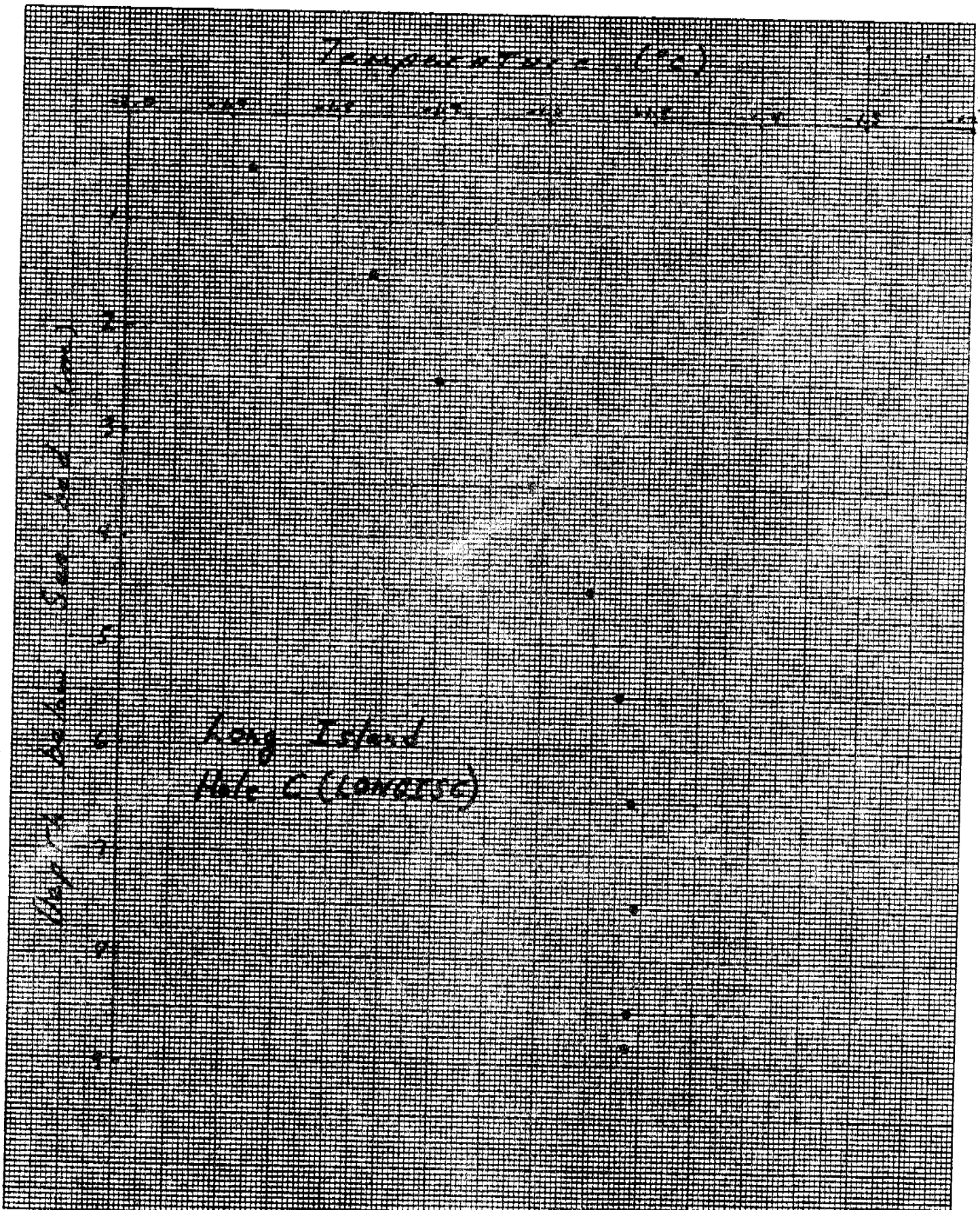


Figure 15. Measured temperature profile in Long Island hole B (LONGISB) on June 10, 1979, 23 days after drilling.

46 1513

NEOPHEL & ESSER CO. MADE IN U.S.A.



Long Island  
Hole C (LONGISC)

Figure 16. Extrapolated temperature profile for Long Island hole C (LONGISC).

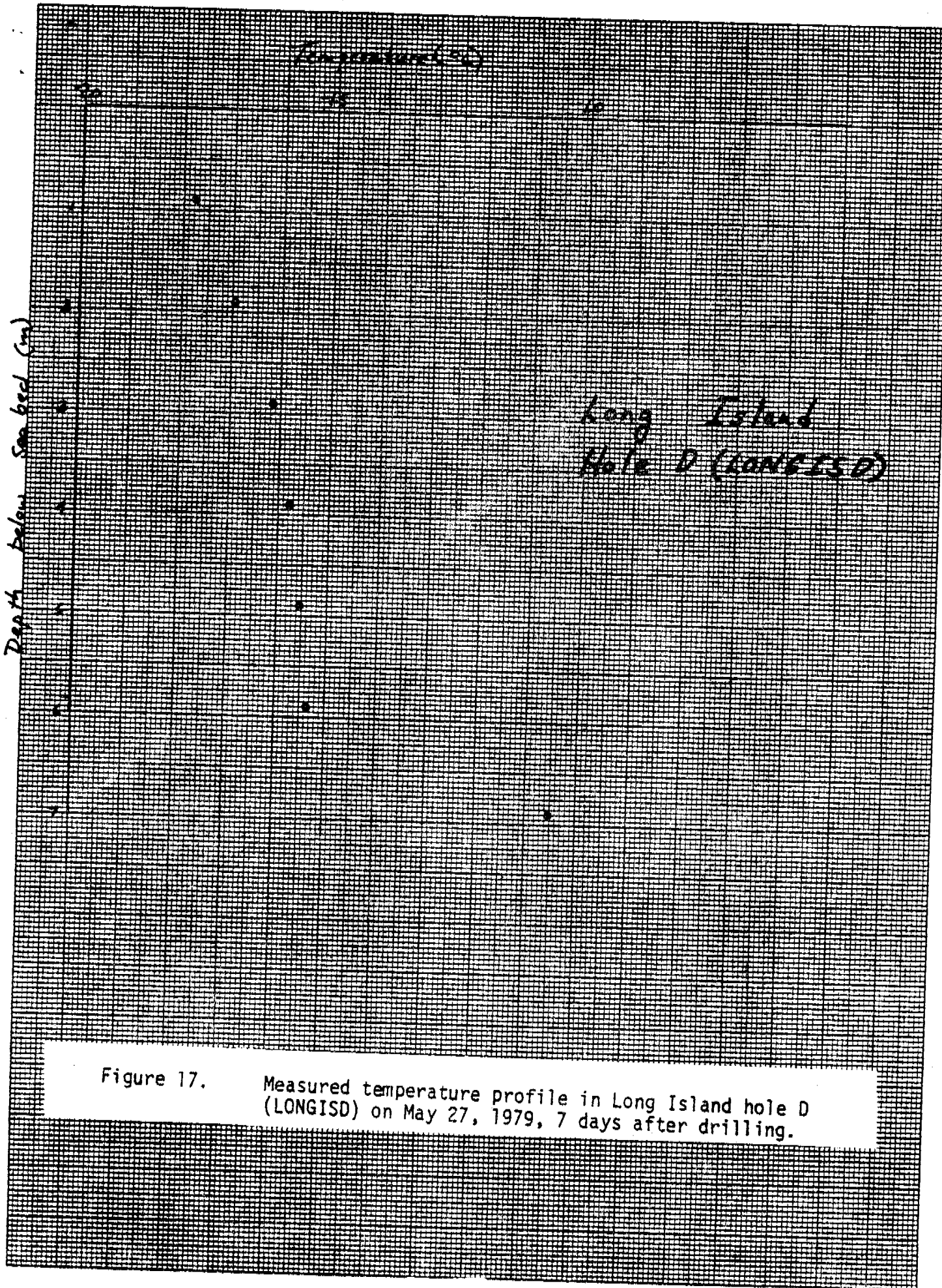
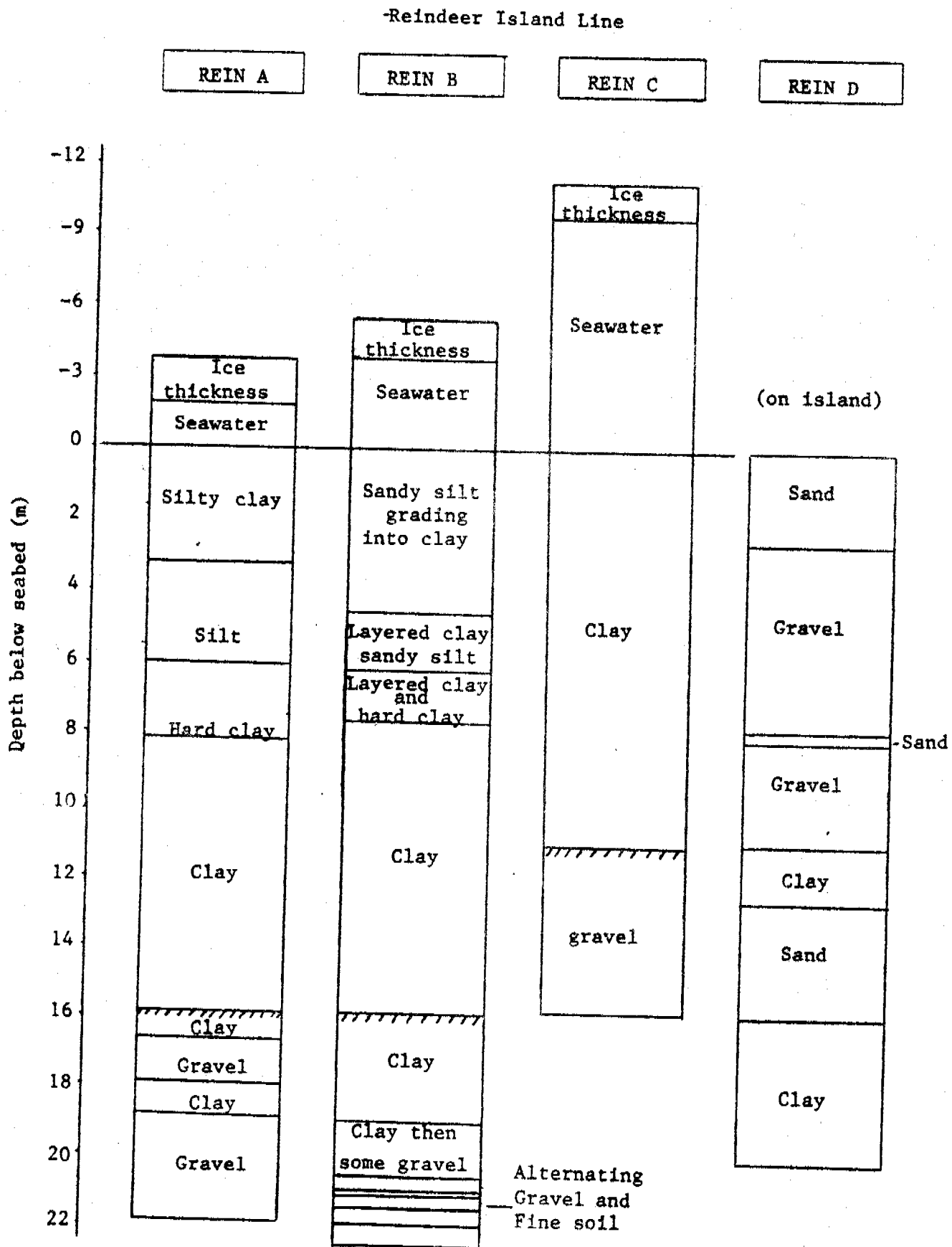


Figure 17. Measured temperature profile in Long Island hole D (LONGISD) on May 27, 1979, 7 days after drilling.

Figure 18. Lithology of the Reindeer Island holes A, B, C and D as determined by rotary-jet drilling.  
- Drill Hole Logs



Ice bonded permafrost table



46 1513

K&E 10 X 10 TO THE CENTIMETER KEUFFEL & ESSER CO. MADE IN U.S.A.

550

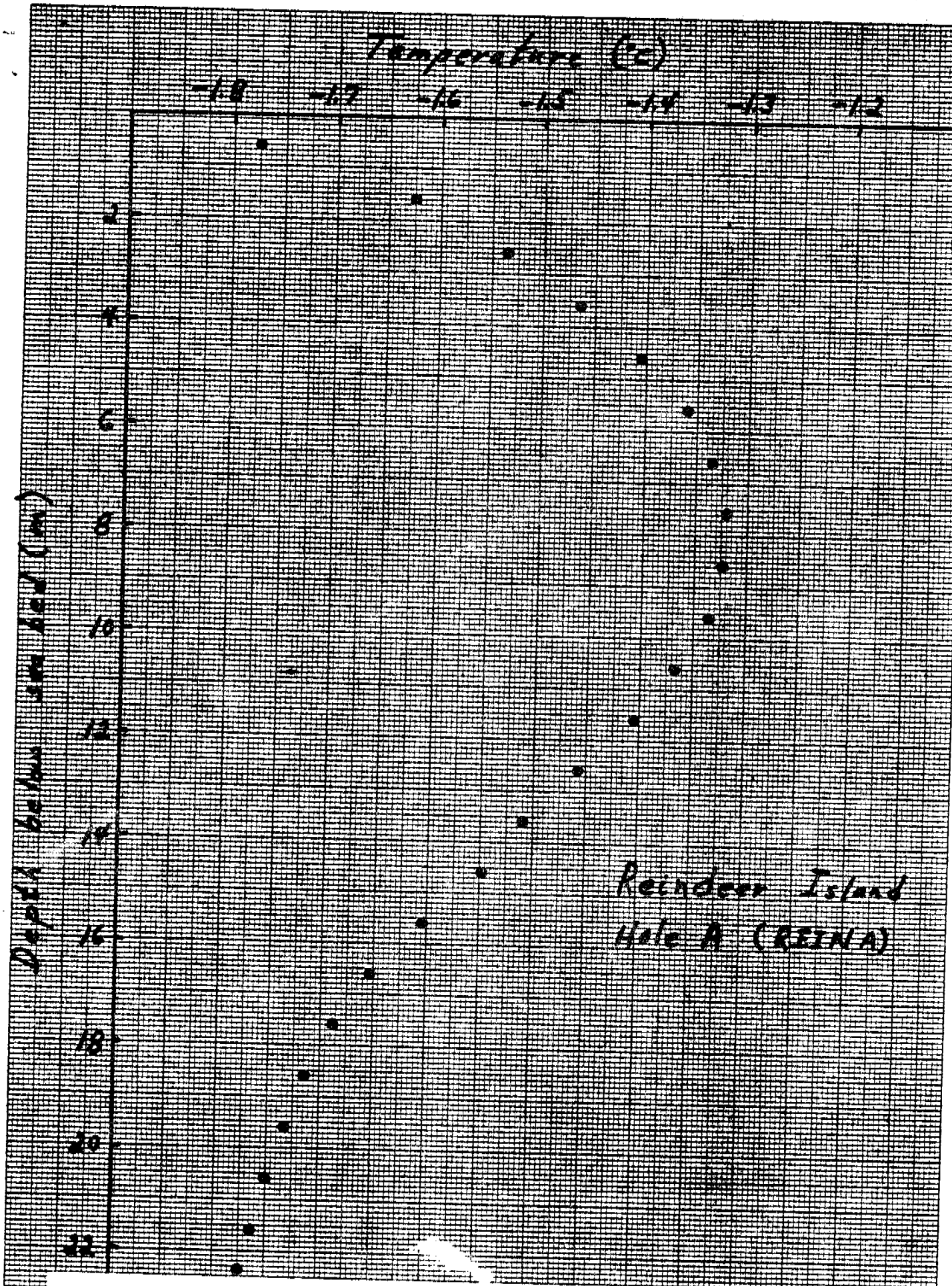


Figure 19. Measured temperature profile in Reindeer Island hole A (REINA) on May 24, 1979, 19 days after drilling.

REINDEER ISLAND

790527

09.08

HOLE BEINGS

BELFEN

CABLE

OLD TAN

BRIDGE

TEMPERATURE (°C)

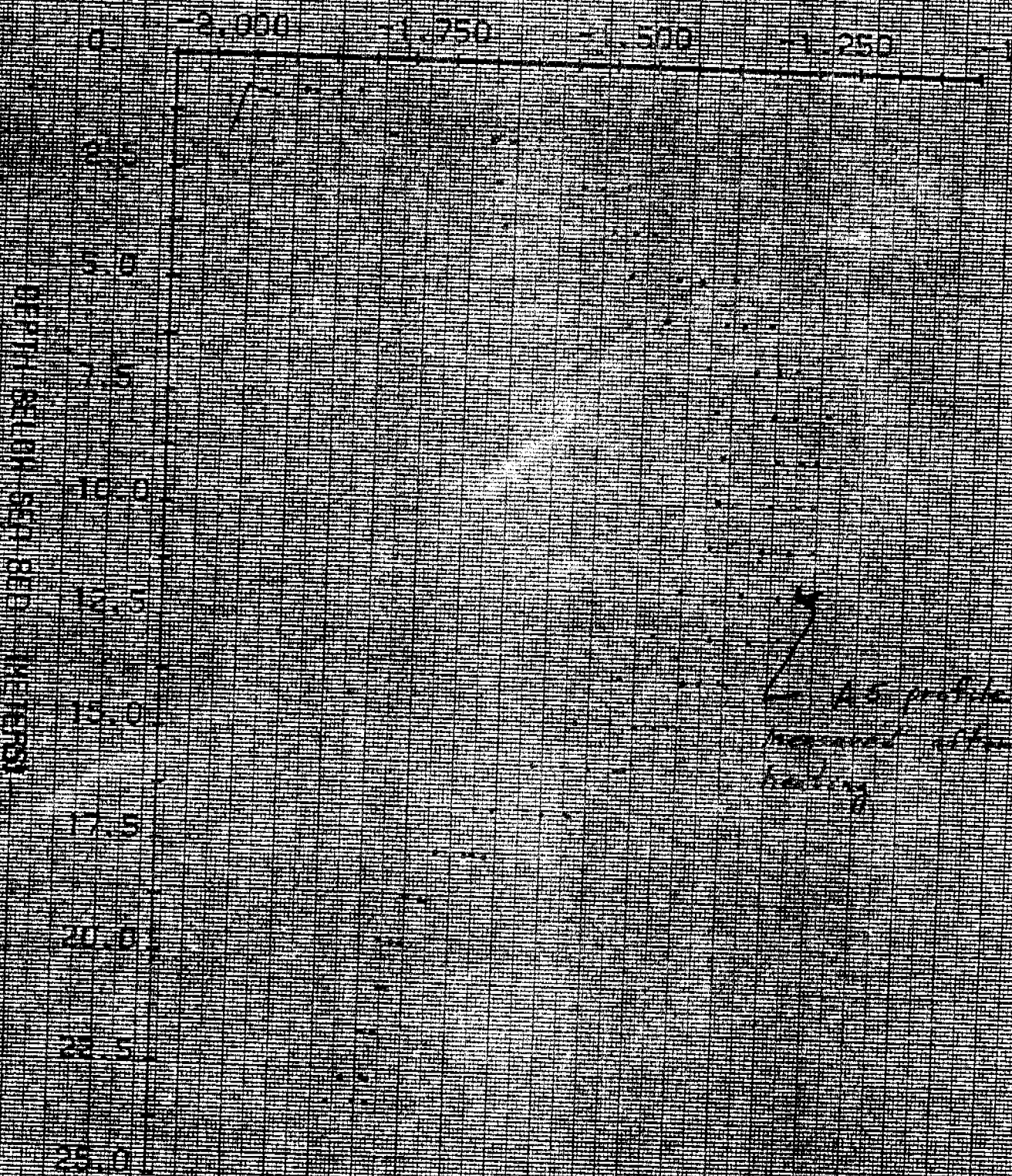


Figure 20. Measured temperature profiles in Reindeer Island hole A (REINA) after the hole was heated for a period of 76 minutes.

REIN

Temperature (°C)

1.8 1.6 1.4 1.2 1.0 0.8 0.6 0.4

Depth below sea level (m)

20 15 10 5 0 5 10 15 20 25 30 35 40 45 50 55 60 65 70 75 80 85 90 95 100

Reindeer Island  
Hole B (REINB)

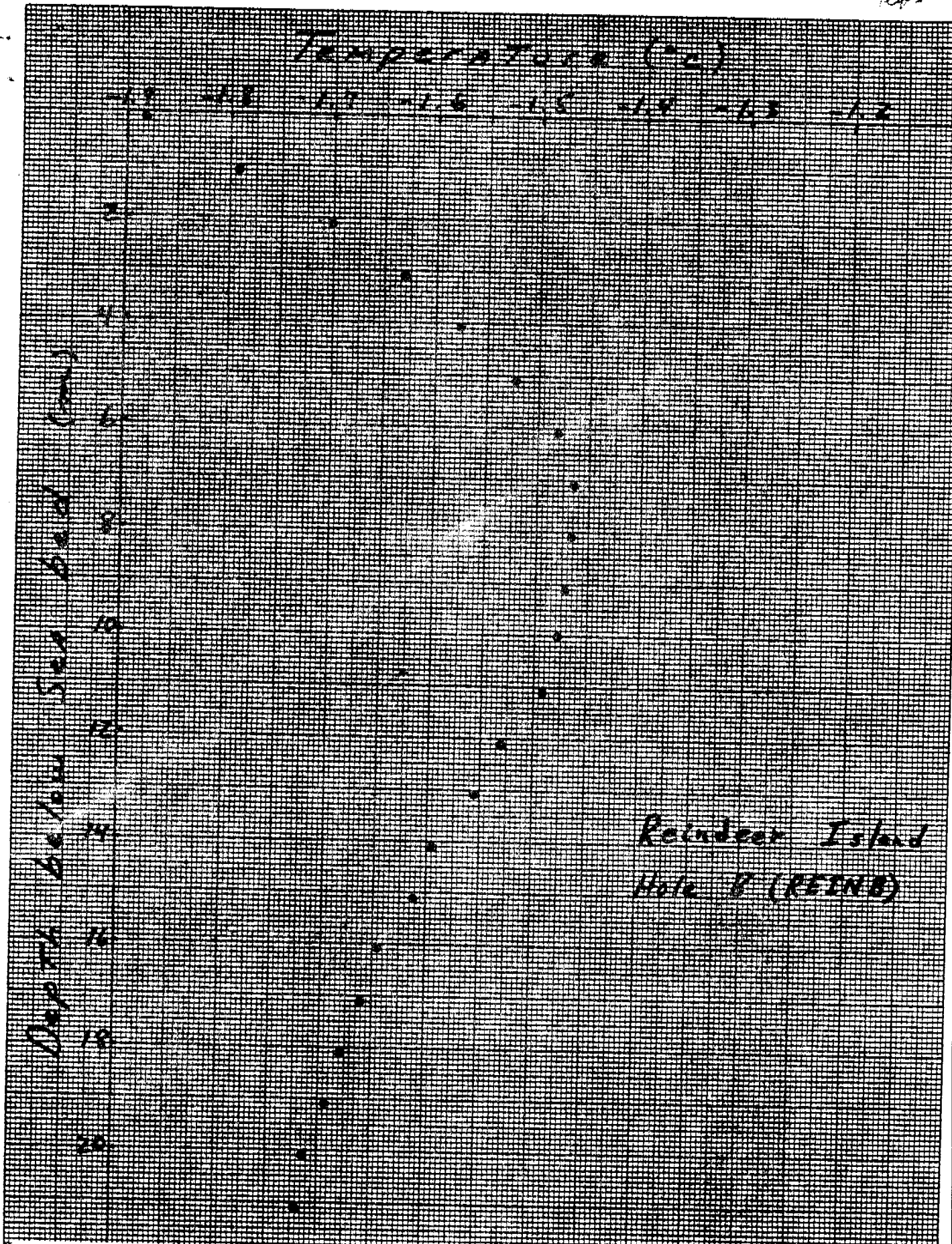


Figure 22. Extrapolated temperature profile for Reindeer Island hole B (REINB).

46 1513

K&E 10 X 10 TO THE CENTIMETER 18 X 25 CM. KEUFFEL & ESSER CO. MADE IN U.S.A.

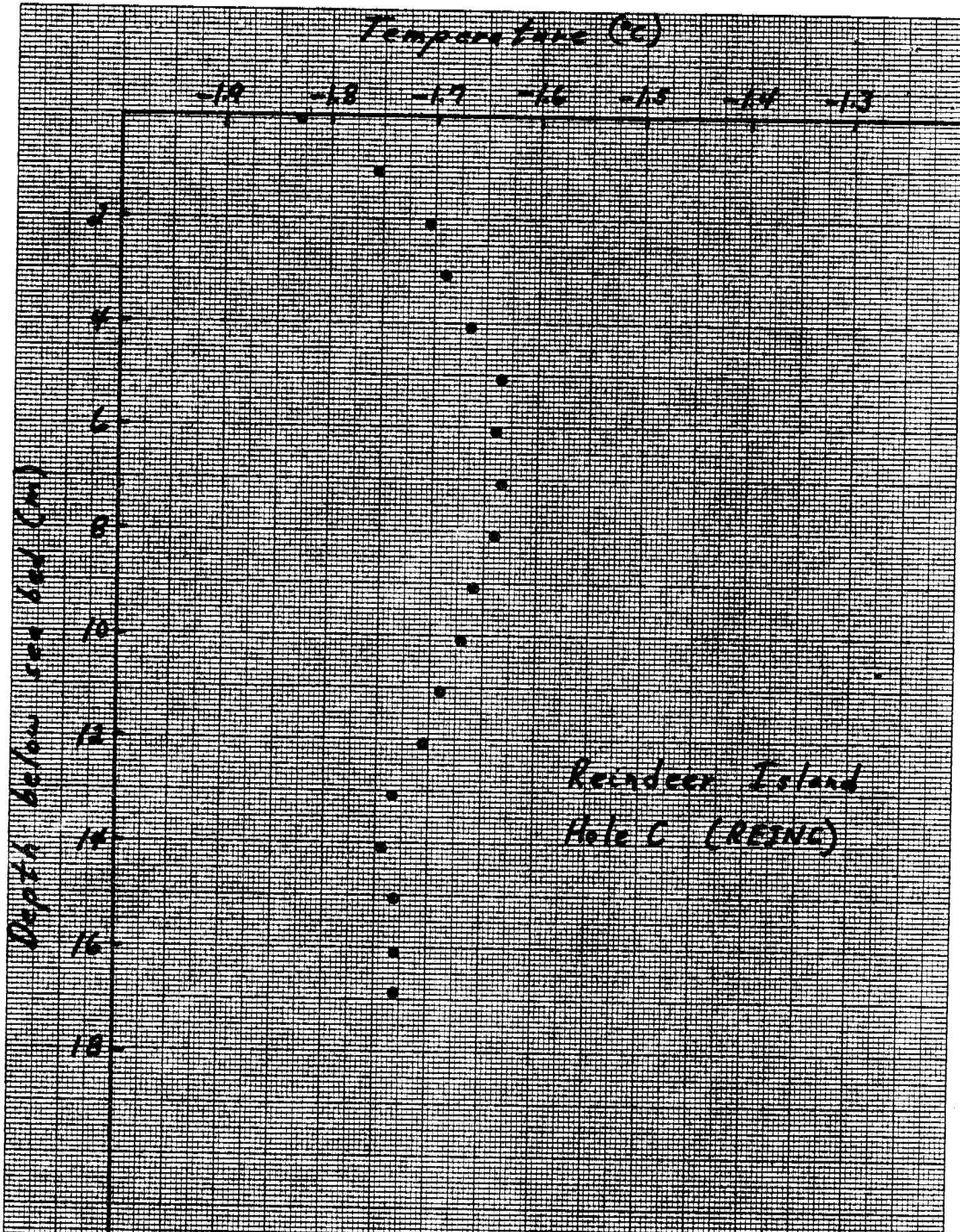


Figure 23. Measured temperature profile in Reindeer Island hole C (REINC) on May 29, 1979, 25 days after drilling.

REINDEER ISLAND 790530 10-00 HOLE REINCO  
 79-3 CABLE OLD LAN BRIDGE  
 TEMPERATURE (°C)

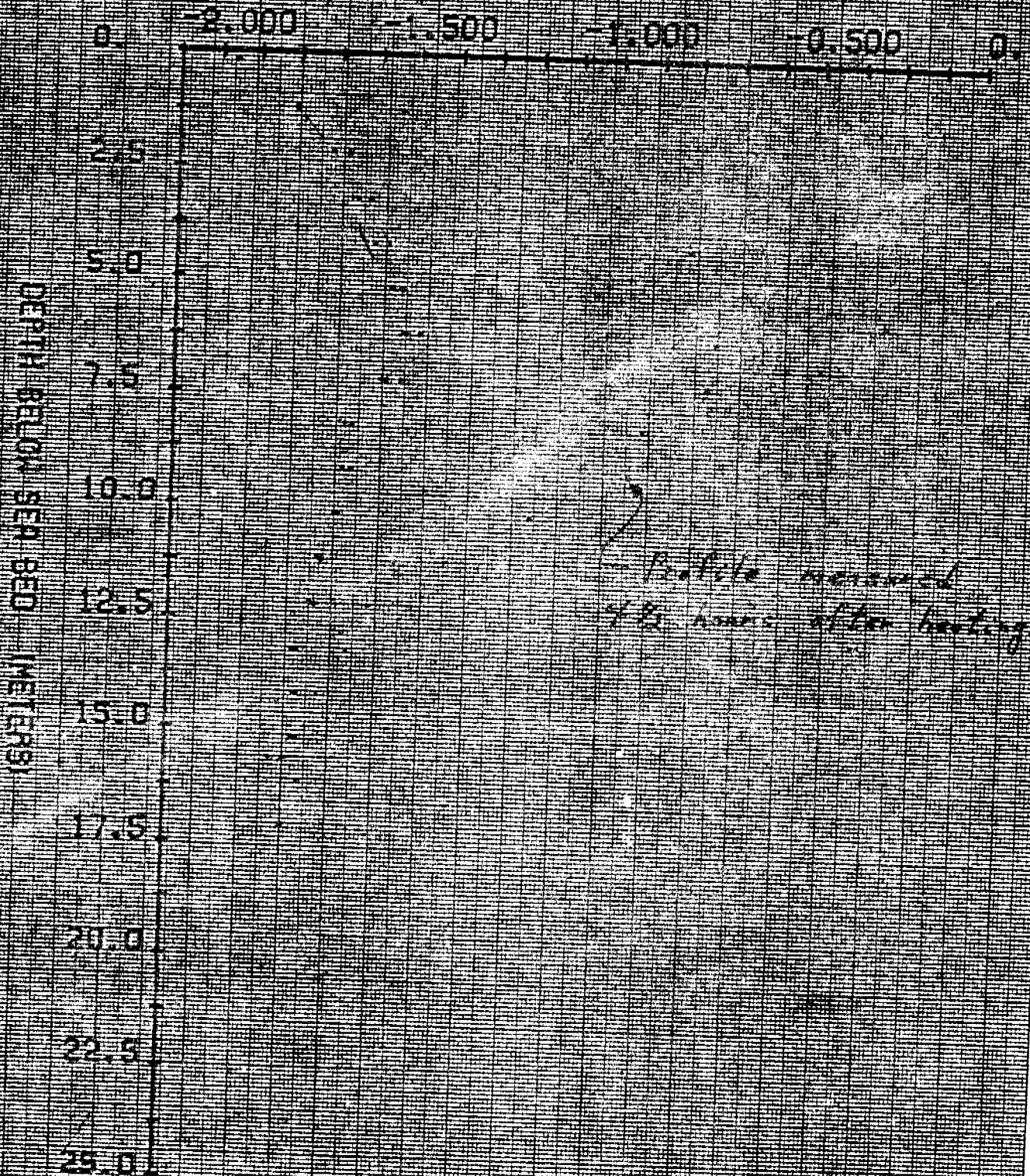


Figure 24. Measured temperature profiles in Reindeer Island hole C (REINC) after the hole was heated for a period of 120 minutes.

LN T  
LPS

Reindeer  
Hole C

Figure 25.

Graph of the  $\ln(t/t_0)$  vs. temperature (see Equation 1) for Reindeer Island hole C (REINC) which demonstrates the return to equilibrium for selected depths after heating the borehole for 120 minutes.

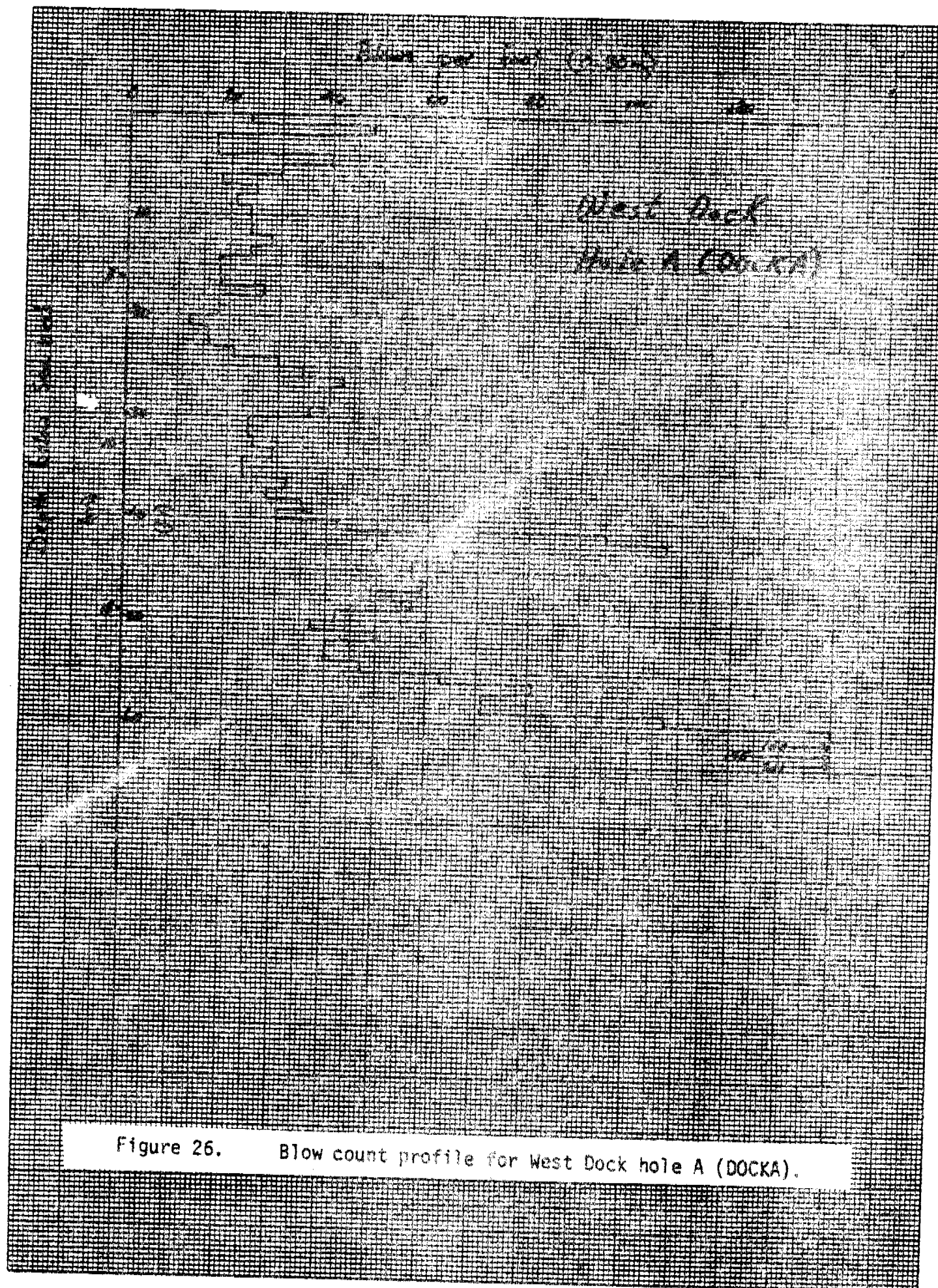


Figure 26. Blow count profile for West Dock hole A (DOCKA).

40 1010

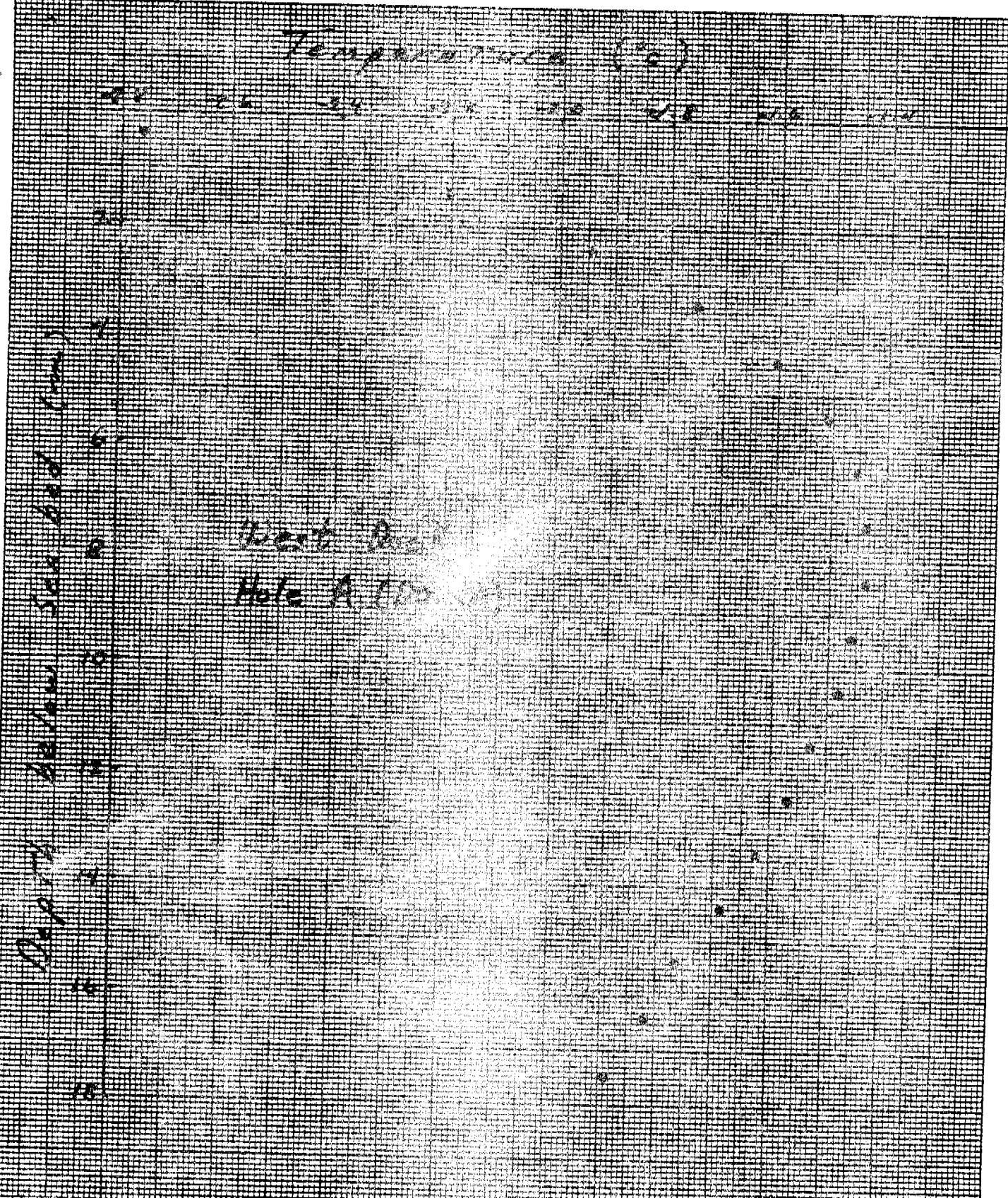
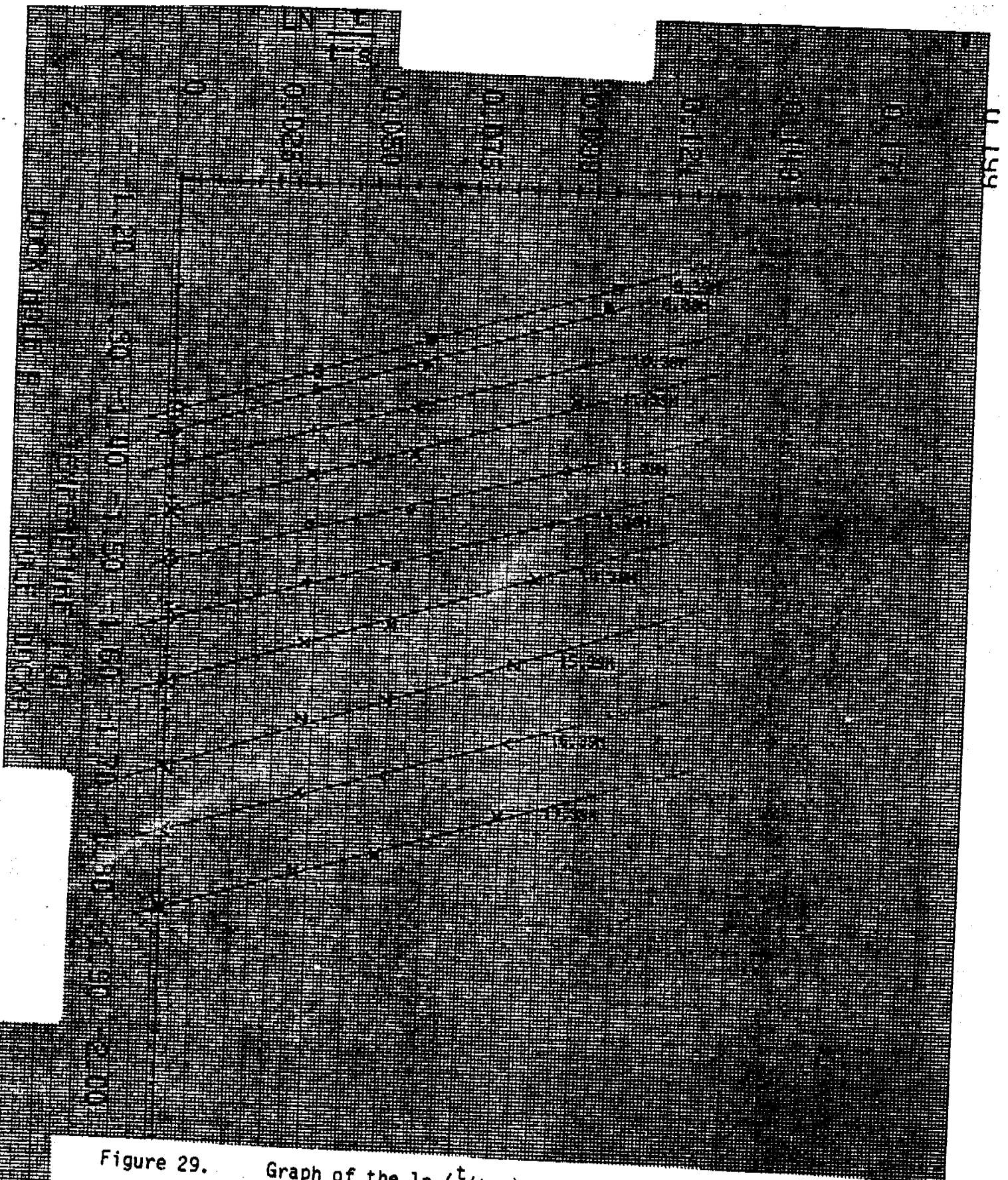


Figure 27. Extrapolated temperature profile for West Dock hole A (DOCKA).







U 159

Figure 29. Graph of the  $\ln (t/t-s)$  vs. temperature (see Equation 1) for West Dock hole A (DOCKA) which demonstrates the approach to equilibrium after heating the borehole for 15 minutes.

46 1513

10 X 30 TO THE CENTIMETER 18 X 25 CM.  
KUEFFEL & ESSER CO. MADE IN U.S.A.



Figure 30. Blow count profile for West Dock hole B (DOCKB).

-2.4 -2.2 -2.0 -1.8 -1.6 -1.4 -1.2

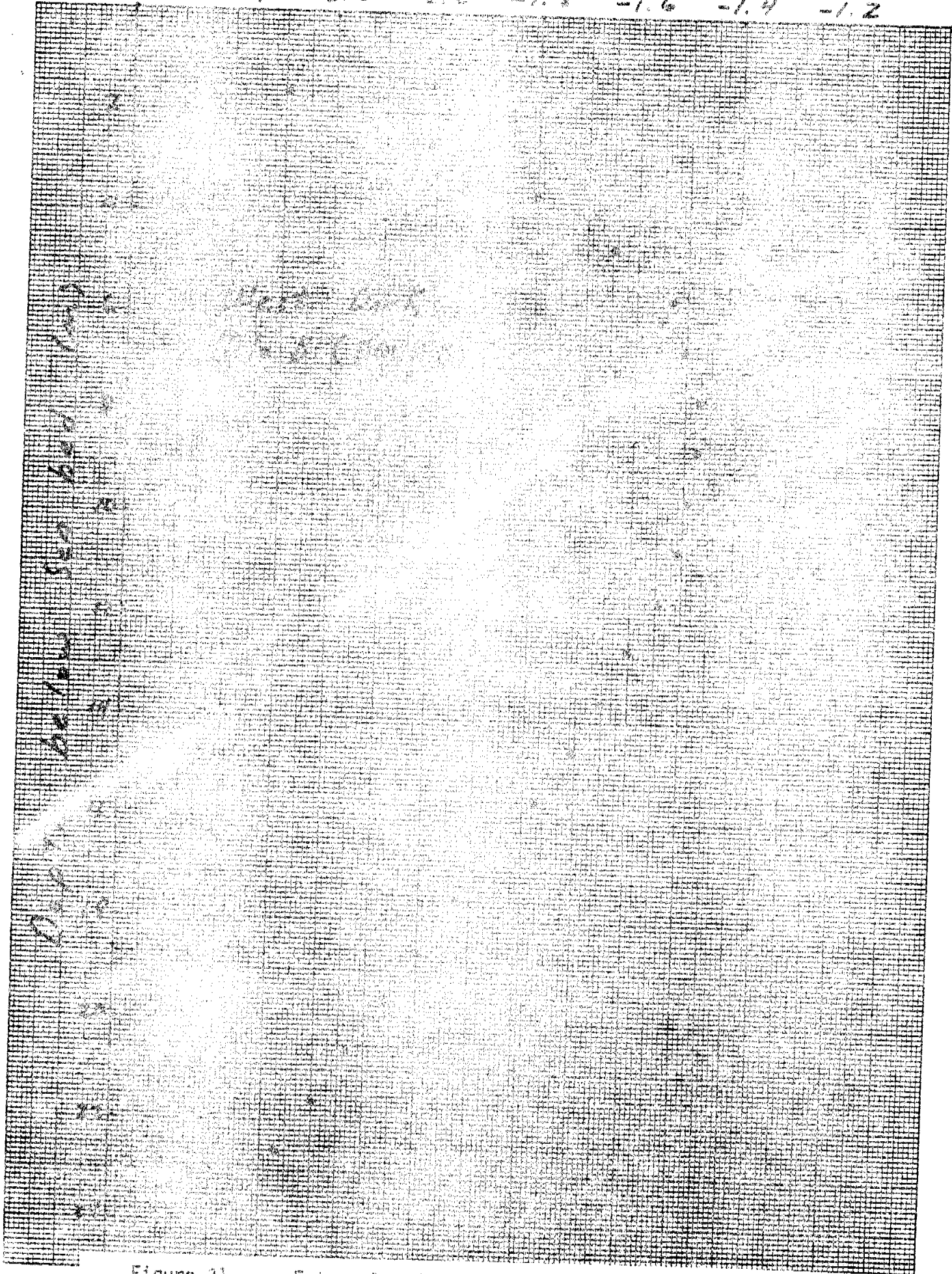


Figure 3). Extrapolated temperature profile for West Dock hole B (DOCKB).

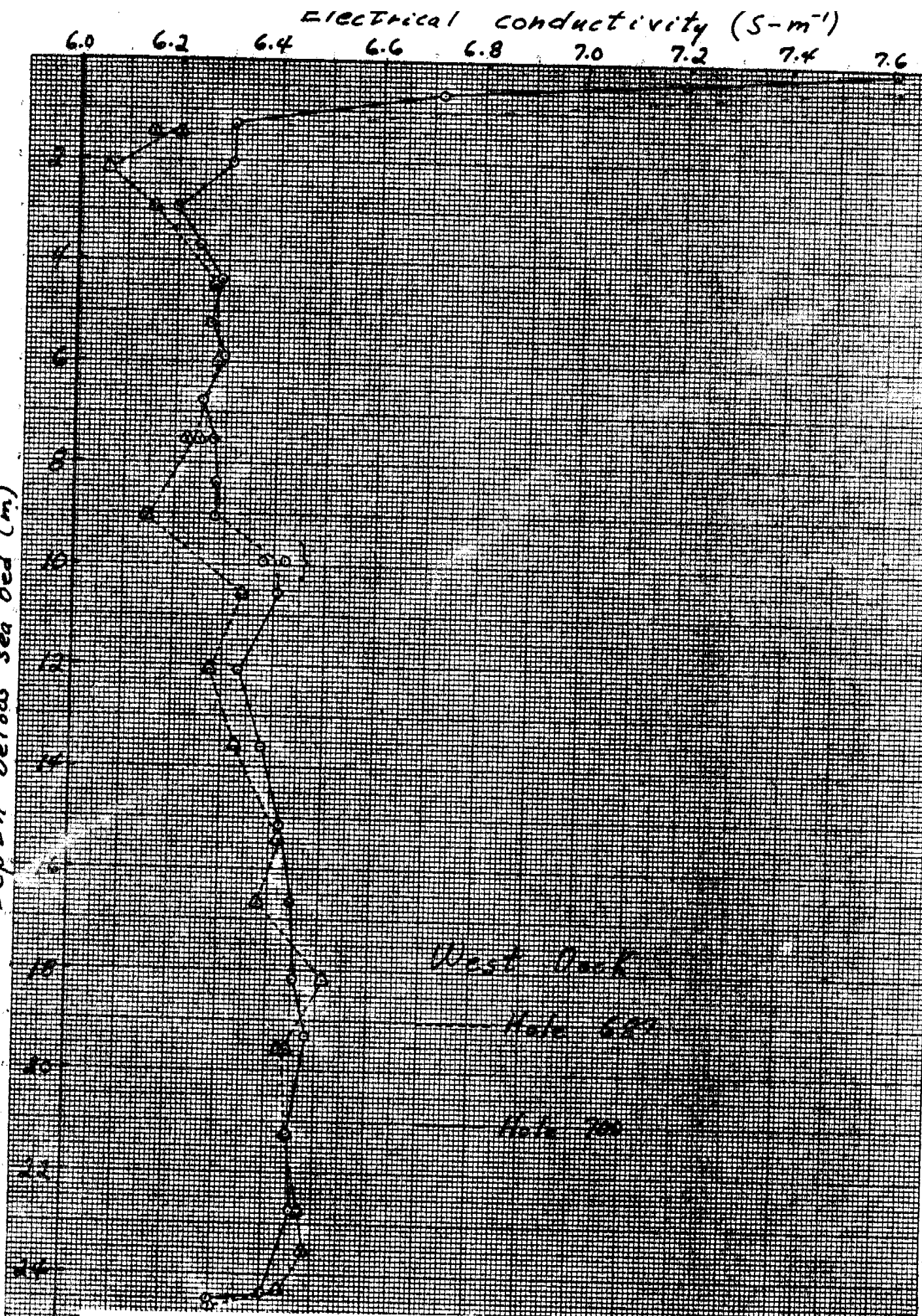
46 1513

REDFIELD & ESSER CO. MADE IN U.S.A.

K&E 10 X 10 TO THE CENTIMETER 18 X 25 CM. KEUFFEL & ESSER CO. MADE IN U.S.A.

46 1513

Depth below sea bed (m)



562

Figure 32. Electrical conductivity profiles of interstitial pore water samples from West Dock, Hole 620, and Hole 700.

TABLE 1

Hole Designation	Approximate Location and/or Offshore Distance	Water Depth (m)	Sea Ice Thickness (m)	Placement Method	Time of Placement Yr. Mo. Da.	Total Depth Below Seabed (m)	Notes
Flaxman I., Hole A	0.893 km south of Leffingwell's cabin	2.2	1.75	rotary-jet	790511	13.4	Lithology, temperature
Flaxman I., Hole B	0.165 km offshore from spit, bearing N2°E from Leffingwell's cabin	3.2	2.10	rotary-jet	790513	17.2	Lithology, temperature borehole experiments
Flaxman I., Hole C	0.684 km offshore from spit, bearing N2°E from Leffingwell's cabin	6.1	2.01	rotary-jet	790512	28.3	Lithology, temperature
Jeanette I., Hole A	= 1 km NE of Jeanette I.,	7.5	1.72	rotary-jet	790501	30.0	"
Jeanette I., Hole B	= 1 km true north of dive site 11 which has coordinates of 70° 19.25'N 147° 35.4'W	6.8	1.83	rotary-jet	790502	15.4	"
Point Brower, Hole C	70° 17.3'N 147° 44.3'W = 1.6 km NE of Pt. Brower	3.4	1.85	rotary-jet	790503	21.9	"
Long Island Hole A	0.315 km N25°E of VABM on Long Island 70° 28.9'N 148° 50.5'W	3.6	2.30	rotary-jet	790517	13.3	"
Long Island Hole B	0.600 km N25°E of VABM on Long Island 70° 29.0'N 148° 51.0'W	5.8	2.30	rotary-jet	790518	12.8	"
Long Island Hole C	70° 29.5'N 148° 50.4'N = 1.8 km N25°E of VABM on Long Island	9.7	2.00	rotary-jet	790519	11.0	"

564

Long Island Hole D	70° 30.7'N 148° 45.5'W = 3.2 km N25°E of VABM on Long Island	14.0	1.40	rotary-jet	790520	7.0	"
Dock Hole A	0.700 km offshore N32°E from North Prudhoe Bay State #1 well	1.8	1.82	driving	790514	20.87	Lithology, temperature, borehole experiments
Dock Hole B	0.689 km offshore N32°E from North Prudhoe Bay #1 well	1.8	1.82	driving	790526	-	Lithology, temperature
Dock Hole C	0.701 km offshore N32°E from North Prudhoe Bay #1 well	1.8	1.75	"	790515	27.45	Salinity samples
Dock Hole D	0.687 km offshore N32°E from North Prudhoe Bay State #1 well	1.8	1.80	"	790523-24	27.20	Salinity Samples
Dock Hole E	0.837 km offshore N32°E from North Prudhoe Bay State #1 well	1.8	1.76	"	790526	18.81	Soil samples
Dock Hole F	All at 0.700 km offshore N32°E from North Prudhoe Bay State #1 well	1.8	1.85	"	790528	9.60	Interstitial water velocity experiment "
Dock Hole G		1.8	1.85	"	790528	12.80	
Dock Hole H		1.8	1.85	"	790528	9.60	
Dock Hole I		1.8	1.85	"	790528	12.80	
Reindeer I., Hole A	0.352 km N9°E from the USGS Tower on Reindeer Island	3.8	1.93	rotary-jet	790505	23.5	Lithology, temperature, borehole experiments
Reindeer I., Hole B	0.744 km N10°W from the USGS Tower on Reindeer Island 70° 29.0'N 148° 21.14'W	5.4	1.90	"	790505	23.46	Lithology, temperature

Reindeer I., Hole C	70° 29.7'N 148° 20.83' W = 2.6 km N9°E from the USGS Tower on Reindeer Island	11.5	1.91	rotary-jet	790504	15.03	Lithology, temperature, borehole experiments
Reindeer I., Hole D	N250°E and = 300 m from the USGS tower on Reindeer Island, = 4 m from the shoreline	-	-	rotary-jet	790831	20	Lithology, temperature



TABLE 2

Thermal conductivity values for Flaxman Island hole B (FLAXB)  
(5-15 m depths) as determined from the borehole heating experiment

<u>Depth (m)</u>	<u><math>K(\frac{W}{m^{\circ}K})</math></u>
5.15	2.0
6.15	2.0
7.15	1.9
8.15	1.4
9.15	2.6
10.15	2.3
11.15	1.7
12.15	1.7
13.15	1.8
14.15	1.7
15.15	2.4

TABLE 3

Thermal conductivity values for West Dock hole A (DOCKA) as determined from the borehole heating experiment

<u>Depth (m)</u>	<u><math>K(\frac{W}{m^{\circ}K})</math></u>
1.39	2.5
2.39	3.1
3.39	2.5
4.39	3.0
5.39	3.4
6.39	3.3
7.39	3.2
8.39	3.8
9.39	3.8
10.39	4.3
11.39	4.2
12.39	4.6
13.39	4.3
14.39	3.8
15.39	3.6
16.39	4.3
17.39	4.2

TABLE 4

Electrical conductivities of interstitial pore water samples  
from West Dock holes C (701) and D (687)

<u>Hole 687</u>			<u>Hole 700</u>		
Sample Number	Depth (m)	Electrical Conductivity (S-m <sup>-1</sup> )	Sample Number	Depth (m)	Electrical Conductivity (S-m <sup>-1</sup> )
687-0	under ice	0.00	700-1	.09 m	7.609
687-1	2.95	1.43	700-2	.39	7.198
	below ice		700-3	.64	6.719
687-2	2.19	6.064, 6.059	700-4	1.27	6.310
687-3	2.95	6.149, 6.160	700-5	2.03	6.307
687-4	4.48	6.275	700-6	2.94	6.197
687-5	6.01	6.282, 6.278, 6.283	700-7	3.69	6.243
			700-8	4.36	6.287
687-6	7.53	6.248, 6.226	700-9	5.22	6.269
687-7	9.06	6.148, 6.142	700-10	5.88	6.296
687-8	10.58	6.342, 6.332	700-11	6.74	6.257
687-9	12.11	6.277, 6.277	700-12	7.52	6.276
687-10	13.63	6.337, 6.324	700-13	8.39	6.281
687-11(6')	15.46	6.422	700-14	9.05	6.282
687-12(4')	16.68	6.382	700-15	9.91	6.380
687-13	18.21	6.513	700-16	9.91	6.422
687-14(4 1/2')	19.58	6.430, 6.455	700-17	10.57	6.408
687-15	21.26	6.44, 6.451	700-18	12.10	6.332
687-16	22.78	6.469, 6.477	700-19	13.62	6.380
687-17	23.54	6.483, 6.484	700-20	15.14	6.420
687-18	24.31	6.445, 6.424	700-21	16.67	6.445
687-19	24.62	6.306, 6.300	700-22	18.19	6.453
			700-23	19.31	6.480
			700-24	21.24	6.448
			700-25	22.76	6.465
			700-26	24.39	6.406
			700-26A		6.399
			700-27	24.48	6.295

TABLE 5

Hydraulic conductivity values at holes 687 and 701

<u>Hole 687</u>		<u>Hole 701</u>	
<u>Depth (m)</u>	<u>Hydraulic Conductivity (m-a<sup>-1</sup>)</u>	<u>Depth (m)</u>	<u>Hydraulic Conductivity (m-a<sup>-1</sup>)</u>
1.43	0.2 to 0.5	127 m	1.8
2.19	0.2	2.03	0.6
2.95	1.1	2.94	1.7
4.48	1.6	3.69	2.8
6.01	4.6	4.36	4.8
7.53	5.3	5.22	5.7
9.06	7.0	5.88	7.4 to 54
10.58	14	6.74	11
12.11	2.6	7.52	28 to 171
13.63	0.1 to 1.0	8.39	4.8
15.46	9.2	9.05	2.2
16.68	11	9.91	4.4 to 11
18.21	6.6	10.57	17
19.58	4.4	12.10	2.0
21.26	13	13.62	3.4
22.78	9.2	15.14	6.1
23.54	7.9	16.67	11
24.31	4.8	18.19	7.0
		19.31	2.6
		21.24	18
		22.76	3.1
		24.39	2.7
		24.48	10*

\*Not corrected for proximity of impermeable phase boundary.

## X. ACKNOWLEDGEMENTS

We want to acknowledge the cheerful and effective assistance of Robert Fisk, Richard Gaffi, Mark Smith, Rod March and the NOAA helicopter crews. Logistic support was provided by OCSEAP and by the Naval Arctic Research Laboratory. Part of the research reported here was supported by the National Science Foundation under NSF Grant No. DPP77-28451.

APPENDIX A

Subsea permafrost temperature data - 1979 field season

1

FLAXMAN ISLAND  
 HOLE FLAXA1  
 790513  
 10:15:00

79-2            CABLE  
 L&N NEW       BRIDGE

TIME	DEPTH (M)	R (OHMS)	T (C)
10.30	0.31	12494.0	-2.152
10.32	1.31	12449.0	-2.071
10.35	2.31	12307.0	-1.812
10.40	3.31	12166.0	-1.551
10.52	4.31	12078.0	-1.387
10.60	5.31	12046.0	-1.327
10.62	6.31	12043.0	-1.321
10.65	7.31	12045.0	-1.325
10.72	8.31	12077.0	-1.385
10.77	9.31	12077.0	-1.385
10.82	10.31	12043.0	-1.321
10.85	11.31	12000.0	-1.240
10.95	12.31	12028.0	-1.293
11.02	13.28	12065.0	-1.363

QUINCY ISLAND  
 GOLF FLASKS  
 12:00:00

	DEPTH	CABLE BRIDGE	R (OHMS)	T (C)
12.77	.31		12530.0	-2.217
12.78	1.31		12423.0	-2.023
12.81	2.31		12295.0	-1.790
12.83	3.31		12174.0	-1.570
12.82	4.31		12099.0	-1.408
12.87	5.31		12048.0	-1.331
12.88	6.31		12038.0	-1.312
12.72	7.31		12052.0	-1.338
12.77	8.31		12073.0	-1.378
12.87	9.31		12100.0	-1.428
12.92	10.31		12115.0	-1.456
12.97	11.31		12130.0	-1.484
14.02	12.31		12143.0	-1.509
14.03	13.31		12123.0	-1.471



FLAXMAN ISLAND  
HOLE FLAXB1  
790515  
14:06:00

79-1                    CABLE  
L&N NEW                BRIDGE

TIME	DEPTH (M)	R (OHMS)	T (C)
14.55	0.15	12336.0	-1.833
14.60	1.15	12331.0	-1.824
14.67	2.15	12318.0	-1.800
14.73	3.15	12345.0	-1.850
14.80	4.15	12387.0	-1.926
14.87	5.15	12486.0	-2.105
14.95	6.15	12620.0	-2.345
15.00	7.15	12733.0	-2.545
15.07	8.15	12801.0	-2.665
15.12	9.15	12923.0	-2.877
15.18	10.15	13056.0	-3.106
15.25	11.15	13166.0	-3.294
15.32	12.15	13267.0	-3.464
15.37	13.15	13362.0	-3.623
15.47	14.15	13496.0	-3.845
15.60	15.15	13786.0	-4.318
15.67	16.15	13934.0	-4.395

FLAXMAN ISLAND  
HOLE FLAXB2  
790513  
13:10:00

79-1  
L&M NEW

CABLE  
FRIDGE

TIME	DEPTH (M)	R (OHMS)	T (C)
13.25	0.15	12289.0	-1.747
13.32	1.15	12289.0	-1.747
13.37	2.15	12316.0	-1.797
13.42	3.15	12333.0	-1.828
13.48	4.15	12400.0	-1.950
13.53	5.15	12521.0	-2.168
13.65	6.15	12652.0	-2.402
13.75	7.15	12771.0	-2.612
13.82	8.15	12891.0	-2.822
13.88	9.15	13016.0	-3.038
13.93	10.15	13133.0	-3.238
14.00	11.15	13246.0	-3.429
14.08	12.15	13359.0	-3.618
14.13	13.15	13447.0	-3.764
14.23	14.15	13584.0	-3.990
14.30	15.15	13735.0	-4.236
14.35	16.15	13809.0	-4.355
14.42	16.57	13835.0	-4.397

1

FLAXMAN ISLAND  
HOLE FLAXB3  
790524  
17:14:0079-2  
L&M NEW CABLE  
BRIDGE

TIME	DEPTH (M)	R (OHMS)	T (C)
17.30	0.15	12275.0	-1.753
17.35	1.15	12266.0	-1.736
17.42	2.15	12297.0	-1.793
17.47	3.15	12316.0	-1.829
17.53	4.15	12403.0	-1.987
17.58	5.15	12528.0	-2.213
17.67	6.15	12659.0	-2.447
17.75	7.15	12793.0	-2.684
17.82	8.15	12911.0	-2.890
17.88	9.15	13049.0	-3.128
18.03	10.15	13147.0	-3.296
18.00	11.15	13258.0	-3.484
18.07	12.15	13364.0	-3.662
18.12	13.15	13467.0	-3.833
18.18	14.15	13580.0	-4.019
18.25	15.15	13705.0	-4.223
18.32	16.15	13783.0	-4.350
18.50	16.61	13819.0	-4.408

FLAXMAN ISLAND  
HOLE FLAXB4  
790529  
15:08:00

79-2  
L&M NEW          CABLE  
                         BRIDGE

TIME	DEPTH (M)	R (OHMS)	T (C)
15.18	0.15	12287.0	-1.775
15.25	1.15	12276.0	-1.755
15.30	2.15	12296.0	-1.792
15.35	3.15	12319.0	-1.834
15.42	4.15	12402.0	-1.985
15.50	5.15	12535.0	-2.226
15.55	6.15	12663.0	-2.454
15.60	7.15	12799.0	-2.695
15.65	8.15	12919.0	-2.904
15.73	9.15	13030.0	-3.096
15.78	10.15	13149.0	-3.299
15.85	11.15	13262.0	-3.491
15.90	12.15	13366.0	-3.665
15.97	13.15	13471.0	-3.840
16.05	14.15	13587.0	-4.031
16.10	15.15	13710.0	-4.231
16.13	16.15	13790.0	-4.361
16.28	16.61	13824.0	-4.416

FLAXMAN ISLAND  
HOLE FLAX85  
790529  
18:43:0079-2  
L&N NEW      CABLE  
                 BRIDGE

TIME	DEPTH (M)	R (OHMS)	T (C)
18.77	0.15	12005.0	-1.250
18.82	1.15	11632.0	-0.533
18.87	2.15	11903.0	-1.056
18.92	3.15	11664.0	-0.596
18.97	4.15	11396.0	-0.066
19.00	5.15	12001.0	-1.242
19.03	6.15	12152.0	-1.525
19.07	7.15	12140.0	-1.503
19.10	8.15	12098.0	-1.425
19.13	9.15	12159.0	-1.538
19.17	10.15	12163.0	-1.546
19.20	11.15	12165.0	-1.550
19.23	12.15	12226.0	-1.663
19.27	13.15	12249.0	-1.705
19.30	14.15	12264.0	-1.733
19.33	15.15	12443.0	-2.060
19.37	16.15	13054.0	-3.137
19.40	16.61	13374.0	-3.678

FLAXMAN ISLAND  
 HOLE FLAX36  
 790530  
 10:01:00

79-2                    CABLE  
 L&M NEW               BRIDGE

TIME	DEPTH (M)	R (OHMS)	T (C)
10.08	0.15	12271.0	-1.746
10.13	1.15	12274.0	-1.751
10.13	2.15	12295.0	-1.790
10.27	3.15	12273.0	-1.749
10.32	4.15	12339.0	-1.870
10.40	5.15	12421.0	-2.020
10.47	6.15	12545.0	-2.244
10.52	7.15	12675.0	-2.476
10.59	8.15	12753.0	-2.614
10.67	9.15	12938.0	-2.937
10.72	10.15	13046.0	-3.123
10.77	11.15	13122.0	-3.253
10.83	12.15	13228.0	-3.433
10.88	13.15	13337.0	-3.617
10.95	14.15	13448.0	-3.802
11.00	15.15	13615.0	-4.077
11.05	16.15	13715.0	-4.240
11.15	16.61	13777.0	-4.340

1

FLAXMAN ISLAND  
HOLE FLAXB7  
790530  
12:20:00

79-2            CABLE  
L&N NEW       BRIDGE

TIME	DEPTH (M)	R (OHMS)	T (C)
12.40	0.15	12266.0	-1.736
12.47	1.15	12270.0	-1.744
12.52	2.15	12289.0	-1.779
12.60	3.15	12220.0	-1.652
12.65	4.15	12336.0	-1.865
12.70	5.15	12432.0	-2.040
12.75	6.15	12559.0	-2.269
12.80	7.15	12692.0	-2.506
12.85	8.15	12775.0	-2.652
12.90	9.15	12954.0	-2.965
12.95	10.15	13061.0	-3.149
12.98	11.15	13138.0	-3.281
13.05	12.15	13241.0	-3.455
13.10	13.15	13349.0	-3.637
13.15	14.15	13457.0	-3.817
13.20	15.15	13619.0	-4.083
13.23	16.15	13714.0	-4.238
13.32	16.61	13775.0	-4.337

FLAXMAN ISLAND  
HOLE FLAX38  
790530  
15:34:00

79-2                    CABLE  
L&N NEW                BRIDGE

TIME	DEPTH (M)	R (OHMS)	T (C)
15.53	0.15	12266.0	-1.736
15.63	1.15	12259.0	-1.724
15.77	2.15	12297.0	-1.793
15.82	3.15	12293.0	-1.768
15.83	4.15	12345.0	-1.881
15.95	5.15	12446.0	-2.065
15.98	6.15	12573.0	-2.294
16.05	7.15	12706.0	-2.531
16.12	8.15	12794.0	-2.686
16.23	9.15	12928.0	-2.929
16.28	10.15	13069.0	-3.163
16.33	11.15	13156.0	-3.311
16.40	12.15	13260.0	-3.487
16.47	13.15	13365.0	-3.663
16.52	14.15	13476.0	-3.848
16.58	15.15	13631.0	-4.103
16.67	16.15	13765.0	-4.320
16.73	16.61	13787.0	-4.356



FLAXMAN ISLAND  
HOLE FLAXB9  
790531  
14:42:0079-2  
L&N NEW      CABLE  
                 BRIDGE

TIME	DEPTH (M)	R (OHMS)	T (C)
14.75	0.15	12271.0	-1.746
14.83	1.15	12261.0	-1.727
15.88	2.15	12307.0	-1.812
15.93	3.15	12301.0	-1.801
15.00	4.15	12367.0	-1.922
15.05	5.15	12486.0	-2.138
15.10	6.15	12618.0	-2.374
15.17	7.15	12753.0	-2.614
15.23	8.15	12870.0	-2.819
15.28	9.15	13020.0	-3.079
15.35	10.15	13118.0	-3.246
15.40	11.15	13219.0	-3.418
15.45	12.15	13327.0	-3.600
15.53	13.15	13433.0	-3.777
15.58	14.15	13542.0	-3.957
15.63	15.15	13667.0	-4.162
15.73	16.15	13754.0	-4.303
15.80	16.61	13799.0	-4.375

FLAXMAN ISLAND  
 HOLE FLAXC1  
 790515  
 11:15

79-1  
 NEW L&N  
 CABLE  
 BRIDGE

TIME	DEPTH (F)	R (OHMS)	T (C)
11.45	0.	12346.0	-1.851
11.55	1.00	12301.0	-1.769
11.65	2.00	12230.0	-1.639
11.70	3.00	12215.0	-1.611
11.75	4.00	12209.0	-1.600
11.80	5.00	12228.0	-1.635
11.92	6.00	12251.0	-1.677
11.97	7.00	12278.0	-1.727
12.02	8.00	12312.0	-1.789
12.07	9.00	12347.0	-1.853
12.12	10.00	12379.0	-1.911
12.13	11.00	12404.0	-1.957
12.23	12.00	12439.0	-2.020
12.30	13.00	12472.0	-2.080
12.37	14.00	12502.0	-2.134

FLAXMAN ISLAND  
HOLE FLAXC2  
790518  
09:32:00

79-1            CABLE  
L&N NEW       BRIDGE

TIME	DEPTH (M)	R (OHMS)	T (C)
9.85	0.	12341.0	-1.842
9.92	1.00	12305.0	-1.776
9.97	2.00	12240.0	-1.657
10.03	3.00	12214.0	-1.609
10.19	4.00	12206.0	-1.594
10.25	5.00	12227.0	-1.633
10.30	6.00	12251.0	-1.677
10.33	7.00	12282.0	-1.734
10.42	8.00	12317.0	-1.798
10.48	9.00	12351.0	-1.860
10.53	10.00	12383.0	-1.919
10.58	11.00	12416.0	-1.979
10.82	12.00	12447.0	-2.035
10.87	13.00	12483.0	-2.100
10.93	14.00	12512.0	-2.152
11.00	15.00	12542.0	-2.206

FLAXMAN ISLAND  
 HOLE FLAXC3  
 770524  
 14:30:00

79-2 CABLE  
 L&M NEW BRIDGE

TIME	DEPTH (M)	R (OHMS)	T (C)
14.72	0.	12316.0	-1.828
14.73	1.00	12273.0	-1.749
14.85	2.00	12219.0	-1.650
14.99	3.00	12187.0	-1.590
14.95	4.00	12186.0	-1.589
15.03	5.00	12209.0	-1.631
15.10	6.00	12237.0	-1.683
15.17	7.00	12265.0	-1.735
15.22	8.00	12300.0	-1.799
15.27	9.00	12334.0	-1.861
15.32	10.00	12366.0	-1.920
15.33	11.00	12398.0	-1.978
15.43	12.00	12428.0	-2.033
15.50	13.00	12461.0	-2.092
15.55	14.00	12496.0	-2.156
15.53	15.00	12521.0	-2.201
15.73	16.00	12553.0	-2.258
15.80	16.70	12600.0	-2.342

FLAYMAN ISLAND  
HOLE FLAXC4  
790529  
15:06:00

79-3                    CABLE  
OLD L&N                BRIDGE

TIME	DEPTH (M)	R (OHMS)	T (C)
15.10	0.	12223.0	-1.847
15.15	1.00	12175.0	-1.758
15.20	2.00	12123.0	-1.662
15.25	3.00	12091.0	-1.602
15.28	4.00	12091.0	-1.602
15.32	5.00	12112.0	-1.641
15.35	6.00	12138.0	-1.690
15.33	7.00	12170.0	-1.749
15.42	8.00	12205.0	-1.814
15.45	9.00	12239.0	-1.877
15.48	10.00	12269.0	-1.932
15.52	11.00	12302.0	-1.993
15.62	12.00	12333.0	-2.049
15.65	13.00	12368.0	-2.113
15.67	14.00	12399.0	-2.170
15.68	15.00	12426.0	-2.219
15.72	16.00	12456.0	-2.273
15.75	17.00	12487.0	-2.329
15.78	18.00	12506.0	-2.363

POINT BROWER  
HOLE JEANCI  
790526  
09:15

	79-2 NEW L&N	CABLE BRIDGE	
TIME	DEPTH (M)	R (OHMS)	T (C)
9.65	0.34	11702.0	-0.670
9.68	1.34	11747.0	-0.757
9.73	2.34	11816.0	-0.890
9.80	3.34	12015.0	-1.269
9.87	4.34	12007.0	-1.254
9.92	5.34	12023.0	-1.284
9.98	6.34	11995.0	-1.231
10.07	7.34	12033.0	-1.303
10.12	8.34	12055.0	-1.344
10.17	9.34	12079.0	-1.389
10.22	10.34	12104.0	-1.436
10.28	11.34	12126.0	-1.477
10.33	12.34	12141.0	-1.505
10.40	13.34	12163.0	-1.546
10.45	14.34	12179.0	-1.576
10.53	15.34	12202.0	-1.618
10.62	16.34	12220.0	-1.652
10.63	17.34	12240.0	-1.688
10.72	18.14	12253.0	-1.712

POINT BROWER  
HOLE JEANC2  
790609  
11:00

79-2  
NEV L&N

CABLE  
BRIDGE

TIME	DEPTH (M)	R (OHMS)	T (C)
11.47	0.34	11690.0	-0.646
11.52	1.34	12037.0	-1.310
11.57	2.34	12063.0	-1.359
11.62	3.34	12041.0	-1.318
11.65	4.34	12020.0	-1.278
11.75	5.34	12034.0	-1.304
11.85	6.34	12010.0	-1.259
11.92	7.34	12016.0	-1.271
11.97	8.34	12047.0	-1.329
12.02	9.34	12071.0	-1.374
12.07	10.34	12094.0	-1.417
12.12	11.34	12121.0	-1.468
12.17	12.34	12137.0	-1.497
12.23	13.34	12152.0	-1.525
12.28	14.34	12167.0	-1.553
12.33	15.34	12188.0	-1.592
12.38	16.34	12211.0	-1.635
12.45	17.34	12231.0	-1.672
12.50	18.34	12249.0	-1.705
12.55	19.34	12268.0	-1.740
12.60	20.34	12289.0	-1.779
12.65	21.04	12302.0	-1.803

JEANETTE ISLAND  
HOLE JEANBI  
790506  
15:20:00

79-3                    CABLE  
L&M NEW                BRIDGE

TIME	DEPTH (M)	R (OHMS)	T (C)
15.45	0.75	12182.0	-1.766
15.58	1.75	12112.0	-1.635
15.55	2.75	12067.0	-1.551
15.70	3.75	12027.0	-1.476
15.82	4.75	11998.0	-1.422
15.90	5.75	11985.0	-1.397
15.93	6.75	11988.0	-1.403
16.02	7.75	11997.0	-1.420
16.08	8.75	12002.0	-1.429
16.13	9.75	12017.0	-1.457
16.18	10.75	12038.0	-1.497
16.37	11.75	12059.0	-1.536
16.43	12.75	12080.0	-1.576
16.47	13.75	12104.0	-1.620
16.55	14.75	12129.0	-1.667
16.62	15.26	12146.0	-1.699



JEANETTE ISLAND  
HOLE JEANB2  
790502  
16:37:00

	79-3 L&N NEW	CABLE BRIDGE	
TIME	DEPTH (M)	R (OHMS)	T (C)
16.62	0.75	12180.0	-1.762
16.70	1.75	12114.0	-1.639
16.30	2.75	12066.0	-1.549
16.88	3.75	12028.0	-1.478
16.95	4.75	12000.0	-1.425
17.00	5.75	11993.0	-1.412
17.05	6.75	11989.0	-1.405
17.17	7.75	11993.0	-1.412
17.27	8.75	12004.0	-1.433
17.30	9.75	12023.0	-1.469
17.35	10.75	12044.0	-1.508
17.42	11.75	12066.0	-1.549
17.47	12.75	12088.0	-1.591
17.52	13.75	12109.0	-1.630
17.57	14.75	12133.0	-1.675
17.62	15.28	12147.0	-1.701

HANFORD ISLAND  
 11/20/67  
 70511  
 11:00

TIME  
 217.18  
 218.18  
 219.18  
 220.18  
 221.18  
 222.18  
 223.18  
 224.18  
 225.18  
 226.18  
 227.18  
 228.18  
 229.18  
 230.18  
 231.18  
 232.18  
 233.18  
 234.18  
 235.18  
 236.18  
 237.18  
 238.18  
 239.18  
 240.18  
 241.18  
 242.18  
 243.18  
 244.18  
 245.18  
 246.18  
 247.18  
 248.18  
 249.18  
 250.18  
 251.18  
 252.18  
 253.18  
 254.18  
 255.18  
 256.18  
 257.18  
 258.18  
 259.18  
 260.18  
 261.18  
 262.18  
 263.18  
 264.18  
 265.18  
 266.18  
 267.18  
 268.18  
 269.18  
 270.18  
 271.18  
 272.18  
 273.18  
 274.18  
 275.18  
 276.18  
 277.18  
 278.18  
 279.18  
 280.18  
 281.18  
 282.18  
 283.18  
 284.18  
 285.18  
 286.18  
 287.18  
 288.18  
 289.18  
 290.18  
 291.18  
 292.18  
 293.18  
 294.18  
 295.18  
 296.18  
 297.18  
 298.18  
 299.18  
 300.18

TIME	DEPTH (M)	P (CM'S)	T (C)
18.72	1.75	12000.0	-1.799
18.73	1.75	12143.0	-1.693
18.83	1.75	12140.0	-1.594
18.93	1.75	12056.0	-1.531
18.97	4.75	12024.0	-1.471
18.98	5.75	12005.0	-1.435
18.97	6.75	12002.0	-1.429
18.98	7.75	12003.0	-1.431
18.17	8.75	12014.0	-1.452
18.23	9.75	12030.0	-1.432
18.31	10.75	12052.0	-1.523
18.35	11.75	12072.0	-1.561
18.41	12.75	12093.0	-1.600
18.47	13.75	12115.0	-1.641
18.53	14.75	12137.0	-1.682
18.53	15.25	12148.0	-1.702

JEANETTE ISLAND  
 HOLE JEAN A1  
 790506  
 11:11:00

79-3  
 L&M NEW CABLE  
 BRIDGE

TIME	DEPTH (M)	R (OHMS)	T (C)
11.18	0.60	12183.0	-1.767
11.23	1.60	12132.0	-1.673
11.28	2.60	12103.0	-1.619
11.35	3.60	12067.0	-1.551
11.43	4.60	12060.0	-1.538
11.53	5.60	12052.0	-1.523
11.63	6.60	12040.0	-1.501
11.70	7.60	12038.0	-1.497
11.77	8.60	12047.0	-1.514
11.82	9.60	12057.0	-1.533
11.87	10.60	12067.0	-1.551
11.97	11.60	12086.0	-1.587
12.00	12.60	12097.0	-1.607
12.03	13.60	12101.0	-1.615
12.10	14.60	12106.0	-1.624
12.13	15.60	12107.0	-1.626
12.20	16.60	12106.0	-1.624
12.32	17.60	12114.0	-1.639
12.57	18.60	12110.0	-1.637
12.62	19.60	12111.0	-1.639
12.70	20.60	12122.0	-1.654
12.77	21.60	12135.0	-1.678
12.90	22.60	12146.0	-1.699
13.08	23.60	12163.0	-1.730
13.12	24.60	12162.0	-1.728
13.17	25.60	12175.0	-1.753
13.22	26.60	12183.0	-1.767
13.27	27.60	12138.0	-1.777
13.33	28.60	12192.0	-1.784
13.40	29.60	12202.0	-1.803
13.70	30.30	12197.0	-1.793

JEANETTE ISLAND  
HOLE JEAN12  
790509  
09:36:00

79-3 CABLE  
L&N NEW BRIDGE

TIME	DEPTH (M)	R (OHMS)	T (C)
9.64	0.60	12137.0	-1.775
9.67	1.60	12140.0	-1.688
9.72	2.60	12107.0	-1.626
9.74	3.60	12078.0	-1.572
9.87	4.60	12062.0	-1.542
10.29	5.60	12053.0	-1.525
10.33	6.60	12047.0	-1.514
10.37	7.60	12045.0	-1.510
10.43	8.60	12054.0	-1.527
10.50	9.60	12062.0	-1.542
10.57	10.60	12074.0	-1.564
10.63	11.60	12083.0	-1.581
10.70	12.60	12092.0	-1.598
10.80	13.60	12097.0	-1.607
10.83	14.60	12101.0	-1.615
11.05	15.60	12101.0	-1.615
11.10	16.60	12104.0	-1.620
11.13	17.60	12113.0	-1.637
11.27	18.60	12123.0	-1.656
11.30	19.60	12124.0	-1.658
11.35	20.60	12130.0	-1.669
11.40	21.60	12144.0	-1.695
11.47	22.60	12149.0	-1.704
11.53	23.60	12167.0	-1.738
11.63	24.60	12161.0	-1.727
11.70	25.60	12185.0	-1.771
11.73	26.60	12190.0	-1.780
11.73	27.60	12195.0	-1.790
11.83	28.60	12198.0	-1.795
11.83	29.60	12210.0	-1.817
12.02	30.24	12184.0	-1.769

JEANETTE ISLAND  
HOLE JEANA5  
790531  
11:28:00

79-3  
L&N NEW CABLE  
BRIDGE

TIME	DEPTH (M)	R (OHMS)	T (C)
11.50	0.60	12186.0	-1.773
11.55	1.60	12148.0	-1.702
11.58	2.60	12115.0	-1.641
11.62	3.60	12087.0	-1.589
11.65	4.60	12069.0	-1.555
11.72	5.60	12056.0	-1.531
11.73	6.60	12049.0	-1.518
11.83	7.60	12048.0	-1.516
11.83	8.60	12055.0	-1.529
11.95	9.60	12065.0	-1.548
12.00	10.60	12074.0	-1.564
12.07	11.60	12083.0	-1.581
12.10	12.60	12094.0	-1.602
12.13	13.60	12103.0	-1.619
12.17	14.60	12105.0	-1.622
12.22	15.60	12109.0	-1.630
12.25	16.60	12117.0	-1.645
12.32	17.60	12125.0	-1.660
12.35	18.60	12131.0	-1.671
12.38	19.60	12138.0	-1.684
12.42	20.60	12147.0	-1.701
12.45	21.60	12153.0	-1.712
12.48	22.60	12162.0	-1.728
12.52	23.60	12169.0	-1.741
12.57	24.60	12175.0	-1.753
12.60	25.60	12183.0	-1.767
12.63	26.60	12189.0	-1.779
12.67	27.60	12197.0	-1.793
12.70	28.60	12203.0	-1.804
12.75	29.60	12211.0	-1.819
12.82	30.21	12197.0	-1.793

LONG ISLAND  
HOLE LONGISAI  
790520  
09:09

79-1 CABLE  
REV. L&M BRIDGE

TIME	DEPTH (M)	R (OHMS)	T (C)
9.70	0.	12371.0	-1.897
9.75	0.97	12299.0	-1.765
9.83	1.97	12211.0	-1.603
9.92	2.97	12152.0	-1.494
9.95	3.97	12111.0	-1.418
10.05	4.97	12086.0	-1.371
10.13	5.97	12064.0	-1.330
10.18	6.97	12057.0	-1.317
10.23	7.97	12052.0	-1.307
10.30	8.97	12059.0	-1.321
10.35	9.97	12063.0	-1.328
10.42	10.97	12065.0	-1.332
10.47	11.97	12060.0	-1.322
10.50	12.67	11984.0	-1.130

LONG ISLAND  
HOLE LONGISA2  
790527  
09:34

79-2                    CABLE  
NEW L&N                BRIDGE

TIME	DEPTH (M)	R (OHMS)	T (C)
9.70	0.	12353.0	-1.896
9.77	0.97	12290.0	-1.781
9.85	1.97	12190.0	-1.596
9.92	2.97	12136.0	-1.496
9.98	3.97	12097.0	-1.423
10.03	4.97	12072.0	-1.376
10.08	5.97	12052.0	-1.338
10.15	6.97	12038.0	-1.312
10.20	7.97	12036.0	-1.308
10.25	8.97	12039.0	-1.314
10.30	9.97	12040.0	-1.316
10.35	10.97	12043.0	-1.321
10.42	11.97	12055.0	-1.344
10.52	12.67	11985.0	-1.212

LONG ISLAND  
 HOLE LONGISA3  
 790530  
 11:40

79-3 CABLE  
 CLE L&M BRIDGE

TIME	DEPTH (M)	R (OHMS)	T (C)
11.93	0.	12037.0	-1.501
11.98	0.97	12217.0	-1.836
12.03	1.97	12120.0	-1.656
12.08	2.97	12059.0	-1.542
12.12	3.97	12015.0	-1.459
12.15	4.97	11988.0	-1.408
12.18	5.97	11965.0	-1.365
12.22	6.97	11951.0	-1.338
12.25	7.97	11947.0	-1.331
12.28	8.97	11948.0	-1.333
12.32	9.97	11952.0	-1.340
12.37	10.97	11955.0	-1.346
12.40	11.97	11963.0	-1.361
12.43	12.07	11953.0	-1.342



LONG ISLAND  
HOLE LONGISB1  
790610  
08:17

79-2 CABLE  
NEW L&N BRIDGE

TIME	DEPTH (M)	R (OHMS)	T (C)
8.45	0.	12301.0	-1.801
8.50	1.00	12200.0	-1.615
8.57	2.00	12141.0	-1.505
8.62	3.00	12096.0	-1.421
8.69	4.00	12068.0	-1.368
8.75	5.00	12045.0	-1.325
8.82	6.00	12034.0	-1.304
8.87	7.00	12030.0	-1.297
8.93	8.00	12035.0	-1.306
8.98	9.00	12036.0	-1.308
9.03	10.00	12039.0	-1.314
9.12	10.80	12052.0	-1.338

LONG ISLAND  
HOLE LONGISCI  
790521  
15:00

79-1 CABLE  
NEW L&N BRIDGE

TIME	DEPTH (M)	R (OHMS)	T (C)
15.19	0.49	12314.0	-1.793
15.16	1.49	12290.0	-1.749
15.22	2.49	12250.0	-1.675
15.28	3.49	12209.0	-1.600
15.33	4.49	12165.0	-1.518
15.38	5.49	12145.0	-1.481
15.47	6.49	12123.0	-1.440
15.52	7.49	12099.0	-1.395
15.52	8.49	12105.0	-1.407
0.	8.82	12112.0	-1.420

LONG ISLAND  
HOLE LONGISC2  
790527  
14:20

79-2            CABLE  
NEW L&N       BRIDGE

TIME	DEPTH (M)	R (OHMS)	T (C)
14.50	0.49	12323.0	-1.841
14.57	1.49	12274.0	-1.751
14.63	2.49	12240.0	-1.688
14.68	3.49	12192.0	-1.600
14.73	4.49	12160.0	-1.540
14.78	5.49	12143.0	-1.509
14.85	6.49	12131.0	-1.486
14.92	7.49	12121.0	-1.468
14.95	8.49	12122.0	-1.469
15.05	8.82	12126.0	-1.477

LONG ISLAND  
HOLE LONGISC3  
790530  
14:30

79-B  
OCT L5N

CABLE  
BRIDGE

TIME	DEPTH (M)	R (OHMS)	T (C)
14.60	0.49	12221.0	-1.843
14.63	1.49	12181.0	-1.769
14.67	2.49	12144.0	-1.701
14.70	3.49	12098.0	-1.615
14.73	4.49	12066.0	-1.555
14.77	5.49	12047.0	-1.519
14.80	6.49	12039.0	-1.504
14.83	7.49	12035.0	-1.497
14.87	8.49	12038.0	-1.503
14.90	8.82	12037.0	-1.501

1  
LONG ISLAND  
HOLE LONGISD1  
79527  
16:50

79-2  
NEW L&N      CABLE  
                 BRIDGE

TIME	DEPTH (M)	R (OHMS)	T (C)
17.05	0.90	12289.0	-1.779
17.13	1.90	12245.0	-1.698
17.18	2.90	12202.0	-1.618
17.23	3.90	12181.0	-1.579
17.23	4.90	12167.0	-1.553
17.35	5.90	12159.0	-1.538
0.	6.85	11900.0	-1.051

DOCK HOLE A  
 DOCK HOLE DOCK A1  
 790516  
 11:25

72-1  
 NEW L&M

CABLE  
 BRIDGE

TIME	DEPTH (F)	R (OHMS)	T (C)
11.75	0.39	12862.0	-2.771
11.48	1.39	12535.0	-2.193
11.98	2.39	12384.0	-1.921
12.03	3.39	12269.0	-1.710
12.17	4.39	12188.0	-1.561
12.23	5.39	12139.0	-1.470
12.23	6.39	12110.0	-1.416
12.33	7.39	12095.0	-1.388
12.33	8.39	12095.0	-1.388
12.51	9.39	12101.0	-1.399
12.60	10.39	12125.0	-1.444
12.65	11.39	12150.0	-1.490
12.70	12.39	12175.0	-1.537
12.82	13.39	12207.0	-1.596
12.87	14.39	12240.0	-1.657
12.97	15.39	12280.0	-1.731
13.00	16.39	12315.0	-1.795
13.07	17.39	12356.0	-1.870

DOCK HOLE A  
HOLE DOCKA2  
790519  
14:50

79-1  
OLD L&M  
CABLE  
BRIDGE

TIME	DEPTH (M)	R (OHMS)	T (C)
15.15	1.39	12538.0	-2.202
15.18	2.39	12394.0	-1.942
15.25	3.39	12284.0	-1.741
15.32	4.39	12200.0	-1.587
15.33	5.39	12152.0	-1.498
15.38	6.39	12121.0	-1.440
15.43	7.39	12109.0	-1.418
15.47	8.39	12109.0	-1.418
15.52	9.39	12120.0	-1.438
15.55	10.39	12137.0	-1.470
15.60	11.39	12160.0	-1.513
15.65	12.39	12185.0	-1.559
15.70	13.39	12214.0	-1.613
15.75	14.39	12247.0	-1.673
15.82	15.39	12290.0	-1.753
15.85	16.39	12322.0	-1.811
15.95	17.39	12362.0	-1.884

DOCK HOLE A  
HOLE 0001A3  
790520  
09:00

79-3  
OIL L&H

CABLE  
BRIDGE

TIME	DEPTH (M)	R (OHMS)	T (C)
9.17	1.39	12402.0	-2.175
9.20	2.39	12267.0	-1.928
9.25	3.39	12160.0	-1.730
9.37	7.39	11994.0	-1.420
9.43	12.39	12069.0	-1.561
9.50	17.39	12244.0	-1.886



DOCK HOLE A  
HOLE DOCKA4  
790520  
11.24

79-3  
OLD L&N CABLE  
BRIDGE

TIME	DEPTH (M)	R (OHMS)	T (C)
11.57	1.39	12255.0	-1.906
11.62	2.39	12159.0	-1.729
11.70	3.39	12029.0	-1.486
11.75	4.39	11980.0	-1.393
11.90	5.39	11930.0	-1.299
11.95	6.39	11919.0	-1.278
12.02	7.39	11902.0	-1.245
12.12	8.39	11926.0	-1.291
12.17	9.39	11935.0	-1.308
12.28	10.39	11964.0	-1.363
12.33	11.39	11983.0	-1.399
12.38	12.39	12017.0	-1.463
12.48	13.39	12044.0	-1.514
12.57	14.39	12072.0	-1.566
12.72	15.39	12115.0	-1.647
12.77	16.39	12155.0	-1.721
12.82	17.39	12192.0	-1.790

DOCK HOLE A  
 HOLE DECK A5  
 790520  
 13:05

79-3  
 OLD L&M

CABLE  
 BRIDGE

TIME	DEPTH (M)	R (OHMS)	T (C)
13.32	1.39	12329.0	-2.042
13.37	2.39	12209.0	-1.821
13.47	3.39	12095.0	-1.609
13.52	4.39	12038.0	-1.503
13.60	5.39	11989.0	-1.410
13.65	6.39	11963.0	-1.361
13.72	7.39	11947.0	-1.331
13.77	8.39	11954.0	-1.344
13.83	9.39	11967.0	-1.369
13.92	10.39	11989.0	-1.410
13.97	11.39	12011.0	-1.452
14.02	12.39	12039.0	-1.504
14.27	13.39	12068.0	-1.559
14.33	14.39	12097.0	-1.613
14.38	15.39	12135.0	-1.684
14.43	16.39	12173.0	-1.755
14.50	17.39	12213.0	-1.829

DOCK HOLE A  
HOLE DOCKA6  
790520  
15:40

72-B CABLE  
OLD L&N BRIDGE

TIME	DEPTH (M)	R (OHMS)	T (C)
16.22	1.39	12364.0	-2.106
16.27	2.39	12232.0	-1.864
16.32	3.39	12117.0	-1.650
16.57	4.39	12053.0	-1.531
16.62	5.39	12008.0	-1.446
16.73	6.39	11978.0	-1.390
16.78	7.39	11966.0	-1.367
16.85	8.39	11972.0	-1.378
16.90	9.39	11981.0	-1.395
16.95	10.39	12001.0	-1.433
17.00	11.39	12023.0	-1.474
17.05	12.39	12048.0	-1.521
17.10	13.39	12077.0	-1.576
17.13	14.39	12107.0	-1.632
17.17	15.39	12146.0	-1.704
17.22	16.39	12183.0	-1.773
17.33	17.39	12223.0	-1.847

DOCK HOLE 3  
HOLE DOCK 31  
790527  
20:54

79-3  
NEW L&N  
CABLE  
BRIDGE

TIME	DEPTH (M)	R (OHMS)	T (C)
21.13	0.63	12688.0	-2.632
21.19	0.63	12753.0	-2.797
21.20	1.63	12443.0	-2.244
21.23	2.63	12283.0	-1.952
21.27	3.63	12169.0	-1.741
21.32	4.63	12087.0	-1.589
21.33	5.63	12040.0	-1.501
21.36	6.63	12010.0	-1.444
21.43	7.63	11999.0	-1.423
21.47	8.63	11999.0	-1.423
21.50	9.63	12006.0	-1.437
21.53	10.63	12023.0	-1.469
21.53	11.63	12048.0	-1.516
21.50	12.63	12074.0	-1.564
21.53	13.63	12103.0	-1.619
21.57	14.63	12143.0	-1.693
21.70	15.63	12181.0	-1.764
21.77	16.63	12217.0	-1.830
21.80	17.63	12252.0	-1.895
21.85	18.63	12292.0	-1.968
21.83	19.63	12329.0	-2.034
21.93	20.63	12367.0	-2.106
21.97	21.63	12409.0	-2.182
22.02	22.63	12447.0	-2.251
22.05	23.63	12485.0	-2.319
22.10	24.63	12529.0	-2.399

DOCK HOLE B  
HOLE DOCKB2  
790529  
21:19

79-3 CABLE  
OLD L&N BRIDGE

TIME	DEPTH (M)	R (OHMS)	T (C)
21.47	0.63	12804.0	-2.892
21.50	0.63	12786.0	-2.860
21.53	1.63	12459.0	-2.278
21.60	2.63	12299.0	-1.987
21.65	3.63	12185.0	-1.777
21.70	4.63	12103.0	-1.624
21.75	5.63	12053.0	-1.531
21.78	6.63	12025.0	-1.478
21.83	7.63	12010.0	-1.450
21.87	8.63	12008.0	-1.446
21.93	9.63	12019.0	-1.467
21.98	10.63	12035.0	-1.497
22.02	11.63	12057.0	-1.538
22.05	12.63	12082.0	-1.585
22.08	13.63	12111.0	-1.639
22.13	14.63	12147.0	-1.706
22.17	15.63	12186.0	-1.779
22.20	16.63	12223.0	-1.847
22.23	17.63	12258.0	-1.912
22.28	18.63	12298.0	-1.985
22.32	19.63	12334.0	-2.051
22.37	20.63	12375.0	-2.126
22.40	21.63	12414.0	-2.197
22.43	22.63	12452.0	-2.266
22.43	23.63	12492.0	-2.338
22.53	24.63	12538.0	-2.420

DOCK HOLE 3  
 HOLE DOCK 33  
 790601  
 10:14

79-1  
 OLD LB                      CABLE  
                                  BRIDGE

TIME	DEPTH (M)	R (OHMS)	T (C)
10.50	0.63	12797.0	-2.830
10.55	0.63	12771.0	-2.834
10.62	1.63	12460.0	-2.280
10.63	2.63	12305.0	-1.998
10.73	3.63	12191.0	-1.788
10.79	4.63	12109.0	-1.634
10.93	5.63	12051.0	-1.527
10.98	6.63	12031.0	-1.489
10.92	7.63	12016.0	-1.461
10.98	8.63	12016.0	-1.461
11.03	9.63	12025.0	-1.478
11.07	10.63	12038.0	-1.503
11.12	11.63	12057.0	-1.538
11.13	12.63	12084.0	-1.589
11.23	13.63	12114.0	-1.645
11.30	14.63	12147.0	-1.706
11.35	15.63	12186.0	-1.779
11.40	16.63	12225.0	-1.851
11.45	17.63	12261.0	-1.917
11.50	18.63	12301.0	-1.991
11.57	19.63	12335.0	-2.053
11.63	20.63	12377.0	-2.130
11.65	21.63	12413.0	-2.195
11.75	22.63	12453.0	-2.267
11.82	23.63	12495.0	-2.343
11.87	24.63	12538.0	-2.420

01 188 131 ANP  
 HOLE SERIAL  
 720502  
 13:12:00

70-1  
 100 CM.      ABLE  
                  RIDGE

TIME	DEPTH (M)	R (OHMS)	T (C)
13.43	0.60	12150.0	-1.725
13.63	1.60	12080.0	-1.576
13.72	2.60	12035.0	-1.491
13.77	3.60	12006.0	-1.437
13.83	4.60	11985.0	-1.397
13.95	5.60	11963.0	-1.355
14.00	6.60	11950.0	-1.331
14.05	7.60	11940.0	-1.312
14.22	8.60	11952.0	-1.335
14.25	9.60	11975.0	-1.378
14.37	10.60	11985.0	-1.397
14.55	11.60	12001.0	-1.427
14.65	12.60	12029.0	-1.480
14.70	13.60	12043.0	-1.516
14.75	14.60	12064.0	-1.546
14.78	15.60	12090.0	-1.594
14.88	16.60	12135.0	-1.678
14.95	17.60	12164.0	-1.732
15.00	18.60	12176.0	-1.754
15.03	19.60	12180.0	-1.762
15.15	20.60	12186.0	-1.773
15.13	21.60	12192.0	-1.784
15.30	22.60	12199.0	-1.797
15.35	23.60	12155.0	-1.715

REINDEER ISLAND  
 HOLE REID42  
 790510  
 13:15

TIME	DEPTH (M)	R (OHMS)	T (C)
13.53	0.60	12164.0	-1.732
13.55	1.60	12085.0	-1.585
13.80	2.60	12036.0	-1.493
13.85	3.60	12003.0	-1.431
13.90	4.60	11977.0	-1.382
13.93	5.60	11957.0	-1.344
14.00	6.60	11943.0	-1.318
14.10	7.60	11939.0	-1.310
14.18	8.60	11943.0	-1.318
14.23	9.60	11967.0	-1.363
14.32	10.60	11986.0	-1.399
14.35	11.60	12000.0	-1.425
14.42	12.60	12022.0	-1.467
14.47	13.60	12037.0	-1.495
14.53	14.60	12052.0	-1.523
14.56	15.60	12084.0	-1.583
14.68	16.60	12116.0	-1.643
14.73	17.60	12130.0	-1.669
14.80	18.60	12154.0	-1.714
14.85	19.60	12170.0	-1.743
14.92	20.60	12179.0	-1.760
15.00	21.60	12187.0	-1.775
15.08	22.60	12196.0	-1.792
15.13	23.60	12154.0	-1.714



REINDEER ISLAND  
 HOLE REINA3  
 790514  
 16:05

75-1 CABLE  
 REV L&T BRIDGE

TIME	DEPTH (M)	R (OHMS)	T (C)
17.33	0.60	12290.0	-1.749
17.43	1.60	12228.0	-1.635
17.53	2.60	12177.0	-1.541
17.58	3.60	12136.0	-1.464
17.70	4.60	12100.0	-1.397
17.75	5.60	12075.0	-1.351
17.82	6.60	12057.0	-1.317
17.87	7.60	12052.0	-1.307
18.92	8.60	12052.0	-1.307
18.00	9.60	12065.0	-1.332
18.07	10.60	12091.0	-1.380
18.12	11.60	12111.0	-1.418
18.18	12.60	12132.0	-1.457
18.23	13.60	12153.0	-1.496
18.30	14.60	12175.0	-1.537
18.35	15.60	12199.0	-1.581
18.40	16.60	12232.0	-1.642
18.45	17.60	12256.0	-1.686
18.52	18.60	12275.0	-1.721
18.57	19.60	12287.0	-1.743
18.62	20.60	12296.0	-1.760
18.72	21.60	12306.0	-1.778
18.82	22.60	12316.0	-1.797
18.87	23.02	12317.0	-1.798

REINDEER ISLAND  
 HOLE REIMA4  
 790524  
 09:24

79-2  
 NEW L&N

CABLE  
 BRIDGE

TIME	DEPTH (M)	R (OHMS)	T (C)
9.67	0.60	12270.0	-1.744
9.73	1.60	12206.0	-1.626
9.80	2.60	12158.0	-1.537
9.85	3.60	12119.0	-1.464
9.95	4.60	12088.0	-1.406
10.00	5.60	12063.0	-1.359
10.08	6.60	12050.0	-1.335
10.13	7.60	12043.0	-1.321
10.18	8.60	12044.0	-1.323
10.23	9.60	12051.0	-1.336
10.32	10.60	12068.0	-1.358
10.37	11.60	12088.0	-1.406
10.42	12.60	12116.0	-1.458
10.47	13.60	12143.0	-1.509
10.52	14.60	12164.0	-1.548
10.58	15.60	12194.0	-1.603
10.70	16.60	12221.0	-1.653
10.75	17.60	12240.0	-1.688
10.82	18.60	12254.0	-1.714
10.87	19.60	12264.0	-1.733
10.93	20.60	12274.0	-1.751
10.98	21.60	12281.0	-1.764
11.08	22.35	12287.0	-1.775

REINDEER ISLAND  
 HOLE REINA5  
 790527  
 09:08

BELFEN            CABLE  
 OLD L&N        BRIDGE

TIME	DEPTH (M)	R (OHMS)	T (C)
9.33	0.60	15003.0	-1.771
9.38	1.60	14851.0	-1.548
9.47	2.60	14774.0	-1.434
9.50	3.60	14786.0	-1.451
9.80	4.60	14683.0	-1.298
9.35	5.60	14652.0	-1.251
10.02	6.60	14629.0	-1.217
10.10	7.60	14603.0	-1.177
10.13	8.60	14613.0	-1.192
10.17	9.60	14614.0	-1.194
10.20	10.60	14613.0	-1.192
10.23	11.60	14625.0	-1.211
10.27	12.60	14639.0	-1.232
10.30	13.60	14688.0	-1.305
10.35	14.60	14729.0	-1.366
10.40	15.60	14765.0	-1.420
10.43	16.60	14812.0	-1.490
10.50	17.60	14890.0	-1.605
10.55	18.60	14933.0	-1.669
10.58	19.60	14947.0	-1.689
10.63	20.60	14962.0	-1.711
10.67	21.60	14970.0	-1.723
10.70	22.60	14979.0	-1.736
10.83	23.14	14986.0	-1.746

REINDEER ISLAND  
HOLE REIM A6  
790527  
12:51

WELFEN            CAPLE  
OLD L&N          BRIDGE

TIME	DEPTH (M)	R (OHMS)	T (C)
12.95	0.60	15042.0	-1.828
13.00	1.60	14874.0	-1.582
13.03	2.60	14798.0	-1.469
13.07	3.60	14754.0	-1.404
13.08	4.60	14712.0	-1.341
13.12	5.60	14676.0	-1.287
13.13	6.60	14645.0	-1.241
13.25	7.60	14631.0	-1.220
13.30	8.60	14625.0	-1.211
13.43	9.60	14626.0	-1.212
13.52	10.60	14633.0	-1.223
13.57	11.60	14641.0	-1.235
13.60	12.60	14669.0	-1.277
13.63	13.60	14705.0	-1.331
13.67	14.60	14741.0	-1.384
13.70	15.60	14772.0	-1.431
13.75	16.60	14810.0	-1.487
13.83	17.60	14880.0	-1.591
13.87	18.60	14931.0	-1.666
13.97	19.60	14950.0	-1.693
14.00	20.60	14960.0	-1.708
14.02	21.60	14970.0	-1.723
14.05	22.60	14975.0	-1.730
14.17	23.14	14975.0	-1.730

REINDEER ISLAND  
 HOLE REINA7  
 790527  
 16:40:00

TIME	DEPTH (M)	SELFEN	CABLE	T (C)
		OLD L&N	BRIDGE	
16.95	0.60		15051.0	-1.841
17.00	1.60		14890.0	-1.605
17.03	2.60		14814.0	-1.493
17.05	3.60		14769.0	-1.426
17.10	4.60		14732.0	-1.371
17.13	5.60		14691.0	-1.310
17.17	6.60		14665.0	-1.271
17.20	7.60		14649.0	-1.247
17.23	8.60		14645.0	-1.241
17.25	9.60		14650.0	-1.248
17.35	10.60		14656.0	-1.257
17.33	11.60		14671.0	-1.280
17.47	12.60		14697.0	-1.319
17.52	13.60		14718.0	-1.350
17.62	14.60		14758.0	-1.410
17.68	15.60		14795.0	-1.465
17.73	16.60		14833.0	-1.521
17.92	17.60		14897.0	-1.616
17.90	18.60		14934.0	-1.670
17.87	19.60		14957.0	-1.704
18.00	20.60		14969.0	-1.721
18.05	21.60		14981.0	-1.739
18.10	22.60		14997.0	-1.762
18.15	23.14		15009.0	-1.780

REINDEER ISLAND  
HOLE REINA8  
790529  
08:55

BELFEN            CABLE  
OLD L&N          BRIDGE

TIME	DEPTH (M)	R (OHMS)	T (C)
9.77	0.60	15100.0	-1.912
9.82	1.60	14976.0	-1.732
9.87	2.60	14885.0	-1.598
9.92	3.60	14879.0	-1.589
9.97	4.60	14770.0	-1.428
10.05	5.60	14740.0	-1.383
10.08	6.60	14704.0	-1.329
10.15	7.60	14696.0	-1.317
10.18	8.60	14691.0	-1.310
10.22	9.60	14693.0	-1.313
10.25	10.60	14700.0	-1.323
10.30	11.60	14722.0	-1.356
10.33	12.60	14745.0	-1.390
10.37	13.60	14771.0	-1.429
10.45	14.60	14807.0	-1.483
10.48	15.60	14842.0	-1.534
10.52	16.60	14875.0	-1.583
10.55	17.60	14922.0	-1.652
10.58	18.60	14947.0	-1.689
10.62	19.50	14969.0	-1.721

REINDEER ISLAND  
HOLE REINBI  
790508  
10:05

79-3  
NEW L&N

CABLE  
BRIDGE

TIME	DEPTH (M)	R (OHMS)	T (C)
10.23	0.12	12203.0	-1.804
10.32	1.12	12124.0	-1.658
10.43	2.12	12093.0	-1.600
10.48	3.12	12069.0	-1.555
10.53	4.12	12044.0	-1.508
10.62	5.12	12023.0	-1.469
10.72	6.12	12010.0	-1.444
10.83	7.12	12014.0	-1.452
10.90	8.12	12014.0	-1.452
10.97	9.12	12019.0	-1.461
11.00	10.12	12021.0	-1.465
11.13	11.12	12035.0	-1.491
11.23	12.12	12059.0	-1.536
11.30	13.12	12076.0	-1.568
11.33	14.12	12091.0	-1.596
11.38	15.12	12106.0	-1.624
11.42	16.12	12123.0	-1.656
11.43	17.12	12147.0	-1.701
11.52	18.12	12165.0	-1.734
11.58	19.12	12177.0	-1.756
11.67	20.12	12192.0	-1.784
11.85	21.12	12170.0	-1.743
11.92	22.12	12127.0	-1.663

REINDEER ISLAND  
HOLE REINB2  
790510  
13:30

79-3  
NEW LSN      CABLE  
                 BRIDGE

TIME	DEPTH (M)	R (OHMS)	T (C)
9.48	0.12	12220.0	-1.836
9.53	1.12	12149.0	-1.704
9.75	2.12	12109.0	-1.630
9.78	3.12	12079.0	-1.574
9.83	4.12	12053.0	-1.525
9.93	5.12	12028.0	-1.478
10.00	6.12	12014.0	-1.452
10.07	7.12	12009.0	-1.442
10.12	8.12	12014.0	-1.452
10.17	9.12	12017.0	-1.457
10.22	10.12	12021.0	-1.465
10.28	11.12	12031.0	-1.484
10.37	12.12	12058.0	-1.534
10.45	13.12	12074.0	-1.564
10.48	14.12	12091.0	-1.596
10.65	15.12	12108.0	-1.628
10.75	16.12	12136.0	-1.680
10.85	17.12	12146.0	-1.699
10.95	18.12	12155.0	-1.715
11.03	19.12	12166.0	-1.736
11.15	20.12	12180.0	-1.762
11.33	21.12	12169.0	-1.741
11.42	22.12	12134.0	-1.676



REINDEER ISLAND  
HOLE REINB3  
790523  
14:56

79-2  
NEW L&N

CABLE  
BRIDGE

TIME	DEPTH (M)	R (OHMS)	T (C)
15.60	0.12	12336.0	-1.865
15.65	1.12	12282.0	-1.766
15.70	2.12	12237.0	-1.683
15.75	3.12	12200.0	-1.615
15.83	4.12	12171.0	-1.561
15.90	5.12	12143.0	-1.509
15.95	6.12	12124.0	-1.473
16.00	7.12	12115.0	-1.456
16.07	8.12	12118.0	-1.462
16.19	9.12	12120.0	-1.466
16.23	10.12	12123.0	-1.471
16.30	11.12	12129.0	-1.482
16.35	12.12	12139.0	-1.501
16.43	13.12	12165.0	-1.550
16.55	14.12	12185.0	-1.587
16.62	15.12	12198.0	-1.611
16.68	16.12	12217.0	-1.646
16.78	17.12	12227.0	-1.664
16.87	18.12	12238.0	-1.685
16.97	19.12	12249.0	-1.705
17.02	20.12	12258.0	-1.722
17.08	21.12	12260.0	-1.725
17.13	22.12	12257.0	-1.720

REINDEER ISLAND  
HOLE REIN34  
790529  
11:27

BELFEN            CABLE  
OLD L&N          BRIDGE

TIME	DEPTH (M)	R (OHMS)	T (C)
11.53	0.12	15093.0	-1.918
11.62	1.12	15027.0	-1.822
11.87	2.12	14962.0	-1.727
11.93	3.12	14915.0	-1.658
11.97	4.12	14879.0	-1.605
12.02	5.12	14842.0	-1.550
12.05	6.12	14815.0	-1.510
12.08	7.12	14813.0	-1.507
12.12	8.12	14807.0	-1.499
12.15	9.12	14812.0	-1.506
12.18	10.12	14818.0	-1.515
12.27	11.12	30828.0	-1.530
12.33	12.12	14849.0	-1.561
12.37	13.12	14873.0	-1.596
12.40	14.12	14897.0	-1.632
12.43	15.12	14911.0	-1.652
12.47	16.12	14933.0	-1.685
12.50	17.12	14944.0	-1.701
12.53	18.12	14960.0	-1.724
12.57	19.12	14966.0	-1.733

HANSEER ISLAND  
 POLYETHYLENE  
 798507  
 09:29

79-  
 NET L&B      CABLE  
                  BRIDGE

TIME	DEPTH (M)	R (OHMS)	T (C)
09.07	0.00	12170.0	-1.743
09.15	1.00	12159.0	-1.723
09.32	2.00	12140.0	-1.688
09.37	3.00	12120.0	-1.650
09.93	4.00	12109.0	-1.630
10.25	5.00	12107.0	-1.626
10.30	6.00	12110.0	-1.632
10.37	7.00	12116.0	-1.643
10.42	8.00	12123.0	-1.656
10.47	9.00	12129.0	-1.667
10.52	10.00	12137.0	-1.682
10.55	11.00	12147.0	-1.701
10.63	12.00	12148.0	-1.702
10.78	13.00	12142.0	-1.691
10.97	14.00	12140.0	-1.688
11.02	15.00	12176.0	-1.754
11.08	16.00	12172.0	-1.747
11.12	17.00	12171.0	-1.745

REINDER ISLAND  
 HOLD BEING  
 790509  
 17:30

79-  
 NEW LOG. CABLE  
 BRIDGE

TIME	DEPTH (M)	R (OHMS)	T (C)
13.73	0.08	12166.0	-1.736
13.78	1.08	12173.0	-1.749
13.82	2.08	12145.0	-1.697
13.93	3.08	12124.0	-1.658
14.12	4.08	12114.0	-1.639
14.20	5.08	12109.0	-1.630
14.35	6.08	12111.0	-1.634
14.42	7.08	12117.0	-1.645
14.58	8.08	12110.0	-1.632
14.82	9.08	12128.0	-1.665
14.83	10.08	12139.0	-1.686
14.92	11.08	12145.0	-1.697
15.03	12.08	12146.0	-1.699
15.18	13.08	12177.0	-1.756
15.23	14.08	12176.0	-1.754
15.30	15.08	12166.0	-1.736
15.32	16.08	12160.0	-1.725
15.37	17.08	12165.0	-1.734

NEW ZEALAND ISLAND  
CABLE REPAIR  
270122  
15:35

79-1  
NEW LINE CABLE  
BRIDGE

TIME	DEPTH (F)	R (OHMS)	T (C)
15.30	0.00	12330.0	-1.322
15.35	1.00	12271.0	-1.714
15.39	2.00	12265.0	-1.703
15.42	3.00	12256.0	-1.686
15.45	4.00	12243.0	-1.662
15.48	5.00	12231.0	-1.640
15.50	6.00	12231.0	-1.640
15.52	7.00	12235.0	-1.648
16.00	8.00	12238.0	-1.653
16.05	9.00	12243.0	-1.662
16.10	10.00	12250.0	-1.675
16.15	11.00	12255.0	-1.685
16.20	12.00	12266.0	-1.705
16.25	13.00	12284.0	-1.738
16.30	14.00	12288.0	-1.745
16.35	15.00	12285.0	-1.740
16.40	16.00	12283.0	-1.736
16.45	16.80	12285.0	-1.740

REINDEER ISLAND  
HOLE REINC4  
790529  
08:55

79-3  
NEW L&N

CABLE  
BRIDGE

TIME	DEPTH (M)	R (OHMS)	T (C)
9.55	0.08	12217.0	-1.830
9.62	1.08	12177.0	-1.756
9.67	2.08	12150.0	-1.706
9.75	3.08	12141.0	-1.689
9.30	4.08	12128.0	-1.665
9.85	5.08	12112.0	-1.635
9.92	6.08	12115.0	-1.641
9.98	7.08	12111.0	-1.634
10.03	8.08	12115.0	-1.641
10.08	9.08	12124.0	-1.658
10.13	10.08	12131.0	-1.671
10.18	11.08	12141.0	-1.689
10.25	12.08	12150.0	-1.706
10.30	13.08	12165.0	-1.734
10.35	14.08	12170.0	-1.743
10.42	15.08	12164.0	-1.732
10.48	16.08	12163.0	-1.730
10.53	16.83	12163.0	-1.730

REINDEER ISLAND  
ICE REINGS  
790529  
17:40

79-3  
GLD LSN

CABLE  
BRIDGE

TIME	DEPTH (M)	R (OHMS)	T (C)
17.80	0.08	12145.0	-1.703
17.83	1.08	12010.0	-1.450
17.85	2.08	11793.0	-1.037
17.87	3.08	11731.0	-0.917
17.88	4.08	11634.0	-0.729
17.90	5.08	11660.0	-0.779
17.92	6.08	11598.0	-0.658
17.93	7.08	11608.0	-0.678
17.95	8.08	11690.0	-0.838
17.97	9.08	11706.0	-0.869
17.98	10.08	11832.0	-1.112
18.00	11.08	12007.0	-1.444
18.02	12.08	12040.0	-1.506
18.03	13.08	12069.0	-1.561
18.05	14.08	12105.0	-1.628
18.13	15.08	12055.0	-1.534

REINDEER ISLAND  
 GULE REINCA  
 790530  
 10:14

79-3                    CABLE  
 OLD L&A                BRIDGE

TIME	DEPTH (M)	R (OHMS)	T (C)
10.37	0.08	12234.0	-1.867
10.40	1.08	12150.0	-1.712
10.43	2.08	12080.0	-1.581
10.48	3.08	12050.0	-1.525
10.52	4.08	12024.0	-1.476
10.55	5.08	12004.0	-1.439
10.60	6.08	11980.0	-1.393
10.63	7.08	12006.0	-1.442
10.67	8.08	12067.0	-1.557
10.70	9.08	12068.0	-1.559
10.73	10.08	12082.0	-1.585
10.77	11.08	12102.0	-1.622
10.80	12.08	12111.0	-1.639
10.83	13.08	12134.0	-1.682
10.87	14.08	12131.0	-1.677
10.90	15.08	12129.0	-1.673



REINDEER ISLAND  
HOLE REINC7  
790530  
13:01

79-3                      CABLE  
OLD L&N                  BRIDGE

TIME	DEPTH (M)	R (OHMS)	T (C)
13.15	0.08	12231.0	-1.862
13.22	1.08	12152.0	-1.716
13.25	2.08	12101.0	-1.621
13.30	3.08	12069.0	-1.561
13.33	4.08	12045.0	-1.516
13.37	5.08	12018.0	-1.465
13.40	6.08	11999.0	-1.429
13.43	7.08	12025.0	-1.478
13.47	8.08	12078.0	-1.578
13.50	9.08	12079.0	-1.579
13.53	10.08	12088.0	-1.596
13.57	11.08	12107.0	-1.632
13.60	12.08	12115.0	-1.647
13.63	13.08	12139.0	-1.691
13.67	14.08	12137.0	-1.688
13.70	15.08	12133.0	-1.680
13.73	16.08	12126.0	-1.667
13.77	17.03	12149.0	-1.710

REINDEER ISLAND  
HOLE REINC8  
790530  
15:45

79-3  
OLD L&N

CABLE  
BRIDGE

TIME	DEPTH (M)	R (OHMS)	T (C)
15.78	0.08	12234.0	-1.867
15.82	1.08	12151.0	-1.714
15.85	2.08	12102.0	-1.622
15.90	3.08	12077.0	-1.576
15.93	4.08	12057.0	-1.538
15.97	5.08	12022.0	-1.472
16.02	6.08	12006.0	-1.442
16.05	7.08	12034.0	-1.495
16.08	8.08	12083.0	-1.587
16.12	9.08	12080.0	-1.581
16.15	10.08	12091.0	-1.602
16.18	11.08	12111.0	-1.639
16.22	12.08	12119.0	-1.654
16.25	13.08	12142.0	-1.697
16.28	14.08	12139.0	-1.691
16.32	15.08	12139.0	-1.691
16.35	16.08	12129.0	-1.673
16.38	17.03	12149.0	-1.710

1  
REINDEER ISLAND  
HOLE REINC9  
790531  
09:27:00

79-3            CABLE  
OLD L&N        BRIDGE

TIME	DEPTH (M)	R (OHMS)	T (C)
9.83	0.08	12230.0	-1.860
9.90	1.08	12156.0	-1.723
9.97	2.08	12122.0	-1.660
10.03	3.08	12101.0	-1.621
10.12	4.08	12090.0	-1.600
10.18	5.08	12056.0	-1.536
10.23	6.08	12046.0	-1.518
10.28	7.08	12068.0	-1.559
10.33	8.08	12090.0	-1.600
10.40	9.08	12092.0	-1.604
10.47	10.08	12099.0	-1.617
10.52	11.08	12114.0	-1.645
10.58	12.08	12124.0	-1.664
10.63	13.08	12140.0	-1.693
10.70	14.08	12137.0	-1.688
10.75	15.08	12138.0	-1.690

APPENDIX B

Subsea Permafrost - Summary of the Results of Probing, Thermal,  
Chemical and Hydrological Measurements and Analyses for  
RU253, 255 and 256, 1975-1979.

\*See main body of report for references and figures.

## Introduction

Subsea permafrost was formed on Alaska's continental shelves in the Bering, Chukchi and Beaufort Seas during emergent periods when sea levels were lower (e.g. - 100 m below present sea level about 18,000 years ago). These continental shelves have been subsequently inundated by rising sea levels and, more recently, by shoreline erosion in the presence of a static sea level. As a result, subsea permafrost is relic in nature, its presence and distribution being determined by sea bed boundary conditions (temperature and salinity), transport processes (heat and salt), and by the thermal and hydrological properties of the sea bed sediments. It appears to underlie most of the Beaufort Sea shelf, parts of the Chukchi Sea shelf and possibly some favorable parts of the Bering Sea shelf. It poses both engineering and scientific challenges that have been taken up seriously only in the last decade or less in Alaska, after an initial interest in the 1950's. University of Alaska research began in 1974 with support from the Sea Grant Program and the Alaska Oil and Gas Association (Rogers and others, 1975; Osterkamp, 1975; Osterkamp and Harrison, 1976a, b; Harrison and Osterkamp, 1976a, 1978b). The first non-proprietary work at Prudhoe Bay was carried out in April and May 1975 with support from the Sea Grant Program, the Alaska Oil and Gas Association, and OCSEAP (Osterkamp and Harrison, 1976, a,b). Since 1976 our research has been sponsored by OCSEAP and the National Science Foundation.

The spring 1975 work was carried out with the help of a conventional drill rig, crew and tracked supporting vehicles; two subsequent programs by CRREL-USGS and the USGS Conservation Division have been similar except on a larger scale. Since 1975 our approach has been to develop lightweight sled or aircraft portable drilling and probing equipment. The capabilities of this equipment are discussed in the next section. It cannot do everything a drill rig can, but because of its speed and portability it can provide large amounts of data in areas where it would be extremely expensive to mobilize a drill rig. The portability has allowed us to work in many areas; throughout the Beaufort Sea Lease Sale area; Harrison Bay, and Elson Lagoon in the Beaufort Sea, near Barrow and in the Hope Basin area of the Chukchi Sea, and in the Norton Sound area of the Bering Sea.

## Development of equipment and methods

A considerable effort, carried out largely with NSF support, has been put into the development of lightweight and efficient equipment and techniques for drilling, probe emplacement and in situ sampling and measurements in subsea permafrost. The drilling methods, basically driving and rotary-jetting, and other techniques are described in Section V of this report. The depth capability varies, but is on the order of 35 m into the sea bed. A partial list of the types of information that can be obtained at a given depth is as follows:

1. Soil type - soil samples are not taken but the soil type can often be determined from the behavior of the rotary-jetting rig or by recovery of soil fragments from driving tips or probes.

2. Presence of ice-bonded or ice-bearing permafrost.
3. Soil interstitial water properties - interstitial water samples can be obtained.
4. Soil hydraulic conductivity - this is basically the permeability.
5. Soil thermal conductivity.
6. Presence of ice - this can often be determined even if the sediments are not well ice-bonded.
7. Temperature and mean annual temperature at the sea bed.

Usually we do not attempt to determine all of this information in a given hole. Occasionally some of our holes have been located to extend information obtained from holes drilled and sampled with drill rigs or to provide ground truth to check the seismic interpretations of Rogers and Morack or Sellman et al. Other observations and measurements such as the details of nearshore bathymetry and sea ice thickness and the boundary conditions at the sea bed and their seasonal and regional variability have been made as well. Information such as shoreline retreat rate, thaw rate at the ice-bonded permafrost table and the nature of the heat and mass transport processes can often be inferred. This approach provides the necessary data and information on subsea permafrost properties and processes which can be used as an aid in the interpretation of seismic data and to infer its distribution and characteristics in a general way.

#### Processes

An understanding of the physical processes is basic to understanding the distribution and properties of subsea permafrost, and to the application of predictive thermal models in the Beaufort (Lachenbruch 1977) and Chukchi (Harrison, Dalley and Osterkamp, 1977) Seas.

A major portion of our NSF support has been focused on the study of the heat and mass transport processes that occur in subsea permafrost. The main goal of the work is to answer the following question: When onshore permafrost is inundated by the ocean due to shoreline erosion or sea level change, what happens, and how fast? A partial answer is that it depends upon the temperature and permeability. If temperature is negative, as it is over the Beaufort Sea shelf, salt must be transported to the ice-bearing permafrost through the developing thawed layer beneath the sea bed. If permeability is high, it can be shown that the soil interstitial water is gravitationally unstable and starts to convect, or to circulate through the soil, allowing rapid salt transport and rapid thawing characteristic of the Prudhoe Bay West Dock area. If permeability is low, convection cannot occur, and salt transport probably takes place by the extremely slow process of molecular diffusion, which results in the very slow thawing characteristic of the area outside the barrier islands at Prudhoe Bay. More details are given in section VI and VII and much remains to be learned. A more rigorous discussion including the effects of heat transport by moving interstitial water, boundary conditions at the thawed, frozen boundary, the coupling between heat and mass transport processes, etc., is given by Harrison and Osterkamp (1978 and 1979) or Osterkamp and Harrison (1978).

Another important process-related idea is that of partial freezing. Salt is obviously the new and important variable in subsea permafrost, and salty sediments may be partially frozen, with the fraction of the interstitial H<sub>2</sub>O in the liquid phase in coarse-grained soils due to the presence of dissolved salts being given approximately by the ratio of the initial freezing temperature of the water to the actual temperature (Harrison 1972, for example). In fine-grained soils additional unfrozen pore water due to soil particle effects may also be present. Such ice-bearing sediments may or may not be ice-bonded mechanically. Ice-bearing but ice-unbonded or partially bonded sediments have been observed in a seasonally active layer beneath the sea bed (Harrison and Osterkamp, 1979). Ice-bearing but ice-bonded sediments seem to be more common but they probably often contain liquid phase as well (Osterkamp and Harrison, 1976).

### Distribution and Properties

#### A. General Remarks

We have obtained data on subsea permafrost throughout the Beaufort Sea lease sale area (see Figure 1 of section V), Harrison Bay, Elson Lagoon, and in the Chukchi Sea at Barrow and near Kotzebue. Subsea permafrost, as defined by temperature regimes colder than 0°C, was found in all holes placed in the Beaufort and Chukchi Seas. Ice-bearing permafrost was found or was implied by negative temperature gradients in all holes except a hole in the Chukchi Sea near NARL. While most of these holes were within a few km of shore several were more than 25 km offshore. It should be noted that ice-bonded permafrost was found within 8 m of the seabed in a hole 5.9 km north of Reindeer Island where the water depth was about 17 m. Since subsea permafrost is relic, its thickness at a given site depends (among other things) upon its thickness at the time the ocean inundated that site. Consideration of the thickness of onshore permafrost suggests that it can vary by a factor of 2-3 for similar thermal boundary conditions. For example, the western segment of the arctic coastal plain has permafrost thicknesses on the order of 300 m while the eastern portion has thicknesses in excess of 600 m. There are large local variations, and the onshore permafrost may be perforated by thaw bulbs under large lakes and rivers. The above considerations, along with information from thermal modeling suggest that subsea permafrost is present over most of the shelf area of the Beaufort Sea, that its thickness may be highly variable even on a local basis, that it generally thins seaward, that it may contain perforations from paleo-lakes and rivers, and that the thickness of the unbonded permafrost at the sea bed is highly variable and probably controlled by soil type. Thermal modeling also suggests that most of this permafrost is relatively warm, probably within one or two degrees of its melting point.

We have also found that where the sea ice freezes to the sea bed and/or where there is restricted sea water circulation under the ice, an active layer up to a few meters in thickness may be present. This active layer may be underlain by a talik at distances of a few hundred meters or more offshore.

The properties of subsea permafrost are controlled by soil type, ice content, temperature and concentration of salts in the pore water or pore ice. Temperature and salt concentration vary strongly with the physical setting. Three different settings exist; where ice freezes to the sea bed, producing a cold annual active layer, where there is restricted circulation of sea water under the ice which may cause partial seasonal freezing of the sea bed, and where there is normal sea water under the ice. The effect of these settings is to cause substantial differences in the sea bed boundary conditions for the underlying permafrost, and resulting differences in thaw rates. In the cold, near-shore region, for example, little thawing takes place, and ice-bonded material is usually found a meter or two below the seasonally active layer at the sea bed. The data are sparse so far, but different conditions will obviously be expected in more complex settings involving estuaries, recently inundated lake and river beds, sites where sea ice ridges ground annually, etc.

Some brief remarks about specific geographic areas are made in what follows. Much of the information used in the discussion came from our boreholes, but some of the results of other OCSEAP investigators are implied. As noted earlier, a complete synthesis of current OCSEAP projects has not yet been undertaken.

#### B. Beaufort Sea Lease Sale Area

Figure 1 shows the locations of holes drilled in the lease sale area with additional information given in our OCSEAP reports of 1975-1979. Information is also available from other OCSEAP investigators and from the 1979 USGS offshore drilling program. There are large gaps in the data base; however some trends are emerging. While there is considerable variation in soil types, both regionally and in vertical profiles, it appears that the shallow sediments to the west of a line from Prudhoe Bay to Reindeer Island are primarily coarse (sands and gravels). To the east of this line the shallow sediments are relatively fine consisting of silts and clays which are sometimes very compact or consisting of a relatively thick layer of fine-grained sediments overlying sands and gravels. Generally, the ice-bearing or ice-bonded permafrost is close to the sea bed (within a few 10's of meters) in the fine-grained sediments and much deeper in the coarse-grained sediments.

A line of holes offshore from Long Island has shown that fine-grained sediments near the sea bed thin seaward and are underlain by sands and gravels.

The North Prudhoe Bay State-Reindeer Island line seems to be underlain by ice-bonded permafrost along its entire length. Nearshore in water of 2 m or less depth, where cold temperatures prevail, ice-bonded permafrost is separated from the sea bed only by a thin seasonal active layer. 500 m or so from shore, a thawed layer about 20 m thick has developed beneath the sea bed, which thickens rapidly seaward, particularly inshore of Reindeer Island, under what Hopkins suggests may be a paleo-river valley. Along this line the sediments are relatively permeable, and the rapid thawing that is taking place under the prevailing negative temperature regime seems to be due to rapid salt transport provided by large scale convection of the soil interstitial water in the thawed layer.



Offshore from Reindeer Island the situation is entirely different, and ice-bonded permafrost is found at shallow depths, typically 5 to 15 m beneath the sea bed. This condition seems to exist at least 6 km beyond the island, and probably further. The survival of ice so near the sea bed in material that has been inundated so long ( $\approx 10,000$  years), seems to be due to diffusive salt transport through the thawed layer, caused by an overlying cap of impermeable clay which prevents convection of the soil interstitial water.

One hole just off the Sagavanirktok River Delta apparently confirms Rogers and Morack's seismic interpretation with ice-bonded permafrost a few tens of meters below the sea bed. A hole offshore from Pt. Brower in 3 m of water probably encountered ice-bonded permafrost 5 1/2 m from the sea bed, and evidence for a thin layer of ice was found in this hole at the 16.2 m depth. A thicker layer of ice ( $\approx 1/2$  m) was also found in a nearby USGS hole somewhat farther offshore. These findings suggest that massive ice may still be present in these fine-grained soils some distance offshore.

A deep section of fine-grained sediments ( $>35$  m) was found offshore of Jeanette Island with ice-bonded permafrost at the 13.7 m depth.

Offshore from Flaxman Island, the sediments were fine-grained with the ice-bonded permafrost relatively close to the sea bed. There was a layer of fine-grained sediments 9.4 m thick just inshore of Flaxman Island underlain by sands and gravels.

#### C. Harrison Bay

Two holes were drilled in eastern Harrison Bay. Although shallow, these are of interest because, as noted earlier, they are near a possible onshore geologic boundary. Sands and gravels reminiscent of conditions in western Prudhoe Bay were found near Oliktok; fine-grained sediments were found south of Thetis Island.

#### D. Barrier Islands

Holes have been drilled on Reindeer, Stump, Cottle and Flaxman Island, in the Beaufort Sea. As at other sites, we have tried to overlap some areas covered by OCSEAP seismic studies by Rogers and Morack; pre-OCSEAP data, notably by Lewellen near Tapkaluk Island, and by industry on Reindeer Island also exist.

The vegetated tundra remnant portion of Cottle Island shows firm ice-bonded permafrost to the 6 m penetrated. This situation is probably typical of such islands. The Reindeer and Stump Island holes show that on the unvegetated islands the permafrost regime can be complex, varying irregularly both with depth and lateral position. Coarse-grained soils were predominant on Cottle and Stump Islands and fine-grained soils on Reindeer and Flaxman Islands.

#### E. Elson Lagoon

Eight holes were drilled and several additional probes were placed off Tekegokrok Point in Elson Lagoon near Barrow, (Osterkamp and Harrison,

1978; Harrison and Osterkamp, 1977). This line of holes shows, in an area of active shoreline retreat, the transition from cold near-shore conditions, where the ice freezes to the sea bed, to the warmer conditions in deeper water maintained by the presence of normal sea water under the ice. A seasonally active permafrost layer at the sea bed is well documented here. Pre-OCSEAP data in the Lagoon area also exist (Lewellen, 1973, 1974, 1976; Rogers and others, 1975). A thawed layer of generally increasing thickness can be traced out from shore under the sea bed.

Several curious features exist. The soils are fine-grained and generally two or three orders of magnitude less permeable than at Prudhoe Bay, although an extremely permeable aquifer was found at one site. Despite low permeability and negative sea bed temperatures, the thaw rates are an order of magnitude or two faster than in the clays off Prudhoe Bay, suggesting that fairly rapid salt transport through the thawed layer may occur, although this transport is not as efficient as at the West Dock.

#### F. Chukchi Sea

Little direct information about permafrost beneath the Chukchi Sea shelf exists, except as obtained from a total of five shallow near-shore holes at NARL, Barrow, and in the southeastern Chukchi Sea. Those at NARL show thermal evidence for a long-stable shoreline, and probably any ice-bearing permafrost there exists only very close to shore and is due to the proximity of the cold emergent land. The situation is quite different in the southeastern Chukchi Sea, where the holes show decreasing temperature with depth, the effect of shoreline recession, and indirect evidence for ice at depth. All holes so far are confined to within a few hundred meters from shore.

It seems entirely possible that permafrost might be widespread beneath the Chukchi Sea, because the entire area has been emergent and exposed to cold temperatures several times, and most recently only ~18,000 years ago. We have tried to face the question of the large scale permafrost distribution, using sea level history, seismic data, onshore borehole, geologic and oceanographic data, and simple theory. (Harrison, Dalley, and Osterkamp, 1976). This indirect approach suggests that in the southeastern Chukchi Sea site of the proposed Hope Basin sale - permafrost may now be absent beneath the deeper waters of the region, although it may well survive in areas shallower than 15-30 m. The borehole data indicate that it probably exists in many near-shore areas. Elsewhere in the Chukchi Sea, except at Barrow, the situation is even less clear. What has been done so far by our indirect approach in the Chukchi Sea provides a good background, but is not a substitute, for field observations.

#### Implications for Development

The distribution and some of the characteristics of subsea permafrost can be inferred from our boreholes. However, as noted above, the great variability in conditions and soil types makes the extrapolation of borehole data to large areas highly uncertain. The implication is that any offshore development will require site specific studies to define the local permafrost regime.

Sediment type appears to be one of the controlling factors that determines the presence or absence of ice-bonded permafrost near the sea bed. In coarse-grained sediments where the water depth is 2-3 m or greater we would not expect to encounter ice-bonded permafrost near the sea bed (i.e. within about 10 - 20 m). Where the water depth is less than about 2 m, ice-bonded permafrost and possibly massive ice may be encountered near the sea bed. In fine-grained sediments, independent of water depth, ice-bonded permafrost and massive ice may be found near the sea bed. The implications are that in coarse-grained sediments where the water depths are greater than 2-3 m it will probably not be necessary to design structures and pipelines for ice-bearing or ice-bonded soils. In addition, these coarse-grained sediments usually make good foundation material. In coarse-grained soils at water depths <2m and in fine-grained soils at all water depths it may be necessary to design offshore structures and pipelines for ice-bearing or ice-bonded soils. These considerations also suggest that offshore excavations for gravel or borrow material will have to take into account the presence or absence of ice-bonded permafrost. An example occurs north of Reindeer Island where a 10 m thick layer of compact clay was found underlain by frozen sands and gravels which would be very difficult to excavate even if the clays could be removed efficiently.

During our 1975 field season we identified the presence of highly concentrated brines in the near-surface sediments where the sea ice was frozen to the bottom. These brines could cause corrosion problems for pipelines and foundations.

Ice-bonded permafrost may be expected to be encountered within a few meters of the sea bed near-shore where the sea ice freezes to the sea bed. This may make it difficult to transect this region of actively thawing permafrost, where massive ice may be present, with pipelines or tunnels. A solution that we proposed during the Barrow Synthesis meeting in February 1977 was to construct a causeway out to the 2-3 m water depth and to bring the pipeline up through the causeway and then onshore along the causeway. However, these causeways will create other problems that must be resolved.

Gravel islands have been suggested as drilling platforms. Our studies of ice-bearing permafrost suggest that it may not be possible to develop sufficient ice-bonding within the islands to bond these islands to the sea bed thus reducing the shearing forces they can withstand.

Temperature measurements and theory suggest that subsea permafrost is very warm, probably within 1-2°C of its melting point. In addition, the pore water may be somewhat salty. These considerations suggest that production boreholes may never freeze-back at depth in the permafrost. On the other hand, a large thaw bulb will develop around them, and the resulting loading of the casings may be severe. Although oil is being successfully produced through the permafrost onshore at Prudhoe Bay, conditions tend to be quite different offshore, and substantial and probably expensive changes in techniques may be required.

APPENDIX C

Sediment-laden sea ice: The role of frazil  
and anchor ice in its formation and development.

by

T. E. Osterkamp

and

J. P. Gosink

SEDIMENT-LADEN SEA ICE: THE ROLE OF FRAZIL AND ANCHOR ICE  
IN ITS FORMATION AND DEVELOPMENT

by

T. E. Osterkamp

and

J. P. Gosink

Summary

Numerous observations over the past century have shown that nearshore ice often contains a significant amount of sediment -- sometimes much more than exists in the water column. Recent winter diving operations have confirmed these observations and have provided additional information on the nature of sediment-laden sea ice. It now appears that sediment-laden sea ice may play an important role in biological productivity, sediment transport processes and sea ice characteristics. Also, if sediments can be entrained in the ice cover then pollutants such as drilling muds, cuttings, oil, dredge spoils etc. can also be entrained. The important questions are:

1. What are the characteristics and distribution of sediment-laden sea ice?
2. What are the mechanisms by which sediments, and also pollutants can be entrained in sea ice?
3. What are the sediment sources, transport trajectories and transport distances?

Answers to these questions, as well as others, will be required before the implications of sediment entrainment in the sea ice cover for resource development can be resolved. The following is a summary of observations

on light transmission through the sea ice cover (Osterkamp, 1971), water and sea bed temperature measurements made during March, 1979, thin section analyses of ice cores obtained during March and November, 1979, and theoretical modeling of potential mechanisms for sediment entrainment in sea ice. Our results must be considered tentative since we have not completed the analyses however, preliminary indications based on a limited number of observations and ice cores are:

1. The sea bed did not appear to be frozen (ice-bonded) nor was any anchor ice observed on or in the sea bed.
2. A small amount of sediment in the ice cover can drastically reduce the light intensity under the ice. Clear sea ice had an extinction coefficient of  $\approx 0.01 \text{ cm}^{-1}$  while ice containing two thin layers of sediment had an extinction coefficient of  $\approx 0.10 \text{ cm}^{-1}$  or about an order of magnitude greater.
3. Cores taken from ice with a smooth surface contained less sediment than cores taken from ice with a rough or broken surface.
4. Ice crystals in cores from smooth ice were larger than ice crystals in cores from rough ice.
5. The sediment in the sea ice was found to reside at grain boundaries, intersections of 3 or more grains, and in or around bubbles. In one case the sediment seemed to be interior to an ice crystal.
6. The sediment particles appear to be clay, silt, and in one case fine sand. Plant debris, possibly of a peat origin, were often found in the thin sections.

7. The sediment particles in the ice occurred in flocs -- not as individual particles. These flocs appeared to contain numerous, perhaps  $10^1 - 10^3$  sediment particles.
8. Theoretical modeling of potential sediment entrainment mechanisms suggests several mechanisms that may act singly or in concert to entrain sediments in a sea ice cover. These include:
  - (a) Sediment entrainment during ice cover formation and development from derived frazil ice and sheet ice forms during periods of high turbulence (storms).
  - (b) Sediment entrainment and deposition from frazil ice formed in open water (as in leads or in a broken ice cover).
  - (c) Sediment entrainment by "katabatic" flow of a dense cold brine formed nearshore and draining downslope (offshore) where suspension of sediments and frazil ice formation can occur. Flow velocities may reach  $10 \text{ cm s}^{-1}$ , 3 1/2 km from shore according to our theoretical calculations. Sediment trapped in the frazil ice could then be deposited on the underside of an ice cover and/or incorporated into an ice cover.
  - (d) Anchor ice formation and subsequent flotation and incorporation of anchor ice containing bottom sediments into an ice cover or deposition under the ice cover.
  - (e) Discharge of sediment laden anchor ice from rivers into estuaries and subsequent incorporation into the sea ice cover.

It appears that 8(a) may be the most viable mechanism for sediment entrainment in a sea ice cover but that other mechanisms may also be operating. We are not considering the case of bottom gouging with subsequent incorporation of bottom material into the ice cover.

### Results and Discussion

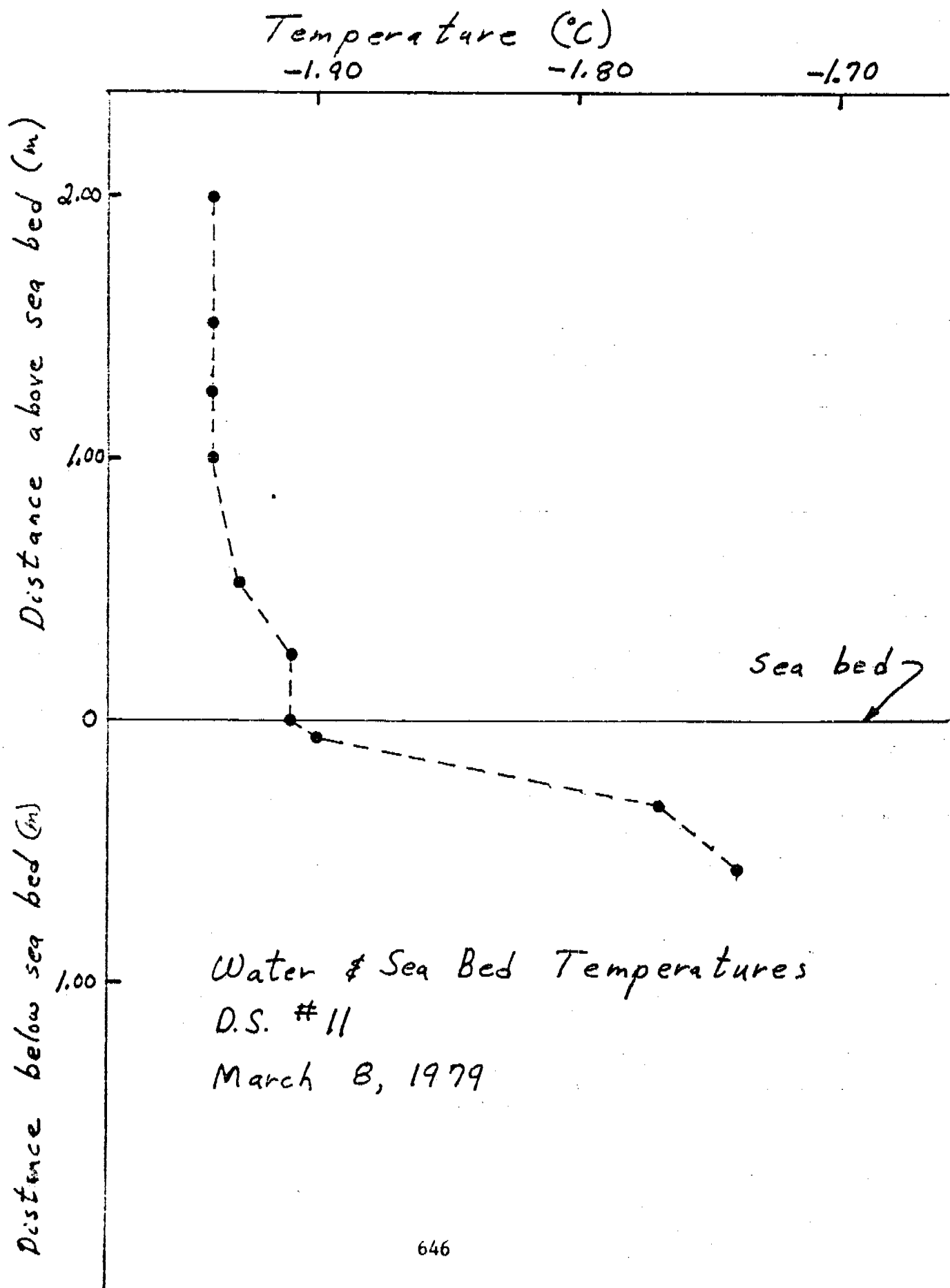
#### A. Water and Sea Bed Temperature Data

During late winter of 1979 we constructed a stainless steel probe 1/2 m in length, and  $\approx$  1 cm in diameter, containing 3 thermistor sensors. This probe was used to obtain precise temperature measurements in the water column and 1/2 m into the sea bed at DS #11 during March, 1979. Figure 1 shows the temperature profile obtained from these measurements. The temperature in the water column was constant at about  $-1.94^{\circ}\text{C}$  warming to about  $-1.91^{\circ}\text{C}$  at the sea bed. This warmer layer existed in the water column within  $\approx$  1.2 m of the sea bed. The temperature gradient in the sea bed is consistent with a water column temperature of  $-1.94^{\circ}\text{C}$  and suggests that the slight warming near the sea bed must have occurred a short time prior to the measurements ( $< 1$  day before). It is not known whether this warming was due to the presence of the diving hole or was the result of a natural process. A few salinity measurements were made by the divers (Dunton et al.,) but these were not sufficiently precise to determine if equilibrium conditions existed under the ice cover.

The sea bed was a very stiff silty clay with about 50-60% of the surface covered by pebbles and cobbles. There were also several 1/2 m diameter "pools" of soft mud in lenses 1-3 cm thick and several small accumulations of coarse, poorly sorted sand to granule size material on the surface (Reimnitz, personal communication).

The sea bed did not appear to be frozen (ice-bonded), judging from the temperature measurements and the penetration of the probe, although





precise measurements of the pore water salinity and a knowledge of soil particle effects would be required to confirm this observation. There were no observations of anchor ice growing on or in the sea bed during the diving operations.

#### B. Crystal Structure of Sediment-Laden Sea Ice

We obtained several short cores ( $\approx 1/2$  m) and samples of sediment-laden sea ice from the vicinity of DS #11 during March and November, 1979. These ice samples were returned to our laboratory in the frozen state. Horizontal and vertical thin sections were cut from the samples and photographed under both ordinary and polarized light. Figures 2 and 3 are photographs of these thin sections. These thin sections are presently being examined to determine grain size, nature of the sediment inclusions, position and distribution of the sediments in the ice etc. Our results must be considered tentative until we can complete the analysis. Preliminary results based on a limited number of cores are:

1. Cores taken from ice with a smooth surface contain less sediment than cores taken from ice with a rough or broken surface.
2. Ice crystals in cores from smooth ice are much larger, generally, than ice crystals in cores from rough ice. In smooth ice, some of the crystals exceeded a cm in maximum dimensions while in rough ice the crystals were usually less than a few mm in maximum dimensions with many less than 1 mm.
3. The sediment in the sea ice was found to reside at grain boundaries, intersections of 3 or more grains, and in bubbles. In one case, the sediment appeared to be interior to an ice crystal.

4. The sediment particles appear to be clay, silt, plant debris (possibly of peat origin) and, in one case, fine to medium sand. Table 1 shows the sediment concentrations in 4 ice cores obtained near DS #11.
5. The sediment particles in the ice occurred in flocs -- not as individual particles. These flocs contained numerous sediment particles, perhaps  $10^1 - 10^3$ . Floc sizes for the entrained sediments were usually on the order of a few tenths millimeter or less in maximum dimensions although a few flocs were found to be  $\approx 1$  mm in maximum dimensions.

#### C. Reduction of Light Intensity by a Sediment-Laden Sea Ice Cover

The reduction of light intensity by sea ice containing sediments was measured by Osterkamp (1971). Some of his data has been replotted in Figure 4 for two places in the sea ice cover, one (F-1) where the sea ice did not contain visible sediments and one (F-2) where two distinct, thin layers of sediment were found at the 23 cm and 33 cm depths. Figure 4 shows that the light extinction when sediments were present was substantially greater than sea ice without sediments. The extinction coefficient for clear ice was about  $0.01 \text{ cm}^{-1}$  compared to  $\approx 0.10 \text{ cm}^{-1}$  for the ice containing sediments. The amount of sediments in the ice was not measured but our impression was that while the ice appeared "dirty" the amount of sediments entrained in it was not large.

We conclude that relatively small amounts of sediments entrained in a sea ice cover can drastically reduce the light intensity under the ice cover.

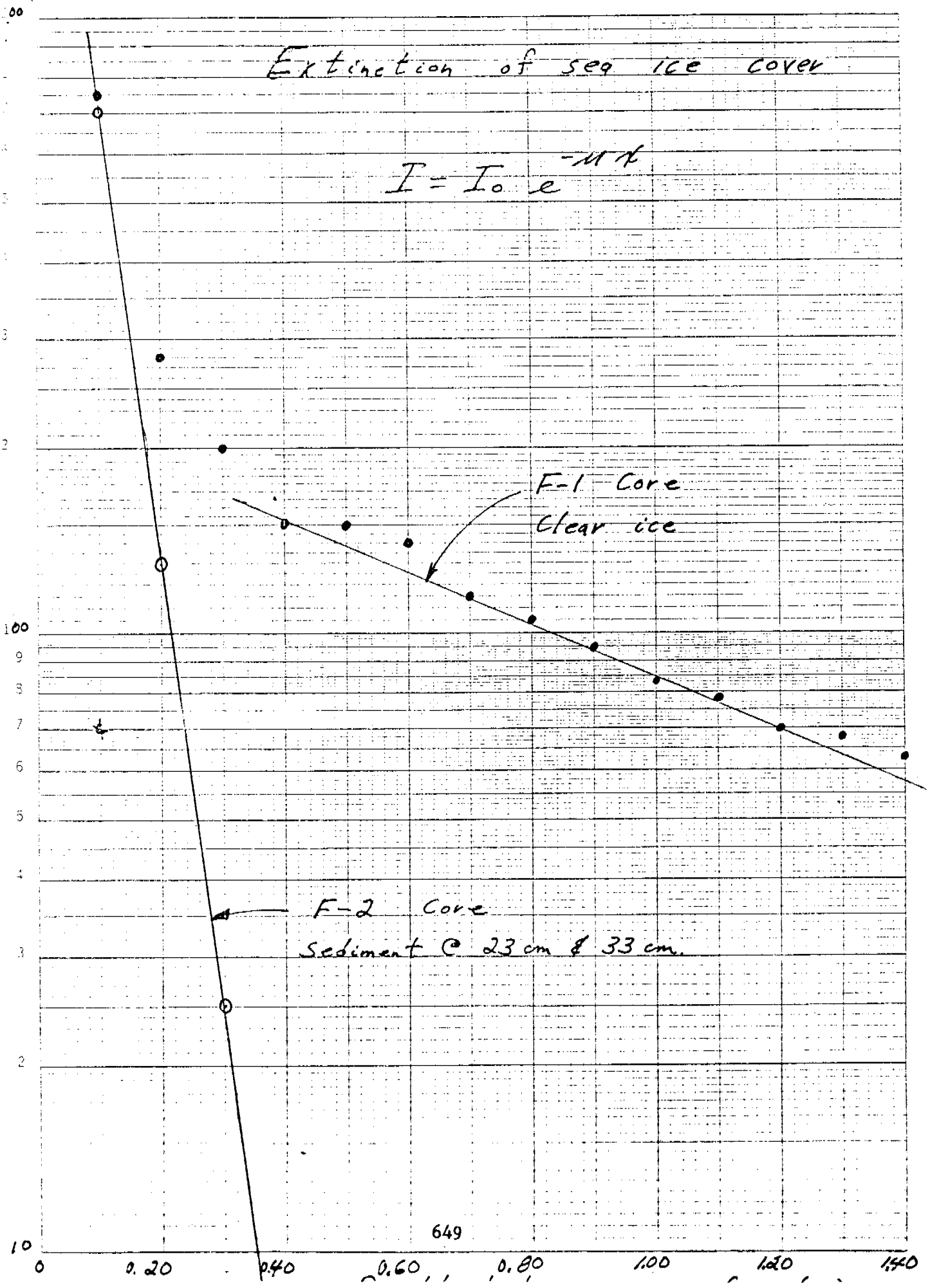
#### D. Potential Mechanisms for Sediment Entrainment in Sea Ice

This is an attempt to define potential mechanisms for sediment entrainment in an ice cover. Its purpose is to focus attention on what

Ln Photocell current (mA)

# Extinction of sea ice cover

$$I = I_0 e^{-kx}$$



TYPE 2 KEUFFEL & ESSER CO. MADE IN U.S.A.

may be the most likely mechanisms and also to provide basic information to divers, biologists, geologists and others on underwater ice formation and the ways in which it can result in entrainment of sediment in an ice cover. The mechanisms we consider involve frazil ice in some form or at some stage of development. We do not include such mechanisms as rafted sediments in highly deformed ice nor the case where ice freezes to the sea bed by conductive heat transfer. We also recognize that many details of frazil ice formation are poorly known which, in turn, hinders our understanding of potential mechanisms. Frazil ice is defined to be thin disc crystals which grow in supercooled water and other ice forms derived from these discs or which are later stages in the evolutionary history of these discs (e.g. grease ice, frazil slush, shuga, frazil pans, frazil floes etc.) The mechanisms defined herein could act singly or in concert to entrain sediments in the ice cover. In general, the present observations and data are too fragmentary to decide on the relative importance of a mechanism or a combination of mechanisms. The following is a discussion of mechanisms according to the degree of turbulence in the water since it seems to be agreed that the observations can best be explained by events that cause turbulence and suspension of sediments in the water columns. We proposed these mechanisms at the Seattle "slush ice" meeting and have benefitted from the discussions at that meeting. Two additional mechanisms; frazil ice billows (S. Martin) and frazil ice formation in a broken ice cover (M. Coon) were also proposed at the Seattle meeting.

1. "Katabatic" flow and bottom water formation

The possibility of a cold density current formation exists on the shallow, sloped sea bed of the Beaufort Sea Shelf, especially near shore.

This phenomenon could be initiated by saline plumes associated with surface heat loss. We anticipate that these plumes would be of maximum strength (i.e. flux density per unit surface area) during periods of high heat loss such as low air temperature over open water. When the plumes attain sufficient strength, the conditions exist for frazil ice growth at depth and also suspension of bottom sediments or continued suspension of bottom sediments as after a storm. Simple models of this process show that downslope salinity plume velocities may reach  $5 \text{ cm sec}^{-1}$  within 1 km of shore and  $10 \text{ cm s}^{-1}$  within 3.5 km of shore (Gosink and Osterkamp, unpublished). This process provides both the heat sink at depth necessary for frazil ice growth and the bottom friction required to suspend fine sediments. It is postulated that sediment particles may adhere to frazil ice particles or be trapped in frazil flocs and subsequently entrained in the ice cover. This process could also lead to anchor ice formation with subsequent incorporation of sediments into the ice cover by the processes noted in 4 below. The mechanism suggests that the nearshore bottom currents should be downslope along the sea bed and that a return flow (upslope) should exist under the ice cover.

The theoretical analysis follows closely standard theory for gravity driven density currents. The primary difference is in the determination of the "buoyancy flux", -- the excess weight flux. This quantity is conserved in standard density current theory when a constant point source of mass flux is assumed. For example, a cold river influx into a bay or snow avalanche may be modeled as point source.

The source of excess weight flux for the katabatic case, however, is the uniform radiative heat loss. Similarly, a density current in the

nearshore area may be initiated by a uniform distribution of salinity plumes -- a rain of excess mass flux formed by rejection of brines during ice formation. If pancake ice, frazil floes, grease ice, etc. are randomly distributed in the nearshore area and ice growth proceeds laterally from these configurations, then it is reasonable to assume that salinity plumes are uniformly distributed at the sea surface.

When these assumptions are made, the excess mass flux transported past any offshore and downslope location increases linearly with distance from the shore. Hence velocities in katabatic flow, and in the present case of brine currents, will increase downstream. In particular, for a constant slope and brine flux, it may be readily shown that velocity increases as the cube root of distance offshore. For surface heat loss of  $1.8 \times 10^{-2} \text{ cal cm}^{-2} \text{ s}^{-1}$  (typical loss at  $T_{\text{air}} = -24^\circ\text{C}$ ) and slope angle of  $2^\circ$ , this theory predicts velocities of  $10 \text{ cm s}^{-1}$  at 3.5 km from shore. It should be noted that this estimate is formulated by assuming total rejection of salt during ice formation. However, a brine rejection of 40% causes a reduction in velocity of only 74%.

These bottom velocities may be compared with observed values (B. Matthews, personal communication) from 5 to 15 cm/sec directed offshore. Critical velocities for suspension of unconsolidated fine grain material are of the order of  $10\text{-}15 \text{ cm s}^{-1}$ . These velocities may be reached by the bottom current within 1 km of shore when surface heat loss is  $6.5 \times 10^{-2} \text{ cal cm}^{-2} \text{ s}^{-1}$ .

## 2. Frazil formation in open water and subsequent deposition under an adjacent ice cover

Density driven convection plumes in open water may carry frazil ice crystals downwards into the water column. Calculations show that vertical water

velocities may be on the order of  $10 \text{ cm s}^{-1}$ . When no currents are present these plumes would deposit the frazil under the adjacent ice cover in a Gaussian distribution. When currents are present, the frazil would be deposited downstream of the open water. Protrusions of ice from under the ice cover would accelerate frazil deposition on the upstream side of these ice projections. It is conceivable that some of the sediment in the water would be swept out by adhesion to frazil crystals or by inclusion in frazil flocs and subsequently be deposited along with the frazil. Coon (Seattle slush ice meeting) suggests a similar mechanism where a broken ice cover could behave as an area of partially open water and could therefore give rise to frazil formation and deposition by the above processes and also by inclusion of sediment in the frazil slush formed between ice pieces.

Standard plume theory may be used to model the velocity and density distributions for a given surface heat loss. For a surface heat loss of  $2 \times 10^{-2} \text{ cal cm}^{-2} \text{ s}^{-1}$  and a well mixed column, this theory predicts downward plume velocities of 2 to  $10 \text{ cm s}^{-1}$  depending upon the area of ice formation. Assuming that ice growth occurs mainly at the edge of ice floes, pancakes, frazil conglomerates, or a broken ice cover, convection plumes are enhanced during the period of formation of the ice cover.

Frazil particles carried down by salinity plumes may be expected to grow whenever the water column is slightly supercooled. Laboratory studies indicate that the growth rate for frazil particles may be proportional to the square root of the water-ice particle relative velocity. Since the frazil particles are slightly buoyant, there exists a non-zero relative velocity between the particles and the plume. However, when the



downward force on a particle is exactly balanced by the net buoyant force, the frazil particle reaches its maximum depth. Initial estimates indicate that for relative velocities of  $0.5 \text{ cm s}^{-1}$ , a typical frazil disc diameter of  $\approx 0.1 \text{ cm}$  may be expected at maximum depth.

It is expected that the horizontal distribution of frazil particles in a salinity plume is similar to the horizontal distribution of velocity in the plume, -- a Gaussian distribution. Hence, in the absence of cross currents, frazil particles may be deposited under the ice cover as a Gaussian distribution. Where a cross current exists, they will be carried downstream of the open water and deposited there. A simple model of this deposition process, for smooth bottom ice, predicts an exponentially decaying distribution of frazil with downstream distance from the lead edge. Where rough ice is found, frazil would probably be deposited preferentially on the upstream side of an underwater ice projection.

The time scale for formation of salinity plumes and convection cells depends critically upon the stability of the water column, in particular upon the existing salinity gradient. When the water column is very stably stratified, say with a density difference of 1% over 1 meter, and surface heat loss is  $\approx 2 \times 10^{-2} \text{ cal cm}^{-2} \text{ s}^{-1}$  it may be shown that the time required for formation of convection cells is of the order of 10 to 40 days. However, when the water column is well mixed, say  $10^{-5}\%$  density differences over 1 meter, then the penetration time scale to a depth of 10 meters is less than 1 hour. Hence the development of convection cells is rapid when the sea water is unstratified, for example, after a storm, or in the nearshore area where the water is well mixed due to shear.

#### 4. Sediment entrainment by ice formation on or in the sea bed (anchor ice)

When ice forms on or in the sea bed, subsequent flotation of that ice can result in the incorporation of sea bed sediments into the ice cover. There are three potential mechanisms for this type of ice formation. The first, and perhaps most significant mechanism is that of anchor ice formation on the sea bed. This mechanism has been observed in both fresh water and sea water. Generally, frazil ice deposits on the sea bed forming anchor ice which freezes to the sea bed. Flotation of the anchor ice by buoyancy (resulting from increased ice growth) or by breaking of ice bonds by partial melting at the sea bed raises sea bed material to the surface where it floats or is incorporated into the underside of an existing ice cover. A second mechanism involves estuaries where the sea bed sediments may be freshened by fresh water flow during the summer. Flow reduction during freeze-up may lead to a cold sea water wedge intruding over the freshened sediments. Since these sediments contain fresh water that would freeze near 0°C, ice could form in the sediments. Sediment entrainment and flotation would occur as above. A third mechanism involves sea bed freezing in very shallow water where the ice does not freeze to the sea bed but where restricted circulation exists. Brine concentration and consequent reduction of under ice water temperatures may lead to freezing of normal salinity pore water in the sea bed. This phenomena has already been observed (Osterkamp and Harrison, 1980). Again, flotation could occur as above.

The nature of the sediments incorporated into the ice cover would be identical to those on the sea bed although ice movement after flotation may cause some confusion on this point. Generally, these mechanisms would be expected to give rise to entrainment and transport of coarser material such

as rocks, pebbles, gravel, kelp, mollusks, etc. This appears to be a unique way to suspend and transport these coarser materials, although its relative importance is unknown.

5. Sediment entrainment during ice cover formation at times of high turbulence

Under calm sea conditions, sea ice forms as a sheet ice cover which has relatively smooth air-ice and ice-water interfaces. As the turbulence in the water column increases due to wind and currents the resulting ice cover becomes quite different in nature. Frazil ice forms in the turbulent water and then evolves into a series of derived ice forms that eventually freeze together constituting the initial ice cover. These derived frazil ice forms are usually frazil slush or grease ice, frazil billows, shuga, pancakes, pans, floes and brash ice although pancakes, pans, floes and brash ice can also be formed by the breaking of a thin ice cover. The ice cover that evolves from frazil slush or grease ice, frazil billows and shuga would typically have a surface relief on the order of centimeters while the ice cover evolved from pancakes, pans, floes and brash ice would have a surface relief of tens of centimeters or more. Under conditions of extreme turbulence, as during a severe storm, the resulting ice cover may be a combination of all these ice types. Additional ice forms such as "rough ice", pressure ridges, shear ridges, ice piles etc. may develop with surface relief of meters to 10's of meters. The resulting ice cover may consist of broken ice chunks, pancakes, pans and floes embedded in a congealed frazil slush with open water holes and leads that may eventually freeze over with sheet ice under less turbulent conditions at a later time.

The underside of this ice cover would have a widely varying relief and nature somewhat similar to the upper surfaces . Specifically, the underside of the ice cover may have smooth areas, projections of broken ice and frazil pans, "rough ice", ridge keels etc. In addition, once the ice cover has formed the decaying turbulence may allow frazil ice crystals suspended in the water column to deposit in a slushy layer under the ice cover.

The turbulence that produces frazil ice can also suspend sediment in the water column. This sediment would be mixed throughout these frazil ice forms and trapped in them. It may also be possible for the frazil ice to sweep sediment particles from the water column by surface tension and adhesive forces thus concentrating the sediment in the ice cover. When the ice cover has been initiated, the sediment would be incorporated into it. We believe that the above described mechanism may be primarily responsible for the incorporation of fine-grained sediment into the sea ice cover.

#### 6. Discharge of sediment laden anchor ice, formed in rivers, into the ocean

It is well-known that sediment incorporated into anchor ice in rivers can be suspended and transported downstream. Usually the sediment is coarse material (gravel). Where rivers flow into the ocean, this sediment laden anchor ice can become part of the sea ice cover (Benson and Osterkamp 1975). Obviously this mechanism would be most important in estuaries or near rivers that carry anchor ice into the ocean.

#### Needs for Further Study

There are three crucial questions that must be answered before we can assess the importance of sediment-laden sea ice to problems of resource

development. These are:

1. What are the characteristics and distribution of sediment-laden sea ice?
2. What are the mechanisms by which sediments, and also pollutants, can be entrained in sea ice?
3. What are the transport trajectories and transport distances for sediment entrained in sea ice?

Answers to 1. above could be obtained by a wide-ranging coring program which would include studies of crystal structure and entrained sediments and diving at selected sites. Our thin section analysis at D.S. #11 is limited to this one site although we plan to obtain sea ice cores with entrained sediments in Norton Sound, Chukchi Sea and at several places in the Beaufort Sea during April and May of this field season (1980).

Answers to 2 above could be obtained by a field program designed to determine the types and stages of ice cover development as they relate to sediment entrainment mechanisms. Measurements of the temperature, salinity currents and sediment concentrations in the water column before, during and just after ice cover initiation when coupled with information from 1 above should define the mechanisms of sediment entrainment and help to answer questions on potential pollution entrainment in the sea ice cover. Answers to 3 above could be obtained by studying the mineralogy of sea ice sediments with comparison to the local sea bed sediments. It may also be possible to tag the sediments with a tracer before freeze-up and to relocate them in the ice after freeze-up to determine the transport trajectories and transport distances.

Other important questions have been delineated by the participants of the Seattle slush ice meeting and the winter studies synthesis

meeting. These are outlined in the documentation of those meetings.

#### Acknowledgements

We are indebted to many individuals for help during our field studies and for discussions on this problem. In particular, we would like to thank K. Dunton, E. Reimnitz, S. Naidu, R. Gaffi, J. Hanscom, C. Stephens and the participants of the Seattle slush ice meeting.

## References

1. Osterkamp, T. E. (1972). Properties of ice in the Colville River area. In, Baseline data study of the Alaskan arctic aquatic environment, report R72-3, Inst. of Marine Science, University of Alaska, Fairbanks, Alaska.
2. Osterkamp, T. E. and W. D. Harrison, (1980). Annual report, RU 253, 255, 256, OCSEAP, Arctic Project Office, University of Alaska, Fairbanks, Alaska.
3. Benson, C. S. and T. E. Osterkamp, (1974). Underwater ice formation in rivers as a vehicle for sediment transport. In, Oceanography of the Bering Sea, D. W. Hood and E. J. Kelley, eds., Inst. of Marine Science, University of Alaska, Fairbanks, Alaska.

Table 1: Sediment concentrations in 4 ice cores obtained near DS #11 in November, 1979. These concentrations were measured by Dr. S. Naidu.

<u>Core</u>	<u>Depth (cm)</u>	<u>Concentration (mg-ℓ<sup>-1</sup>)</u>
AV	0-7	209
	8-15	123
	17-24	92
	26-33	98
	35-42	221
	43-50	110
BV	1-7	37
	9-15	66
	17-24	44
	26-33	43
	34-40	281
	41-49	127
CV	51-59	192
	2-8	260
	10-16	352
	19-24	52
	26-32	42
	34-40	41
DV	42-bottom	57
	2-8	142
	10-17	732
	19-25	596
	28-35	87
	37-42	53
43-bottom	96	



### List of Figures

- Figure 1: Temperature profile in the water column and sea bed at DS #11.
- Figure 2: Photographs of thin sections of sediment-laden sea ice illustrating their fabric.
- Figure 3: Micro-photographs of thin sections of sediment-laden sea ice showing the sediment inclusions.
- Figure 4: Natural logarithm of photocell current which is proportional to the light intensity vs. depth in normal and sediment-laden sea ice.

## APPENDIX D

Ice coverage and temperature data in the Chukchi Sea  
used to assess the presence and distribution of  
subsea permafrost.

Table 1.

Ice cover data in areas bounded by 1° of longitude and 30' of latitude. The boundaries of the areas are given in the first two columns. Percent ice cover in each half monthly period is given in the other columns. Parts I and II of the table are for the southern and northern Chukchi Sea respectively, as defined by latitude 69°N.

## PART I

N Boundary	W Boundary	J	F	M	A	M	J	J	A	S	O	N	D											
66°	168°	60	80	60	80	80	60	80	40	40	20	10	0	0	0	0	0	0	0	0	20	40	60	40
66°	169°	60	60	80	80	80	60	60	40	40	40	10	10	0	0	0	0	0	0	0	40	40	60	40
66°	170°	100	40	80	80	80	60	60	40	40	20	10	0	0	0	0	0	0	0	0	60	20	(60)	(60)
66°30'	162°	100	100	60	80	80	80	100	80	60	60	40	20	10	0	0	0	0	20	20	40	40	(60)	(60)
66°30'	163°	100	100	60	80	0	0	100	80	60	60	40	20	10	0	0	0	0	20	20	40	40	(60)	(60)
67°	163°	100	100	60	80	80	80	100	80	60	60	40	20	10	0	0	0	0	20	20	40	40	(60)	(60)
66°30'	164°	100	100	60	80	80	80	100	80	60	60	40	20	10	0	0	0	0	20	20	40	20	(60)	(60)
67°	164°	100	100	60	80	80	80	100	80	60	60	40	20	10	0	0	0	0	20	20	40	20	(60)	(60)
67°	165°	100	100	60	60	80	80	100	80	40	60	40	20	10	0	0	0	0	0	20	20	(60)	(60)	
66°30'	166°	100	100	60	60	80	80	80	60	40	60	40	20	10	0	0	0	0	0	0	20	40	(60)	(60)
67°	166°	100	100	60	60	80	80	80	60	40	60	40	20	10	0	0	0	0	0	0	20	40	(60)	(60)
66°30'	167°	100	100	60	60	80	80	80	60	40	60	20	10	0	0	0	0	0	0	0	20	40	40	60
67°	167°	100	100	60	60	80	80	80	60	40	60	20	10	0	0	0	0	0	0	0	20	40	40	60
66°30'	168°	60	80	60	80	80	80	80	60	40	40	20	10	0	0	0	0	0	0	0	20	40	40	60
67°	168°	60	80	60	80	80	80	80	60	40	40	20	10	0	0	0	0	0	0	0	20	40	40	60
66°30'	169°	60	60	60	80	80	80	80	60	40	40	20	10	0	0	0	0	0	0	0	40	40	40	60
67°	169°	60	60	60	80	80	80	80	60	40	40	20	10	0	0	0	0	0	0	0	40	40	40	60

N Boundary	W Boundary	J	F	M	A	M	J	J	A	S	O	N	D												
66°30'	170°	100	100	60	80	80	40	60	40	40	20	10	0	0	0	0	0	0	0	0	60	20	40	40	
67°	170°	100	100	60	80	80	40	60	40	40	20	10	0	0	0	0	0	0	0	0	60	20	40	60	
67°	170°40'	100	100	60	80	80	40	60	40	40	20	10	0	0	0	0	0	0	0	0	60	20	40	(60)	
67°30'	164°	100	100	60	80	80	80	100	80	40	40	40	10	10	0	0	0	0	0	0	40	60	(100)	(100)	
67°30'	165°	100	100	60	80	80	80	80	60	40	20	20	10	10	0	0	0	0	0	0	20	60	(100)	(100)	
68°	165°	100	100	60	80	80	80	80	60	40	20	20	10	10	0	0	0	0	0	0	20	60	(100)	(100)	
67°30'	166°	100	100	60	60	80	80	60	60	40	20	20	10	10	0	0	0	0	0	0	20	60	(100)	(100)	
68°	166°	100	100	60	60	80	80	60	60	40	20	20	10	10	0	0	0	0	0	0	20	60	(100)	(100)	
67°30'	167°	100	80	60	60	80	80	80	40	40	20	20	10	10	0	0	0	0	0	0	20	40	40	(100)	
68°	167°	100	80	60	60	80	80	60	40	40	20	20	10	10	0	0	0	0	0	0	20	40	40	(100)	
67°30'	168°	100	60	60	60	80	60	80	40	40	20	20	10	0	0	0	0	0	0	0	50	70	40	(100)	
68°	168°	100	60	60	80	80	60	80	40	40	20	20	10	10	0	0	0	0	0	0	50	70	40	(100)	
67°30'	169°	100	60	60	80	80	60	80	40	40	20	20	10	0	0	0	0	0	0	0	60	60	40	(100)	
68°	169°	100	60	60	80	80	60	80	40	40	20	20	10	10	0	0	0	0	0	0	60	60	40	(100)	
67°30'	170°	100	60	60	80	80	40	80	40	40	20	20	10	0	0	0	0	0	0	0	(40)	60	(100)	(100)	
68°	170°	100	60	60	80	80	60	80	40	40	20	20	10	10	0	0	0	0	0	0	(40)	60	(100)	(100)	
67°30'	170°40'	100	80	80	80	80	60	80	(60)	20	20	20	10	0	10	0	0	0	0	0	(40)	(40)	(100)	(100)	
68°30'	166°	100	60	60	60	80	80	60	40	40	20	20	10	10	0	0	0	0	0	0	20	40	40	(100)	
69°	166°	100	60	60	60	80	80	80	60	40	60	20	10	10	0	0	0	0	0	0	20	20	40	60	(100)
68°30'	167°	100	60	60	80	80	80	60	40	40	20	20	10	10	0	0	0	0	0	0	20	20	40	40	(100)

N Boundary	W Boundary	J	F	M	A	M	J	J	A	S	O	N	D											
69°	167°	100	60	80	100	80	80	60	60	40	20	20	10	10	0	0	0	0	0	20	20	40	40	(100)
68°30'	168°	100	60	80	100	80	60	80	40	40	20	40	10	10	0	0	0	0	0	20	20	40	40	(100)
69°	168°	100	60	80	100	80	60	80	60	40	20	40	10	10	0	0	0	0	0	20	20	40	40	(100)
68°30'	169°	100	80	80	100	80	60	60	40	40	20	40	10	10	0	0	0	0	0	0	(40)	40	40	(100)
69°	169°	100	80	80	100	80	60	60	60	40	20	40	10	20	10	0	0	0	0	0	(40)	40	40	(100)
68°30'	170°	100	80	100	100	80	60	(80)	(60)	20	20	40	10	10	10	0	0	0	0	0	(40)	40	(40)	(100)
69°	170°	100	80	100	100	80	60	(80)	(60)	20	40	40	10	40	10	0	0	0	0	0	(40)	(40)	(40)	(100)
68°30'	170°40'	100	80	100	100	80	60	(80)	(60)	10	20	40	10	(10)	10	0	0	0	0	0	(40)	40	(40)	(100)
69°	170°40'	100	80	100	100	80	60	(80)	(60)	10	40	40	10	(10)	10	0	0	0	0	0	(40)	40	(40)	(100)

## PART II

N Boundary	N Boundary	J	F	M	A	M	J	J	A	S	O	N	D												
71°	161°	(100)	(100)	80	60	80	80	80	60	60	40	60	60	30	20	10	10	10	20	40	40	60	60	(100)	(100)
71°	162°	(100)	(100)	80	60	80	80	80	60	40	40	60	60	20	10	10	20	10	40	40	20	60	60	(100)	(100)
71°	163°	(100)	(100)	80	80	80	(100)	80	60	20	20	60	40	20	10	10	20	10	40	40	20	60	60	(100)	(100)
70°30'	163°	(100)	(100)	80	80	80	(100)	80	60	60	20	60	40	20	10	10	20	10	0	20	10	60	60	(100)	(100)
71°	164°	(100)	(100)	80	80	80	(100)	80	80	20	20	60	20	20	10	10	20	20	40	20	10	40	60	(100)	(100)
70°31'	164°	(100)	(100)	80	80	80	(100)	80	80	40	20	60	20	20	10	10	20	10	40	10	10	40	60	(100)	(100)
71°	165°	(100)	(100)	80	100	(100)	(100)	80	80	40	20	40	20	20	10	20	20	10	10	10	10	40	80	100	(100)
70°30'	165°	(100)	(100)	80	100	(100)	(100)	80	80	40	20	40	20	20	10	0	20	20	10	20	10	40	80	100	(100)
71°	166°	(100)	(100)	80	100	(100)	(100)	80	80	40	20	20	20	20	20	10	20	10	10	20	10	20	80	100	(100)
70°30'	166°	(100)	(100)	80	100	(100)	(100)	80	80	40	20	20	20	20	10	0	20	10	10	10	10	20	80	100	(100)
71°	167°	(100)	(100)	80	100	(100)	(100)	80	80	60	20	20	40	20	20	10	10	(10)	(10)	20	(10)	20	60	100	(100)
70°30'	167°	(100)	(100)	80	100	(100)	(100)	80	80	40	20	20	40	20	20	0	10	(10)	0	10	(10)	20	60	100	(100)
71°	168°	(100)	(100)	80	100	(100)	(100)	80	80	60	40	40	20	40	20	10	10	(10)	0	0	(10)	40	60	100	(100)
70°30'	168°	(100)	(100)	80	100	(100)	(100)	80	80	40	40	40	20	40	20	10	10	(10)	0	0	(10)	40	60	100	(100)
70°31'	169°	(100)	(100)	100	100	(100)	(100)	80	80	40	40	60	20	60	10	10	10	10	0	0	(10)	60	60	(100)	(100)
71°	170°	(100)	100	100	100	(100)	(100)	80	80	40	60	(60)	20	40	10	10	10	(10)	0	0	(10)	60	(60)	(100)	(100)
70°30'	170°	(100)	100	100	100	(100)	(100)	80	80	40	60	(60)	20	60	10	10	0	(10)	0	0	(10)	60	(60)	(100)	(100)
72°	163°	(100)	(100)	80	100	(100)	(100)	100	100	80	(60)	60	60	60	40	10	20	10	10	20	20	40	60	100	(100)
71°30'	166°	(100)	(100)	100	100	(100)	(100)	100	100	(100)	(100)	80	(80)	60	40	10	20	10	10	20	20	40	60	100	(100)
72°	167°	(100)	(100)	100	100	(100)	(100)	100	100	(100)	(100)	80	(80)	60	40	10	20	10	10	20	20	60	60	100	(100)
71°30'	167°	(100)	(100)	80	100	(80)	(80)	80	80	40	40	40	20	30	20	10	10	10	0	0	10	40	60	100	(100)

N Boundary	W Boundary	J	F	M	A	M	J	J	A	S	O	N	D												
72°30'	165°	(100)(100)	100	100	(100)(100)	100	100	(100)(100)	80 (80)	60	60	20	40	20	20	40	40	60	80	100	(100)				
72°	160°	(100)(100)	80	60	80	80	80	60	40	60	60	40	20	10	10	10	10	40	40	60	60	(100)(100)			
71°	160°	(100)	60	80	80	80	80	80	60	40	40	60	60	40	20	10	10	10	10	40	40	60	60	(100)(100)	
70°	164°	(100)(100)	60	80	80	80	80	80	80	40	80	40	40	20	10	0	0	10	0	10	10	40	80	(100)(100)	
70°	165°	(100)(100)	60	80	80	80	100	80	60	40	20	20	20	10	0	10	10	0	10	10	20	80	80	(100)	
69°30'	165°	(100)(100)	60	80	80	80	100	80	60	60	20	20	20	10	0	10	10	0	10	10	20	80	80	(100)	
70°	166°	(100)	40	60	100	80	80	80	80	10	20	20	20	10	0	10	10	0	10	10	20	80	80	(100)	
69°30'	166°	(100)	40	60	100	80	80	80	60	10	20	20	20	10	0	10	10	0	10	20	20	80	60	(100)	
70°	167°	(100)	40	80	100	80	80	80	80	10	20	20	20	20	0	0	10	0	10	10	20	60	80	(100)	
69°30'	167°	(100)	60	80	100	80	80	80	60	10	20	20	20	10	0	0	10	0	10	10	20	60	60	(100)	
70°	168°	(100)	60	80	100	80	80	80	80	10	40	40	20	40	10	0	0	10	0	10	10	20	60	80	(100)
69°30'	168°	(100)	60	80	100	80	80	80	80	10	20	40	20	40	10	0	0	0	0	10	10	20	60	60	(100)
70°	169°	(100)	60	80	100	80	80	80	80	10	40	60	20	60	10	0	0	0	0	0	10	40	(60)	(100)(100)	
69°30'	169°	(100)	60	80	100	80	80	80	80	10	40	40	20	60	10	0	0	0	0	0	10	40	(60)	(80)(100)	
70°	170°	(100)	80	100	100	80	80	80	80	20	40	60	20	60	10	10	0	0	0	0	0	60	(60)	(100)(100)	
69°30'	170°	(100)	80	100	100	80	80	80	80	10	40	60	10	60	10	0	0	10	0	10	10	40	80	(100)(100)	

Estimated monthly mean temperatures, as compiled from actual temperature measurements, in areas bounded by 1° of longitude and 30' of latitude. The boundaries of the areas are given in the first two columns. Pairs of numbers are listed. The first is the mean in °C; the second (in parentheses) is the number of measurements upon which it is based. Parts I and II of the table are for the southern and northern Chukchi Sea respectively, as defined by latitude 69°N.

PART I

N Boundary	W Boundary	J	F	M	A	M	J	J	A	S	O	N	D
66°	168°							1.8 (5)	11.2 (3)				
66°	169°							3.2 (9)	4.4 (53)	3.8 (16)	4.4 (8)		
66°	170°								1.7 (14)	1.4 (4)	0.9 (1)		
66°30'	162°								3.1 (8)				
67°	163°					-1.8 (5)			4.1 (11)				
66°30'	163°		-1.7 (2)						2.9 (26)				
67°	164°		-1.8 (6)						8.2 (34)	6.6 (6)			
66°30'	164°		-1.8 (2)						8.5 (17)				
67°	165°		-1.8 (11)						7.4 (13)	8.5 (8)			
67°	166°		-1.8 (1)					7.6 (1)	8.5 (18)	7.3 (3)	4.2 (2)		
66°30'	166°								10.0 (1)				
67°	167°								6.9 (20)	7.7 (1)	5.1 (1)		
66°30'	167°								8.9 (3)				
67°	168°							3.3 (1)	6.5 (22)	6.2 (1)	3.4 (1)		

699



N Boundary	W Boundary	J	F	M	A	M	J	J	A	S	O	N	D
66°30'	168°								9.4 (21)	7.4 (2)	5.7 (3)		
67°	169°							3.4 (1)	4.9 (16)	3.7 (3)	3.0 (2)		
66°30'	169°							2.0 (3)	3.9 (27)	5.3 (1)	3.2 (4)		
67°	170°								3.7 (3)	1.1 (1)	2.8 (1)		
66°30'	170°							3.2 (1)	3.3 (1)		1.8 (2)		
67°	170°40'							2.4 (2)		1.7 (1)			
67°30'	164°								7.1 (70)	6.8 (2)			
68°	165°		-1.8 (1)						9.3 (13)	5.5 (2)			
67°30'	165°		-1.7 (1)						7.5 (32)	6.6 (5)			
68°	166°								5.3 (99)	7.4 (1)			
67°30'	166°						0.1 (5)		6.0 (21)	6.4 (2)	3.8 (3)		
68°	167°						0.3 (3)		4.2 (64)	3.0 (2)			
67°30'	167°								3.6 (20)	4.6 (2)			
68°	168°								3.0 (28)				
67°30'	168°								3.0 (21)	2.5 (3)	3.3 (1)		
68°	169°								3.1 (11)	2.6 (2)			
67°30'	169°								3.1 (9)	1.7 (2)	4.0 (2)		
68°	170°								3.3 (1)		3.3 (1)		

670

	N Boundary	W Boundary	J	F	M	A	M	J	J	A	S	O	N	D
	67°30'	170°								3.1 (4)		2.1 (2)		
	67°30'	170°40'								1.9 (2)	1.5 (1)			
	69°	166°								6.9 (2)				
	68°30'	166°								10.2 (2)				
	69°	167°		-1.9 (2)				2.6 (2)		6.9 (17)	5.8 (2)	1.0 (2)	-1.8 (1)	
	68°30'	167°								8.0 (23)	7.3 (1)			
	69°	168°		-1.9 (2)				0.1 (3)		5.2 (22)	3.8 (4)			
671	68°30'	168°						1.4 (1)		5.2 (26)	3.2 (1)	1.7 (1)		
	69°	169°		-1.9 (3)						3.4 (20)	3.5 (2)			
	68°30'	169°								2.9 (10)	3.1 (1)	2.9 (1)		
	69°	170°		-1.9 (2)						2.4 (6)	1.3 (2)			
	68°30'	170°							--	--	--			
	69°	170°40'			-1.9 (2)					1.4 (4)	1.1 (1)			
	68°30'	170°40'										1.7 (2)		

## Part II

N Boundary	W Boundary	J	F	M	A	M	J	J	A	S	O	N	D
71°	161°								2.2 (32)	5.2 (4)			
71°	162°								2.8 (2)	2.2 (3)			
71°	163°							-1.2 (7)	3.6 (5)	4.4 (7)			
70°30'	163°								6.6 (4)	5.6 (2)	3.9 (4)		
71°	164°							-1.6 (2)		4.4 (2)			
70°30'	164°							-1.1 (4)	4.6 (10)	6.8 (18)	4.2 (6)		
71°	165°								1.2 (12)	4.6 (6)			
70°30'	165°							0.5 (13)	3.7 (5)	5.8 (15)	2.8 (3)		
71°	166°							-1.6 (1)	1.4 (21)	3.6 (2)			
70°30'	166°							-1.5 (1)	0.9 (2)	3.6 (11)	6.4 (6)		
71°	167°							-1.8 (1)	2.0 (20)	3.7 (2)	1.8 (1)		
70°30'	167°							-1.5 (8)	2.9 (12)	3.0 (3)	2.7 (1)		
70°	168°								-0.6 (11)				
70°30'	168°							-0.9 (1)	0.8 (11)	3.2 (2)	1.9 (2)		
70°30'	169°								-1.4 (8)	-1.7 (1)	1.8 (1)		
71°	170°									0.7 (4)			
70°30'	170°								3.6 (1)	0.4 (2)			
71°	170°40'							-1.2 (1)					
72°	163°								-1.8 (1)				
71°30'	166°							-0.5 (2)		0.9 (1)			

	N Boundary		J	F	M	A	M	J	J	A	S	O	N	D
	72°	15°								-1.4 (5)				
	71°30'	16°								-1.8 (8)				
	72°	16°							-1.7 (7)					
	71°	16°							0.3 (7)	3.1 (20)	1.8 (1)			
	70°	16°							5.7 (6)	4.2 (7)	2.4 (2)			
	70°	15°							2.6 (6)	3.2 (4)	4.3 (6)	3.4 (1)		
	69°30'	15°		-1.9 (1)						4.2 (9)	7.1 (1)	1.8 (2)		
	70°	16°							-1.8 (1)	2.9 (9)	7.1 (4)	0.7 (1)		
673	69°30'	16°								6.4 (10)	7.1 (1)	0.6 (2)		
	70°	15°							-1.6 (3)	2.6 (21)	4.8 (5)	3.6 (2)		
	69°30'	17°							2.0 (7)	6.0 (21)	7.0 (2)	1.6 (2)		
	70°	16°		-1.9 (1)					-0.1 (8)	3.7 (5)	3.7 (3)	3.4 (4)		
	69°30'	18°							0.5(14)	5.2 (11)	4.5 (2)	3.0 (1)	0.2 (2)	
	70°	19°							-1.7 (2)	1.4 (6)	3.3 (1)			
	69°30'	19°		-1.8 (1)					-0.7 (3)	3.3 (6)	3.6 (1)	3.2 (1)		
	70°	20°								1.9 (2)	4.1 (1)			
	69°30'	20°								-1.7 (4)	2.6 (3)	2.7 (1)		

Reference List for Chukchi Sea Bottom Temperature

- Acona, August, 1974, National Oceanographic Center - Bathythermograph listing.
- AEIDC, 1975. "Plate 14 Oceanography" in Chukchi Sea: Bering Strait-Icy Cape Physical and Biological Character of Alaskan Coastal Zone and Marine Environment. Sea Grant Report 75-10, University of Alaska.
- Alpha Helix, 1974. Institute of Marine Science Cruise 778.
- Alverson, D. L., and Wilimovsky, N. J., 1966. "Fishing Investigation of the Southeastern Chukchi Sea" in Environment of Cape Thompson Region, Alaska. N. J. Wilimovsky and J. N. Wolfe, Eds., U.S. Atomic Energy Commission Report PNE-461, pp. 843-860. M.V. John N. Cobb, 1959.
- Anonymous, 1954. Oceanographic Cruise to the Bering and Chukchi Seas, Summer, 1949. Part IV: Physical Oceanographic Studies, Vol. 2. Data Report. Oceanographic Section, USNEL and Pacific Oceanographic Group, Canada. HMCS Cedarwood 1949.
- Atka, 1956. National Oceanographic Data Center - Bathythermograph Listing.
- Bell Helicopter, 1977, National Oceanographic Center - Bathythermograph listing.
- Bloom, G. L., 1964. "Water Transport and Temperature Measurements in the Eastern Bering Strait, 1953-1958." J. Geophys. Res., Vol. 69, No. 16, pp. 3335-3354.
- Burton Island, 1960. National Oceanographic Data Center - Bathythermograph listing.
- Burton Island, 1961. National Oceanographic Data Center - Bathythermograph listing.
- Burton Island, 1966. National Oceanographic Data Center - Bathythermograph listing.
- Chelsea, 1967. National Oceanographic Data Center - Bathythermograph listing.
- Discoverer, 1976, National Oceanographic Center - Bathythermograph listing.
- Eldorado, 1956. National Oceanographic Data Center - Bathythermograph listing.

- Fleming, R. H., and staff, 1961. Physical and Chemical Data for the Eastern Chukchi and Northern Bering Seas. Dept. of Oceanography, Univ. of Washington, Technical Report 69. Brown Bear Cruise 236, 2 August to 1 September, 1959; Brown Bear Cruise 268, 26 July to 28 August, 1960. The Brown Bear Cruise of 1960 is also on the National Oceanographic Data Center Bathythermograph listing and in R. H. Fleming and D. Heggarty, "Oceanography of the Southeastern Chukchi Sea" in Environment of the Cape Thompson Region, Alaska, N. J. Wilimovsky and J. N. Wolfe, Eds.
- Garrison, G. R., and Becker, P., 1975. Marginal Sea Ice Zone Oceanographic Measurements Bering and Chukchi Seas, 1973 and 1974. Applied Physics Laboratory, A Division of the Univ. of Washington. APL-UW 7505. Burton Island 1973; Burton Island 1974; Staten Island 1974.
- Garrison, G. R., and Becker, P., 1976. The Barrow Submarine Canyon: A Drain for the Chukchi Sea. J. Geophys. Res., Vol. 81, No. 24, p. 4445.
- Garrison, G. R., and Pence, E. A., 1973. Studies in the Marginal Ice Zone of the Chukchi and Beaufort Seas. A report on Project MIZPAC-71B, Applied Physics Laboratory, A Division of the Univ. of Washington. APL-UW 7223. Northwind 1972.
- Garrison, G. R., Pence, E. A., and Feldman, H. R., 1973. Studies in the Marginal Ice Zone of the Chukchi Sea. Acoustic and Oceanographic Data for 1972. Applied Physics Laboratory, A Division of the Univ. of Washington. APL-UW 7309. Staten Island 1972.
- Harmony, 1967. National Oceanographic Data Center - Bathythermograph listing.
- Husby, D. M., 1969. Report of Oceanographic Cruise USCGS Northwind Northern Bering Sea-Bering Strait-Chukchi, July 1967. U.S. Coast Guard Oceanographic Report 24. Northwind 1967.
- Husby, D. M., and Hufford, G. L., 1971. Oceanographic Investigation of the Northern Bering Sea and Bering Strait, 8-21 June 1969. U.S. Coast Guard Oceanographic Report 42. Northwind 1969.
- Husby, D. M., and Hufford, G. L., 1971. Oceanographic Investigation of the Northern Bering Sea and Bering Strait, 8-21 June 1969. U.S. Coast Guard Oceanographic Report 42. Northwind, 8-21 June 1969.
- Kinney, P. J., Burrell, D. C., Arhelger, M. E., Loder, T. C., and Hood, D. W., 1968. Chukchi Sea Data Report: USCGS Northwind, July-August 1968; USCGS Staten Island, July-August 1969. Institute of Marine Science, Univ. of Alaska. Northwind 1968. This information is also on the National Oceanographic Data Center Bathythermograph listing and the Institute of Marine Science Cruise 751 listing.
- Lachenbruch, A. H., Green, G. W., and Marshall, B. V., 1966. "Permafrost and the Geothermal Regimes" in Environment of the Cape Thompson Region Alaska. N. J. Wilimovsky and J. N. Wolfe, Eds., U.S. Atomic Energy Commission Report PNE-481, pp. 149-163.

- LaFond, E. C., Dietz, R. S. and Pritchard, D. W., 1949. Oceanographic Measurement from the USS Nereus on a Cruise to the Bering and Chukchi Seas, 1947. U.S. Navy Electronics Laboratory, San Diego, California. USS Nereus 1947.
- LaFond, E. C., and Pritchard, D. W., 1952. Physical Oceanographic Investigation in the Eastern Bering and Chukchi Seas During the Summer of 1947. J. of Marine Res., Vol. 11, No. 1, pp. 69-86.
- Moana Wave, 1976, National Oceanographic Data Center - Bathythermograph listing.
- Northwind, 1958. National Oceanographic Data Center - Bathythermograph listing.
- Northwind, 1959. National Oceanographic Data Center - Bathythermograph listing.
- Northwind, 1961. National Oceanographic Data Center - Bathythermograph listing.
- Northwind, 1962. National Oceanographic Data Center - Bathythermograph listing. Oceanographic Cruise USCGC Northwind, Bering and Chukchi Seas, July-September 1962. U.S. Coast Guard Oceanographic Report 1, 1964.
- Northwind, 1963. National Oceanographic Data Center - Bathythermograph listing.
- Northwind, 1964. National Oceanographic Data Center - Bathythermograph listing.
- Northwind, 1966. National Oceanographic Data Center - Bathythermograph listing.
- Osterkamp, T. E., and W. D. Harrison, 1978. Subsea Permafrost: Probing, Thermal Regime and Data Analysis, OCSEAP Annual Report, Reporting Period April 1, 1977 to March 31, 1978.
- Pathfinder, 1954. National Oceanographic Data Center - Bathythermograph listing.
- Saur, J. F. T., Tully, J. P., and LaFond, E. C., 1954. Oceanographic Cruise to the Bering and Chukchi Seas, Summer 1949. Part IV: Physical Oceanographic Studies, Vol. 1, Descriptive Report. U.S. Navy Electronics Laboratory, San Diego, California. HMCS Cedarwood, 1949; USS Baya 1949; USS Epce 1949.
- Scholl, D. W., and Sainsbury, C. L., 1961. "Marine Geology and Bathymetry of the Chukchi Shelf Off the Ogotoruk Creek Area, Northwest Alaska" in Geology of the Arctic, Gilbert O. Raasch, pp. 718-732.

- Seasounder, July 1977, National Oceanographic Data Center - Bathythermograph listing.
- Staten Island, 1961. National Oceanographic Data Center - Bathythermograph listing.
- Storis, 1954. National Oceanographic Data Center - Bathythermograph listing.
- Surveyor, 1962. National Oceanographic Data Center - Bathythermograph listing.
- Surveyor, August 1977, National Oceanographic Data Center - Bathythermograph listing.
- Wilimovsky, N. J., 1953. Inshore Temperature and Salinity Data During Open Water Periods, Point Barrow, Alaska, 1951-1953, 14 pp. Available from NARL library.
- Wilimovsky, N. J., 1954. Inshore Temperature and Salinity Data During Open Water Period, Point Barrow, Alaska, 1954, 5 pp. Available from NARL library.



